

Sonja Phillipp, Bernd Leiss, Axel Vollbrecht,
David Tanner & Agust Gudmundsson (Hrsg.)

11. Symposium
„Tektonik, Struktur- und Kristallogenie“
Zusammenfassungen der Tagungsbeiträge



Geowissenschaftliches Zentrum
der Georg-August-Universität
Göttingen

22.-24. März 2006



Universitätsdrucke Göttingen

Sonja Philipp, Bernd Leiss, Axel Vollbrecht, David Tanner & Agust
Gudmundsson (Hrsg.)

11. Symposium „Tektonik, Struktur- und Kristallingeologie“

Except where otherwise noted, this work is
licensed under a [Creative Commons License](#)



erschienen im Universitätsverlag Göttingen 2006

Sonja Philipp, Bernd Leiss, Axel
Vollbrecht, David Tanner & Agust
Gudmundsson (Hrsg.)

11. Symposium „Tektonik, Struktur- und Kristallingeologie“

Zusammenfassung der
Tagungsbeiträge



Universitätsverlag Göttingen
2006

Bibliografische Information der Deutschen Bibliothek

Die Deutsche Bibliothek verzeichnet diese Publikation in der Deutschen Nationalbibliographie; detaillierte bibliografische Daten sind im Internet über <<http://dnb.ddb.de>> abrufbar.

Diese Publikation wird außerdem über die Publikationsplattform GEO-LEO *e-docs* verfügbar sein <<http://geoleo.sub.uni-goettingen.de/geoleo/www-docs/>>.

Anschriften der Herausgeber

Geowissenschaftliches Zentrum
der Universität Göttingen
Abteilung Strukturgeologie und Geodynamik
Goldschmidtstr. 3, D-37077 Göttingen
<http://www.gzg.uni-goettingen.de/struktur/>

Titelbild: Deformierter und migmatisierter Metasediment-Xenolith (NE' Gunnebo, Västervik-Gebiet, SE-Schweden), aufgenommen von Ralf Klischies.

Dieser Xenolith gehört zu den metasedimentären Einheiten der Västervik-Formation, die unterschiedliche Grade von Migmatisierung zeigen. Solche Schollen treten in großer Anzahl am Nordufer des Verkebäcksviken in einem mittelkörnigen Granit auf, der vermutlich als Anatexit bei der Migmatisierung des Rahmengesteins entstanden ist. Anhand des dextral ausgelenkten Metasediment "Sigmaklasten" ist deutlich zu erkennen, wie der Granit sein eigenes Ausgangsmaterial deformiert.

© 2006 Universitätsverlag Göttingen
Umschlaggestaltung: Hans-Werner Hilse, David Tanner
Satz und Layout: David Tanner
ISBN 3-938616-40-7

Inhaltsverzeichnis

Vorwort		1
Almeida, H.L., Ruiz, A.S. & Vollbrecht, A.	Poster	
<i>Microfabrics and textures of quartzites of the Indiavaí-Lucialva shear zone, SW Amazonian Craton: preliminary conclusions</i>		3
Andrew, R. & Gudmundsson, A.	Poster	
<i>Holocene shield volcanoes in Iceland</i>		6
Angerer, T. & Greiling, R.O.	Vortrag	
<i>Rock fabrics in palaeo-weathering profiles below basement-cover interfaces (AMS-study on drill cores from the Caledonian margin, Central Sweden)</i>		9
Beck, A., de Wall, H. & Kück, J.	Vortrag	
<i>Lithologierekonstruktion von submarinen Einheiten des Mauna Kea Vulkans mit bohrlochgeophysikalischen Messungen der magnetischen Suszeptibilität, HSDP Bohrung, Hawai'i</i>		12
Bense, F., Ertl, G., Battaglia, M. & Vollbrecht, A.	Poster	
<i>GPS-gestützte Kartierung gravitativer Massenverlagerungen an der Röt/ Muschelkalk-Grenze im Göttinger Wald</i>		16
Bissen R. & Henk A.	Poster	
<i>Felsmechanische Untersuchungen am Hauptrogenstein (bjHR) der Vorbergzone des südlichen Oberrheingrabens</i>		18
Brodhag, S., Herwegh, M., Berger, A. & Pfiffner, A.	Vortrag	
<i>Gekoppeltes Kornwachstum in polymineralischen Gesteinen</i>		20
Burchardt, S., Gudmundsson, A. & Krumbholz, M.	Poster	
<i>Tektonische Entwicklung des Geitafell-Vulkans, Südost-Island</i>		21
Burchardt, S., Gudmundsson, A. & Philipp, S.L.	Poster	
<i>Dyke emplacement in Tenerife (Canary Islands): Field studies and numerical models</i>		24

Burchardt, S., Kracke, T., Molli, G. & Leiss, B.	Poster	
<i>Regional fold structure analysis in the Eastern Alpi Apuane, Northern Apennine</i>		25
Buurman, N. & Reuther, C.-D.	Poster	
<i>Erkundung von Erdfallstrukturen in der Metropolregion Hamburg und Lüneburg mit dem Georadar (Ground Penetrating Radar)</i>		27
Chatziliadou, M, Hilgers, C. & Sindern, S.	Vortrag	
<i>Fracture sealing in limestones, a microstructural and mineralogical study</i>		30
Cotza, G., Thöni, M. & Grasemann, B.	Poster	
<i>Structural investigations of the W termination of the ‘Schneeberg Zug’ — Austroalpine Unit, Southern Tyrol: Results from a crustal scale shear zone</i>		33
Davaa, B., Geerds, P., Vogler, M. & Henk, A.	Poster	
<i>Evolution of the Tamtsag Basin / NE-Mongolia — part II: structure and hydrocarbon potential</i>		34
Deckert, H. & Gessner, K.	Poster	
<i>Application of Photogrammetry in Geology: 3D Investigation of Rock Fracture Distributions</i>		36
Deckert, H. & Ring, U.	Vortrag	
<i>Relevance of viscous flow in accretionary wedges</i>		38
Doman, D., Riller, U. & Hofmann, K.	Vortrag	
<i>Deformation mechanisms in the eastern Sudbury Igneous Complex, Canada: Evidence for meteorite impact into an active orogen</i>		40
Dresmann, H., Spottke, I., Timar-Geng, Z. Wetzels, A. & Fügenschuh, B.	Poster	
<i>A further step toward a thermochronological 3-D model of the SE Black Forest</i>		42
Dunkl, I., Danišik, M., Picotti, V., Frisch, W. von Eynatten, H. & Castellarin, A.	Vortrag	
<i>(U-Th)/He thermochronology — methodology and a case study: dating of faulting in the Southern Alps</i>		45
Dworazik, N., Auer, A., Martin, U., Németh, K., de Wall, H. & Rolf, C.	Poster	
<i>Magnetische Charakteristik von Pyroklastika des Ság-hegy Vulkan Komplex, Kleine Ungarische Tiefebene</i>		48
Ebert, A., Herwegh, M. & Pfiffner, A.	Vortrag	
<i>Entwicklung einer fluidbeeinflussten Scherzone am Beispiel der Glarner Hauptüberschiebung (Schweiz)</i>		50

Ehrlich, R., Sverdrup, E., Øye, V., Smørdal Lien, K. & Færseth, R.	Vortrag	
<i>Quantification and sensitivity of fault seal parameters demonstrated in an integrated reservoir modelling work flow. A case study on the Njord Field, Halten Terrace, Norway</i>		52
Fischer, M., Hansen, B.T. & Kleinhanns, I.C.	Poster	
<i>Geochemische Klassifikation und Sm-Nd Isotopensystematik proterozoischer Metasedimente des Baltischen Schildes (Västervik Region, SE-Schweden)</i>		56
Freitag, R., Jähne, F., Gaedicke, C. & Krbetschek, M.	Poster	
<i>Deformationsanalyse und mechanische Kopplung eines aktiven fore-arcs in Raum und Zeit, Kamtschatka, Russische Föderation</i>		58
Friese, N., Krumbholz, M., Burchardt, S. & Gudmundsson, A.	Poster	
<i>Strukturgeologische Analysen des Thingvellir Spaltenschwarms, Süd-west Island</i>		61
Geerdts, P., Vogler, M., Davaa, B. & Henk, A.	Poster	
<i>Evolution of the Tamtsag Basin / NE-Mongolia — part I: basin fill</i>		63
Gessner, K., Jones, P.A. & Wilde, A.S.	Vortrag	
<i>Strain Localisation, Fracturing and Hydrothermal Mineralisation: Numerical Models of the Mount Isa Copper Deposit, Australia</i>		66
Glotzbach, C., Spiegel, C., Rahn, M. & Reinecker, J.	Poster	
<i>Perturbation of isotherms below topography: constraints from tunnel transects through the Alps, Gotthard road tunnel</i>		67
Greiling, R.O., Lichtenberger, M. & Obermeyer, H.	Vortrag	
<i>Electromagnetic radiation (EMR) and its interpretation in terms of stresses in the lithosphere</i>		70
Grimmer, J.C.	Poster	
<i>Very high anisotropies of the magnetic susceptibility in ductile shear zones: first quantitative results from a metamorphic nappe in the Central Scandinavian Caledonides, Sweden</i>		72
Gröger, H., Tischler, M., Fügenschuh, B. & Schmid, S.M.	Vortrag	
<i>The timing of polyphase Miocene tectonics in Northern Romania</i>		73
Gross, CJ	Poster	
<i>Grain coarsening and hydrothermal alteration in metacarbonates of the Damara Orogen, Namibia</i>		75
Gudmundsson, A. & Geyer, A.	Poster	
<i>Effects of damage-zone thickness on fault displacement</i>		79

Gudmundsson, A. & Philipp, S.L.	Poster	
<i>How stress transfer between volcanic and seismic zones affects volcanic and earthquake activity</i>		81
Hauten, S., Handy, M.R. & Dobmeier, C.	Poster	
<i>Feldspar deformation in greenschist facies shear zones (Aar-Massif, Switzerland)</i>		84
Heinemann, N, Giba, M. & Stipp, M.	Poster	
<i>Scherzonen- und Schuppenbildung am Kontakt von Aarmassiv und Helvetikum im Bereich der Engelhörner, Berner Oberland (Schweiz)</i>		85
Hilgers, C., Bücker, C. & Urai, J.	Vortrag	
<i>Fossil overpressures compartments? A case study from the Eifel area and some general aspects</i>		87
Hilgers, C., Pennock, G., Schlöder, Z., Burgila, S. & Urai, J.	Poster	
<i>Microstructures of fibrous halite veins</i>		90
Hirt, A.M., Schmidt, V., McEnroe, S., Heidelbach, F. & Robinson, P.	Poster	
<i>Magnetic fabric in ilmenite-rich norites of the Bjerkreimer-Sokndal Layered Intrusion, Norway</i>		91
Hoffmann, S., Müller, C., Philipp, S.L. & Gudmundsson, A.	Poster	
<i>Strukturgeologische Geländestudie im Mittleren Buntsandstein zur Nutzung als geothermisches Reservoir</i>		93
Ibele, T. & Behrmann, J.H.	Poster	
<i>Deformation und Kinematik der Lechtal-Decke im nordwestlichen Rätikon, Nördliche Kalkalpen (Vorarlberg, Österreich)</i>		96
Jähne, F. & Freitag, R.	Vortrag	
<i>Remote Sensing Analyses of Neotectonic Active Regions in East-Kamchatka</i>		98
Jonas, P.S. & Ranten, C.D.	Poster	
<i>The significance of fractures in Europe</i>		101
Kenkmann, T.	Vortrag	
<i>The fate of sandstone during impact cratering: shock compaction, cataclastic flow, and granular fluidization</i>		103
Kiechl, E., Rabitsch, R., Gaich, H., Kurz, W. & Winkler, G.	Poster	
<i>Die hydrogeologische Wirksamkeit von Störungen am Beispiel des Talhof-Störungs-System (Ostalpen, Österreich)</i>		106
Klein, T., Zulauf, G., Craddock, J. & Glodny, J.	Vortrag	
<i>Methodische Untersuchungen am Kreta-Detachment (Kreta, Griechenland): Anzeichen für eine alpidische Metamorphose der Hangendscholle</i>		108

- Klimczak, C. & Riller, U. Poster
Deformation of the Onaping Formation in the NE-lobe of the Sudbury Igneous Complex, Canada: Evidence for fold adjustment flow in the core of a km-scale fold 111
- Koehn, D., Renard, F., Toussaint, R., Schmittbuhl, J. & Passchier, C. Vortrag
Die dynamische Entwicklung von Styloliten 112
- Kouankap, N.G.D. Poster
Textures in mylonitised granite from Banefo area in the central part of the Cameroon Central Shear Zone (central Africa) — Kinematics and gradian deformation indicators 113
- Kouankap, N.G.D. Poster
Neotectonic markers in the Panafrikan belt formations of Cameroon: elements of interpretation and their environmental impacts 115
- Kouankap, N.G.D. & Sylvestre, G. Vortrag
A new practical and economical technique for the obtention of high quality thin section photographs with the help of a simple optical microscope 116
- Krumbholz, M., Friese, N., Burchardt, S. & Gudmundsson, A. Poster
Fluidtransport entlang von Störungen und Klüften im Gebiet des Hengill-Vulkans, SW-Island 119
- Kühn, A. & Austrheim, H. Poster
Metastability and HP metamorphism at fluid deficient conditions, an example from the Bergen Arcs (Western Norway) 121
- Kühn, A., Glodny, J. & Ring, U. Poster
Oligocene emplacement of the Eclogite Zone of the central Tauern Window, Eastern Alps, Austria 122
- Laukamp, C. & Angerer, T. Poster
Eo-Alpine imbrication of Middle Austroalpine units in the Gurktal Alps, Carinthia — questioning the existence of the Upper Austroalpine Murau Nappe 123
- Laukamp, C., Petzel, V. & Bechstädt, T. Vortrag
Structural control of fluid flow on a carbonate platform margin: an example from the Otavi Mountainland, Namibia 125
- Leiss, B. & Ullemeyer, K. Poster
Neue Perspektiven der Texturanalytik von Gesteinen mit konventioneller Röntgenbeugung 128
- Letourneur, L. & Gudmundsson, A. Poster

- Asymmetrical deformation of the Piton de la Fournaise (Réunion Island) summit cone* 130
- Liebl, C., Kuntcheva, B., Kruhl, J.H. & Kunze, K. Poster
Effect of crystallography and temperature on the development of quartz high-angle grain boundaries in metamorphic rocks 132
- Liu, J. & Cao, S. Vortrag
Change of deformation mechanisms during low temperature flow of rocks — observation from micron to nanometer scales 135
- Lögering, M.J., Kolb, J., Meyer, F.M. & Schwarzbauer, J. Vortrag
Paläofluide in störungskontrollierten Bruchsystemen der Aachener Geothermie-Bohrung 137
- Mora, A., Parra, M. & Strecker, M. Vortrag
The role of penetrative deformation in orogenic processes. An example from the Eastern Cordillera of Colombia 141
- Müller, M., Grasemann, B., Edwards, M.A., Draganits, E., Voit, K., Igl-seder, C., Zámolyi, A. & Petrakakis, K. Poster
Extensional crustal-scale shear zones in the Western Cyclades (Kea, Greece) 143
- Nagel, T. & Buck, R. Vortrag
Über die mechanischen Ursachen von parallelen Abschiebungen 145
- Neubert, J., van der Klauw, S. & Kley, J. Poster
Microfabrics and deformation processes in magmatic veins of the Thuringian Forest, Germany 146
- Nitzsche, T., de Wall, H. & Rolf, C. Poster
Strukturanalyse juveniler Fragmente in Vulkaniklastika des Messel Maar-Diatremes 151
- Nüchter, J.-A. and Stöckhert, B. Vortrag
Fracturing and vein formation in the middle crust - a record of co-seismic loading and post-seismic stress relaxation 155
- Otto, M, Hirt, A.M., Leiss, B., Schmidt, V. & Walter, J.M. Poster
Correlation of magnetic fabric and crystallographic preferred orientations of naturally deformed carbonate — mica rocks from the Alpi Apuane in Italy and the Damara Orogen in Namibia 156
- Peternell, M. & Kruhl, J.H. Vortrag
Crystal distribution patterns and their anisotropy behaviour in igneous rocks: towards an automated quantification, first results 159
- Pfaar, R., Leiss, B., Molli, G. & Walter, J.M. Poster
Gefügecharakterisierung von Calcitmyloniten und Marmoren bezüglich

<i>senkrecht zueinander stehender Falteinteilstrukturen, Alpi Apuane, Italien</i>		161
Philipp, S.L. & Gudmundsson, A.	Poster	
<i>Gypsum veins as hydrofractures in layered and faulted mudstones: implications for reservoir permeability</i>		164
Philipp, S.L., Oelrich, A., Müller, C., Hoffmann, S., Bartelsen, T., Thäter, D. & Gudmundsson, A.	Poster	
<i>Strukturgeologische Studien als Beitrag zum Erfolg tiefergeothermischer Projekte</i>		167
Pleuger, J., Roller, S., Walter, J.M., Jansen, E. & Froitzheim, N.	Vortrag	
<i>Kinematik des Deckenkontaktes zwischen der Combinzone und der Zermatt-Saas-Zone (Penninische Decken, Westalpen) und deren Bedeutung für die Exhumierung der Zermatt-Saas-Zone</i>		170
Rambousek, C., Grasemann, B., Petrakakis, K., Edwards, M.A., Iglseder, C. & Zamolyi, A.	Vortrag	
<i>The Serifos Metamorphic Core Complex (Greece) — kinematic investigations of the southern detachment mylonites</i>		172
Renk, D., de Wall, H., Martin, U. & Nemeth, K.	Poster	
<i>Einfluss der Zusammensetzung von Titanomagnetit auf die Anisotropie der magnetischen Suszeptibilität — Fallstudie an einem Dyke-Sill Komplex in Ungarn</i>		173
Reuther, C.-D. & Moser, E.	Vortrag	
<i>Empirische Feldstudien über elektromagnetische Emissionen in Gesteinen unter aktiven Krustenspannungen</i>		177
Richter, P., Ring, U., Willner, A.P. & Leiss, B.	Vortrag	
<i>Structural contacts in the Late Paleozoic accretionary wedge of central Chile and their tectonic significance for the evolution of the accretionary complex</i>		179
Riller, U.	Vortrag	
<i>Origin of Central Andean collapse calderas</i>		180
Riller, U., Götze, H.-J., Schimdt, S., Hongn, F. & Ivan, P.	Poster	
<i>Identification of upper-crustal discontinuities using dip curvature analysis of isostatic residual gravity: examples from the central Andes</i>		181
Roeser, G., Behrmann, J.H. & Kopf, A.	Vortrag	
<i>Geotechnical characterization of trench- and slope sediments off Southern Chile: preliminary results</i>		182
Ruedrich & Vollbrecht	Poster	
<i>Geowissenschaftliche Bedeutung von Mikrorissen in Kristallingesteinen</i>		185

Sachau, T. & Koehn, D.	Poster	
<i>Influence of viscosity on the growth of high pressure phases in computer experiments</i>		187
Scherler, D., Kenkmann, T. & Jahn, A.	Vortrag	
<i>Structural record of an oblique impact: the central uplift of the Upheaval Dome impact structure, Utah, USA</i>		188
Schmatz, J., Vrolijk, P., Urai, J.L., Giese, S., Ziegler, M. & van der Zee, W.	Poster	
<i>Experimental study of the evolution of fault gouge in layered sand-clay sequences</i>		191
Schmidt, V. Hirt, A.M., Burlini, L., Leiss, B. & Walter, J.M.	Vortrag	
<i>Measurement of calcite crystallographic-preferred orientations by magnetic anisotropy and comparison to diffraction methods</i>		194
Schmidt, V., Hirt, A.M. & Rosselli, P.	Poster	
<i>Separation of magnetic subfabrics by high-field, low-temperature torque measurements</i>		196
Scholz, K., Urai, J.L., Trautwein, U. & Kukla, P.	Vortrag	
<i>Microstructural analysis of the RWTH-1 cores in thin-sections</i>		196
Schreurs, G., Giese, J., Berger, A. & Gnos, E.	Poster	
<i>The role of the Ranotsara Zone in southern Madagascar for Gondwana correlations</i>		198
Schneider, S. & Rosenberg, C.	Poster	
<i>Kinematics of the SEMP-fault in the western Tauern Window (Stillupp Valley)</i>		201
Schulz, B., Krenn, E., Finger, F. Brätz, H & Klemd, R.	Poster	
<i>Cadomian and Variscan metamorphic events in the Léon Domain (Armorican Massif) resolved by trace element analysis in monazite and garnet</i>		203
Schwarz, M.	Vortrag	
<i>Evolution and structure of the Upper Rhine Graben — quantitative insights from numerical modelling approaches</i>		205
Seib, N., Kley, J., Freitag, R. & Voigt, T.	Poster	
<i>Die neogene Entwicklung des zentralen Tien Schan, Kasachstan. Erste Ergebnisse von Apatit-Spaltspurdaterungen und morphotektonischer Analyse von Satellitendaten</i>		207
Seidel, T., Leiss, B., Küster, Y., Ullemeyer, K. & Schramm, M.	Poster	
<i>Texturanalysen von Halitmyloniten aus den Salzstrukturen Gorleben, Morsleben und Teutschenthal</i>		211

- Siemes, H., Klingenberg, B., Rybacki, E., Naumann, M., Walter, J.M., Jansen, E. & Kunze, K. Poster
Mikrostruktur und Textur nach Scherverformungsversuchen an Hämatiterzen 214
- Steenken, A., Siegesmund, S., López de Luchi, M., Rapalini, A & Wemmer, K. Vortrag
Syn-kinematic magma ascent and batholith inflation (Sierra de San Luis/Argentina) 216
- Steffes, E., Riller, U. & Doman, D. Poster
Deformation der karbonatischen Espanola-Formation im zentralen Teil der Sudbury-Impaktstruktur, Kanada 220
- Stipp, M. Tullis, J. & Behrens, H. Vortrag
The effect of water, temperature and strain rate on the dislocation creep microstructure, recrystallized grain size and flow stress of quartz 222
- Streit, V., de Wall, H & Dietl, C. Poster
Magnetische Suszeptibilitätsmessungen an Gängen vom Ostrand des Hauzenberger Granitplutons — Bayerischer Wald 224
- Tanner, D.C., Lohr, T., Krawczyk, C.M., Oncken, O., Endres, H., Samiee, R., Trappe, H. & Kukla, P. Poster
Kinematic 3D Retro-Deformation of Fault Blocks Picked from 3D Seismics 226
- Timar-Geng, Z., Henk, A. & Wetzel, A. Poster
Two-dimensional finite element models of convective heat transfer in the upper crust — implications for the interpretation of fission-track data 228
- Trepmann, C.A. & Spray, J.G. Vortrag
Microstructural evidence of impact-induced crystal-plastic deformation and post-shock annealing of quartz 229
- Trepmann, C.A., Stöckhert, B., Dorner, D., Küster, M. & Röller, K. Poster
Quartz microstructures in nature and experiment — evidence of rapid plastic deformation and subsequent annealing 232
- Ullemeyer, K. & Behrmann, J.H. Vortrag
Neutron time-of-flight texture measurements in Dubna: Status and developments 233
- Ustaszewski, M., Pfiffner, A. & Herwegh, M. Vortrag
Neotectonics in the Swiss Alps — A late Alpine to postglacially active fault at the Gemmi Pass 235
- Vahle, C., Kontny, A., Dietze, F. & Audunsson, H. Poster
Discrimination of different volcanic rock units by magnetic properties

— <i>geothermal field at Reykjanes peninsula (SW-Iceland)</i>	238
Voit, K., Grasemann, B., Edwards, M.A., Müller, M., Iglseder, C., Petrakakis, K. & Exner, U. <i>Kinematics and deformation structures in a crustal-scale shear zone on Kea (W. Cyclades, Greece)</i>	Poster 239
Vollbrecht, A., Leiss, B. & Thust, A. <i>Komplexe Verformung von Metaquarziten im Umfeld kleinräumiger Granitintrusionen — Ergebnisse einer Vorstudie im Paläoproterozoikum der Västervik Region (SE-Schweden)</i>	Poster 240
Wagner, L., Lohr, T., Tanner, D.C., Krawczyk, C.M. & Oncken, O. <i>Structural investigation and strain analysis of a polyphase flower structure in the Lower Saxony Basin, Germany</i>	Poster 243
Wittek, A., Riller, U., & Hecht, L. <i>The importance of lithological heterogeneity of the Onaping Formation for understanding post-impact deformation of the Sudbury Impact Structure, Canada</i>	Poster 246
Zámolyi, A., Grasemann, B., Draganits, E., Petrakakis, K., Iglseder, C., Rámbousek C., Exner, U., Voit, K. & Müller, M. <i>Late stage evolution of the Serifos Metamorphic Core Complex (Cyclades, Greece)</i>	Poster 248
Zander, I. <i>Tertiäre Landoberflächen in Mitteldeutschland als Anzeiger tektonischer Bewegungen — Eine Rekonstruktion mittels Einsatz von Geo-Informationssystemen</i>	Poster 249
Autorenverzeichnis	257
Adressenverzeichnis	261

Vorwort

Seit nunmehr 20 Jahren findet regelmäßig alle zwei Jahre das Symposium ‚Tektonik — Strukturgeologie — Kristallingeologie‘ (TSK) statt. Die Tagung soll insbesondere jungen Nachwuchswissenschaftlern die Möglichkeit bieten, ihre Ergebnisse zu diskutieren und einem breiten Fachpublikum vorzustellen. Dies ist natürlich besonders attraktiv, wenn auch die ‚alten Hasen‘ der Zunft eifrig dabei sind.

In diesem Jahr wird schon TSK 11 — nach Tübingen, Erlangen, Graz, Frankfurt, Salzburg, Freiberg, Freiburg und Aachen nun zum zweiten Mal nach 1994 wieder in Göttingen durchgeführt. Wir freuen uns, auch dieses Mal wieder ein vielseitiges Tagungsprogramm präsentieren zu können. Die vorgestellten Arbeiten befassen sich mit Geländebeobachtungen, Laboranalysen und -experimenten bis hin zu Computermodellierungen. Im Maßstab reichen sie vom submikroskopischen Bereich bis hin zu ganzen Orogenen. Dabei werden sowohl duktile als auch spröde Deformationsprozesse beleuchtet. Regionale Geologie ist ebenso Thema wie auch eher angewandte Fragestellungen.

Um die einzelnen Beiträge schnell auffinden zu können, wurden diese alphabetisch nach Erstautoren geordnet. Aus Zeitgründen konnte nur der kleinere Teil der mehr als einhundert eingegangenen Beiträge in das Vortragsprogramm aufgenommen werden. Auf parallele Vortragssitzungen haben wir bewusst verzichtet. Besonderen Raum für anregende Diskussionen sollen auch die thematisch zusammengestellten Postersitzungen bieten, für die wir spezielle Zeiten eingeräumt haben. Hierzu werden Poster jeweils vorher im Plenum kurz vorgestellt.

Die eingegangenen Manuskripte wurden, wie bei TSK üblich, für die Publikation keinem Gutachterverfahren unterzogen. Daher sind die jeweiligen Autoren allein für den Inhalt verantwortlich.

Wir wünschen allen Teilnehmenden anregende Diskussionen und interessante Kontakte sowie einen schönen Aufenthalt in der ‚Stadt, die Wissen schafft‘!

Göttingen, im Februar 2006

Sonja Philipp
Bernd Leiss
Axel Vollbrecht
David Tanner
Agust Gudmundsson

Microfabrics and textures of quartzites of the Indivaí-Lucialva shear zone, SW Amazonian Craton: preliminary conclusions *Poster*

Harrison Lima de Almeida¹ Amarildo Salina Ruiz¹ Axel Vollbrecht²

Introduction

The purpose of this contribution is to present preliminary results regarding the kinematics and deformation conditions of the Indivaí-Lucialva Shear Zone, based on the analysis of the texture and microfabrics of related quartzites.

Geological setting

The Amazonian Craton consists of older Archean cores related to a larger accretionary event represented by the formation of several province belts (Teixeira et al. 1989; Tassinari et al. 2000). The tectonic evolution of the SW Amazonian Craton, in particular, has been attributed the formation of an accretionary complex, Proterozoic in age (Rodonia-San Ignacio Orogeny). Although that division was based on geochronologic data, lineaments have been proposed as structural limits between several terranes. Saes (1999) proposed that the Santa Helena and Jauru (Alto Jauru, Geraldes et al., 2001) terranes were separated by the Indivaí-Lucialva shear zone (ILSZ). The ILSZ constitutes an important mega structure which deformed units of the Jauru terrain and parts of the limit east of the Santa Helena terrain (Fig. 1). Based

¹ Dep. Geologia Geral, Universidade Federal de Mato Grosso-ICET/DGG ² Geowissenschaftliches Zentrum der Georg-August-Universität Göttingen (GZG)

on field studies and Ar-Ar muscovite ages, Ruiz (2005) and Ruiz et al. (2005) have demonstrated that the ILSZ was formed during an extensional tectonic event, possibly associated with the rearrangement of collided blocks related to the Sunsás Orogeny (ca. 900 Ma).

The Indivaí-Lucialva Shear Zone

The Indivaí-Lucialva Shear Zone (ILSZ) strikes NW-SE over a distance of about 100 km separating magmatic rocks from a metavolcanic-metasedimentary sequence. In the studied area (Fig. 1) rocks which display a distinct mylonitic fabric frequently contain feldspar porphyroclasts and garnet. In addition, quartz-rich tectonites, former quartzites, developed along the ILSZ. The mylonitic foliation (S_{myl}) of these mylonitic quartzites, marked by aligned muscovite flakes and strongly flattened small quartz grains, is subparallel to the margins of the shear zone which strikes 315–330° and dips with angles between 60° and 70° to the east-northeast. Shear sense criteria are usually abundant mainly in gneisses which have retained evidence of mylonitization at mesoscale. Moreover, the rocks show a well-developed stretching lineation which is defined mainly by elongated grains of quartz and muscovite laths. The dip angles of this lineation typically vary between about 50° and 70°. The ILSZ clearly exhibits a normal fault kinematic, i.e. a top-to-the-NE movement, juxtaposing the Santa Helena Batholith against metavolcanic-metasedimentary sequences and orthogneisses of the basement.

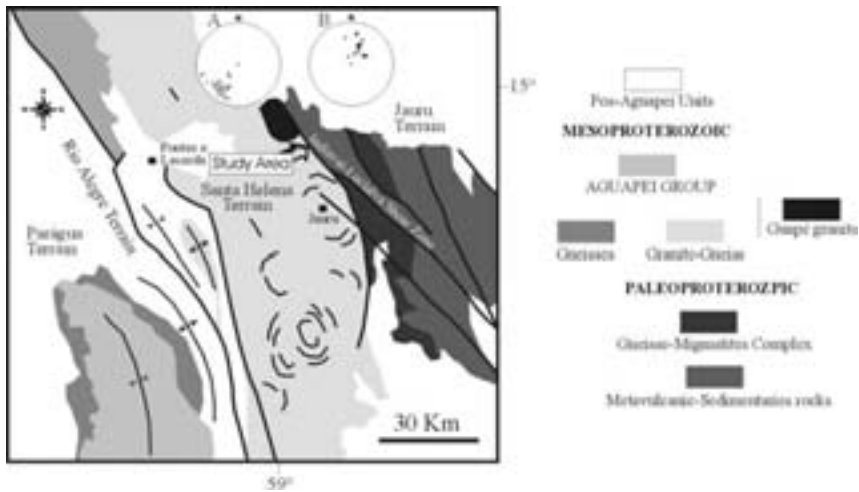


Figure 1: Geological sketch map of the SW Amazonian Craton. The stereoplots display the poles to the mylonitic foliation s_{myl} (A) and stretching lineation L (B), measured within the ILSZ; modified after Ruiz (2005).

Microfabrics

In all the analyzed quartzites, quartz forms polycrystalline aggregates consisting of inequigranular grains with very irregular interlobate grain boundaries. The average quartz grain size scatters between 0.3 and 1.4 mm (Fig. 2A). The occurrence of dissection microstructures (Urai et al. 1986) with the consequent formation of isolated ‘island’ grains, has also been observed in the several thin sections (Fig. 2A). Such microstructures are interpreted as resulting from fast migration of grain boundaries, correlated with the regime 3 microstructure of Hirth & Tullis (1992) which indicates high-temperature (HT) conditions during mylonitisation. In addition, other features pointing to grain boundary migration like dragging and pinning microstructures (Jessel, 1987) have been observed. Microstructures representing a subsequent intracrystalline defor-

mation include deformation bands and irregular subgrains. Frequently, two sets of deformation bands are developed (‘chessboard patterns’; Fig. 2B) indicating HT crystal plasticity (e.g., Kruhl, 1996). Muscovite occurs as solid inclusions in quartz or along the quartz grain boundaries. In the first case, muscovite consists of boudinaged single crystals elongated parallel to the mylonitic foliation (Fig. 2C). It also displays deformation (kink) bands, particularly within larger grains. Kinematic indicators, e.g. mica and tourmaline displaying distinct asymmetric fish-structures, point to a top-to-the-ENE (normal) sense of shear (Fig. 2D). Altogether, grain boundary migration has to be assumed here as the main mechanism of dynamic recrystallization.

Quartz textures

As a start, quartz *c*-axis textures (crystallographic-preferred orienta-

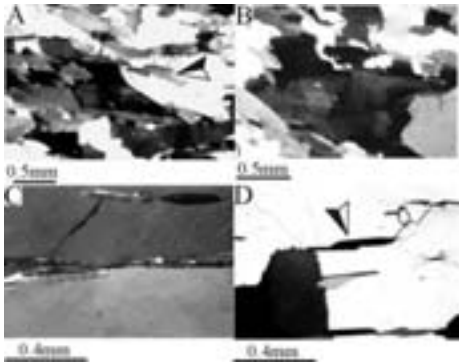


Figure 2: Deformation microstructures in mylonitic quartzite. A. Quartz grains with irregular shape and lobate boundaries. The arrow points to an isolated 'island' grain. B. Two sets of deformation bands in quartz ('chessboard patterns'). C. Tourmaline (top) and muscovite grains (middle) showing boudinage. D. Tourmaline micro fish (arrow) documenting a top-to-the-east sense of shear when reoriented to the field.

tions) have been measured for three selected quartzite mylonite samples (Fig. 3). The quartz c -axis patterns are complex with a more or less pronounced asymmetry with respect to the reference directions (s_{myl} and L) indicating a predominance of non-coaxial deformation. The c -axis maxima close to s_{myl} suggest that prism slip in $\langle a \rangle$ or $[c]$, which is generally attributed to HT deformation regimes (e.g. Mainprice et al. 1986), has significantly contributed to the texture development. Only sample C shows, in addition, a significant concentration of $\langle c \rangle$ -axes sub-normal to s_{myl} pointing to basal slip at lower temperatures. Intermediate positions of maxima are probably related to combined prism and basal slip in connection with complex deformation geometries (e.g. Garbutt & Teyssier, 1991). According to Stipp et al. (2002) complex pole figure of this

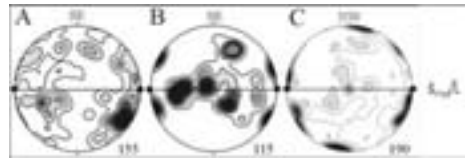


Figure 3: Quartz c -axis textures of three selected quartzite mylonites (A, B, C) from the ILSZ; horizontal line-trace of s_{myl} ; dots — direction of L ; trace of s_{myl} is oriented with respect to geographic directions; Schmidt net, lower hemisphere.

kind are typical for HT deformation of quartz polycrystals. As related to the field, the obliquity of the patterns indicates a top-to-the-NE sense of shear.

Conclusions

Based on both characteristic quartz microstructures and quartz c -axis textures the knowledge about the deformation conditions within the ILSZ could be improved. The microfabrics and intracrystalline structures of quartz indicate HT deformation with dominant grain boundary migration recrystallization and subsequent weak plastic deformation producing two sets of deformation bands in many grains. Deformation in a HT deformation regime is also confirmed by typical quartz c -axes textures which, in addition, reflect a strong component of non-coaxial strain.

Acknowledgements The research was supported by CNPQ Grant 350565/2004-0 and FAPEMAT Grant 3.2.2.33/02-2004.

References

- Garbutt JM & Teyssier C (1991) Prism <c>-slip in quartzites of the Oakhurst Mylonite Belt, California. *Journal Structural Geology* 13: 657–666
- Geraldes MC, Van Schmus W, Condie KC, Bell S, Teixeira W & Babinski M (2001) Proterozoic geologic evolution of the SW part of the Amazonian Craton in Mato Grosso state, Brazil. *Precambrian Research* 11: 91–128
- Hirth G & Tullis J (1992) Dislocation creep regime in quartz aggregates. *Journal Structural Geology* 2: 145–159.
- Jessel MW (1987) Grain-boundary migration microstructure in a naturally deformed quartzite. *Journal Structural Geology* 9: 1007–1014
- Kruhl JH (1996) Prism- and basal-plane parallel subgrain boundaries in quartz: a microstructural geothermobarometer. *Journal Metamorphic Geology* 14: 581–589
- Mainprice D, Bouchez JL, Blumenfeld P & Tubia JM (1986) Dominant c-slip in naturally deformed quartz: implications for dramatic plastic softening at high temperature. *Geology* 14: 819–822
- Ruiz AS (2005) Evolução geológica do sudeste do Cráton Amazônico: região limítrofe Brasil-Bolívia. PHD Thesis. Unesp, Rio Claro, 250pp
- Ruiz AS, Simões LSA, Almeida HL, Misson, AG & Manzano, JC (2005) Análise estrutural do batólito Santa Helena: implicações sobre a evolução tectônica do SW do Cráton Amazônico durante as orogenias San Ignácio-Rondoniano e Sunsás-Aguapeí. X Simpósio Nacional de Estudos Tectônicos. Curitiba, Brasil, 411–414
- Saes G (1999) Evolução tectônica e paleogeográfica do aulacógeno Aguapeí (1.2–1.0 Ga) e dos terrenos do seu embasamento na porção sul do Cráton Amazônico. PHD Thesis. Usp, São Paulo, 135 pp
- Stipp M, Stünitz H, Heilbronner R, Schmid S (2002) The eastern Tonale fault zone: a ‘natural laboratory’ for crystal plastic deformation of quartz over a temperature range from 250 to 700°C. *Journal Structural Geology* 24: 1861–1884
- Tassinari CG, Bettencourt JS, Geraldes MC, Macambira MB & Lufon JM (2000) The Amazonian Craton. In: Cordani U, Milani EJ, Thomaz Filho A & Campos DA (ed) *Tectonic Evolution of South América, I International Geological*, Rio de Janeiro, Brazil, 41–95
- Teixeira W, Tassinari CG, Cordani UG, Kawashita K (1989) A review of the geochronology of the Amazonian Craton: tectonic implications. *Precambrian Research* 42: 213–227
- Urai JL, Means WS & Lister G (1986) Dynamic recrystallization of minerals. *Geophysical Monographs* 36: 161–199

Holocene shield volcanoes in Iceland *Poster*

Ruth Andrew¹ Agust Gudmundsson¹

Introduction

Holocene shield volcanoes (lava shields) are common in Iceland, but they are restricted in space and time. As regards space, most of the shield volcanoes in Iceland occur within two bands in the West and North Volcanic Zones (Fig. 1). There are no shields in the East Volcanic Zone apart from the island of Surtsey. The shields are mostly at the margins of or outside the volcanic systems (Fig. 2). As regards time, many Holocene shield volcanoes formed some 5000–10000 years ago during early post-glacial time. Apart from the shield on top of the island of Surtsey, there are no known shields in Iceland younger than about 3500 B.P.

Formation

The formation of shield volcanoes follows a general pattern. The eruption begins with a fissure that subsequently

¹ Dept. Structural Geology and Geodynamics, University of Göttingen, Germany



Figure 1: Map of Iceland with shield volcanoes and fissure marked as circles and lines respectively. The Neovolcanic Zone is also shown as the darker shaded area, and the main ice caps are marked.

becomes concentrated at several vents, which generate overlapping shields. A single vent, the last one to remain active, generates a main shield which buries the earlier overlapping smaller shields. The shield volcano itself consists of two main morphological units; a central cone and a lava apron. The cone is generally roughly symmetrical,

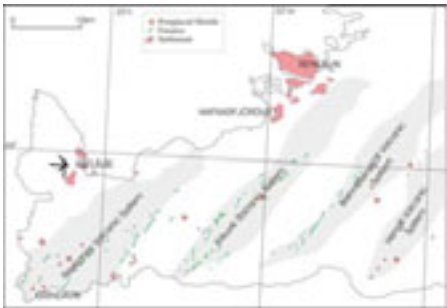


Figure 2: The Reykjanes Peninsula with its volcanic systems and their postglacial shields and fissures shown. Note the location of many shield volcanoes on the outskirts or outside of volcanic systems. Keflavik Airport is also shown along with the main settlements of the peninsula.

and the apron roughly a circular shape, though both are affected by topography (Rossi, 1996). There is no caldera collapse associated with Icelandic shield volcanoes, since they are supplied with magma from elongated reservoirs at the boundary between the crust and upper mantle.

Composition

In Iceland, the shield volcanoes are mainly of two compositions, olivine-tholeiite basalt and picrite basalt, both of which are primitive basalts. The magma composition is determined by the local pressure and temperature conditions, as well as the composition of the rock undergoing partial melting. Rossi (1996), who documented 40 to 50 Holocene shield volcanoes in Iceland and made a detailed study of 31 found all the shield volcanoes to be monogenetic. Of the 31 shields studied in detail, 24 are olivine-tholeiite basalts and 7 picrite basalts. This indicates that the conditions for the formation of olivine-tholeiite shields are more commonly satisfied than the conditions for picrite shields.

Picrite magma is a primary magma from the mantle. During the waning stages of the last glaciation and the early postglacial period, magma of this composition migrated up under the volcanic zones of the Reykjanes Peninsula at exceptionally high rates. This high rate of migration is attributable to the decrease in lithostatic pressure as a result of the rapid melting of the glaciers. Later in the postglacial period, the picrite magma is thought to have been trapped by the lighter olivine-tholeiite magma that subsequently accumulated in the upper parts of the magma reservoirs (Gudmundsson, 1986).



Figure 3: Skjaldbreiður shield volcano in the West Volcanic Zone.

Shields and Fissures

The volumes of shield volcanoes differ from those of fissure eruptions within the same volcanic system. The average lava volume of Holocene shield eruptions is much larger than the average lava volume of Holocene fissure eruptions. For example, on the Reykjanes Peninsula the mean eruptive volume of 101 volcanic fissures is about 0.1 cubic kilometers, whereas that of 26 shields is about 1 cubic kilometre. A typical large Holocene shield volcano on the Reykjanes Peninsula is Skjaldbreiður, which has a volume of around 15 cubic kilometers (Fig. 3). There is also a correlation between the compositions of the two types of eruption; the fissures produce more-evolved basalts, commonly tholeiite or quartz-tholeiite.

Conclusions

Here we present conceptual and numerical models as to how the stress changes related to the deglaciation may, partly at least, explain four related volcanotectonic features in Iceland. First, how high-density basaltic magmas were able to reach the surface to form the shields. Second, why most of the shields formed

in the early part of the postglacial period, with hardly any formed during the past 3500 years. Third, why many of the shields formed at the margins of the volcanic systems to which they are associated rather than at their centres. And, fourth, why the shields became confined to the West and North Volcanic Zones, with essentially no shields in the East Volcanic Zone.

References

- Gudmundsson A (1986) Mechanical aspects of postglacial volcanism and tectonics of the Reykjanes Peninsula, Southwest Iceland. *Journal of Geophysical Research* 91, 12711–12712.
- Rossi MJ (1996) Morphology and mechanism of eruption of postglacial shield volcanoes in Iceland. *Bulletin of Volcanology* 57, 530–540.

Rock fabrics in palaeo-weathering profiles below basement-cover interfaces (AMS-study on drill cores from the Caledonian margin, Central Sweden) *Vortrag*

Thomas Angerer¹

Reinhard O. Greiling¹

Basement-cover-interfaces are important crustal boundaries. In many cases they act as detachment horizons. Criteria like pre-erosional basement characteristics, intensity of palaeo-weathering and post-erosional processes during burial stage lead to a huge variety of observable alteration and fabric features of basement-cover-interfaces, which may influence the shear-strength.

Unconformity-parallel planar fabrics in the weathering profile were facilitated by palaeo-alteration and later processes (Angerer 2005 unpubl. data). Such fabrics may be a factor for lowering the shear-strength (e.g. Wintsch et al. 1995). The probably ubiquitous existence of those fabrics at basement-cover-interfaces is investigated in case studies by means of AMS-fabric analysis, which is a sensitive indicator of rock fabric changes.

The present case study is based on sections from two drill cores across the erosional unconformity between Fennoscandian Granite (Revsund) and Cambrian Gärdsjön Fm. (Långviken SGU 73007 and Hara 79002, see Fig. 1) (petrographic descriptions in Gee, 1978 and Gee et al. 1982).



Figure 1: Geological overview of the Central Caledonides. Marked are the two drill hole localities.

Hara SGU 79002 drill core

In the Hara drill core, the basement-cover-interface is reached at 180 m drill depth. The upper part of the basement is a 5.5 m thick tectonic slice with weathered and brecciated granite. The footwall of this slice is a shear surface with a foliated cataclasite and a thin graphitic black shale horizon. Below the slice there is a gradual change downward from strongly weathered to fresher granite. This can be considered as a primary palaeo-weathering profile below an erosional unconformity. The samples are paramagnetic with very low bulk susceptibility (κ_{bulk}) values. Dark granitic samples are graphite bearing and clay rich due to weathering and/or brittle

¹ Geologisch-Paläontologisches Institut, Universität Heidelberg, Im Neuenheimer Feld 234

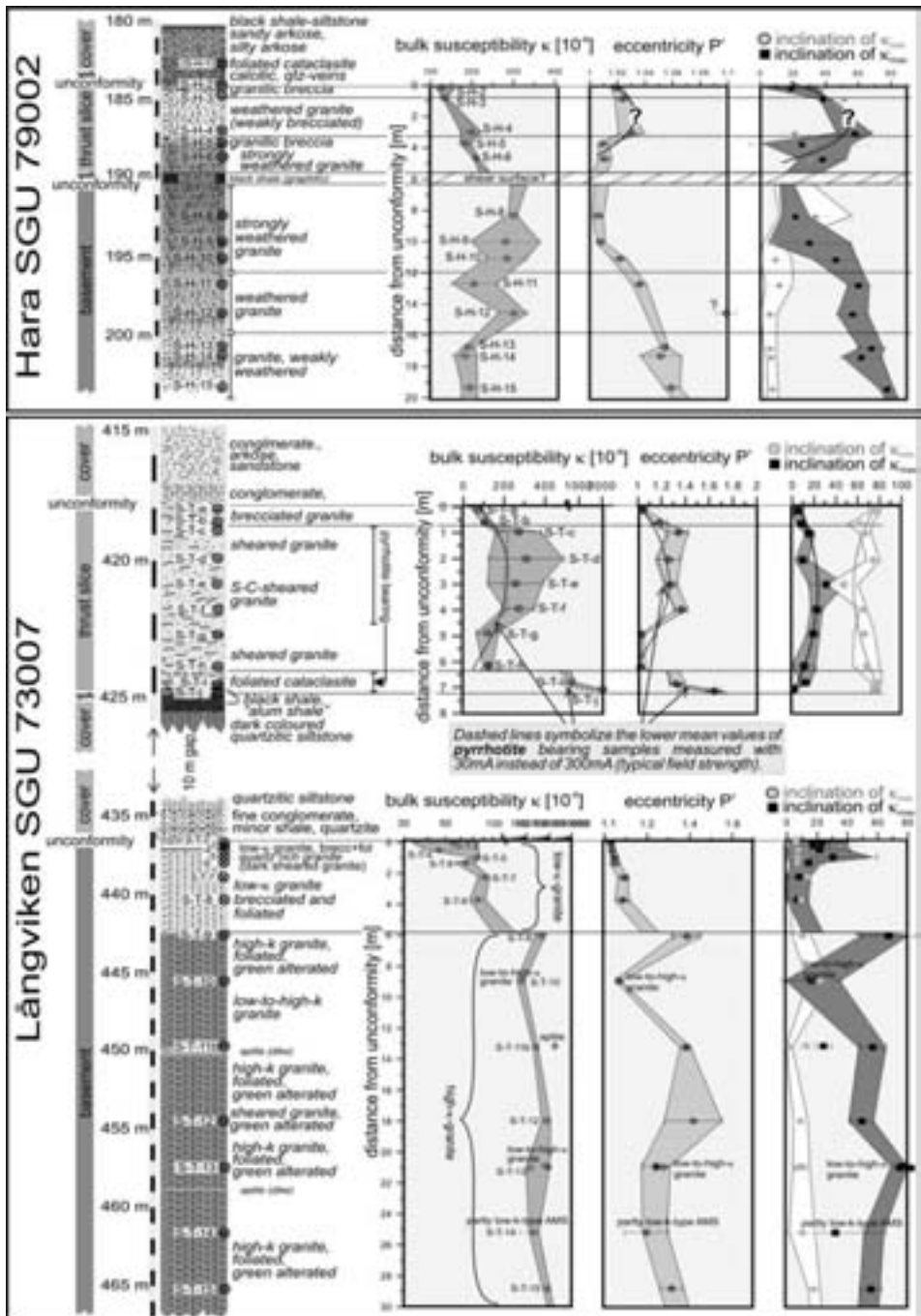


Figure 2: Compilation of the AMS-parameters bulk susceptibility (κ_{bulk}), eccentricity (P^*) and inclination of magnetic foliation (κ_{min} = surface pole) and magnetic lineation (κ_{max}) in dependance of distance from unconformity.

brittle deformation. The feldspar-to-clay alteration during weathering is a process that increased the bulk susceptibility. Both magnetic foliation and lineation are steep in the granite. Whereas the foliation inclination remains relatively stable, the lineation inclination decreases considerably together with eccentricity P' and shape factor T (latter not visualized here) towards the black shale horizon. These changes of parameters, especially the systematic lowering of the lineation inclination, can be best explained with a multi-phase superposition of unconformity-related fabrics (see Fig. 2, upper part).

Långviken SGU 73007 drill core

The autochthonous granite in the Långviken drill core below 437 m drill depth is divided into a more strongly weathered and brecciated zone down to 6 m below the unconformity (low- κ -granite) and a relatively fresher zone further below (high- κ -granite). The transition is rather discrete. However, there are parts of low- κ - inside the high- κ -granite. The high- κ -granite is magnetite bearing (large crystals of up to 2 mm), whereas the low- κ -granite is free of magnetite, but bearing Fe-clay and hematite as the susceptibility-dominating phases.

With the decrease of κ_{bulk} , P' decreases, as well. The magnetic lineation is steep in the high- κ -granite and changes to shallow in the low- κ -granite (see Fig. 2, lower part.) The magnetic foliation remains sub-parallel to the steep primary gneissic foliation. The change of the magnetic fabric towards the unconformity reveals characteristics like in the Hara drill core, therefore similar superposition processes can be assumed. In the Långviken drill core, 12 m above

the basement-cover-unconformity, the sequence is cut by a thrust, which transported a slice of granitic basement (7 m thick) with overlying cover sediments. It is a detached uppermost part of the autochthonous granite. Pyrrhotite appears dispersed in the deformed matrix of the central part and the cataclastic part in form of small irregular crystals (0.02 mm). This has an impact on κ_{bulk} and P' , because of the magnetic field dependence of pyrrhotite. However, the AMS-ellipsoid shaping effect of pyrrhotite is not important compared to the rock fabric defining shear-deformation.

Through the entire slice the granite is sheared in a ductile way and altered with a green colour. Both footwall and hanging-wall of the granite are cataclastically deformed. The distinct rock foliation is pronounced and flat-lying towards the top and bottom. Magnetic foliation parallels the main petrographic foliations. In the centre part of the sheared granite, fabrics are slightly steeper and partly composed by two sets of surfaces. The deformation gradient through the slice can be traced by κ_{bulk} , by P' , which reaches 70% in the lower cataclasite, and by the inclination of the magnetic lineation. Towards both rims of the sheared granite, the magnetic lineation becomes shallow, which is clearly caused by simple shear deformation (see Fig. 2, middle part).

Systematic unconformity-related magnetic fabrics

The results show how useful AMS is to trace even cryptic flat-lying fabrics in weathered granite, which apparently can be developed below basement-cover-interfaces. In both profiles unconformity-related fabric change is

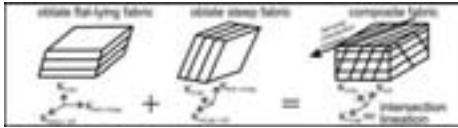


Figure 3: This sketch explains the change of AMS trajectories when a secondary fabric superposes a primary one. Here, the primary fabric is a flat-lying diagenetic feature and the secondary is the steep Caledonian gneissic foliation. In case of the Långviken allochthonous slice, the secondary fabric is a flat-lying fabric, which was induced by simple shear during thrust tectonics.

traceable: towards the unconformity the magnetic lineation decreases its inclination, whereas magnetic foliation stays stable and AMS-ellipsoid shapes become less pronounced (general decrease of eccentricity P'). The AMS fabrics resulted from a superposition of a prominent steep fabric (gneissic foliation) and a cryptic flat-lying one (see Fig. 3). The flat-lying fabric is a diagenetic pure shear feature (flattening), produced during the burial stage. It was facilitated by palaeo-weathering, which produced mainly clay minerals.

The AMS-trends are independent of κ_{bulk} , which behaves differently in the two cores, due to the different alteration properties of the paramagnetic (Hara) and ferromagnetic *s.latu* (Långviken) phases. The allochthonous basement slices are examples for the detachment of the uppermost basement parts, featuring unconformity parallel slip. The flat-lying fabric may have facilitated propagation of Caledonian detachments sub-parallel with this fabric during orogenic deformation. Apparently, burial compaction (pure shear) and lateral slip (simple shear) can produce quite similar AMS-fabrics.

References

- Gee DG, Kumpulainen R & Thelander T (1978) The Tasjön Décollement, central Swedish Caledonides. SGU Serie C Nr. 742: p 35
- Gee DG, Snäll S & Stejskal V, (1982) SGU Alunskifferprojektet - Prospekteringsrapport BRAP 82502.
- Wintsch RP, Christofferson R & Kronenberg AK (1995) Fluid-rock reaction weakening of fault zones. J Geophys Res 100(B7):13021–13032

Lithologierekonstruktion von submarinen Einheiten des Mauna Kea Vulkans mit bohrlochgeophysikalischen Messungen der magnetischen Suszeptibilität, HSDP Bohrung, Hawai'i Vortrag

Andre Beck¹ Helga de Wall¹
Jochem Kück²

Einführung

Als Teil des International Continental Drilling Projects (ICDP), wurde von März bis September 1999 im Rahmen des Hawai'i Scientific Drilling Projects (HSDP) die etwa 3109 m tiefe HSDP-2 Bohrung in der Nähe von Hilo auf Big Island, Hawai'i niedergebracht. Die mit einem Durchmesser von 98 mm (3.85") durchgehend gekernte Bohrung, durchteuft sowohl die subaerischen Einheiten des Mauna Loa, als auch die darunter liegenden submarinen Laven des Mauna Kea. Ab etwa 1080 m Teufe wurden die jüngsten, während der Entwick-

¹ Institut für Geologie, Pleicherwall 1, 97070 Würzburg ² Geo-Forschungs-Zentrum Potsdam, Telegrafenberg, 14473 Potsdam

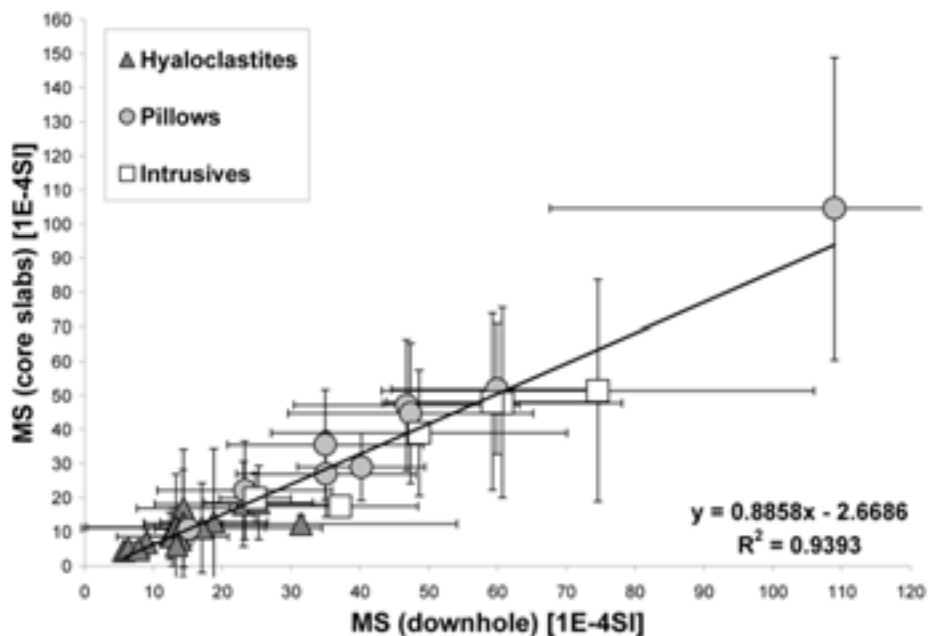


Abbildung 1: Crossplot der MS Mittelwerte aus Bohrloch- und Kernmessungen für die einzelnen im Logintervall erfassten lithologischen Einheiten (Für die eingefügte Trendlinien wurde das Bestimmtheitsmaß R^2 sowie die für den Zusammenhang der Werte daraus abgeleitete Gleichung errechnet).

lung dieses Vulkans abgelagerten submarinen Laven erbohrt. Die Verteilung von Hyaloklastiten, Pillowlaven, massiver Intrusiva sowie sedimentärer Ablagerungen, wurde durch die lithologische Beschreibung des durchgehend geförderten Kernprofils von DePaolo et al. (1999) aufgenommen. Verschiedene Autoren, wie z.B. Bücker et al. (1999) oder Helm-Clark et al. (2004) haben bereits gezeigt, dass sich Messungen der natürlichen Gammastrahlung (GR), die üblicherweise sehr gut zur lithologischen Einteilung von Gesteinen herangezogen werden können, in vergleichbaren Bohrungen nur sehr bedingt zur primären Unterscheidung basaltischer Gesteinseinheiten eignen. Dies ist vor al-

lem auf die sehr geringe Variation des K-, U- und Th-Gehalts der Basalte zurückzuführen. Daher wurden von der Operational Support Group (OSG) des GFZ-Potsdam im November 2002 bohrlochgeophysikalische Messungen in dem 98 mm Bohrloch in einem Bereich von etwa 1830 bis 2615 m durchgeführt. Diese wurden speziell zum Test einer Bohrlochsonde zur Messung der magnetischen Suszeptibilität (MS) im Rahmen des DFG-Projektes Wa 1015/4 angesetzt. Dazu wurde die MSdH-2 Sonde der OSG, hergestellt von der Fa. Antares GmbH (Stuhr, Germany) eingesetzt.

Qualitätskontrolle der MS Messung

In einem ersten Schritt wurden die erfassten MS Daten einer genauen Qualitätskontrolle, vor allem in Bezug auf eventuelle fehlerhafte Einflüsse durch Bohrlocherweiterungen, unterzogen. Die genaue Bohrlochgeometrie und -beschaffenheit wurde auf der Grundlage von Daten aus einer 1999 von der University of Hawai'i durchgeführten 1-arm Kalibermessung (CAL) ermittelt. Anhand der Häufigkeitsverteilung der gemessenen CAL Daten zeigt sich eine sehr hohe Qualität und Stabilität des Bohrloches. Bei einem nominellen Bohrlochdurchmesser von 98 mm (3.85"), ergibt die Kaliberauswertung einen durchschnittlichen Durchmesser von 115 mm. Dies kombiniert mit der visuellen Auswertung des CAL-Logs führte zur Einteilung der Bohrung in einen stabilen Bohrlochbereich bis 115 mm, indem etwa 85% aller aufgenommenen CAL-Werte liegen. Dennoch neigen vor allem die erbohrten Intrusiva sowie die Pillowlaven häufiger zu stärkeren Bohrlochausbrüchen bis ca. 160 mm, was eine genaue Qualitätskontrolle der aufgenommenen MS Daten erfordert. Diese wurde durch den Vergleich von MS Loggingdaten mit MS Kerndaten durchgeführt. Die MS Kernmessungen wurden an Bohrkernhälften ausgewählter Profile der HSDP-2 mit einem Handkappameter KT-5 (Fa. Agico Inc., Brno, Czech Republic) durchgeführt und freundlicherweise von Herrn Dr. Carsten Vahle, Universität Heidelberg zur Verfügung gestellt. Der Vergleich dieser Daten führt zu einer sehr guten Übereinstimmung der errechneten MS Mittelwerte für die einzelnen lithologischen Einheiten (siehe Abb. 1). Als Ergebnis der Qualitätskontrolle kann also fest-

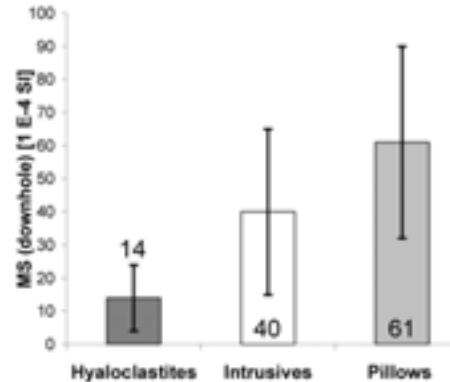


Abbildung 2: MS Mittelwerte und Standardabweichung der im Logintervall erfassten Gesteinsarten.

gehalten werden: Bei Messung der MS mittels der MSdH-2 Sonde, kann in der HSDP Bohrung, wenn ein Durchmesser von 160 mm nicht überschritten wird, generell auf die Korrektur der Logantworten verzichtet werden!

Auswertung der MS Daten

Hyaloklastite sind generell durch niedrige mittlere MS Werte charakterisiert ($14 \pm 10 \times 10^{-4}$ SI). Durch Laboranalysen kann dies auf das Vorherrschen von paramagnetischen Mineralen sowie den nur sehr geringen Gehalten an feinkörnigem Magnetit zurückgeführt werden. Intrusive Einheiten ($61 \pm 29 \times 10^{-4}$ SI) und Pillowlaven ($40 \pm 25 \times 10^{-4}$ SI) zeigen dagegen signifikant höhere, allerdings sehr stark schwankende MS Werte, was auf unterschiedliche Volumenanteile an Titanomagnetit und Schwankungen in seiner Zusammensetzung (Kontny et al. 2003) zurückzuführen ist. Die Messung der MS birgt damit eine sehr gute Möglichkeit zwischen den verschiedenen im HSDP-2 Profil erbohrten basaltischen Gesteinen zu unterscheiden (siehe

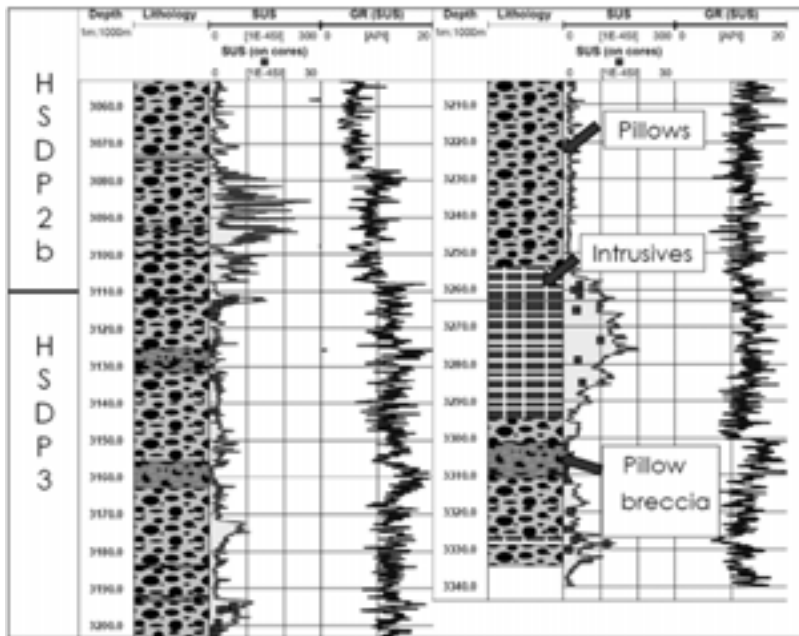


Abbildung 3: MS Log und mittels diesem angepasstes und rekonstruiertes Litholog der HSDP-3 (SUS=MS).

Abb. 2). Diese Ergebnisse stimmen sehr gut mit MS Messungen die an Kernhälften ausgewählten Profelsektionen durchgeführt wurden (Kontny et al. 2003, Vahle 2005) überein.

Lithologierekonstruktion für die HSDP 3 — Bohrung anhand von MS Daten

Von November 2004 bis Februar 2005 wurde die bestehende HSDP-2 Bohrung auf 3340 m vertieft (HSDP-3). Die Bohrung wurde ebenfalls mit einem Durchmesser von 98 mm, allerdings mit geringerem Kerngewinn niedergebracht. Dadurch konnte eine lithologische Gliederung nur deutlich ungenauer durchgeführt werden. Um die anhand der Kerninformationen gewonnene lithologische Gliederung zu ergänzen oder ggf. zu ver-

bessern sowie um die bei der HSDP-2 gewonnenen Ergebnisse anzuwenden, wurden im April 2005 Messungen der MS an den Bohrkernen und im Bohrloch durchgeführt. Die an ausgewählten Profilen des Kernmaterials der HSDP-3 mit dem KT-5 durchgeführten MS Messungen halfen zur Korrelation des von der OSG erstellten MS Logs. Mittels des erhaltenen MS Logs konnte die Lithologie dargestellt, rekonstruiert und ergänzt werden (siehe Abb. 3.). Dies verdeutlicht ein weiteres Mal die gute Nutzbarkeit von MS Daten zur Rekonstruktion von Lithologien in submarinen Basalten. Die bohrlochgeophysikalische Messung der magnetischen Suszeptibilität sollte folglich einen integralen Bestandteil von Bohrlochmesskampagnen an Bohrprojekten in submarinen Vulkanen darstellen.

Literatur

- Bücker CJ, Cashman KV & Planke S (1999) 5. Data Report: Physical and Magnetic Characterization of AA and Pahoehoe Flows: Hole 990 A. In: Larsen HC, Duncan RA, Allan JF & Brooks K (eds.) (1999) Proc. ODP, Scientific Results, 163. College Station (TX), 41–49
- DePaolo DJ, Thomas DM, Stolper EM & Garcia MO (1999) Hawai'i Scientific Drilling Project: core logs and summarizing data. Report, California Institute of Technology, Pasadena.
- Helm-Clark CM, Rodgers DW & Smith RP (2004) Borehole geophysical techniques to define stratigraphy, alteration and aquifers in basalt. *J. Appl. Geophys.*, 55, 3–38
- Kontny A, Vahle C & de Wall H (2003) Characteristic magnetic behavior of subaerial and submarine lava units from the Hawai'i Scientific Drilling Project (HSDP-2). *G3*, 4 (2), 8703, DOI:10.1029/2002GC000304
- Vahle C (2005) Aufbau und Entwicklung des Vulkans Mauna Kea anhand von gesteinsmagnetischen und magneto-mineralogischen Untersuchungen an Kernen des 'Hawai'i Scientific Drilling Project' (HSDP-2). Inaugural-Dissertation zur Erlangung der Doktorwürde, Naturwissenschaftlich-Mathematische Gesamtfakultät, Ruprecht-Karls-Universität Heidelberg, pp 285

GPS-gestützte Kartierung gravitativer Massenverlagerungen an der Röt/ Muschelkalk-Grenze im Göttinger Wald *Poster*

Frithjof Bense¹ Gabriele Ertl¹ Maurizio Battaglia¹ Axel Vollbrecht¹

Gravitative Massenverlagerungen entlang der Muschelkalkschichtstufe gehören zur natürlichen Morphodynamik.

¹ Geowissenschaftliches Zentrum der Georg-August-Universität Göttingen, Goldschmidtstr. 1-3, D-37077 Göttingen, Germany

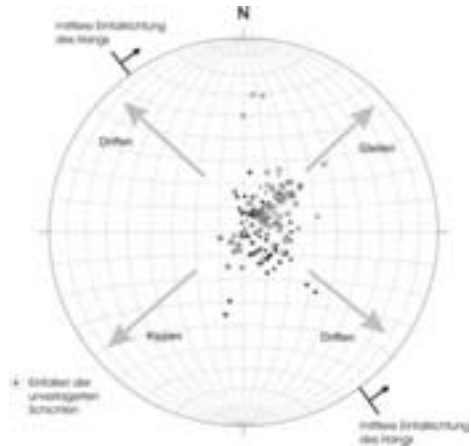


Abbildung 1: Schichtflächenpole von gravitativ verlagerten Schollen des Unteren Muschelkalks sowie ungestörter Bereiche (Schmidt'sches Netz, untere Halbkugel). Ausgehend von der ungestörten Lagerung ist eine Erhöhung des Einfallswinkels bei gleich bleibender Einfallrichtung Ergebnis einer hangwärtigen Rotationsbewegung (Gleiten), eine Erniedrigung des Einfallswinkels oder die Umkehrung der Einfallrichtung ist Resultat einer talwärtigen Rotation (Kippen). Eine Änderung des Einfallswinkels und der Einfallrichtung erfolgt durch Driften (nach Ertl, 2005).

Durch die unterschiedliche Erosionsresistenz der relativ inkompetenten Ton- und Mergelsteine des Röt und der direkt darüber anstehenden widerstandsfähigeren Kalkgesteinen des Unteren Muschelkalks hat sich ein Steilhang im Übergang dieser Einheiten ausgeprägt. Ein unruhiges Relief des Schichtstufenhangs zeugt an vielen Stellen von gravitativen Massenverlagerungen.

Zur detaillierten Kartierung dieser gravitativen Massenverlagerungen am Hünstollen im Göttinger Wald (10 km nordöstlich von Göttingen) wurden Zweifrequenz-GPS-Messungen

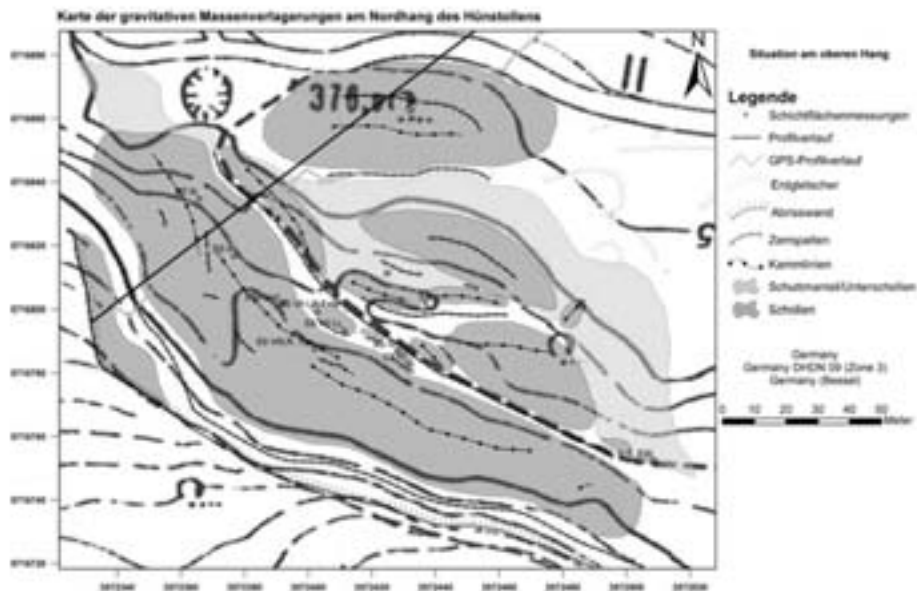


Abbildung 2: Karte der gravitativen Massenverlagerungen am Hünstollen (aus Bense, 2005).

durchgeführt. Mittels differentieller Korrektur der gesammelten GPS-Daten konnte eine horizontale Präzision der Positionsbestimmung von bis zu 10 cm auf freier Fläche und bis zu 40 cm im Wald erreicht werden. Zusammen mit Schichtflächenmessungen ermöglichen die gesammelten Daten eine hochauflösende Darstellung einzelner Strukturelemente (Abb. 2), Rückschlüsse auf die stattgefundenen Bewegungsabläufe (Abb. 1) sowie eine relative zeitliche Zuordnung der einzelnen Rutschkörper. Die Verlagerungen im bearbeiteten Gebiet gehören der Historischen Generation nach Ackermann (1959a&b) an. Eine weitere Eingrenzung in das Ältere oder Jüngere Stadium der Historischen Generation kann anhand der Morphologie nicht eindeutig durchgeführt werden.

Die Auswertung der Schichtflächendaten ergab eine Vorherrschaft von Driftgleit- und Kriechbewegungen. Kippbewegungen treten lediglich untergeordnet auf. Anzeichen auf jüngste Verlagerung oder ein künftiges Ereignis (z.B. aufreißende Spalten) finden sich im bearbeiteten Gebiet nicht. Rezente Bewegungen finden, neben Kriechbewegungen der Schutthänge, lediglich an einzelnen Schollen statt. Die Bewegungen beschränken sich auf das Abstürzen, Driften und Gleiten kleinerer Gesteinspakete. Darüber hinaus zeigen sich an der Abrisswand Anzeichen von Verteilung einzelner Gesteinstürme sowie Kippbewegungen kleinerer Gesteinseinheiten. Die überwiegend deutlich ausgeprägten Erdgletscher befinden sich in einem Zustand zunehmender Konsoli-

dierung und zeigen lediglich Anzeichen langsamer Fließ- oder Kriechbewegungen. (Bense, 2005; Ertl, 2005)

Als Hauptursache der Verlagerungen im bearbeiteten Gebiet können mit hoher Wahrscheinlichkeit kollabierte Hohlräume angeführt werden, welche durch Gipsauslaugung im Untergrund entstanden sind (Wilczewski & Steinmetz, 2003). Die Gipsauslaugung im bearbeiteten Gebiet ist durch das Auftreten mehrerer Dolinen und Erdfälle dokumentiert.

Da im Arbeitsgebiet innerhalb der Röt-schichten noch Gips angetroffen wurde, ist davon auszugehen, dass die Auslaugung von Gips im Untergrund weiterhin stattfinden kann und somit die Voraussetzung der Massenverlagerungen am Hünstollen nach wie vor gegeben ist. Aus diesem Grund muss der Hünstollen als Gebiet latenter Massenverlagerung angesehen werden.

Danksagung Wir danken K. Wemmer und T. Heinrichs für anregende Diskussionen während einer gemeinsamen Geländebegehung.

Literatur

- Ackermann E (1959a) Der Abtragungsmechanismus bei Massenverlagerungen an der Wellenkalk-Schichtstufe. Zeitschrift für Geomorphologie 3: 193-226
- Ackermann E (1959b) Der Abtragungsmechanismus bei Massenverlagerungen an der Wellenkalk-Schichtstufe. Zeitschrift für Geomorphologie 3: 283-304
- Bense F (2005) Gravitative Massenverlagerungen an der Röt/Muschelkalk-Schichtstufe im Göttinger Wald - Eine GPS-gestützte Strukturkartierung am Nordhang des Hünstollens (W-Abschnitt). Unveröffentlichte Bachelorarbeit, Georg-August-Universität Göttingen, Göttingen, pp 85
- Ertl G (2005) Gravitative Massenverlagerungen an der Röt/Muschelkalk-Schichtstufe im

Göttinger Wald - Eine GPS-gestützte Strukturkartierung am Nordhang des Hünstollens (E-Abschnitt). Unveröffentlichte Bachelorarbeit, Georg-August-Universität Göttingen, Göttingen, pp 56

Wilczewski N, Steinmetz S (2003) Rutschungen an der Grenze Buntsandstein/Muschelkalk, Göttinger Arbeiten zu Geologie und Paläontologie Sb5: 121-123

Felsmechanische Untersuchungen am Haupttrogenstein (bjHR) der Vorbergzone des südlichen Oberrheingrabens

Poster

Raphael Bissen¹ Andreas Henk¹

Einleitung

Der Haupttrogenstein ist im Ober-Bajocium, im Braunen Jura ϵ (bjHR), gebildet worden. Im Bereich des südlichen Oberrheingrabens ist der Haupttrogenstein als hellgrauer bis hellbräunlicher, schräggeschichteter bis massiger Kalkoolith ausgebildet. Die Gesamtmächtigkeiten dieser durch Mergelbänke und Schill-Lagen gegliederten Einheit reichen von 40 m bis ca. 80 m. Durch mehrere große Steinbrüche der Kalkindustrie ist der Haupttrogenstein in der Vorbergzone hervorragend aufgeschlossen. Mit Uniaxial- und Triaxialexperimenten sollen felsmechanische Kennwerte für den Haupttrogenstein bestimmt werden, auch in Hinblick auf die mögliche zukünftige Nutzung als Heisswasseraquifer für die Gewinnung geothermischer Energie.

¹ Geologisches Institut der Albert-Ludwigs-Universität Freiburg i. Br.

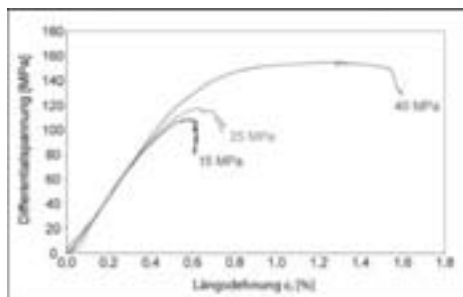


Abbildung 1: Druck-Stauchungslinien-Diagramm für den Probenatz Merdingen 1.

Uniaxial- und Triaxialversuche

Die Untersuchungen wurden an zylinderförmigen Probenkörpern mit einem Durchmesser von 100 mm durchgeführt. Die Proben wurden direkt im Gelände mit einem mobilen Kernbohrgerät gewonnen. Das Probenmaterial stammte aus dem Hauptrogenstein (b_jHR) des Steinbruchs ‚Am Ostberg‘ bei Herbolzheim sowie aus dem Kalkwerk der Fa. Mathis nahe Merdingen am Tuniberg. Anhand von Uniaxialversuchen wurden Verformungs- bzw. Elastizitätsmodul, Druckfestigkeit und Poissonzahl bestimmt, während in Spaltzugversuchen die Zugfestigkeiten gemessen wurden. Darüber hinaus wurden in Triaxialversuchen bei Manteldrücken von 15, 25 und 40 MPa Kohäsion und Winkel der inneren Reibung bestimmt.

Für die uniaxiale Druckfestigkeit ergaben sich Werte von 21–89,8 MPa, die V- bzw. E-Module lagen bei 27–34 GPa und die Poissonzahl erreichte Werte von 0,25–0,32. Die Spaltzugversuche lieferten Werte von 2,64–5,66 MPa. Die triaxialen Druckversuche lieferten kritische Scherspannungen von 48–68 MPa bei Manteldrücken von 15, 25 und 40 MPa, eine Kohäsion von 22 MPa,

einen Winkel der inneren Reibung von $28,5^\circ$ und ein E-Modul von 25–28 GPa (Abb. 1). Für die Auswertung der Messergebnisse wurden zwei verschiedene Methoden verwandt: Mohr’scher Spannungskreis (MohrView 2.0) und Spannungspfade (MS Excel). Beide Methoden lieferten sehr ähnliche Ergebnisse. Aufgrund von Stärken und Schwächen der Einzelverfahren stellte eine Kombination der beiden Methoden die zuverlässigste Art der Auswertung dar. Die hohe Variationsbreite bei den uniaxialen Druckfestigkeiten lässt sich dadurch erklären, dass die Proben aus Herbolzheim, mit Festigkeiten von 21–45 MPa, eine stärkere Beeinträchtigung durch Verkarstungsvorgänge erfahren haben als das Probenmaterial aus Merdingen. Zusätzlich wurden die Proben aus Herbolzheim parallel, die aus Merdingen jedoch senkrecht zur Bankung erbohrt. Aufgrund dessen war eine 10–20% niedrigere Festigkeit für das Material aus Herbolzheim zu erwarten. Die Proben aus dem Kalkwerk der Fa. Mathis zeigen ihrerseits eine durch die Herkunft aus zwei verschiedenen Bänken bedingte Variation der uniaxialen Druckfestigkeit, wobei eine Bank Werte von 53,8–55,8 MPa, die andere Festigkeiten von 79,5–89,8 MPa erreichte. Eine makroskopische Erklärung hierfür konnte nicht gefunden werden. Unterschiedliche Ausbildung im Bindemittelbereich oder präexistente Risse im Gestein liefern mögliche Erklärungen.

Gekoppeltes Kornwachstum in polymineralischen Gesteinen

Vortrag

Sabine Brodhag¹ Marco Herwegh¹
Alfons Berger¹ Adrian Pfiffner¹

Bei Temperaturerhöhung tritt in einem kristallinen Festkörper Kornwachstum auf; die treibende Kraft hierfür entspricht einer Reduktion der Oberflächenenergie. Die Parameter, die das Kornwachstum in monomineralischen Stoffen, wie zum Beispiel in Metallen beeinflussen, wurden in der Vergangenheit eingehend studiert. In der Natur sind Gesteine aber meistens polymineralisch, was ein ungleich komplexeres Wachstumsverhalten mit sich bringt. Bei Gesteinen mit einer dominanten Matrixphase und mengenmäßig untergeordneten Sekundärphasen muss eine Interaktion zwischen Matrixphase und Sekundärphasen auftreten, damit beide Phasengruppen wachsen können und somit eine Korngrößenzunahme im Gesamtgefüge stattfinden kann.

Um dieses gekoppelte Kornwachstum in natürlichen Gesteinen besser verstehen zu können, wurden Karbonatgesteine mit unterschiedlichem Sekundärphasengehalt entlang von Temperaturprofilen in der kontaktmetamorphen Aureole des Adamello Plutons in Norditalien beprobt. Die Proben stammen aus den Calcare di Angolo, bei denen es sich um unreine Karbonate, die mit Mergellagen alterieren, handelt. Hauptphase dieser Gesteine ist Kalzit, daneben gibt es einen variierenden Zweitphasengehalt an Glimmern, Quarz, Erzen und teilweise Feldspäten und Amphibolen. Letztere treten als Reaktionsprodukte erst in Kontaktnähe auf.

¹ Institut für Geologie, Universität Bern, Schweiz

Es zeigt sich, dass mit abnehmender Distanz zum Intrusionskontakt eine Zunahme der Korngröße von Kalzit und Sekundärphasen in allen polymineralischen Karbonaten auftritt. Dabei hängt die Korngrößenzunahme des Gesamtgefüges nicht nur vom Kalzit ab, sondern im Wesentlichen von dessen Sekundärphasen. Denn diese beeinflussen das Wachstum der Matrixphase durch ihre Anzahl und Verteilung im Gestein. Je höher der Sekundärphasengehalt, umso stärker werden die Kalzitkorn Grenzen durch diese beim Wachstum behindert. Wenn die treibenden Kräfte für das Kalzitkornwachstum größer sind als die rückhaltenden Kräfte der Sekundärphasen, werden letztere vom Kalzit überwachsen und somit eingeschlossen. Im umgekehrten Fall werden die Kalzitkorn Grenzen durch die Sekundärphasen zurückgehalten, was in einer kleineren Kalzitkorngröße resultiert. Infolge Diffusion zwischen den Sekundärphasen entlang Kalzitkorn Grenzen können die Sekundärphasen weiter wachsen. Dies führt zur Abnahme der Anzahl der Sekundärphasen und somit einer Zunahme der Distanz zwischen den Sekundärphasen, wodurch weiteres Kornwachstum beim Kalzit ermöglicht wird. Dieses Kalzitwachstum ist also direkt von demjenigen der Sekundärphasen abhängig, weshalb man auch von gekoppeltem Kornwachstum spricht. Die Tatsache, dass grosse Sekundärphasen Kalzitkorn Grenzen fixieren und gleichzeitig kleinere als Einschlüsse in Kalzitkörnern auftreten, erlaubt eine Abschätzung der treibenden Kräfte für das Kalzitkornwachstum bei unterschiedlichen Temperaturen. Als Funktion des Metamorphosegrades variieren nicht nur die Größe der Sekundärphasen, sondern auch die Sekundärphasenmineralogie, da Mine-

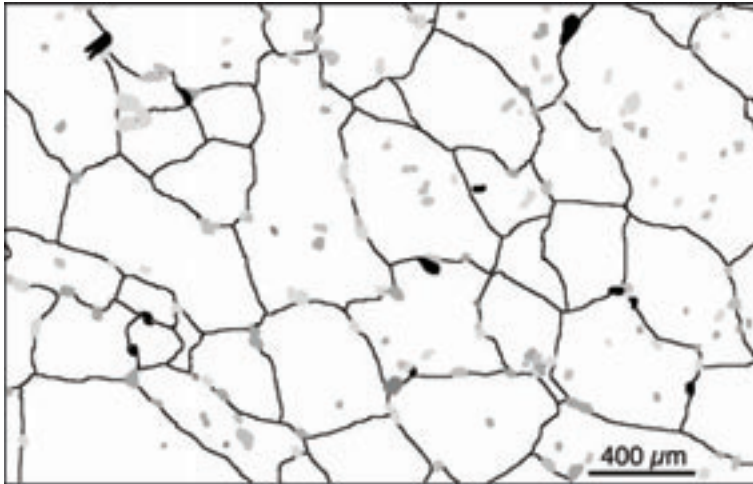


Abbildung 1: bearbeitete Dünnschliffprobe aus nächster Nähe des Kontaktes. Relativ große Amphibole (schwarz) sowie weitere große Zweitphasenkörner wie Glimmer, Quarz, Erze und Feldspäte (verschiedene Graustufen) befinden sich an den Kalzitkornengrenzen (schwarze Linien), während kleinere Körner jeder Phase in den Kalziten (weiss) eingeschlossen sind.

ralreaktionen auftreten. So entsteht bei hohen Temperaturen beispielsweise Tremolit als eine Sekundärphase. Sein Auftreten ist in diesen Bereichen immer auf die Korngrenze oder, als Einschluss, auf den äußersten Randbereich der Kalzitkörner beschränkt. Dies bedeutet, dass der Tremolit erst in einem späten Kalzitwachstumsstadium entstanden und eingeschlossen worden ist. Infolgedessen kann Typ und Ort von eingeschlossenen Sekundärphasen verwendet werden, um das Kalzitkornwachstum in eine relative Zeit-Temperaturskala einzuhängen.

In diesem Sinne gewährt das Studium von Sekundärphasen beeinflussten Aggregaten wichtige neue Erkenntnisse bezüglich der Prozesse und resultierenden Gefüge von polymineralischen Gesteinen.

Tektonische Entwicklung des Geitafell-Vulkans, Südost-Island *Poster*

Steffi Burchardt¹

Agust Gudmundsson¹

Michael Krumbholz¹ Nadine Friese¹

Der Geitafell-Vulkan ist ein erloschener tertiärer Zentralvulkan (Stratovulkan) in Südost-Island. Aufgrund tiefer glazialer Erosion ist das Innere des Vulkans bis hinab zur erloschenen krustalen Magmakammer aufgeschlossen. Das bietet die einmalige Möglichkeit, die Infrastruktur und die tektonische Entwicklung eines typischen isländischen Zentralvulkans zu untersuchen.

Der Geitafell-Vulkan besteht aus einer

¹ Abteilung Strukturgeologie und Geodynamik, Geowissenschaftliches Zentrum Göttingen, Goldschmidtstraße 3, 37077 Göttingen

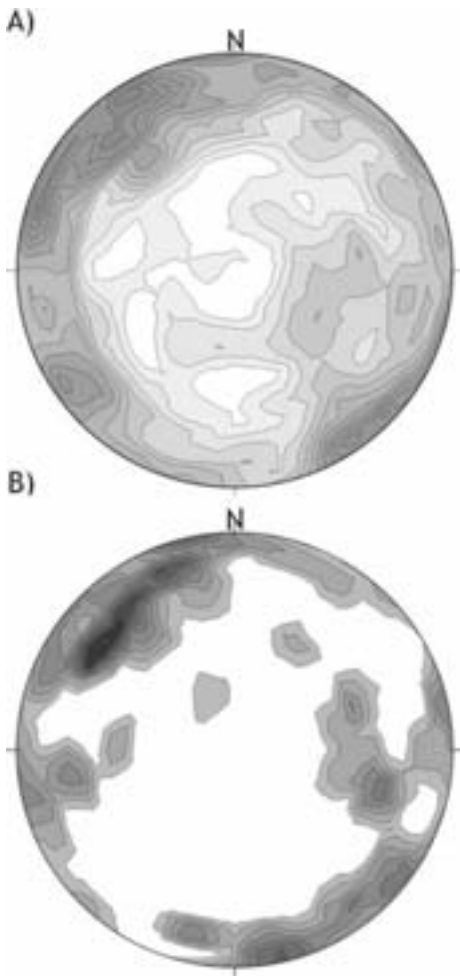


Figure 1: Stereographische Projektion (untere Hemisphäre) von A) 1087 Klüften und B) 48 Gängen und Kegelgängen in den Gabbros im Geitafell-Vulkan.

Abfolge von eruptiven Materialien unterschiedlicher mechanischer Eigenschaften wie zum Beispiel basaltische Laven, Hyaloklastite und saure Extrusiva. Im Kern des Vulkans ist der obere Teil einer erloschenen krustalen Magmakammer in Form mehrerer Gabbrokörper aufgeschlossen. Im di-

rekten Kontakt mit der Magmakammer befindet sich ein sehr dichter Schwarm von Kegelgängen, die von der Magmakammer injiziert wurden, als der Geitafell-Vulkan von etwa 5 bis 6 Ma aktiv war (Fridleifsson, 1983).

Um unser Verständnis über die vulkanotektonische Entwicklung des Zentralvulkans zu verbessern, wurden im Geitafell-Gebiet mehr als 500 Gänge und Kegelgänge, 400 Mineralgänge und etwa 1100 Klüfte gemessen. Die Analyse der Orientierung der Kegelgänge zeigt eine kreisförmige Verteilung der Streichrichtungen mit einem Maximum in N-S-Richtung. Die Analyse des Kluft- und Mineralgangsystems innerhalb der Gabbrokörper zeigt zwei senkrecht zueinander stehende Hauptstreichrichtungen: NNW-SSE und ENE-WSW. Die meisten Klüfte in den Gabbros sind Abkühlungsklüfte (Säulenklüfte), die sich bildeten, als der äußere Teil der Magmakammer abkühlte und sich verfestigte. Die Übereinstimmung zwischen den Richtungen von Klüften und Mineralgängen deutet an, dass Abkühlungsklüfte als Wegsamkeiten für geothermale Fluide, die durch die abgekühlte, äußere Hülle der der Magmakammer zirkulierten, dienten. Des Weiteren zeigt die Orientierung von 48 Gängen, die die Gabbros schneiden, dass einige Klüfte als Wegsamkeiten für die spätesten Gänge und Kegelgänge, die von der Magmakammer injiziert wurden, genutzt wurden. Diese spät gebildeten Gänge passierten auf ihrem Weg in den Kegelgangschwarm eine abgekühlte, aber immer noch heiße Hülle der Magmakammer. Die Zahl der Gänge, die den Gabbro schneiden, ist jedoch niedrig im Vergleich mit der Zahl der Gänge im Kegelgangschwarm. Luftbilder und Geländebeobachtungen

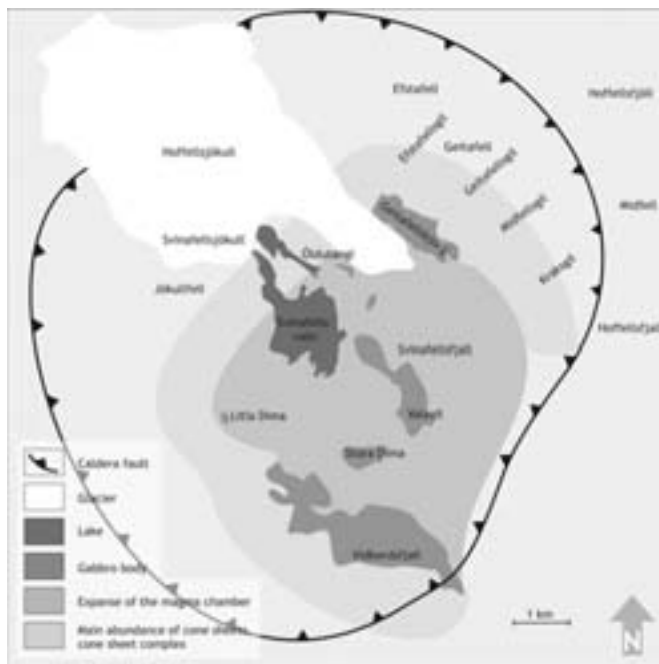


Figure 2: Rekonstruktion der Geometry der Magmakammer basierend auf den Aufschlüssen von Gabbros und Kelgelgangschwärmen. Der Geitafellsbjörg-Gabbro und der Vidbordsfjall Gabbro befinden sich im direkten Kontakt mit sehr dichten Kelgelgangschwärmen. Der maximale Durchmesser der rekonstruierten Magmakammer war etwa 7 km. Geologie basierend auf Fridleifsson (1983).

zeigen, dass die Magmakammer im Kern des Geitafell-Vulkans sill-förmig war und einen Durchmesser von etwa 7 km besaß. Die Geometrie der Magmakammer und die mechanischen Eigenschaften der Hauptschichten, die den Geitafell-Vulkan aufbauen, wurden in numerischen Modellen verwendet, um das lokale Spannungsfeld um die Magmakammer zu simulieren. Die Resultate erlauben uns, die Intensität und Geometrie des Kelgelgangschwarms zu erklären.

Zusätzlich wurden numerische Modelle erstellt, um die Bildung der Caldera im Geitafell-Vulkan zu erklären. Geländebeobachtungen von Fridleifsson (1983) zeigen, dass die Caldera einen

Durchmesser von etwa 8 bis 10 km besitzt. Die numerischen Modelle deuten darauf hin, dass die Aufwölbung des Magmareservoirs an der Kruste-Mantel-Grenze unter der sill-förmigen Magmakammer zum Caldera-Kollaps im Geitafell-Vulkan geführt hat.

Literatur

Fridleifsson, GO (1983) The Geology and the Alteration History of the Geitafell Central Volcano, Southeast Iceland. Ph.D. thesis, Grant Institute of Geology, University of Edinburgh, pp 371

Dyke emplacement in Tenerife (Canary Islands): Field studies and numerical models

Poster

Steffi Burchardt¹

Agust Gudmundsson¹

Sonja L. Philipp¹

Dykes are magma-driven extension fractures and the main conduits for magma in volcanic eruptions. To understand the mechanics of dyke emplacement is thus essential to assess volcanic hazards. To improve the understanding of the processes of dyke initiation from shallow magma chambers and dyke propagation through a mechanically-layered crust, field measurements and observations from Tenerife (Canary Islands) are used and compared with the results from numerical models.

Careful studies of 550 dykes in three profiles in the Anaga massif (Tenerife) include measurements of dyke geometry and orientation. The results of these measurements show that dykes have been injected from a deep-seated reservoir during the shield-building phase. Furthermore, the dyke attitudes agree with the main axial trends of Tenerife that are preserved in the old massifs of Teno, Anaga, and Roque del Conde. In addition, it has been observed that most studied dykes did not reach the surface to feed volcanic eruptions but became arrested.

Using data from field studies in Tenerife, numerical models on the effects of a mechanically layered crust on the stress fields around magma chambers of different geometries and around a propaga-

ting dyke were made. These models use the finite element program ANSYS and the boundary element program BEASY. The numerical models of the stress field around circular and sill-like magma chambers show that a mechanically layered crust is likely to arrest many dykes injected from a magma chamber. The numerical models indicate that, for the given loading conditions, most dykes either turn into sills at contacts between layers of contrasting mechanical properties or, more likely, become arrested. Stress-field homogenisation is presumably a necessary condition for a dyke to be able to reach the surface to feed a volcanic eruption.

The field studies and numerical models also indicate that the geometry of the tip of an arrested dyke depends much on the mechanical properties of the arresting layer. When a dyke is arrested on meeting a soft layer the dyke tip will be blunt. By contrast, a dyke arrested on meeting a stiff layer will have a rather sharp tip. The numerical models on dyke propagation also show that the main tensile stress concentration can be expected around the dyke tip. Only if the tensile stresses at the dip of a dyke exceeds the tensile strength of the host-rock, has the dyke a chance of propagating to shallower crustal levels or, eventually, to the surface.

¹ Geowissenschaftliches Zentrum der Georg-August-Universität Göttingen, Abteilung Strukturgeologie und Geodynamik, Goldschmidtstr. 3, 37077 Göttingen

Regional fold structure analysis in the Eastern Alpi Apuane, Northern Apennine

Poster

Steffi Burchardt¹ Tobias Kracke¹ Giancarlo Molli² Bernd Leiss¹

The Alpi Apuane represent a large tectonic window within the Northern Apennine in Italy. In this area, not only a complete succession of the tectonic units of the Northern Apennine can be studied, but also the structures that result from at least two Alpine deformational events.

The rocks of the Alpi Apuane have been deposited from Triassic to Tertiary times on the Hercynian basement of the passive continental margin of the Apulian plate. The sedimentary succession included meta-dolostones, marbles, metacherts, schists, and turbiditic arenites. During late Oligocene more internal units (the Tuscan Nappe together with the overlying Ligurides and Sub-Ligurides) were thrust over the External Tuscan Domain (Alpi Apuane). The Alpi Apuane stratigraphic sequence was subject to greenschist facies metamorphism and severe deformation within a crustal scale shear zone. Kilometre-scale tight recumbent folds developed during a first deformation event (D_1). The successive crustal shortening resulted in a further tightening of folds and the formation of an antiformal stack geometry with a central culmination. This late phase of D_1 produced a curving of N-S (Apenninic) trending folds towards an E-W (anti-Apenninic) trend (Fig. 1a). During Miocene the over-

thickened antiform underwent gravitational collapse resulting in the refolding of D_1 structures producing D_2 open and back folds.

The studied field area is located in the Eastern Alpi Apuane between Arni and Isola Santa in an area of anti-Apenninic trending D_1 folds. The purpose of this study is to contribute to an understanding of

1. how the anti-Apenninic fold trend is developed in the Eastern Alpi Apuane,
2. how the D_2 deformational event influenced the D_1 folds in the area, and
3. how the anti-Apenninic fold trend developed.

Hence, field work focussed on the structural analysis of folds at all scales (from kilometre-scale to micro-scale).

In the field area, D_1 folds are commonly highly non-cylindrical and sometimes even sheathfold-like. This fold geometry can be found in thin sections, hand specimen, to outcrop- and /cartographic scale. The development of D_2 structures showing sub-horizontal axial planar crenulation cleavage is to a great extent dependent on the lithology and on the orientation and the intensity of the development of D_1 structures. The results of our studies suggest that the anti-Apenninic is due to a complex interference pattern between two generations of isoclinal sheath-like folds (D_1 and Late D_1) refolded by later collapse folds associated to a sub-horizontal crenulation cleavage (regional D_2).

References

- Burchardt S (2005) Report of the structural geology map of the Eastern Monte Fredone area, Alpi Apuane, Northern Apennine,

¹ Geowissenschaftliches Zentrum Göttingen, Goldschmidtstraße 3, 37077 Göttingen, Deutschland ² Dipartimento di Scienze della Terra, Università Pisa, Italien



Figure 1: a) Geological setting of the Alpi Apuane region. Apuane Unit: Pz//Tr = Paleozoic to Triassic metavolcanics, phyllites, quartzites and metaconglomerates, Tr/J = Upper Triassic to Liassic carbonate platform deposits, K/T = Cretaceous to Tertiary phyllites and metasandstones. The axial surfaces of D₁ folds show two different trends: Apenninic and anti-Apenninic. Map by courtesy of G. Molli (modified after Carmignani & Kligfield 1990). b) Structural geology map of the area between Arni and Isola Santa in the Eastern Alpi Apuane. The main fold trend of D₁ folds is anti-Apenninic. Modified from Burchardt (2005).

Italy. University of Göttingen, unpublished
Diplom mapping thesis, pp 168

Carmignani & Kligfield (1990) Crustal extension in the Northern Apennines: the transition from compression to extension in the Alpi Apuane core complex. *Tectonics*, 9, 1275–1303

Erkundung von Erdfallstrukturen in der Metropolregion Hamburg und Lüneburg mit dem Georadar (Ground Penetrating Radar) *Poster*

Nils Buurman¹ C.-D. Reuther¹

Der oberflächennahe geologische Untergrund Norddeutschlands wird durch das Auftreten zahlreicher Salzvorkommen geprägt. Während der Triaszeit und des unteren Juras herrschte ein E-W gerichtetes, extensives tektonisches Regime vor. Durch zusätzliche Umlagerung klastischer Sedimente wurden darunter liegende Salzmassen permischen Alters (Zechstein) aus Tiefen von bis zu 5000 Metern an die Erdoberfläche empor gepresst. Durch diesen Salzaufstieg wurden darüber liegende mesozoische Schichten durchschlagen, randlich der Salzdiapire deformiert und teilweise mitgeschleppt. Eine letzte Phase salztektonischer Aktivitäten während der oberen Kreide und des unteren Tertiärs zeichnet sich zum einen durch weiteren Salzaufstieg aus und zum anderen durch horizontale Einengung der Salzstöcke. Begleitgesteine der Salze, wie Gips, Anhydrit, und Karst, sowie Tertiäre und Quartäre Ablagerungen überlagern die Salzstöcke mit unterschiedlichen Mächtigkeiten.

Das humide Klima Norddeutschlands begünstigt natürliche Auslaugungsprozesse (Subrosion) der Evaporite durch Grundwasser. Je nach Tiefenlage des Salzpiegels (Salzstock Lüneburg: -20 bis -40 m; Salzstock Othmarschen-Langenfelde (Hamburg): ca 0 bis -250 m) kann es zu intensiver

Hohlraumbildung im tieferen Untergrund kommen. Die fortschreitende Vergrößerung einer solchen Höhle steht in Abhängigkeit zur Intensität der Lösungsprozesse, während die Stabilität des Hohlraumes zusätzlich von der Materialbeschaffenheit abhängt. So können feste Gesteine oder bindige Böden zwar ein stabiles Höhlendach bilden, jedoch ist bei andauernden Lösungsprozessen langfristig ein statisches Versagen des Höhlendaches unvermeidlich. Der damit verbundene Kollaps und die Verfüllung des Hohlraumes mit Sediment spiegelt sich häufig in Form von sub-zirkularen und konischen Einsturzröhren oder weitläufigen morphologischen Trichtern an der Erdoberfläche wieder. Die Terminologie der Erdfälle wird anhand der Subsidenzrate gewählt. Man unterscheidet in der Hauptsache zwei Typen von Erdfällen: zu einen den *dropout-type*, welcher durch schlagartiges Versagen des Höhlendaches und einem abrupten Kollaps der Erdoberfläche charakterisiert ist, und zum anderen der *suffosion-type*, welcher eine langsame Verfüllung der Höhle durch Spalten im Höhlendach und ein allmähliches Nachsackens der Erdoberfläche nach sich zieht. Während der *dropout-type* in der Regel immer mit einem hohen Georisiko eingeschätzt werden muss, hängt die Georisikenabschätzung bei dem *suffosion-type* von der Subsidenzrate, dem Massenverlust und der räumlichen Ausbreitung der Subsidenzstruktur ab. Gewöhnlich werden die morphologischen Depressionen durch Erosionsprozesse mit Sediment oder Wasser wiederverfüllt, während im tieferen Untergrund die Lösungsprozesse der Evaporite weiter voranschreiten. Da die höhlenreichen Deckgesteine den ganzen Salzdom überlagern, treten

¹ Geologisch Paläontologisches Institut, Universität Hamburg, Bundesstraße 55, 20146 Hamburg, Germany

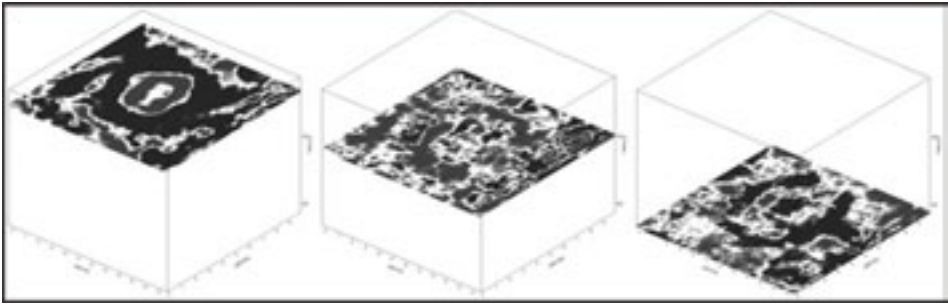


Abbildung 1: GPR-Daten: 3D-Darstellung eines verborgenen Erdfalles (*dropout-type*) in Hamburg; die Zeitfenster entsprechen jeweils Tiefen von 1.1, 5.5 und 11.2 m.

Erdfälle meist räumlich weit verteilt auf und erstrecken sich entlang von lösungsbegünstigten Bereichen wie Verwerfungen oder dem Kontakt zwischen Salzstockrand und Grundgebirge.

Für die Gewährleistung der Standsicherheit von Gebäuden, Industrieanlagen, Verkehrswegen etc. in urbanen Gebieten, ist das Wissen über die Stabilität des Untergrundes von entscheidender Wichtigkeit. Aktive Erdfallregionen wie in der Metropolregion Hamburg und in der Stadt Lüneburg bürgen ein erhöhtes Georisiko für die gesamte Infrastruktur in sich. In den vergangenen zwei Jahrhunderten wurden im Stadtgebiet Hamburgs ca. vierzig potentielle Erdfallerscheinungen dokumentiert. Die meisten von ihnen befinden sich am SW-Rand des Othmarschen-Langenfelde Diapir (OLD). Dabei handelt es sich überwiegend um eine Vielzahl kleinräumiger Strukturen des *suffosion-type*, welche innerhalb einer N-S streichenden Depression, der Bahrenfelder Senke, auftreten. Zur Aufnahme der räumlichen Ausbreitung und der Darstellung des Deformationsstils der im Untergrund verborgenen Kollapsröhren und Einsturztrichter benutzen wir das Georadar (GPR). Obwohl die langsame Kriechbe-

wegung des Untergrundes ein nur moderates Georisiko darstellt, zeigen vor allem Hausfassaden und Straßenbeläge in der betroffenen Umgegend sichtbare Schäden. GPR-Untersuchungen verdeutlichen, dass Kellerbereiche, Fundamente und Straßen direkt oberhalb von verborgenen Abbruchkanten, Gleitflächen und Bereichen starker Bodenunruhe errichtet worden sind. Sedimentäre Strukturen im zentralen Bereich der Erdfälle dokumentieren unterschiedliche Deformationsereignisse, was auf eine Reaktivierung, also eine wiederholte Abfolge von Oberflächeneinbrüchen mit anschließender Wiederverfüllung an ein und der selben Lokalität hinweist. Die Reaktivierung lässt sich durch anhaltende Lösungsprozesse im tieferen Untergrund erklären. Eine zweite weitläufige Depression oberhalb des westlichen Randes des OLD, die Flottbeker Senke, streicht ebenfalls in N-S Richtung. Ihr nordwestlicher Rand zeigt steile morphologische Stufen im Gelände, welche direkt zum Erdfallzentrum eines *dropout-types* hin abfallen. Während des letzten Jahrhunderts wurden hier drei Einsturzbeben dokumentiert (1928, 1963, 2000). GPR-Daten belegen anhand von verborgenen Abbruchkanten

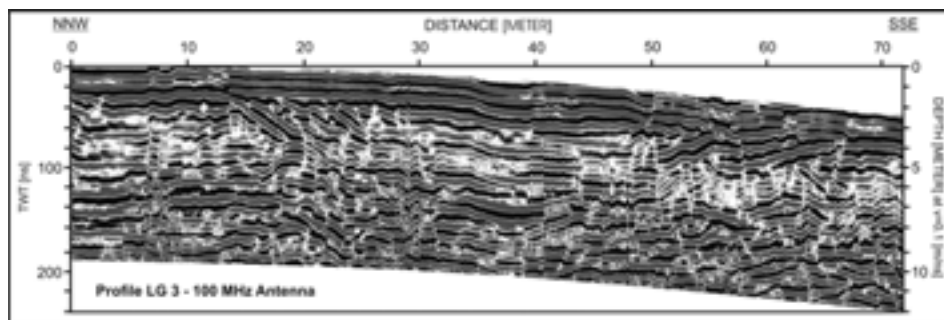


Abbildung 2: GPR-Profil: verborgene Abbruchkanten innerhalb des Einsturztrichters eines Erdfalles (*suffosion-type*) in Lüneburg.

im Untergrund die wahre Ausbreitung der Subsidenzstruktur auch außerhalb des Einsturztrichters. Dort gelegene Gebäude und Fahrbahnen zeigen anhaltende oder wiederkehrende Setzungsschäden und bestätigen eine aktive Bewegung des oberflächennahen Untergrundes auch zwischen den plötzlich auftretenden Einsturzereignissen.

Eine weitere Feldstudie im westlichen Stadtbereich Lüneburgs zeigt eine gravierende Gefährdung eines Wohngebietes und der gesamten Infrastruktur. Geologisch liegt der Bereich des Michaelis Friedhofes und das Wohngebiet ‚Ochtmisser Kirchstieg‘ oberhalb des Kontaktes zwischen triasischem Grundgebirge und dem nördlichen Salzstockrand. Angefangen mit einer ca. 90 cm breitem Einsturzröhre wurden in den Jahren zwischen 2002 und 2004 Subsidenzraten bis zu 20 cm pa. gemessen. Andauernde Oberflächenabsenkungen führten zur Ausbildung einer morphologischen Senke mit einem Durchmesser von 30 bis 50 m. Die weiträumige dreidimensionale Kartierung des betroffenen Bereiches mit dem GPR und einer Erkundungstiefe von ca. 10 m zeigt Abbruchkanten im Untergrund, welche sich noch nicht bis an die Erdoberfläche

durchgepaust haben. Die im Untergrund verborgenen Strukturen lassen einen Durchmesser von mindestens 90 m erkennen. Darüber liegende Gebäude und Kellerwände sind stark beschädigt, Fundamente sanken unter den Grundwasserspiegel ab. Ebenso sind starke Straßenschäden und defekte Versorgungsleitungen für Gas und Wasser die Folge, ein Einfamilienhaus musste bereits evakuiert werden.

In betroffenen Gebieten der aktiven Bodensenkung kann neben permanenten Nivellierungsarbeiten der Einsatz des GPR einen wichtigen Beitrag zur Georisikenabschätzung liefern. Durch hoch auflösende 3D-Kartierungen des Untergrundes kann die aktuelle Geometrie und die Größe der Gesamtstruktur abgebildet werden. Langzeitbeobachtungen in Gebieten mit hohen Subsidenzraten und signifikanten Massenverlusten können durch wiederholte Messungen die fortschreitende räumliche Ausweitung der Strukturen darstellen und Erkenntnisse über den genauen Bewegungsmechanismus im Untergrund liefern. Paläoböden und Sedimentfazien können durch Korrelation zusätzlicher Bohrungen in den GPR-Daten als Radarfazien verifiziert werden. Nur eine

genaue Kenntnis über den strukturellen und sedimentären Aufbau des Untergrundes erlaubt eine seriöse Georisikenschätzung gefährdeter Gebiete und kann bei der Ergreifung von Präventivmaßnahmen zum Schutze von Gebäuden, Infrastruktur und der Bevölkerung helfen.

Dank Diese Studien werden im Zuge des Projektes: HADU — Hamburg-A Dynamic Underground vom BMBF im Programm Geotechnologien gefördert.

Fracture sealing in limestones, a microstructural and mineralogical study *Vortrag*

Maria Chatziliadou¹
 Christoph Hilgers² Sven Sindern¹

Introduction

Fractures significantly enhance the flow rate in rocks, if fracture density is high (Taylor 1999, Cox et al. 2001). This leads to rapid flux along a hydraulic gradient from high to low pressure reservoirs, and is represented in rocks as veins. Veins are precipitates from supersaturated fluid, and are formed by a change in pressure, temperature or geochemistry. The solubility of vein forming minerals such as quartz, calcite or halite is generally low and thus large (and sometimes unreasonable) fluid volumes are required to account for the precipitated mass. Rapid ascent of solution may explain the high supersaturation needed to seal fractures, ei-

ther by fluid flow along deep reaching faults due to seismic ruptures, or mobile hydrofractures driven by pressure gradients in fluid filled fractured at deeper crustal sections (Bons 2001, Miller 2002). The vein microstructure is a unique tool to unravel the fracture sealing process. The most indicative microstructures are fractured minerals, which were sealed by a fluid of different composition. The repeated presence of fluid and solid host rock inclusions in fibrous, stretched crystal type veins (minerals which extend across the vein and into the host rock) also indicate repeated fracture-sealing processes (Ramsay 1980), although their presence is not a sufficient criteria (Hilgers 2005). In this study, we outline the different fault sealing processes associated in a still seismic zone. The faults are located in Carboniferous limestones, and thus present an analogue for fault sealing processes in hydrocarbon reservoirs and an in-depth study of seismogenic faults.

Geological Setting

We studied lower Carboniferous limestones, which are truncated by subvertical, dm-wide calcite veins. These platform limestones are located on the NE-limb of the Stavelot-Venn Anticline, which is part of the Variscan fold and thrust belt. Our study area is the quarry Hastenrath, which is located app. 50 m SW of the seismogenic Sandgewand normal fault. Calcite veins locally contain lead- and zinc-sulfide ores and strike NW-SE parallel to the normal fault. We compare our results of core data derived from the deep drilling project RWTH-1, a 2543 m deep well drilled in 2004 in the city centre of Aachen. The core contains 20 m of in-

¹ Institut für Mineralogie und Lagerstättenlehre, RWTH-Aachen, Germany ² Geologie-Endogene Dynamik, RWTH-Aachen, Germany

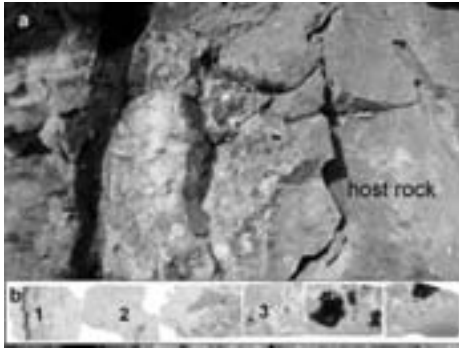


Figure 1: (a). A calcite vein with Pb-Zn mineralization, Hastenrath Quarry. The rim of the vein shows fragments of hydrothermal dolomite and euhedral galena crystals. The central part of the vein is filled with organic material (36% C). (b). Horizontal section of the vein shows three fluid generations.

tensely deformed upper Devonian limestones at 1420 m depth. These limestones also contain different sets of calcite veins, but are devoid of ore mineralization.

Microstructure and mineralogy

Hastenrath

The Hastenrath quarry exposes several approx. 20 cm wide subvertical veins in limestone with some first localised dolomitisation. Macroscopically, the veins show three to four different, symmetrically arranged cements.

#1 is close to the host rock, a pink hydrothermal dolomite precipitated next to the host rock. The dolomite is a tectonic dilational breccia, which is cemented with calcite. The cathodoluminescence shows fragments of euhedral calcite crystals outlined by different colours, and large areas where grains do not match with the variations in luminescence. Such calcite grains consist

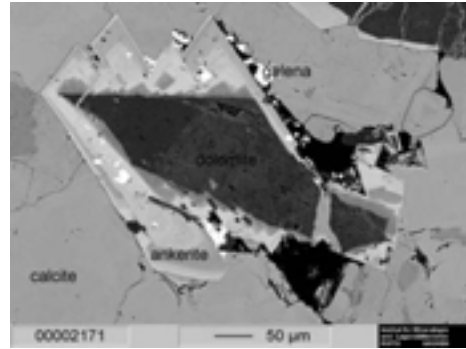


Figure 2: Microprobe image of a broken fragment of dolomite with an ankerite seam. Galena is also present in the patchwork calcite matrix.

of subangular fragments of dark and orange luminescence. Calcite twin morphology indicates temperatures of approx. 250°C. Dolomite is overgrown by euhedral ankerite. Euhedral to subhedral galena crystals up to 1 cm in diameter indicate a later timing of growth. Euhedral quartz has a solid inclusion rich rounded centre and is present in all phases of zone #1.

The intermediate zone #2 shows up to 2 cm twinned calcite grains of twin type II which indicate a temperature of 150–300°C. The cathodoluminescence shows a pattern which does not correspond to calcite grain boundaries. The central zone #3 is sealed with small twinned calcite crystals with a thin sphalerite vein. The sphalerite shows zones with high cadmium content. Both zone #1 and #3 contain chalcopyrite within and around galena and sphalerite. Locally, organic material is emplaced in the central part of the vein. Vitrinite reflectance gives <150°C.

RWTH Aachen

The core material from the RWTH-1

well contains up to 0.3 cm thick veins in dolomite. The host rock indicates a late diagenetic dolomitisation with zoned Fe-rich seams around dolomite crystals. Two different quartz phases precipitates in the pores, as indicated by a blue luminescence (restricted to the host rock) and a later brown luminescence in veins and host rock. Pyrite crystals growth in the pores of the host rock as bacterial degradation in reduced milieus. The vein consists of dolomite of dark brown luminescence, transected and surrounded by bright orange calcite. Euhedral quartz crystals (brown luminescence) are present in dolomite, calcite and are enriched along the vein wall interface.

Conclusions

The sealed fractures show similar fluid events and -sequences in upper Devonian (RWTH-1) and lower Carboniferous (Hastenrath) limestones with an early dolomite vein, fractured and resealed by calcite and late euhedral quartz. The veins in Hastenrath show an even more complex sealing history because they contain beside brecciated dolomite and calcite, euhedral ankerite overgrowth, galena (approx. 150°C), euhedral quartz, calcite, sphalerite (approx. 150°C) and calcite, later filled with organic material <150°C. Galena and sphalerite are associated with chalcopyrite. The geochemistry of the dolomite is different in both localities, indicating either a different fluid systems or strong influence of the host rock. Similar fluid types at both localities may suggest a homogeneous fluid system. However, marked differences exist between hydrothermal mineral products of both localities. The complex fluid system in Hastenrath shows that the same

fracture was sealed during different fluid events, possibly associated with normal faulting.

Literatur

- Bons, PD (2001) The formation of large quartz veins by rapid ascent of fluids in mobile hydrofractures. *Tectonophysics* 336(1-4), 1-17
- Cox SF, Knackstedt MA & Braun, J (2001) Principles of structural control on permeability and fluid flow in hydrothermal systems. *Reviews in Economic Geology* 14, 1-24
- Hilgers C & Urai, JL (2005) On the arrangement of solid inclusions in fibrous veins and the role of the crack-seal mechanism. *Journal of Structural Geology* 27(3), 481-494
- Miller SA (2002) Properties of large ruptures and the dynamical influence of fluids on earthquakes and faulting. *Journal of Geophysical Research* 107(B9), 2182, doi:10.1029/2000JB000032
- Ramsay JG (1980) The crack-seal mechanism of rock deformation. *Nature* 284(5752), 135-139
- Sander B (1948) Einführung in die Gefügekunde der geologischen Körper. Erster Teil: Allgemeine Gefügekunde und Arbeiten im Bereich Handstück bis Profil. UND Zweiter Teil: Die Korngefüge. Springer, Wien
- Sibson RH (2004) Controls on maximum fluid overpressure defining conditions for mesozonal mineralisation. *Journal of Structural Geology* 26, 1127-1136
- Stoneley R (1983) Fibrous calcite veins, overpressures and primary oil migration. *AAPG Bulletin, Geological Notes*, 1427-1428
- Taylor WL (1999) Fluid flow in discrete joint sets: Field observations and numerical simulations. *Journal of Geophysical Research* 104(B12), 28,983-29,006

Structural investigations of the W termination of the ‘Schneeberg Zug’ — Austroalpine Unit, Southern Tyrol: Results from a crustal scale shear zone *Poster*

Gianluca Cotza¹ Martin Thöni²
Bernhard Grasemann¹

The Austroalpine microplate traces the Alpine collision event between the Africa-related southern Alpine realm and the European continent. The southern margin of this microplate, the basement to the north of Meran (including Texel unit and Schneeberg Zug) is characterized by regional eo-Alpine high-pressure metamorphism (Hoinkes & Thöni, 1987). PT conditions decrease from SE (Texel unit) to the pre-alpine basement in the NW.

The HP Rocks were exhumed within a ca. 15 km broad SW-NE-striking, NW-dipping high strain zone (Sölva et al. 2001). The high-pressure Texel crystalline is tectonically underlain by the Campo unit in the south and overlain by the Ötztal-Stubai Basement in the north(west). The Schneeberg Zug forms an up to 5 km thick shear zone at its base, representing the study area. It shows normal-sense kinematics and separates pre-Alpine basement rocks in the hanging wall from high-pressure rocks in the footwall, the Texel unit. These were emplaced on top of pre-Alpine basement rocks (Campo unit) by an eo-Alpine ductile thrust.

¹ Department of Geodynamics and Sedimentology, Structural Processes Group University of Vienna, Althanstraße 14, Vienna A-1090, Austria ² Centre for Earth Sciences, University of Vienna, Laboratory for Geochronology, Althanstraße 14, Geozentrum 2A449, A-1090 Wien, Austria

Lithologically the western termination of the Schneeberg Zug comprises characteristic garnet micaschists, marble layers, amphibolites, quartzites, hornblende-garnet-schists and calc-schists. These lithologies are called *Bunte Serie* (Mauracher, 1981) and differ from the polyphase adjacent Texel unit and the polymetamorphic basement rocks in the hanging wall due to their lithological content and their monometamorphic evolution.

Petrological and geochronological investigations on the eastern continuation of these characteristic metapelitic rocks evidence the time of garnet growth during D₁ close to the Cretaceous pressure peak. Sm-Nd isochron data of these continuously zoned garnets yielded crystallization ages between 90 and 95 Ma.

Preliminary structural investigations yielded four major deformation events: D₁ produced a compositional layering and a mylonitic foliation; generally this ductile deformation in the northwestern portion of the Schneeberg Zug is characterized by contemporaneous shearing and folding forming isoclinal folds with axes oriented parallel to the NW-SE plunging stretching lineation. Deformation stage D₂ formed tight folds with steep NW to WSW plunging axes and NW to W dipping axial planes, which re-fold the D₁ related structures. Deformation stage D₃ is characterized by a crenulation with NW-plunging axes and NW-dipping axial planes. Lower greenschist-facies shear-zones dipping to the W and with shear sense top to W-WNW represent the last ductile event. They crosscut the older structural inventory. Brittle deformation evidences normal faulting reactivating the NW dipping main foliation as well as related dextral strike slip movement.

Geochronological data and structural investigations indicate a continuous eo-Alpine tectono-metamorphic evolution, which started at high grade conditions homogeneously distributed over the whole shear zone. With decreasing temperature conditions the deformation progressively partitioned into distinct shear zones.

References

- Habler G (2004) Exhumation in the eo-Alpine high-pressure belt of the Eastern Alps: Petrological, structural and geochronological investigations of high-pressure metamorphic rocks. Dissertation. Fakultät für Naturwissenschaften und Mathematik der Universität Wien
- Hoinkes G & Thöni M (1987) New findings of eclogites within the eo-Alpine amphibolite grade area of the Ötztal basement. *Terra cognita* 7(96)
- Mauracher J (1981) Alpidische und voralpidische Metamorphose und Strukturprägung am Westende des Schneebergerzuges. (Ötztales Alpen). *Mitt. Ges. Geol.-Bergbaustud.* 27, 244–245
- Sölva H, Thöni M, et al. (2001) Emplacement of eo-Alpine high-pressure rocks in the Austroalpine Ötztal complex (Texel group, Italy/Austria). *Geodinamica Acta* 14, 345–360
- Thöni M (1999) A review of geochronological data from the Eastern Alps. *Schweiz. Mineral. Petrogr. Mitt.* 79, 209–230

Evolution of the Tamtsag Basin / NE-Mongolia — part II: structure and hydrocarbon potential *Poster*

Buyan Davaa¹ Peter Geerdts¹ Marc Vogler¹ Andreas Henk¹

Introduction

The Tamtsag basin in NE Mongolia is part of a widespread basin system which formed during Late Jurassic and Cretaceous times (Graham et al. 2001, Qing-Ren et al. 2003). It is filled with continental sediments and volcanics which can reach up to 4 km in thickness. Rifting and subsequent basin inversion led to a complex basin geometry characterized by several horst and graben structures. The geodynamic causes for regional basin formation are discussed controversially and several hypothesis ranging from orogenic collapse via subduction rollback to collision-induced rifting have been put forward.

Scientific research on the Mesozoic basins in Mongolia has so far concentrated on the East Gobi basin to the southwest (Graham et al. 2001, Prost 2004, Johnson et al. 2004) and some work has also been published on the Hailar Basin (Qing-Ren et al. 2003), the northeastward continuation of the Tamtsag Basin into China. Fundamental data on the fill and tectonics of the Tamtsag Basin in between is still missing. This is partly due to poor exposure as most of the basin fill is covered by Cenozoic sediments and only locally, near the borders faults, rocks are accessible for surface investigations.

¹ Geologisches Institut, Universität Freiburg Albertstraße 23b, D-79104 Freiburg



Figure 1: Schematic petroleum system chart of the Tamtsag Basin

However, recent discoveries of oil in the Tamtsag and Hailar Basins have resulted in intense exploration activity and a strong interest in the area.

This contribution describes the results of a field campaign in Fall 2005 focusing on the structure and hydrocarbon potential while a companion paper (Geerds et al. this volume) deals with the fill of the Tamtsag Basin.

Tectonics

The Tamtsag Basin is an approximately 300 km long and 80 km wide ENE-trending fault-controlled structure. The basin architecture is characterized by uplifted fault blocks in the central parts and graben-like structures to the North and South, close to main basin bounding faults. In the nearby East Gobi Basin, Prost (2004) distinguished five structural episodes: (1) pre-Jurassic north-east shortening, (2) Middle Jurassic to Early Cretaceous north-east directed extension, including rifting, (3) late Early Cretaceous north-south shortening, that led to the basin inversion on already existing normal faults, (4) Middle-Cretaceous uplift and erosion,

and finally (5) east-west directed shortening and dextral movement on north-east trending faults.

Field work concentrated on the western margin of the basin where sufficient outcrops for structural analysis are available. The large-scale structural elements, i.e. the major faults, follow the regional ENE trend. Of particular interest are ridges composed of Mesozoic magmatic rocks which are uplifted relative to the surrounding Cretaceous sedimentary basin fill and strongly resemble positive flower structures. For example, one of the ridges is crosscut by several faults striking 20° , thus forming an angle of 40° to the principle basin axis. Most are normal or reverse faults with an additional strike-slip component.

Hydrocarbon potential

Oil has recently been found in block XIX of the Tamtsag Basin. Reservoirs are located in sandstones of the Lower Cretaceous Tsagaantsav and Zuunbayan Formations. Source rocks are situated in the same stratigraphic units and total organic carbon contents in the corresponding shales reach up to 3%. Trans-

pression at the end of the Lower Cretaceous formed structural traps, e.g. tilted fault blocks and anticlinal folding, as well as stratigraphic traps beneath the related unconformity.

In order to get a quantitative understanding of petroleum formation in the Tamtsag Basin the subsidence and thermal histories of various wells are modelled. This requires a complete reconstruction of the sedimentation and uplift history, i.e. the thickness and age of the eroded, and hence missing, strata has to be estimated. Using shale compaction data derived from sonic logs and the method of Magara (1976), respectively, it can be found that the rocks of the Tamtsag basin were once buried 350–800 m deeper than today. Comparison with the regional evolution indicates that this maximum burial occurred during late Lower Cretaceous time prior to deposition of Upper Cretaceous Saynshand formation. This burial history forms the basis for maturity modelling using the software Petromod1D of IES, Jülich. The thermal history model is calibrated against observed vitrinite reflectance data. Modelling results show heating of the source rocks, the critical moment, i.e. the onset of oil migration as well as the time of peak oil generation. For example, the oldest source rocks of the Tsagaantsav formation reach maximum temperatures of up to 136°C during the late Lower Cretaceous at about 118 Ma bp. Petroleum systems modelling will be extended to 2D and basin-wide sections to provide quantitative information for future exploration in blocks XX, XXI and XXII.

Acknowledgements Financial support by Deutsche Forschungsgemeinschaft is gratefully acknowledged. ‘Min-

eral and Petroleum Authorities of Mongolia’ kindly supported our work in the Tamtsag Basin.

References

- Graham SA (2001) Sedimentary record and tectonic implications of Mesozoic rifting in Southeast Mongolia: Geological Society of America Bulletin, 1561–1578
- Johnson CL, Greene TJ, Zinniker DA, Moldawan JM, Hendrix MS & Carrol AR (2003) Geochemical characteristics and correlation of oil and nonmarine source rocks from Mongolia: The American Association of Petroleum Geologist Bulletin 87, 817–846
- Magara K (1976) Thickness of removed sedimentary rocks, paleopore pressure, and paleotemperature, southwestern part of Western Canada Basin: The American Association of Petroleum Geologist Bulletin 60, 554–565
- Prost GL (2004) Tectonics and hydrocarbon systems of the East Gobi basin, Mongolia: The American Association of Petroleum Geologist Bulletin, 88(4), 483–513

Application of Photogrammetry in Geology: 3D Investigation of Rock Fracture Distributions *Poster*

Hagen Deckert¹ Klaus Gessner²

Geology as a science has an important visual component and the knowledge of any geologist is deeply linked to visual experience of rock outcrops, thin sections and analytical images. One of the shortcomings of most geological images such as maps, cross sections and outcrop photographs is that they are 2D,

¹ Institut für Geowissenschaften, Johannes Gutenberg-Universität, Becherweg 21, 55099 Mainz, Germany ² School of Earth and Geographical Sciences, University of Western Australia, 35 Stirling Highway, Crawley WA 6008, Australia

while processes geologists are interested in are typically occurring in 3D space. The 3D geometry of faults, fractures and joints is crucial to quantify geological processes related to fracture mechanics, such as hydrothermal mineralization and ground water flow, but also geotechnical problems such as rock mass stability. A number of studies have shown that some geological structures can be described with a scale invariant, fractal distribution. So far these observations on which these findings are based were restricted to one and two dimensions and has been difficult to obtain a full spatial geometric picture of fracture sets from rock outcrops, because much of the rock is not directly accessible. However, without taking into account the spatial distribution of geological structures the true geometry of joint patterns cannot be fully described and scaling laws, fractal or not, cannot be derived.

We present images of joint patterns based on datasets acquired by digital photographs which are processed to three dimensional images using the photogrammetry software Siro3D. This technique allows to obtain a highly accurate 3D picture of the visible outcrop. The spatial pattern of joints in nature is investigated using the software SiroJoint. For the analysis of joint systems a large data set was collected from the Heavitree Quarzite at Ormiston Gorge, near Alice Springs. The Heavitree Quartzite is fragmented by a spectacularly regular three-dimensional joint pattern, which is repeated at different scales and therefore represents a perfect laboratory for our investigations (Hobbs 1993). Siro3D generates a spatially fully referenced 3D image from overlapping digital images, such that each pixel of the image is assigned spa-

tial coordinates. The software SiroJoint routinely constructs planes from the intersection of the rock-face with the linear trace of planar features (Poropat 2001). It provides stereographic plots of structural elements and additionally measures joint persistence, area, and joint spacing. Our measurements allow to analyse geometrical scaling relationships of joint sets with high accuracy and will help explore the character of their 3D complexity.

Several hundred joint planes were defined with SiroJoint in an Ormiston Gorge outcrop. Three different joint sets can be distinguished. Joint set one and two are characterized by steeply inclined planes with joint spacings ranging between 2 cm to 40 cm and 2 cm to 10 m respectively. Both joints sets depict a power law distribution in joint spacing/frequency plots. The third set is defined by a subhorizontal orientation. It shows a very regular spacing in the meter scale and lacks an exponential distribution. We intend to use the results as a basis to compare observed fracture pattern with those generated by computational methods like Iterated Function Systems. This might help to understand how physical rock properties influence the spatial complexity of fracture systems and develop constitutive scaling relationships for certain rock types.

References

- Hobbs BE (1993) The Significance Of Structural Geology In Rock Mechanics, Chapter 2, in: Comprehensive Rock Engineering 1, Hoek E, Hudson J & Brown ET (eds.), Pergamon Press, 25–62.
- Poropat GV (2001) New methods for mapping the structure of rock masses, Australian Institute of Mining and Metallurgy, Conference Proceedings EXPLO2001. Huntersvalley, NSW, Australia.

Relevance of viscous flow in accretionary wedges *Vortrag*

Hagen Deckert¹ Uwe Ring²

The orogenic wedge model (Davis et al. 1983; Platt 1986) marks a conceptual breakthrough in understanding the growth and long-term evolution of accretionary wedges. The characteristic rheology of subduction-related accretionary wedges is thought to change from Coulomb to viscous when the wedge becomes thicker than ca. 15 km, a transition that may influence the stability and dynamics of these wedges. Platt (1986) proposed that viscous flow may trigger extensional faulting in the upper rear part of the wedge and Wallis et al. (1993) argued that viscous flow may cause vertical ductile thinning of the rear part of the wedge.

Material fluxes control the geometric shape of an accretionary wedge (Brandon et al. 1998; Platt 1986). Frontal accretion and erosion both tend to drive the wedge into a subcritical condition as the taper angle of the wedge is progressively reduced. This leads to horizontal shortening across the wedge. If underplating is dominantly controlling the flow field in the wedge and frontal accretion or erosion at the rear of the wedge are small, the wedge is supercritically tapered and leading horizontal extension. Horizontal extension leads to a subhorizontal foliation and may eventually lead to normal faulting in the rear-part of the wedge. Despite the importance of these issues, there remains a paucity of detailed informa-

tion about ductile deformation and how viscous flow influences the stability of subduction-related accretionary wedges. Strain measurements are an instrument to address whether viscous flow strongly influences the deformation in accretionary wedges. They provide direct information about the kinematics of ancient orogenic belts. Additionally, they allow understanding important tectonic processes in subduction wedges such as the pattern of flow within the wedge.

We focus on deformation analysis on a suite of samples from the Otago wedge exposed in the South Island of New Zealand. The Otago accretionary wedge offers a unique opportunity to study the tectonic evolution of a typical subduction-related accretionary complex. Its across-strike length of ca. 600 km makes it one of the largest exposed ancient accretionary wedges on Earth. Pressure and temperature estimates indicate that our samples are representative of deformation conditions to depths as great as ca. 35 km. This is similar to maximum depths observed for subducting slabs beneath modern fore-arc highs.

The deformation measurements show that the strain magnitude is generally small in the Otago wedge. The γ_{oct} values, a measure of the distortion a sample experienced (independent from the strain geometry), range from 0.34–3.87 for the R_f/ϕ strains, 1.01–4.28 for XTG strains across the whole suite of the Otago rock pile, and 0.08–0.70 for the absolute strains obtained from low metamorphic grade rocks. The Otago samples are characterized by considerable volume strain that increases from the lower textural zones towards the high-grade interior of the wedge.

Our strain results are inconsistent with

¹ Institut für Geowissenschaften, Johannes Gutenberg-Universität, Becherweg 21, 55099 Mainz, Germany ² Department of Geological Sciences, University of Canterbury, Christchurch, New Zealand

the models which advocate supercritically tapering of accretionary wedges and that supercritical tapering eventually triggers normal faulting. Taking averages of our strain measurements, a residence time in the wedge of 35 Myr, burial depths of 30 km, coaxial deformation and a depth-dependent rate for ductile deformation, we calculate vertically-averaged strain rates. Because the principal strain axes of the tensor average are all inclined, the vertical averaging changes the principal stretches. The horizontal principal stretch parallel to the 160° -striking Otago wedge becomes 0.79, that for across strike 0.88 and for vertical strain 0.44. Averaged strain rates are $-1.44 \cdot 10^{-16} \text{ s}^{-1}$ for parallel-strike horizontal strain, $-6.2 \cdot 10^{-17} \text{ s}^{-1}$ for across-strike horizontal strain, and $-8.02 \cdot 10^{-16} \text{ s}^{-1}$ for vertical strain. The strain rates are related to volume loss and to the efficiency with which dissolved chemicals are advected away. The rates are similar to the ones calculated by Bolhar & Ring (2001) and Ring & Richter (2004) for the Franciscan wedge. These strain rates are orders of magnitude smaller than the $1 \cdot 10^{-14} \text{ s}^{-1}$ strain rates assumed by Platt (1986). Thus, our data imply that the Otago wedge could not shorten horizontally fast, and hence could not have steepened up its surface slope. The fact that shortening was accompanied by volume loss has another important and interesting consequence. Even if a case was envisioned in which horizontal shortening was fast enough to steepen up the surface slope of the wedge, the volume loss would not necessarily change the wedge geometry into a supercritical configuration triggering normal faulting. As a consequence of the slow strain rates and the high vol-

ume loss, viscous flow probably was not fast enough to significantly influence the stability of the wedge and to form a supercritically tapered wedge.

References

- Bolhar R & Ring U (2001) Deformation history of the Yolla Bolly terrane at Leech Lake Mountain, Eastern belt, Franciscan subduction complex, California Coast Ranges. *Geological Society of America Bulletin* 113: 181–195
- Brandon MT, Roden-Tice MK & Garver JI (1998) Late Cenozoic exhumation of the Cascadia accretionary wedge in the Olympic Mountains, NW Washington State. *Geological Society of America Bulletin* 110: 985–1009
- Davis D, Suppe J and Dahlen FA (1983) Mechanics of fold-and-thrust belts and accretionary wedges. *Journal of Geophysical Research* 88: 1153–1172
- Platt JP (1986) Dynamics of orogenic wedges and the uplift of high-pressure metamorphic rocks. *Geological Society of America Bulletin* 97: 1037–1053
- Ring U & Richter PP (2004) Normal faulting at convergent plate boundaries: Mylonitic extensional fabrics in the Franciscan subduction complex in Del Puerto Canyon, California, revisited. *Tectonics* 23: art. no. TC2006
- Wallis SR, Platt JP & Knott SD (1993) Recognition of syn-convergence extension in accretionary wedges with examples from the Calabrian arc and the Eastern Alps. *American Journal of Science* 293: 463–495

Deformation mechanisms in the eastern Sudbury Igneous Complex, Canada: Evidence for meteorite impact into an active orogen *Vortrag*

Daniel Doman¹ Ulrich Riller¹ Kai Hofmann²

The 1.85 Ga Sudbury Igneous Complex (SIC) in central Ontario is now widely considered to be the erosional remnant of a deformed paleo-horizontal impact melt sheet, about 2.5 km in thickness. Deformed impact melt breccias of the Onaping Formation and post-impact metasedimentary rocks overlie the layered SIC, which in turn rests on shocked Archean basement and Paleoproterozoic cover rocks. The main mass of the Igneous Complex is subdivided from top to bottom into granophyre, quartz-gabbro and norite layers. Previous workers considered non-cylindrical folding and NW-directed reverse faulting as the main structural processes that formed the asymmetric, syn-formal geometry of the SIC apparent in map view and seismic section. Structural studies support this model in the southern part of the impact structure, where greenschist-facies metamorphic tectonites of the South Range Shear Zone (SRSZ) accomplished structural uplift of the southern SIC by NW-directed reverse shearing. However, little evidence for pervasive ductile strain has been reported from the weakly metamorphosed eastern part of the SIC, the East Range, which is characterised by steep basal dips and max-

imal curvature in plan view. The objective of this study is to assess the structural inventory of the East Range in terms of post-emplacment deformation mechanisms. Our interpretation is based on published and newly acquired structural data.

Planar mineral shape fabrics of cumulate plagioclase and pyroxene are developed in the intermediate quartz-gabbro and lower norite layers of the southern East Range SIC. Microstructures show little intracrystalline deformation in quartz. Euhedral cumulate plagioclase retains an angular outline indicating magmatic mineral fabric development. This magmatic foliation is concordant to SIC contacts or large-scale discontinuities in their vicinity (Fig. 1). Magmatic fabrics are observed rarely in the northern portion of the East Range. Here, tectonic foliations and S-C fabrics are developed sporadically at, and concordant to, brittle structures striking N-S. A weak tectonic foliation defined by chlorite that replaces magmatic minerals is developed in the upper granophyric SIC of the NE-lobe that connects the SIC's North and East Ranges via a 105° arc. This foliation grades into a shape-preferred orientation of primary, i.e., magmatic, mafic minerals observed in the lower granophyre and underlying layers of the SIC. Mineral fabrics observed in the NE-lobe SIC are concordant to metamorphic foliations developed in the overlying Onaping Formation breccias. Both foliations strike parallel to the NE-Lobe's acute bisectrix and, thus, display an axial-planar geometry typical for fabrics formed in the core of a buckle fold (Fig. 1). Brittle structures including centimetre-scale shear-fractures to kilometre-scale fault-zones are observed in the eastern

¹ Humboldt-Universität zu Berlin, Museum für Naturkunde, Invalidenstrasse 43, D-10115 Berlin ² Freie Universität Berlin, Institut für Geologische Wissenschaften, Malteserstrasse 74-100, D-12249 Berlin

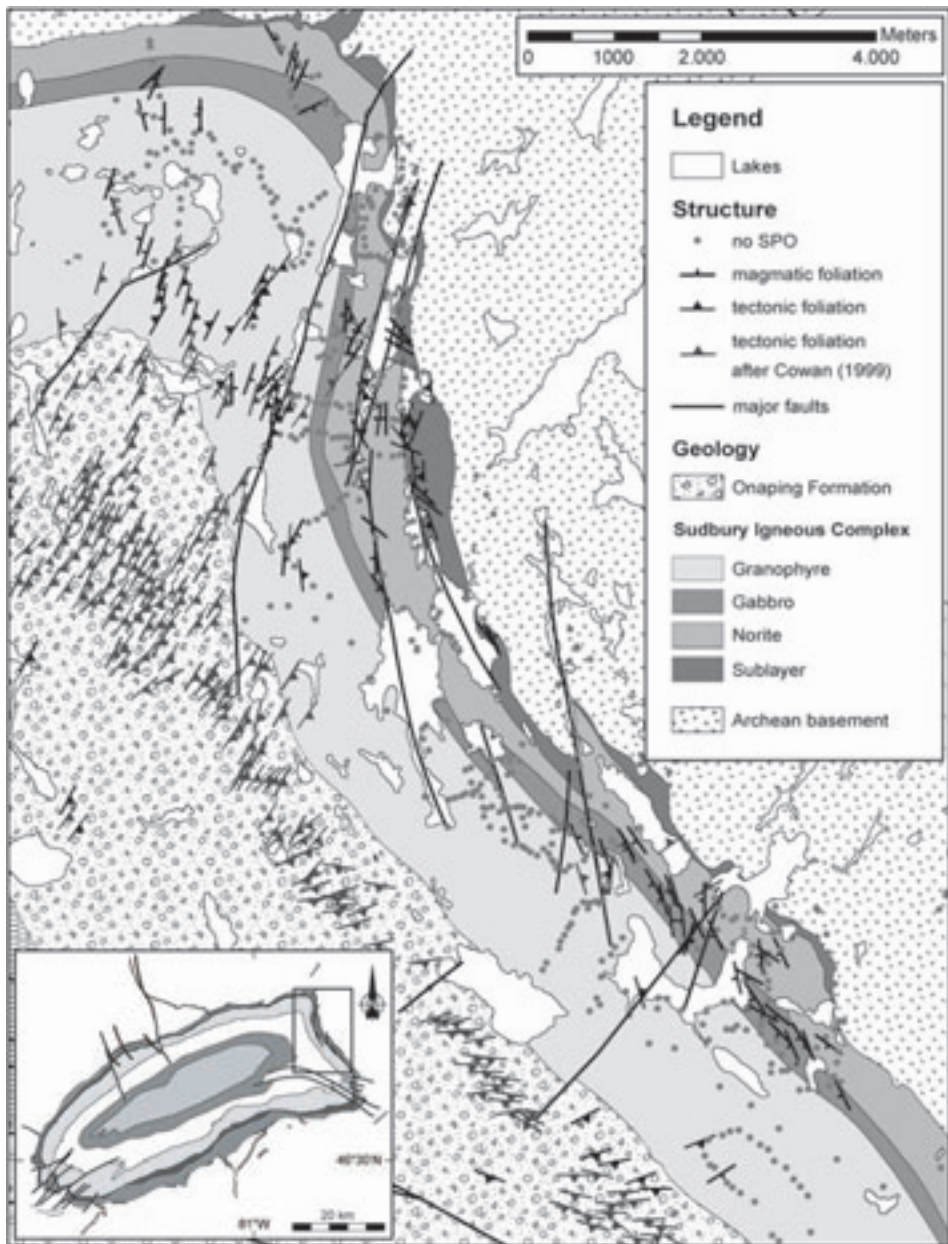


Figure 1: Strike and dip directions of magmatic and tectonic foliations in the East Range SIC and overlying Onaping Formation.

SIC and its host rocks. Large-scale faults striking N-S cut the NE-lobe's eastern limb causing variable magnitudes of strike separation of SIC contacts. Centimetre- to metre-scale, brittle faults and chlorite-filled brittle-ductile shear-zones occur pervasively in the eastern SIC, often causing centimetre-scale offset of markers. Microstructures from first-order fault-zones indicate deformation at, and below, greenschist-facies metamorphic conditions.

The concordance of magmatic and tectonic mineral shape fabrics in the NE-lobe indicates progressive deformation of the SIC during cooling from the magmatic state to lower greenschist-facies metamorphic conditions. Syn-magmatic deformation of the SIC suggests that it was emplaced during ongoing orogenic deformation. Furthermore, maximum principal stress directions inferred from inversion of fault-slip data collected in the Onaping Formation are orthogonal to metamorphic foliation surfaces at the same localities. This points to a similar deformation regime in the Onaping Formation during ductile and brittle deformation. The concordance of magmatic, metamorphic and brittle fabrics is explained best by a single progressive deformation event that was active while the SIC cooled and solidified. The lack of pervasive ductile deformation fabrics in the East Range SIC can be explained by rapid cooling of the impact melt sheet (within 100–500 ka) with respect to natural tectonic strain rates. While the geometry of mineral fabrics in the study area is compatible with large-scale, non-cylindrical folding, the low levels of ductile deformation suggest that shape-change of the eastern SIC

has been accomplished mainly by discontinuous deformation. This deformation mechanism may have accomplished bulk NW-SE shortening that was accommodated by reverse shearing within the SRSZ, resulting in large strike separations of SIC contacts observed in the western part of the impact structure. By contrast, the eastern SIC may have accomplished such shortening by brittle-ductile, non-cylindrical folding at the eastern terminus of the SRSZ. The complex post-impact deformation pattern of the central Sudbury Structure results from impact into an active orogen.

References

- Cowan EJ (1999) Magnetic constraints on the initial geometry of the Sudbury Igneous Complex: a folded sheet or a basin-shaped igneous body? *Tectonophysics* 307, 135-162

A further step toward a thermochronological 3-D model of the SE Black Forest *Poster*

Horst Dresmann¹ Ina Spottke¹ Zoltan Timar-Geng² Andreas Wetzel¹ Bernhard Fügenschuh³

Fission-track (FT) data always depend on the thermal history of a 3-D geological complex. Therefore it is expedient to display FT data sets in 3-D models. Such a model in which tectonic, sedimentological and hydrological features are combined can greatly improve

¹ Geologisch-Palaeontologisches Institut, University of Basel, Switzerland ² Geologisches Institut, University of Freiburg, Germany

³ Institut für Geologie und Palaeontologie, University of Innsbruck, Austria

the interpretation of the palaeo-thermal pattern derived from FT analyses.

Since 1988 several FT studies have been conducted in the Black Forest (BF) (Michalski 1988, Wyss 2000, Timar-Geng et al. 2004, 2005). Timar-Geng et al. (2006) analyse the crystalline basement and the Permian Rotliegend beneath the Mesozoic units in the Tabular Jura (TJ) east of Basel, Switzerland, using samples taken from the three Nagra boreholes at Kaisten, Riniken and Leuggern.

In particular Timar-Geng et al. (2005, 2006) characterise the thermal history of this pre-Mesozoic basement. For the BF they estimate at least one heating phase during the lower and middle Mesozoic while similar heating could not be observed in northern Switzerland. However, the FT-data in both regions show moderate to rapid cooling during the Cretaceous and Lower Eocene, which was followed by an Upper Eocene heating event.

The software package GOCAD (Geological Objects Computer-Aided Design) was used to build a digital elevation model (DEM), which provide a new detailed view of these FT data sets. The model is located about 20 km east of Basel, Switzerland, and extends over an area of about 21 km by 24 km and spans a vertical height difference of about 2 km.

The data sets described above along with two additional FT analyses from the Buntsandstein which lies directly on the BF crystalline, were compiled and plotted at their topographic heights in the DEM.

The FT central-ages (Galbraith & Laslett 1993) of this region range between 25 ± 2 Ma and 98 ± 6.5 Ma. The topographic positions extend between

–1412 m at the Borehole Riniken and 960 m in the BF with mean sea level as a reference.

FT central-age isochron surfaces were drawn in order to visualize the thermal evolution within the model range. Because the FT central-ages also correspond to a closure temperature, these surfaces can also be considered an isotherm. The FT closure temperature of apatite is about $90 \pm 30^\circ\text{C}$ (Laslett et al. 1987). Therefore each surface shows the position and shape of the ca. 90°C isotherm of a specific age.

This 3-D model points out an important difference in the thermal evolution of the BF und the TJ. The vertical distance between the isothermal surfaces increases from north to south. Between 90 Ma and 60 Ma the ca. 90°C isotherm drops at the Kaisten borehole by 1000 m while in the same time span in the BF a lowering of the same isotherm by 300 m can be observed. In the eastern part of the model this feature is not as marked as in the west but nevertheless it is observable.

To explain this entirely different thermal evolution it is necessary to turn to the tectonic and other geological features of the region. South of the exposed BF crystalline and beneath the TJ there lies an old Variscan structure: the Permo-Carboniferous trough (PCT). This trough strikes in WSW-ENE direction and extends from Lake Constance to the Bresse Graben and contains up to 6000 m of Palaeozoic sediments. Additionally, some Variscan fault structures strike in WNW-ESE direction and cut both the BF and the PCT, for example the Eggberg Fault and the Vorwald Fault. Beside the tectonic structures the hydrological characteristics played an important role during

the palaeo-thermal evolution. Circulating hot fluids controlled the thermal pattern. Variscan faults were often reactivated during the Mesozoic (e.g. Wetzel et al. 2003) and also during the formation of the Upper Rhine Graben. (e.g. Illies 1967) These faults are the major water-conducting features in the crystalline basement of the BF, joints and fracture networks are tributaries. Below the aquifers within the Mesozoic of the TJ, the PCT trough sediments predominantly act as an aquitard. Only the border faults of the trough were important pathways for fluids (Thury 1994).

Considering the Mesozoic sedimentological history of the region it is unlikely that fault movements are responsible for the different palaeo-thermal pattern of the BF and the TJ. Only different magnitudes of heat flow caused by hydrothermal circulating fluids can explain the 'warm' BF crystalline in comparison to the 'cold' basement of the TJ at the transition between the Mesozoic and Tertiary.

References

- Galbraith RF & Laslett GM (1993) Statistical models for mixed fission track ages. *Nucl. Tracks* 21, 459–70
- Illies JH (1967) Development and tectonic pattern of the Rhinegraben. *Thr Rhinegraben progress report 1967*
- Laslett GM, Green PF, Duddy IR & Gleadow AJW (1987) Thermal annealing of fission tracks in apatite 2. A quantitative analysis. *Chemical Geology (Isotope Geoscience Section)* 65:1–13
- Michalski I (1987) Apatit-Spaltspuren-Datierungen des Grundgebirges von Schwarzwald und Vogesen: Die post-variszische Entwicklung. Unpubl. doctoral dissertation, Heidelberg, pp 125
- Thury M, Gautschi A, Mazurek M, Müller WH, Naef H, Pearson FJ, Vomvoris S & Wilson W (1994) Geology and hydrogeology of the crystalline basement of Northern Switzerland. *Nagra Technischer Bericht, NTB 93–01*, Baden
- Timar-Geng Z, Fügenschuh B, Schaltegger U & Wetzel A (2004) The impact of the Jurassic hydrothermal activity on zircon fission track data from the southern Upper Rhine Graben area. *Schweizerische Mineralogische und Petrographische Mitteilungen* 84, 257–269
- Timar-Geng Z, Fügenschuh B, Wetzel A & Dresmann H (2005) Low-temperature thermochronology of the flanks of the southern Upper Rhine Graben. *International Journal of Earth Sciences* (in press)
- Timar-Geng Z, Fügenschuh B, Wetzel A & Dresmann H (2006): The low-temperature thermal history of northern Switzerland as revealed by fission track analysis and inverse thermal modelling. *Eclogæ Geologicae Helvetiæ*. (submitted)
- Wetzel A, Allenbach R & Allia V (2003) Reactivated basement structures affecting the sedimentary facies in a tectonically 'quiescent' epicontinental basin: an example from NW Switzerland. *Sedimentary Geology* 157:153–172
- Wyss A, (2001) Apatit Spaltspur Untersuchungen in der Vorwaldscholle (SW-Deutschland). Unpubl. diploma thesis, Univ. Basel, pp 69

(U-Th)/He thermochronology — methodology and a case study: dating of faulting in the Southern Alps *Vortrag*

István Dunkl¹ Martin Danišik² Vincenzo Picotti³ Wolfgang Frisch²
Hilmar von Eynatten¹ Alberto Castellarin³

History of He thermochronology

The radiogenic ⁴He isotope is continuously forming in the lithosphere mainly by the alpha-decay of U, Th and Sm. This decay process was discovered already at the beginning of the 20th century, and the first U/He dating was made by Rutherford (1905). Although his result indicated that the dimensions of the Earth's history ranges to millions of years, the U/He method was used only scarcely later on because the minerals are usually not closed to the decay product. The helium is extremely mobile and diffuse through the crystal lattices. Thus, the apparent U/He ages were always younger than the radiometric ages determined by other isotope geochronometers like U/Pb, Rb/Sr or K/Ar. The current renaissance of the method has been started at the end of eighties, when H. Lippolt, P. Zeitler, K. Farley and their co-workers have described the parameters of diffusion of some uranium-bearing minerals (e.g. Lippolt & Weigel 1987, Zeitler et al. 1987). It turned out that the (U-Th)/He apparent ages do carry meaningful geological information. The closure temperature of the most widely used apatite-He system is around 70°C. Thus, by the usage of this

¹ University of Göttingen, Germany ² University of Tübingen, Germany ³ University of Bologna, Italy

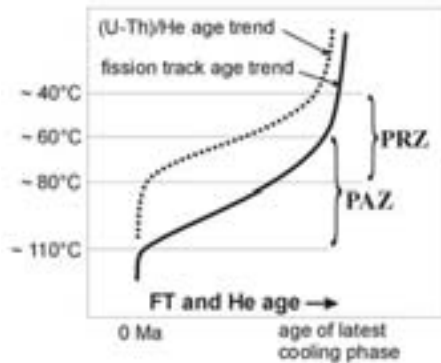


Figure 1: Schematic vertical trend of apatite FT and He ages in the uppermost part of the lithosphere in a tectonically stagnating block (after Stockli et al. 2000).

mineral/method pair it became possible to date low-temperature geological processes, which were undatable by other geochronometers.

Typical applications

The vertical trends of apparent fission track (FT) and He ages in a stagnating lithosphere show convergence to the age of the latest exhumation phase at the surface and they have total reset (= zero age) at the depth where the temperature does not allow the accumulation of decay products and nuclear tracks (Fig. 1). In between these values there is a gradually changing section where the apparent ages are the result of the balance of continuous accumulation of decay products and their disappearance. This transitional section is called as 'partial annealing zone' (PAZ) in the fission track thermochronology and 'helium partial retention zone' (PRZ), which is defined as a temperature range where between 5% and 95% of the He is retained in a crystal. The rapid expansion of the application of (U-Th)/He

method in different fields can be related to its low closure temperature.

- This allows determining the final phase of exhumation of structural blocks in the upper crust (e.g. Stockli et al. 2000).
- In ideal conditions (proper granitoid lithology, possibility of 3D sampling in a high mountains, in a subsurface mine or in boreholes) the sensitivity of the He-thermochronology allows to date and determine the magnitude of vertical offset along faults (McInnes et al., 1999).
- In cratonic areas, where the typical lithologies are high-grade rocks and the sedimentary record is usually poor the post-orogenic thermal events can be well recorded by apatite fission track and He-thermochronology.
- Not only cooling and exhuming geodynamic scenarios, but the early phase of burial warming of sedimentary basins can also be well dated. This has prominent importance in the hydrocarbon prospecting, because the temperature range of He reset in apatite corresponds to the beginning of 'oil-window'.
- The depth of the ca. 70°C isotherm depends on the geothermal gradient, the local surface morphology and the areal variation of rate of erosional removal. This opens the door for apatite He-thermochronology in geomorphological and morphotectonic studies (House et al. 1997).

Methodology

The (U-Th)/He age determination is performed on single or more crystals in multiple aliquots. Only completely clear, mineral and fluid inclusion free crystals are datable. Crystals with fissures and damaged external surface have to be avoided. The documentation of the dimensions and shape of the crystals is crucial. By the radioactive decay the alpha-particles has significant kinetic energy and 'jump' ca. 20–30 µm through the lattice of apatite crystals. Consequently, the rim of the crystals is depleted as the part of helium atoms is ejected from the crystals. This causes a predictable loss, but this can be corrected by consideration of the dimensions and shape (surface/volume ratio) of the dated crystals. After the selection, the crystals are degassed in a full-metal vacuum oven and the released helium is purified from the reactive gases by getters. The He content is measured by mass spectrometer using isotope dilution. The mother elements (U, Th and Sm) are measured after the dissolution of the degassed crystals by ICP-MS.

Our case study in the Dolomites

The Dolomites of the eastern Southern Alps were formed from the Permian-Triassic sedimentary cover of the slightly deformed South Alpine in the Tertiary. The different parts of the Dolomites have suffered two times Alpine deformation, and the shortening process is actually still active along the southernmost thrusts. The immediate dating of the deformation is possible only in the southern zones, where sediments are involved in the thrusts, while the northern areas no or rather scarce geological evidences exists on the timing of structural evolution.



Figure 2: Simplified geological map of Dolomites with the apatite ages, where FT chronometer suffered minor reset, but the more sensitive He ages indicate Late Miocene exhumation.

The isotope geochronological dating is also difficult because the sedimentary successions are dominantly composed of carbonate rocks. We could use only the Triassic volcanic dikes and tuff horizons for thermochronology. The apatite fission track ages are ranging between 210 and 6 Ma. The oldest ages indicate the presence of slightly reset areas and date the exhumation of some structural blocks to be Late Miocene. The apatite (U-Th)/He ages are younger than the FT ages in every sample. In the western Dolomites, where the Neogene thermal reset is not detected by the apatite fission track thermochronometer, the He ages show Late Miocene reset (Fig. 2) due to the lower closure temperature of the later method. From the significant contrast between the FT and He ages we can conclude that the dated stratigraphic horizons were deeper than the total reset depth of He method but shallower than the reset depth of the FT method

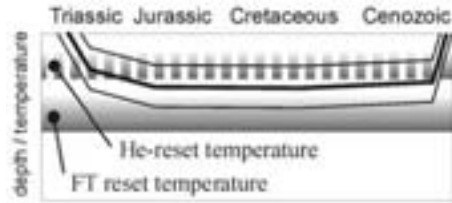


Figure 3: Schematic burial history of the samples from western Dolomites. The thick black line represents the position of the dated samples. They were in a hotter environment than the helium retention temperature, but below the complete FT reset temperature.

between the Late Triassic and Late Miocene. We suppose that beyond the general Miocene uplift of the Dolomites mainly the displacements along the Stava Line and Schio-Vicenza Fault or Bassano Thrust are responsible for the exhumation of Passo Feudo and Recoaro area, respectively. Figure 3 shows a supposed burial path for the samples presented in Figure 2.

References

- Lippolt HJ & Weigel E (1987) ^4He diffusion in ^{40}Ar -retentive minerals. *Geochim. Cosmochim. Acta*, 52, 1449–1458
- McInnes BIA, Farley KA, Sillitoe RH & Kohn B (1999) Application of apatite (U-Th)/He thermochronometry to the determination of the sense and amount of vertical fault displacement at the Chuquicamata porphyry copper deposit, Chile. *Economic Geology*, 94, 937–948
- Stockli DF, Farley KA & Dumitru, TA (2000) Calibration of the apatite (U-Th)/He thermochronometer on an exhumed fault block, White Mountains, California. *Geology* 28, 983–986
- Zeitler PK, Herczeg AL, McDougall I & Honda M (1987) U-Th-He dating of apatite: a potential thermochronometer. *Geochim. Cosmochim. Acta*, 51, 2865–2868

Magnetische Charakteristik von Pyroklastika des Ság-hegy Vulkan Komplex, Kleine Ungarische Tiefebene

Poster

Nina Dworazik¹ Andreas Auer¹
Ulrike Martin¹ Karoly Németh² Helga de Wall¹ Christian Rolf³

Der Ság-hegy Vulkan Komplex befindet sich in dem Vulkanfeld der Kleinen Ungarischen Tiefebene. Eine ³⁹Ar/⁴⁰Ar Datierung ergab ein Alter von $5,42 \pm 0,06$ Ma für den Ság-hegy (Wijbrans et al. 2004). Die Entwicklung des Vulkans weist zwei verschiedene Ereignisse auf. Als erstes trifft aufsteigendes Magma auf meteorisches Wasser in einer fluvio-lakustinen Umgebung (fuel-coolant interaction FCI). Die FCI von Wasser bzw. wassergesättigtem Sediment und Magma führte zur Bildung eines phreatomagmatischen Tuffrings. Nachdem das Wasserangebot aufgebraucht war, füllte sich das Innere des Tephrrings mit einem Lavasee. Lokal kollabierte der Tuffring, so dass Lava aus dem See herausfließen konnte. Durch die Anlage eines Steinbruches im zentralen Bereich des Vulkankomplexes ergibt sich ein 3-D Aufschluss mit hervorragenden Einblick auf die Intrusionsbeziehungen von Förderdykes, Sills und Überresten des Lavasees (Martin & Németh, 2004). Die pyroklastischen Gesteine enthalten massive und geschichtete Einheiten mit Lapilli, Lapillituff/Tuff sowie pyroklastische Breccien. Die variierenden Proportionen der Nebengesteinsklasten wei-

sen auf eine Aufnahme des Nebengesteins während der Eruption. Juvenile Klasten bestehen hauptsächlich aus eckigen, blockigen Sideromelan (glass shards) mit nahezu gleichen Formen und einem geringen Anteil an Tachylit. Softsedimentdeformation und akkretionäre Lapilli sind ein Beleg für die große Menge an Wasser, die sich in dem System befand. Dünen- und Antidünenschichtung, Rinnen- und Pool Strukturen, Gradierungs- und Sortierungseigenschaften deuten an, dass der Tuffring graduell von base surge und eingeschalteten fallout Ablagerungen aufgebaut wurde.

Nach der phreatomagmatischen Phase füllte sich der Krater mit einem Lavasee, dessen Morphologie durch die Tephra Ablagerungen begrenzt wurde. Am Kontakt zu den Pyroklastika entwickelte sich ein cm-mächtiger abgekühlter Rand, der plattige (zweibelförmige) Klüftung zeigt. In die angrenzenden Schichten intrudierte eine große Anzahl an Dykes und Sills. Diese Intrusivkörper durchschlagen generell die pyroklastischen Einheiten im gesamten Vulkankomplex. Wenn die pyroklastischen Einheiten eine große Menge an Wasser beinhalteten, so kam es zum mingling der Gänge mit der nassen Tephra und so zur Ausbildung von Peperiten. Die obersten Einheiten waren mächtige Lavaströme, die alle darunter liegenden Einheiten überdeckten. Allerdings wurden diese Gesteine bereits abgebaut. Übrig geblieben ist nur ein großer strombolianischer Schlackenkegel, der mit seinem auffälligen Förderdyke die höchste Ebene des Steinbruches darstellt. Hiermit bietet sich eine sehr gute Möglichkeit, die Beziehung zwischen der Platznahme von Dykes und Sills und deren Geometrieübergängen von vertikal bis

¹ Institut für Geologie, Julius-Maximilians-Universität Würzburg, Pleicherwall 1 D-97070, Germany ² Geological Institute of Hungary, 14 Stefania St., Budapest H-1143, Hungary ³ Leibniz Institute for Applied Geoscience, Stillweg 2, D-30655 Hannover, Germany

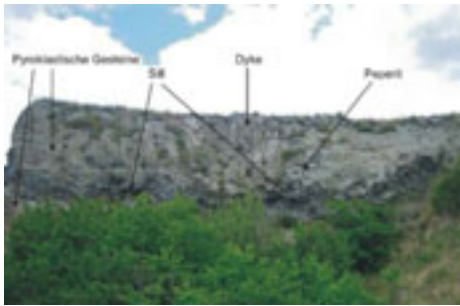


Abbildung 1: Ein Sill und Dyke Komplex in den pyroklastischen Einheiten des Säghegy. Die Sills sind vorzugsweise entlang einer Diskordanz der Tuffring Sequenz intrudiert.

schichtparallel zu untersuchen. Die Ausdehnung der Intrusivkörper reicht von Mächtigkeiten im cm-Bereich von kleinen Apophysen des Lavasees in die pyroklastischen Gesteine bis zu mehrere Meter mächtigen Dykes und Sills.

In dieser Studie sollen die magnetischen Charakteristika einer Sektion von pyroklastischen Gesteinen, die von Dykes und Sills abgeschnitten wird, untersucht werden. Vorläufige Ergebnisse zeigen, dass die magnetische Suszeptibilität aller pyroklastischen Einheiten im Bereich der ferrimagnetischen Suszeptibilität liegt und von $(2 - 20 \times 10^{-3} \text{ SI})$ variiert. (Abb. 1).

Die magnetische Anisotropie ist generell niedrig (kleiner als 5%) und in dem Feld für oblate Geometrie, in geschichteten Tuffen ist eine signifikant höhere (5 bis 10%) aber auch oblate Anisotropie festzustellen (Abb. 2).

Die magnetische Lineation zeigt einen gleich bleibenden NE (020) gerichteten Materialtransport für die gesamte Abfolge. Die Intensität der magnetischen Remanenz der pyroklastischen Einheiten ist relativ hoch mit Werten von

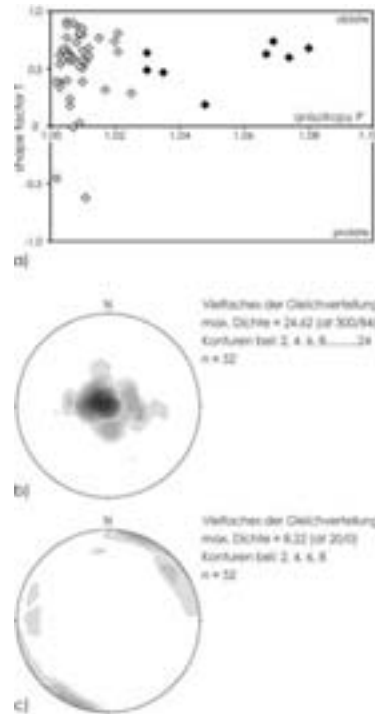


Abbildung 2: a) zeigt ein Jelinek-Diagramm der pyroklastischen Gesteine, die in dem oblaten Geometrie Feld plotten, die Tufflagen (schwarz) weisen eine höhere Anisotropie als die restlichen Einheiten (grau) auf. b) und c) präsentieren die Orientierung der b) magnetischen Foliationspole und c) magnetischen Lineation der pyroklastischen Einheiten mit einem NE (020) gerichteten Materialtransport für die gesamte Abfolge.

1 bis 15 A m^{-1} und die Proben zeigen eine stabile magnetische Remanenz, die auf Anwesenheit nur eines Remanenztyps (Thermoremanente Magnetisierung) hinweist. Die MDF Werte reichen von 30 bis 160 mT. Der Feldvektor hat eine steile Inklination, was mit der Paläofeldrichtung übereinstimmt. Die Einheiten zeigen ausschließlich inverse Polaritäten. Die insgesamt sehr stabilen

natürlichen Remanenzen deuten auf eine Ablagerung der Pyroklastika bei hohen Temperaturen hin.

Dagegen streut die Remanenzrichtung in den Dykes und Sills erheblich und weist Geometrien von steilen bis flachen Orientierungen auf mit starken Variationen in der Deklination. Die Koerzitivität der magnetischen Träger ist signifikant niedriger als in den Pyroklastika mit MDF Werten, die von 8 bis 30 mT in den Dykes und von 15 bis 30 mT in den Sills reichen. Es ist jedoch bemerkenswert, dass abgesehen von einem geringen Anteil einer viskosen Komponente, der Remanenzvektor auch in den Dykes und Sills nur durch die Anwesenheit eines einzigen Remanenztyps charakterisiert ist, wie aus Zijderfeld Projektionen abgeleitet werden kann. Die deutliche Abweichung in den Remanenzrichtungen der in etwa altersgleichen Gangintrusionen von den Pyroklastika bedarf einer weiteren detaillierten Untersuchung.

Literatur

- Martin U & Németh K (2004) Ság-hegy tuff ring. *Geologica Hungarica*. In: *Geologica Hungarica Series geologica Tomus 26*. Geological Institute of Hungary, Budapest, 159–163
- Wijbrans J, Németh K, Martin U & Balogh K (2004) $^{39}\text{Ar}/^{40}\text{Ar}$ geochronology of a Miocene phreatomagmatic volcano field in the western Pannonian Basin. *Earth and Planetary Science Letters* [in press]

Entwicklung einer fluidbeeinflussten Scherzone am Beispiel der Glarner Hauptüberschiebung (Schweiz) Vortrag

Andreas Ebert¹ Marco Herwegh¹
Adrian Pfiffner¹

Lokalisierung unter retrograden Deformationsbedingungen kann häufig in großmaßstäblichen Scherzonen beobachtet werden. Dabei nimmt die Scherzonenbreite kontinuierlich ab. Gleichzeitig passt sich das Gefüge (Korngröße, Kornform, Kornorientierung, Zwillingdichte, kristallographische Orientierung, usw.) den neuen Umgebungsbedingungen (Temperatur, Spannung und Verformungsrate) an. Die Glarner Hauptüberschiebung in den Ostschweizer Alpen ist ein gutes Beispiel, um das Ausmaß und die Entwicklung einer Verformungslokalisierung zu bestimmen. In der Vergangenheit wurde sie detailliert in Hinblick auf ihre Isotopenverteilung und daraus resultierenden Fluidbewegungen und Überprägungen untersucht. Dies erlaubt das Zusammenspiel der Lokalisierung und der Fluidüberprägung zur Zeit der Platznahme der Glarnerdecke zu bestimmen. Im Fall der Glarner Hauptüberschiebung wurde permischer Verrucano über den sedimentären infrahelvetischen Komplex (Flysch und mesozoische Karbonate) geschoben. Dabei entstand zwischen dem Hangenden und Liegenden der bekannte Lochseiten Kalkmylonit. Die alpinen peak-metamorphen Bedingungen lagen im Bereich der Anchizone (230°C) im Norden und der Grünschieferfazies (350°C) im Süden.

Entlang der Überschiebungsbahn wurden im Abstand von wenigen Kilome-

¹ Institut für Geologie, Universität Bern, Schweiz

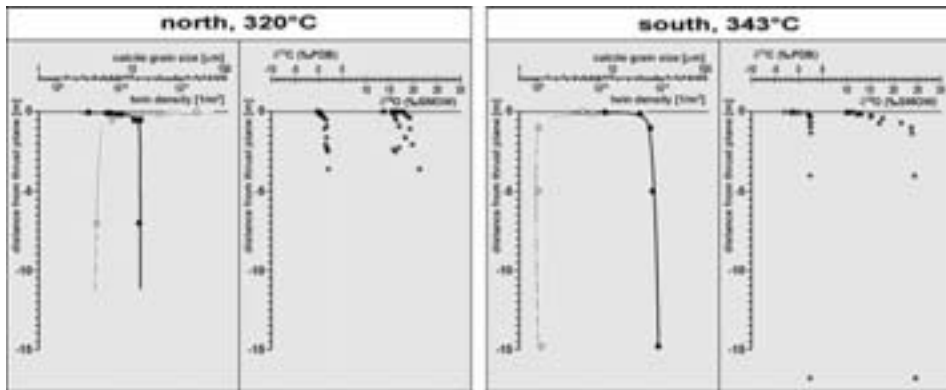


Abbildung 1: Änderung der Korngröße (schwarze Punkte), der Zwillingdichte (weiße Punkte), der Kohlenstoff-Isotope (+) und der Sauerstoff-Isotope (x) in Abhängigkeit der Distanz zur Überschiebungsbahn für ein nördliches und südliches Profil. Beachten Sie die Zunahme der mittleren Korngröße von Nord nach Süd. Isotopendaten von Badertscher (2001).

tern Probenserien vertikal zur Scherbahn genommen. Dabei wurde beginnend am Kontakt zum Verrucano bis zu 20 m tief beprobt, wobei nahe am Kontakt im Dezimeter-Bereich beprobt wurde. Alle Proben zeigen stabilisierte Korngefüge, welche durch ein temperatur- und spannungskontrolliertes Wechselspiel von korngrößenreduzierenden Mechanismen und Kornwachstum charakterisiert sind. Als Konsequenz nimmt die mittlere Korngröße von Nord nach Süd zu, wobei sie aber gleichzeitig senkrecht zur Scherbahn abnimmt (Abb. 1). Die Zwillingdichte verhält sich entgegengesetzt zur Korngröße. Sie nimmt mit abnehmender Distanz zur Überschiebung zu (Abbildung 1). Änderungen der stabilen Isotope in vertikalen Profilen zeigen übereinstimmende Trends (Badertscher, 2001). $\delta^{13}\text{C}$ und $\delta^{18}\text{O}$ -Werte nehmen simultan mit der Korngröße zur Überschiebungsbahn hin ab (Abb. 1). Zusammen mit synkinematischen Adern zeigen diese Isotopenänderungen, dass während

der Deformation Fluide vorhanden gewesen sein müssen und das Gefüge beeinflusst haben.

Diese Änderungen im Mikrogefüge lassen sich nur mit veränderten Deformationsbedingungen während der Überschiebung erklären. Bedingt durch die Exhumation kühlte sich der ganze Deckenstapel ab. Dadurch änderten sich die Temperatur, Spannung und Verformungsrate welche wiederum einen Einfluss auf die Deformationsmechanismen und somit auch auf das Gefüge hatten. Als Konsequenz lokalisierte die Scherzone zunehmend, mit dem Ergebnis, dass die Scherzonenbreite kontinuierlich abnahm. Eine Texturabschwächung zur Überschiebungsbahn hin, wie auch die kleineren Korngrößen deuten auf einen Wechsel von Deformationsprozessen hin. Mit zunehmender Lokalisierung nahm der Anteil an korngrößenkontrollierter Deformation zu, während der Anteil an Dislokationskriechen abnahm. Die erhöhte/leichtere Überprägung der Isotopensignatur zur Scher-

zone hin kann mit folgenden Punkten erklärt werden: (a) dynamische Rekristallisation mit Korngrenzwandern erleichtert den Einbau von fremden Isotopen, (b) lokalisierungsbedingte kleinere Korngrößen vergrößern die Permeabilität und damit den Fluidfluß und (c) höhere finite Verformung in lokalisierten Scherzonenbereichen führt zu einer längeren Equilibrierungszeit zwischen Fluid und Mylonit.

Die allerspätsten Lokalisierungsstrukturen in der Glarner Hauptüberschiebung spiegeln spröde Bedingungen wieder. Diese sind scharfe planare Bänder/Brüche, die alle alten Strukturen durchschlagen und entweder mit Gesteinsmehl oder einer extrem feinkörnigen Matrix gefüllt sind. Desweiteren findet man lokal tektonische Brekzien.

Literatur

Badertscher N (2001) Deformation mechanisms and fluid flow along the Glarus overthrust, eastern Helvetic Alps, Switzerland. PhD Thesis, Université de Neuchâtel, Switzerland, pp 286

Quantification and sensitivity of fault seal parameters demonstrated in an integrated reservoir modelling work flow. A case study on the Njord Field, Halten Terrace, Norway *Vortrag*

Ralf Ehrlich^{1,3} Einar Sverdrup^{1,3}
Vibeke Øye² Jorunn Sjøholm² Kari Smørdal Lien² Roald Færseth²

The primary objective of this paper is to present a fault seal case study from the Njord Field, offshore Norway. The study utilised analogue field studies as well as core descriptions and petrophysical well data in order to evaluate the sealing potential of large to medium scale faults that segment the reservoir. Dynamic data and 4D seismic information was used to calibrate the results

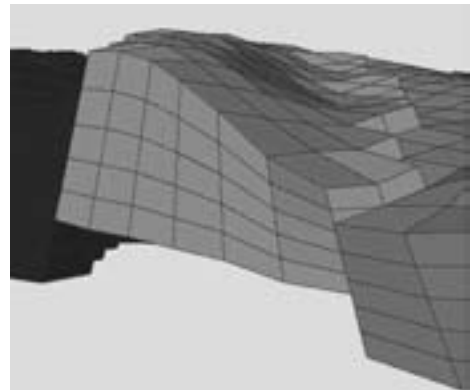


Figure 1: Reservoir simulator grid. Fault zones will be represented as grid cell boundaries with no volume.

through multiple fault seal scenarios.

¹ Roxar AS, PO Box 165 Skøyen, N-0212 Oslo, Norway ² Norsk Hydro ASA, PO Box 7190 Bergen, Norway ³ present address: Ener Petroleum ASA, Lysaker Torg 5, 1325 Lysaker (Oslo), Norway

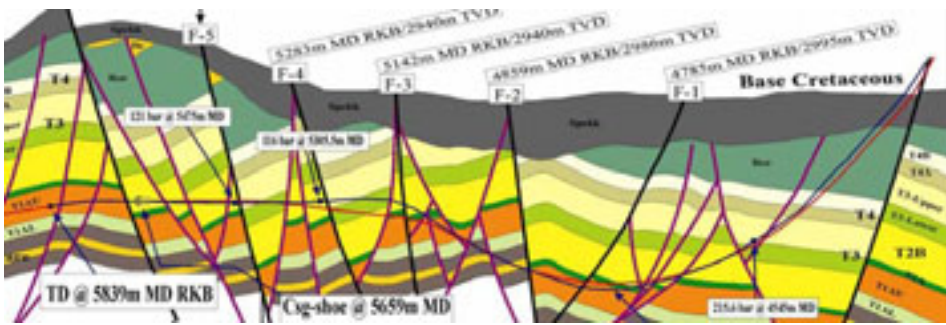


Figure 2: Cross section through a part of the Njord field showing intensive faulting and reservoir segmentation

The study was performed using the FaultSeal module of Irap RMS.

Intensive faulting has in nearly all cases a strong influence on fluid flow in reservoirs. As methods to investigate fault seal have evolved and the tools are becoming integrated in the reservoir modelling work flows, the effect of faults now have an increased influence in numerical models of reservoir communication. Also, several recent articles have increased our understanding of faults and their effect on fluid flow in different types of lithology and reservoirs (e.g. Yielding et al. 1997, Manzcocchi et al. 1999, Sperrevik et al. 2002). In reservoirs where faults form complex fault patterns and comprise effective seals, a good representation of the faults requires the three-dimensional geometry, displacement pattern, fault zone thickness variation and deformation characteristics. In current reservoir simulator grids, such properties must be captured in a regularised coarse grid on the grid cell boundaries (Fig. 1).

The Njord Field is one of the most challenging oil fields offshore Norway, particularly in terms of prediction of structural deformation and flow communication (Dart et al. 2004, Rivenæs et al.

2005). The field is located on the Halten Terrace, ca. 130 km NW of Kristiansund, Norway. The reservoir sequence of the Lower Jurassic Tilje Formation is approximately 120 m thick, and comprises alternating sandstones and shales, which were deposited in a tidal to estuarine paleoenvironment (Dalland et al. 1988). The structural development of the field is defined by several rifting phases throughout the Triassic, Jurassic and Early Cretaceous (Blystad et al. 1995, Ehrlich & Gabrielsen 2003). The field is structurally deformed by a complex pattern of segmented and linked extensional faults, which have led to a high degree of compartmentalization in the reservoir zone (Fig. 2).

Since production start-up in 1997, dynamic well data, 4D seismic surveys, and tracer data have shown that faults have a significant effect on fluid flow and communication patterns within the Njord field. Faults with displacement in excess of 25 meters are commonly regarded as sealing in relation to production timescales (Dart et al. 2004). The sealing mechanism on these faults has been assumed to be caused by shale/clay smearing. Previous unpublished studies have shown that the most



Figure 3: Fault core (ca. 1 m thick) consisting of sand lenses, fault gouge, and smeared coal and shale. The fault throw is approximately 15 m. Locality: Hartley Steps, Northumberland, England

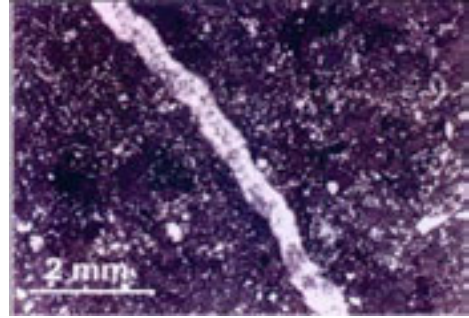


Figure 4: Micro-fault cemented by calcite

important factors in fault seal assessments of the Njord field are the stratigraphy involved in faulting as well as the fault throw. Analogue field studies have therefore focussed on the mechanisms of incorporating incompetent lithology from the host rock into fault zones, and to quantify the sealing capacity of such faults (Fig. 3). Dynamic well data from the Njord field, however, show that the pressure differences across the faults are higher than those predicted from analyses of clay/shale smear. Based on core observations and measurements, it is concluded that cementation processes have been active along the faults and have increased the fault seal capacity for the faults in the Njord Field (Fig. 4). In cases where cementation processes act along faults, fault seal analysis evaluating smear effects only become ambiguous.

This study focussed on integrating the fault seal calculations in a common reservoir modelling workflow in order to quickly investigate the effects of changing fault seal parameters and algorithms with respect to reservoir performance (Figure 5). The fault seal module of

RMS has the ability to create and organize a large number of fault rock property predictions, and to export final results for reservoir simulation. The algorithms include Shale Gouge Ratio (SGR), Shale Smear Factor (SSF), Clay Smear Potential (CSP), and user-defined SGR curves, as well as the published algorithms of Manzocchi et al. (1999) and Sperrevik et al. (2002). The module supports stair-step implementation of faults, and include numerous and advanced cell face visualization that allow answers to be viewed and checked. The results from this study demonstrate the importance of evaluating the deformation mechanisms of fault prior to fault seal analyses, and the effect of a geological fault seal tuning process. The study further shows the value of integrating fault seal as one work task in a reservoir modelling work flow, enabling multiple sensitivity runs and rapid assessment of the fault seal results. The integrated workflow will certainly encourage an even tighter communication between geologists and reservoir engineers.

References

Blystad P, Brekke H, Færseth RB, Larsen BT,

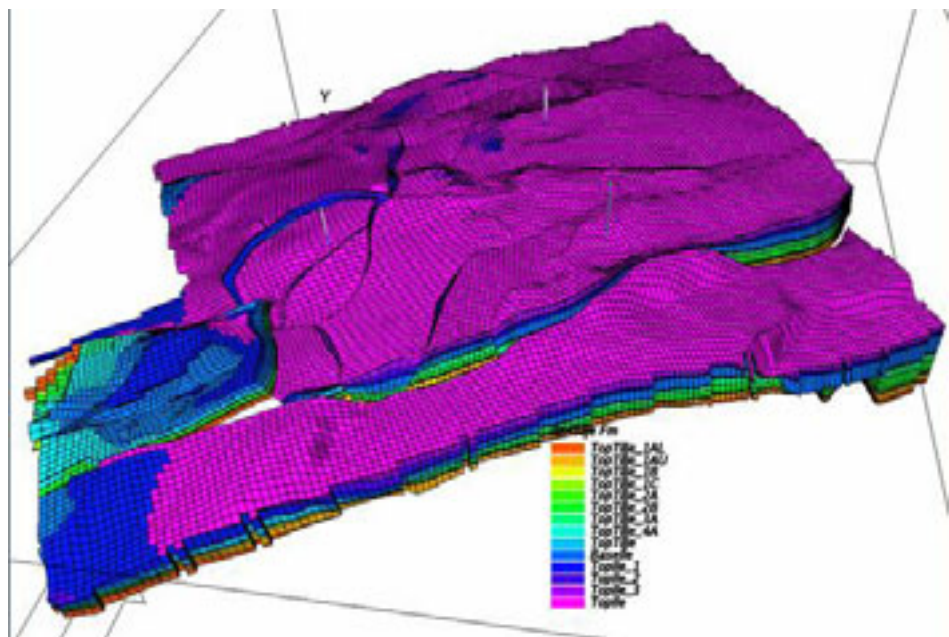


Figure 5: 3D grid of the east flank, Njord Field

- Skogseid J & Tørudbakken B (1995) Structural elements of the Norwegian continental shelf: Part II. The Norwegian Sea Region. Norwegian Petroleum Directorate Bulletin, 8
- Dalland A, Worsley D & Ofstad K (1988) A lithostratigraphic scheme for the Mesozoic and Cenozoic succession offshore mid- and northern Norway. Norwegian Petroleum Directorate Bulletin, 4
- Dart C, Cloke I, Herdlevær Å, Gillard D, Rivenæs JC, Otterlei C, Johnsen E & Ekern A (2004) Use of 3D visualization techniques to unveil complex fault patterns for production planning: Njord field, Halten Terrace, Norway. In: Daviers RJ, Cartwright JA, Stewart SA, Lappin M & Underhill JR (eds.) 2004. 3D Seismic Technology: Application to the Exploration of Sedimentary Basins. Geological Society, London, Memoirs, 29, 249–261
- Ehrlich R & Gabrielsen, RH (2004) The complexity of a ramp-flat-ramp fault and its effect on hanging-wall structuring: an example from the Njord oil field, offshore mid-Norway. *Petroleum Geoscience*, 10, 305–317
- Manzocchi T, Walsh JJ, Nell P & Yielding G (1999) Fault transmissibility multipliers for flow simulation models. *Petroleum Geoscience* 5, 53–63.
- Rivenæs JC, Otterlei C, Zacheriassen E, Dart C & Sjøholm J (2005) A 3D stochastic model integrating depth, fault and property uncertainty for planning robust wells, Njord Field, offshore Norway.
- Sperrevik S, Gillespie PA, Fisher QJ, Halverson T & Knipe RJ (2002) Empirical estimation of fault rock properties. In: Koestler AG & Hunsdale R (eds) *Hydrocarbon Seal Quantification*, NPF Special Publication 11, 109–125 Elsevier, Amsterdam
- Yielding G, Freeman B & Needham T (1997) Quantitative fault seal prediction: AAPG Bulletin, 81, 897–917

Geochemische Klassifikation und Sm-Nd Isotopensystematik proterozoischer Metasedimente des Baltischen Schildes (Västervik Region, SE-Schweden) *Poster*

Mario Fischer¹ Bent T. Hansen¹
Ilka C. Kleinhamns¹

Die Västervik Region liegt an einer Haupt-Terran-Grenze im Baltischen Schild. Im NE schließen sich die Einheiten des Südsvecofennischen Vulkanitgürtels mit Altern $>1,85$ Ga an, im SW folgen die Granitoide des Transskandinavischen Magmatitgürtels (TMZ) mit Altern $<1,85$ Ga. Die Metasedimente der Västervik Formation bilden die stratigraphisch älteste Einheit der Västervik Region. Ihre Stellung in Bezug auf die svecofennischen Metasedimente des Bothnischen Beckens ist noch unklar. Sie können nach ihren mineralogischen Paragenesen in vier Gruppen klassifiziert werden: reine Quarzite, glimmerführende Quarzite, Glimmerquarzite und quarzitisches Gneise. Vermutlich zeitgleich mit der Intrusion der großvolumigen Granitoidmagmen ab 1.85 Ga wurde die Västervik Formation amphibolitfazial überprägt. Dies führte innerhalb der Metasedimente zur Bildung von Cordierit, Sillimanit und Andalusit sowie akzessorischem Granat. Der Beginn der Sedimentation ist begrenzt durch das Vorkommen detritischer Zirkone mit Altern ab 1.87 Ga. Etwa 75% der gemessenen detritische Zirkone zeigt eine Altersgruppierung von 1,8 bis 2,1 Ga, die restlichen 25% zeigen archaische U/Pb-Alter von 2,8 bis

3,0 Ga (Claesson et al. 1993, Sultan et al. 2005).

Die Nd-Isotopensignaturen der Proben zeigen eine sehr homogene Mischung und Schüttung der Sedimente mit subparallelem Verlauf der Nd-Entwicklungslinien und einem sehr engen TDM (Nd) Altersspektrum von 2,2 bis 2,4 Ga. Diese Ergebnisse deuten auf ein konstantes Mischungsverhältnis von proterozoischen und archaischen Anteilen hin. Zusätzlich zeigen die REE-Muster der Proben eine Anreicherung der LREE gegenüber den HREE, so dass Zirkon als kontrollierende Phase für die REE ausgeschlossen werden kann. Damit ist davon auszugehen, dass die Proben nicht nur archaische Zirkone in sich tragen, sondern dass effektiv archaisches Detritusmaterial eingetragen wurde. Weiterhin zeigt die mineralogische Zusammensetzung der Proben keine Korrelation mit den TDM (Nd). Die Modellalter hängen weder mit dem Sortierungs- noch mit dem Reifegrad der Metasedimente zusammen. Dieses deutet wiederum auf ein sehr konstantes Mischungsverhältnis archaischer und proterozoischer Anteile hin.

Der archaische Detritusanteil kann als Tracer benutzt werden, um herauszufinden wo die Liefergebiete der Sedimente liegen. Als mögliche Liefergebiete des archaischen Detritus kommen der Ukrainische Schild (Sarmatia) und die Archaische Domäne im NE-Teil des Baltischen Schildes (Fennoscandia) in Frage. Der Ukrainische Schild kann auf der Grundlage eines geotektonischen Modells der Kollisionszone zwischen Fennoscandia und Sarmatia als Quelle des archaischen Detritus ausgeschlossen werden. Demnach befanden sich zum Zeitpunkt der Ablagerung der Västervik Formation zwei Inselbögen und ein mittel-

¹ Geowissenschaftliches Zentrum der Universität Göttingen, Goldschmidtstr. 3, 37077 Göttingen, Germany

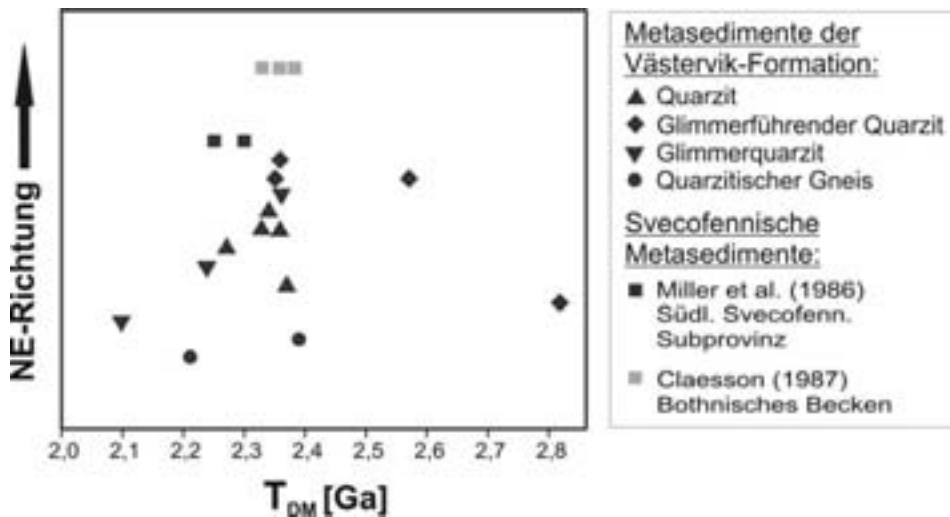


Abbildung 1: Zusammenhang zwischen Modellalter (T_{DM}) und geographischer Position der Metasedimente der Västervik Formation und svecofennischer Metasedimente. Die Auftragung der geographischen Position ist nicht maßstabsgerecht. Mantelmodell (DM) nach Nägler & Kramers (1998).

ozeanischer Rücken zwischen den beiden Kontinenten (Skridlaite et al. 2003). Falls das archaische Sedimentmaterial aus dem NE-Teil des Baltischen Schildes abstammt, sollten sich aufgrund der abnehmenden Distanz zum Liefergebiet in NE-Richtung höhere Modellalter ergeben. In Abbildung 1 sind die Modellalter der Metasedimente der Västervik Formation zusammen mit Modellaltern von Metasedimenten aus dem Bereich der südlichen Svecofennischen Subprovinz (Miller et al. 1986) und des Bothnischen Beckens (Claesson 1987) gegen ihre Position in nordöstlicher Richtung aufgetragen. Den Erwartungen entsprechend liegen die Metasedimente mit den höchsten Modellaltern am weitesten Richtung NE. Die Probe mit dem höchsten Modellalter von 2,8 Ga ist eine Schwermineralseife. Nach den Ergebnissen dieser Arbeit stammt das detritische Material der Västervik Formation sehr wahr-

scheinlich von Liefergebieten aus dem NE-Teil des Baltischen Schildes ab.

Literatur

- Claesson S (1987) Nd Isotope Data on 1,9–1,2 Ga Old Basic Rocks and Metasediments from the Bothnian Basin, Central Sweden. *Precambrian Res.* 35, 115–126
- Claesson S, Huhma H, Kinny PD & Williams IS (1993) Svecofennian detritical zircon ages — implications for the Precambrian evolution of the Baltic Shield. *Precambrian Res.* 64, 109–130
- Miller RG, O’Nions RK, Hamilton PJ & Welin E (1986) Crustal residence ages of clastic sediments, orogeny and continental evolution. *Chem. Geol.* 57, 87–99
- Nägler THF & Kramers JD (1998) Nd isotopic evolution of the upper mantle during the Precambrian: models, data and the uncertainty of both. *Precambrian Res.* 91, 233–252
- Skridlaite G, Willingshofer E & Stephenson R (2003) P-T-t modelling of Proterozoic terranes in Lithuania: geodynamic implications for accretion of southwestern Fennoscandia. *Geol. Fören. Stockholm Förh.* 125, 201–211

Sultan L, Claesson S & Plink-Björklund P (2005) Proterozoic and Archean ages of detrital zircon from the Paleoproterozoic Västervik Basin, SE Sweden: Implications for provenance and timing of deposition. Geol. Fören. Stockholm Förh. 127, 17–24

Deformationsanalyse und mechanische Kopplung eines aktiven fore-arcs in Raum und Zeit, Kamtschatka, Russische Föderation

Poster

Ralf Freitag¹ Fabian Jähne¹
 Christoph Gaedicke² Matthias
 Krbetschek³

Seit dem Mesozoikum wächst die kontinentale Kruste am aktiven Plattenrand von Kamtschatka durch Akkretion allochthoner Terrane. Dieses Wachstum manifestiert sich in der differenziellen Exhumierung und Hebung tektonischer Blöcke innerhalb des Akkretionskeils, parallel zum Kamtschatka-Graben. Die Kinematik der Exhumierung soll mittels strukturgeologischer und neotektonischer Deformationsanalyse erfasst und mit thermochronologischen Untersuchungen an Apatiten bis etwa ins Untere Pliozän quantifiziert werden.

Bedingt durch diese differenzielle Hebung und durch Meeresspiegelschwankungen kommt es zur Ausbildung zahlreicher rezenter mariner und alluvialer Terrassen auf Kamtschatka. Die absolute Altersdatierung dieser Terrassen bietet die Möglichkeit, den relativen vertikalen Versatz und die absoluten He-

bungsbeträge der tektonischen Blöcke bis in rezente Phasen hochauflösend zu dokumentieren.

Ziel des Projektes ist, den Zusammenhang zwischen Unterplattenkonvergenz (Geometrie, Richtung, Geschwindigkeit) und Oberplattendeformation, also die seismische und mechanische Kopplung zwischen Unter- und Oberplatte entlang des Kamtschatka-Grabens zu charakterisieren. Der aktive Plattenrand von Kamtschatka bietet mit seiner global einzigartigen Geometrie und über lange Zeiträume gleich bleibenden (?) Subduktionsparametern eine herausragende Möglichkeit, aus der Oberplattendeformation und der Art des akkretierten Materials auf den Einfluss von Konvergenz und Beschaffenheit (z.B. Alter, Segmentierung, Material, Rauigkeit) der subduzierenden Unterplatte zu schließen.

Am aktiven Plattenrand von Kamtschatka wird die Unterplatte im Bereich des Aleutenbogens segmentiert und unter Kamtschatka subduziert. Die Verformung wird an mehreren dextralen Blattverschiebungen in der Komandorsky Scherzone aufgeteilt (Abb. 1). Die Konvergenzgeschwindigkeit der einzelnen Unterplattensegmente nimmt von 7.9 cm a⁻¹ im Süden (Pazifische Platte PAC) ab auf 0 cm a⁻¹ im Norden (Nordamerikanische Platte NAM). Durch die unterschiedlichen Konvergenzgeschwindigkeiten kommt es zur differenziellen Hebung im fore-arc von Kamtschatka. Störungsbegrenzte tektonische Blöcke werden gehoben und gegeneinander versetzt. Die Exhumierungs- und Hebungs(?) -Raten korrelieren mit der Konvergenzgeschwindigkeit (Abb. 2, 3). Die Hebungsraten der individuellen Oberplattensegmente können durch die Datierung quartärer mariner und allu-

¹ Universität Jena ² Bundesanstalt für Geowissenschaften und Rohstoffe ³ Sächsische Akademie der Wissenschaften

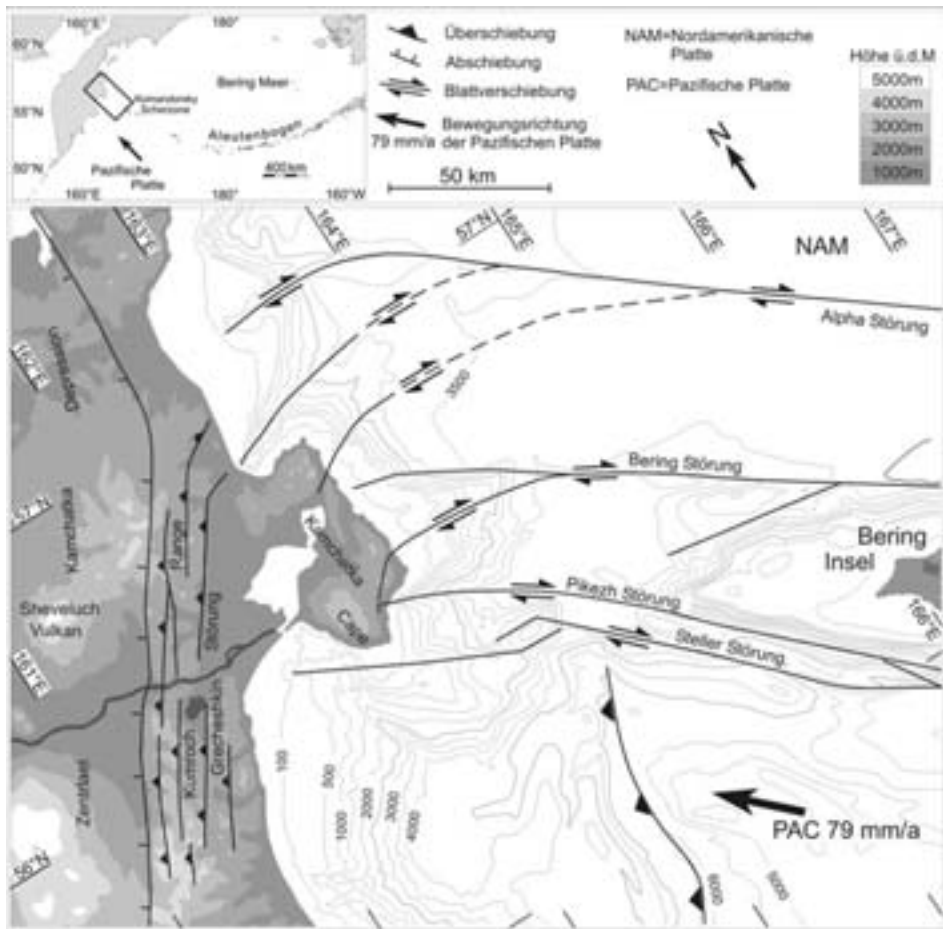


Abbildung 1: Strain partitioning in der Komandorsky-Scherzone. Einige der Blattverschiebungen (z.B. Pikezh-Störung) setzen sich an Land fort und biegen dort um (horse tail structure), erfassen also auch die Oberplatte. Die Konvergenzgeschwindigkeit der Unterplatte nimmt von N nach S hin zu. Die einzelnen Späne zwischen den Störungen konvergieren also mit unterschiedlicher Geschwindigkeit.

vialer Terrassen (Abb. 4) ermittelt und daraus die Verkürzung der Oberplatte rekonstruiert werden.

Das Verhältnis von Konvergenz der Unterplatte zu Oberplattenverkürzung wird als kinematische Kopplung bezeichnet. Der Charakter der kinematischen Kopplung an dem Plattenkontakt zwischen Ober- und Unterplatte hat

einen wesentlichen Einfluss auf die Generierung oft schwerster subduktionsbezogener Erdbeben. Wenn die Plattenkonvergenz gleich dem Versatz auf der Subduktionsüberschiebung ist, ist die kinematische Kopplung minimal und die Oberplatte wird nicht deformiert. Bei sehr starker kinematischer Kopplung ist der Versatz auf der Subdukti-

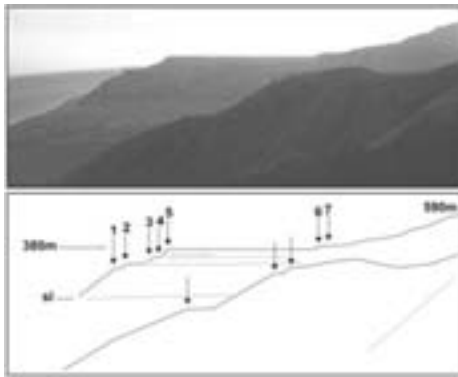


Abbildung 2: Blick nach S über die Pikezh Störung. Mindestens sieben Terrassenstufen bis in 380 m Höhe sind erkennbar.

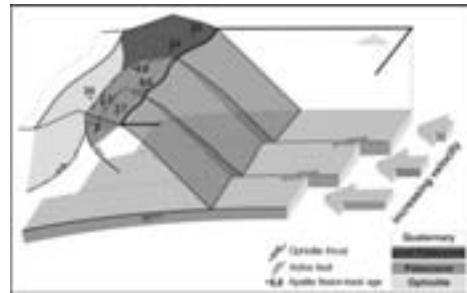


Abbildung 4: Der schematische Schnitt durch Ober- und Unterplatte vor Kamchatka zeigt die Abhängigkeit der Exhumierungs- und Hebungs(?) -Raten im fore-arc von der Konvergenzgeschwindigkeit der einzelnen Unterplattensegmente.

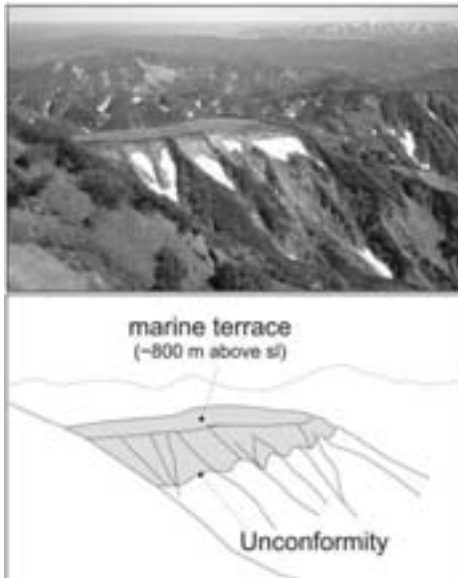


Abbildung 3: Marine Terrasse in etwa 800 m Höhe. Sie sitzt diskordant dem Paläo-Relief auf.

onsüberschiebung gering und der Großteil der Plattenkonvergenz wird durch die Verkürzung der Oberplatte kompensiert. Eine Schlüsselfrage für das Verständnis von Subduktionserdbeben ist,

wie viel Versatz durch langsames, aseismisches ‚Kriechen‘ und wie viel durch plötzliche Erdbeben generiert wird. Die energiereichsten Beben überhaupt sind subduktionsbezogen (z.B. Alaska 1964, M 9.2, Kamtschatka 1952, M 9.0).

Zur Quantifizierung der Oberplatten-deformation hat sich eine Kombination aus strukturgeologischer Kartierung und thermochronologischen Untersuchungen als geeignet erwiesen. Aus Zeit-Temperatur-Pfaden der Gesteine im fore-arc und den Exhumierungsraten störungsbegrenzter, tektonischer Blöcke soll ein kinematisches Modell der Ostküste Kamtschatkas entwickelt werden. Durch die Analyse der Höhenlage und der Expositionsalter (sub-)recenter Terrassenflächen und durch neotektonische Analysen (Fernerkundung, Geländebe-funde) kann das kinematische Modell des auch rezent tektonisch sehr aktiven fore-arcs bis in jüngste Zeit hinein hoch-auflösend validiert werden.

Zur Untersuchung der Abhängigkeit zwischen Konvergenzgeschwindigkeit und Reaktion des fore-arc (Abb. 4) ist Kamtschatka weltweit außerordentlich

gut geeignet, da die Pazifische Platte genau orthogonal zum Plattenrand konvergiert. Dort werden störende Einflüsse wie schiefe Subduktion (Verformungsaufteilung), Subduktion eines aktiven Rückens oder schief konvergierende Transformstörungen vermieden.

Strukturgeologische Analysen des Thingvellir Spaltenschwarms, Südwest Island

Poster

Nadine Friese¹ Michael Krumbholz¹
Steffi Burchardt¹
Agust Gudmundsson¹

Der Holozäne Thingvellir Spaltenschwarm ist Teil des 60 km langen Hengill Vulkansystems, das sich in der Westvulkanischen Zone in Island befindet und ein etwa 9000 Jahre altes basaltisches Lavafeld nördlich des Sees Thingvallavatn durchquert (Abb. 1).

Dieser Spaltenschwarm enthält einige der größten postglazialen Verwerfungen und Brüche, die in der Riftzone Islands anzutreffen sind. Das Zentrum des Hengill Vulkansystems bildet der 0.8 Ma alte gleichnamige Vulkan. Der Gipfel des Vulkans ist durchzogen von NE-SW streichenden Abschiebungen, von denen einige bis zum See Thingvallavatn verfolgt werden können. Der Thingvellir Spaltenschwarm wird von nahezu vertikalen Zugbrüchen und geöffneten Abschiebungen dominiert (Abb. 2).

Diese Strukturen sind en-échelon und

¹ Abteilung Strukturgeologie und Geodynamik, Geowissenschaftliches Zentrum Göttingen, Goldschmidtstraße 3, 37077 Göttingen



Abbildung 1: (a) Schematische geologische Karte Islands (nach Gudmundsson, 2006). Rahmen markiert den in (b) markierten Teilausschnitt. NVZ: Nordvulkanische Zone; EVZ: Ostvulkanische Zone; WVZ: Westvulkanische Zone; SISZ: Südisländische Seismische Zone. (b) Vereinfachte geologische Übersichtskarte des Thingvellir Grabens in Südwest Island (nach Gudmundsson, 1987)

subparallel zueinander angeordnet und streichen im Mittel N29°E. Die Längen der Brüche variieren zwischen 360 m und 7700 m; die Sprunghöhen reichen von 0.5 m bis zu 40 m. Entlang der westlichen Grabenverwerfung, Almannagja, wurde eine maximale Öffnung des Bruchs von 68 m gemessen.

Während tektonischer Studien im Pleistozänen Hengill Gebiet an einem etwa 7 km langen E-W streichenden Profils wurden mehr als 60 Störungen, davon



Abbildung 2: Mit Grundwasser gefüllte, an der Oberfläche vertikale Störung. Die Öffnungsweite beträgt etwa 10 m. Blickrichtung nach NNE



Abbildung 3: NE–SW streichende Abschiebungen im Hengill Gebiet. Blickrichtung E, Kraftwerk Nesjavellir in der Bildmitte

35 große Abschiebungen gemessen. Die Abschiebungen in diesem Gebiet streichen NE–SW und sind an der Oberfläche subvertikal (Abb. 3). Die maximale Sprunghöhe beträgt 160 m, gemessen an einer Abschiebung, die den nordwestlichen Hang des Hengill Vulkans durchschneidet. Mehr als 85% aller gemessenen Abschiebungen zeigen Versatzbeträge kleiner als 25 m. Die Abschiebungen mit den größten Beträgen treten im und nahe dem westlichen Teil des Hengill Systems auf. So kann zum Saemundsson (1967) zum Beispiel eine Sprunghöhe von mehr als 240 m entlang einer Abschiebung südwestlich des Sees Thingvallavatn ermitteln, und schätzte für einige Verwerfungen im Nordwesten des Sees, im Gebiet Botnssalur, Beträge von über 400 m. Messungen anhand von Luftbildern (mit Hilfe eines Stereomikrometers) bestätigten diese Geländedaten. An der Abschiebung Jorukleif, im Südwesten des Untersuchungsgebietes, wurden Sprunghöhen von 210 m gemessen. Es kann eine direkte Korrelation zwischen dem Alter der Gesteine und den Verwerfungsbeträgen festgestellt werden. So liegt die Abschiebung

Jorukleif in dem Gebiet, wo einige der ältesten Gesteine des Hengill Gebietes anzutreffen sind.

Ein 30 km langes Profil, welches einen Schnitt von 3 Ma alten Pliozänen Gesteinen am Fjord Hvalfjörður bis hin zu den Holozänen Lavafeldern des Thingvellir Spaltenschwarms repräsentiert, wurde von Forslund & Gudmundsson (1991) systematisch aufgenommen. Danach durchziehen 156 Abschiebungen mit einem durchschnittlichen Streichen von N37°E das Gebiet. Die durchschnittliche Sprunghöhe beträgt 10 m; die maximal gemessene Sprunghöhe beträgt 150 m. Der Einfallswinkel der Quartären Störungen beträgt im Mittel 75°. Sie sind somit steiler als diejenigen, die in den Tertiären Gebieten angetroffen werden können, welche einen durchschnittlichen Einfallswinkel von 69° aufzeigen.

Diese struktureologischen Daten implizieren, dass das Spannungsfeld, welches die Holozäne Entwicklung des Thingvellir Fissure Swarm maßgeblich beeinflusste, mindestens seit den letzten 3 Ma gleich bleibend war.

Das dominierende NE Streichen aller Strukturen im Extensionsgebiet Islands ergibt eine Ausrichtung der maximalen Zugrichtung von 110–130°. Dieser Trend geht in etwa konform mit dem derzeitigen geodätischen Vektor.

Literatur

- Forslund T, Gudmundsson A (1991) Crustal spreading due to dikes and faults in southwest Iceland. *J. Struct. Geol.* 13: 443–457
- Saemundsson, K (1967) Vulkanismus und Tektonik des Hengill Gebietes in Südwest Island. *Acta Naturalia Islandica Vol II*, pp 105

Evolution of the Tamtsag Basin / NE-Mongolia — part I: basin fill *Poster*

Peter Geerds¹ Marc Vogler¹ Buyan Davaa¹ Andreas Henk¹

Introduction

The Tamtsag Basin in NE Mongolia is part of a widespread basin system which formed during Late Jurassic and Cretaceous times (Graham et al. 2001, Qing-Ren et al. 2003). It is filled with continental sediments and volcanics which can reach up to 4 km in thickness. Rifting and subsequent basin inversion led to a complex basin geometry characterized by several horst and graben structures. The geodynamic causes for regional basin formation are discussed controversially and several hypothesis ranging from orogenic collaps via subduction rollback to collision-induced rifting have been

¹ Geologisches Institut, Universität Freiburg Albertstrasse 23b, D-79104 Freiburg, Germany

put forward. Scientific research on the Mesozoic basins in Mongolia has so far concentrated on the East Gobi Basin to the south (Graham et al 2001, Prost 2004, Johnson 2004) and some work has also been published on the Hailar Basin (Qing-Ren et al. 2003), the northeastward continuation of the Tamtsag Basin into China. Fundamental data on the fill and tectonics of the Tamtsag Basin in between is still missing. This is partly due to poor exposure as most of the basin fill is covered by Cenozoic sediments and only locally, near the bordering faults, rocks are accessible for surface investigations. However, recent discoveries of oil in the Tamtsag and Hailar Basins have resulted in intense exploration activity and a strong interest in the area. This contribution describes the results of a field campaign in fall 2005 focusing on the basin fill while a companion paper (Davaa et al. this volume) deals with the basin structure and hydrocarbon potential of the Tamtsag Basin.

Basin fill

So far little has been published on the stratigraphy of the Tamtsag Basin. A comparative synopsis of the Mesozoic stratigraphy in the adjacent basins is given by Qing-Reng et al. (2003).

Basement rocks consist of metamorphics and intrusives of Permian to Devonian age. Triassic strata is missing. Basin subsidence commenced in the Lower-Middle Jurassic with sedimentation of alluvial/fluvial conglomerates, sandstones and intercalating coalbeds. Voluminous Upper Jurassic volcanics with sedimentary interbeds are known from the Tamtsag Basin and also found in the Hailar and Erlian Basins. Using mainly borehole data,

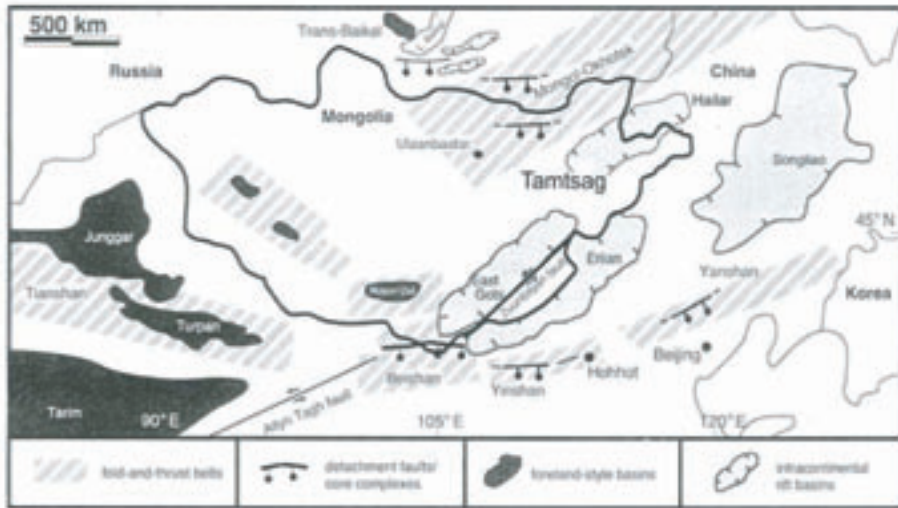


Figure 1: Location of the Tamtsag Basin and adjacent Mesozoic basins (Graham et al. 2001)

Neves (2000) identified a Lower Cretaceous, clastic, continental rift-fill with fluvio-deltaic conglomerates and sandstones. Volcanics occur. A general fining upward-trend leads into deep water, lacustrine mudstones and shales overlain by Upper Cretaceous fluvial-lacustrine mudstone-sandstone facies. Clastic Cenozoic deposits of conglomerates, sandstones, and mudstones cover most parts of the basin, concealing the Mesozoic units.

At the western margin the filling of the Tamtsag Basin is accessible at surface and two areas have been mapped in detail to get an insight view of the lithologies and depositional environments of the basin fill.

In one of the areas mapped the pre-rift basement rocks of the Tamtsag Basin are exposed. They consist of low- to high-grade contact-metamorphic schists and turbidites with basaltic interlayers of presumably Devonian to Permian

age. Contact metamorphism was caused by voluminous granitic intrusions. The syn-rift sequence in the area can be divided into a volcano-sedimentary and an effusive volcanic unit. The former consists of large scale, proximal ignimbrite deposits which are overlain by terrestrial, fluvial and lacustrine sediments (conglomerates, breccias, sand- / silt- / mudstones), frequently interfingering with volcanic rocks (tuffs, ignimbrites). There is a strong lateral lithologic change in this unit across the mapping area. It is conformably overlain by lavas of basaltic-basaltic to andesitic composition, presumably indicating a time of enhanced basin extension. K/Ar-dating of this unit is in preparation to provide a radiometric age and exact stratigraphic position, respectively. The effusive volcanics are concordantly followed by units of terrestrial-sedimentary origin, with conglomerates, sand-, silt-, and mudstones



Figure 2: Preliminary stratigraphic column of mapping area 1.

rich in plant fossils and containing a unit of black shale that could serve as a potential source rock. Furthermore, volcanics (rhyolite, tuffites) are found in this unit.

The second mapping area covers more than 70 square kilometers and is located southeast of the one described above, closer to one of the main basin-bounding faults. Most of the area is covered by Cenozoic sediments. The central part is an uplifted structure providing good outcrops. It comprises no basement rocks, but a thick volcanic sequence of rhyolite, andesite and two basalt generations, possibly of Late Jurassic to Early Cretaceous age. Field observations show that the rhyolitic volcanics are overlain by andesite. Basalts cross-cut the rhyolite and andesite and, hence,

are of younger age. The center of the ridge is formed by a dome-like structure of rhyolitic composition. The magmatic units are overlain by a well rounded, possibly basal conglomerate. The second, younger basalt overlies the conglomerate. This indicates two separate stages of volcanic activity. A lens of marine carbonate sediment with crinoidal fossils was found intercalating with the basalt. The stratigraphic position of this unit remains unclear and requires further investigations as so far no marine sediments have been described from the Tamtsag Basin.

Acknowledgements Financial support by the Deutsche Forschungsgemeinschaft is gratefully acknowledged. ‘Mineral and Petroleum Authorities of Mongolia’ kindly supported our work in the Tamtsag Basin.

References

- Qing-Ren M et al. (2003) Tectonics of the late Mesozoic wide extensional basin system in the China–Mongolia border region. In: Basin Research 15, 397–415
- Graham SA et al. (2001) Sedimentary record and tectonic implications of mesozoic rifting in southeast Mongolia. In: Geological Society of America Bulletin, 113/12, 1560–1579
- Prost GL (2004) Tectonics and hydrocarbon systems of the East Gobi basin, Mongolia. In: The American Association of Petroleum Geologists Bulletin 88(4) 483–513
- Johnson CL (2004) Polyphase evolution of the East Gobi basin: Sedimentary and structural records of Mesozoic-Cenozoic intraplate deformation in Mongolia. In: Basin Research 16, 79–99
- Neves R et al. (2000) Mongolia, Tamtsag Basin, evidence for widespread, high quality, mature Lower Cretaceous Source Rock. Abstract, AAPG International Conference & Exhibition.

Strain Localisation, Fracturing and Hydrothermal Mineralisation: Numerical Models of the Mount Isa Copper Deposit, Australia *Vortrag*

Klaus Gessner^{1,2} P.A. Jones³
A.S. Wilde⁴

There is substantial need in mineral exploration to understand the structural controls on ore deposition for these types of deposits in order to predict the localities of new ones. Application of basic principles of rock mechanics, and numerical simulations of deformation and fluid flow processes provide fundamental insights to Proterozoic hydrothermal mineralization at Mount Isa, Australia. The rheology of layered meta-sedimentary rocks, and the orientation and position of these layered rocks relative to major fault systems were the key controls on ore deposition. Rock deformation is a crucial requirement for creating fluid pathways and depositional sites in post-metamorphic hydrothermal ore systems, since metamorphism creates a largely impermeable wall rock. Compositional layering in the host rock partitioned mechanical behaviour and strain, leading to selective permeability generation and focussing of fluid flow during separate hydrothermal events. Differences in physical property values between shale and siltstone lead to a significant variation in

deformation behaviour and changes in deformation related permeability. From field and mine observations it is reasonable to assume that the shale layers had less cohesion and a lower friction angle, but higher tensile strength than the siltstone layers. A layering of these rock types is thus likely to lead to a partitioning effect known as shear-lag, which occurs when ongoing stretching in the weak phase of a two-layer composite reduces s_3 , resulting in a preferential partitioning of tensile stresses into the strong phase. This rheological contrast may be the reason why a number of large copper and lead-zinc-silver deposits in the Mount Isa area are hosted by a single rock unit, the Urquhart shale. According to our model fine-grained carbonaceous shale layers preferentially failed by plastic shearing, whereas meta-siltstones remained elastic or failed in tension, depending on the magnitude of deformation and the pore fluid pressure. If lead-zinc silver mineralization is assumed to have occurred early orogenic or late syngenetic in consolidated and lithified sedimentary rocks, the pelitic layers of the Urquhart shale would have deformed plastically, becoming more permeable than elastically deforming siltstones. A second hydrothermal event occurred after the metamorphic peak of the (ca. 1590–1550 Ma) Isan orogeny. Numerical simulations suggest that during this late orogenic event the orientation of layering and the proximity to major fault systems controlled fracturing and permeability increase in the Urquhart shale. Deformation patterns similar to the observed extent of dilation and brecciation occur in the case of E–W shortening and top-to-E simple shearing. These geometries correspond to the second and third

¹ Computational Geoscience, CSIRO Exploration and Mining, PO Box 1120, Bentley WA 6102, Australia ² Earth Systems Modelling, School of Earth and Geographical Sciences, The University of Western Australia, Crawley WA 6009, Australia ³ School of Earth Sciences, James Cook University Townsville QLD 4811, Australia ⁴ School of Earth Sciences, Monash University Clayton, VIC 3400, Australia

deformation events recognized at Mount Isa, during which meta-siltstone layers in the Urquhart shale failed in tension and massive silicification occurred. The fractured siltstones provided pathways for an upward flowing, over-pressured basement fluid, from which quartz was deposited during cooling. An oblique strike-slip strain geometry corresponding to the fourth major deformation event, localized strain in steeply-dipping pre-existing fault zones, and again, in the mechanically anisotropic Urquhart shale. The reactivation of steep structures provided access to surface derived fluids during a third hydrothermal event, causing the precipitation of dolomite followed by chalcopyrite ore. The change from regional contraction and simple-shear to strike-slip changed the hydraulic architecture significantly, favouring upward flow, lithostatic fluid pressures and hydro-fracturing in the former case, and access to surface-derived fluids in the latter. These findings support a sequential model for copper mineralization at Mount Isa, where alteration from a reduced basement fluid preceded introduction of a surface-derived oxidized metal-bearing brine.

Perturbation of isotherms below topography: constraints from tunnel transects through the Alps, Gotthard road tunnel *Poster*

Christoph Glotzbach¹ Cornelia Spiegel¹ Meinert Rahn² John Reinecker¹

Introduction

For many years it has been known that near surface isotherms are influenced by the topography (Lees 1910). Recently, a number of studies were pursued to quantify the effect of topography on low temperature isotherms (e.g. Stüwe et al. 1994, Mancktelow & Grasemann 1997). The magnitude of perturbation depends on several parameters: exhumation rate, geothermal gradient, wavelength and amplitude of topography, and finally by the age of surface relief change (Braun 2002).

Modelled perturbation

To obtain a rough impression of perturbation of near surface isotherms, a 2-D modelling approach following Stüwe & Hintermüller (2000) was applied to a profile intersecting the Aar and Gotthard massifs along the Gotthard road tunnel. Assuming steady state topography, wavelength of 20 km, a temporally and spatially constant exhumation rate of 1 mm y^{-1} , a geothermal gradient of 20°C km^{-1} , and height, slope and aspect dependent ground surface temperatures, the modelling results reveals significant perturbation of the near-surface isotherms (Fig. 1).

¹ Institut für Geowissenschaften, Eberhard-Karls-Universität Tübingen ² Hauptabteilung für die Sicherheit der Kernanlagen, Villigen-HSK, CH

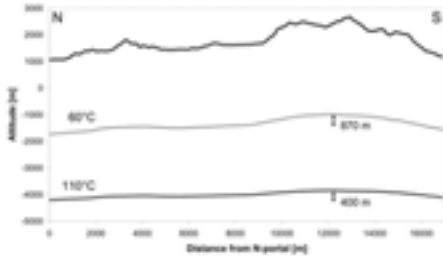


Figure 1: Results of 2-D modelling along the Gotthard road tunnel, showing the topography of the tunnel-transect, and the modelled 60°C and 110°C isotherms.

The modelled 60°C and 110°C isotherms are perturbed by 870 and 400 m respectively, suggesting that the isotherm-perturbation effect significantly influences the apatite fission track (AFT), and particularly the (U-Th)/He-system. To verify these modelled prediction, our study aims to directly measure perturbation of isotherms below topography by applying low-temperature thermochronology (zircon fission track, AFT and (U-Th)/He analysis). We therefore sampled three tunnel transects through the Alps (Gotthard and Mont Blanc road tunnels and Lötschberg railway tunnel), as well as their corresponding surface lines. The investigated regions are characterised by pronounced topography and rapid present-day surface uplift rates in the range of 1 mm y^{-1} (Kahle et al. 1997).

Measure perturbation

AFT data from the literature (Schaer et al. 1975; Wagner et al. 1977) and own data were projected from within a corridor of 1 km along the tunnel-axis (Fig. 2). By linear interpolation of the AFT-ages, isochrones (here the 9, 8, 7 and 6.5 My isochrones) can be esti-

mated. The modelled isotherms (Fig. 1) and estimated isochrones (Fig. 2) show comparable perturbations correlating with topography. For palaeotopographic investigations the sample density has been increased along the tunnel transect. Currently, the AFT-age density is too low for palaeotopographic interpretations.

Implications for age-elevation relationships (AER)

Exhumation rates are routinely deduced from age-elevation relationships (i.e. from AFT-ages plotted *vs.* sample elevation). This approach, however, is based on the assumption of flat-lying isotherms. For perturbed isotherms, exhumation rates deviated from AERs are overestimated (Stüwe et al. 1994). Fig. 3a shows conventional AERs from the Gotthard and Aar massifs, yielding exhumation rates of 0.45 mm y^{-1} and 0.54 mm y^{-1} , respectively. Simplified 3-D modelling of the 110°C-isotherm, based on equations and input parameters mentioned above, yields modified AERs, plotted against the distance from present elevation to the modelled 110°C-isotherm (Fig. 3b).

In contrast to other correction approaches (e.g. Reiners et al. 2003), this procedure allows to correct every AFT-sample separately, accounting for their specific spatial topographic location. The resulting ‘real’ exhumation rates are about 10% lower than the apparent exhumation rates revealed from conventional AER, yielding 0.42 mm y^{-1} for the Gotthard massif and 0.46 mm y^{-1} for the Aar massif.

Future investigations

Samples collected from three tunnel systems and their corresponding surface traces will be analysed by AFT, zircon fission track, and apatite (U-Th)/He thermochronology. This will allow to estimate the effect of isotherm-perturbation on these thermochronologic systems. The existing thermochronologic model will be refined, and different kind of models shall be tested for their consistency with the growing amount of low thermochronological data.

References

Braun J (2002) Quantifying the effect of recent relief changes on age-elevation relationships. *Earth Planet Sci Lett* 200:331–343

Kahle H-G, Geiger A, Bürki B, Gubler E, Marti U, Wirth B, Rothacher M, Gurtner W, Beutler G, Bauersima I & Pfiffner OA (1997) Recent crustal movements, geoid and density distribution: Contribution from integrated

satellite and terrestrial measurements. In: Pfiffner et al (eds) *Results of NRP 20; deep structure of the Swiss Alps*. Birkhäuser Verlag, Basel, 251–259

Lees CH (1910) On the shape of the isotherms under mountain ranges in radioactive districts. *Proc R Soc London A* 83, 295–317

Mancktelow NS & Grasemann B (1997) Time-dependent effects of heat advection and topography on cooling histories during erosion. *Tectonophysics* 270, 167–195

Reiners PW, Zhou Z, Ehlers TA, Xu C, Brandon MT, Donelick RA & Nicolescu S (2003) Post-orogenic evolution of the Dabie Shan, eastern China, from (U-Th)/He and Fission-Track Thermochronology. *American Journal of Science* 303, 489–518

Schaer JP, Reimer GM & Wagner GA (1975) Actual and ancient uplift rate in the Gotthard region, Swiss Alps: A comparison between precise levelling and Fission-Track Apatite age. *Tectonophysics* 29, 293–300

Stüwe K, White L& Brown R (1994) The influence of eroding topography on steady-state isotherms. Application to fission track analysis. *Earth Planet Sci Lett* 124, 63–74

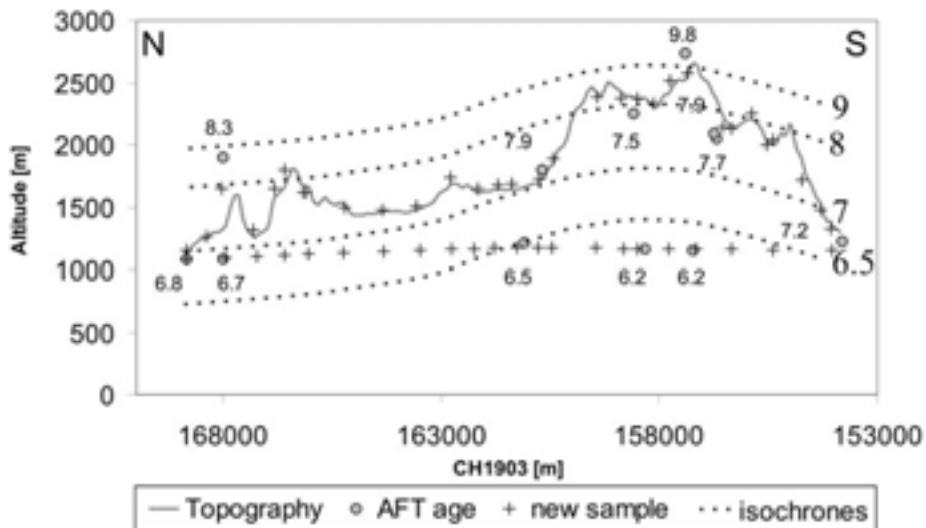


Figure 2: Sample pattern, available AFT-ages and interpolated isochrones along the Gotthard road tunnel transect.

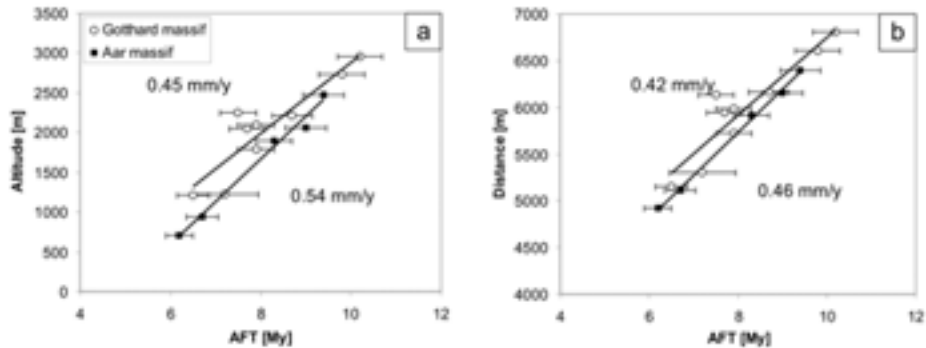


Figure 3: AFT-ages for the Gotthard and Aar massifs, plotted against their sampling altitude, yielding a clear age elevation relationship (a) and the same AFT-ages plotted against the distance from present elevation to the modelled 110°C-isotherm (b).

Stüwe K & Hintermüller M (2000) Topography and isotherms revisited: the influence of laterally migrating drainage divides. *Earth Planet Sci Lett* 184:287-303.

Wagner GA, Reimer GM & Jäger E (1977) Cooling ages derived by apatite fission track, mica Rb-Sr and K-Ar dating: the uplift and cooling history of the Central Alps. *Mem Ist Geol Mineral Univ Padova* 30, 1–27

Electromagnetic radiation (EMR) and its interpretation in terms of stresses in the lithosphere *Vortrag*

Reinhard O. Greiling¹ Marco Lichtenberger¹ Hennes Obermeyer²

Electromagnetic radiation (EMR) as measured at the surface of the lithosphere or underground shows preferred

¹ Geologisch-Paläologisches Institut, Heidelberg University, Im Neuenheimer Feld 234, 69120 Heidelberg, FR Germany

² Gesellschaft für Erkundung und Ortung, Yorckstraße 36, 76185 Karlsruhe, FR Germany

orientations, which can be related to microcracks and other brittle structures at micro and nano scales (see Bahat et al. 2005 and references therein). During the last years, numerous studies showed the applicability of EMR measurements for the determination of active fractures and stress orientations. EMR is determined with a ‘Cerescope’, which picks up EMR signals at frequencies from 5–50 kHz (Obermeyer, 2005) with a ferrite aerial and processes them electronically so that the results can be displayed on a screen or copied to a computer.

With the help of oriented EMR measurements, intensity variations are determined, which can be related to preferred crack fracture orientations. From this information, orientations of the principal stresses can be calculated. In addition, the intensity of the EMR is related to stress magnitudes. Several EMR measuring methods with the Cerescope can be applied to study regional and local stress fields. For horizontal measurements the aerial is moved in a horizontal circle. Every 5 degrees a measurement is taken. The entire hori-

zontal measurement consists of 72 readings, which are illustrated in a polar diagram. Calculating the directions of the cracks from EMR intensities, the principal directions of the horizontal principal stresses can be determined. For Linear measurements the aerial is moved along a straight or curved line in this method. Every metre (can also be any other distance) a measurement is taken. Using this method it is possible to find loci of high stresses, such as active faults, where stress accumulates. It is also appropriate to find loci of possible rock burst in underground facilities. If several linear measurements are arranged in grids it is possible to map the orientation of structures such as faults, where stress is accumulated. Cross section measurements can only be applied in long underground excavations such as tunnels. The measurements are undertaken along the cross section of the tunnel and are oriented normal to the tunnel's long axis. Beginning with a vertical orientation of the aerial every 5 degrees a measurement is taken until a full circle of 360 degrees consisting of 72 measurements is completed. Fractures around tunnels originate from a secondary stress field which is induced by the regional stress field and the empty space of the tunnel. This secondary stress field is described by radial, tangential and shear stresses. Shear stresses are most likely produce fractures, since shear strength is much smaller than compressive strength. Therefore, the EMR measured in cross section measurements is proportional to shear stress of the secondary stress field. By determining the shear stress distribution along the long axis of the tunnel it is possible to calculate directions and magnitudes

of the regional stresses, which induce the secondary stress field. The tunnels in which this technique can be applied have to be curved and need to have a maximum overburden of at least 75 m and a minimum overburden of less than 20 m. These parameters are necessary to produce shear stress distribution along the tunnels' long axis from which regional stresses can be determined reliably and with small standard deviations.

In order to build up experience and a comprehensive database, EMR is determined in different regions and different tectonic environments. Two examples will be presented, one from the shoulder of the Upper Rhine rift (Odenwald) and one from northern Sweden and adjacent Norway.

In the example from the Odenwald (tunnel at Wald-Michelbach), EMR results are generally compatible with published data on the regional stress field (azimuth of major horizontal principal stress 103°). In addition, a minor N-S tensional component and the influence of local faults can be discerned.

In the investigated area of Scandinavia the regional stress field as determined from EMR is uniform, the major horizontal principal stress has a ENE–WSW orientation. Published results from different stress determination methods applied on the eastern coast of Sweden show a major horizontal principal stress with NE–SW orientation.

At the Steinfjellet road tunnel residual stresses with a maximum of 3 times the regional stress magnitude are found at a thrust contact, which represents the Caledonian suture between Baltica and Laurentia. There, the major horizontal principal stress has a NW–SE orientation.

References

- Bahat D, Rabinovitch A & Frid V (2005) Tensile Fracturing in Rocks — Tectonofractographic and Electromagnetic Radiation Methods. Springer Verlag, Berlin Heidelberg, pp 569
- Obermeyer H (2005) Measurement of Natural Pulsed Electromagnetic Radiation (EMR) with the Cerescope, Ceres GmbH, Staffort, pp 8

Very high anisotropies of the magnetic susceptibility in ductile shear zones: first quantitative results from a metamorphic nappe in the Central Scandinavian Caledonides, Sweden *Poster*

J.C. Grimmer¹

Shear zones in the Seve crystalline basement nappes of the central Scandinavian Caledonides contributed to exhumation and translation of these high-grade metamorphic rocks. The Seve unit is considered to represent the former distal passive margin of the continent Baltica, which was subducted beneath an island arc during Ordovician times and subsequently collided with the continent Laurentia during Silurian and early Devonian times. Strongly textured mylonitic garnet mica schists with well developed mica fish and S–C-fabrics from a shear zone within the Seve unit show unusual high anisotropies of the magnetic susceptibility (AMS). The corrected degrees of anisotropy of the magnetic susceptibility (P') range from 1.78

to 4.24. Bulk susceptibilities range from 2.8×10^{-3} to 96.9×10^{-3} . The shape factors range from 0.32 to 0.62, documenting an oblate shape. Magnetic foliation is subparallel with metamorphic foliation. Magnetic lineation scatters due to permutations of the maximum and intermediate principal susceptibility axes. Temperature-dependent susceptibility measurements identify magnetite as the carrier of the bulk susceptibility. The temperature dependent susceptibility curves indicate a minor contribution of iron carbonates. Such high anisotropies from natural samples have not yet been documented elsewhere. These high anisotropies result from apparently flattened magnetite. The relatively incompetent mylonite is 'sandwiched' between competent mafic-ultramafic rocks and localizes deformation. A multidisciplinary quantitative approach involving rock magnetic studies, geochemical data, digital image analysis, and X-ray texture goniometry (XTG) is carried out.

A section across this ductile shear zone was sampled systematically from top to bottom over a vertical distance of ca. 0.8 m (six samples). The bulk susceptibility and the degree of AMS increase from top to bottom. With the exception of one sample this coincides with increasing total Fe-content. Other samples from exposures of similar lithologies also exhibited high anisotropies ($2.59 < P' > 4.15$). Magnetite grains occur as inclusions in mica and garnet as well as in the fine-grained quartz-mica matrix. Grain sizes range from a few μm to ca. 0.5 mm. First digital image analysis of SEM-pictures (x–z-sections) of a high-AMS sample shows ca. 2% modal magnetite with a mean ellipticity of 3.3 and with ellipticities of up to 16.7. Statis-

¹ Geologisch-Paläontologisches Institut, Ruprecht-Karls Universität Heidelberg, Im Neuenheimer Feld 234, 69120 Heidelberg



Figure 1: Tectonic map of the study area.

tically, the long axis of the magnetite grains is oriented subparallel with the S-planes. The magnetite grains can be thus used as kinematic indicators. The bulk susceptibility k and the anisotropy P' show a clear positive log-rhythmic correlation. The log-rhythmic relationship can be expressed by the general equation $P' = a \cdot \log k + b$. The geological meaning of the parameters a and b is not yet clear. These parameters could be a quantitative expression for: 1) the modal magnetite content, 2) the distribution density of magnetite, and 3) the degree of deformation of magnetite grains and the associated shape.

The timing of polyphase Miocene tectonics in Northern Romania Vortrag

Heike R. Gröger¹ Matthias Tischler¹
 Bernhard Fügenschuh² Stefan M. Schmid¹

This study addresses the polyphase Miocene tectonic evolution in the Maramures area (northern Romania, Fig. 1) by combining field observations, stratigraphic arguments and fission-track analysis (Tischler et al. in press). Fission-track analysis has been carried out on basement sam-

¹ Geologisch Paläontologisches Institut, Universität Basel, Bernoullistrasse 32, 4056 Basel, Switzerland ² Institut für Geologie und Paläontologie, Universität Innsbruck, Innrain 52, Bruno Sander Haus, 6020 Innsbruck, Austria

ples from the Rodna horst, situated in the East Carpathians (Bucovinian nappes). This area was affected by Cretaceous medium- to low-grade metamorphism, followed by post-collisional exhumation and renewed moderate thermal overprint due to the deposition of Eocene to Early Miocene sediments.

Based on paleostress analyses of meso-scale structures, three main tectonic phases can be distinguished in the study area, all of which are post-date the earliest Miocene (Aquitanian, 20.5 Ma, Fig. 2). In late Early Miocene (Burdigalian) the Pienide nappes, non-metamorphic flysch series, were emplaced onto the Paleogene to Early Miocene sedimentary cover of the Bucovinian nappes. Emplacement of the Pienides is consistently SE-directed and dominated by brittle thrusting while folding is of subordinate importance only. The curved map appearance of the thrust contact is due to lateral ramps and tear-off faults, accentuated by later folding. This early Miocene thrust contact was sinistrally offset later on along the Bogdan-Voda fault (Fig. 1).

Activity along the Bogdan-Voda fault started in Middle Miocene times as a sinistral transpressive fault related to the formation of open NW-SE trending folds in the sedimentary units. In a next stage (late Middle Miocene to Late Miocene) kinematics along the coevally active Bogdan-Voda fault and its eastern prolongation, the Dragos-Voda fault, formed one through going fault, characterised by sinistral transtension. Towards the east the left lateral offset along the main fault is continuously reduced by coevally active SW-NE trending normal faults (e.g. Greben fault, Fig. 1), thus terminating the Dragos-Voda fault in an extensional horsetail

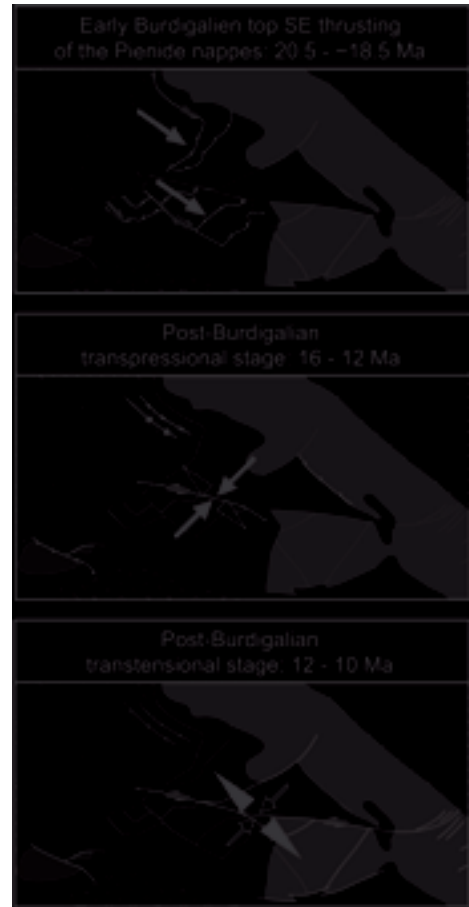


Figure 2: The three main Miocene tectonic phases observed in the study area.

splay. The main activity along the Bogdan-Voda fault ends at about 10 Ma, as is indicated by almost unaffected Neogene volcanics. In the western part of the study area, along the Bogdan-Voda fault, sedimentary and volcanic rocks provide timing constraints for the deformation. In the Eastern part of the study area, along the Dragos Voda fault, only basement units and Paleogene sediments crop out. Therefore the fault activity is indirectly dated

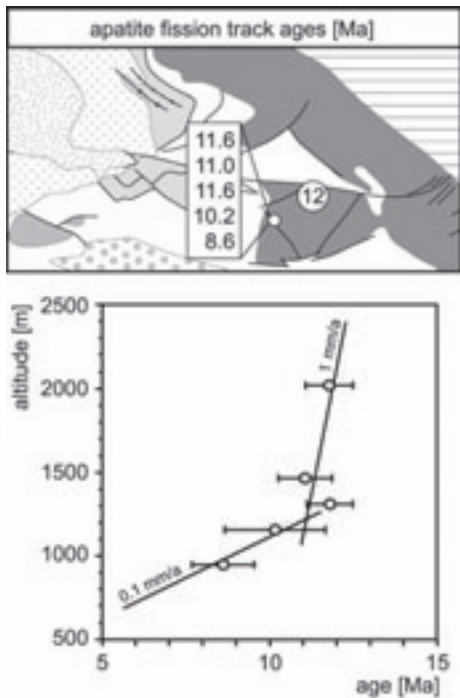


Figure 3: Apatite fission track data from the Rodna horst (encircled datum point from Sanders 1998) together with altitude *vs.* age diagram.

and inferred from the cooling history of the syn-kinematically exhumed Rodna horst. A vertical profile covering about 1000 m of altitude difference has been sampled for apatite fission-track analysis. Burial by Eocene to Oligocene sediments led to full annealing of apatite in the Rodna Horst, and all samples yielded Middle to Late Miocene cooling ages (8.6–11.6 Ma, see also Sanders 1998, Fig. 3). The altitude *vs.* age relationship indicates enhanced exhumation between 12–11 Ma with exhumation rates of at least 1 mm a^{-1} , while a fast decrease in the rate of exhumation to around 0.1 mm a^{-1} is observed after 10 Ma (Fig. 3).

Our fission-track data suggest enhanced exhumation of the Rodna horst between 12–10 Ma, i.e. during the stratigraphically dated transtensional sinistral strike-slip phase.

Literatur

Sanders C (1998) Tectonics and erosion: competitive forces in a compressive orogen. A fission track study of the Romanian Carpathians. Ph.D. thesis, Free University of Amsterdam, 204 p.

Tischler M, Gröger HR, Fügenschuh B & Schmid SM (in press) Miocene tectonics in the Maramures area (Northern Romania)-implications for the Mid-Hungarian fault zone. *Journal of international Earth Sciences*.

Grain coarsening and hydrothermal alteration in metacarbonates of the Damara Orogen, Namibia

Poster

Christian J. Gross¹

Introduction and geological background

Grain coarsening is a process that occurs in a wide variety of rock types. The application of grain growth theory to natural geologic materials has its beginnings in the theoretical foundations of the metallurgical and material sciences. Two types of grain growth can be statistically defined: 1) normal grain growth describing a uniform grain structure and 2) abnormal grain growth, where some grains grow more rapidly in size at the

¹ GZG, Goldschmidstr. 3, 37077 Göttingen, Germany

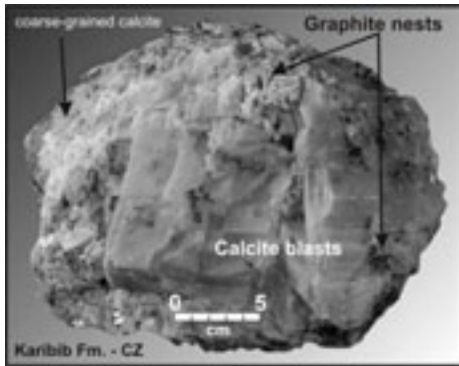


Figure 1: Large rhombohedral calcite blasts in a matrix of coarse-grained calcite with evenly distributed nests of graphite.

expense of matrix grains, thus creating a bimodal grain size distribution. This study aims to understand the grain coarsening phenomenon in metacarbonate rocks, to determine the mechanisms involved and to elucidate the role of fluids (e.g. hydrothermal alteration).

Metacarbonate units exhibiting coarsely crystalline fabrics, representing abnormal grain growth, and hydrothermal alteration have been investigated from two major geologic formations of the Damara Orogen (Namibia). The study sites are located in two distinct tectono-stratigraphic zones with different tectonic and metamorphic histories. The Central Zone (CZ) is characterized by crustal-scale dome structures, extensive platform carbonates, numerous granitic intrusions, major shear zones and Karoo-age dolerite dike swarms. Amphibolite to granulite facies metamorphic conditions prevailed in the CZ. Shown in Figure 1 is a typical example of abnormal grain growth in a white graphite-bearing calcite marble of the Karibib Formation. Large rhombohedral calcite blasts are visible in a coarse-

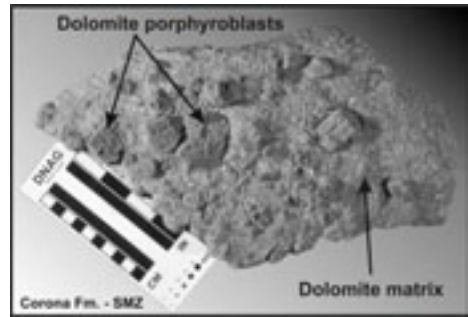


Figure 2: Metadolomite marble showing large dolomite porphyroblasts embedded in a matrix of medium-grained dolomite.

grained calcite matrix with graphite forming nests distributed throughout. Local lenses of grey calcite marble occur showing similar grain growth characteristics, but without graphite nests. Peak metamorphic temperatures in the graphite-bearing calcite reached 760° C (Walter 2004). Late-stage cataclastic and mylonitic deformation accompanied by hydrothermal alteration overprints the coarse-grained calcite marbles.

In the Southern Margin Zone (SMZ) where metadolomites of the Corona Formation were investigated, greenschist facies conditions prevailed with differences in style of deformation and hydrothermal alteration. Carbonates are differentiated into siliceous dolomites, talc-bearing dolomites, a dark dolomite mylonite and a medium-grained dolomite marble with large dolomite porphyroblasts (Fig. 2). Field evidence for extensive hydrothermal alteration is present as hydrothermal dolomite veins, hydrothermal quartz veins, extensive alteration in contact zones and bleaching of the dark dolomite mylonite.

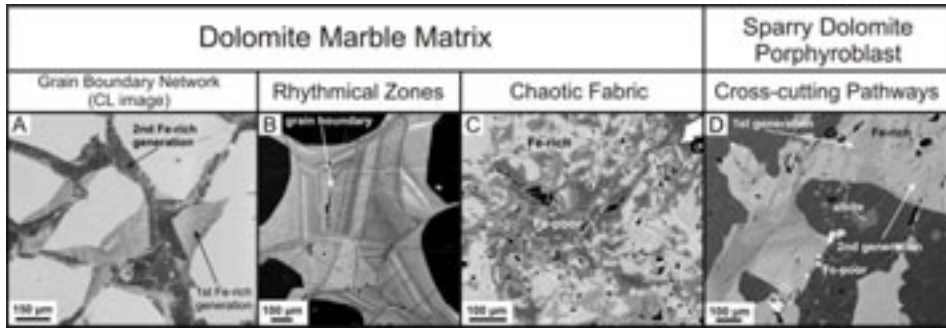


Figure 3: Classification of zonation types in the dolomite marble. A) CL image of the dolomite matrix depicting the two grain-boundary parallel Fe-rich zonations. B) Rhythmical growth zones indicating paleo-porosities. C) Local chaotic fabric of Fe-rich and Fe-poor dolomite. D) Fe-rich pathway (two generations) cut across the porphyroblast. Minor rhythmical zonations are also visible. Note: Pictures B-D represent back-scatter electron images.

Fabrics and microstructures

The graphite-bearing calcite marble of the CZ exhibits a wide variety of microstructures and fabrics. In the coarse-grained matrix domain, calcite shows irregular grain shapes characterized by serrated, interpenetrating grain boundaries. Some microstructural features include leftover grains, twin-free bulges migrating into neighboring grains and examples of relic triple-point grain boundaries undergoing transformation. Twinning occurs in varying degrees, with twin-boundary migration also observable. Contacts between matrix and blasts are curved and irregular. Thin flakes of graphite (3–4 mm in size) occur along grain contacts, in small clusters and occasionally in the large calcite blasts. Calc-silicate minerals occur in thin layers or clusters. When present in greater concentration, grain coarsening appears hindered.

In optical cathodoluminescence microscopy (CL), the coarse-grained calcite matrix and calcite blasts show homogeneous red CL colors with very low

to medium luminescence. Calcite showing very bright luminescence occurs as cross-cutting micro-veins. The etch experiments reveal a qualitative map of dislocation densities. In the calcite marble etching occurred primarily along grain boundaries and formed trains of etch pits aligned parallel to twin boundaries.

The dolomite marble from the SMZ exhibits a somewhat granoblastic fabric with a visible shape-preferred orientation. The dolomite matrix grains range from flattened (a small percentage) to elongated in shape, where grain boundaries can be straight or show fine irregularities. Dolomite porphyroblasts appear anhedral in thin section. Relatively large numbers of very fine-grained inclusions of albite clusters, talc, quartz and pyrite are found in the dolomite porphyroblasts. The interface or contact zone between matrix and porphyroblast is usually irregular and indentations of dolomite matrix grains into the porphyroblast are locally observable as well as leftover grains. Bulk neutron texture

analysis revealed a moderate to strong crystallographic preferred orientation in the dolomite matrix.

The density of etch pits appears greater in the porphyroblast as compared to the matrix, with some etch grooves creating curved traces in the dolomite porphyroblast. SEM also reveals relatively open grain boundaries in the matrix dolomite after etching.

Evidence for extensive grain-scale fluid-rock interaction is visible by CL in the dolomite marble. The CL color in unaltered matrix grains as well as in the porphyroblast is yellow-orange, whereas the Fe-rich areas exhibit various shades of brown. Figure 3 shows a classification of the types of zonation microstructures present in the matrix and porphyroblast. In the dolomite matrix an interconnected network of Fe-/Mn-rich zones, creating two distinct generations, occurs parallel the grain boundaries (Fig. 3A). Complex rhythmical zonations with alternating bands and sharp boundaries occur in some parts of the matrix (Fig. 3B). Chaotic CL fabric patterns occur locally and destroy the matrix grains and the grain-boundary zonations (Fig. 3C). In the dolomite porphyroblast (Fig. 3D), the Fe-rich alteration is represented by cross-cutting pathways also forming two generations. Furthermore, zoned albite clusters with dark cores and blue rims are always associated with the Fe-rich zonations. Those in the matrix are unzoned.

Discussion and conclusion

All the data indicates that the grain coarsening in the graphite-bearing calcite marbles is the result of regional metamorphism due to granitic intrusions (e.g. static recrystallization, Evans et al. 2001). The dominant mechanism

responsible for the grain growth in the calcite marble is grain boundary migration, as is evident by the types of microstructures and fabrics observable in thin section.

Cathodoluminescence observations of the graphite-bearing calcite marble indicate that hydrothermal alteration was limited to a late-stage event. Microveins of brightly luminescent calcite (zoned and unzoned) are associated with the fluids accompanying cataclastic deformation and are not connected to the grain coarsening process. Fluid inclusions within the coarse calcite matrix and the calcite blasts have a composition similar to that of seawater. Fluids released by the granitic intrusions must have played a role in the coarsening process, since in theory the rate of grain growth and grain boundary mobility would be much slower under dry conditions.

The grain coarsening, porphyroblast growth and alteration in the dolomite marble is somewhat problematic. The dolomite porphyroblasts could be either younger or older than the coarsened matrix. The relic grain boundaries and possible leftover grains suggest the porphyroblast is younger, whereas embayments of matrix grains into the porphyroblast could suggest an older age. Furthermore, the grain coarsening and porphyroblast growth could have occurred earlier than the hydrothermal alteration, since the Fe-rich zones cross-cut the porphyroblast. On the other hand, the CL zonations may represent evidence for fluid-enhanced grain coarsening and thus the mechanism of growth is solution/precipitation. Fluid inclusion data from dolomite veins point to highly saline solutions present during hydrothermal alteration.

The sequence of events for the hydrothermal alteration represented by the Fe-/Mn-rich zonation network can be separated out into five stages of a continuous process. Stage I introduces two Fe-/Mn-rich fluid generations. In Stage II intergranular pore spaces are created which are then filled in by rhythmically zoned dolomite (Stage III). Formation of a second generation of pore spaces occurs in Stage IV caused by corrosion of the original rock fabric. This leads to the precipitation of dolomite (Stage V) represented by the local chaotic CL fabric. All these events represent episodic fluid influxes possibly caused by seismic events, since the carbonate unit lies in close proximity to a thrust fault.

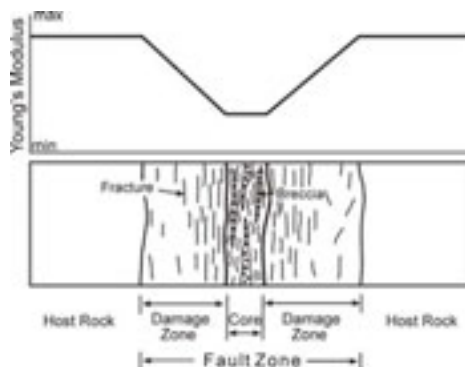


Figure 1: Fault zones consist of two main mechanical units: a comparatively thin core and a much thicker damage zone. The effective Young's modulus (stiffness) gradually decreases from the host rock to the boundary between the core and the damage zone.

References

- Evans B, Renner J & Hirth G (2001) A few remarks on the kinetics of static grain growth in rocks. *Int J Earth Sci* 90, 88–103
- Walter J (2004) Fabric development, electrical conductivity and graphite formation in graphite-bearing calcite marbles from the Central Damara Belt, Namibia. PhD Thesis, Georg-August University of Göttingen, pp 289

Effects of damage-zone thickness on fault displacement

Poster

Agust Gudmundsson¹ Adelina Geyer²

When viewed as ideal elastic cracks, seismogenic faults are often modeled as

¹ Department of Structural Geology and Geodynamics, Geoscience Center, University Göttingen, Goldschmidtstrasse 3, D-37077 Göttingen, Germany ² Institute of Earth Science, Jaume Almera, Barcelona, Spain

mode II or mode III cracks in semi-infinite elastic bodies or half spaces. These models normally assume the rock to be homogeneous and isotropic. Such assumptions may be justified and necessary when using closed-form analytical solutions for fault displacement. They are not justified, however, when we attempt to understand fault-displacement profiles along earthquake rupture sites or in paleofault studies. This follows because crustal segments hosting faults are, as a rule, not homogeneous and isotropic, but rather heterogeneous and anisotropic. In particular, the fault rocks commonly form layers or units parallel with the fault plane. Also, the mechanical properties of the rocks next to the fault change as the fault develops (Gudmundsson 2004). During repeated earthquakes in a seismogenic fault zone, two main rock units develop around the fault plane. One unit is the core, located next to the fault plane and normally composed of soft (low Young's modu-

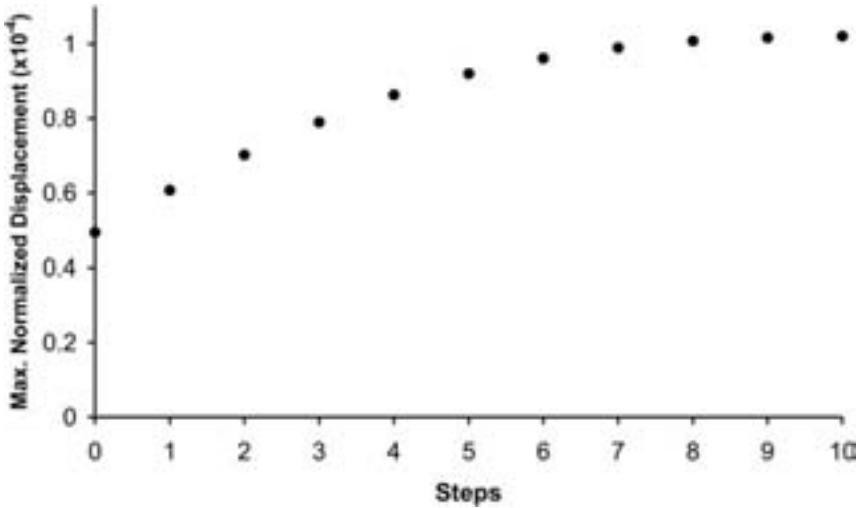


Figure 2: Boundary-element model of fault displacement when the damage-zone thickness is gradually increased in 10 steps, showing the maximum normalized displacement (MND) in the fault center in each of the steps. Here $MND = 10^4 \frac{MD}{FL}$, where MD is the maximum displacement and FL the fault length, both expressed in model length units.

lus) breccia, gouge, and other cataclastic rocks. The other unit is the damage zone, containing some cataclastic rocks but characterized by fractures of various types. Field studies show that the fracture frequency in the damage zone is often quite variable, but normally decreases with distance from the core-damage zone boundary; similar results are obtained for microfaults in laboratory experiments (Shimada 2000). The higher the fracture frequency, the lower will be the effective Young's modulus (stiffness) in a direction perpendicular to the main fracture trend. The Young's modulus of a damage zone thus normally decreases on approaching the fault core (Fig. 1). On the basis of variations in fracture frequency, the damage zone associated with a fault can commonly be divided into several sub-zones or units, each with a different effective stiffness (Gudmundsson & Bren-

ner 2003).

Field studies also show that as the fault zone evolves the core and the damage zone both increase in thickness. A fault zone composed of units (core and damage zone) with stiffnesses that are different from those of the host rock develops local stresses that may be very different from the far-field stresses (Gudmundsson & Brenner 2003).

Using these observations as a basis, we present numerical results on how the fault slip in a fault zone, for given fault geometry and loading conditions, may change when the thickness of its damage zone increases. Our results indicate that when the damage-zone thickness gradually increases, the maximum displacement on the fault also increases (Fig. 2). It follows that the fault slip generated during a particular earthquake, including the postseismic slip, may gradually increase with increasing damage-zone

thickness. Thus, for an active seismogenic fault of constant rupture (trace) length, the ratio of the maximum displacement to the rupture length should decrease with time. These theoretical results are supported by field observations.

Acknowledgments This work was supported by a grant from the European Commission through the project Prepared (EVG1-CT-2002-00073 PREPARED).

References

- Gudmundsson A (2004) Effects of Young's modulus on fault displacement. *C.R. Geoscience* 336, 85–92
- Gudmundsson A & Brenner SL (2003) Loading of a seismic zone to failure deforms the nearby volcanoes: a new earthquake precursor. *Terra Nova* 15, 187–193
- Shimada M (2000) *Mechanical Behavior of Rocks under High Pressure Conditions*. Balkema, Rotterdam

How stress transfer between volcanic and seismic zones affects volcanic and earthquake activity

Poster

Agust Gudmundsson¹ Sonja L. Philipp¹

Oceanic transform faults and ridge segments form a network where mechanical interaction is to be expected (Fig. 1). In particular, dike emplacement in ridge segments is likely to affect earthquake activity in the adjacent transform faults

¹ Department of Structural Geology and Geodynamics, Geoscience Centre, University of Göttingen, Goldschmidtstraße 3, D-37077 Göttingen

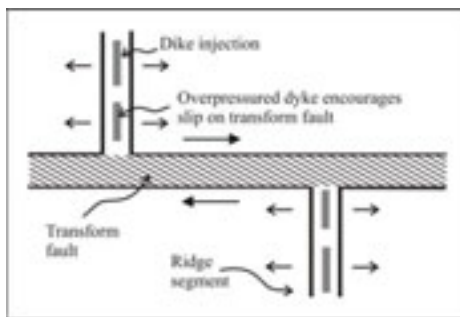


Figure 1: Ocean-ridge segments and transform fault forms an interconnected fracture system, where stress changes in one fracture (say, due to dike injection in a ridge segment) may be expected to be partly transferred to the adjacent fractures (here, transform faults).

through processes such as stress transfer. Similarly, strike-slip displacement across transform faults may trigger dike injections and, eventually, eruptions in the adjacent ridge segments. For obvious reasons, direct observations of the possible mechanical interaction between submarine transform zones and ridge segments at mid-ocean ridges are difficult.

The subaerial seismic zones of Iceland, however, are in clear spatial connections with the adjacent volcanic zones (Fig. 2). These zones, therefore, provide excellent opportunities to study stress transfer between volcanic and seismic zones (Gudmundsson 2000). At the junctions with the Kolbeinsey Ridge in the north and the Reykjanes Ridge in the south, there are ocean-ridge discontinuities that host one or more seismic zones (Fig. 2). The northern discontinuity is referred to as the Tjörnes Fracture Zone (TFZ), a transform fault that is partly exposed on land as the Husavik-Flatey Fault (HFF). The southern dis-

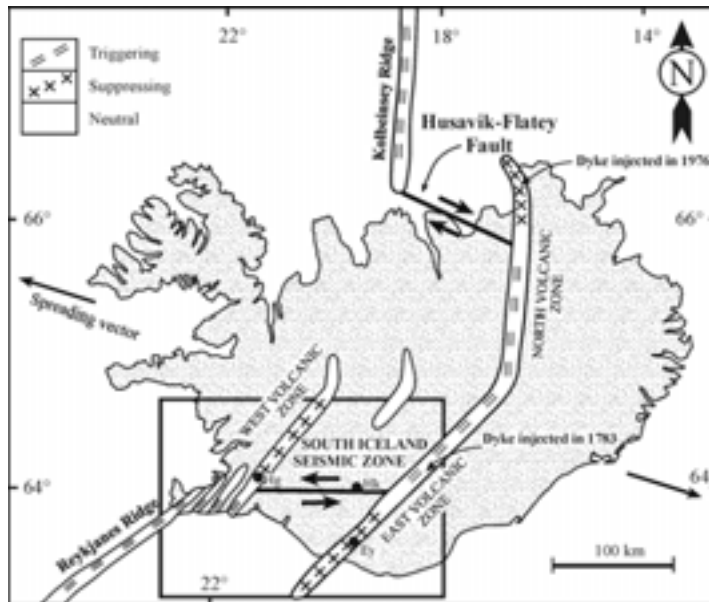


Figure 2: The Husavik-Flatey Fault (HFF) is the main structure of the Tjornes Fracture Zone which connects the North Volcanic Zone to the Kolbeinsey Ridge. HFF is an oceanic transform fault. By contrast, the South Iceland Seismic Zone (SISZ) is a zone of high shear stress concentration between the overlapping West and East Volcanic Zones (modified from Gudmundsson and Brenner 2003).

continuity is referred to as the South Iceland Seismic Zone (SISZ). It is a zone where most of the seismogenic faulting occurs on conjugate strike-slip faults. The largest earthquakes in Iceland, reaching M7.1–7.3, occur on strike-slip faults in the TFZ and the SISZ.

In the SISZ, major destructive earthquakes occur at intervals of 80–100 years, the largest events reaching M7.1–7.3 (Gudmundsson and Brenner 2003). Although the zone is E–W trending, with an overall sinistral movement, most of the earthquakes are associated with NNE and ENE-trending strike-slip faults. We present numerical models indicating that when the SISZ is loaded to failure, stresses are transferred to, and

concentrate at, its ends: tensile in the northeast and southwest quadrants and compressive in the northwest and southeast quadrants. These model results agree with observations made when the SISZ was loaded to failure in June 2000, resulting in two M6.6 earthquakes. For several years prior to the June 2000 earthquakes, compression, uplift and intense earthquake swarms (some events exceeding M4) occurred in two active composite volcanoes, Hengill and Eyjafjallajökull, located in the quadrants of compressive stresses (Fig. 3). Most of this earthquake activity came to an end following the June 2000 earthquakes.

Also, in the decades prior to the June 2000 earthquakes, the Hekla Volcano (Fig. 3), located in one of the quad-

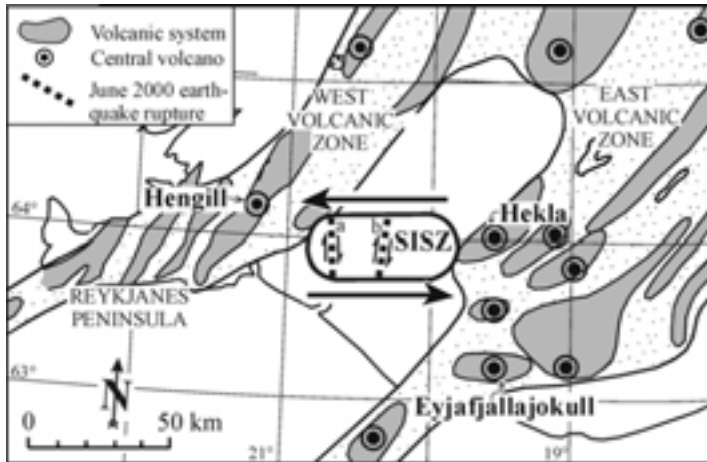


Figure 3: Location of the central volcanoes of Hengill, Hekla, and Eyjafjallajökull in relation to the South Iceland Seismic Zone (SISZ). Also indicated is the overall sinistral movement across the zone, as well as the two faults (a, b) associated with the June 2000 earthquakes (modified from Gudmundsson & Brenner 2003).

rants of tensile stress, erupted unusually frequently. These composite volcanoes (with shallow magma chambers) act as ‘soft inclusions’ at which stresses transferred from the SISZ become concentrated. Deformation and seismicity in Eyjafjallajökull and Hengill and the unusually high eruption frequency in Hekla may thus be used as precursors to large earthquakes in the SISZ.

In South Iceland, stress is also transferred from the volcanic zones to the seismic zone. For example, stress transfer from the overpressured 27 km-long feeder dike of the 1783 Laki eruption to the nearby SISZ triggered the 1784 earthquake sequence, the largest historical one (that is, for the past 1100 years) in the SISZ. Thus, the largest historical eruption in Iceland, Laki 1783, triggered its largest historical earthquake sequence.

In contrast to the SISZ, the TFZ is a well-developed oceanic transform fault

(Fig. 2). Its main structure is the HFF, an active dextral fault, partly exposed on land in North Iceland. Dike injection in 1976 in the North Volcanic Zone during the Krafla Fires (1975–1984) resulted in a nearly two-decade suppression of earthquake activity in the HFF (Fig. 2).

For regional dikes, such as those injected during the Laki 1783 and the Krafla 1976 eruptions, the magmatic overpressure may reach tens of megapascals. Part of the overpressure associated with the dikes is transferred as compressive stress to the nearby seismic zones, the SISZ and the HFF. The models presented here indicate that when the dike-generated horizontal displacement is opposite to the normal displacement across the adjacent seismic zone, earthquakes are suppressed. By contrast, when the dike-generated displacement is consistent with the normal displacement across the adjacent seismic

zone, earthquakes are triggered (Fig. 2).

References

- Gudmundsson A (2000) Dynamics of volcanic systems in Iceland. *Annual Reviews of Earth and Planetary Sciences* 28, 107–140
- Gudmundsson A & Brenner SL (2003) Loading of a seismic zone to failure deforms nearby volcanoes: a new earthquake precursor. *Terra Nova* 15, 187–193

Feldspar deformation in greenschist facies shear zones (Aar-Massif, Switzerland)

Poster

Sarah Hauten¹ Mark R. Handy¹
Christoph Dobmeier¹

Granitic gneisses of the Central Aar Granite host a shear zone network that formed at greenschist facies conditions. The work area is located in the Bächlital (Grimsel area, Central Switzerland) and was chosen for the analysis of shear zones because of the weakly anisotropic fabric of the host gneisses. Contrary to previous publications (e.g. Choukroune & Gapais, 1983), none of these host rocks are undeformed. They contain a penetrative foliation (S_1) that strikes consistently ENE-WSW with a steep dip of around 70° to the south. This foliation is overprinted by the aforementioned shear zone network, which was the main focus of this study. The granitic gneisses are predominantly equigranular, but locally contain feldspar augen. Albite, quartz, magmatic K-feldspar, biotite, chlorite

and epidote make up the rock. Albite is the dominant plagioclase mineral, reflecting the greenschist facies metamorphic overprint. Partial chloritization of biotite is associated with the segregation of a Ti-phase. Calcium from the K-feldspar was used for the formation of epidote. The shear zone network comprises major, dm to km long shear zones which are interconnected by minor, cm to dm long shear zones. The major shear zones are oriented predominantly NE–SW and have a cm-wide mylonitic to ultramylonitic centre which is bounded on either side by cm to m long fractures that run parallel to the shear zone centre in intervals of meters to decimeters. The minor shear zones are not preferentially oriented and reach lengths of several centimeters to decimeters. They do not always show a distinct shear component and sometimes end as cracks before reaching the next major shear zone.

Four stages of feldspar deformation during the shear zone development could be observed in thin section:

1. Discrete, intracrystalline microfaults form conjugate sets. Although some of these microfractures run parallel to the cleavage planes, the majority runs oblique to them. Bent twin lamellae represent the beginning stages of microfracturing. Rotated microphacoids (fragments bordered by the microfractures) are the end result;
2. Dynamic recrystallisation characterized by serrate grain boundaries and core-mantle structure of feldspar grains. What processes leading to this recrystallisation are unclear and are still under investigation. Cracks filled with

¹ Freie Universität Berlin, Department of Earth Sciences, Malteserstr. 74-100, 12249 Berlin

small feldspar grains and pressure shadows of K-feldspar clasts point to pressure solution as a relevant process in this stage. Electron microprobe analysis revealed that some fractures are filled with K-feldspar which is chemically distinct from the host K-feldspar (e.g. higher Ba content). Progressive subgrain rotation is also commonly observed in feldspar grains. Some subgrain aggregates show a crystallographic preferred orientation;

3. Recrystallised aggregates become more prevalent and grains start to creep, leading to a mylonitic fabric;
4. The transition to the fourth, ultramylonitic stage is not well defined.

The aim of my work is to understand the mechanisms of the feldspar deformation in the four stages that lead to the ultramylonitic final stage. The results I have presented in this abstract are preliminary.

Scherzonen- und Schuppenbildung am Kontakt von Aarmassiv und Helvetikum im Bereich der Engelhörner, Berner Oberland (Schweiz)

Poster

Niklas Heinemann¹ Marc Giba¹
Jochenl Fiseli¹ Michael Stipp¹

Das Untersuchungsgebiet umfasst den Nordrand des Aarmassivs, die autochthone und paraautochthone sedimentäre Bedeckung des Aarmassivs, den

¹ Geologisches Institut, Universität Freiburg, Albertstr. 23b, D-79104 Freiburg

ultrahelvetischen Wildflysch und den Südrand der Wildhorndecke. Das Aarmassiv besteht aus dem Innertkirchener Granit und Granitgneis und den sogenannten Mischgneisen. Lokal sind präalpine mylonitische Scherzonen ausgebildet. Die sedimentäre Bedeckung des Aarmassivs beginnt mit einem geringmächtigen permotriassischen Aufarbeitungshorizont des kristallinen Untergrundes aus Quarz-Glimmerschiefern, Arkosen und Konglomeraten. Darüber folgt die mehrere hundert Meter mächtige mesozoische Abfolge. Im Arbeitsgebiet tritt an der Basis der massige, hell bis rötlichgelb verwitternde Rötildolomit hervor. Im Hangenden liegen die kalkigen Schichten des Doggers sowie das Argovien. Darüber folgen die mächtigen Kalkserien des Malm (Quintner Kalk) und der unteren Kreide (Oehrlikalk), welche die Steilwände der Engelhörner aufbauen. In den paraautochthonen Schuppen auf der Nordseite der Engelhörner beginnt die Abfolge erst mit dem unteren Malm. Als jüngste Einheit treten dort allerdings auch Tertiäre Schichten auf, welche überwiegend aus kalkhaltigen Sandsteinen, Brekzien und Tonschiefern bestehen. Als nur wenige Meter mächtiger dunkler bis schwarzer, glimmerführender Tonschiefer ist der allochthone ultrahelvetische Wildflysch zwischen den paraautochthonen Schuppen und der Wildhorndecke eingeklemmt. Die Wildhorndecke wird im Arbeitsgebiet von den Einheiten des Doggers aufgebaut. Die Zuordnung des Doggers zur Wildhorndecke ist allerdings nicht immer eindeutig. Westlich des Arbeitsgebietes in der Umgebung von Grindelwald werden Einheiten des Doggers z.T. auch dem Ultrahelvetikum zugerechnet (Günzler-Seiffert & Wyss 1938).

Die lithologische Kartierung, aber auch die Zuordnung der Lithologien zu den tektonischen Einheiten basiert im Wesentlichen auf den ausgezeichneten Vorarbeiten (z.B. Arbenz & Müller 1920; Günzler-Seiffert & Wyss 1938; Müller 1938; Büchi 1980). Ziel unserer Untersuchungen ist es, die Kinematik sowie die relative zeitliche Abfolge der einzelnen Groß- und Kleinstrukturen genauer zu bestimmen und die strukturelle Gliederung des Arbeitsgebietes mit den von Burkhard (1988) definierten Deformationsphasen zu korrelieren. Bei den strukturgeologischen Untersuchungen konzentrieren wir uns auf zwei Fragestellungen:

1. Welche Auswirkungen haben die alpidischen Scherzonen im Aarmassiv auf die überlagernden sedimentären Deckeinheiten?
2. Unter welchen rheologischen Bedingungen erfolgte die Deckenüberschiebung und Schuppenstapelung, und wurden diese Scherzonen bei ihrer späten Steilstellung reaktiviert?

Die meisten tektonischen Kontakte im Arbeitsgebiet sind steil gestellt oder überkippt, was auf die mehrphasige Deformationsgeschichte infolge der alpinen Kollision zurückzuführen ist. Im Wesentlichen lassen sich drei Deformationsphasen unterscheiden, die den von Günzler-Seiffert (1943) und Burkhard (1988) definierten Phasen im Zeitraum von Oligozän und Miozän entsprechen. Nach der Platznahme der Ultrahelvetischen Decken wurde in der Prabé Phase (ca. 38–30 Ma, Burkhard 1988) die Wildhorndecke überschoben. Einhergehend mit der Deckenüberschiebung fand eine isoklinale Faltung der sedimentären

Einheiten statt. Während dieser Phase oder wahrscheinlich erst in der nachfolgenden Kiental Phase (30–20 Ma, Burkhard 1988) wurden die parautochthonen Schuppen gebildet und gestapelt. Die Karbonate an den Kontakten sind meist mylonitisiert, während die quarzreichen Tertiär-Gesteine kataklastisch deformiert sind. Dieses deutet auf niedriggradige Metamorphosebedingungen im Kontaktbereich von Aarmassiv und Helvetikum hin (ca. 300°C; vgl. Burkhard 1990, Herwegh & Pfiffner 2005). Bei der Schuppenbildung wurden die Granite und granitischen Gneise des Aarmassivs z.T. mit in die Deformation einbezogen und randlich gefaltet. Eine der Schuppencherzonen innerhalb der parautochthonen Sedimente ist die ‚Weissenbach Störung‘ am Kontakt von Malmkalk zu tertiärem Sandstein. Die Kalke sind mylonitisiert im direkten Kontakt zu Kataklastiten, in welche Pseudotachylite eingedrungen sind. Es ist mikrostrukturell noch zu klären, ob tatsächlich Kalkmylonite, Kataklastite und Pseudotachylite gleichzeitig gebildet wurden oder ob beispielsweise die Pseudotachylite auf eine späte Reaktivierung der Schuppencherzonen nach der Steilstellung zurückzuführen sind. Die Steilstellung und Überkipfung der Schuppencherzonen erfolgte während der fortschreitenden Heraushebung des Aarmassivs und der Exhumation des helvetischen Deckenstapels in der Grindelwaldphase (20–0 Ma, Burkhard 1988). Das Aarmassiv wurde dabei durch interne Verformung und Überschiebung parallel zur Einengungsrichtung verkürzt. Dabei wurden präalpine Scherzonen reaktiviert, und es bildeten sich grünschieferfazielle Mylonite aus (z.B. Marquer & Gapais 1985). Wir vermuten, dass

die Aarmassiv-Scherzonen auch im Arbeitsgebiet erst nach und nicht wie von Büchi (1980) postuliert bereits vor der Deckenplatznahme (re-)aktiviert wurden. Diese Scherzonen überprägen nämlich die z.T. tektonisierten Kontakte von Aarmassiv und autochthoner Sedimentbedeckung. Die Deformation der Kontakte ist gekennzeichnet durch zerscherzte Sediment-Schuppen des Perms bis Doggers und einer mehr oder weniger starken mylonitischen Foliation, die wohl der Deckenplatznahme zugeordnet werden kann. Die Aarmassiv-Scherzonen reichen meist nur wenige Meter in die autochthone Bedeckung hinein. Darüber haben sich allerdings Faltenstrukturen entwickelt, wie z.B. die Falten des Rötidolomites an der Basis der Engelhörner im Urbachtal. Es kann hier also davon ausgegangen werden, dass sich über den Kristallin-Sedimentkontakt hinweg ‚Fault-bend folding‘ Strukturen, also an Störungen gebundene Falten, ausgebildet haben. Diese Strukturen sind ebenfalls ein deutlicher Hinweis darauf, dass Aarmassiv und helvetische Deckeinheiten infolge der alpinen Kollision intensiv gemeinsam deformiert worden sind.

Literatur

- Arbenz, P & Müller F (1920) Ueber die Tektonik der Engelhörner bei Meiringen und den Bauder paraautochthonen Zone zwischen Engelberg und Grindelwald. *Eclogæ geol. Helv.* 16, 111–115
- Büchi E (1980) Geologie der autochthonen Sedimentbedeckung des Aar-Massivs im Urbachtal bei Innertkirchen. Lizentiatsarbeit, Universität Bern, pp 102
- Burkhard M (1988) L'Helvétique de la bordure occidentale du massif de l'Aar (Évolution tectonique et métamorphique). *Eclogæ geol. Helv.* 81 (1), 63–114
- Burkhard M (1990) Duktile deformation mechanisms in micritic limestones naturally deformed at low temperatures (150–350°C). In: Knipe RJ & Rutter EH (Eds.), *Deformation Mechanisms, Rheology and Tectonics*, Geological Society Special Publication 54, 241–257
- Günzler-Seiffert H & Wyss R (1938) Geologischer Atlas der Schweiz 1:25000. Blatt 396 Grindelwald (Atlasblatt 13), Erläuterungen
- Günzler-Seiffert H (1943) Beweise für passive Tektonik im Berner Oberland. *Eclogæ geol. Helv.* 36(2), 219–223
- Herwegh M & Pfiffner OA (2005) Tectonometamorphic evolution of a nappe stack: A case study of the Swiss Alps. *Tectonophysics* 404, 55–76
- Marquer D, Gapais D & Capdevila R (1985) Chemical behavior and orthogneissification of a granodiorite in greenschist facies, Aar Massif, Central Alps. *Bulletin de Mineralogie*, 108 (2), 209–221
- Müller F (1938) Geologie der Engelhörner, der Aareschlucht und der Kalkkeile bei Innertkirchen (Berner Oberland). *Beitr. geol. Karte Schweiz*, NF 91

Fossil overpressures compartments? A case study from the Eifel area and some general aspects Vortrag

Christoph Hilgers¹ Carsten Bückler²
Janos L. Urai¹

Introduction

Fluid overpressures are well known from hydrocarbon exploration in many sedimentary basins. They can reach almost lithostatic values, and may cause the fracturing of rock. Fracturing allows the discharge of fluid overpressure, and fluid flows along a hydraulic gradient towards a low pressure reservoir. Different mechanisms may cause the precipitation from the fluid, such as a fluid

¹ Geologie-Endogene Dynamik, RWTH-Aachen, Germany ² Shell E&P, Houston, USA

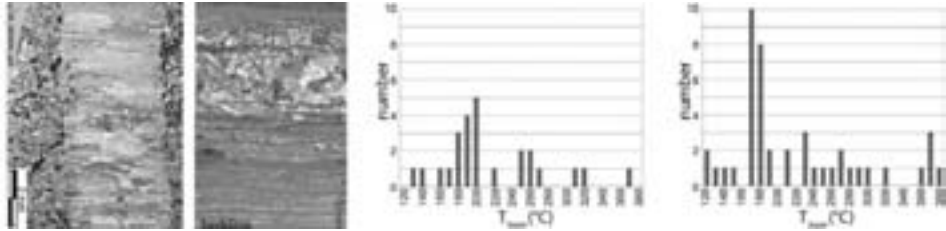


Figure 1: (a) The vein microstructure of #1 shows stretched crystals, which can laterally evolve towards an elongate-blocky microstructure grown syntaxially. b) Vein set #2 is blocky and was deformed plastically by dynamic recrystallisation. c, d) Fluid inclusion data show maximum temperatures of about 370°C for both vein sets #1 (c) and #2 (d).

pressure drop, a variation of temperature at the low pressure reservoir, or a different rock type inducing different Eh-pH conditions. Such precipitates in fractures are called veins, which often display paleo-fluid overpressures in rocks. In this study, we present some results from Devonian clastic sedimentary rocks of the Eifel area. Results are compared with other sedimentary basins to highlight some general aspects.

Geological setting

The lower Devonian rocks exposed along the shore of the Rursee water reservoir are Siegenian Upper Rurberger beds and Emsian Klerfer and Heimbacher beds to the NE. They are located on the SE-flank of the NE-plunging Variscan Venn-Anticlinorium. Both units expose shales, siltstones and sandstones deposited in the subsiding Devonian Eifel Basin.

Meso- and microstructural data

Two different vein sets are oriented subnormal (#1) and parallel (#2) to bedding, respectively. Both sets are filled with quartz. Vein set #1 is restricted to sandstone layers, and rarely continues into the enclosed shale beds.

Their shape is sigmoidal on fold limbs, and their orientation in accordance with flexural slip along the bedding planes. The vein microstructure of #1 shows an elongate-blocky to fibrous microstructure. Fibrous grains continue across the vein (stretched crystals) and contain solid and fluid inclusions arranged parallel to the vein wall interface. Meso- and microstructural observations indicate vein formation prior or syn-folding, veins opened in incremental steps (crack-seal mechanism). Vein set #2 is located at the shale-sandstone interface and can be traced for several tens of metres. It generally truncates #1 and thus post-dates the bedding-normal veins. Locally, vein set #2 cuts through the hanging-wall and is associated with small thrusts. The blocky quartz grains of vein set #2 exhibit extinct undulose and are recrystallised by grain boundary migration and sub-grain rotation. The quartz grains of the host rock, however, are elongated (overgrowth, fringes and dissolution along the cleavage planes), but generally optically undeformed. This indicates that pressure solution was the dominant deformation mechanism in the host rock. Modelling the subsidence of the upper Rurberg beds using published data

of burial temperatures (vitrinite reflectance, illite crystallinity etc., e.g. von Winterfeld 1994) indicates rapid burial down to 7–8 km depth prior to the onset of Variscan compression and subsequent basin inversion. This accounts for the up to approx. 6.5 km thick lower Devonian sedimentary pile deposited in the Eifel Basin, and fluid overpressure generation during subsidence and the onset of Variscan compression (Fig. 2).

Discussion and Conclusion

Field and microstructural observations of vein sets #1 and #2 are consistent with our modelled overpressure generation due to basin evolution (Fig. 2). Bedding normal veins #1 are restricted to the competent sandstone layers and formed in an already competent rock, as shown by transgranular fractures and the absence of compaction features associated with vein set #1. Repeated crack-seal increments and the variation of paleo-temperatures suggest that veins were subsequently opened and re-sealed during subsidence. Stretched crystals are oriented normal to the vein wall, indicating extension normal to bedding. Vein formation requires tensile fracturing of the sandstone with the maximum principal stress oriented normal to bedding, which is consistent with vein formation during subsidence at high fluid overpressures and low differential stress. Bedding-parallel vein set #2 truncates set #1 and cuts through the hanging wall associated with small thrusts. This indicates a reorientation of the principal stresses between #1 and #2. Vein set #2 is folded in accordance with the Variscan folds exposed on the shore, but parasitic folds of the veins are absent. This suggests that vein set #2 represents the first compressional event asso-

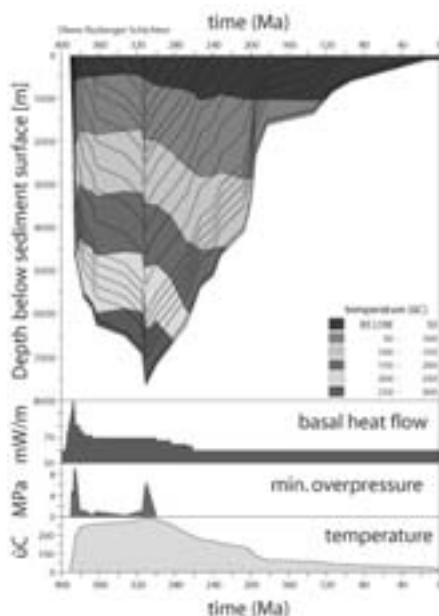


Figure 2: Subsidence curve of the Lower Devonian upper Rurberg beds.

ciated with Variscan deformation. The vein system of the Eifel Basin is consistent with results from other sedimentary basins, which may also include microstructural aspects.

References

- von Winterfeld, C-H (1994) Variszische Deckentektonik und devonische Beckengeometrie der Nordeifel — Ein quantitatives Modell. PhD Thesis, RWTH Aachen, Aachen, 319 pp.

Microstructures of fibrous halite veins *Poster*

Christoph Hilgers¹ Gill Pennock²
 Zsolt Schlöder¹ Stansilaw Burliga³
 Janos L. Urai¹

Introduction

Halite veins hosted in clastic sedimentary rocks are frequently observed next to evaporite layers. Their microstructure can be enhanced by gamma irradiation and etching, which can be used to infer the deformation mechanism of halite (e.g. Howard & Kerr 1960, Schleder & Urai 2005). In this study, we present results from gamma-decorated vein microstructures of fibrous halite veins hosted in claystone.

Data

Samples were taken in the Klodawa salt mine in Poland and the Hengelo mine in the Netherlands. Both locations expose halite veins with a white and orange colour. The halite host rock, which is the source of halite precipitated in the vein, is located centimeters to meters away from the veins. The vein microstructure is fibrous with variable fibre diameters, and slightly widens towards the vein-wall interface. This indicates antitaxial vein growth from the centre towards the wall and precipitation of new material on both sides of the vein. Fibre grain boundaries are straight and not serrated. Irradiated samples show that some fibres consist of subgrains, which formed during growth.

¹ Geologie-Endogene Dynamik, RWTH-Aachen, D-52056 Aachen, Germany

² Utrecht University, Faculty of Earth Sciences, 3508 TA Utrecht, The Netherlands

³ Wrocław University, Department of Structural Geology, ul. W. Cybulskiego 32, 50-205 Wrocław, Poland

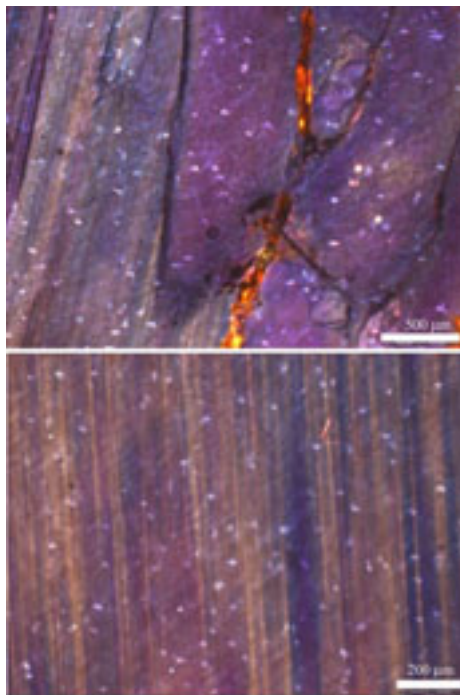


Figure 1: Gamma-irradiated fibrous halite veins show different fibre widths ranging between millimeters to microns. Micron-scale fibres are growth subgrains, while deformation subgrains are absent in the vein. Klodawa mine, Poland.

Overall, the vein is devoid of deformation subgrains. Repeated solid- or fluid inclusion bands have not been observed in the veins, which would point to the crack-seal mechanism causing vein opening (see also Hilgers & Urai 2005 for similar conclusion on antitaxial gypsum and calcite veins).

EBSD analysis suggests a random texture (Fig. 2), which is also apparent in colored maps showing the crystal directions of the grains. Thus, significant growth competition is absent and grains continue to grow regardless of their crystallographic orientation. Growth in an

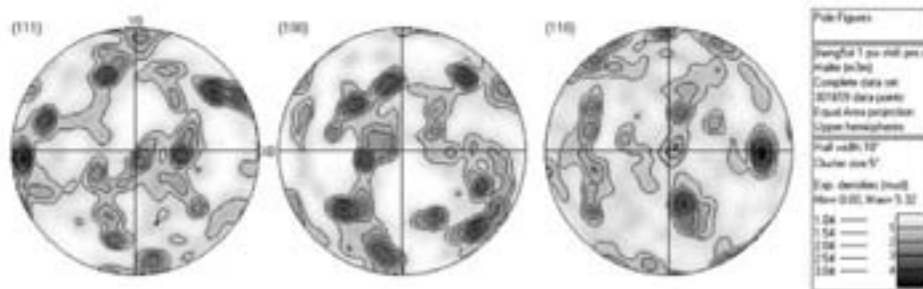


Figure 2: The fibrous halite vein from Hengelo shows a random texture (137 grains measured).

open vug would result in euhedral crystals and significant growth competition, while randomly oriented fibrous grains require contact with the wall rock during growth (Hilgers et al. 2001).

Conclusion

Fibrous antitaxial halite veins formed in extension fractures in claystone. Microstructural indicators for repeated crack-seal mechanism are absent, and thus veins may rather have formed during a continuous growth process. The bulk permeability of the fractured rock was low even if the vein aperture reaches several centimetres, because a random crystallographic texture of the vein microstructure requires close contact between the growing vein and the host rock.

References

- Hilgers C, Koehn D, Bons PD & Urai JL (2001) Development of crystal morphology during uniaxial growth in a progressively widening vein: II. Numerical simulations of the evolution of antitaxial fibrous veins. *Journal of Structural Geology*, 23, 873–885
- Hilgers C & Urai JL (2005) On the arrangement of solid inclusions in fibrous veins and the role of the crack-seal mechanism. *Journal of Structural Geology*, 27(3), 481–494

Howard & Kerr, RC (1960) Blue halite. *Science*, 132(3443), 1886–1887

Schleder Z & Urai JL (2005) Microstructural evolution of deformation-modified primary halite from the Middle Triassic Röt Formation at Hengelo, The Netherlands. *International Journal of Earth Sciences*, 94, 941–955

Magnetic fabric in ilmenite-rich norites of the Bjerkreim-Sokndal Layered Intrusion, Norway *Poster*

Ann M. Hirt¹ Volkmar Schmidt¹
Suzanne McEnroe² Florian
Heidelbach³ Peter Robinson²

Introduction

The Bjerkreim-Sokndal (BKS) is a layered intrusion, located in the Mid-Proterozoic Egersund anorthosite-norite province within the Sveconorwegian province of the Baltic Shield, south Norway. The layered intrusion formed

¹ Institute of Geophysics, ETH Hoenggerberg, CH-8093 Zurich, Switzerland ² Geological Survey of Norway, N-7040, Trondheim, Norway ³ Bayerisches Geoinstitut, University of Bayreuth, 95440 Bayreuth, Germany

by influxes of more primitive magma into more evolved magma to produce six Megacyclic units (MCU), each of which can be divided into up to six subunits. From bottom to top in each megacycle the rocks consist of early plagioclase-rich norites, intermediate hemo-ilmenite-rich norites and later magnetite-rich norites. Aeromagnetic maps over the intrusion show large negative and positive anomalies. A negative anomaly with amplitude to -13000 nT at 60 m above ground is associated with hemo-ilmenite-rich norite layer MCU IVe. This layer IVe contains plagioclase, orthopyroxene, hemo-ilmenite, magnetite, and minor clinopyroxene, biotite, apatite and sulfides. Multi-domain (MD) magnetite makes up 2–3% of the rock.

The negative magnetic anomaly associated with MCU IVe reaches its most negative value on the east limb of the Bjerkreim Lobe near Heskestad. The anomaly at Heskestad is part of a longer negative anomaly, which follows MCU IVe for more than 20 km around a large syncline. The average NRM intensity decreases from 25 A M^{-1} along the east fold limb to 10 A M^{-1} towards the hinge area to 7 A M^{-1} at the hinge. The BKS has a penetrative deformation fabric within the syncline with the weakest deformation found in the hinge area and the strongest on the east limb. Electron backscatter diffraction (EBSD) was used to determine the lattice-preferred orientation (LPO) of orthopyroxene and ilmenite. The (100)-planes of the orthopyroxenes are found to lie parallel to a foliation in the rock, which is sub-parallel to the cumulate layering. Orthopyroxene c-axes form the steep lineation within the foliation plane.

The anisotropy of magnetic susceptibil-

ity (AMS) was measured for samples that were taken at five locations from the eastern limb to the hinge area of the syncline to investigate if the change in NRM intensity could be related to magnetic fabric.

Magnetic Fabric

The AMS of the norite samples was measured in low fields with an AGICO KLY-2 susceptibility bridge at room temperature (293 K) and liquid nitrogen temperature (77 K). At room temperature the AMS ellipsoid is triaxial with a grouping of maximum axes down-dip in the foliation plane and minimum axes sub-parallel to the pole to foliation. The degree of anisotropy is lower in the hinge area compared to localities on the limb of the syncline. The average, low-field susceptibility increases by a factor of 2.2 to 3.2 at low temperature, which indicates that both ferromagnetic and paramagnetic minerals are responsible for the low-field susceptibility. This grouping becomes less distinct at low temperature; the shape remains triaxial although the degree of anisotropy increases. There is also a slight change in the orientation of the ellipsoid at 77 K, which may be related to the increased contribution of the paramagnetic phases to the magnetic susceptibility at low temperature, and this will be discussed in conjunction with the mineral fabric. To understand better which mineral fraction is controlling the AMS at the two temperatures, i.e., the ferromagnetic or paramagnetic, the AMS was measured subsequently in high-fields with a torque magnetometer at 293 K and 77 K on selected samples. The torque is dominated by the ferromagnetic phases at both temperatures. The orientation of the ferromagnetic ellip-

soid is at 293 K is in agreement with the orientation of the low-field AMS. The paramagnetic AMS is similar is tilted slightly with respect to the ferromagnetic AMS, but both are triaxial in shape. At 77 K the orientation of the ferromagnetic subfabric rotated clockwise with respect to its orientation at 293 K. Magnetite is the dominant carrier of the susceptibility anisotropy. It must be noted that magnetite undergoes a transition in its crystallographic structure from cubic to lower symmetry below the Verwey transition at approximately 120 K. Above the Verwey transition magnetite is dominated by shape anisotropy, i.e., shape of the magnetite grains, whereas below the Verwey transition, magnetite is dominated by a strong crystalline anisotropy. The change in magnetic fabric will be discussed in the context of the mineral fabric of orthopyroxene and ilmenite.

Strukturgeologische Geländestudie im Mittleren Buntsandstein zur Nutzung als geothermisches Reservoir

Poster

Stefan Hoffmann¹

Müller¹ Sonja L. Philipp¹ Agust Gudmundsson¹

Christian
Agust

Zur Nutzung von Erdwärme aus Teufen zwischen 2–5 km werden häufig Systeme aus einer Injektions- und Förderbohrung („Dublekton-System“) genutzt. Dabei wird durch die Injektionsboh-

rung ein Fluid in den Untergrund verpresst, welches sich erhitzt und durch die Förderbohrung wieder an die Oberfläche gelangt. Ein wesentlicher Parameter für die produktive Nutzung von solchen Dublekton-Systemen ist eine hohe Permeabilität der Gesteine im Untergrund. Häufig werden in solchen geothermischen Reservoiren die Wegsamkeiten für Fluide von Brüchen kontrolliert, die bereits vorhanden sind oder künstlich erzeugt werden müssen (hydraulische Stimulation). Deshalb ist die Kenntnis über existierende Bruchgeometrien sowie Vernetzung der Bruchsysteme von fundamentaler Notwendigkeit zur Abschätzung der Permeabilität von geothermischen Reservoiren. Seismische Verfahren und Bohrkernanalysen besitzen im Allgemeinen dafür eine zu geringe Auflösung. Daher bieten sich dreidimensionale Rekonstruktionen des Bruchsystems aus analogen Obertageaufschlüssen an (vgl. Philipp et al. 2005; 2006).

Detaillierte strukturgeologische Geländestudien wurden dazu in Aufschlüssen des Mittleren Buntsandsteins in Bad Karlshafen (bei Höxter) und Reinhausen (bei Göttingen) durchgeführt.

Die Sandsteine des Mittleren Buntsandsteins wurden während der Trias im gesamten Norddeutschen Becken abgelagert. In Niedersachsen ist der Buntsandstein südlich des Harzes in weiten Arealen an der Oberfläche aufgeschlossen. Nördlich des Harzes ist der Mittlere Buntsandstein von jüngeren Sedimenten überdeckt und in geothermisch interessanten Teufen von ca. 3 km anzutreffen. Der Mittlere Buntsandstein ist durch einen sohlbankzyklischen Aufbau im gesamten Beckenbereich charakterisiert (Bachmann et al. 1999). Diese beginnen jeweils mit mächtigen Basissandstei-

¹ Geowissenschaftliches Zentrum der Georg-August-Universität, Abteilung Strukturgeologie und Geodynamik, Goldschmidtstr. 3, 37077 Göttingen

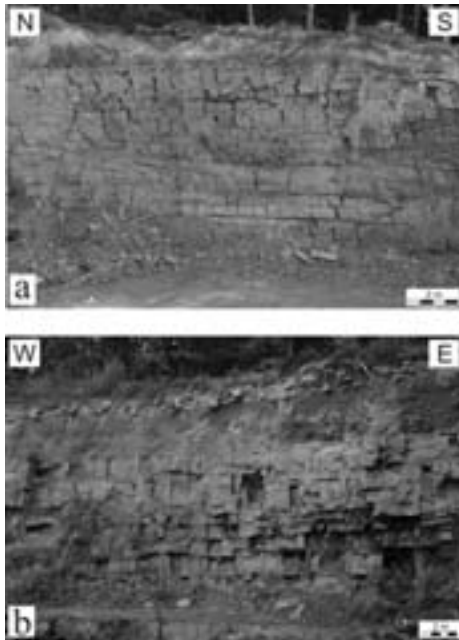


Abbildung 1: Aufschluss im Mittleren Buntsandstein bei Bad Karlshafen: a) Die N-S streichenden Klüfte bilden durch recht geradlinig verlaufende Kluftflächen relativ glatte Aufschlusswände; b) Die W-E streichenden Klüfte sind meist schichtgebunden, so dass Aufschlusswände mit deutlich hervorspringenden Bereichen entstehen.

nen, die im Hangenden in eine geringmächtigere Wechselfolge aus Sandstein-Bänken und Ton-/Schluffsteinen übergehen. Die Aufschlüsse dieser Gelände-studie decken diese unterschiedliche Fazies ab: Der Aufschluss in Reinhausen entspricht den mächtigen Basissandsteinen, hingegen ist in Bad Karlshafen die heterogene Wechselfolge aufgeschlossen. In den Geländeuntersuchungen soll untersucht werden, in wieweit Materialkontraste zwischen sandigen und tonig/schluffigen Gesteinsschichten die Bruchausbreitung beeinflussen.

In beiden Aufschlusslokalitäten tritt ein

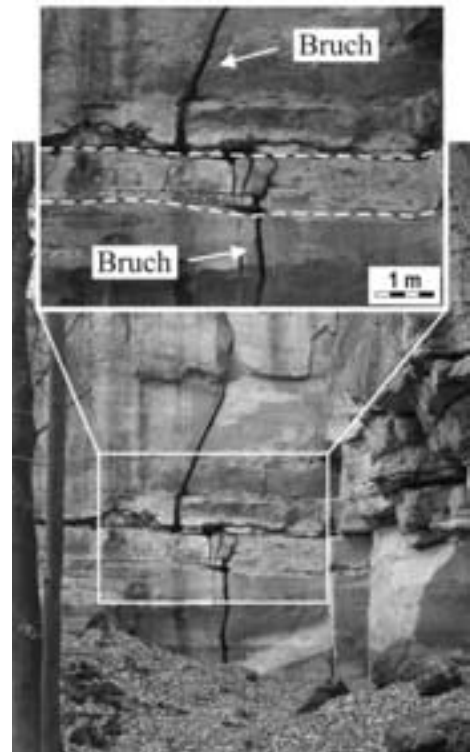


Abbildung 2: Abgelenkte oder gestoppte Bruchausbreitung in geschichteten Gesteinen (Reinhausen): dünne Tonschichten (weißgestrichelt) zwischen mächtigen Sandsteinschichten beeinflussen die Bruchausbreitung.

orthogonales Kluftsystem mit einer N-S und einer W-E streichenden Kluftchar auf (vgl. Philipp et al. 2006). Im Aufschluss in Bad Karlshafen setzen sich die N-S streichenden Klüfte oft durch mehrere Schichten fort. Diese Kluftchar weist eine geringe Richtungs- und Einfallstreue auf und bildet im Aufschluss meist auch sehr glatte Wände aus (Abb. 1a). Die Klüfte der W-E streichenden Schar sind hingegen schichtgebunden und zeigen eine weit größere Richtungsstreuung. Die Eigenschaf-

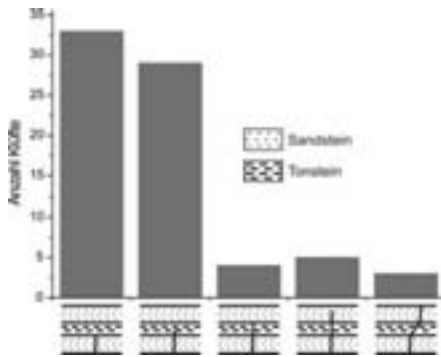


Abbildung 3: Terminationsverhalten von 74 Klüften an einer Tonschicht in Reinhausen. Die Tonschicht fungiert als Spannungsbarriere und stoppt die meisten Klüfte.

ten dieser zweiten Kluftchar führen zu Aufschlusswänden mit deutlich hervorspringenden Bereichen (Abb. 1b).

Im Vergleich zu Bad Karlshafen zeigen die dickbankigen Sandsteinschichten in Reinhausen größere Kluftabstände. Dies deutet auf einen Zusammenhang zwischen Bankmächtigkeit und Klufterhäufigkeit hin. Die meist groß-dimensionierten Klüfte reagieren überaus empfindlich auf dünne Tonsteinschichten (Abb.2). Tonsteinschichten können als Spannungsbarriere fungieren und den Verlauf von Klüften beeinflussen oder sogar terminieren.

Aus den Geländeuntersuchungen geht hervor, dass die Bruchausbreitung von der Schichtmächtigkeit und entscheidend vom Materialkontrast der unterschiedlichen Schichtpakete abhängt. Die Geländebeobachtungen zeigen, dass schon geringmächtige Lagen von Tonstein viele Klüfte stoppen oder ihren Verlauf ändern können (Abb. 3).

Anscheinend aber entspricht die mechanische Schichtung nicht immer der sedimentären Schichtung, wie zum Beispiel in Bad Karlshafen. Mehrere Schichten

können eine Einheit bilden und sich wie eine einzelne Schicht verhalten (Philipp et al. 2005). Diese Klüfte sind geothermischen Reservoiren von großer Bedeutung, da sie zusammenhängende Bruchnetzwerke bilden können und zu einer erhöhten Permeabilität des Reservoirs führen. Ein solches Bruchnetzwerk würde in einem geothermischen Reservoirgestein zu einem erwünscht hohen Fluidfluss führen.

Anscheinend aber entspricht die mechanische Schichtung nicht immer der sedimentären Schichtung. So bilden im Aufschluss in Bad Karlshafen mehrere Schichten häufig eine Einheit, die sich wie eine einzelne Schicht bei der Kluftausbreitung verhalten (Philipp et al. 2005). Diese Klüfte sind in geothermischen Reservoiren von großer Bedeutung, da sie zusammenhängende Bruchnetzwerke bilden und zu einer erhöhten Permeabilität des Reservoirs führen können. Ein solches Bruchnetzwerk würde im Mittleren Buntsandstein zu einer erwünscht hohen Permeabilität führen.

Danksagung Wir danken der Deutschen Bundesstiftung Umwelt für ein Promotionsstipendium für C. Müller, sowie den Steinbruchbetrieben Bunk und Niemeyer für den Zugang zu den Aufschlussflächen.

Literatur

- Bachmann GH, Beutler G, Hagedorn H & Hauschke N (1999) Stratigraphie der Germanischen Trias. In: Hauschke N & Wilde V (Hrsg.). Trias - Eine ganz andere Welt. Pfeil Verlag, München, S. 81–104
- Philipp SL, Oelrich A, Müller C, Hoffmann S, Bartelsen T, Thäter D & Gudmundsson A (2006): Strukturgeologische Studien als Beitrag zum Erfolg tiefegeothermischer Projekte. (in diesem Band)

Philipp SL, Hoffmann S, Müller C & Gudmundsson A (2005) Verringerung des Fündigkeitsrisikos für tiefegeothermische Projekte durch strukturgeologische Geländestudien und Numerische Modell. Geothermische Jahrestagung 2005, Unterschleißheim: 113–124

Deformation und Kinematik der Lechtal-Decke im nord-westlichen Rätikon, Nördliche Kalkalpen (Vorarlberg, Österreich) *Poster*

Tobias Ibele¹ Jan H. Behrmann¹

Diese Arbeit beschäftigt sich mit dem strukturellen Bau und der tektonischen Entwicklung der Lechtal-Decke im nord-westlichen Rätikon am Westende der Nördlichen Kalkalpen (NKA). Die Daten und Interpretationen beziehen sich zum Einen auf den gesamten Bereich der NKA im Rätikon westlich des Brandnertals und zum Anderen auf ein detailliert kartiertes Teilgebiet zwischen dem südlichen Brandnertal und dem südlichen Gamperdonatal. In- und außerhalb dieses Kartiergebiets konnten in Aufschlüssen der Arosazone, die das lokale Unterlager der Nördlichen Kalkalpen darstellt, kinematische Daten von Scherbändern erhoben werden. Auf der Basis der eigenen Arbeiten und publizierten Geologischen Karten der Region (Allemann 1985, Heissl 1965) wurde ein NW–SE-Profil durch das westliche Rätikon konstruiert und bilanziert. Die Anlage des Profils erfolgte senkrecht zum Überwiegenden Streichen der Großstrukturen die einen ausgeprägten

Schuppen- und Faltenbau zeigen. Das Kartiergebiet enthält die gesamte Abfolge der Nördlichen Kalkalpen vom skythischen Buntsandstein bis zu den oberkretazischen Kreideschiefern, sowie Gesteine der Arosazone. Das Strukturinventar des Kartiergebiets zeigt eine vorwiegend NW-gerichtete Vergenz in den tieferen Einheiten und eine vorwiegend N- bis NE-gerichtete Vergenz in den höheren Einheiten. Die beiden Domänen unterschiedlicher Vergenz sind durch den Horizont der karnischen Raibler-Schichten voneinander getrennt. Dabei ist in Bereichen, in denen die Raibler-Schichten größere Mächtigkeiten aufweisen der Vergenzkontrast zwischen prä- und postkarnischen Einheiten geringer als in Bereichen in denen die Raibler-Schichten stark reduzierte Mächtigkeiten aufweisen.

Die Strukturdaten der Arosazone im westlichen Rätikon zeigen überwiegend einen NW-gerichteten Transport des tektonisch Hangenden. Im Norden, wo Arosazone die Nördlichen Kalkalpen von Rhenodanubischem Flysch und nicht von der mittelpenninischen Falknis-Decke trennt, zeigt sich dagegen ein NE-gerichteter Transport des tektonisch Hangenden. Da der Rhenodanubische Flysch nach dem Mittelpenninikum überfahren wurde (Frisch 1979, Oberhauser 1995), zeigt sich hier möglicherweise ein Wechsel der tektonischen Verkürzungsrichtung mit der Zeit von NW nach NE.

Im Kartiergebiet wurden Raumdaten von insgesamt 123 Harnischen aufgenommen. Diese Daten wurden erst nach tektonisch sinnvollen Gruppen getrennt, und daraufhin eine Paläospannungsanalyse mit der RDM (Right Dihedra Method; Angelier & Mechler 1977) und der P/T-Achsen Methode (Marrett &

¹ Geologisches Institut, Universität Freiburg, Albertstr. 23B, D-79104 Freiburg

Allmendinger 1990) durchgeführt. Beide Methoden ergaben im Wesentlichen ähnliche Ergebnisse. Mit Ausnahme weniger lokaler Abweichungen zeigen alle Datensätze eine SE-NW gerichtete Orientierung der größten kompressiven Hauptnormalspannung (σ_1). Die ermittelte räumliche Anordnung der drei Hauptnormalspannungen zeigt nur für die Daten aus der Arosazone eine überschiebende Kinematik. Die Übrigen Daten zeigen abschiebende Kinematik. Die relativ homogene Orientierung der Paläospannungsachsen weist auf ein regionales Ereignis hin.

Die Profilbilanzierung wurde in zwei Einzelschritten vorgenommen: Eine spät-orogene Verkürzung des gesamten Profils, und eine vorhergehende interne Verkürzung und Verschuppung der Nördlichen Kalkalpen. Für den ersten Schritt wurde eine Einengung von 37% ermittelt. Er reflektiert eine späte tektonische Phase, die im Liechtensteiner Valorschtal Rhenodanubischen Flysch mit einschuppt und dem gesamten Profil die Geometrie einer weitspannigen Synform gibt. Im zweiten Bilanzierungsschritt wurden die einzelnen Schollen und innerhalb dieser das prä- und das post-karnische Gesteinspaket jeweils getrennt voneinander bilanziert. Dabei wurden verschiedene Verkürzungsbeträge zwischen 10% und 30% ermittelt. Die Bilanzierung musste für jede Scholle einzeln vorgenommen werden, da auf den die Schollen trennenden Störungen größere Seitenverschiebungsbeträge anzunehmen sind. Die aus der Profilbilanzierung ermittelten Verkürzungsbeträge nehmen entlang des Profils von Nordwesten nach Südosten ab. Auch die Übereinstimmung der entzerrten Zustände von prä- und post-karnischen Einheiten nimmt in diesem Verlauf ab. Der Grund

hierfür könnte in der nach Südosten zunehmenden Differenzierung in überwiegend NW-gerichtete Einengung im prä-karnischen Stockwerk und mit der Zeit zunehmende Einengung in NE-Richtung nur im post-karnischen Stockwerk zu suchen sein. Aus dem Befund einer mit der Höhe des tektonischen Stockwerks zunehmenden Rotation der Einengungsrichtung im Kartiergebiet folgt für den SE-Teil des Profils eine mit der Profilhöhe zunehmend senkrecht zur Profilebene gerichtete Einengungskomponente und somit eine zunehmende Unmöglichkeit korrekter Bilanzierung. Dieser zweite Bilanzierungsschritt reflektiert die frühe Kalkalpen interne Verkürzung und die Deformation während der Überfahung der Mittel- und Nordpenninischen Einheiten durch die NKA.

Im Kartiergebiet zeigt sich eine Vergenzänderung von NW nach NNE mit zunehmender stratigraphischer Höhe, aus den kinematischen Daten der Arosazone zeigt sich eine Vergenzänderung von W nach NE mit der Zeit. Da der nordwestliche Teil des bilanzierten Profils eine bessere Übereinstimmung zwischen den unterschiedlichen stratigraphischen Niveaus zeigt als der Südöstliche, scheint die NE-gerichtete Bewegung den nordwestlichen Teil des Gebirges ‚en-bloc‘, im Südöstlichen Teil aber nur die höheren Einheiten erfasst zu haben.

Zur späten tektonischen Phase gehört die Einschuppung des Rhenodanubischen Flyschs im Valorschtal, und die Bildung der Harnische im Rahmen eines konvergent überschiebenden Regimes. Die gleichzeitige Bildung der weitspannigen Synkinalstruktur des Gesamtprofils und die dadurch verursachte Ankipfung des in ihrem Südflügel befindlichen Kartiergebiets führt möglicherweise dazu, dass eine aufschiebende Kine-

matik der im Kartiergebiet vorgefundenen Harnische sich im heutigen Kartierbefund als überwiegend abschiebende Kinematik darstellt. Diese letzte Phase ist NW- bis N-gerichtet. Dafür sprechen die dem Kartenbild entnommene Aufschlußgeometrie des eingeschuppten Flysches im Valorschtal und die aus den Harnischdaten ermittelte Orientierung der Paläospannungsachsen. Deshalb konnte das in NW-SE-Richtung angelegte Profil für diese tektonische Phase gut bilanziert werden.

Literatur

- Allemann F (1985) Geologische Karte des Fürstentums Liechtenstein. 1:25.000. Hrsg.: Regierung des Fürstentums Liechtenstein. 1985.
- Angelier J & Mechler P (1977) Sur une methode graphique de recherche des contraintes principales egalement utilisable en tectonique et en seismologie: la methode des diedres droits. *Bull Soc geol France*, 19/6, 1309–1318
- Frisch W (1979) Tectonic Progradation and Plate Tectonic Evolution of the Alps. *Tectonophysics*, 60, 121–139
- Heissel W, Oberhauser R, Reithofer O, & Schmidegg O (1965) Geologische Karte des Rätikon. Maßstab 1:25.000. Hrsg.: Geol. Bundesanstalt Wien, Wien 1965
- Marrett R & Allmendinger RW (1990) Kinematic analysis of fault-slip data. *Journal of Structural Geology*, 12/8, 973–986
- Oberhauser R (1995) Zur Kenntnis der Tektonik und der Paläogeographie des Ostalpenraumes zur Kreide-, Paläozän- und Eozänzeit. *Jb. Geol. Bundesanstalt in Wien*, 138/2, 369–432

Remote Sensing Analyses of Neotectonic Active Regions in East-Kamchatka *Vortrag*

Fabian Jähne¹ Ralf Freitag¹

Introduction

The tectonic history of the Kamchatka Peninsula is dominated by continuous accumulation and amalgamation of terranes with different origins, which were delivered by convergence between the Pacific plate and in former times, the Kula plate against Eurasia (Freitag, 2002). The Kronotsky and Cape Kamchatka Peninsulas show that the collision of terranes and the resulting tectonics are still important for major parts of East-Kamchatka. While the collision of the Kronotsky Peninsula is sorely influenced by the convergence of the Pacific plate, the Cape Kamchatka Peninsula is affected by the collision of the Aleutian Arc with Kamchatka, what gives the opportunity to compare two different processes that resulted in the amalgamation of terranes to Kamchatka.

Data, analyse methods & object of work

In this work, neotectonic structures along the east coast of Kamchatka were analysed in detail. The study area includes the Kronotsky Peninsula, the Cape Kamchatka Peninsula and a part of the Kumroch Range that lies between them (Fig. 2). The available remote sensing data (Landsat TM7, ASTER, SRTM) were examined by the analysis of lineaments, terraces (Fig. 1), spectral properties and drainage networks all over the study areas. The analyse

¹ Friedrich-Schiller-Universität Jena — Institut für Geowissenschaften, Burgweg 11, 07749 Jena

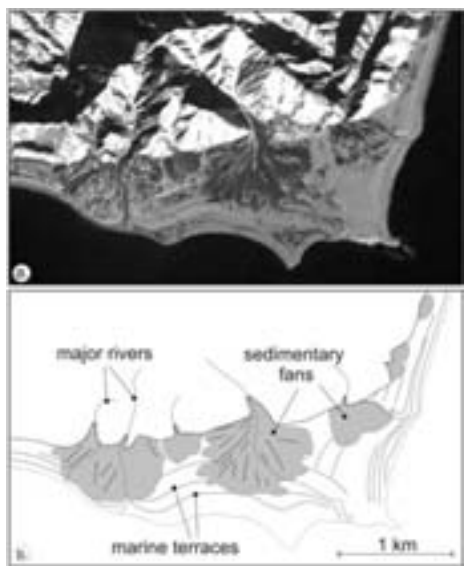


Figure 1: a.: detail image (Landsat TM7) of south-eastern Cape Kamchatka; b.: this interpretation of TM7 data show sedimentary fans which covers coastlines and marine terraces. (R. Freitag)

methods were chosen on the basis of their applicability to neotectonic structures and the available dataset. As no absolute ages of the terraces are available yet and because of the low resolution DEMs, only relative uplift could be determined for the study area. The result of all applied methods is a block-model of neotectonic active regions of eastern Kamchatka.

Results of remote sensing analysis

The results indicate that the Kronotsky and Cape Kamchatka Peninsulas are related to different neotectonic kinematics (Fig. 2). Both are also moving relatively to the Kumroch Range. But the applied analyses reveal that the style of deformation of the Kronotsky Peninsula has more similarities with the Kumroch

Range as the Cape Kamchatka Peninsula.

The results of terrace analysis imply that the Cape Kamchatka Peninsula is divided into several small parts with different vertical movement. A major part of horizontal shortening on the Cape Kamchatka Peninsula seems to be relieved in differential rock uplift along the east coast. The lineament and terrace analysis clearly show a segmentation of the peninsula. This segmentation is mainly caused by the impact of the Komandorsky strike-slip zone, whose faults form horsetail structures on Cape Kamchatka (Fig. 2). To the south of the peninsula the evidences for neotectonic activity increase. The southern part of the peninsula differs in topography, as well as in geology and the development of terraces from the northern and central parts of Cape Kamchatka. The neotectonics of Cape Kamchatka indicate that it can be associated to the Aleutian Arc.

The Kronotsky Peninsula seems to be less deformed by active tectonics than Cape Kamchatka. This Peninsula is probably uplifted en bloc. Several large thrust faults along the west side of the Peninsula indicate the collision of the Kronotsky-Terran with the accretionary wedge of East-Kamchatka (Fig. 2). The central part of the Kronotsky Peninsula is displaced to the NW along strike-slip faults and is interpreted to act as an 'indenter'. Young E-ENE striking lineaments which occur in Neogene volcanics (Railway Ridge) in the NW of Kronotsky are assumed to represent active dip-slip faults, which can be interpreted as Riedel shears with respect to the indenter. From this assumption an active displacement of the indenter can be inferred.

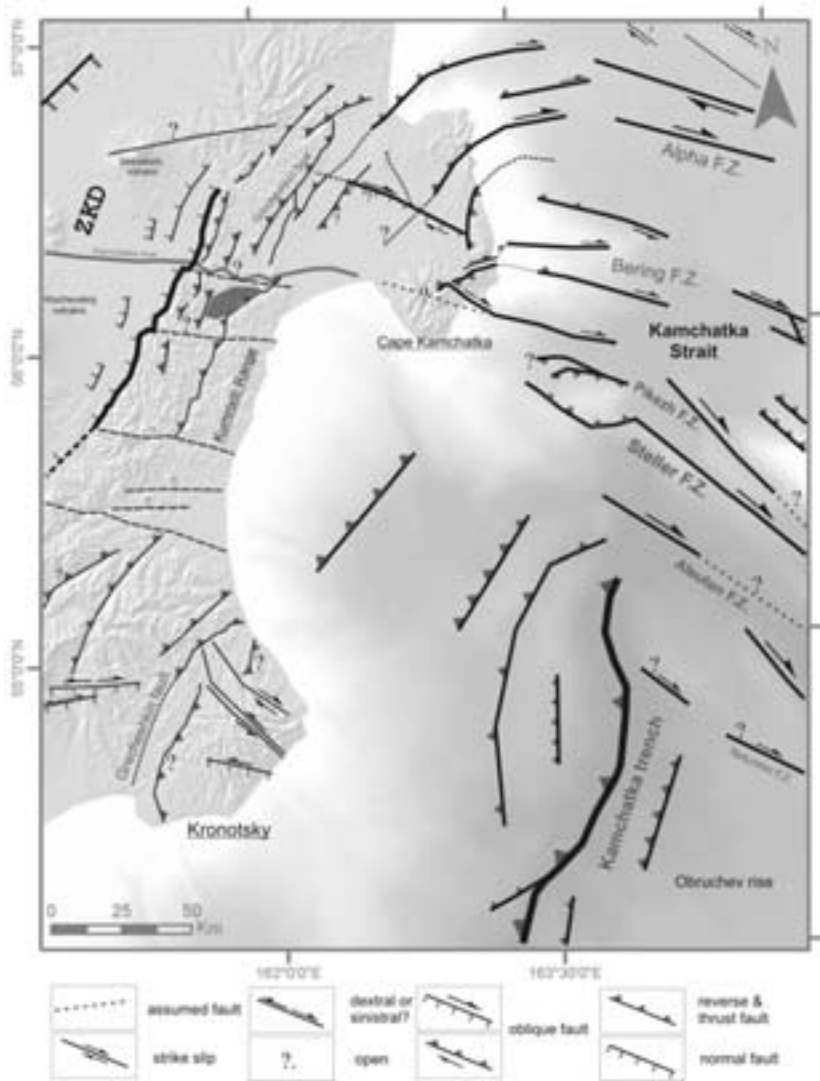


Figure 2: tectonic overview of eastern Kamchatka and the western Aleutian arc

The structure and uplift of the Kumroch Range (Fig. 2), between the Kronotsky and Cape Kamchatka Peninsulas, is interpreted to result from the subduction of the Pacific plate beneath East-Kamchatka. The Kumroch Range and the submarine accretionary wedge are

dominated by NE-NNE striking thrust faults. From the analysis of terraces it is suggested that this part of the Kumroch Range is uplifted *en bloc*.

References

- Freitag R, Gaedicke C, Baranov B & Tsukanov N (2001) Collisional processes at the junction of the Aleutian-Kamchatka arc: New evidence from fission track analysis and field observations. *Terra Nova* 13: 433-442
- Freitag R (2002) Inselbogenentwicklung im Kamchatka — Aleuten Kreuzungsbereich. Dissertation, Scientific Technical Report STR02/09, GFZ Potsdam
- Gaedicke C, Baranov B, Seliverstov N, Alexeiev D, Tsukanov N & Freitag R (2000) Structure of an active arc-continent collision area: the Aleutian-Kamchatka junction. *Tectonophysics* Vol. 325, 63-85
- Jähne F (2005) Fernerkundliche Analyse neotektonisch aktiver Gebiete in Ostkamchatka. Diplomarbeit, FSU Jena, Institut für Geowissenschaften
- Seliverstov N.I. (1998) Structure of the ocean floor around Kamchatka and geodynamic of the Kuril-Kamchatka / Aleutian junction area. *Nauchny Mir, Moscow*, (in Russian)



Figure 1: Measurement of the outcrop length l of data point 2 (see text)

The significance of fractures in Europe *Poster*

Philipp S. Jonas¹ Colin D. Ranten¹

Analytical modelling of geological fractures is now at an exciting stage. In view of the ever-mounting amount of fracture data available, and the need for a European overview of the state of the art, we correlate fractures from across the continent. In order to achieve relevant and meaningful statistics, the dataset of millions of entries was down-sampled to filter out inadequate and irrelevant values. The resulting data³ are the object of this study. For each fracture there exist measurements on the strike (s), dip (d), outcrop trace length or height (l) and aperture or thickness (a) (Fig. 1).

¹ Fractured Institute of Studies, 00007 Gutingi

² Institute of Near-Trivial Geological Studies, 34587 Altenbrunslar ³ 3 data

The data are: 1) An earthquake fracture (formed in the June 17th earthquake of M6.6 in the South-Iceland-Seismic-Zone) from a Pleistocene basaltic lava flow near Eyvik, South Iceland (s 163, d 90, l 30 m, a 0.47 m),

2) a calcite vein from a horizontal outcrop of limestone layer (Blue-Lias-Formation, Lower Jurassic), Kilve, Somerset Coast, Southwest England (s 095, d 73, l 2.1 m, a 0.0045 m), and

3) a joint from a vertical section in a quarry in sandstone (Solling-Formation, Middle Buntsandstein, Lower Triassic) from Bad Karlshafen, Central Germany (s 166, d 90, l 0.48 m, a 0.0025 m).

All the fractures are extension fractures. Although there is still some discussion about shear joints being sheared joints, but shear joints are shear nonsense. Whatever, the present fractures are ex-

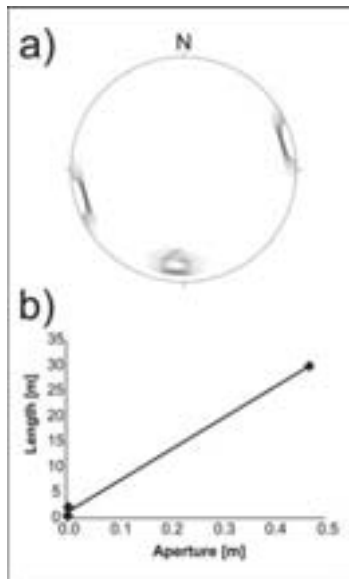


Figure 2: Meaningful presentation of our data. a) strike and dip density contours, b) scatter plot of aperture versus length)

tension fractures.

Figure 2a shows the density contours of the strike and dip measurements in a Schmidt-net stereo projection (equal area, equatorial projection, lower hemisphere). The average fracture strike is 141.33 (N38.67W), the average dip is 84.33. From the strike direction we infer the orientation of the minimum principal compressive stress (maximum principal tensile stress), σ_3 , as being 51.33°. The average aperture (thickness) of the fractures is 0.159 m; the average length is 10.86 m.

A scatter plot of aperture versus outcrop length (Fig. 2b) shows that the two variables are related to each other. Linear regression of the present data — with the aperture as the dependent variable y , the length as the independent variable x — results in the equation $y = 61.554x + 1.073$. The coefficient

of determination is $R^2 = 0.998$. With such a high correlation coefficient the correlation must be significant (but we would rather not run a statistical test with so few data points). This means that 99.8% of the variation in aperture is linearly related to the variation in outcrop length, and only 0.02% of the data variability cannot be explained by a linear regression.

We now use these data to calculate the fluid overpressure that formed these fractures (even if we do not know if they are hydrofractures, maybe they are, maybe not; the earthquake fracture from Iceland probably isn't, but who cares?). For a fluid-filled extension fracture modelled as a through crack there is a nice equation to calculate the static fluid overpressure (we don't present the equation here; we have the solution, it would not even be too long to print in this abstract, but we are too lazy to write all the symbols). And even if we don't care if the outcrop length is the controlling dimension, we still use this equation. For Young's modulus we use an average value of 79.157 GPa (based on an uneducated guess) and for Poisson's ratio a value of 0.2497 (ditto). Using the average aperture and outcrop length presented above, we obtain an average fluid overpressure of 617.99 MPa.

From this overpressure we can infer the depth to the source of the fluid that formed these fractures. Using an *in situ* tensile strength 579.7 kPa (yielding an upper limit for the excess pressure of the source rock and one fourth of the maximum differential stress), an average rock density of 2468 kg m⁻³ and an average fluid density of 975.12 kg m⁻³ (some water, some oil, some gas) we obtain a depth of 42000.10 m below the present

surface.

This signifies that these fractures originated at depths somewhat greater than that of Moho beneath Europe, that is, in the lithospheric mantle. Extrapolating these significant results to the rest of our planet, it follows that there must thus be a lot of fluid in the mantle. Even if extrapolation to the moon, other planets, or beyond our solar system is maybe not valid, these results are not only significant but very important, and obviously extremely interesting.

Remarks

This work is not funded by anyone. Who should care about this nonsense? Anyway, we like doing field work in the sunshine. This is why we selected localities particularly in SW-England and Iceland . . .

We could have written this text in German. However, we felt that it sounds much more scientific in English, doesn't it?

The data presented here are original data from our field note books. The calculations are based on real equations that in fact are useful. The statistics and the conclusions presented here, however, are maybe not quite matching any scientific standards.

The fate of sandstone during impact cratering: shock compaction, cataclastic flow, and granular fluidization *Vortrag*

Thomas Kenkmann¹

Impact of solid bodies is the most fundamental of all processes that have taken place on the terrestrial planets in our Solar system (Shoemaker 1977). On Earth, impact cratering was the dominant geologic process during the period of the early heavy bombardment until 3.8 Ga. A constant asteroid impact flux exists since that time. Although deformation of the crust by meteorite impacts is now subordinate with respect to tectonics, it represents an important, but often underestimated fraction of the bulk crustal deformation. Short-term deformation during hypervelocity impact events differs in many respects from standard tectonics: Unique conditions exist at pressures above the so-called Hugoniot elastic limit (HEL) of a particular mineral or rock. This state of compression is reached in a shock wave that propagates from the point of impact. Shock waves travel at supersonic velocity, heat and irreversibly deform the rock, and cause a residual motion of the material they have passed, which ultimately leads to the formation of parabolically shaped crater cavity of much larger extent than the projectile diameter. At pressure above the HEL minerals are subjected to shock metamorphism. For instance, the HEL of quartz is in the range of 3–5 GPa, pending on crystallographic orientation. With increasing

¹ Institut für Mineralogie, Museum für Naturkunde, Humboldt-Universität Berlin, Invalidenstrasse 43, 10115 Berlin

shock pressure, quartz first displays reduction in refraction indices and birefringence (10–35 GPa). Localized amorphization occurs in this pressure interval along certain crystallographic directions and leads to the formation of so-called *Planar Deformation Features* (PDF) in which small stishovite crystals can form. PDFs are among the most important diagnostic features to prove the existence of ancient impact structures. Above 35 GPa quartz is completely transformed to amorphous glass while keeping its initial shape (diaplectic glass). Clusters of coesite can grow within this solid-state glass. Above 50 GPa quartz melted upon pressure release, as indicated by the formation of schlieren and vesicles. Vaporization of quartz is completed at about 100 GPa upon pressure release (Stöfler & Langenhorst 1994). The volume of rock affected by shock metamorphism increases unproportionally strong with increasing crater size. Since pressure decays with increasing distance from the point of impact, the zone of shocked rock is surrounded by a zone in which deformation by strong pressure waves occurs without indications of shock metamorphism. Deformation products of this area comprise cataclastites, monomictic and polymictic breccias, dikes, pseudotachylites, and variously faulted and folded rocks. The period of deformation during initial compression, and the subsequent excavation flow and crater modification at ambient pressure is in the order of seconds to minutes, pending on crater size. However, even in this short period the physical boundary conditions for deformation change in time and space and lead to a complex deformation path in which reversals in motion direction are com-

mon. A general characteristic of deformation during excavation is a radial symmetric, divergent, outward and upward directed flow. This is followed by an inward directed, convergent flow that dominates the gravity-driven crater collapse (Kenkmann 2002). Here, the deformation history of porous sandstone during impact cratering is presented. These rocks were investigated experimentally (Kenkmann 2006), and in the deeply eroded Upheaval Dome impact crater, Utah (Kenkmann 2003, Kenkmann et al. 2005). We can distinguish three stages of deformation: (i) deformation above the HEL of quartz, (ii) deformation at confining pressure below the HEL, (iii) deformation at fluctuating ambient pressure during the excavation and modifications stage of the cratering process:

- i) Porous rocks behave differently in shock waves with respect to non-porous, dense rocks. Before the rock can be pervasively compressed, the pore space must collapse. Thus, a large amount of shock wave energy is spent for compaction prior to compression. This leads to reduced shock magnitudes, unusually high target heating, and more rapid shock decay. Since volume and size of the crater depend on shock magnitude and the decay in shock pressure with distance, the resulting crater will be smaller than a crater in a dense rock with the same bulk density. In weakly-shocked porous sandstone (<10 GPa) pore closure is accomplished by brittle fracturing of grains, in moderately and strongly shocked rocks, pore space collapse is accomplished by jetting, the extrusion of melted streams of hot

SiO₂ material into the pores (Kieffer et al. 1976). PDF formation is relatively rare in porous sandstone. Most of the shock metamorphosed rock volume will be ejected from the crater.

- ii) At pressures below the HEL shock metamorphism of quartz does not occur. But the attenuated shock wave still provides a considerable pressure and initiates a cataclastic flow within porous sandstones. Distributed cataclastic flow is defined as a microscopically brittle process in which a material's coherence is reduced by pervasive microcracking that affects the entire rock. The distributed cataclastic flow in the sandstones is initiated by grain crushing, collapse of pore space, and subsequent intergranular shear. An important result of the deformation at high confining pressure is that the cohesive sandstone is transformed to a non-cohesive sand by pervasive, delocalized intergranular cracking. Hence, further deformation is controlled by frictional properties rather than the fracture toughness of the rock.
- iii) It is well-known that the strength properties of rocks are temporarily strongly reduced after the shock wave has passed through the rocks. Disturbances of the shock wave lead to strong residual seismic noise and vibrations behind a shock wave; a process which is called acoustic fluidization (Melosh 1979). The basic idea of acoustic fluidization is that seismic vibrations of grains, fragments, or blocks within the target result in fluctuations of the overburden pressure, which leads to slip

events in periods of low pressures and reduced frictional strength. In terms of rheology the fluidized rock can be described with the properties of a Bingham plastic material (Melosh & Ivanov 1999), which is characterized by a linear viscous behavior after a yield strength is exceeded. Deformation at such fluctuating ambient pressures allows dilatancy and a rearrangement of grains in periods of unloading. Hence, the cataclastically deformed sandstones behave like unconsolidated sand and most likely deform in a pervasive granular flow. A macroscopic result of granular flow of sandstones during impact crater collapse is the formation of large sandstone dike networks, which occur, e.g. in the center of the Upheaval Dome impact crater, Utah. These dikes show extreme thickness variations, blind terminations and frequent embranchments at nodular-like points and indicate an almost complete loss of internal coherence during deformation. Fluidized sandstone accommodates space incompatibilities that arise from the deformation of more competent target rocks.

References

- Shoemaker EM (1977) In: Roddy DJ et al. (eds) *Impact and explosion cratering*, Pergamon Press, New York, 1–10
- Stöffler D & Langenhorst F (1994) *Meteoritics*, 29, 155–181
- Kenkmann T 2002, *Geology*, 30, 231–234
- Kenkmann T, Thoma K & the MEMIN team (2006) *LPSC*, 37, #1587
- Kenkmann T (2003) *EPSL*, 214, 43–58
- Kenkmann T, Jahn A, Scherler D & Ivanov, BA (2005) *GSA Spec. Pap.*, 384

- Kieffer SW, Phakey, DP & Christie, JM (1976)
Contrib Min Petrol 59, 41–93
- Melosh HJ, (1979) J Geophys Res 84, 7513–7520
- Melosh HJ & Ivanov BA (1999) Annu. Rev. Earth Planet Sci 27, 385–415

Die hydrogeologische Wirksamkeit von Störungen am Beispiel des Talhof-Störungssystem (Ostalpen, Österreich) *Poster*

Eva Kiechl¹ Robert Rabitsch¹
Heiko Gaich¹ Walter Kurz¹
Gerfried Winkler²

In der oberen Kruste sind Störungszonen üblicherweise aus komplexen Netzwerken von diskreten Brüchen unterschiedlicher Genese zusammengesetzt. Sie stellen daher meist maßgebliche Zonen bevorzugter unterirdischer Wasserwegigkeiten dar. Außerdem sind sie somit wesentlich für die hydrogeologische Beurteilung von Gebirgskörpern, da massive Wassereinträge im Untertagebau sehr häufig an Störungszonen gebunden sind.

Solche Störungszonen zeigen für gewöhnlich eine räumlich-zeitliche Entwicklung vom Ausgangsgestein zu vollständig ausgeprägten Störungszonen mit einer internen strukturellen Gliederung (Protolith — damage zone — fault core).

Die hydraulische Bewertung von Störungen ist ein wesentlicher Eingangsparameter für eine numerisch hydraulische

Modellierung von Gebirgskörpern. Hierfür ist es notwendig das hydraulische Verhalten und die Wirksamkeit der verschiedenen Bereiche der Störung zu beschreiben und für die modellhafte Umsetzung mit hydraulischen Kenngrößen zu belegen.

Das Ziel der Arbeit ist eine Korrelation von strukturgeologischen Parametern mit hydraulischen Parametern (k_f , T , ...). Dies kann als eine hydraulische Kalibration der einzelnen Störungsklassen in Verbindung mit Wasserdurchlässigkeit angesehen werden

Für eine Fallstudie wurde als Testgebiet das Talhof-Störungssystem im Nordostteil der Ostalpen (Semmering-Raxgebiet, Österreich) gewählt. Diese subvertikale, ca. E–W streichende Talhof-Störung zeigt links-lateralen Versatz und schneidet permo-triassische Sequenzen (Quarzite, Karbonate) der unterostalpinen Einheiten, welche den unteren Teil einer permomesozoischen Cover-Sequenz bilden. Im Untersuchungsgebiet zeigen sie eine sub-vertikale Lagerung und streichen E–W bis NE–SW. Diese Gesteinseinheiten sind durch unterschiedliche Rheologie und daher unterschiedlichem Deformationsverhalten charakterisiert. Im bearbeiteten Bereich schneidet die Talhofstörung die primäre Quarzit-Karbonatabfolge spitzwinkelig. Bruchhafte Strukturen in den Karbonaten sind charakterisiert durch die Bildung von diskreten Brüchen (Scher- und Extensionsbrüche) und zementierten tektonischen Breckzien. Innerhalb der Quarzite ist der Protolith durch beinahe vollständige Auflockerung bis zur Bildung von kohäsionslosen Kakiriten gekennzeichnet.

Kartierungen im Kleinmaßstab (Lithologie, Bruchstrukturen), und die

¹ Institute of Applied Geosciences, Graz, Austria ² Joanneum Research, Institute of Water Resources Management, Graz, Austria

detaillierte Untersuchung repräsentativer Aufschlussbereiche (incl. der Aufnahme von Scan-lines) geben Detailinformationen über die Geometrie des Bruchsystems. Für die hydraulische/hydrogeologische Auswertung und Analyse werden in erster Linie die richtungsgebundenen Kluftvolumina bestimmt. Hierfür werden Kluftsystemparameter wie Raumlage, Öffnung, linearer Durchtrennungsgrad sowie kumulative Öffnungsparameter (z.B. Auflockerung des Gebirges, relativer Anteil an Porenvolumen) u.dgl. aufgenommen und mittels statistischer Methoden (Clustering — hierarchisch, fuzzy c-mean) nach objektiven Kriterien ausgewertet. Die Kakirite werden auch mittels labormäßige Porositätsmessungen untersucht, um Rückschlüsse über Speicherverhalten und Durchlässigkeiten zu erhalten. Auf Basis dieser Daten können bestimmte Domänen definiert werden, denen jeweils spezifische hydraulische Wirksamkeiten zugeordnet werden kann.

Bei der statistischen Auswertung muss besonders auf die in unterschiedlicher Qualität und Maßstab vorliegenden Datensätzen zwischen den ober- und untertägig erhobenen und aufgenommenen Parametern Rücksicht genommen werden. Ebenso muss ein gemeinsamer Bewertungsschlüssel zwischen strukturgeologischer Gebirgsbeschreibung und hydrogeologischer Bewertung hinsichtlich Konsistenz und Vergleichbarkeit erarbeitet werden. Dies ist vor allem notwendig, um geologisch erhobene Parameter in bestehende hydrologische/hydrogeologische Berechnungs- und Modellierungsverfahren zur Ermittlung von Speichervolumina und hydrographischen Einzugsgebieten einfließen lassen zu können.

Als Resultat der statistischen Auswertungen werden die Parameter in Gruppen bzw. Klassen unterteilt. Weitere Unterteilungen bzw. Klassifizierungen, unter anderem in Hinblick auf unterschiedliche Auswirkungen auf verschiedene lithologische Einheiten, sind Bestandteile der statistischen Auswertung. In weiterer Folge werden die Ergebnisse der statistischen Auswertungen (objektiv) der subjektiven hydrogeologischen Gesamtbeschreibung der Störungen interpretativ gegenübergestellt. Zudem können die ermittelten hydraulischen Kennwerte den errechneten Porositäten und Kluftvolumina der Störungen gegenüber gestellt und verglichen werden. Dies stellt auch einen wesentlichen Bearbeitungsschritt in der Ausweisung hydrographischer Einzugsgebiete in Festgesteinskörpern dar, da Störungen einen wesentlichen Einfluss in Bezug auf deren Erstreckung und Ausdehnung haben. In Verbindung mit hydrologischen Daten (Wasserbilanz) sind die somit wichtige zusätzliche Eingangsdaten für die Berechnung von Bergwasserzutritten (Spitzenzutritte und Beharungsmengen) vorhanden.

Methodische Untersuchungen am Kreta-Detachment (Kreta, Griechenland): Anzeichen für eine alpidische Metamorphose der Hangendscholle

Vortrag

Thomas Klein¹ Gernold Zulauf¹ John Craddock² Johannes Glodny³

Einführung

Die Insel Kreta bildet den südlichen Rand der externen Helleniden, welche üblicherweise in zwei Deckenstapel untergliedert werden: Die unteren Decken (Plattenkalk und Phyllit-Quarzit-Einheit) sind durch eine alpidische HP-Metamorphose (Oligozän/Miozän) gekennzeichnet (Seidel et al. 1982, Jolivet et al. 1996), welche im Hangenden bislang nicht nachgewiesen wurde. Die Oberen Decken (i.w. Tripolitza- und Pindos-Einheit) bestehen aus karbonatischen Gesteinen und sind für eine petrologische PT-Abschätzung ungeeignet. Aufgrund des Gesteinshabitus wurden sie als unmetamorph eingestuft. Schlußfolgernd wird der Kontakt der beiden Stapel seit etwa zwanzig Jahren als krustales Megadetachment („Kreta-Detachment“) aufgefaßt (Jolivet et al. 1996, Fassoulas et al. 1994, Kiliass et al. 1994), wobei Versatzbeträge von über 100 km angenommen werden (Ring et al. 2001, 2001).

Ziel dieser Arbeit ist es Gemeinsamkeiten und Unterschiede der unmittelbar an das Detachment angrenzenden Einheiten herauszuarbeiten, um Rück-

schlüsse auf die tatsächliche Signifikanz der Störungszone zu ziehen.

Methoden

Es wurden neben der röntgenographischen Bestimmung der Illitkristallinität (IK) zusätzlich Kalzitwillinge zur Temperaturabschätzung herangezogen. Die IK wurde an luftgetrockneten Texturpräparaten mit standardisierter Belegungsichte ermittelt. Die Umrechnung der gemessenen Halbhöhenbreiten erfolgte mittels CIS-Standardisierung (Warr und Rice 1994). Kalzitwillings-Thermometrie (Burkhard 1993, Ferrill et al 2004) erfaßt im Gegensatz zur IK eher das Temperaturregime während einer Deformation.

Die Verformung der Gesteine ließ sich im Falle der Phyllit-Quarzit-Einheit E-Kretas mit der R_f/ϕ - und der (normalisieren) Fry-Methode quantifizieren.

Um die Raumlage der prinzipiellen Verformungsachsen in Tripolitza- und Phyllit-Quarzit-Einheit zu rekonstruieren, wurde die statistische Orientierung der Kalzitwillinge im geographischen Referenzrahmen probenweise erfaßt (n. Grohng 1972). Streß- und Strainellipsoid sind in bei fehlender Vorzugsorientierung der Kalzite kongruent (Burkhard 1993). Streßmagnituden wurden mit dem Kalzitwillingsintensitäts-Paläopiezometer nach Rowe und Rutter (1990) bestimmt. Die erzielten Absolutwerte für den differentiellen Stress erscheinen zwar zu hoch, sollten jedoch untereinander vergleichbar sein.

Ergebnisse

Die Geländebefunde zeigen für E-Kreta, dass in beiden Einheiten bruchhafte Verformung stattfand. Die basalen Anteile der Tripolitza-Einheit sind dabei vollständig brekziiert. Auf Klasten

¹ Johann Wolfgang Goethe-Universität, Senckenberganlage 32-34, 60325 Frankfurt am Main ² Macalaster College, Geol. Dept., St. Paul, 1600 Grand Ave., Mn 55105 ³ GeoForschungsZentrum Postdam, Telegrafenberg C2, 14473 Potsdam

der kataklastisch überprägten Phyllit-Quarzit-Einheit treten spröde Strömungen und Kalzitfaserminerale mit Top-SW Kinematik auf. Während die Tripolitza-Einheit in der Regel steile Abschiebungen, teilweise aber auch horizontale Bruchflächen mit assoziierten Riedel-Scherflächen aufweist, treten in den darunterliegenden triassischen Rotsedimenten zudem E-W streichende Dehnungsrisse, Abschiebungen (z.T. listrisch), Knickbänder, und N-S verlaufende Streckungslineare auf.

In W-Kreta konnten in den basalen Anteilen der Tripolitza-Einheit Top-WNW-Bewegungen nachgewiesen werden, womit die Streckungsfaser parallel zur den dortigen Faltenachsen verläuft. Die Brekzierung ist deutlich schwächer, das Gestein meist homogranular mikroparitisch. An der Probenlokalität Falasarna (W-Küste) kam es zum metamorphen Wachstum von Hellglimmern. Da dies eine Ausnahme ist, ist der Metamorphosegrad der Tripolitza-Einheit am einfachsten mit den klassischen Methoden zur Intensitätsabschätzung einer niedergradigen Metamorphose bestimmbar.

Deren Anwendung zeigt ebenfalls, dass eine schwachmetamorphe Überprägung der Tripolitza-Einheit vorliegt. Selbst die Kalzitverzwillingung fand in beiden Einheiten etwa unter gleichen Bedingungen statt, wobei jedoch für einen Großteil der kretischen Gesteine gilt, dass nur dünne Zwillinge auftreten, wie sie für Temperaturen weit unter 200°C charakteristisch sind.

Speziell in E-Kreta erscheint die Phyllit-Quarzit-Einheit zudem auch diagenetische Anteile zu beinhalten, wobei die Tripolitza-Einheit hier anchizonale Bedingungen erfuhr, was eine inverse Metamorphose impliziert. Die fehlende me-

tamorphe Überprägung im Liegenden der Tripolitza-Einheit ist durch die sehr niedrige Illitkristallinitäten, niedrigen Partikel- und Matrixstrain, durch Kalzit- und Quarz-Mikrogefügen und relativ hohe Differentialspannungen belegt (vgl. Zulauf et al. 2002). Von einer retrograden Überprägung der Phyllit-Quarzit-Einheit im Zuge der Störungsaktivität ist laut Jolivet et al. (1996) abzusehen.

Deswegen sind Deckenbewegungen in E-Kreta die wahrscheinlichste Ursache. Das Vorhandensein einer jungen kompressiven Tektonik mit Deckenbewegungen wird aber vor allem durch die Tatsache gestützt, dass dort unmittelbar im Liegenden der Tripolitza-Einheit Neogene Anteile vorkommen, was mit keinem Detachment-Modell erklärbar ist (s.a. Fortuin 1977).

In W-Kreta ist eine inverse Metamorphose zwar nicht nachweisbar, doch auch hier erscheint der in der Literatur postulierte Metamorphosesprung überzogen, da sowohl in der Tripolitza-Einheit als auch in der Phyllit-Quarzit-Einheit anchi- bis epizonale Illitkristallinitäten gemessen wurden.

Die metamorphen Hellglimmer in W-Kreta zeigen zudem ähnliche Phengit-Gehalte, wie Gesteine der Phyllit-Quarzit-Einheit. Trotz des Fehlens einer kritischen Paragenese ist dieses ein Hinweis auf unterschätzte Druckbedingungen. U.a. aufgrund sehr geringer Korngrößen gelang es nicht ein robustes Rb/Sr-Alter zu gewinnen. Die ermittelte vier-Punkt Isochrone liefert mit $19 \pm 2,5$ Ma (MSWD = 9,8) jedoch ein Isotopen-Alter, welches den Ar-Ar Altern der Phyllit-Quarzit-Einheit W-Kretas entspricht.

Die Kalzitstrainanalysen zeigen, dass in Tripolitza-Einheit und Phyllit-Quarzit-

Einheit im wesentlichen schichtparallele (subhorizontale) Einengung stattfand, wobei vertikale Einengung ebenfalls vorkommt. Die statistischen Mittelwerte der Einheiten sind dabei nahezu identisch. Trotzdem deutet eine starke Streuung der Straintensoren auf eine polyphase Deformation unter einem sich änderenden Streßfeld hin.

Zusammenfassung und Schlußfolgerungen

Kreta wurde in den zurückliegenden beiden Dekaden als ein, im Rahmen der durch roll-back der ozeanischen Kruste Gondwanas induzierten Ägäischen Extension exhumierte, ‚kalter‘ metamorpher Kern-Komplex interpretiert. Dabei wurde als wesentlicher Mechanismus der Exhumierung der kretischen HP-Gesteine ein Megadetachment unmittelbar oberhalb der Phyllit-Quarzit-Einheit erwägt. Die vorliegenden Daten belegen jedoch einen wesentlich geringeren Metamorphose-Sprung, was sich auch mit jüngsten Literaturdaten deckt. In E-Kreta liegt sogar eine inverse Metamorphose vor. Dabei ist festzustellen, dass der Zeitpunkt der thermischen Überprägung in der Tripolitza-Einheit mit den Abkühlaltem der Phyllit-Quarzit-Einheit identisch ist. Auch zeigen die Geländebefunde nicht selten eine von den Literaturdaten abweichende Kinematik unmittelbar am Störungskontakt.

Die rezente Geländesituation ist damit wesentlich besser durch eine Tektonik zu erklären in der Kompression und Extension einander abwechselten, es zwar zur Exhumierung von HP Gesteinen kam, aber auch Krustenstapelung in kleinerem Maßstab stattfand. Dabei sind weder Magnituden noch die Raumlagen der Hauptnormalspannungen in einem

hohen Krustenstockwerk für alle Lokalitäten auf Kreta identisch gewesen. Ein ‚Kreta-Detachment‘ kann damit weder Ursache noch alleiniger Mechanismus der Exhumierung der HP-Gesteine Kretas sein. Offenbar ist die gesamte Extension entgegen bisheriger Vermutungen viel stärker delokalisiert und verteilt sich über ein Netz von Störungen innerhalb der Phyllit-Quarzit-Einheit. Die kataklastische Störungszone unmittelbar zwischen Tripolitza- und Phyllit-Quarzit-Einheit ist zumindest in E-Kreta durch Kompression entstanden.

Literatur

- Burkhard M (1993) Calcite twins, their geometry, appearance and significance as stress-strain markers and indicators of tectonic regime - a review. *Journal of Structural Geology*, 15(3-5): 351-368
- Fassoulas C, Kiliass A & Mountrakis D (1994) Postnappe stacking, extension and exhumation of high-pressure, low-temperature rocks in the island of Crete, Greece. *Tectonics* 13(1): 127-138
- Ferrill DA, Morris AP, Evans MA, Burkhard M, Groshong RH & Onasch CM (2004) Calcite twin morphology: a low-temperature deformation geothermometer. *Journal of Structural Geology*, 26(8): 1521-1529
- Fortuin A R (1977) Stratigraphy and sedimentology of the Neogene deposits in the Ierapetra Region, Eastern Crete. GUA Papers of Geology (PhD thesis, Univ. of Utrecht), 8, pp 164
- Groshong R H (1972) Strain calculated from twinning in calcite. *Geol Soc Am Bull*, 83(7): 2025-2038
- Jolivet L, Goffe B, Monie P, Truffert LC, Patriat M & Bonneau M (1996) Miocene detachment in Crete and exhumation P-T-t paths of high-pressure metamorphic rocks. *Tectonics*, 15(6): 1129-1153
- Kiliass A, Fassoulas C & Mountrakis D (1994) Tertiary extension of continental crust and uplift of Psiloritis metamorphic core complex in the central part of the Hellenic Arc (Crete, Greece). *Geologische Rundschau*, 83: 417-430

- Ring U & Reischmann T (2002) The weak and superfast Cretan detachment, Greece: exhumation at subduction rates in extruding wedges. *Journal of the Geological Society*, 159: 225–228
- Ring U, Lawyer PW & Reischmann T (2001) Miocene high-pressure metamorphism in the Cyclades and Crete, Aegean Sea, Greece: Evidence for large-magnitude displacement on the Cretan detachment. *Geology*, 29(5): 395–398
- Rowe KJ & Rutter EH (1990) Paleostress estimation using Calcite twinning — experimental calibration and application to nature. *Journal of Structural Geology*, 12(1): 1–17
- Seidel E, Kreuzer H & Harre W (1982). A late Oligocene/early Miocene high pressure belt in the external Hellenides. *Geologisches Jahrbuch*, E23: 165–206
- Warr LN & Rice AHN (1994) Interlaboratory standardization and calibration of clay mineral crystallinity and crystallite size data. *Journal of Metamorphic Geology*, 12(2): 141–152
- Zulauf G, Kowalczyk G, Krahl J, Petschick R & Schwanz S (2002) The tectonometamorphic evolution of high-pressure low-temperature metamorphic rocks of eastern Crete, Greece: constraints from microfabrics, strain, illite crystallinity and paleodifferential stress. *Journal of Structural Geology*, 24(11): 1805–1828

Deformation of the Onaping Formation in the NE-lobe of the Sudbury Igneous Complex, Canada: Evidence for fold adjustment flow in the core of a km-scale fold

Christian Klimczak¹ Ulrich Riller²

The synformal geometry of the 1.85 Ga Sudbury Igneous Complex (SIC), an impact melt sheet resulting from large-magnitude meteorite impact, attests to post-impact deformation. However, in contrast to the overlying Onaping Formation, a heterolithic impact melt breccia, the SIC shows little evidence for pervasive ductile strain. This pertains in particular to its NE-lobe characterized by a curvature of about 100° in plain view. This curvature has been interpreted either as a fold or as a primary feature. In order to test these scenarios, a detailed structural analysis was conducted in the core of the NE-lobe, which consists of rocks of the Onaping Formation.

Structural measurements and lithological observations made at a total of 700 stations collectively led to the construction of a detailed structural map of the Onaping Formation in the NE-lobe. The map displays a non-systematic fold pattern evident by individual units of the Onaping Formation, which from bottom to top are known as the Basal, the Grey, the Green and the Black Members. The fold pattern of these units is characterized by elongate domes and basins, the axes of which trend approximately NE–SW. These axes are

¹ Freie Universität Berlin, Institut für Geologische Wissenschaften, Malteser Strasse 74-100, D-12249 Berlin ² Humboldt-Universität Berlin, Institut für Mineralogie, Invalidenstrasse 43, 10115 Berlin

collinear to the uniformly SW-dipping planar mineral shape fabrics suggesting that the formation of these fabrics is genetically related to that of the domes and the basins. Near km-scale structural discontinuities, which in the field and digital elevation models are evident by their strong gradients in topography, the strike of the mineral fabrics generally matches that of the discontinuities. In terms of scale and structures developed, deformation of the Onaping Formation in the core of the NE-lobe is, therefore, highly heterogeneous.

Based chiefly on the shape-preferred alignment of metamorphic minerals, the intensity of shape fabrics was visually estimated. Fabric intensity is strongest at the top of the Onaping Formation but decreases dramatically towards its contact with the SIC. This intensity gradient corresponds well with the size of matrix minerals as well as with granitoid and metasedimentary fragments, which increases toward the base of the Onaping Formation. Apart from this lithologically controlled correspondence, shape fabric intensity is maximal in the central portion of the NE-lobe and, along with the axial-planar geometry of the planar mineral fabrics, attest to generation of the NE-lobe by folding of the SIC around a south-westerly plunging axis. During such folding, deformation of the mechanically less competent Onaping Formation was accomplished heterogeneously, evident by the highly variable fold geometry and shape fabric intensity. Such heterogeneous deformation is typical for fold-adjustment rock flow in fold hinge zones of mechanically more competent rocks, i.e., the SIC.

Die dynamische Entwicklung von Styloliten Vortrag

Daniel Koehn¹ François Renard²
Renaud Toussaint³ Jean Schmittbuhl³
Cees Passchier¹

Stylolite sind raue Lösungssäume, die sich in einer großen Zahl von natürlichen Gesteinen bilden. Sie werden häufig verwendet um die Kompaktion von sedimentären Becken abzuschätzen und die Hauptspannungsrichtung zu finden. Allerdings sind die meisten Beschreibungen von Styloliten qualitativ und wir wissen nicht viel über ihre dynamische Entwicklung und den Einfluss der Spannung auf die Entwicklung der Rauigkeit. Wir präsentieren numerische Simulationen mit deren Hilfe wir die dynamische Entwicklung von Styloliten untersuchen und erforschen, welchen Einfluss Heterogenitäten, Oberflächenenergien und Spannungen auf die Entwicklung der Rauigkeit haben. Die meisten numerischen Simulationen werden mit dem Programm *Elle* durchgeführt, wobei ein Partikelnetzwerk für elastische Interaktionen verwendet wird und das Auflösen mit einem thermodynamisch/kinetischen Ansatz gerechnet wird. Wir vergleichen diesen diskreten Ansatz mit einer analytischen linearen Herleitung und einem Kontinuumsansatz, der eine Langevin Gleichung für das Auflösen eines heterogenen elastischen Mediums im Kontakt mit einer Flüssigkeit verwendet. Die Ergebnisse der numerischen Simulationen werden mit der Statistik von natürlichen

¹ Tectonophysics, Institut of Geosciences, University of Mainz, Becherweg 21, 55099 Mainz, Germany ² LGIT-CNRS-Observatoire, Université J. Fourier BP 53, F-38041 Grenoble, France ³ IPG Strasbourg, UMR 7516 CNRS, 5 Rue Descartes, F-67084 Strasbourg Cedex, France

Styloliten verglichen. Wir zeigen, dass Elastische- und Oberflächenenergien ein Abflachen der Fläche bewirken, was beweist, dass Heterogenitäten die Rauigkeit hervorrufen. Die durchschnittliche Höhe des Styloliten wächst mit einem Wachstumsexponenten von 0.6, so dass das Wachstum mit der Zeit langsamer wird. Oberflächenenergie und elastische Energie produzieren zwei ‚selbst-ähnliche‘ also pseudo-fraktale Bereiche. Die Oberflächenenergie dominiert im Mikrobereich mit einem Rauigkeitsexponenten von etwa 1.0 und die elastische Energie im Makrobereich mit einem Exponenten, der kleiner 1.0 ist (0.8 bis 0.5). Im elastischen Bereich werden die Stylolite wegen des kleinen Exponenten flacher, je größer der Bereich ist, den man betrachtet. Die charakteristischen ‚Stylolitzähne‘ entwickeln sich nur im elastischen Bereich. Der Wechsel vom Bereich der Oberflächenenergie zum Bereich der elastischen Energie ist bestimmt durch einen Schnittpunkt, der von dem absoluten Wert der Spannung abhängt, so dass Stylolite vielleicht als Spannungsindikatoren verwendet werden können.

Textures in mylonitised granite from Banefo area in the central part of the Cameroon Central Shear Zone (central Africa) — Kinematics and gradian deformation indicators *Poster*

Nono Gus D. Kouankap¹

The North Equatorial Panafrican belt is constituted by orthogneissified metamorphic and magmatic sets linked to tectonometamorphic events of the neoproterozoic orogeny. This belt whose formations are situated in the North of the Congo craton is divided into three distinct geodynamic domains: a southern domain, a northern domain and a central domain. The deformation and metamorphism relationships are a function of the different geodynamic domains of the belt.

The central domains, to which belongs the Banefo region, is affected by large strike-slip faults among which is the central Cameroonian shear zone. This domain is marked out by numerous syn-tectonic granitoids. At Banefo (NE Bafoussam, West Cameroon), those massifs are mainly constituted by mylonitised orthogneisses and granites of various degrees. The country rock is made up of gneiss and amphibolite. In the Banefo massifs, the orthogneiss is the least deformed petrographic unit. It shows a heterogranular granoblastic texture with a mineral assemblage formed by quartz, K-feldspars, biotite, etc., within the orthogneiss, remains of magmatic fluidity can still be observed marked by feldspar megacrystal.

¹ Université de Yaoundé I, Département des Sciences de la Terre, BP : 812 Yaoundé-Cameroun

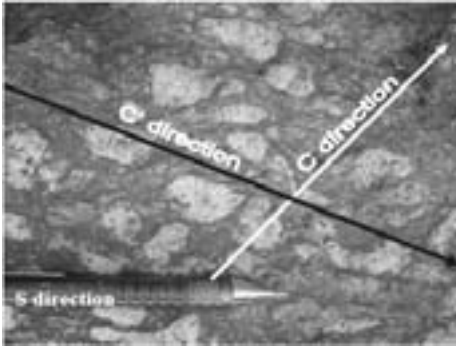


Figure 1: C/S/C' structure

Field observations reveal a net progression of the intensity of deformation of orthogneisses to ultramytonitised granites having an identical chemical composition as the orthogneisses. The mylonitisation is marked by a reduction in grain size, in the percentage of the megacrystals of feldspars and by the flattened, elongated and stretched forms of minerals, with the main ones including:

- orthoclase, which is present as elongated crystals with sigmoidal and elliptical shapes, with oblique fissuration planes at the long axes of the mineral;
- quartz which is in the form of rubans and xenomorphic stretched crystals;
- biotite which is less abundant, with crystals disposed parallelly at the borders of orthoclase clasts, the latter showing shadow zones with quartz grains.

The organization of those minerals in the rock forms the S/C' structure whose identification in the field permitted to determine the sinistral trend of the shear movement.

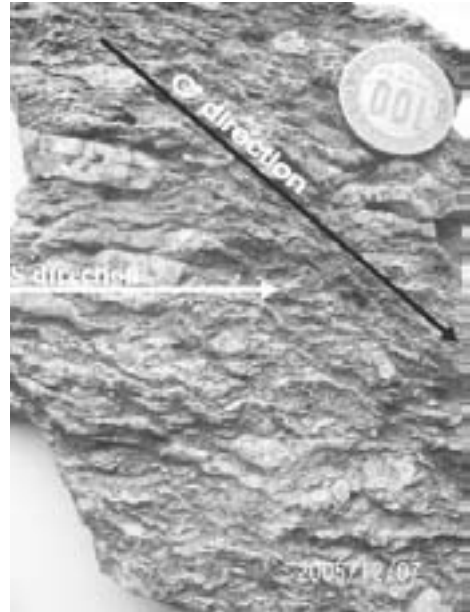


Figure 2: S/C' structure

These S/C' structures evolve with the intensity of the deformation; from the orthogneisses where they are observed, they pass to mylonites *sensu stricto* with S/C/C' structures (Fig. 1) and finally to the ultramytonites where one observes the S/C' structure in which C is parallel and confused with S (Fig. 2). The gradian of the deformation is marked by stretched crystals of quartz, by the reduction of the sizes and proportions of feldspar megacrystals. This has implications at the level of orthogneissification of structures, reduction of the angle between S and C, the increase in the density of C and the appearance of the C' plane, such that in the ultramytonites, S is almost parallel to C and the angle between C and C' attains its maximum.

Neotectonic markers in the Panafrican belt formations of Cameroon: elements of interpretation and their environmental impacts *Poster*

Nono Gus D. Kouankap¹

The North equatorial Panafrican Belt, whose Cameroonian formations are dated between 650 and 400 million years, and which are located in the North of the Congo Craton, is subdivided in to three major geodynamic domains: a north Cameroon domain, a central Cameroon domain and a south Cameroon domain. These major domains are generally, particularly the central domain, affected by great strike-slip faults in which the most important are the central cameroonian shear zone and the Sanaga fault.

Studies that establish the order of occurrence of geological events, generally performed in these domains and particularly at Banefo area (West Cameroon) reveal markers of recent tectonics (post panafrican) that affect the granitogneissic basement. They include:

- i) pseudotachytes observed in the regions of Yaoundé, Tibati, Edea, and Banefo (Fig. 1);
- ii) Net and fresh stries of movement observed on the quartzofeldspathic injections sampled in some faults in the Banefo locality (Fig. 2).

The impact of the repeated action of this fault on the environment is expressed by:

- the fissuration of the tarred road at the level of the Banefo road cut,

¹ Université de Yaoundé I, Département des Sciences de la Terre, BP : 812 Yaoundé-Cameroun



Figure 1: pseudotachylites

in the same direction as the major fractures of this locality;

- the crumbling of gneissified massifs in the Banefo Region in 1955, preceding a series of local minor earth tremors;
- fissuration, in parallel directions, of houses in some urban areas of the Yaoundé town; capital of the Republic of Cameroon (Fig. 3);

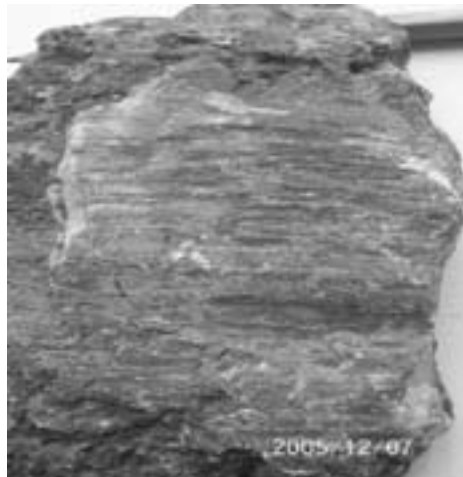


Figure 2: Stries of movement.



Figure 3: Fissurations of the houses.

- the most recent regional earth tremor (March 2005) recorded along the Sanaga Fault, which was registered right at Yaoundé situated 70 km away from the fault.

The tectonic processes that occur in the North Equatorial Panafrican belt since the end of panafrican orogeny (400 My) to the present day can be explained in the context of the neotectonic processes. The causes of the neotectonics, according to Ngako (1999), might be due to the processes of progressive peneplanation of the Panafrican reliefs by erosion, thus controlling the mechanism of isostatic rising of the crust/mantle interface from the end of the orogeny.

The genetic link existing between the pseudotachytes and the seismic faults coupled with the recorded minor earth tremors make the geotectonic environment of these areas a non-aseismic one, and for this reason, a particular attention should be focussed in the study of those major accidents in order to predict, monitor and take the necessary measures to minimize the consequences

of an eventual natural seismic catastrophe in this environment which seems aseismic.

A new practical and economical technique for the obtention of high quality thin section photographs with the help of a simple optical microscope

Vortrag

Nono Gus D. Kouankap¹ Ganno Sylvestre¹

Microscopic study is an indispensable step in the determination of the petrographic characteristics of rocks. In Cameroon just like in most developing countries, simple polarizing microscopes of the 20th Century constitute the only available material for macroscopic studies. A major difficulty encountered in the use of these instruments resides in the realisation of photographs of the different parts of the thin section that require illustrations. The technique that has been used upto now has been inefficient and unsatisfactory. Faced with this recurrent situation, we thought of setting up a new, semi-modern, practical and very economical technique for photographing the thin section.

The setup that has existed till present day consists of an 'Euromex' microscope with eyepiece fixation plates (removable eyepiece plate). The principle consists of removing the eyepiece plate and then fixing a second one which is specially conceived, for, it bears a metallic tube

¹ Université de Yaoundé I, Département des Sciences de la Terre, BP : 812 Yaoundé-Cameroun

on which can easily be connected an argentic or classical camera, that is, using films. Once the camera is connected, the part of the thin sections to be filmed is carried out through a fastidious set up step of the image, for, it is the eye piece of the camera that is used rather than that of the camera; the zoom of the camera is fixed. Once the setup of the image is over, room light has to be eliminated so as to avoid any influence on the quality of the films. Moreover, the source of light of the microscope should neither be too low, nor too sharp, because on this factor strictly depends the quality of the photographs. All these problems suppose that, for the realisation of good quality photographs, it is better to proceed at night while putting off all room lights (electricity).

However, after having thoroughly respected all the above constraints and obligations related to light, it is very recurrent that after having realised the pictures, one still obtains empty negatives during the process of development. This is because the camera was unable to fix a single image. As a result, in order to increase the chances of obtaining images, several photographs are usually taken on one single section, while modifying the intensity of the light source after each film. With this technique, we succeeded in obtaining few images whose quality was highly denatured by light. The few images were then later on scanned so as to have a numerical version. It should however be noted here that due to the low resolution power of the scanner, the exact nature of the original photograph is not reproduced. Finally, mediocre to poor quality photographs are obtained.

This method, which is long, fastidious and expensive, is a serious obstacle in

the progress of most research works of geologists in third world countries. This is because it is not only a time consuming technique, but also a non-reassuring one. The final product is only lightly satisfactory. Because of the above constraints, it was necessary to revolutionize the method.

Faced with the persisting difficulties, the establishment of a new technique of microscopic photography was then envisaged. The setup is based on the polarizing microscope, a numerical camera and an adapter.

- the polarizing microscope can either be monocular or binocular;
- the adapter is a hollow cylinder or a plastic cylinder whose diameter is greater than that of the objective of the numerical camera, with its height varying between 3 and 5 cm. The adapter should also have a diameter which is slightly greater than or equal to that of the eyepiece of the microscope. The adapter plays the role of extension of the eyepiece thereby facilitating movements (translational movements) of the zoom (objective) of the camera.
- numerical cameras of all sorts can be used so long as their objectives have diameters which are close to that of the eyepiece of the polarizing microscopes.

The principle consists to:

- Place the thin section on the mineral plate and choose suitable sections to be filmed
- fix the adapter on the eyepiece of the polarizing microscope

- insert the zoom (objective) of the numerical camera inside the adapter
- Progressively move the camera so that the light source from the eyepiece of the microscope should pass inside the objective of the camera (coincide the objective of the camera with the eyepiece of the microscope).
- Once the previous step is properly done, the zone of the thin section to be filmed will be seen on the screen of the numerical camera. At this point in time, the zoom can be readjusted for the best quality photograph to be obtained.

The advantages are:

- the section to be filmed is visible on the screen of the camera;
- after filming, the photo is immediately observable and if its quality is not very good, it is possible to cancel the picture and to repeat the process on the same zone of the thin section;
- the pictures obtained are of very high quality and directly transferable to a computer without further scanning, as in the previous case, for the various manipulations. Moreover, with the aid of modern software programs, it is possible to improve the quality of those images in the computer.
- The method is relatively easier, faster and cheaper.

However, the only obstacle or inconvenience encountered in the new technique resides in the determination of the scale

of the photographs. This is because it is difficult to determine the rate of enlargement or reduction of the camera's objective as well as that of the computer. In order to overcome the obstacle, the following steps have been proposed:

- On each section to be filmed, choose a given mineral, mark it and measure its dimensions with the help of the graduations on the crossed nicols. The obtained value is termed initial dimension (D_i) or real dimension.
- After computer processing and printing of the photographs, the marked minerals are then measured again and the obtained value is termed final dimension (D_f).
- The scale of the photo is the ratio of the real dimension to the final dimension $E = D_i/D_f$

The proposed method enables to obtain high quality photographs, but, it however remains rudimentary, for it requires much skills and manipulations. Moreover, the polarizing microscope does not offer durable observations; it will be necessary to construct a more practical and less expensive microscope on which is incorporated a numerical camera that will meet up with the expectations of all. Thus, microscopic observations will be carried out for longer periods of time (because the light will no longer exhaust the eyes with time) and in groups, thus permitting constructive discussions.

Fluidtransport entlang von Störungen und Klüften im Gebiet des Hengill-Vulkans, SW-Island *Poster*

Michael Krumbholz¹ Nadine Friese¹ Steffi Burchardt¹ Agust Gudmundsson¹



Abbildung 1: Das geothermische Kraftwerk Nesjavellir im Hengill-Vulkansystem. Die Abschiebungen im Hintergrund streichen N30°E.

Das Holozäne Hengill-Vulkansystem liegt in der aktiven Westvulkanischen Zone in Südwestisland. Es beinhaltet den Hengill-Zentralvulkan, der sich südlich des Sees Thingvallavatn befindet, und ist eines der aktivsten geothermischen Systeme Islands (Abb. 1). Die aktuelle Spreizungsrate in der Westvulkanischen Zone liegt zwischen 3 und 7 mm a⁻¹ bei einer Subsidenzrate von 1 mm a⁻¹ (Tryggvason 1982; La Femina et al. 2005). Das Hengill-Vulkansystem ist 60–70 km lang und zwischen 5 und 10 km breit. Struktureologisch wird das Gebiet von großen NNE-streichenden Abschiebungen dominiert.

Der Hengill-Vulkan selbst liegt in der Nähe des Tripelpunktes zwischen der Reykjanes-Halbinsel, der Westvulkanischen Zone und der Südisländischen Seismischen Zone. Diese besondere plattentektonische Konfiguration ist eine der Ursachen für die sehr hohe seismische Hintergrundaktivität. So wurden allein in dem Zeitraum zwischen 1994 und 1998 mehr als 80.000 Erdbeben kleiner Magnitude im Gebiet um den Hengill registriert (Vogfjord et al. 2005). Ungefähr die Hälfte davon zeigte Herdflächenlösungen, die auf Abschiebungen und auf Seitenverschiebungen zurückzuführen sind. Die Seitenverschiebungen bilden in diesem Gebiet ein konjugiertes System von NNE-streichenden dex-

tralen und ENE-streichenden sinistralen Störungen. Die andere Hälfte der Erdbeben fand vorzugsweise in Hochtemperaturgebieten statt und zeigt Herdflächenlösungen, die charakteristisch für Extensionsversagen verursacht durch zirkulierende geothermale Wässer sind (Foulger 1988).

Das Hauptziel dieser Untersuchung ist, das Verständnis für die Bruchentwicklung und die Fluidtransportmechanismen im Hengill-Gebiet zu verbessern. Dieses Verständnis ist notwendig, um realistischere Modelle über den Fluidtransport in den geothermischen Feldern erstellen zu können und um bessere Prognosen über ihre Lebensdauer zu ermöglichen. Weiterhin soll der Kenntnisstand über den Einfluss von Wässern auf Erdbebenentstehung untersucht werden, da in diesem Gebiet die meisten Erdbeben durch Fluidüberdruck ausgelöst werden.

Für diesen Zweck wurden mehr als 2000 Klüfte, 1000 Mineralgänge und 29 großskalige Abschiebungen am Hengill-Vulkan gemessen (Abb. 2). Die großen Abschiebungen, die eine Grabenstruktur bilden, streichen im Mittel N30°E.

¹ Geowissenschaftliches Zentrum Göttingen, Goldschmidtstraße 3, 37077 Göttingen

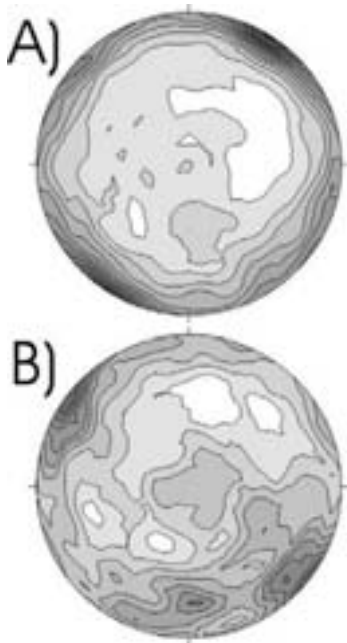


Abbildung 2: Stereographische Projektion (untere Hemisphäre) von A) 2044 Klüften and B) 972 Mineralgängen. Die Klüftscharren sind senkrecht und parallel zum Verlauf der Grabenstruktur. Die Hauptschar der Mineralgänge streicht NE-SW, während die untergeordneten Gangscharen E-W streichen bzw. subhorizontal liegen.

Der gemessene vertikale Gesamtversatz über diese 29 entlang eines Profils gemessenen großen Abschiebungen beträgt mehr als 1200 m. Die Klüfte im Untersuchungsgebiet besitzen zwei Hauptrichtungen. Eine Klüftschar streicht parallel (NE-SW) zum Hengill-Vulkansystem während die zweite Klüftschar genau senkrecht (NW-SE) dazu ausgerichtet ist. Die NE-SW verlaufenden Klüfte wurden bevorzugt von den zirkulierenden geothermalen Wässern als Leiter benutzt und liegen heute zum großen Teil als Mineralgänge vor. Diese Klüftschar wurde bevorzugt von

den Wässern benutzt, da sie senkrecht zur maximalen Zugspannung, also senkrecht zum örtlichen Spreizungsvektor, ausgerichtet war. Zusätzlich zu dieser NE-SW streichenden Schar von Mineralgängen haben sich zwei untergeordnete Gangscharen entwickelt. Eine von ihnen streicht E-W und fällt nach Süden ein, die zweite Schar ist subhorizontal. Da die E-W streichenden Mineralgänge nicht mit dem regionalen Spannungsfeld erklärt werden können, wäre es möglich, dass sie mit dem konjugierten System von Seitenverschiebungen in Zusammenhang stehen. Dieses System von Seitenverschiebungen ist vermutlich die Ursache für die häufigen Erdbeben im Gebiet des Hengill-Vulkans.

Literatur

- Foulger GR (1988) Hengill triple junction, SW Iceland, 2. Anomalous earthquake focal mechanisms and implications for process within the geothermal reservoir and at accretionary boundaries. *J. Geophys. Res.* 93, 13507-13523
- La Femina PC, Dixon TH, Malservisi R, Árnadóttir T, Sturkell E, Sigmundsson F & Einarsson P (2005) Geodetic GPS measurements in south Iceland: Strain accumulation and partitioning in a propagating ridge system, submitted to *JGR*
- Tryggvason E (1982) Recent ground deformation in continental and oceanic rift zones. *Continental and Oceanic Rifts, Geodynamic Series*, 8, 17-29
- Vogfjörd KS, Hjaltadóttir, S & Slunga, U (2005) Volcano-tectonic interaction in the Hengill region, Iceland during 1993-1998. *Geophys. Res. Abstracts* 7, EGU05-A-09947

Metastability and HP metamorphism at fluid deficient conditions, an example from the Bergen Arcs (Western Norway) *Poster*

Alexander Kühn¹ Haakon Austrheim²

In the Lindæs Nappe, Bergen Arcs Western Norway, Precambrian granulites facies anorthosites ($P < 10$ kbars, $T = 800^\circ\text{C}$) and their Caledonian eclogite ($P < 17$ kbars, $T = 700^\circ\text{C}$) and amphibolite facies equivalents alternate on meter scale. It has recently been suggested by Camacho et al. (2005) that the granulite facies anorthosites, remained at low temperatures (350°C) and were only locally heated to 700°C and reacted to eclogites by spasmodic hot fluids. This is in contrast to previously published models (Austrheim 1987) where the fluid-triggered mineral reactions in a terrain that was at 700°C during the Caledonian Orogeny. In the latter model the dry granulites metastably survive the Caledonian HP/HT metamorphic event at 425 Ma.

In pristine granulites, occurring adjacent (less than 1 m distance) to the completely eclogitised parts, visible Caledonian metamorphism is very limited. Reactions are confined to local (15 m wide kyanite, zoisite, garnet and K-feldspar aggregates and feathery intergrowth of K-feldspar and zoisite growing on plagioclase-plagioclase grain boundaries. In addition 0.1 to 0.5 mm thick coronas are observed around spinel and corundum that is embedded in plagioclase (Fig. 1). During progres-

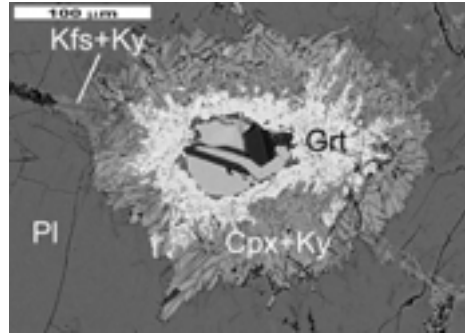


Figure 1: Eclogite facies garnet-omphacite-kyanite corona around spinel/corundum embedded in a plagioclase groundmass within an otherwise unreacted granulite facies anorthosite. The grain boundaries between plagioclase grains show tiny growth of K-feldspar and kyanite.

sive reaction/fluid availability these reaction rims (coronas) become thicker and change their mineral assemblage from garnet, omphacite, kyanite to omphacite, amphibole, kyanite. In addition to these changes, plagioclase transforms to an increasing amount of fine-grained zoisite and phengite needles. The little H_2O needed to facilitate these transformations is provided from the breakdown of primary hydrous phases like scapolite and hornblende that are typically found in the granulites.

Based on the above described textural and chemical characteristics (e.g. the occurrence of omphacite and garnets rich in Alm and Grs component, distinctly different to the granulite facies mineral compositions), that can be observed in the most pristine granulites we suggest that these coronas and can be assigned to the Caledonian metamorphism. This in turn means that also the least reacted granulites record the same P-T conditions as are recorded in the adjacent eclogites but not the same fluid

¹ Institut für Geowissenschaften, Becherweg 21, Universität Mainz, D-55099 Mainz, Germany ² Physics of Geological Processes (PGP), University of Oslo, PO Box 1048 Blindern, 0136 Oslo, Norway

conditions. The little water needed to balance the zoisite formation on the micro scale can be balanced by the breakdown of hydrous primary phases (hornblende and scapolite). These ‘granulite facies’ anorthosites remained fluid deficient compared to their fully equilibrated eclogite facies equivalents. Fluid deficiency and meta-stability at metamorphic conditions as recorded by the nearby eclogites explain the observed close occurrence of granulites and eclogites.

The granulites from the eclogitised areas in the Lindæs Nappe contain sufficient amounts of fluid to record the high-pressure event on the microscale. However, these signs of metamorphism are easily miss-interpreted as of lower grade origin. Extending our observations to a completely dry bulk composition it is inferred that such a rock will miss all signs of the Caledonian metamorphism and that the first metamorphic mineral assemblage will first form when fluid is introduced.

References

- Austrheim A (1987) Eclogitization of lower crustal granulites by fluid migration through shear zones. *Earth and Planetary Science Letters* 81, 221–232
- Camacho A, Lee JKW, Hensen BJ & Braun J (2005) Short-lived orogenic cycles and the eclogitisation of cold crust by spasmodic hot fluids. *Nature* 435, 1191–1196

Oligocene emplacement of the Eclogite Zone of the central Tauern Window, Eastern Alps, Austria *Poster*

Alexander Kühn¹ Johannes Glodny²
Uwe Ring³

The EZ is an approximately 20 km long and 2–3 km wide coherent unit of the Tauern Window in the Eastern Alps. It is sandwiched between the Venediger- and the Glockner Nappe. While rocks in the EZ experienced HP metamorphic conditions (24 kbar/650°C), rocks from the underlying Venediger Nappe and the overlying Glockner Nappe only record lower alpine metamorphic conditions with peak pressures not exceeding 10 and 8 kbar, respectively. While metamorphism in the EZ is well dated with an average age of 31.5 ± 0.7 Ma (Glodny et al. 2005) the final emplacement of these different nappes is still under debate.

Thrusting of the EZ on top of the underlying Venediger Nappe is documented by top-N shear-sense indicators in carbonaceous mica schists and mylonites from the Dorfertal. The internal structure of the EZ is characterized by N-vergent folds at the 100 m to km scale. Fold axial planes are moderately to steeply dipping. The upper boundary of the EZ at its contact with the Glockner Nappe is characterized by blueschist to greenschist facies carbonate bearing mylonites. Stretching lineations in the ENE-striking mylonites dip on average 20° to the ENE indicating sinistral shear

¹ Institut für Geowissenschaften, Becherweg 21, Universität Mainz, D-55099 Mainz, Germany ² GeoForschungsZentrum Potsdam, Telegrafenberg C2, D-14473 Potsdam, Germany ³ Department of Geological Sciences, University of Canterbury, Christchurch 8004, New Zealand

with a slight extensional component.

Two carbonate mylonites from the Dorfertal, (samples EIS 14a and 14b; calcite, dolomite, muscovite, paragonite, tourmaline and rare garnet) yielded Rb/Sr mineral isochron ages between 30.5 ± 0.8 Ma and 29.1 ± 0.5 Ma, interpreted to date the final thrust emplacement of the EZ above the Venediger Nappe. The youngest ages are obtained from the most fine-grained muscovites in these mylonites, which are further characterised by particularly high Sr concentrations. This may be due to a change of the Sr partition coefficient between carbonate and muscovite during progressive deformation and coeval decompression, related to the aragonite to calcite phase transition. A Rb/Sr mineral isochron age of 31.4 ± 0.4 Ma from a mafic schist from the base of the Glockner Nappe (Seekopfscharte, sample EIS11) directly above the EZ dates blueschist facies metamorphism and sinistral shearing within the Glockner Nappe. Rb/Sr data from carbonate-dominated mylonites (sample EIS 6; calcite, dolomite, muscovite, rare amphibole and epidote), marking the upper boundary of the EZ in the Timmeltal provide a deformation age of 31.2 ± 0.7 Ma.

Our data indicate that top-N thrusting at the base and large-scale folding of the EZ was coeval with sinistral strike-slip faulting at its upper boundary and eclogite-facies metamorphism in the EZ. The data also indicate that today's nappe architecture must have been established in less than 2 Ma after the eclogite facies metamorphism in the EZ. Very fast exhumation of the EZ was accomplished in a transpressional setting, which might explain why the exposed EZ is such a small unit.

References

- Glodny J, Ring U, Kühn A, Gleissner P & Franz G (2005) Crystallization and very rapid exhumation of the youngest Alpine eclogites (Tauern Window, Eastern Alps) from Rb/Sr mineral assemblage analysis. *Contributions to Mineralogy and Petrology* 149, 699–712

Eo-Alpine imbrication of Middle Austroalpine units in the Gurktal Alps, Carinthia — questioning the existence of the Upper Austroalpine Murau Nappe *Poster*

Carsten Laukamp¹ Thomas Angerer¹

Structural analysis of Paleozoic Middle and Upper Austroalpine (MAA, UAA) units of the Gurktal Nappe Complex (GNC) in combination with electron microprobe analyses of multiphase garnets reveal a complex Variscan and Alpidic tectonometamorphic evolution of the GNC. Our study is focussed on the UAA 'Murau Nappe' and its tectonic transition to the MAA respectively to the overlying UAA Stolzalpen Nappe. The 'Murau Nappe' may rather be interpreted as a major zone of imbricate thrust slices of the underlying and overlying units than a distinct nappe.

The tectonometamorphic evolution of the MAA and UAA units in the GNC comprises the following events:

- i) D₁: pre-Alpine (Variscan), anchizonal to greenschist-facies metamorphism of the MAA (⁴⁰Ar/³⁹Ar-ages on micas of the western GNC

¹ Geologisch-Paläontologisches Institut, Universität Heidelberg, Im Neuenheimer Feld 234

- about 315–310 Ma; Neubauer et al. 1999),
- ii) D₂: after subduction of the North-Penninic ocean thrusting of the Austroalpine units during Cretaceous times west- to northwestwards over the North-Penninic and Helvetic units,
 - iii) D₃: Paleogene movement of thrusts to the north/northwest (v. Gosen 1989), and
 - iv) syn- to post-D₃: transition of the N–S-compressional regime to E–W-extension, causing sliding of the extruding wedge of the Murals from the Tauern Window eastwards towards the Pannonian Basin (Ratschbacher et al. 1991a,b) from Eocene/Oligocene to Middle Miocene times.

The ‘Murau Nappe’ (Stohwasser 1947/1956) was postulated because of two Mesozoic units (Stangalm respectively Pfannock unit) separating the nappe from the underlying MAA and overlying Stolzalpen Nappe. The occurrence of Mesozoic units, however, is locally restricted; therefore the ‘Murau Nappe’ as a distinct thrust unit is not confirmed yet.

The analyses on spessartine-rich garnets indicate upper greenschist-facies to epidote-amphibolite-facies in the phyllitic micaschists and epidote-amphibolite-facies in the phyllites, which are presumably related to the pre-Alpine peak-metamorphism. The carbonate dominated suite (Murau Limestones) displays conditions of higher greenschist-facies and has been tectonically imbricated between the overlying phyllitic micaschists and the overlying phyllites during D₂.

The Stolzalpen Nappe lacks Variscan ductile structures (v. Gosen 1989). During the Eo-Alpine orogeny the Stolzalpen Nappe overthrusts the MAA and the direction of movement changes from top-NW (syn-D₂) to top-E/NE (syn-D₃). A NW- to SW-dipping penetrative cleavage (S₃) is attributed to the late phase of the Eo-Alpine orogeny (D₃) and is a ubiquitous feature of all MAA- and UAA-units in the central Gurktal Alps. Linked to D₃ is a retrogressive overprint (diaphthoresis) of the MAA and ‘Murau Nappe’ under low to high greenschist-facies conditions. The Stolzalpen Nappe is not affected by this retrogression. The boundary ‘Murau Nappe’ and Stolzalpen Nappe appears to be transitional with respect to lithology and metamorphic grade. Locally a tectonic boundary is defined by chloritoid-bearing quartzitic mylonites (Angerer et al. 2000), indicating a thrust zone, with lower greenschist facies metamorphism.

Except for the Murau Limestones a continuous metamorphic gradient from MAA to the Stolzalpen Nappe was established during the Eo-Alpine orogeny. The Murau Nappe appears as a continuous shear zone, incorporating less deformed imbricate slices of the Murau Limestones. No discrete tectonic boundary between MAA and ‘Murau Nappe’ has been observed in the central GNC.

The results of our study lead to a reinterpretation of the ‘Murau Nappe’ as a major shear zone generated during the Eo-Alpine thrusting of the Stolzalpen Nappe over the MAA. Concerning the central GNC we conclude, that the genetic term ‘Murau Nappe’ for the lower UAA unit between MAA and Stolzalpen Nappe is not valid. Instead, its reinterpretation

pretation as a major shear zone ('Murau shear zone'), genetically belonging to the MAA, generated during Eo-Alpine overthrusting of the Stolzalpen Nappe, is favoured. The Mesozoic Stangalm unit is interpreted as a local sequence imbricated during the northward movement of the MAA units.

References

- Angerer T, Laukamp C & Leonhard A (2000) Strukturgeologische Untersuchungen in den Teileinheiten des Gurktaler Deckensystems (Ostalpen) und seines Kontaktes zum Mittelostalpin. *Terra Nostra* 2000/5: 4–5
- v. Gosen W (1989) Gefügeentwicklungen, Metamorphosen und Bewegungen der ostalpinen Baueinheiten zwischen Nockgebiet und Karawanken (Österreich). *Geotekt Forsch* 72, pp 247
- Neubauer F, Hoinkes G, Sassi FP, Handler R, Höck V, Koller F & Frank W (1999) Pre-Alpine metamorphism of the Eastern Alps. *Schweiz Min Petr Mitt* 79, 41–62
- Ratschbacher L, Merle O, Davy Ph & Cobbold P (1991a) Lateral extrusions in the Eastern Alps, Part 1: Boundary conditions and experiments scaled for gravity. *Tectonics* 10, 245–256
- Ratschbacher L, Frisch W, Linzer H-G & Merle O (1991b) Lateral extrusions in the Eastern Alps, Part 2: Structural analysis. *Tectonics* 10, 257–271
- Stowasser H (1947/1956) Zur Schichtfolge, Verbreitung und Tektonik des Stangalm-Mesozoikums (Gurktaler Decke). *Jb Geol B-A* 99, 75–199

Structural control of fluid flow on a carbonate platform margin: an example from the Otavi Mountainland, Namibia *Vortrag*

Carsten Laukamp¹ Volker Petzel²
 Thilo Bechstädt¹

Fault inversion and alteration influence fluid pathways over the period of deformation and thereafter. Relationships between the formation and site of ore deposits can be established if the stages of deformation can be linked to specific hydrothermal events. In order to find new indications on the genesis and distribution of known and eventual further base metal mineralisation in the Otavi Mountainland (OML) in northern Namibia, we started a cement-stratigraphic and detailed structural investigation.

The OML is positioned in the north-eastern part of the Damara belt, on the northern tip of a foreland fold and thrust belt. The ENE-trending belt in northern central Namibia results from the pan-African collision of the Congo with the Kalahari Craton. The pan-African tectonic evolution of the OML is summarised in Fig. 1. Sedimentary lithologies in the OML consist of the Neoproterozoic Damara sequence with the siliciclastic and volcanoclastic Nosib Group at the bottom, overlain by the Otavi Group carbonates and the molasse-like Mulden Group. Deposition proceeded from Cryogenian to late Ediacaran or early Cambrian (Frimmel et al. 2004, amongst others).

¹ Geologisch-Paläontologisches Institut, Universität Heidelberg, Im Neuenheimer Feld 234

² Geological Survey of Namibia, 1 Aviation Road, Windhoek, Namibia

Mining stage	deposition/age	met.	def.	structures OML	min.
	Mulden Group 780 - 740 Ma			thrusting (steep, normal)	
Continental convergence in Karakoram region	Osage Group (Shank. Fac.) (711-630 Ma)		D1	unstable growth faults F1 (NW-SE axis) F2 (NW-SE axis) F3 (SE-NW axis) F4 (SE-NW axis) F5 (SE-NW axis) F6 (SE-NW axis) F7 (SE-NW axis) F8 (SE-NW axis) F9 (SE-NW axis) F10 (SE-NW axis) F11 (SE-NW axis) F12 (SE-NW axis) F13 (SE-NW axis) F14 (SE-NW axis) F15 (SE-NW axis) F16 (SE-NW axis) F17 (SE-NW axis) F18 (SE-NW axis) F19 (SE-NW axis) F20 (SE-NW axis) F21 (SE-NW axis) F22 (SE-NW axis) F23 (SE-NW axis) F24 (SE-NW axis) F25 (SE-NW axis) F26 (SE-NW axis) F27 (SE-NW axis) F28 (SE-NW axis) F29 (SE-NW axis) F30 (SE-NW axis) F31 (SE-NW axis) F32 (SE-NW axis) F33 (SE-NW axis) F34 (SE-NW axis) F35 (SE-NW axis) F36 (SE-NW axis) F37 (SE-NW axis) F38 (SE-NW axis) F39 (SE-NW axis) F40 (SE-NW axis) F41 (SE-NW axis) F42 (SE-NW axis) F43 (SE-NW axis) F44 (SE-NW axis) F45 (SE-NW axis) F46 (SE-NW axis) F47 (SE-NW axis) F48 (SE-NW axis) F49 (SE-NW axis) F50 (SE-NW axis) F51 (SE-NW axis) F52 (SE-NW axis) F53 (SE-NW axis) F54 (SE-NW axis) F55 (SE-NW axis) F56 (SE-NW axis) F57 (SE-NW axis) F58 (SE-NW axis) F59 (SE-NW axis) F60 (SE-NW axis) F61 (SE-NW axis) F62 (SE-NW axis) F63 (SE-NW axis) F64 (SE-NW axis) F65 (SE-NW axis) F66 (SE-NW axis) F67 (SE-NW axis) F68 (SE-NW axis) F69 (SE-NW axis) F70 (SE-NW axis) F71 (SE-NW axis) F72 (SE-NW axis) F73 (SE-NW axis) F74 (SE-NW axis) F75 (SE-NW axis) F76 (SE-NW axis) F77 (SE-NW axis) F78 (SE-NW axis) F79 (SE-NW axis) F80 (SE-NW axis) F81 (SE-NW axis) F82 (SE-NW axis) F83 (SE-NW axis) F84 (SE-NW axis) F85 (SE-NW axis) F86 (SE-NW axis) F87 (SE-NW axis) F88 (SE-NW axis) F89 (SE-NW axis) F90 (SE-NW axis) F91 (SE-NW axis) F92 (SE-NW axis) F93 (SE-NW axis) F94 (SE-NW axis) F95 (SE-NW axis) F96 (SE-NW axis) F97 (SE-NW axis) F98 (SE-NW axis) F99 (SE-NW axis) F100 (SE-NW axis)	
	Mineralization I Mulden Group 680 - 640 Ma				
Collision of Kalkat and Congo Plate	M1 (reg. Met. peak 620Ma)		D2a	thrusting (steep, normal)	
			D2b	thrusting (N-S, NE-SW)	
			D2c	thrusting (N-S, NE-SW)	
Late or post-Damaran uplift in northern zone of Damara Orogen	M2 (reg. Met. ca. 487 - 455)		D3	normal faults (NW-SE, N-S, NE-SW)	
Late Damaran reactivation of Damara Lineaments			post-D3	strike slip?	
	Mineralization II				

Figure 1: Tectonic evolution of the OML (ages after Frimmel et al. (1996), Frimmel (2004), Goscombe et al. (2004), Haack and Martin (1983), Haack et al. (1980), Hoffmann et al. (2004))

The present study focuses on the north-western OML, southwest of the mining town of Tsumeb. The dominating structure in this area is the NW-SE striking Guinas Fault. The Guinas Fault is a shear zone that divides an area, which is different in sense of stratigraphic features, the grade of pre-, syn- and post-Damaran deformation and the type and grade of mineralisation. The northern area is enriched by Cu-rich base metal sulphides, whereas the southern area is almost barren.

The carbonate successions in the Guinas Fault area are part of the Tsumeb Subgroup (upper Otavi Group, lithozones T4–T8). North of the Guinas Fault the massive dolomites of the Hüttenberg Formation (T6–T8) are unconformably overlain by conglomerates and sandstones of the lower Mulden Group. South of the Guinas Fault T6 and lower

T7 show almost the same stratigraphy, but instead of the laminated dolomites, there are thin laminated and thick bedded limestones with intercalated mass flow breccias. Total thickness of the T7 in the south is about 600 m, but in the north only about 35 m (Petzel, 1993). This huge difference in thickness could either be caused by (1) tectonic nappe stacking in the south, (2) lateral facies change obliterated by the thrusting or (3) due to growth faulting during the deposition of the Hüttenberg Formation. Mass flow breccia lenses embedded in the laminated limestones of the T7 lithozone exist only southwest of the Guinas Fault. Clasts of carbonate sediments from the northeastern area are enclosed in the mass flows. Restricted to the northeast there are algal reefs pointing to shallow marine conditions, whereas the mass flows and the dark limestones and shales might have been deposited at a slope just south of the Guinas Fault. Therefore the origin of the Guinas Fault as a growth fault along an unstable slope at the southwestern margin of a carbonate platform is possible. Similar growth faults have been reported from the central OML.

Differences in the deformation south and north of the Guinas Fault are even bigger. South of the Guinas Fault our study examined a wide range of Damaran deformations. Bedding parallel first cleavage S_1 is marked by thin chert layers, which are isoclinal folded around an NW–SE axis. The second cleavage cuts S_1 and small scale thrusts and nappe stacking evolve. Therefore nappe stacking is evident south of the Guinas Fault, but only on a minor scale and tectonic thinning of the limestone units might have partly neutralized the greater thickness of the stacked

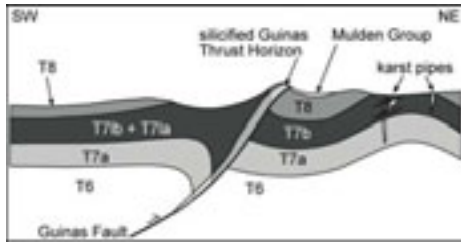


Figure 2: transect of the Guinas Fault and the upper Tsumeb Subgroup (Hüttenberg Fm., T6–T8); not to scale

T7-litho-units. A major lateral facies change is not likely, because the small dimension of thrusting is not sufficient to obliterate the major facies change. The hanging wall of the Guinas Fault itself is a thrust horizon, which is made up of a highly silicified oolitic dolomite. Silicification happened in a late stage or even after the main phase of the north-eastward thrusting (D_2) along this horizon.

A transect through the Guinas Fault (Fig. 2) shows a displacement of the carbonates of the upper Tsumeb Subgroup (T6–T8, Hüttenberg Formation) along the Guinas Thrust. The carbonates are thrust over the Mulden siliciclastics, indicating that the thrusting is of an Early Cambrian age developed during D_2 . Karst pipe structures, filled by Mulden siliciclastics, are common hosts for mineralisation in the northern OML, like the Tsumeb Pipe, which is deformed by Damaran tectonics. Karstification down to the middle Tsumeb Subgroup occurs preferred at fractures, which are related to the syn- D_2 folding event. The Guinas Fault has been involved again during the late Damaran uplift (D_3), as minor normal faulting along the floor thrust of the silicified thrust horizon can be referred to D_3 .

Applying our data to the base metal mineralisation in the northwestern OML, we find implications for the formation and alteration of ore bodies. Deposition of primary base metal mineralisation has started at the latest during the deposition of the lower Mulden siliciclastics (ca. 580–540 Ma) and before the peak metamorphism of the Damaran orogenesis in the OML (ca. 535 Ma). Ages of around 530 Ma (Kamona et al. 1999) may indicate an upper age of the primary mineralisation or its syn-Damaran remobilisation (Fig. 1). Adequate conduits for mineralising fluids could have been the Guinas Fault/Thrust itself, stratigraphic horizons of higher porosity in the Tsumeb Subgroup and karst structures in the upper levels (Fig. 2). In a later stage of the Damaran orogenesis (Fig. 1) hydrothermal fluids could have moved along these pathways to the area north of the Guinas Fault, whereas the distribution to the south was prevented by the syn- D_{2b} silicified Guinas Thrust horizon that acted down to the lower Tsumeb Subgroup as a dam for the ascending fluids (Fig. 2). The result is a highly-deformed, almost barren area in the south, the inverted Guinas Growth Fault and the silicified Guinas Thrust Horizon in the center and the less deformed Uris-Tsumeb-mining area with all the base metal sulphide deposits, as a precursor for further supergene Cu- and V-enrichments in the north.

References

- Frimmel HE, Klätzli US& Siegfried PR (1996) New Pb-Pb single zircon age constraints on the timing of Neoproterozoic glaciation and continental break-up in Namibia. *J Geol* 104, 459–469

- Frimmel HE (2004) Neoproterozoic sedimentation rates and timing of glaciations — a southern African perspective. In: Eriksson PG, Altermann W, Nelson DR, Mueller WU, Catuneanu O (eds) *The Precambrian Earth: Tempos and Events*. Elsevier Amsterdam 459–472
- Goscombe B, Gray D & Hand M (2004) Variation in Metamorphic Style along the Northern Margin of the Damara Orogen, Namibia. *J Petr* 45(6), 1261–1295
- Haack U & Martin H (1983) Geochronology of the Damara Orogen - A Review. In: Martin H, Eder FW (eds) *Intracontinental Fold Belts*. Springer Heidelberg pp 945
- Haack U, Gohn E & Klein JA (1980) Rb/Sr Ages of Granitic Rocks Along the Middle Reaches of the Omaruru River and the Timing of Orogenetic Events in the Damara Belt (Namibia). *Contrib Mineral Petrol* 74, 349–360
- Hoffmann K-H, Condon DJ, Bowring SA & Crowley JL (2004) U-Pb zircon date from the Neoproterozoic Ghaub Formation, Namibia: Constraints on Marinoan glaciation. *Geology* 32(9), 817–820
- Petzel VFW (1993) Progress report on exploration conducted in the Tsumeb Grant Area. M46/3/132A Gold Fields Namibia Ltd
- Kamona AF, Leveque J, Friedrich G & Haack U (1999) Lead isotopes of the carbonate-hosted Kabwe, Tsumeb, and Kipushi Pb-Zn-Cu sulphide deposits in relation to Pan African orogenesis in the Damaran-Lufilian fold belt of Central Africa. *Min Dep* 34(3), 273–283

Neue Perspektiven der Texturanalytik von Gesteinen mit konventioneller Röntgenbeugung *Poster*

Bernd Leiss¹ Klaus Ullemeyer²

Technische Entwicklungen und verbesserte Messmethoden haben in den vergangenen 15 Jahren in der Gesteinstexturanalyse zu einer zunehmenden Nutzung vor allem der Elektronen- und Neutronenbeugung geführt. Dabei ist die Anwendung der Röntgentexturanalyse in der Geologie in den Hintergrund getreten. Neue technische Optionen dieser Methode, wie sie zum Beispiel für die Qualitätskontrolle in der Siliziumchipherstellung entwickelt worden sind, haben noch keinen Eingang in die Gesteinstexturanalyse gefunden. Steht die volumenbezogene Gesamttexturanalyse im Vordergrund, so hat die Röntgenbeugung spezifische Vorteile. Gegenüber der Elektronenbeugung am Rasterelektronenmikroskop (Backscatter Electron Diffraction) ist keine aufwendige Probenpräparation notwendig und es kann ein wesentlich größeres Probenvolumen erfasst werden. Gegenüber der Neutronenbeugung ist die Röntgenbeugung wesentlich kostengünstiger und die zur Verfügung stehende Messzeit ist im Prinzip unbeschränkt.

Nachteile der Röntgentexturanalyse sind die notwendige Messdatenkorrektur aufgrund der Defokussierung des Messstrahls im Verlauf der Messung (Ullemeyer & Weber 1994), die unter Umständen schlechte Auflösung bezüglich Gitterabstand d , und das gegenüber der Neutronenbeugung wesentlich ge-

¹ Geowissenschaftliches Zentrum Göttingen, Goldschmidtstraße 3, 37077 Göttingen

² Geologisches Institut, Universität Freiburg, Albertstr. 23B, 79104 Freiburg

ringere messbare Probenvolumen. Die Anwendung der Röntgentexturanalyse war daher klassischerweise auf monophase und feinkörnige Gesteine beschränkt.

Um diese Nachteile der Röntgentexturanalyse kostengünstig zu minimieren, wurde für die Abteilung Strukturgeologie und Geodynamik des Geowissenschaftlichen Zentrums der Universität Göttingen ein neues Röntgentexturgoniometer auf der Basis von neu entwickelten standardisierten Bauteilen für die Gesteinstexturanalyse individuell konfiguriert und die Messdatenauswertestrategie angepasst:

- Glasfaserkapillaren (Polykapillare) ermöglichen eine Parallelisierung des Primärstrahls auf einen maximalen Durchmesser von 7 mm bei nur geringem Intensitätsverlust. Damit ist ein vergleichsweise großes Probenvolumen in kurzer Zeit messbar
- die hohe Strahlintensität erlaubt in Kombination mit entsprechenden Kollimatoren auf der Sekundärseite trotz kurzer Messzeiten eine hohe d -Wert-Auflösung
- eine zusätzliche Kreuzblende auf der Sekundärseite erlaubt die Verkleinerung des Messstrahls und damit individuelle Strahlgeometrien bei spezifischen Fragestellungen (z.B. Messung lokaler Texturen)
- ein in X und Y verfahrbarer Probentisch erlaubt Translationsbewegungen, um das genutzte Probenvolumen zu erhöhen, lokale Texturen automatisiert innerhalb eines 100×100 mm großen Rasters zu messen, oder mehrere Proben nacheinander automatisch zu messen

- der Probentisch erlaubt Probengrößen mit bis zu 20 cm Durchmesser und 24 mm Höhe

Durch diese erweiterten Anwendungsmöglichkeiten der Röntgentexturanalytik auf grobkörnigere und/oder polymineralische Gesteine und die lokale Texturanalyse per Rastermessung, sowie die gleichzeitige Erhöhung des Proben-durchsatzes werden wesentlich umfangreichere Datensätze erzeugt. Des Weiteren hängt die Qualität der resultierenden Polfiguren stark von der zuverlässigen Korrektur des Defokussierungseffekts ab. Die bewährte empirische Korrektur mit Hilfe regelloser Pulvermessungen soll beibehalten werden, denn sie erlaubt auch die Korrektur von Kornformeinflüssen, die z.B. bei Polfigurmessungen an Schichtsilikaten bei sehr kleinen Streuwinkeln erheblichen Einfluss haben (Ullemeyer & Weber 1994). Auch kleinere Justierungsfehler beim Probeneinbau können unter Umständen nachträglich korrigiert werden. Da der Defokussierungseffekt von mehreren Parametern abhängt (Strahldimensionen, Streuwinkel, Kornformanisotropie), muss für routinemäßige Korrekturen eine umfangreiche Datenbank zur Verfügung stehen. Aufgrund der schnellen und automatisierten Messungen ist die Erstellung und Aktualisierung der Datenbank unproblematisch.

Mit Hilfe von Texturmessungen senkrecht zueinander stehender Schnittlagen ist die Güte der Defokussierungskorrekturen sehr gut abschätzbar: bis zu einem Kippwinkel von 70° ist die Korrektur unproblematisch und je nach Anforderung an die Messung oft bis 80° hinreichend genau. Die hier nur im Reflexionsmodus messbaren experimentelle Röntgentexturpolfiguren sind jedoch generell unvollständig. Um vollständige Polfigu-

ren zu erzeugen gibt es zwei Herangehensweisen:

- i) ist erkennbar, dass in den Ausfallsbereichen keine wesentlichen Texturinformationen enthalten sind (Bereiche unter ein mal die Gleichverteilung), lassen sich fehlende Daten durch Extrapolation berechnen
- ii) die Daten aus drei senkrecht zueinander stehender Schnittlagen werden kombiniert.

Da alle bekannten Programme für die quantitative Texturanalyse mit unvollständigen Polfiguren umgehen können, kann alternativ auf die Vervollständigung der Polfiguren verzichtet werden. Die dann erforderliche größere Zahl an Eingabepolfiguren kann aufgrund der Geschwindigkeit der Messungen leicht gewonnen werden.

Die Kombination neuer Messoptionen aufgrund weiter entwickelter technischer Komponenten mit optimierten Korrekturfunktionen und der vergleichsweise kostengünstige Betrieb erweitern die Anwendungsmöglichkeiten der an sich konventionellen Röntgentexturanalytik enorm und ermöglichen damit auch die Bearbeitung neuer Fragestellungen in den Geowissenschaften. Bezüglich der nutzbaren Probenvolumina bewegt sich die Röntgentexturanalytik in der vorgestellten Konfiguration im mm- bis cm-Bereich und steht damit zwischen der Elektronen (μm bis mm)- und Neutronenbeugung (cm-Bereich). Die Röntgentexturanalytik sollte bei entsprechenden Texturanalyseanforderungen wieder stärker berücksichtigt werden.

Literatur

Ullemeyer K & Weber K (1994) Correction of phyllosilicate (002) X-ray pole fig-

re measurements. In: Textures of Geological Materials (eds. Bunge et al.), DGM Informationsgesellschaft-Verlag, Oberursel, pp 83

Asymmetrical deformation of the Piton de la Fournaise (Réunion Island) summit cone *Poster*

Ludovic Letourneur¹
Agust Gudmundsson¹

Piton de la Fournaise (Réunion Island) is an active basaltic shield volcano in the south-western part of the Indian Ocean. The activity consists essentially of lava being issued from two rift zones close to the summit cone. The summit cone has been monitored since 1980 by the OVPF (Volcanological Observatory of Piton de la Fournaise). Geodetic data and radar interferometry show a systematic asymmetric pattern of deformation associated with all the N-S trending eruptive fissures (Briole et al. 1998, Sigmundsson et al. 1999).

The asymmetric deformation has been interpreted in various ways. The two main models proposed are (1) eastward dip of the dykes, based on inversion of data provided by radar interferometry (Sigmundsson et al 1999), and (2) the existence of a free boundary in the east part of the volcano. The second model allows the accommodation of dykes by eastward displacements, whilst the western part of the volcano is supported by the existing Piton des Neiges (Lénat et al., 1989). However,

¹ Department of Structural Geology and Geodynamics, Geoscience Centre, University of Göttingen, Germany

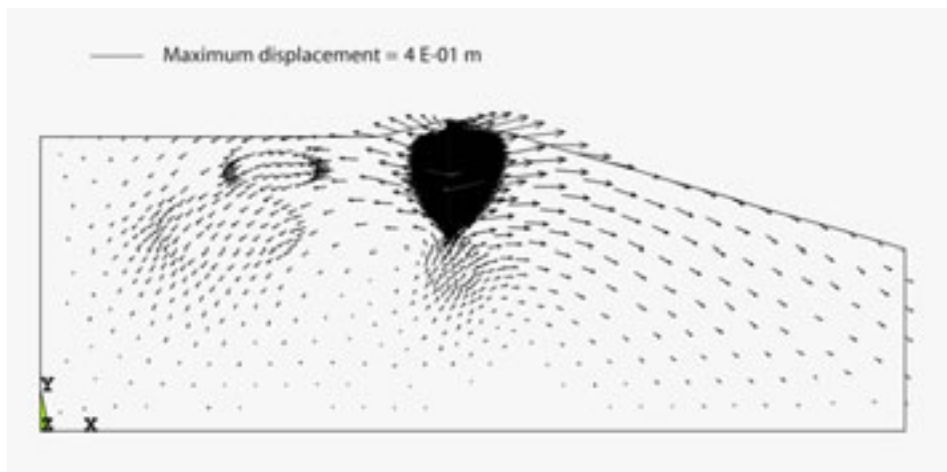


Figure 1: Numerical model showing the displacement triggered by the injection of an overpressured dyke (1 MPa) in the summit cone of an asymmetric volcano. Unit = 1 km

no displacements occur along the eastern coastline of Piton de la Fournaise. The only parts of the volcano affected by deformation are the rift zones and the summit cone. Moreover, geodetic data provided by the new real-time GPS network show that there is an asymmetric deformation of the summit cone prior to eruption (Staudacher 2005). The deformation itself seems to be related to pressure increase in the magma chamber. Absence of permanent displacements during periods of rest (such as 1992–1998) (Briole et al. 1998) support this link between magmatic pressure and deformation.

Here we complement previous deformation studies by the results of several numerical models that aim at understanding the internal processes resulting in deformation of the volcano. We investigate the influence of different parameters such as the topography and the lateral mechanical heterogeneity revealed by gravimetric data and seismic data. We are able to obtain an asymmetric

deformation as resulting from (1) the asymmetric topography of the volcano, and (2) the existence of a pluton under the Plaine des Sables area. The asymmetric topography can explain the major part of the asymmetric deformation, whilst the existence of pluton beneath the Plaine des Sables area arrests the propagation of deformation in the western part of the volcano.

Our models explain the large features of the asymmetric deformation observed during eruptions at Piton de la Fournaise Volcano. Vertical and lateral heterogeneities are very important for understanding the deformation. In the case of Piton de la Fournaise Volcano, absence of deformation on the other parts of the volcano, especially the lower eastern part, whilst the upper part shows much deformation, implies that stresses concentrate primarily in the eastern flank.

References

- Briole P, Bachèlery P, McGuire B, Moss J, Ruegg J-C & Soubraut P (1998) Deformation of Piton de la Fournaise: Evolution of the monitoring techniques and knowledge acquired in the last five years. In: Casale R, et al. (eds) *The European Laboratory Volcanoes, Proceedings of the Second Workshop Santorini, Greece 2 to 4 May 1996*, pp 467–474
- Lénat J-F, Bachèlery P, Bonneville A & Hirn A (1989) The beginning of the 1985-1987 eruptive cycle at Piton de la Fournaise (La Réunion); new insights in the magmatic and volcano-tectonic systems. *J Volcanol Geotherm Res* 36, 209–232
- Sigmundsson F, Durand P & Massonnet D (1999) Opening of an eruptive fracture and seaward displacement at Piton de la Fournaise volcano measured by RADARSAT satellite radar interferometry. *Geophys Res Lett* 26, 533–536
- Staudacher T (2005) *Bulletin de l'observatoire volcanologique du Piton de la Fournaise*, 23 September 2005

Effect of crystallography and temperature on the development of quartz high-angle grain boundaries in metamorphic rocks

Poster

Christoph Liebl¹ Boriana Kuntcheva^{†1}
Jörn H. Kruhl¹ Karsten Kunze¹

Grain boundary migration during dynamic recrystallization of quartz results in grain boundary suturing of various extent. The geometry of the sutured boundaries is affected not only by temperature, strain rate, finite strain and

¹ Tectonics and Material Fabrics Section, Technische Universität München, D-80290 München, Germany ² Geologisches Institut, ETH Zürich, CH-8092 Zürich, Switzerland

[†] Boriana Kuntcheva, 8.10.1971–9.11.2004

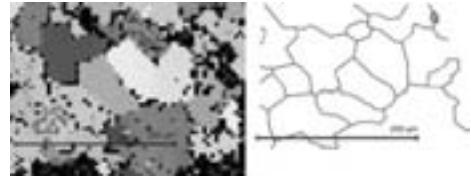


Figure 1: Thin-section outline (right) and orientation image map (OIM) (left) for part of the measured area, obtained as result of the combined beam/stage EBSD measurements; confidence index >0.2; step size 5 micrometer; boundary levels: 15°.

differential stress, but also by internal properties such as the defect distribution and crystallographic orientations. Consequently, the grain boundary geometry may provide information about these conditions and properties.

In continuation of a previous study (Kuntcheva et al.) the complete crystallographic orientation of quartz grain boundaries was measured, based on a combination of electron backscatter diffraction (EBSD) and universal-stage (U-stage) measurements. For this purpose a sample of granite from the northern Aar Massif (Central Alps, Switzerland) was taken, deformed at temperatures up to 300–350°C at the end of the Lepontine event of the Alpine Orogenesis. The former magmatic quartz partly recrystallized dynamically to grains of ca. 50–100 micrometer diameter, with weakly sutured grain boundaries showing no curved but always straight segments (Fig. 1) as typical for quartz grain boundaries in metamorphic rocks (Kruhl & Peternell, 2002). In addition, at grain boundary triple junctions the dihedral angles generally deviate from 120 degree. These observations indicate anisotropy of grain boundary energies.

The measurement of the Aar Massif

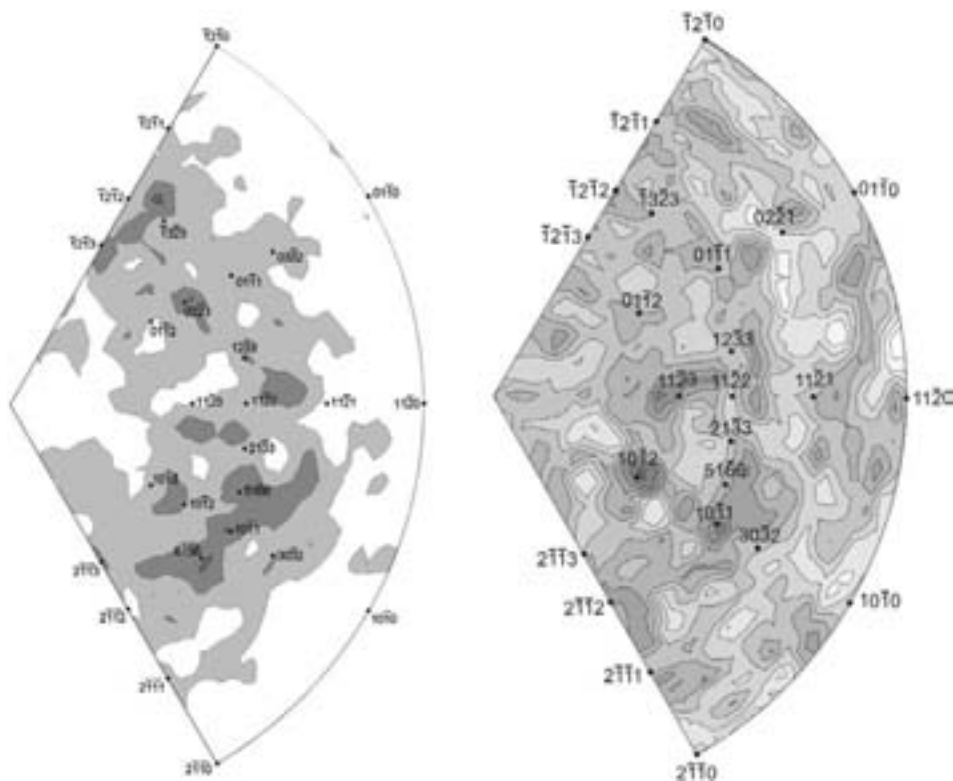


Figure 2: Frequency distribution of quartz grain boundaries (inverse pole figure, Schmid net, upper hemisphere). Each grain boundary is represented with respect to the crystallographic system of both neighbouring grains and, consequently, occurs in two different orientations. For comparison, low-index planes of quartz are indicated. Left: 3320 measurements from a quartzite from the Barrow metamorphic zones of the Scottish Highlands, deformed during increasing temperatures up to mid-amphibolite facies conditions. Contour intervals = $0.5 \times$ uniform distribution, starting at 1. Modified after Kuntcheva et al. Right: 6288 measurements from a granite from the northern Aar Massif (Central Alps, Switzerland), deformed at temperatures up to $300\text{--}350^\circ\text{C}$. Contour intervals = $0.25 \times$ uniform distribution, starting at 1.

granite sample by combined EBSD/U-stage methods led to 3144 quartz grain boundary segments, the orientation of which was calculated with respect to both neighbouring grains so that a final data set of 6288 segment orientations was achieved. In accordance with Kuntcheva et al. the segments do not occupy preferred low-index or coinci-

dence site lattice orientations with respect to both neighbouring grains, i.e., they do not represent special boundaries. They preferentially occupy rhombohedral, trapezohedral and bipyramidal positions, i.e. positions in a ca. $30\text{--}50$ degree girdle to the c-axis, however, to a less extent than the quartz analyzed by Kuntcheva et al. The strongest

maxima in the girdle are near the $(10\bar{1}2)$ plane of quartz, the other two near the $(10\bar{1}1)$ and the $(11\bar{2}3)$ planes. In general, however, positions near the basal and near the prism planes occur, too (Fig. 2, right).

With such a high number of measurements special grain boundary geometries, like triple junctions or zigzag structures, or segment orientations with respect to both neighbouring quartz grains could be investigated on a sufficiently broad data basis. Specifically, the orientations of grain boundary segments at triple junctions show a distinct dependency on the size of the angles at the triple junctions. In general, segments with a preferred crystallographic orientation, with respect to one neighbouring quartz grain, often shows a preferred orientation with respect to the other neighbouring grain, too.

As shown by HRTEM studies on gold crystals, a partly ordered transition from one to the other crystal occurs across straight grain boundary segments (Wolf & Merkle, 1992). Consequently, the atoms across such a boundary are bound in periodically repeated sections, whereas in other sections the crystal is strongly elastically distorted. We suggest that these results may also serve as an explanation for the present observations on quartz grain boundaries.

Together with the previous study by Kuntcheva et al. the present study confirms the preliminary results on the temperature-dependency of the crystallographic control of quartz grain boundaries, based exclusively on universal-stage measurements (Kruhl & Peterzell 2002). At relatively low temperatures, i.e., just above the quartz recrystallization temperature of about 300°C, the grain boundary segments oc-

cupy a broad spectrum of crystallographic orientations with only a weak preference for rhombohedral and trapezohedral positions. However, at mid-amphibolite facies temperatures the segments concentrate in a ca. 30°-50 degree girdle to the c-axis. Further investigations will show if this relationship holds to higher temperatures and represents a general reduction to rather few (meta)stable crystallographic grain boundary orientations with increasing temperatures, which may represent a potential geothermometer. Since the development of sutured grain boundaries is a geologically short process that takes place during and immediately after deformation, the studied quartz grain boundaries can be considered as stabilized post-tectonic textures, with more or less stable crystallographic orientations for the given geological conditions, mainly the temperature immediately after deformation.

Literatur

- Kruhl JH & Peterzell M (2002) The equilibration of high-angle grain boundaries in dynamically recrystallized quartz: the effect of crystallography and temperature. *Journal of Structural Geology* 24: 1125-1137.
- Kuntcheva BT, Kruhl JH & Kunze K (in revision) Crystallographic orientations of high-angle grain boundaries in dynamically recrystallized quartz: first results. *Tectonophysics*.
- Wolf D & Merkle KL (1992) Correlation between the structure and energy of grain boundaries in metals. In: Wolf D & Yip S (ed) *Materials Interfaces*. Chapman & Hall, London, pp 87-150.

Change of deformation mechanisms during low temperature flow of rocks — observation from micron to nanometer scales

Vortrag

Junlai Liu¹ Shuyun Cao¹

Recent studies on nano-materials in materials science revealed that nano-materials may have fantastic features due mainly to size-effect of the materials. For example, nano ceramics may have very high ductility at room temperatures and pressures, even though normal ceramics is easily deformed by brittle fracturing.

What and how much do we know about the nature of nano or nano to micron scale geological materials? What factors contribute to their occurrence? How do they flow at geological conditions and how do they affect the rheology of rocks? Upper crustal deformation is characterized by low temperature flow of rocks under unsteady state, which results in progressive grainsize reduction and leads to the occurrence of micron to nano meter scale materials in fault zones. The examples of naturally-deformed upper crustal rocks presented in the paper help to unravel the importance of nano to micron scale rock materials during the low temperature flow of rocks.

Cataclastically faulted marble, limestone and dolomite from the Autseib fault zone, Namibia, and micro-breccias from detachment fault zones in several metamorphic core complexes (mcc's), e.g. the Whipple mountains mcc in Western USA, Jinzhou mcc, and Huh-

hot mcc in North China are studied with optical microscope, CL microscope, SEM, and TEM. It is shown from the present study that micron to nano scale materials do occur during natural faulting at low temperatures in the upper crust. Macroscopic brittle features are shown primarily by the field occurrence of zones of microbreccias or cataclasites. Angular clasts with straight or irregular boundaries are randomly distributed in extremely fine-grained matrix and they do not show any evidence of preferred dimensional or lattice orientation. There is either clear or vague transition from clasts to matrix along the clast boundaries, which is also clearly shown by SEM studies. The matrix materials are extremely fine grains from micron to nano meter scales. They have optically irregular or vermiculate forms and are either fine clasts of grain aggregates or single grains. At the highest strain zones, rare clasts are observed. Single grains, however, predominate in the matrix and often have polygonal forms. TEM studies reveal great differences in dislocation patterns between coarse-grained clasts and fine-grained matrix. Dislocation substructures are widespread in grains of different sizes and origins. Tangled dislocations are the most common dislocation substructures in coarse-grained clasts, although free dislocations, dipoles, dislocation loops, dislocation walls and irregularly connected dislocations are also observed either jointly or separately in deformed grains in the clasts. A general tendency is that dislocations are more and more regularly organized towards clast boundaries. Tangled and irregularly connected dislocations occur mostly in the central grains of relatively big clasts, while walls of well-organized disloca-

¹ State Key Laboratory of Geological Processes and Mineral Resources, China University of Geosciences, Beijing 100083, China

tions occur mainly near the boundaries, constituting subgrain boundaries. It is shown from TEM observations that tangled dislocations occur mainly in clasts with sizes greater than several tens of microns and well-organized dislocations and subgrains predominate clasts with sizes smaller than that limit. Fine-grains are $0.02\ \mu\text{m}$ to $3\ \mu\text{m}$ in sizes and characterized by polygonal shapes. They have regular and straight boundaries, and are generally dislocation free or contain only very few free dislocations. Grain sizes of the fine grains vary in the range from hundreds of nano meters to tens of microns. The fine grains generally have no preferred dimensional orientation. Due to extremely fine grain sizes their lattice orientation is undetectable.

On the other hand, there are often micropores along grain boundaries between the fine grains. This, together with the cathodoluminescence difference between big clasts and fine matrix may imply the importance of fluid phases during flow of the fault rocks.

The above evidence lead to the following conclusions:

- i) Micron to nano meter scale geological materials are common in highly deformed crystalline rocks. Their occurrence is attributed to unsteady state progressive shearing and grain size reduction along fault zones in the upper crustal level.
- ii) Variation of grain sizes at micron to nano meter scales in rocks has strong effects on the flow of the rocks at natural strain rate and deformation conditions. The grain-size range from $n \times 10^{-1}\ \mu\text{m}$ to $n \times 10^1\ \mu\text{m}$ is an important range
- iii) Variation in deformation mechanisms at micron to nano meter scales is interpreted as the results of grain-size reduction to a very high level at unsteady state and the effects of fluid involvement in the deformation of the extremely fine-grained rock materials. There is a sharp decrease in surface area with grain sizes. Such an increase and fluid flow may both enhance diffusion of atoms or lattice defects towards grain boundaries and from grain to grain. Both effects contribute to the variation of deformation mechanisms of naturally deformed rocks at upper crustal levels.

Paläofluide in störungskontrollierten Bruchsystemen der Aachener Geothermie-Bohrung

Vortrag

M.J. Lögering¹ J. Kolb¹ F.M. Meyer¹
J. Schwarzbauer²

Einleitung

In der vorliegenden Arbeit werden geologische Prozesse im Untergrund des linksrheinischen Rhenoharzynikums und deren Verhältnis zum regional-tektonischen Rahmen anhand der Proben aus der Aachener Geothermie-Bohrung mit dem Schwerpunkt des Fluid- und Stofftransportes untersucht. Die methodische Vorgehensweise basiert auf einer systematischen und detaillierten Bestandsaufnahme der Paläofluide in Form von Flüssigkeitseinschlüssen an Kernmaterial der Bohrung. Im Aachener Raum wurden Untersuchungen von Flüssigkeitseinschlüssen hauptsächlich an postvariszischen Pb-Zn-Gangvorkommen durchgeführt. Die Homogenisierungstemperaturen (T_h) von NaCl-CaCl₂-Lösungen unterschiedlicher Salinität liegen zwischen 70°C und maximal 190°C (Redecke 1992, Stroink 1993, Muchez et al. 1994, Glasmacher 1995). Für die tektonisch-metallogentische Entwicklung des Rheinischen-Schiefergebirges können generell zwei Fluid-Aktivitätsperioden unterschieden werden (Behr et al. 1993). Die im Zuge der variszischen Gebirgsbildung synkinematische Defluidisierung des Orogenkörpers generierte das Fluid-System der ‚Tectonic Brines‘

(1). Diese sind Na-(K)-Cl-betonte Lösungen geringer Salinität mit CO₂, CH₄ und N₂ sowie durch $T_h \leq 350^\circ\text{C}$ gekennzeichnet. Im Gegensatz dazu wurden die meisten postvariszischen Ganglagerstätten des Rheinischen-Schiefergebirges durch ‚Basement Brines‘ (2) gebildet. Diese sind Ca-Na-Cl-Lösungen hoher Salinität mit $T_h \leq 250^\circ\text{C}$ (Behr et al. 1993).

Regionale Geologie

Die 2544 m tiefe Bohrung befindet sich ca. 500 m nordwestlich der Aachener Überschiebung und durchteuft Gesteine des Karbon und Devon. Die untersuchte Kernstrecke von 1391 m bis 1516 m umfasst Gesteine des Ober Devon. Sie besteht aus Ton-Silt-Feinsandstein Wechselfolgen mit zwischengeschaltetem Dolomit, Dolomit- bzw. Kalzitmergel und bioreliktischem Knollenkalk. Ton-Siltbereiche sind mehrfach geschiefert. Die zweite Schieferung ist durch eingeregelter Chlorit gekennzeichnet. Karbonatbereiche sind dolomitisiert. Die Lithologien wurden wiederholt von kataklastischen Deformationsprozessen erfasst. Die Nordost-Südwest streichende Aachener Überschiebung lässt sich nach Westen hin über die Eifel-Überschiebung bis hin zur Faille du Midi-Überschiebung bis nach Belgien verfolgen. Im östlichen Rheinischen Schiefergebirge sind bedeutende variszische Überschiebungen West-Ost gerichtet. Die Pb-Zn Vererzungen im Aachener Raum sind an postvariszische, Nordwest-Südost angelegte Störungszonen gebunden.

Gangpetrographie

Die lithologischen Einheiten werden von unterschiedlich orientierten, teilweise konjugierten Gängen und Gangsysteme-

¹ Institut für Mineralogie und Lagerstättenlehre, RWTH Aachen, Wüllnerstr. 2, D-52056 Aachen ² Lehrstuhl für Geologie, Geochemie und Lagerstätten des Erdöls und der Kohle, RWTH Aachen Lochnerstr. 4-20, D-52056 Aachen

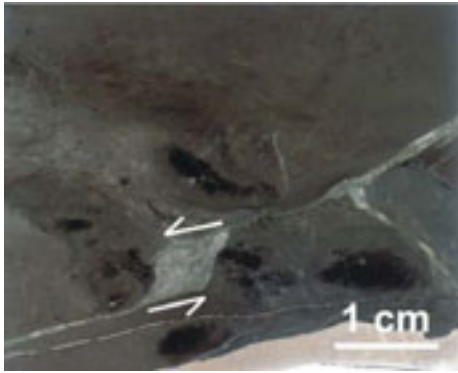


Abbildung 1: Schergang mit befreiender Krümmung (Teufe 1483,84 m)

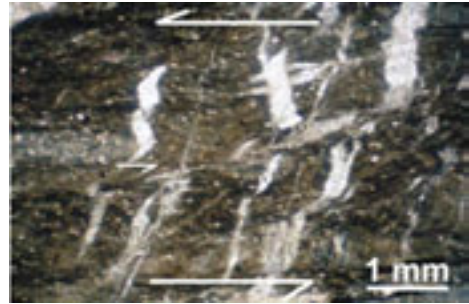


Abbildung 2: Quarz-Karbonat-Gänge als Fiederspalt (Teufe 1433,7 m)

men durchschlagen. Die Gänge zeigen syntaxiale, aber auch antitaxiale Ganggefüge und variieren in der Mächtigkeit von <1 mm bis 3 cm. Drei Gangtypen werden unterschieden:

- i) Quarz-Karbonat Gänge \pm Chlorit \pm Sulfat,
- ii) Karbonat Gänge \pm Chlorit und
- iii) Quarz Gänge \pm Chlorit.

Die hydrothermale Fällung des Mineralinhaltes der Gänge erfolgte mit der episodischen tektonischen Öffnungsbewegung. Die Gänge werden aufgrund der Tektonik und ihrer Geometrie in Schergänge, befreiende Krümmungen (dilational jog) und Fiederspalt gegliedert (Abb. 1 u. 2). Duktile Deformation wird durch die Rekristallisation von Quarz, Kalzit und Dolomit angezeigt. Die Rekristallisation findet hauptsächlich an Gangrändern, aber auch innerhalb der Gänge statt. Durch den bruchkontrollierten Fluidfluss kam es zu hydrothermalen Alteration des Nebengesteins, die vor allem durch Dolomit- und Chloritneubildung gekennzeichnet ist.

Flüssigkeitseinschlusspetrographie

Bei den Flüssigkeitseinschlüssen im Quarz sowie Kalzit und Dolomit handelt es sich um dunkle, CO_2 -reiche und transparente, H_2O -reiche zweiphasige Einschlüsse. Dabei kann im Quarz zwischen ca. 15–30 μm großen, primären Einschlüssen, die isoliert innerhalb von Kristallen auftreten und ca. 4–8 μm großen, sekundären Einschlüssen, die entlang von Trails, Korngrenzen und in Klustern auftreten, unterschieden werden. Die Einschlüsse im Kalzit und Dolomit kommen als Cluster oder isoliert vor. Sie sind überwiegend 2–8 μm , vereinzelt bis zu ca. 25 μm groß und primär eingeschlossen. Sekundäre Einschlüsse im Kalzit und Dolomit sind selten und kommen als Trails vor. Die Einschlüsse zeigen unterschiedliche Homogenisierungstemperaturen, die durch eine Temperaturzunahme vom Zentrum der Gänge ($T_h = 240\text{--}260^\circ\text{C}$) zum Gangrand ($T_h = 330\text{--}360^\circ\text{C}$) gekennzeichnet sind. Gasförmige Inhaltsstoffe von Fluideinschlüssen wurden mittels Gaschromatographie als CO_2 , CH_4 und N_2 bestimmt (Abb. 3).

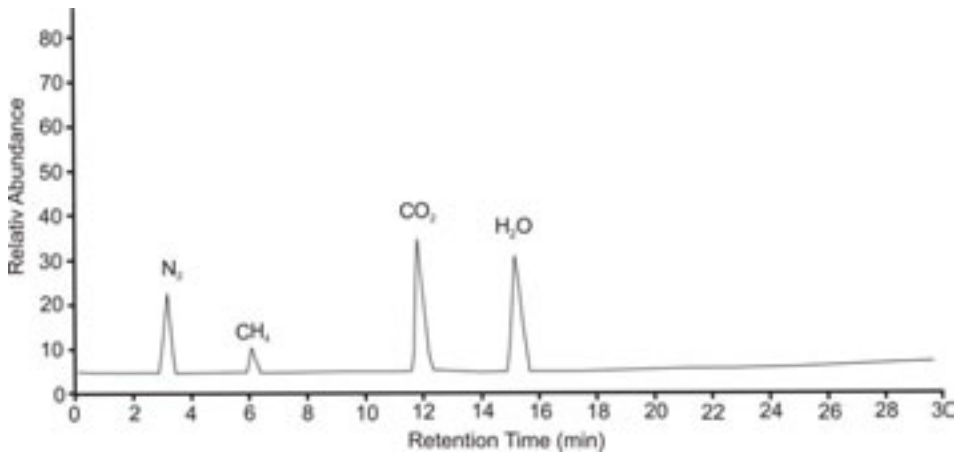


Abbildung 3: Gaschromatogramm der Flüssigkeitseinschlüsse aus einem Quarz-Karbonat Gang

Mikrothermometrie und Geothermometrie

Die Fluide der primären und sekundären Einschlüsse bestehen aus Na-(K)-Cl-haltigen Lösungen mit einer geringen Salinität. Die Homogenisierungstemperaturen sekundärer Einschlüsse in Quarz der Quarz-Karbonatgänge (1) bzw. der Quarzgänge (3) sind mit einer Salinität von ca. 5 Gew.% NaCl-Äq. und Th von 180 bis 230°C relativ einheitlich, während die primären Einschlüsse in den Quarz-Karbonatgängen (1) im höheren Th von 240 bis 380°C streuen und eine Salinität von <4–6 Gew.% NaCl-Äq. aufweisen. In den Karbonatgängen (2) haben die Einschlüsse im Kalzit unterschiedliche Th von 240–280°C und Salzgehalte von <4–5 Gew.% NaCl-Äq. Die Einschlüsse im Dolomit haben eine Salinität um 6 Gew.% NaCl-Äq. und bilden zwei Gruppen mit T_h bei 310°C bzw. 370°C. Die T_h der Einschlüsse in den Quarz-Chlorit Gängen (3) liegen bei 360°C mit einer Salinität von 6–<9 Gew.%

NaCl-Äq. (Abb. 4). Kalzit-Dolomit Geothermometer ergeben Temperaturen ähnlich der mikrothermometrischen Daten primärer Einschlüsse zwischen 280 bis 370°C. Unterschiedliche Chloritthermometer ergeben konsistente Temperaturen zwischen 290 bis 350°C und zeigen mit den Isochoren der primären Fluideinschlüsse im Quarz und Kalzit-Dolomit Drücke von 2 kbar an.

Diskussion

Die sekundären Flüssigkeitseinschlüsse mit geringer Salinität und Homogenisierungstemperaturen von 180°C bis 230°C zeigen ein späteres Reaktivierungsereignis und somit möglicherweise einen postvariszischen Fluidtransport, der mit der regionalen Pb-Zn-Vererzung im Zusammenhang stehen könnte. Die untersuchten primären Flüssigkeitseinschlüsse mit T_h von 240 bis 380°C sind bisher im linksrheinischen Schiefergebirge nicht beschrieben worden. Die Fluide sind Na-(K)-Cl-betonte Lösungen ge-

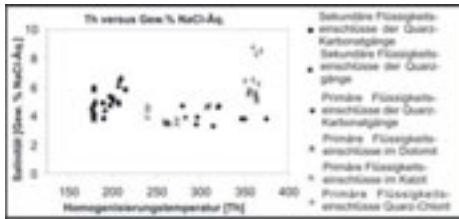


Abbildung 4: Diagramm für die Salinität (Gew.% NaCl-Äq.) Gegen die Homogenisierungstemperatur (T_h) für die Einschlüsse in Quarz-, Kalzit- und Dolomitkristallen

ringer Salinität. Die T_h und die Zusammensetzung der Fluide können aufgrund der gleichen Fluidzusammensetzung direkt mit den ‚Tectonic Brines‘ im variszischen Basement von Mitteleuropa (Behr et al. 1993) korreliert werden. Desweiteren zeigen Ergebnisse der Untersuchungen von Schroyen et al. (2000) und Muechez et al. (2000) im Falten und Überschiebungsgürtel von Ostbelgien sowie in den Varisziden von Belgien und Nordfrankreich ähnliche Homogenisierungstemperaturen und Zusammensetzungen der Fluide.

Die Bohrung befindet sich im Überschiebungsgürtel der Aachen-Überschiebung. Daher erfolgte der Fluidtransport vermutlich entlang der SW-NE gerichteten Aachener Überschiebung während der variszischen Gebirgsbildung. Die hohen Fluidtemperaturen im Zusammenhang mit der nicht weit in das Nebengestein reichenden Alteration lassen auf ein geringes Fluid/Gesteins-Verhältnis schließen und implizieren damit einen kurzzeitigen, episodischen Fluidfluss durch tektonische Öffnungsbewegungen entlang von Scherzonen. Diese Fluide sind durch die primären Einschlüsse der Aachener Geothermie-Bohrung repräsentiert. Dem gegenüber stehen die Fluideinschlüsse von postva-

riszischen Pb-Zn-Gangvorkommen, wobei hier allerdings der Fluidtransport entlang des NW-SE gerichteten postvariszischen Störungssystems verläuft. Die Aachener Geothermie-Bohrung stellt das fehlende Glied zwischen den Untersuchungen an Falten- und Überschiebungsfronten der Eifel-Überschiebung und der Faille du Midi-Überschiebung nach Westen und dem Rheinischen Schiefergebirge nach Osten dar.

Literatur

- Behr HJ, Gerler J, Hein UF & Reutel CJ (1993) Tectonic Brines and Basement Brines in den mitteleuropäischen Varisziden: Herkunft, metallogentische Bedeutung und geologische Aktivität. *Göttinger Arb. Geol. Paläont.* 58, 3–28
- Glasmacher U (1995) Variszische und postvariszische Fluidsysteme. In: Walter R, Glasmacher U & Wolf M, (eds): KW-relevante Eigenschaften potentieller Mutter- und Speichergesteine am Nordrand des Linksrheinischen Schiefergebirges. RWTH Aachen, BMBF-Forschungsprojekt 032 6804 A 5, 01.04.1991-30.09.1994, Teil 5, 1–40
- Muechez P, Slobodnik M, Viaene W & Keppens E (1994) Mississippi Valley-type Pb-Zn mineralization in eastern Belgium: indications for gravity-driven flow. *Geology* 22, 1011–1014
- Muechez P, Sintubin M & Swennen R (2000) Origin and migration pattern of palaeofluids during orogeny: discussion on the Variscides of Belgium and northern France. *Journal of Geochemical Exploration*, 69–70, 47–51
- Redecke, P (1992) Zur Geochemie und Genese variszischer und postvariszischer Buntmetallmineralisation in der Nordeifel und der Niederrheinischen Bucht. RWTH Aachen, Dissertation, pp 159
- Schroyen K & Muechez P, (2000) Evolution of metamorphic fluids at the Variscan fold-and-thrust belt in eastern Belgium. *Sedimentary Geology* 131, 163–180
- Stroink L (1993) Zur Diagenese paläozoischer Sandsteine am Nordrand des Linksrheinischen-Ardennischen Schiefergebirges. Aachener Geowissenschaftliche Beiträge, Band 1, Verlag der Augustinus Buchhandlung, Aachen, pp 190

The role of penetrative deformation in orogenic processes. An example from the Eastern Cordillera of Colombia

Vortrag

Andrés Mora¹ Mauricio Parra¹ Manfred Strecker¹

The Lower Cretaceous units of the Eastern Cordillera of Colombia have been deposited during a stage when the area where nowadays lies a contractional orogen was an actively deforming rift. Therefore, they are syn-rift sedimentary units. These rocks have a unique feature in the Cretaceous sedimentary column of this mountain chain. This is a widespread planar fabric expressed mostly as a penetrative slaty cleavage. This planar fabric is only macroscopically evident in Cretaceous units older than Barremian. Planar fabric (e.g. slaty cleavage) is one of the products of internal or penetrative deformation (i.e. contractional deformation at microscopical scale in rock units). Pressure solution and even cleavage have been recently reported in areas undergoing only subtle burials (Engelder & Marschak 1985). However, in the Eastern Cordillera, the units where planar fabric is evident are the base of a sequence of at least 5 km and they have vitrinite reflectance values up to 2. These data and the formation of clorithoid contemporary with the slaty cleavage, allow us to propose that this planar fabric was developed when the Lower Cretaceous units had an amount of overburden close to the thickness of the entire Cretaceous sequence.

We carried out finite strain measure-

ments using the enhanced normalized Fry method (Erslev 1988) in order to quantify the shortening by internal deformation in various localities in the Eastern Cordillera. For this purpose we used thin sections of sandstones containing macroscopically evident planar fabrics as recommended by Dittmar et al. (1994). In some cases we deduced 3D-strain ellipsoids from individual Fry-method measurements following von Winterfeld & Oncken (1995). In addition we took strike and dip measurements of all the observed structural features observed in the outcrop to carry out a structural and orientation analysis mostly in the same localities where finite deformation was measured. Finally we also produced stratigraphic profiles in some of the locations in order to check relationships between lithology and deformation features.

First finite strain measurements allowed us to quantify an additional amount of shortening by penetrative deformation (i.e. contractional deformation at the microscopical scale that mostly produces slaty cleavage) in the Eastern Cordillera that is locally near 20%. Shortening by internal deformation is localized in the steeply dipping limbs of anticlines, the hinge zones of some synclines and the contractionally reactivated boundaries of former normal faults. As the observed planar fabric (e.g. slaty cleavage) is mostly continuous throughout different lithologies rather than discontinuous cleavage within spaced deformation zones; we assumed that shortening by penetrative deformation is not discrete. Thus, we propose that it represents a homogeneous flattening of the outcropping units in those localities where it is present. We calculated that shortening

¹ Institut für Geowissenschaften, Universität Potsdam, 14415 Potsdam, Germany

by folding in the Eastern Cordillera is close to 20%. This means that shortening by penetrative deformation compared to shortening by folding is not minor.

Orientation analysis of fractures and SiO₂-filled or CaCO₃-filled veins was done when these features were spatially associated with the planar fabric. With the collected data we propose that planar fabric and fractures have been formed mostly at the early stages of folding under a dominant WNW–ESE to E–W compressional stress field. For instance, fractures present in tilted beds only give a consistent pattern of compressional stress if they are restored to a prefolding position. In such cases the obtained direction is coincident with the direction of maximum finite deformation (This direction is assumed to be roughly perpendicular to the plane of slaty cleavage when finite strain measurements are not available at a given location). After restoring the fractures to a prefolding position their dip is vertical and perpendicular to bedding. In the folded state fracture orientation strongly depends on their position within the folded structures. However fracture intensity appears to depend both on structural position and lithology.

In addition, we found the presence of similar sets of fractures with similar orientations in different Lower-Cretaceous lithologies along the stratigraphic sections. However, fractures found in terrigenous pelrites always lack any kind of filling. In contrast when found in terrigenous sandstones they have SiO₂ filling and in carbonates they are filled with CaCO₃. When evaporites are the host rocks of mineralization the veins have the paragenesis of albite, pyrite,

calcite and emeralds. This paragenesis is a guide for emerald exploration and therefore represents the only mineralization of economic interest. In such evaporitic facies, fracture density reaches a maximum. Thus, evidence of mineralization strongly dependent on lithology, allow us to we hypothesize about a closed mineralization system, at least partially. However, by the field evidence the possibility of the influence of fluids coming from outside the formations cannot be discarded completely. In addition, in some of the analyzed localities we have found specific types of deformation, only observed when the sequence is composed of interbedded medium to thick layers of terrigenous mudstones with marls: A close association of slaty cleavage restricted to calcareous beds with CaCO₃-filled veins restricted to adjacent terrigenous mudstones. In such localities both features have been formed under the same stress field. The exposed relationships allow us to propose the following situation. Fluids ascending from terrigenous mudstones to adjacent marls. They ascend due to them being expelled because of a reduction in porosity caused by pressure solution processes. The exposed mineralization scenario would be then a highly autochthonous one.

The paragenesis of the veins associated with evaporites provides the entire Colombian emerald production, which in fact is one of the largest in the world. In such context those veins in the emerald-bearing areas have been dated (Cheilletz et al. 1996) as old as 37 ± 0.1 My in the western flank of the Eastern Cordillera and 65 ± 3 My in its eastern flank. We propose that the mentioned ages are giving a proxy of the age of the kinematic indicators

deduced from fracture and vein orientations. Fluid inclusion studies demonstrate that these mineralizations occurred at more than 250°C (Cheilletz et al 1996). Thus fluid inclusions and vitrinite reflectance data illustrate that at this time exhumation of the Cretaceous rocks was minor or absent.

Mineralization is also present as hydrothermal breccia frequently localized in the hinge zones of folds. In some cases those areas are also the location of intenser finite deformation values. Therefore we propose that mineralization associated with Lower Cretaceous units were formed in presence of high fluid pressure during folding and internal deformation under epithermal conditions. With all the collected evidence it appears that penetrative deformation (Slaty cleavage) is instrumental for mineralization.

Therefore, our contribution shows pieces of evidence supporting that the role of penetrative deformation has been underestimated in the Eastern Cordillera. Penetrative deformation does not only account for important additional crustal shortening in this orogen, but also plays a role in the formation of prolific economic mineral deposits.

References

- Cheilletz A & Giuliani G (1996) The genesis of Colombian emeralds: a restatement. *Mineralium Deposita* 31, 359–364
- Dittmar D, Meyer W, Oncken O, Schievenbusch T, Walter R & von Winterfeld C (1994) Strain partitioning across a fold and thrust belt: the Rhenish Massif, Mid-European Variscides, *Journal of Structural Geology* 16, 1335–1352
- Engelder T & Marshak (1985) Disjunctive cleavage formed at shallow depths in sedimentary rocks. *Journal of Structural Geology* 7, 327–343
- Erslev EA (1995) Normalized center to center strain analysis of packed aggregates. *Journal of Structural Geology* 17, 417–450
- von Winterfeld C & Oncken O (1995) Non-plane strain in section balancing: calculation of restoration parameters. *Journal of Structural Geology* 17, 447–450

Extensional crustal-scale shear zones in the Western Cyclades (Kea, Greece)

Poster

Monika Müller¹ Bernhard Grasemann¹
Michael A. Edwards¹ Erich Draganits³
Klaus Voit¹ Christoph Iglseider¹ András Zámolyi¹ Konstantin Petrakakis²

Intense seismicity and intensely developed active and ancient fault systems are common to the Aegean Region. Extending/thinning crust involves a complex interplay of (1) Gulf of Corinth rift-expansion, (2) west- and south-ward retreat of the Hellenic Trench, (3) west-ward impingement of the Anatolian Platen, and/or (4) propagation of the Anatolian Fault system into the Aegean. New geological/structural investigations on Kea (also known as Tzia), in the Western Cyclades reveal a low angle crustal-scale, detachment-type ductile shear zone probably formed during Miocene extension and thinning of the continental crust.

The area of interest, which lies in north-western Kea, comprises a large-scale de-

¹ Department of Geodynamics and Sedimentology, Structural Processes Group, University of Vienna, A-1090 Vienna, Austria ² Department of Geodynamics and Sedimentology, University of Vienna, A-1090 Vienna, Austria ³ Institute for Engineering Geology, Vienna University of Technology, A-1040 Vienna, Austria

tachment shear zone. Brittle deformation and lithospheric failure in the region includes at least two failure phases: (1) multiple low angle cataclastic fault zones formed within, and parallel to, a regional mylonitic ductile foliation and (2) a widespread system of (sub)vertical cross-cutting steep faults. For low angle extensional faulting, *a priori* co-seismic deformation (i.e. pseudotychylites) is absent and therefore aseismic creep is suggested, is overprinted by younger steep/vertical fault zones.

A several meter thick low angle cataclastic fault zone, with interestingly developed S-C fabrics, separates (i) steeply dipping, minimal deformation-related microstructure, ankeritised dolomite in the hanging wall from (ii) folded (ultra-)mylonitic marbles in the footwall and is regarded as the upper crustal expression of the failure of regionally thinning crust. The locally more than 10 m thick brittle fault zone comprises numerous generations of cataclases ranging from foliated protocataclases with brittle/ductile overprint, incohesive coarse grained fault breccias and partly graphitic fine grained fault gouges. This brittle fault zone locally includes a 2 m thick serpentinitic zone, fractured boudin lenses of opalescent serpentine associated with partly ankeritised (mega-) boudins of dolomites. In the northern part of Kea, this brittle fault zone can be mapped over several kilometres. The faults dip at low angle towards the NNW. Slickensides on brittle faults show consistent NNE-SSW orientations. Shear sense indicators including scaly fabrics and Riedel geometries of secondary fractures consistently indicate south-directed hanging wall displacement direction.

The footwall of the brittle fault zone consists of a several tens of meters thick ultramylonitic shear zone, mainly comprising marbles, phyllites, gneisses and quartzitic schists. The mylonites have a pronounced stretching lineation that has maximum plunge gently towards NNE parallel to the brittle kinematics. Countless textbook examples of a broad range of shear sense indicators (flanking structures, asymmetric boudinage, stable porphyroclasts with monoclinic symmetry, rotated and boudinaged veins) consistently indicate a south-directed, non-coaxial shearing. Beside a pronounced stretching lineation towards NNE specially in one area distinctive lineations and recurvature is observed. However, the most striking structural observation is the upright non-cylindrical folding of the mylonites with fold axes parallel to the stretching lineation. Shearing of these folds into tubular/sheath folds suggests that folding occurred during shearing due to shortening perpendicular to the stretching lineation. The same shortening direction is associated with gentle buckling of the structurally overlying cataclastic zones suggesting that the W-E shortening component accompanied deformation persisting from ductile, to brittle/ductile to brittle conditions.

Several generations of extension gashes filled with calcite, quartz and actinolite are widespread throughout the mylonitic rocks. Locally, some extension gashes with associated flanking folds are rotated into the shearing direction developing trains of elongated boudins. Quantitative kinematic flow analyses suggest an effective shear strain in the orders of several tens of gamma supporting the interpretation of a high-strain shear zone corroborating with the ob-

servation of sheath folds.

The low angle cataclastic fault zones are regarded as the upper crustal expression of the failure of regionally thinning crust. Further investigations will reveal whether steep faults suites may be related to more than one tectonic event and show, for example, a regional genetic link with the actively widening Gulf of Corinth.

In summary, lithological and structural investigations on Kea indicate that the island is a further example of crustal scale shear zone. Preliminary observations suggest that the shear zone bends around the whole island forming a dome-shaped antiform. In analogy to Serifos, a metamorphic core complex to the S of Kea, we speculate that, complementary to the N directed shear zones of Naxos and Paros, the mapped shear zone on Kea is part of an extensional S-directed detachment system.

Über die mechanischen Ursachen von parallelen Abschiebungen Vortrag

Thorsten Nagel¹ Roger Buck²

Gruppen von parallel einfallenden Abschiebungen treten in der Natur sehr häufig und in unterschiedlichsten Dimensionen auf. Existierende, überwiegend experimentelle Arbeiten führen einheitliches Einfallen auf laterale Festigkeitsschwankungen oder, vor allem, auf horizontale Scherspannungen zurück (e.g. Brun et al. 1994, Behn et al. 2002). Einheitliche horizontale Scherspannun-

gen im großen Maßstab werden mit einer konsistenten Fließrichtung in der mittleren und/oder unteren Kruste erklärt. Beobachtungen in einigen der bedeutendsten Rift-Systeme lassen jedoch beide Erklärungen als zentrale Ursache unwahrscheinlich erscheinen. In der Basin-and-Range-Provinz in den westlichen Vereinigten Staaten ändert sich die Einfallrichtung von parallelen Abschiebungen im Streichen der Störungen, so dass strukturelle Domänen mit intern einheitlicher Einfallrichtung entstehen, die von Blattverschiebungen untereinander getrennt werden. Eine solche Geometrie ließe sich nur mit bizarren Fließmustern in der Unterkruste erklären.

Wir präsentieren numerische Extensionsexperimente von sprödem Material, das auf einem linear-viskosen Substrat ruht. Parallele Abschiebungen treten in der oberen Schicht nur dann auf, wenn das Substrat mäßig viskos und nur eine relativ dünne Schicht ist, die eine in der vertikalen Richtung fixierte Untergrenze hat. Mit diesen Randbedingungen bilden sich parallele Abschiebungen auch dann, wenn die Untergrenze scherstressfrei ist. Wir erklären dieses Verhalten mit den Fließeigenschaften von Flüssigkeiten in dünnen viskosen ‚Kanälen‘. Die Wechselwirkung mit einem viskosen Substrat führt in erster Linie dazu, dass die Verformung in der spröden Schicht verteilt ist — die obere Lage wird boudiniert. Wenn der Abstand zwischen einzelnen Brüchen (Boudin-necks) kleiner als die elastische Wellenlänge der oberen Lage ist, minimiert eine Geometrie von einheitlich einfallenden Störungen die viskose Arbeit in der unteren Schicht. Dies ist so, weil in einem viskosen Kanal die zu leistende Arbeit quadratisch von der Entfernung zwischen Quellen und Sen-

¹ Geologisches Institut Bonn ² Lamont Doherty Earth Observatory, Palisades, NY, USA

ken im Fließmuster abhängt und eine Geometrie von parallelen Abschiebungen eben diese Entfernung minimiert.

Desweiteren unterscheiden wir zwei Geometrien, mit denen die spröde Lage in einem ‚Boudin-neck‘ nachgeben kann — einzelne Störungen und lokale Gräben, d.h. zwei entgegengesetzt einfallende Störungen, die sich nahe der Grenze zwischen sprödem und viskosem Material schneiden. Wir beobachten, dass ein hoch viskoses Substrat die Bildung von lokalen Gräben — im Gegensatz zu einzelnen Störungen — begünstigt. Am unteren Ende einer Störung treten im viskosen Material in einem begrenzten Bereich die höchsten Verformungsraten auf. Eine einzelne Störung muss dabei mehr Arbeit leisten als ein lokaler Graben, da es zu einem vertikalen Versatz der beiden Blöcke kommt. Diese ‚Strafe‘ für einzelne Störungen (die andere energetische Vorteile haben) nimmt mit zunehmender Viskosität des Substrats zu. Das heißt, dass das viskose Substrat bei der Bildung von parallelen Abschiebungen (die ja aus einer Folge einzelnen Störungen bestehen) nicht allzu hoch sein darf, da es sonst zur Bildung von einer Serie von Horsten und Gräben kommt. Ein niedrig viskoses Substrat führt jedoch zu weit auseinander liegenden Brüchen, wenn die viskose Lage dick ist oder eine schwimmende Untergrenze (Winkler-foundation) hat. Eine dünne, mäßig viskose Lage verbindet die beiden erforderlichen Eigenschaften, indem sie wenig Widerstand an der Untergrenze einzelner Störungen bietet und dazu die spröde Lage effektiv boudiniert.

In unseren Modell sind parallele Abschiebungen nicht, wie bisher angenommen, auf einheitlichen horizontalen Scherstress, sondern auf vertikale Normalspannungen zurückzuführen,

d.h. auf den Widerstand, den das viskose Substrat vertikalen Blockbewegungen in der spröden Lage entgegengesetzt. Wenn unser Modell richtig ist, würde das für Gebiete wie die Basin-and-Range-Provinz bedeuten, dass die spröde Oberkruste auf einer wenige Kilometer dicken, viskosen mittleren Kruste liegt, die wiederum ein festeres Substrat hat. Die Unterkruste müsste deutlich fester sein als die mittlere Kruste. Es scheint, dass Folgen von parallelen Abschiebungen häufig in dünnen, niedrig viskosen Lagen (etwa Ton oder Salz) wurzeln.

Literatur

- Behn, MD, Lin J & Zuber MT (2002) A continuum mechanics model for normal faulting using a strain-rate softening rheology: Implications for rheological controls on continental and oceanic rifting, *Earth. Planet. Sci. Lett.*, 202, 725–740.
- Brun J-P, Sokoutis D & van den Driessche J (1994) Analogue modeling of detachment fault systems, *Geology*, 22, 319–322.

Microfabrics and deformation processes in magmatic veins of the Thuringian Forest, Germany *Poster*

Jana Neubert^{1,2} Sebastiaan van der Klauw³ Jonas Kley²

Introduction

The research area is located in the Ruhla-Brotterode crystalline complex in

¹ Universidade Federal do Pará, Dep. Geologia, CP 1611, 66017970 Belém, Brazil
² Friedrich-Schiller-University, IGW, Burgweg 11, 07749 Jena, Germany
³ Ercosplan — Ingenieurgesellschaft Geotechnik und Bergbau mbH, Arnstädter Strasse 28, 99096 Erfurt, Germany

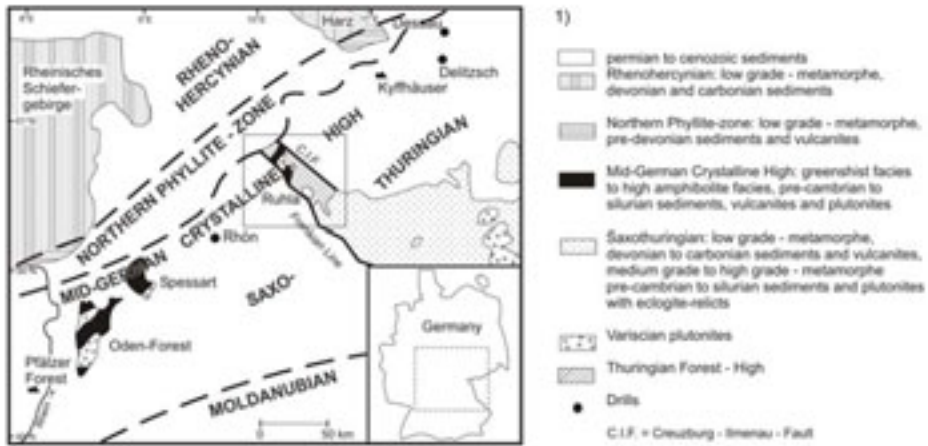


Figure 1: Position of the Mid-German Crystalline High within the variscan orogen (modified after Hansch & Zeh (1999))

the western part of the Thuringian Forest (Germany), about 20 km south-southwest of Eisenach. The investigated outcrops occur at the eastern and western flanks of the valleys north of the villages Trusetal and Hohleborn. Deformed magmatic veins only occur in the Hohleborn area. Both areas have relative fresh outcropping rocks, due to the steep relief, former quarries and fresh road cuts. According to Obst & Katzung (2000) several periods with the formation of magmatic veins with different chemical composition occur in the Ruhla-Brotterode crystalline complex. Presumably older lamprophyric veins and younger doleritic, syenitporphyric and granitporphyric veins have been identified (Obst & Katzung 2000). Benek & Schust (1988) already pointed out that some of these magmatic veins have experienced ductile deformation. The subject of this work is the occurrence of deformed magmatic veins in the Hohleborn area. The contact

to their host rocks, their petrography and their microfabrics have been investigated and related to deformation processes, which led to a better understanding of their deformation conditions within the late- to post-variscan development of the area.

Regional geological framework

The Ruhla-Brotterode crystalline complex is part of the Mid-German Crystalline High (Fig. 1). The Crystalline High is a 50–70 km broad zone striking NE–SW and forms the NW border of the Variscan Saxothuringian zone (Seidel 1995). During the main phase of the Variscan orogeny, in the lower to middle Carboniferous, the Mid German Crystalline High is considered to have been part of the active continental margin of the Saxothuringian (micro)continent (Seidel 1995), which overrode the more northwestern Rheohercynian (micro)continent. This phase continued during upper Carboniferous

time with the segmentation of the Variscan orogen through an E–W extensional stage within Central-Europe. The investigated area lies in the south-eastern part of the Crystalline Complex. Its rocks mainly consist of paragneisses, which are intruded and bordered by numerous permocarboniferous granites and a diorite (Lützner et al., 1997). According to Zeh et al. (1996), the paragneisses are part of the Truse Formation and represent an accretionary wedge. The crystalline rocks are covered by Permotriassic sedimentary rocks and crosscut by numerous E–W to SSE–NNW-trending, magmatic veins. These veins are of basaltic, andesitic and dacitic to rhyolitic nature (Obst & Katzung, 2000) and appear as simple veins, mixed or combined veins (Mädler & Voigt 1994). U–Pb zircon dating of the veins by Brätz (2000) shows ages between 285 ± 5 Ma and 264 ± 7 Ma for undeformed veins and ages between 305–320 Ma and 294 ± 4 Ma for the deformed veins.

Methodology

From 10 oriented samples of deformed veins (2 sections per sample, perpendicular to the foliation) as well as for comparison purposes from 10 samples of macroscopically undeformed vein (1 section per sample) thin sections have been prepared for microscopic structural and petrographical analysis. The sections have been investigated for mineralogical composition, micro-fabrics, deformation structures and deformation intensity through measurement of length-width-relation of quartz crystals (shape preferred orientation, SPO) and extension-relation of feldspars crystals as well as the crystallographic preferred orientation (LPO) of the quartz crystals with

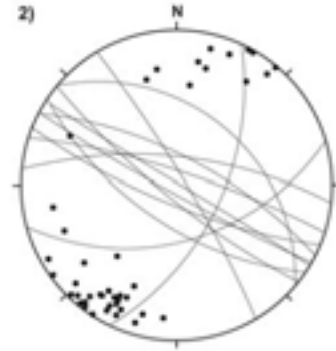


Figure 2: Stereographic projection (lower hemisphere) of vein-host rock contacts of undeformed, magmatic veins in the research area; $n = 44$.

the universal stage. The structural data from veins and host rocks have been evaluated with the program 'Wintek' for integration of the deformed veins within the late to post-variscan context.

Structural Analysis

Figure 2 shows the stereographic projection of the contacts of undeformed magmatic veins with their host rocks. Nearly all veins strike E–W to NW–SE and dip steeply with $65\text{--}85^\circ$ to N–NE respectively SSW–WSW. In contrast the deformed magmatic veins in Figure 3 strike mostly N–S to NE–SW and dip with $40\text{--}65^\circ$ to ENE to SE. The structural inventory of the host rocks (Fig. 4a & 4b) shows a predominance of N–S to NE–SW striking and $30\text{--}75^\circ$ dipping schistosity S_3 and NW–NNE striking $20\text{--}60^\circ$ dipping S_2 which both seem to be partly refolded by B_4 . This leads to the possible directions of $5\text{--}35^\circ$ to ENE–E for B_3 respectively $35\text{--}60^\circ$ to ESE–SSE for B_4 folding axes.

The main rock-forming minerals of the deformed veins own the following char-

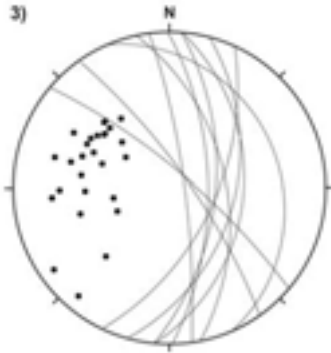


Figure 3: Stereographic projection (lower hemisphere) of vein-host rock contacts of deformed, magmatic veins in the research area; $n = 28$.

acteristics.

- Feldspars (potassic feldspar & plagioclase): microboudinage, sericitisation, fissures (often filled with antitaxial and syntaxial quartz- and feldspar-fibers), incipient fractures, growth rims of quartz parallel and perpendicular to schistosity and in strain shadows of crystals, undulatory extinction & microclincic & myrmekitic structures (pot. feldspar) or uniform extinction and mechanical twins (plagioclase).
- Quartz: occurs as porphyroclast, matrix-quartz or growth-rims. Porphyroclast have a strong elongation (extreme length-wide-relation, long axis parallel to schistosity), undulatory extinction, deformation ribbons, subgrain structures (size ca. 1 mm), recrystallised grains with highly irregular grain boundaries (size 10–15 μm); as coarse strain-shadow of crystals or vein filling; grain size spectrum: coarse / fine matrix = 15–50 μm / 10–

15 μm , strain shadow = ca. 50 μm , growth rim = 100–300 μm .

- Biotite: structures indicating sliding of layer-packages parallel to cleavage or bending with undulatory extinction in extreme fracturing perpendicular to schistosity; single clasts as well as small orientated fragments (frequently marks the schistosity together with chlorite, hematite, sericite and opaque phases), partly strongly altered.

The evaluation of the quartz-elongation and the stretched feldspars in the Flinn-Diagramm shows that the deformation regime is flattening and that the intensity of the quartz deformation (in all directions) is higher than that of the feldspars. The determination of recrystallized grain size of quartz and the calculation of differential stress after Blenkinsop (2000) and Twiss (1977) yielded relative high differential stresses in the range of 95–125 MPa for this flattening deformation stage. The deformation also resulted in the development of a lattice preferred orientation (LPO) of the quartz in the deformed veins. The preferred orientation of the c-axis for isometric and elongate quartz grains is not well defined. Nevertheless the measured quartz c-axes suggest an uniform reorientation with increasing deformation intensity. The c-axis reorientation is to within the plane of the vein internal schistosity.

Conclusions

The investigation shows deformed andesitic and rhyolitic veins with quartz-growth rims mostly orientated parallel to the schistosity. This strongly suggests that a fluid was available during

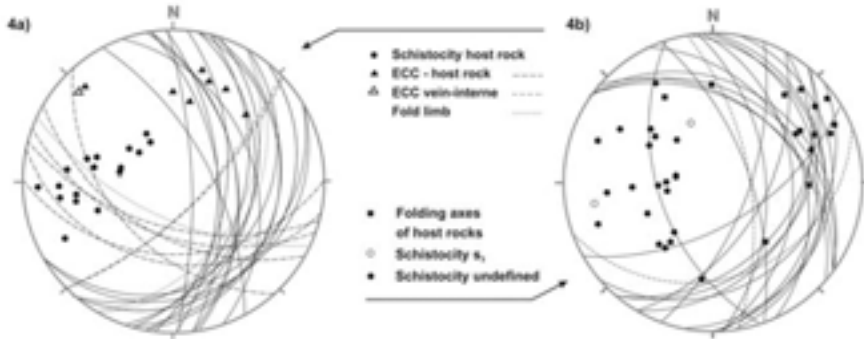


Figure 4: a) and b) Stereographic projection (lower hemisphere) of the host rock structural inventory in the research area; a) of outcrop A, $n = 28$; b) of outcrop B, $n = 35$.

deformation of the veins. The comparison with the position of the main schistosity in the host rocks indicates that the deformed magmatic veins intruded before or during the last deformation phase of the host rocks (D_4). This inference is supported by the nearly parallel orientation of the veins with the shallower schistosity planes of the main schistosity (S_3), the formation of ecc-structures in the deformed veins as well as fabrics of similar deformation intensity within the younger quartz-veins in the host rocks. The different orientation of deformed and undeformed veins also argues for their formation during different time episodes with a changed orientation of σ_3 . The sparse age determinations for the magmatic veins do not contradict this conclusion. The observed micro-fabrics limit the boundary conditions during the deformation to a regime with relative high differential stresses of 95–125 MPa and low temperatures. The microstructures and the LPO of quartz indicate that the vein-deformation took place between the deformation regimes

of low temperature plasticity and dislocation creep of quartz.

References

- Benek R & Schust F (1988) Bemerkungen zur partiellen Gefügedeformation in Magmatitgängen des Ruhlaer Kristallins (Thüringer Wald). *Z. dt. Geol. Wiss.* 16, 801–816
- Blenkinsop, T (2000) Deformation Microstructures and Mechanisms in Minerals and Rocks. Kluwer Academic Publishers Dordrecht, p 150
- Brätz H (2000) Radiometrische Altersdatierungen und geochemische Untersuchungen von Orthogneisen, Graniten und Granitporphyren aus dem Ruhlaer Kristallin, Mitteldeutsche Kristallinzone. PhD-Thesis, Julius-Maximilians-University Würzburg, pp 131
- Hansch R & Zeh A (1999) Metabasites from the Ruhla Crystalline Complex: Evidence for Distinct Pre-Variscan, Plate-tectonic Environments within the Mid-German Crystalline Rise. *Mineralogical Institute of the University Würzburg*, pp 25
- Lütznier H & Seidel G (1997) Ruhlaer Kristallin, Tambacher und Eisenacher Rotliegendebcken (westlicher Thüringer Wald). *Schriftenreihe der Deutschen Geologischen Gesellschaft - Exkursionsführer 'Regionale Geologie von Mitteleuropa'*, pp 34

- Mädler J & Voigt H (1994) Aufbau, Petrographie und Genese eines Systems zusammenhängender Gesteinsgänge am Südrand des Ruhlaer Kristallins westlich Seligenthal / Thüringer Wald (ehemaliger Gieselsberg-Schacht); In: Thüringer Landesanstalt für Geologie — Geowissenschaftliche Mitteilungen von Thüringen, Weimar, pp 321
- Obst K & Katzung G (2000) Die magmatischen Gänge am Südrand des Kristallins von Ruhla-Brotterode (Thüringer Wald) - Herkunft der Magmen, Aufstieg und Platznahme im variszischen Spannungsfeld. Z. dt. geol. Ges. 151, 441–470
- Passchier CW & Trouw RAJ (1998) *Microtectonics*. Springer-Verlag Berlin Heidelberg, pp 289
- Seidel G (1995) *Geologie von Thüringen*. Schweizerbart'sche Verlagsbuchhandlung Stuttgart, pp 555
- Twiss RJ (1977) Theory and applicability of a recrystallized grain size palaeopiezometer. In: *Pure & Applied Geophysics*, 227–244
- Zeh A (1996) *Die Druck-Temperatur-Deformations-Entwicklung des Ruhlaer Kristallins (Mitteldeutsche Kristallinzonen)*. Schweizerbart'sche Verlagsbuchhandlung Stuttgart, pp 212

Strukturanalyse juveniler Fragmente in Vulkaniklastika des Messel Maar-Diatremes *Poster*

Thomas Nitzsche^{1,2} Helga de Wall²
Christian Rolf¹

Einführung

Geophysikalische Untersuchungen im Gebiet der Grube Messel (25 km südlich von Frankfurt) ließen schon vor einigen Jahren eine Maar-Diatrem-Struktur im Untergrund vermuten. Jedoch erst die gekerkte Forschungsbohrung im Jahr 2001 bewies die Existenz eines durch phreatomagmatische Eruptionen gekennzeichneten Maar- Vulkans, der vor ca. 48 Ma aktiv war. Neben den berühmten fossilreichen Ölschiefern wurde im Teufenbereich zwischen –240 m und –370 m unter der Erdoberfläche vulkaniklastisches Material entdeckt. Unterhalb des so genannten Lapillituffs wurden bis zur Endteufe von –433 m Gesteine der Diatrem-Brekzie erbohrt. Um das schwer differenzierbare, vulkanische Gestein *in situ* detaillierter untersuchen zu können, sind gesteinsmagnetische Messungen besonders wertvoll. Hierbei kann die magnetische Suszeptibilität (MS), die Magnetisierbarkeit eines Gesteins, für quantitative und qualitative Analysen sehr hilfreich sein. Die juvenilen Lapilli, an die die ferrimagnetischen Minerale bzw. die magnetischen Träger gebunden sind, sind dabei von besonderem Interesse. Bildanalytische Auswertungen sowohl an Kernen als auch an Dünnschliffen dienen dabei zur Interpretation des Suszeptibi-

¹ Institut für Geowissenschaftliche Gemeinschaftsaufgaben (GGA) Hannover ² Institut für Geologie, Julius-Maximilians-Universität Würzburg

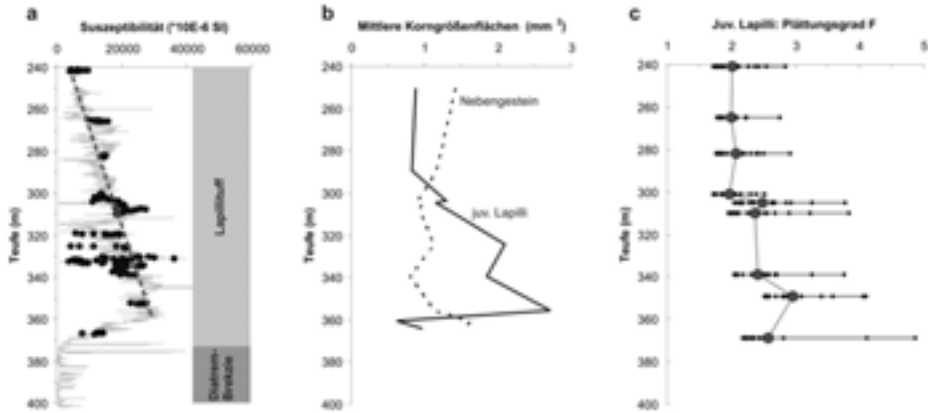


Abbildung 1: a) Messungen der Suszeptibilität im Bohrloch (Daten von T. Wonik, GGA-Institut) und an Einzelproben im Labor, b) Darstellung der bildanalytischen Auswertung für die Zunahme der mittleren Korngrößenflächen der gemessenen Partikel und c) Diagramm des durchschnittlichen Plättungsgrades ($F = \text{Länge}/\text{Höhe}$) juveniler Fragmente.

litätslogs der durchgeführten Bohrlochmessungen. In dieser Studie ist weiterhin ein besonderes Augenmerk dem magnetischen Gefüge der Vulkaniklastika verliehen. Dabei liefern Messungen der Anisotropie der magnetischen Suszeptibilität (AMS) Informationen über die räumliche Anordnung der magnetischen Minerale (Foliation und Lineation) und offenbaren dadurch interne Strukturen des Gesteins.

Suszeptibilität und juvenile Fragmente

Während der Forschungsbohrung im Jahr 2001 wurde die magnetische Suszeptibilität im Bohrloch mit einer Suszeptibilitätssonde mit einer Abtastrate von 5 cm gemessen (Wonik & Bücker 2000). Betrachtet man die MS in Abbildung 1a vom Hangenden zum Liegenden, so steigen diese mit starken Schwankungen, aber mit einem nahezu linearen Trend vom oberen Bereich des Lapillituffs in –250 m Tiefe bis

ca. –360 m im Mittel von 0,01 SI auf Werte bis zu 0,03 SI an. Beim Verlassen der Vulkaniklastika und mit Erreichen der Diatrem-Breccie fällt die Suszeptibilität fast sprunghaft auf geringe bis mittlere Werte ($\ll 0,01$ SI) zurück. Der lineare Trend mit ansteigender Suszeptibilität unter starken Schwankungen der Werte ist auch durch Untersuchungen an Proben im Labor nachvollziehbar und bestätigt worden (Abb. 1a). Der Nebengesteinsanteil innerhalb der Vulkaniklastika beträgt 5–35% und zeigt keine Korrelation mit dem MS-Log. Bildanalytische Untersuchungen an Dünnschliffen des vulkaniklastischen Materials dagegen belegen eindeutig eine Zunahme der mittleren juvenilen Kornflächengrößen bis –360 m, welche mit dem MS-Log sehr gut korrelieren (Abb. 1b). Die ansteigende Suszeptibilität spiegelt somit eine Korngrößenzunahme der juvenilen Fragmente wider. Untersuchungen des Plättungsgrades einzelner juveniler Klatten

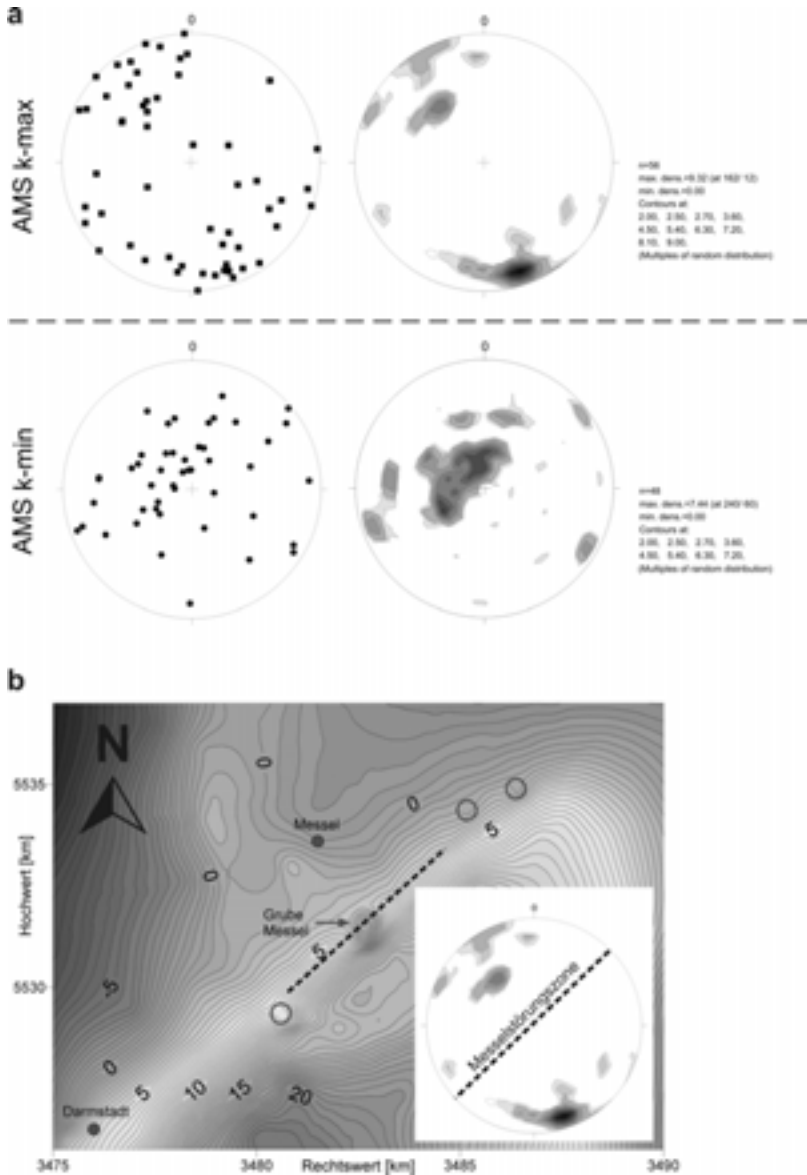


Abbildung 2: a) Rückorientierte k_{max} und k_{min} Achsen im Schmidt'schen Netz mit Projektion in die untere Lagenhalbkugel. Veranschaulicht sind jeweils die Einzelwerte (links) und die Belegungsdichtediagramme (rechts). b) Karte der Schwereanomalien im Umfeld von Messel und weiteren Maar- Vulkanen (Kreise) (nach Bunes et al. 2004). Auffällig ist eine SW-NE orientierte Zone, die den Übergang von geringen zu hohen Schwerewerten darstellt, die sogenannte Messel- Störungszone (Jacoby et al. 2000). Vorzugsrichtung der magnetischen Lineation der Vulkaniklastika von Messel (Schmidt'sches Netz unten rechts).

zeigen oberhalb -300 m sehr ähnliche gemittelte Werte (Abb. 1c). Dagegen liefern die abgelagerten juvenilen Fragmente unterhalb -300 m die höchsten Werte und bilden hier den größten Grad der Abflachung. Paläomagnetische Untersuchungen weisen auf hohe Ablagerungstemperaturen ($>300^\circ\text{C}$) für die untere Hälfte des Lapillituffs hin (Nitzsche et al., im Druck), so dass sich die juvenilen Komponenten hier relative leicht verformen konnten. Die juvenilen Körner erlauben durch ihre Geometrie den Lapillituff bildanalytisch in eine obere und untere Hälfte abzugrenzen. Sie bestimmen die strukturellen Trends des magnetischen Gefüges im Gestein und sind für weitere strukturgenetische Modellierungen essentiell.

Anisotropie der magnetische Suszeptibilität (AMS) der Vulkaniklastika

Trotz des makroskopisch meist strukturlos erscheinenden, vulkaniklastischen Materials, liefert die Methodik der AMS ein ideales Instrument zur Untersuchung des internen Gefüges. In oblaten Gefügen ist die Raumlage der kleinsten Achse des AMS-Ellipsoides (Pol zur magnetischen Foliation, \hat{e}_{\min}) sehr gut definiert, während in prolaten Gefügen die längste Achse des Ellipsoides (magnetische Lineation, \hat{e}_{\max}) in ihrer Raumlage bestimmt ist (Tarling & Hrouda 1993).

Aufgrund der horizontal unorientierten Kerne, mussten die AMS-Daten mithilfe paläomagnetischer Daten (Deklination der natürlich remanenten Magnetisierung (NRM)) rückorientiert werden. Die gefilterten \hat{e}_{\max} Achsen zeigen dabei generell flache Inklinationen. Nach Rückorientierung gruppieren sich die Achsen zu einem subho-

rizontalen NW–SE orientierten Cluster (Abb. 2a). Diese Richtung entspricht ungefähr der tatsächlichen geographischen Orientierung der Lineation des vulkanischen Materials, da die Paläodeklination vor ca. 48 Ma, um nur 10° von der heutigen Deklinationsrichtung abweicht (McElhinny & Lock 1990). Beim Betrachten der \hat{e}_{\min} Deklinationen/Inklinationen macht sich ebenfalls ein Trend bemerkbar (Abb. 2a). Hier erscheinen die Deklinationen in einem NE–SW orientierten Gürtel, mit starker Belegung der steilen Foliationspole und daher überwiegend flacher Orientierung der magnetischen Foliation. Das Gefüge der Vulkaniklastika innerhalb des Messel Maar-Diatrems resultiert möglicherweise aus Überlagerungen einer aus der Kompaktion resultierenden Vertikalspannung mit horizontalen tektonischen Paläospannungen der Rheingrabentektonik.

Gravimetrische Messungen im Gebiet um Messel zeigen einen markanten Gradienten, der auf ein ENE-streichende Krustendiskontinuität schließen lässt (Abb. 2b), und als Messel Störungslinie bezeichnet wird (Jacoby et al. 2000). Die Orientierung der Lineation genau senkrecht zum Streichen der Messel-Störungszone spricht für eine genetische Relation der AMS Lineation zu dieser Störungslinie.

Literatur

- Buness H, Gabriel G, Pucher R, Rolf C, Schulz R & Wonik T (2004) Grube Messel: Die Geophysik blickt unter die Abbausohle. *Natur u. Mus.* 134, 65–76
- Jacoby W, Wallner H & Smilde P (2000) Tektonik und Vulkanismus entlang der Messel-Störungszone auf dem Sprendlinger Horst: Geophysikalische Ergebnisse. *Z. dt. geol. Ges.* 151, 493–510
- McElhinny MW & Lock J (1990) IAGA global

- palaeomagnetic database. Geoph. J. Intern. 101, 763–766
- Nitzsche T (im Druck) Origin of magnetic anomalies in volcanoclastic units of the Messel maar-diatreme (Germany). Z. dt. Gew. Ges.
- Tarling, DH & Hrouda, F (1993) The Magnetic Anisotropy of Rocks; S. 217, London (Chapman & Hall)
- Wonik T & Bücker C (2000) Möglichkeiten der Bohrlochgeophysik im Institut für Geowissenschaftliche Gemeinschaftsaufgaben. Mitteilungen der deutschen geophysikalischen Gesellschaft, Sonderband 3: 41–43

Fracturing and vein formation in the middle crust - a record of co-seismic loading and post-seismic stress relaxation

Vortrag

Jens-Alexander Nüchter¹ Bernhard Stöckhert¹

Metamorphic rocks approaching the crustal scale brittle-ductile transition (BDT) during exhumation are expected to become increasingly affected by short term stress fluctuations related to seismic activity in the overlying seismogenic layer (schizosphere), while still residing in a long-term viscous environment (plastosphere). The structural and microstructural record of quartz veins in low grade – high pressure metamorphic rocks from southern Evia, Greece, yields insight into the processes and conditions just beneath the long-term BDT at temperatures of about 300 to 350°C, with switches between brittle failure and viscous flow as a function of imposed stress or strain rate. The following features are characteristic:

¹ Ruhr Universität Bochum, Institut für Geologie, Mineralogie und Geophysik

- i) The veins crosscut the foliation and all pre-existing structures;
- ii) The veins have formed from tensile fractures, with a typical length on the order of 10^{-1} to 10^1 m. Vein orientation is uniform on the kilometer scale;
- iii) Some veins branch symmetrically with an aperture angle of 30° , which is interpreted to indicate high energy dissipation rates and crack tip propagation velocities approaching the terminal velocity similar to the Raleigh wave speed;
- iv) Fabrics of the vein quartz indicate that the veins formed during a single sealing stage by mineral precipitation in open cavities;
- v) The veins show a low aspect ratio of about 10 to 100 and an irregular or characteristic lenticular shape, which requires distributed ductile deformation of the host rock;
- vi) The sealing quartz crystals reveal a broad spectrum of microstructural features indicative of crystal plastic deformation at temperatures of about 300 to 350°C and high stress.
- vii) Fluid inclusions entrapped in vein quartz reveal a markedly sublithostatic pore fluid pressure during crack sealing.

Fractures propagated in a single step. Therefore, fluid overpressure as the only source of crack-driving energy is excluded. The drop in pore-fluid pressure related to incremental growth would cause arrest of the fracture until recovery. Hydraulic fracturing is therefore expected to result in cyclic vein-ing, which is not observed in the present

case. Opening of the fractures, commencing immediately after crack arrest, was controlled by ductile deformation of the host rock. Vein-parallel shortening is less than about 2%. The structural and microstructural record reflects an isothermal switch from short-term brittle failure at quasi-instantaneous loading to decelerating viscous creep with little strain accumulated. Individual veins are the result of a single sequence of events:

- i) A major stress peak is imposed to the uppermost part of the plastosphere, probably as a consequence of co-seismic loading by fault displacement in the overlying schizosphere (timescale is seconds).
- ii) Fractures presumably initiate after a stage of enhanced stress corrosion with sharpening of earlier blunt flaws, resulting in a rise of the stress intensity factor K_I (timescale is not certain, but estimated to be between seconds and days).
- iii) Flaw sharpness rises abruptly after critical fracture initiation and results in a K_I peak. The fracture propagation velocity increases extremely in this early stage. Dilation during fracturing causes an instantaneous drop in pore fluid pressure; this implies a drop in driving force and consequently an arrest of the fractures. The time span from initiation to arrest must be a few milliseconds.
- iv) After fracture arrest, decelerating viscous deformation during post-seismic stress relaxation causes the opening of the fractures. Sealing of

the fissures to become a vein takes place by precipitation of minerals from the pore fluid percolating into the evolving cavity. This process is estimated to take some time on the order of 10^0 to 10^4 years.

Opening of fractures and development to a vein is therefore interpreted to be a short-term and episodic process during a stage of post-seismic creep. The record of the exhumed rocks provides insight into earthquake related damage in the uppermost plastosphere and transient crustal properties during post-seismic creep and stress relaxation.

Correlation of magnetic fabric and crystallographic preferred orientations of naturally deformed carbonate — mica rocks from the Alpi Apuane in Italy and the Damara Orogen in Namibia

Poster

Michael Otto¹ Ann M. Hirt² Bernd Leiss¹ Volkmar Schmidt² Jens M. Walter³

Scope of the correlation

The anisotropy of magnetic susceptibility (AMS) is a time-efficient method to describe crystallographic preferred orientations of rocks and has been applied in a wide field of sedimentary, metamorphic and magmatic geology. The

¹ Geoscience Centre Göttingen, University of Göttingen, 37077 Göttingen, Germany ² Institute of Geophysics, ETH Zurich, 8093 Zurich, Switzerland ³ Forschungszentrum Jülich, 52425 Jülich, Germany

method, however, suffers from limitations which mainly result from the interference of diamagnetic, paramagnetic and ferromagnetic fabrics (de Wall 2005) — the term ferromagnetism is used in a wider sense here, including e.g. ferrimagnetism. The AMS is an integral parameter which describes a crystallographic preferred orientation as an ellipsoid. The quantitative correlation of the AMS with the crystallographic preferred orientations should help to allow a closer view at the applicability and the limitations of the AMS analysis (see also Schmidt et al. 2006 a, b).

Recent advances in AMS analysis through new methods for phase separation

The separation of ferromagnetic, paramagnetic and diamagnetic partial fabrics has been a subject of research in recent times and has led to several new methods. Martin-Hernandez & Hirt (2001) presented a method for the separation of diamagnetic/paramagnetic and anti-ferromagnetic from the ferromagnetic phase fabrics using high-field torque measurements and different field strengths between 0.1 and 1.7 T. While ferromagnetic magnetization saturates at high fields, paramagnetic/diamagnetic magnetization is proportional to the field strength. So the separation can be calculated from measurements at several fields.

Schmidt et al. (2005, 2006 a,b) developed a method for the separation of paramagnetic from diamagnetic fabric. It is achieved by the comparison of room-temperature and low-temperature (77 K) measurements using the high-field torque method. This method was applied and compared to neutron textures on synthetically-deformed calcite-

mica samples.

Naturally-deformed rocks

To test the application of the new methods on naturally deformed rocks, mica bearing calcite marbles and mylonites from the Alpi Apuane in Italy and dolomite mylonites from the Damara Orogen in Namibia were selected. Selection criteria were varying mica contents and varying intensities/types of their crystallographic-preferred orientations (CPOs). Quantitative texture analyses were carried out by means of the ‘powder and texture diffractometer SV7’ at the research reactor Jülich 2 of the Research Center Jülich (FRJ-2) in Germany. Due to a low absorption coefficient of neutrons in condensed matter, neutron diffraction allows a volume-related quantitative texture analysis of the sample cylinders which were also used for AMS measurements. Only this strategy allows a direct correlation of CPOs with the AMS. AMS measurements were performed at different field intensities (0.8 to 1.7 T) as well as at different temperatures (room temperature and 77 K) in order to separate the different magnetic phases.

Mica shows a relatively strong paramagnetic anisotropy; calcite a weaker diamagnetic anisotropy.

First results

The 30 samples analysed cover a spectrum from fine-grained (0.05 mm) rocks to coarser grain sizes (max. 0.2 mm). In general, grains show isometric to elongated shapes; the grain boundaries vary from relatively straight to irregular and lobate. In the different samples, the mica content covers a range from 0 to ca. 50%.

Texture analyses reveal a large variety of texture types. The carbonate phases show single c-axis maxima, covering a range from weak to very strong intensity maxima. Other samples show distinct to weak c-axis double maxima. Furthermore, some samples show partially developed girdle distributions with moderate to weak intensity. In one case, dolomite displays a completely developed girdle distribution. The mica phases show c-axis preferred orientations covering a range of very weak to very strong single maxima.

The measured AMS tensors are found to represent the crystallographic preferred orientations of calcite and mica detected by neutron diffraction goniometry. Differing directions of the carbonate and mica phase preferred orientations are generally reflected by the directions of the dia- and paramagnetic AMS. In general, the eccentricity of the AMS ellipsoid reflects the intensity and type of the texture.

The AMS of the ferromagnetic phases was found to be often significantly different from the para-/diamagnetic AMS. Magnetite has been identified by acquisition of isothermal remanent magnetization (IRM) and thermal demagnetization of a cross-component IRM. The AMS of magnetite is defined by the grain shape rather than crystallographic orientation. Additional low field AMS measurements give results representing directions which are intermediate between paramagnetic/diamagnetic and ferromagnetic AMS.

Conclusions

The results of this study are based on a large variety of fabric types of carbonate-mica marbles and mylonites, i.e. varying mica content, grain sizes,

grain shapes, types and intensities of the crystallographic preferred orientation. The presented first correlations of the AMS and CPO for the single mineral phases in general demonstrate a good matching. Regarding the comparison of texture types and the AMS, limitations are possible. While single c-axis maxima and girdle-like c-axis distributions can be also distinguished by the AMS, it is obvious that distinguishing between these types and the double c-axis type is not possible at the present stage.

References

- De Wall, H (2005) Die Anisotropie der magnetischen Suszeptibilität — eine Methode zur Gefügeanalyse. *Z. d. dt. Geol. Ges.* 155, 287–298
- Martin-Hernandez F & Hirt AM (2001) Separation of ferrimagnetic and paramagnetic anisotropies using a high-field torsion magnetometer. *Tectonophysics* 337, 209–221
- Hrouda F (1982) Magnetic-anisotropy of rocks and its application in geology and geophysics. *Geophysical Surveys* 5, 37–82
- Lowrie W (1989) Magnetic Analysis of Rock Fabric. In: James, DE *The Encyclopedia of Solid Earth Geophysics*, 698–706
- Schmidt, V, Hirt, AM, Burlini, L & Leiss, B (2005) Crystallographic-Preferred Orientations and Anisotropic Magnetic Susceptibilities in Experimentally Produced Calcite Samples: Deformation Mechanics, Rheology and Tectonics 2005, Zürich, pp 190
- Schmidt V, Hirt AM & Rosselli P (2006a) Separation of magnetic subfabrics by high-field, low-temperature torsion measurements. this volume
- Schmidt V, Hirt AM, Burlini L, Leiss B & Walter JM (2006b) Measurement of calcite crystallographic preferred orientations by magnetic anisotropy and comparison to diffraction methods. this volume

Crystal distribution patterns and their anisotropy behaviour in igneous rocks: towards an automated quantification, first results

Vortrag

Mark Paternell¹ Jörn H. Kruhl¹

Introduction

Since approximately two decades fractal geometry offers tools for the quantification of rock fabrics, and new methods are currently under development to investigate the inhomogeneity of crystal distributions, grain- and phase-boundary patterns as well as their anisotropy behaviour (Kruhl et al. 2004). These methods are now adapted for automated processing and suitable to quantify the inhomogeneity and anisotropy of rock fabrics from macro to microscale. Applications for quantifying inhomogeneity are mainly based on the box-counting and map-counting (Paternell 2002) methods, for anisotropy behaviour mainly based on modified Cantor-dust methods and provide fractal dimensions, fractal-dimension isolines and azimuthal anisotropies of fractal dimension (AAD, Volland & Kruhl 2004). For instance, the results provide information about the local variations of fabric patterns and their prefer orientation behaviour at macro and microscale.

Measurements

Inhomogeneity

Different types of granites from the Tuolumne Batholith (Sierra Nevada, USA), the Piquiri Syenite Massif

(Neoproterozoic basement of southern Brazil) and a fine-grained granite from central China (plates sold by a do-it-yourself store, Munich) have been investigated. Based on digital photographs of flat non-polished, polished and stained surfaces of fine-grained granites, the distributions of phase-boundary patterns for biotite, quartz, plagioclase and K-feldspar have been

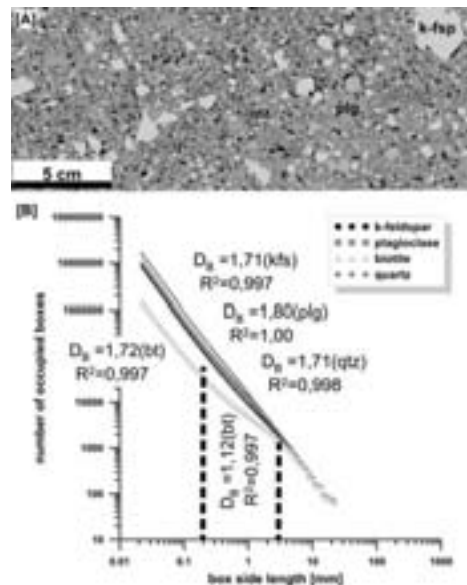


Figure 1: [A] Image of quartz (qtz), plagioclase (plg), K-feldspar (fsp) and bt (black) phases based on data from a stained plate of a fine-grained granite from Central China (plates sold by a do-it-yourself store, Munich). [B] Results of box counting on [A] - the linear relation between the number of occupied boxes and the box-side length plotted in a double-logarithm diagram for all phases shows that the pattern for each face is self-similar. The box dimension (D_B — defined as the slope of the line) for all different patterns is app. the same, except for biotite (marked by the dashed lines).

¹ Tectonics and Material Fabrics Section, Technische Universität München, D-80290 München, Germany

quantified by the box-counting method (Fig. 1). All distributions and patterns are self-similar, and their fractal box-dimensions range from 1.71 to 1.80 for all phases and for all different surfaces of the samples, but they are significantly different within the box-size interval of approx. 0.2 mm to 2 mm for biotite. This indicates the influence of at least two pattern-forming processes during crystallization:

- i) equilibrium crystallization conditions for all minerals, and
- ii) biotite distribution controlled by feldspar, as biotite crystals may have either grown in the remaining spaces or rotated during feldspar growth.

A comparison of manually (highest precision) and automatically digitized crystal distribution and grain-boundary patterns shows no significant differences in fractal-dimension values, and indicates the possibility of fully automated data processing. Box-counting measurements of crystal distribution for hornblende/pyroxene- and feldspar-phases on differently-oriented cuts of a foliated syenite show significantly different box-dimensions for mafic and felsic minerals. This may result either from feldspar having controlled the crystallization and/or orientation of the mafic minerals, or from the influence of early-formed pyroxene cumulates now disrupted and found as schlieren. Otherwise the cut orientation has no influence on the results of the measurements, indicating that the box-counting method is not useful for analyzing anisotropic behaviour of rock patterns.

Anisotropy

Because of the impracticalness of the

box-counting method for analyzing the anisotropic rock pattern behaviour of the syenite, the hornblende/pyroxene and feldspar phases on the differently-oriented cuts are analyzed with a new automated process based on the work of Volland & Kruhl (2004). First results should show different orientation behaviour of;

- i) the mineral phases in relation to the differently-oriented cuts and
- ii) different anisotropic behaviour between the hornblende/pyroxene and the feldspar phases.

The results from the differently-oriented cuts could be potentially useful as a step towards the analyses of 3D anisotropic material as well as the interpretation of the 2D cut effect of such material. Different anisotropic behaviour of different mineral phases in the syenite possibly indicate complex geometrical as well as chemical phase-to-phase interactions caused by either different pattern forming processes, for each phase, during the crystallization of the rock or by different crystallization time during the same process.

Results

The application of box-counting, a classical fractal geometry method for analyzing inhomogeneity distributions indicates:

- i) Stained, polished and even non-polished granite surfaces yield the same information about the rock pattern distribution and, therefore, about the pattern-forming processes of different phases like quartz, feldspars, and opaque phases even if the precision for digitizing the outlines of the different

phases is not the same in different surfaces. Such record forms the basis of automated fractal geometry procedures and, consequently, of detailed pattern analysis of larger areas.

- ii) Pattern differences between different minerals may be detected, even if they are not apparent, and quantified, as a necessary basis for the further investigation of pattern-forming processes.
- iii) Box-counting seems not to be adequate for analyzing the anisotropic behaviour of rock patterns. Thus an automated process based on the Cantor dust method was applied on anisotropic mineral-phases patterns. The results show different orientation behaviour of this pattern due to differently oriented rock cuts and mineral phases, potentially indicating
- iv) complex mineral-phases growth interactions, influenced by one or several pattern forming processes at the same time or at different times, during the crystallisation of the syenite.
- v) Combining fractal and non-fractal data, i.e., chemical and/or mineralogical properties of rocks, may provide even more useful data sets.

References

- Kruhl, JH, Andries, F, Peternell, M & Volland, S (2004) Fractal geometry analyses of rock fabric anisotropies and inhomogeneities. In: Kolymbas, D (ed) *Fractals in Geotechnical Engineering*. Advances in Geotechnical Engineering and Tunnelling 9. Logos, Berlin, 115–135
- Peternell, M (2002) Geology of syntectonic granites in the Itapema Regiona (SE Brazil) — Magmatic structures of the Rio Pequeno Granite (SE Brazil) and analyses with methods of fractal geometry. Unpubl. Diploma Thesis, TU München, pp 90
- Volland, S & Kruhl, JH (2004) Anisotropy quantification: the application of fractal geometry methods on tectonic fracture patterns of a Hercynian fault zone in NW-Sardinia. *Journal of Structural Geology* 26, 1489–1500

Gefügecharakterisierung von Calcitmyloniten und Marmoren bezüglich senkrecht zueinander stehender Falten- teilstrukturen, Alpi Apuane, Italien

Poster

Rüdiger Pfaar¹ Bernd Leiss¹ Giancarlo Molli² Jens M. Walter³

Im nördlichen Teil des Appenin in Italien ist der metamorphe Komplex der Alpi Apuane in Form eines tektonischen Fensters sehr gut aufgeschlossen. Die metamorphen Gesteine der Alpi Apuane — Metakarbonate, Kiesel- und Karbonatschiefer sowie Phyllite — sind aufgrund der Kollision der korsisch-sardischen Mikroplatte mit der italienischen Halbinsel im mm bis km-Maßstab verfaultet worden. Im zentralen Teil der Alpi Apuane biegt das generelle N-S Streichen der Faltenstrukturen in eine E-W Richtung um. Faltenstrukturen mit senkrecht zueinander stehenden Faltenachsen sind charakteristisches Strukturmerkmal u.a. ‘Metamorpher Kernkomplexe’ und Schlüssel

¹ Geowissenschaftliches Zentrum der Universität Göttingen, Goldschmidtstr. 3, 37077 Göttingen ² Dipartimento di Scienze della Terra, Università di Pisa, Via San Maria 53, 56126 Pisa, Italien ³ Forschungszentrum Jülich, 52428 Jülich

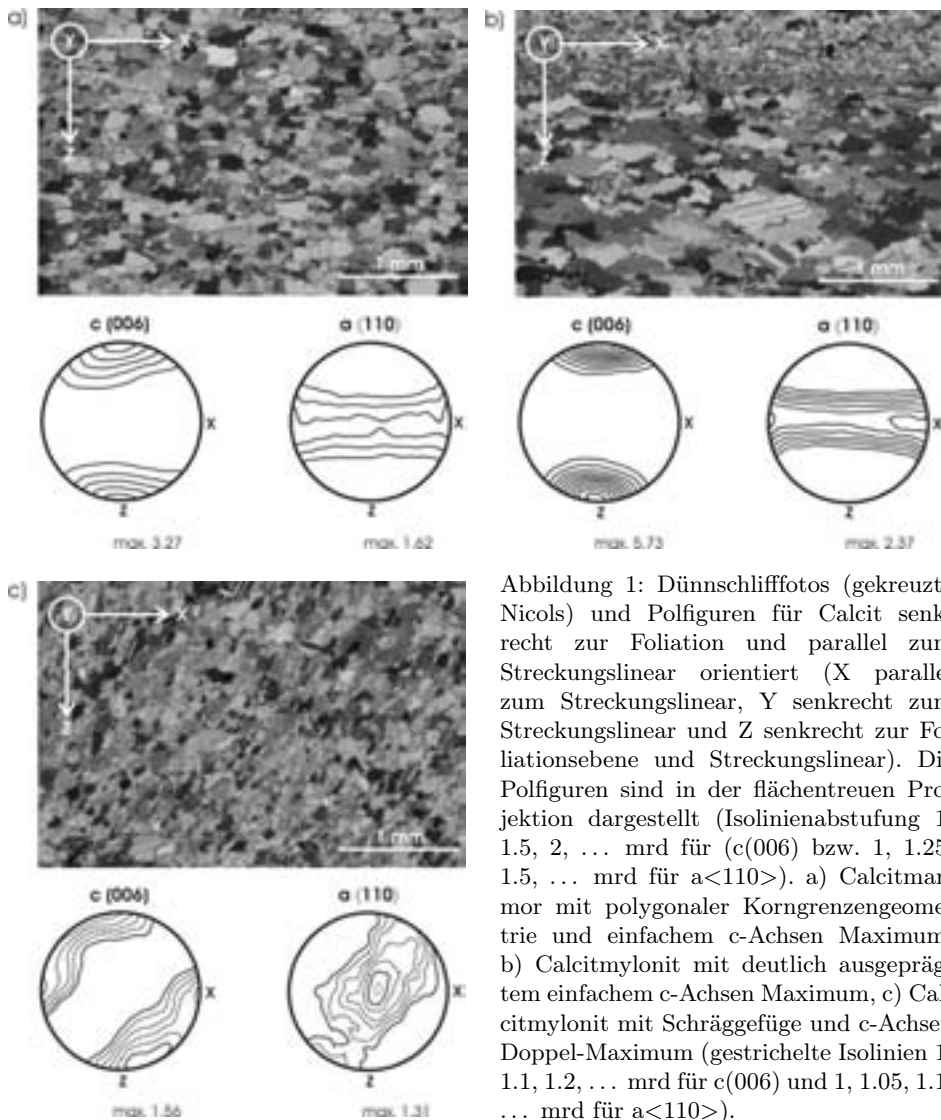
zum Verständnis von Deformationsgeschichte und -mechanismen. Die Entwicklung dieser Strukturen wird kontrovers diskutiert.

Auf der Basis einer vorangegangenen, eigenen Detailkartierung des Umbiegungsbereiches im Maßstab 1:5000, ist es Ziel dieser Arbeit, Kornformgefüge und kristallographische Vorzugsorientierungen (Texturen) mit den makro- und grossmaßstäblichen Gefügen der Falten- teilstrukturen systematisch zu charakterisieren und zu korrelieren. Diese Arbeiten sollen zum einen zum Verständnis der Deformationsgeschichte der Alpi Apuane, aber auch zum generellen Verständnis von Deformationsmechanismen und -prozessen von Karbonaten beitragen. Aufgrund des steilen Reliefs und guter Aufschlussverhältnisse durch zahlreiche Steinbrüche können die Strukturen dreidimensional kartiert und beprobt werden. Die in der ersten Deformationsphase (D_1) eng verfaltete, N-S streichende Synklinale von Arni biegt nach Süden hin innerhalb einer relativ kurzen Distanz von 100 bis 200 m in ein E-W-Streichen um. Der N-S-streichende Teil entspricht dem generellen Streichen innerhalb des Kernkomplexes, das Vorkommen des E-W-streichenden Teils ist lokal begrenzt. Die Streckungslineare sind sowohl im N-S-streichenden als auch im E-W-streichenden Bereich senkrecht zur Faltenachse entwickelt und in lokal auftretenden Scherzonen in Kleinfalten mitverfaltet. Während der späteren zweiten, extensionalen Deformationsphase (D_2) werden die gesamten D_1 -Faltenstrukturen durch offene Falten mit subhorizontal einfallenden Faltenachsenflächen überprägt. Das untersuchte Probenmaterial stammt aus der Einheit der jurassischen Marmore. Die

orientierte Probennahme erfolgte strukturbezogen, d.h. es wurden Proben aus Scherzonen und aus verschiedenen stark verfalteten Bereichen bzw. aus den Falten-schenkeln und den Scharnieren der unterschiedlich streichenden Falteinteilstrukturen entnommen.

Die Korngrößen- und Kornformgefügeanalysen erfolgten mit Hilfe des Polarisationsmikroskops, die Polfigurmessungen für die Texturanalysen wurden am Pulver- und Texturdiffraktometer SV7 am Forschungsreaktor Jülich 2 des Forschungszentrums Jülich (FRJ-2) durchgeführt. Neutronen erlauben aufgrund ihrer geringen Absorption in Materie, die Messung relativ großer Probenvolumina (hier Zylinder mit 3 oder 4 cm Durchmesser und Höhe), was bei den vorliegenden Proben mit relativ großer Korngröße notwendig ist. Ein Überblick der ersten Gefügeanalysen von 10 Proben ergibt folgendes Bild:

In der Regel weisen die Marmore ein Korngrößenspektrum von ca. 0,05 mm bis ca. 0,5 mm auf. Die Körner sind von einer interlobaten bis polygonalen Korngrenzengeometrie gekennzeichnet. Meist ist eine schwache Kornstreckung parallel zum generellen Streckungslinear zu erkennen (Abb. 1a). Die Mylonitproben aus den Scherzonen, weisen ein deutlich breiteres Korngrößenspektrum auf und zwar in Form eines feinkörnigeren (<0,01 mm bis 0,1 mm) und eines grobkörnigeren (0,1 mm bis ca. 1 mm) Lagenbaus. Die Körner sind von einer interlobaten bis verzahnten Korngrenzengeometrie gekennzeichnet. Vor allem die grobkörnigeren Kristalle zeigen eine deutliche Kornlängung (Abb. 1b) mit Kornachsenverhältnissen bis 1:4. Die Kornlangachsen liegen parallel zum Mineralstreckungslinear oder zeigen im Schliff parallel Linear, senkrecht Foliat-



on Kornschräggefüge auf (Abb. 1c).

Es lassen sich in allen, auch in den Marmorproben, kristallographische Vorzugsorientierungen nachweisen. Im Allgemeinen zeigen die Texturen ein zum Teil deutlich ausgeprägtes, einfaches c-Achsen Maximum (Abb. 1b), meist senkrecht zur Foliation orientiert.

Es lassen sich aber auch c-Achsen Doppelmaxima (Abb. 1c) und c-Achsen-Teilgürtel nachweisen.

Diese ersten Ergebnisse zeigen keine eindeutige Korrelation zwischen Korngefügetyp (Marmor oder Mylonit), Kornformtyp (polygonal, Kornlangachsenverhältnis, Korngrenzverzäh-

nungsgrad etc.), dem Texturtyp, den makroskopischen und den regionalen Strukturen. Damit wird offensichtlich, dass die Gefüge die komplexen Verformungs- und Temperaturpfade sehr differenziert aufgezeichnet haben und dass in weiteren systematischen Detailanalysen ein hohes Potenzial steckt, zum Entwicklungsmodell der Alpi Apuane beizutragen.



Figure 1: Reverse fault in the profile at Watchet. There is a network of white gypsum veins on either side of the fault plane, which stops abruptly at a grey siltstone layer and is absent in the overlying mudstones. A gypsum vein follows the fault plane to a higher level than the vein network in the adjacent layers. View southeast; the person provides a scale.

Gypsum veins as hydrofractures in layered and faulted mudstones: implications for reservoir permeability *Poster*

Sonja L. Philipp¹

Agust Gudmundsson¹

Mineral veins and reservoir permeability

Mineral veins form when water solutions passing through fluid-transporting fractures gradually seal the fractures as minerals precipitate. Many mineral veins are hydrofractures, that is, fractures generated at least partly by an internal fluid pressure. For most mineral veins, the fluid generating the hydrofracture is geothermal water. Other hydrofractures include fractures generated by magma (dykes, sills, inclined sheets), oil, gas and groundwater (many joints), as well as man-made hydraulic fractures in petroleum engineering. Hydrofractures are primarily extension fractures (Gudmundsson et al. 2002). The formation of

hydrofractures is one of the two basic mechanisms for the generation and maintenance of permeability, particularly in fluid-filled heterogeneous reservoirs such as those commonly associated with petroleum, groundwater, volcanic and geothermal fields. The other, and better-known, mechanism for permeability development is the formation of shear fractures, that is, faults.

The permeability development in fractured reservoirs, such as those for groundwater, geothermal water and petroleum, depends on fluid overpressure and transport in hydrofractures (Aguilera 1995). It has been proposed that a high fluid pressure in a reservoir can create high temporary permeability through hydrofracturing (Aguilera 1995; Gudmundsson et al. 2002). This hydrofracturing may result in mineral vein networks. Such palaeohydrofractures give information about past fluid

¹ Geowissenschaftliches Zentrum der Georg-August-Universität Göttingen, Abteilung Strukturgeologie und Geodynamik, Goldschmidtstr. 3, 37077 Göttingen

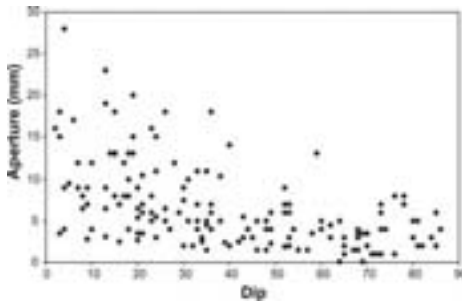


Figure 2: Aperture /dip relationship of 160 gypsum veins measured at Watchet. The thick veins are subhorizontal indicating that the minimum principal compressive stress was oriented vertically at the time of vein formation, a situation occurring during basin inversion.

flow and flow networks. Studying mineral veins is thus important for understanding fluid and mineral transport in rocks and reservoirs.

Faults and gypsum veins in mudstones

Here we present field measurements of mineral veins in coastal sections near the village of Watchet on the Somerset Coast of Southwest England (Fig. 1). The cliffs provide excellent outcrops of subhorizontal to gently dipping red mudstone beds with horizons of nodular gypsum and of siltstone of the Upper Triassic Mercia Mudstone Group.

In the upper part of the red mudstones there are laterally impersistent evaporite-rich horizons, mainly of white nodular gypsum. In part of the studied section west of Watchet Harbour, there are many thin beds of grey-green carbonatic siltstones, as well as nodular gypsum horizons. The beds are dissected by many faults and numerous gypsum veins. In some beds, there are

dense anastomosing networks of fibrous gypsum (satin spar) veins which may have formed during transient hydraulic fracturing (Cosgrove 2001). The exact mechanism for the formation of gypsum veins, however, is still a matter of debate. Proposed mechanisms include mineral precipitation in open fractures, formation due to crystallisation pressure, and hydraulic overpressure (Shearman et al. 1972; Gustavson et al. 1994). Based on 160 measurements, the veins in a dense vein network do not show any preferred orientation. The thickest veins, however, are subhorizontal (Fig. 2), indicating a horizontal orientation of the maximum principal compressive stress during their formation. Thus, the vein networks were partly developed during horizontal basin compression, a stress state which may have existed during basin inversion associated with Alpine Tectonics in the late Cretaceous and early Tertiary. 97 cross-cutting relationships, as well as mostly perpendicular vein fibres, indicate that the veins are primarily extension fractures; that is, they show hardly any evidence of shear displacement. In a 300 m-long profile dissected by (mostly) normal faults with small displacements, 24 faults (out of 28) have veins following them, indicating palaeofluid transport along the fault planes.

Formation of gypsum veins as hydrofractures

Mineral veins form through several related processes: fracturing, mineral dissolution, transport and precipitation. These processes may occur simultaneously and be repeated many times to form a single mineral vein. For a vein to form there must thus be a fluid, a material source, a fracture providing space,

and suitable pressure-temperature conditions for material precipitation. We propose that for the gypsum veins at Watchet water was transported from deeper levels in the sedimentary basin along faults into the mudstones where it got access to nodular anhydrite. The water then dissolved the anhydrite and formed gypsum. The volume increase due to this reaction and the low permeability of the mudstones lead to build-up of high fluid pressure in the nodules that, eventually, created hydrofractures at the ends of their long axes. The resulting hydrofractures connected the gypsum nodules. Calcium-sulphate saturated fluids, transported along the faults, got access to evaporite-free mudstone layers where dense anastomosing vein networks developed. Most veins were arrested during their propagation by layers with contrasting mechanical properties (generating stress barriers). Some veins, however, propagated through the barriers along faults to shallower levels.

Permeability of heterogeneous reservoirs

Our results have important implications for fluid transport in reservoirs and the formation of hydrofractures. The gypsum veins at Watchet indicate hydrofracturing rather late in basin history during inversion and exhumation (Cosgrove 2001). The veins show that fluids from deeper levels in the sedimentary basin can be transported along faults into rather impermeable host rocks. When injected into the host rocks, the overpressured fluids induce new hydrofractures. Provided the host rock has a low permeability and is sealing the nodules, the fluid overpressure is then partly related to the volume change

at the hydration of nodular anhydrite to gypsum. The hydrofractures propagate until they become arrested at layers with contrasting mechanical properties. Individual layers or ‘compartments’ in a fluid reservoir can be connected vertically through faults in which case the reservoir may develop a high temporary permeability. The gypsum veins following many fault planes indicate the faults transported water through the mudstones. This transport, presumably, occurred either during fault slip or through the formation of hydrofractures along the fault planes. Hydrofractures can transport fluids through low-permeability rocks. When the fluids are supersaturated with respect to certain minerals, or when there exists a local material source, mineral veins may form. At Watchet, nodular anhydrite acted as local material source. The present results suggest that high temporary permeabilities can develop in reservoirs not only during early burial but also during basin inversion — and that these permeabilities are primarily due to the formation of hydrofractures.

Acknowledgements We thank Statoil for a PhD-Grant (to AG) for Sonja Philipp, née Brenner.

References

- Aguilera R (1995) Naturally Fractured Reservoirs. PennWell Publishing Company, Tulsa, Oklahoma
- Cosgrove JW (2001) Hydraulic fracturing during the formation and deformation of a basin: A factor in the dewatering of low-permeability sediments. *Am Assoc Petrol Geol Bull* 85, 737–748
- Gudmundsson A, Fjeldskaar I & Brenner SL (2002) Propagation pathways and fluid transport of hydrofractures in jointed and layered rocks in geothermal fields. *J Volc Geotherm Res* 116, 257–278

al. 2002). In der Bruchzone mit zahlreichen Brüchen, meist subparallel zur Störungsfläche orientiert, hängt die Permeabilität der Bruchsysteme besonders vom Vernetzungsgrad der Brüche und dem lokalen Spannungsfeld ab.

In vielen Reservoirgesteinen ist die Matrixpermeabilität gering, so dass Fluidtransport besonders durch Brüche stattfindet (‚bruchkontrollierte Reservoir‘). Fluidtransport zwischen zwei Punkten A und B in einem bruchkontrollierten Reservoir findet gewöhnlich nur dann statt, wenn die Perkolationschwelle erreicht wird, d.h. dass diese Punkte durch ein zusammenhängendes Bruchnetzwerk miteinander verbunden sind (Stauffer & Aharony 1994). Um die Permeabilität von Gesteinen in potentiellen Reservoiren in geothermisch interessanten Tiefen abzuschätzen, sind Prognosen über die Geometrie existierender Brüche (insbesondere deren Orientierung und Öffnungsweite) sowie deren Vernetzung zu Bruchsystemen nötig. Da seismische Verfahren und Bohrkerne dafür nicht ausreichen, sind strukturgeologische Analysen entsprechender Gesteine in Aufschlüssen gleicher Fazies (‚Analoge‘) wichtig. Dabei wird der Schwerpunkt darauf gelegt, wie Gesteinsheterogenitäten (insbesondere die Schichtung) die Bruchausbreitung beeinflussen. Geländestudien in unterschiedlichsten Gesteinen — z.B. auch in natürlichen Paläogeothermiefeldern in Großbritannien und Island (Brenner 2003) — haben gezeigt, dass die mechanische Schichtung der Gesteine (insbesondere Änderungen der Steifigkeit) der wichtigste Parameter für die Bruchausbreitung ist. In mechanisch geschichteten Gesteinen sind Brüche häufig auf einzelne Schichten beschränkt und bilden daher seltener zu-

sammenhängende Bruchnetzwerke. Detaillierte Geländestudien werden daher mit der Bestimmung der mechanischen Gesteinseigenschaften ergänzt.

Weiterhin ist es wichtig, das lokale Spannungsfeld möglichst gut zu kennen. Zum einen hängen die Aktivität von Störungszonen und der damit verbundene Fluidtransport vom vorherrschenden Spannungsfeld ab. Zum zweiten wird durch das lokale Spannungsfeld bestimmt, ob Brüche sich ausbreiten können oder gestoppt werden. Zum dritten bestimmt das Spannungsfeld allgemein, ob Brüche eher geöffnet oder eher geschlossen werden (Abb. 2) und damit ob Fluidtransport durch das Bruchsystem stattfindet. Ist die größte Horizontalspannung, σ_H , parallel zum Streichen eines Bruchs orientiert, wird der Bruch offen gehalten, Fluidtransport wird erleichtert. Ist die größte Horizontalspannung, σ_H , jedoch senkrecht zum Bruchstreichen orientiert, wird der Bruch eher geschlossen, Fluidtransport wird erschwert. Das lokale Spannungsfeld kann erheblich vom regionalen Spannungsfeld abweichen. Gesteine mit unterschiedlichen mechanischen Eigenschaften können das Spannungsfeld auf kleinstem Raum extrem heterogen machen und so die Bruchausbreitung stark beeinflussen (Brenner 2003). Numerische Modelle tragen jedoch erheblich zum Verständnis des lokalen Spannungsfelds sowie der Vernetzung vorhandener und zu schaffender Bruchsysteme und somit des Fluidtransports im Reservoir bei.

Fallstudie: Geothermisches Potential des Buntsandsteins

Im Folgenden präsentieren wir Ausschnitte aus einer derzeit durchgeführten Fallstudie zur Vorhersage von Bruchsystemen und Permeabilitäten

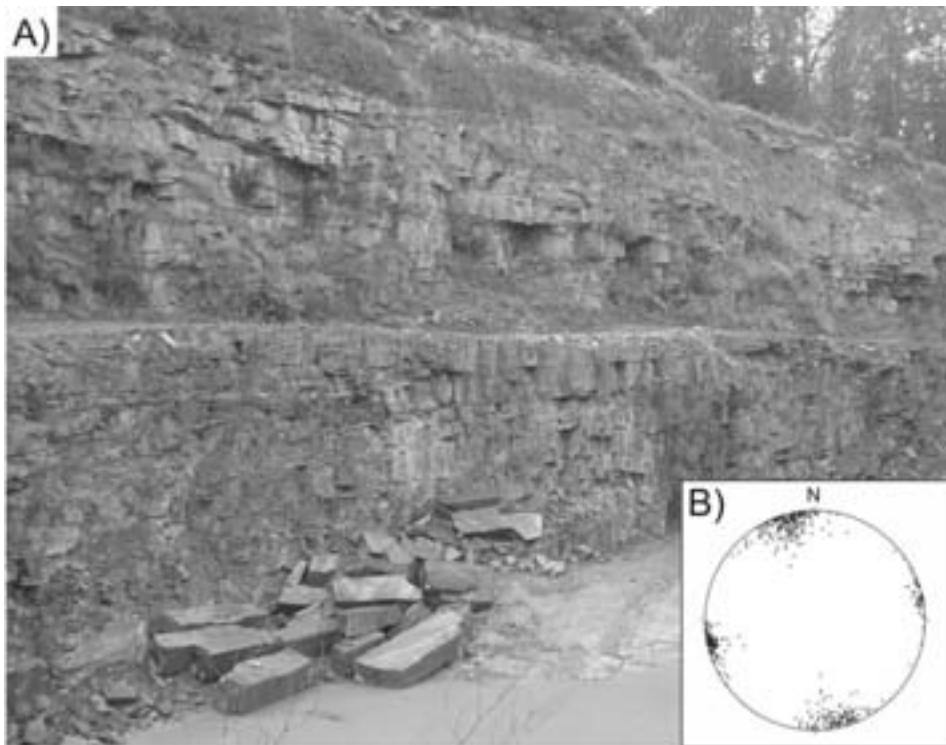


Abbildung 2: Aufschluss im Buntsandstein (Solling-Folge) bei Bad Karlshafen. A) Blick nach NNO, die kurze Bildkante ist etwa 10 m hoch. B) Darstellung von 558 Klüften als Durchstoßpunkte der Flächennormalen im Schmidtschen Netz (flächentreue, äquatoriale Projektion, untere Halbkugel).

im Buntsandstein Niedersachsens (vgl. Hoffmann et al. 2006). Detaillierte Geländestudien wurden in Aufschlüssen der Solling-Folge bei Bad Karlshafen durchgeführt (Abb. 2A). Es liegen zwei orthogonale Kluftscharen (Abb. 2B) mit unterschiedlichen Eigenschaften vor. Von 58 O–W-streichenden Klüften sind 40 (69%) auf einzelne Sandsteinschichten beschränkt. Von 129 N–S-streichenden Klüften hingegen konnten sich 71 (55%) durch mehrere Sandsteinschichten ausbreiten. Schon geringmächtige Lagen von Tonstein können viele Klüfte stoppen. Offenbar ha-

ben die deutlich unterschiedlichen mechanischen Eigenschaften von Tonstein (niedrige Steifigkeit) und Sandstein (höhere Steifigkeit) Einfluss auf die Kluftausbreitung.

Auch wenn es unwahrscheinlich ist, dass das im Steinbruch analysierte Bruchsystem genau dem Bruchsystem entspricht, das in der Tiefe angetroffen werden wird können Prognosen auf das vorhandene Bruchsystem im Untergrund getroffen werden. Weiterhin sind Aussagen zur potentiellen Ausbreitung neu zu schaffender künstlicher hydraulischer Brüche möglich, bzw. dazu, wie sich

vorhandene Brüche durch Stimulation voraussichtlich vernetzen werden. Dazu werden aus den in Geländestudien gewonnenen Daten und Informationen über den Untergrund der angestrebten Bohrung numerische Modelle erstellt. Ähnliche Studien können auch für andere Standorte, Lithologien und Stratigraphien durchgeführt werden. Durch die erläuterten Untersuchungen ist es möglich, optimale Bohrlokalitäten zu bestimmen. Die Wahrscheinlichkeit des Abteufens einer nicht nutzbaren Bohrung wird dadurch minimiert. Ebenso können durch eine geringere Zahl von Bohrungen höherer Effizienz Kosten reduziert werden.

Dank Wir danken der Deutschen Bundesstiftung Umwelt für CMs Promotionsstipendium und der Firma Steinbruch Niemeyer, Bad Karlshafen, strukturgeologische Geländestudien durchführen zu dürfen.

Literatur

- Brenner SL (2003) Field studies and models of hydrofractures in heterogeneous reservoirs. Doktorarbeit, Universität Bergen, Norwegen
- Gudmundsson A, Fjeldskaar I, & Brenner SL (2002) Propagation pathways and fluid transport of hydrofractures in jointed and layered rocks in geothermal fields. *Journal of Volcanology and Geothermal Research* 116, 257–278
- Hoffmann S, Müller C, Philipp SL & Gudmundsson A (2006) Strukturgeologische Geländestudie im Mittleren Buntsandstein zur Nutzung als geothermisches Reservoir (dieser Band)
- Philipp SL, Hoffmann S, Müller C & Gudmundsson A (2005) Verringerung des Fündigkeitsrisikos für tiefengeothermische Projekte durch strukturgeologische Geländestudien und numerische Modelle. *Geothermische Jahrestagung 2005*, 113–124
- Stauffer D & Aharony A (1994) *Introduction to Percolation Theory*. Taylor & Francis, London

Kinematik des Deckenkontaktes zwischen der Combinzone und der Zermatt-Saas-Zone (Penninische Decken, Westalpen) und deren Bedeutung für die Exhumierung der Zermatt-Saas-Zone *Vortrag*

Jan Pleuger¹ Sybille Roller¹ Jens M. Walter² Ekkehard Jansen² Nikolaus Froitzheim¹

Die Grenze zwischen zwei ophiolithischen Decken der penninischen Alpen, der Zermatt-Saas-Zone (unten) und der Combinzone (oben), markiert zugleich einen bedeutenden Sprung der bei der tertiären alpinen Metamorphose maximal erreichten Drücke. Während die Zermatt-Saas-Zone Ultrahochdruckmetamorphose (25–30 kbar/550–600°C, Bucher et al. 2005) erfuhr, erreichte die Combinzone lediglich blauschieferfazielle Bedingungen (13–18 kbar/380–550°C, Bousquet et al. 2004). Vor allem die Polarität des Drucksprunges führte dazu, daß die Deckengrenze zumeist als gewaltige südostvergente Abschiebung interpretiert wurde (z.B. Ballèvre & Merle 1993, Reddy et al. 1999). Strukturgeologische Geländebeobachtungen ergeben jedoch sowohl für das Hangende als auch das Liegende der Combinstörung die folgende kinematische Entwicklung:

- i) Nordwestvergente, überschiebende Scherung (D_1),
- ii) (Süd)westvergente Scherung (D_2),

¹ Geologisches Institut, Universität Bonn, Nufkallee 8, 53115 Bonn ² Mineralogisch-Petrologisches Institut, Universität Bonn, Arbeitsgruppe für Neutronenbeugung, Forschungszentrum Jülich, MIN/ZFR, 52425 Jülich

- iii) Südostvergente, abschiebende Scherung (D_3).

Alle drei Deformationsphasen fanden in beiden Einheiten unter grünschieferfaziellen Bedingungen statt.

Neutronentexturgoniometrische Untersuchungen sind vor allem an Quarziten der Cimes-Blanches-Decke durchgeführt worden, die sich an der Basis der Combinzone befindet und große Versatzbeträge entlang der Combinstörung durch duktile Scherung aufgenommen hat. Die im Rahmen dieser Studie erhaltenen Quarzittexturen lassen insbesondere Rückschlüsse auf die Geometrie der Verformungen D_1 , D_2 und D_3 zu. Sie spiegeln die oben avisierte Verformungsgeschichte wieder und erlauben, zusammen mit Quarzittexturen aus anderen Einheiten, den Geländebeobachtungen und petrologischen sowie geochronologischen Daten, eine detaillierte kinematische Rekonstruktion des penninischen Deckenstapels. Diese zeigt, daß abschiebende Bewegungen entlang der Combinstörung während D_2 und D_3 stattgefunden haben, aber nur geringe Versatzbeträge hatten. Spät während D_1 entstanden jeweils an der Basis der Sesia-Dent Blanche-Decke, der Zermatt-Saas-Zone und der Monte Rosa-Decke drei out-of-sequence-Überschiebungen, die als stark ausgedünnte Liegendschenkel von Deckenfalten aufgefaßt werden können. Nach Abwicklung dieser Falten liegt die Combinzone im Süden über der Sesia-Dent Blanche-Decke, in der Mitte über der Zermatt-Saas-Zone und im Norden über dem Bernhard-Deckensystem (Briançonnais). Die Platznahme der Combinzone fand während früher Stadien von D_1 statt als die Combinstörung eine flache, nordwestgerichtete Überschiebung war. Gleichzeitig mit dieser

Überschiebung war eine Abschiebung an der Basis der Sesia-Dent Blanche-Decke aktiv, so daß diese nach Süden aus dem Deckenstapel extrahiert wurde. Die Extraktion der Sesia-Dent Blanche-Decke bewirkte größtenteils die Exhumierung der Zermatt-Saas-Zone. Nördlich des extrahierten Blocks vereinigten sich in der Combinstörung die Überschiebung und die Abschiebung. Da der Versatzbetrag der Überschiebung größer als der der Abschiebung war, addierten sich die Bewegungen nördlich der Sesia-Dent Blanche-Decke zu einer Überschiebung. Diese transportierte die ursprüngliche Bedeckung der Sesia-Dent Blanche-Decke, von der sich auch die Cimes Blanches-Decke ableitet, so weit nach Norden, daß die ursprüngliche Bedeckung des Briançonnais durch die Cimes-Blanches-Decke ersetzt wurde (siehe auch Sartori & Marthaler 1994). Die Rekonstruktion ergibt, daß die Combinstörung hauptsächlich als Überschiebung aktiv war. Die Exhumierung der Gesteinseinheiten im Liegenden wurde nicht durch Extension, sondern durch vertikale Ausdünnung der Kruste während horizontaler Kontraktion bewirkt.

Literatur

- Ballèvre M & Merle O (1993) The Combin fault: Compressional reactivation of a Late Cretaceous-Early Tertiary detachment fault in the Western Alps. *Schweiz Mineral Petrogr Mitt* 73, 205–227
- Bousquet R, Engi M, Gosso G, Oberhänsli R, Berger A, Spalla MI, Zucali M & Goffé B (2004). Explanatory notes to the map: Metamorphic structure of the Alps Transition from the Western to the Central Alps. *Mitt Österr Miner Ges* 149, 145–156
- Bucher K, Fazis Y, de Capitani C & Grapes R (2005) Blueschists, eclogites, and decompression assemblages of the Zermatt-Saas ophiolite: High-pressure metamorphism of sub-

- ducted Tethys lithosphere. *Am Mineral* 90, 821–835
- Reddy SM, Wheeler J, Butler RWH, Cliff RA, Freeman S, Inger S, Pickles C & Kelley SP (2003) Kinematic reworking and exhumation within the convergent Alpine Orogen. *Tectonophysics* 365, 77–102
- Sartori M & Marthaler M (1994) Exemples de relations socle-couverture dans les nappes penniques du Val d'Hérens *Compte-rendu de l'excursion de la Société Géologique Suisse et de la Société Suisse de Minéralogie et Pétrographie* (25 et 26 septembre 1993). *Schweiz Mineral Petrogr Mitt* 74, 503–509

The Serifos Metamorphic Core Complex (Greece) — kinematic investigations of the southern detachment mylonites

Vortrag

Christian Rambousek¹ Bernhard
Grasemann¹ Konstantin Petrakakis¹
Michael A. Edwards¹ Christoph
Iglseider¹ András Zámolyi¹

The island of Serifos is situated about 100 km SSE of Athens in the Aegean Sea and belongs to the Attic-Cycladic massif. The geology of Serifos is largely characterized by a shallow hornblende-biotite granodiorite pluton that intruded in the late Miocene into a previously deformed (under blueschist conditions) sequence mainly consisting of ortho- and paragneisses, calc-silicate marbles, amphibolites and schists. The pluton has a dome-shaped body occupying the central and southern parts of the island (Salemink 1985). The Serifos MCC is the very western continuation

of a zone of syn- to post tectonic intrusions younging from the East (Naxos, Paros ~12 Ma) to the West (Serifos 9–8 Ma). Whereas the older intrusions in the East show a top to the North geometry, the Serifos MCC has developed a South-directed low-angle detachment fault.

The northern contact of the Serifos pluton is intrusive. In the SE, towards structurally higher levels, a core becomes foliated with increasing intensity and, under greenschist facies conditions, transformed into S-dipping low temperature mylonitic to ultramylonitic rocks with abundant SSW-directed kinematic indicators (SCC' fabrics, sigma and delta clasts, flanking structures and mica fish). This zone forms the main greenschist facies to brittle/ductile detachment of the Serifos MCC. The lineation in these rocks has a remarkably consistent NNE-SSW direction. The foliation however varies and follows the dome shaped structure caused by the exhumation and unloading of the MCC. Quantitative kinematic indicators and micro structures with monoclinic symmetry have been investigated in order to characterize the flow within the main detachment zone. It is well known that in mylonitic zones, an increase in intensity of deformation is normally expressed by a decrease in grain size, accompanied by recrystallisation (Berthé et al. 1979) as it can be observed in the ultramylonitic granodiorites of the SE detachment zone. Here the undeformed core becomes foliated towards the S and, with increasing intensity, turns into a ultramylonite with quartz-feldspar- and biotite-porphyroblasts in a very fine grained matrix.

Rigid objects in rocks undergoing penetrative ductile non-coaxial flow will tend

¹ Department of Geodynamics and Sedimentology, Structural Processes Group, University of Vienna, Austria

to rotate with respect to the kinematic frame of the bulk flow, and disturb the developing foliation pattern at a small adjacent domain. To investigate the rotational behaviour of porphyroblasts in aspect to their shape, thin sections of the ultramylonitic Hbl–Bt granodiorite of the southern detachment were analyzed with the image analysis program Scion Image. Qtz, feldspar and biotite were separately plotted in aspect to their orientation (θ) and the normalized length-width ratio (B^*) of their ideal strain ellipsoid. In contrast to the plastically deforming quartz, the feldspar shows brittle deformation which suggests maximum deformation temperatures of about 350°C. Our microstructural investigation reveals that feldspar grains with variable aspect ratio record no stabilization forming-clast geometries. In contrast Qtz clasts show both: stabilization of grains with high aspect ratio inclined against the shear direction and grains with low aspect ratios with no stable position. Bt always forms textbook examples of mica fish type clast with stable position inclined against the shear direction. These observations from natural mylonites confirm results from analogue and numerical models (e.g. Ceriani et al. 2003, Marques et al. 2005; Schmid & Podladchikov 2005), which suggest a strong dependence of the shape and the clast matrix coupling on the rotational behaviour and stable position of clasts.

References

- Ceriani S, Mancktelow NS & Pennacchioni G (2003) Analogue modelling of the influence of shape and particle/matrix interface lubrication on the rotational behaviour of rigid particles in simple shear. *Journal of Structural Geology*, 25(12), 2005–2021
- Berthé D, Choukroune P & Jegouzo P (1979)

Orthogneiss, mylonite and non coaxial Deformation of granites: The example of the South Armorican Shear Zone. *Journal of Structural Geology* 1, 31–42

- Grasemann B, Petrakakis K, Iglseider C, Ramboisek C, Zamolyi A & Draganits E (2004) The Serifos Metamorphic Core Complex (Western Cyclades, Greece). 5th International Symposium on Eastern Mediterranean Geology, Thessaloniki, Greece. 14-20th April 2004
- Marques FO, Taborda, R & Antunes J (2005) Influence of a low-viscosity layer between rigid inclusion and viscous matrix on inclusion rotation and matrix flow: A numerical study. *Tectonophysics*, 407(1-2), 101
- Salemink J (1985) Skarn and ore formation at Serifos, Greece, as a consequence of granodiorite intrusion. Unpublished PhD Thesis, University of Utrecht
- Schmid DW & Podladchikov YY (2005) Mantled porphyroclast gauges. *Journal of Structural Geology*, 27(3), 571

Einfluss der Zusammensetzung von Titanomagnetit auf die Anisotropie der magnetischen Suszeptibilität — Fallstudie an einem Dyke-Sill Komplex in Ungarn *Poster*

Daniela Renk¹ Helga de Wall¹ Ulrike Martin¹ Karoly Nemeth²

Einführung

In den letzten Jahrzehnten hat die Messung der magnetischen Suszeptibilität im Schwachfeld (üblicherweise bei 300 A m⁻¹) für geologische Arbeiten eine wichtige Rolle eingenommen. Da anhand der Anisotropie der magnetischen

¹ Institut für Geologie, Julius-Maximilians-Universität Würzburg, Pleicherwall 1 D-97070 Germany ² Geological Institute of Hungary, 14 Stefania St., Budapest H-1143, Hungary

Suszeptibilität (AMS) auch schwache Vorzugsorientierungen registriert werden können, ist die AMS eine wichtige Methode zur Bestimmung von Fließrichtungen in magmatischen Körpern. In ferrimagnetischen, basaltischen Gesteinen ist hauptsächlich Titanomagnetit Träger der Information für die AMS. Nach Jackson et al. (1998) und de Wall (2000) variiert die magnetische Suszeptibilität (MS) von Titanomagnetiten stark mit der Mineralzusammensetzung und ist abhängig von der Feldstärke (Amplitude des Wechselfeldes) des angelegten Magnetfeldes.

Diese Arbeit umfasst eine systematische Studie zum Einfluss der Feldstärke für AMS Messungen an Gängen (Dykes und Sills) und Lavaströmen (flows). Variationen in der MS und ihrer Anisotropie können Informationen zur Platznahme und den Fließeigenschaften von Laven beinhalten (Canon-Tapia et al. 1997, Canon-Tapia & Pinkerton 2000). Für eine korrekte Bewertung und Interpretation von Variationen der AMS, muss in Titanomagnetit-haltigen Gesteinen der Einfluss der Feldstärkenabhängigkeit auf die MS und AMS berücksichtigt werden.

Die Studie wurde am Ság-hegy Vulkankomplex in der kleinen ungarischen Tiefebene durchgeführt. Dieser Komplex besteht aus einem phreatomagmatischen Tuffring, der sich im Pliozän bis Miozän bildete. Nachdem die Zufuhr an meteorischem Wasser endete, wechselte der phreatomagmatische Stil zu einem effusiven. Dabei wurde der Tephrring mit einem Lavasee verfüllt und ein Dyke-Sill Komplex intrudierte in die pyroklastischen Einheiten.

Im Gelände wurden Proben von den Dykes und Sills, sowie von Laven aus dem Lavasee und aus den ausgeflossenen La-

vaablagerungen genommen und an diesen die Parameter der AMS bestimmt. Die geochemischen Analysen der Proben ergaben eine basaltische bis trachybasaltische Zusammensetzung und plotten im Diskriminierungsdiagramm im Feld der Intraplattenvulkanite. Proben der Übergangsbereiche (Transitional) von Dykes zu Sills und Intrusiva zu Effusiva wurden gesondert betrachtet. Die MS wurde mit einer KLY-4S Kapabrücke (AGICO, Brno) gemessen.

Ergebnisse

Im Schwachfeld wird eine lineare Beziehung zwischen der Magnetisierung und dem angelegten, magnetischen Feld angenommen. Dies gilt in den hier bearbeiteten Proben nur für Felder kleiner als 100 A m^{-1} , bei einer höheren Feldstärke ist die Beziehung nicht mehr linear (Abb. 1). Um den Einfluss der Feldstärke auf die AMS zu testen, wird ein Datensatz präsentiert, der bei 30 A m^{-1} (lineares Verhalten) und 300 A m^{-1} (nicht-lineares Verhalten) gemessen wurde. Für diese beiden Datensätze sind in Tab. 1 die Volumensuszeptibilität, der Formfaktor (T) und der Grad der Anisotropie

	Dyke	Transitional	Sill	Lava
Anzahl	40	20	20	16
k_{30}	8.7	8.9	6.4	14.4
std-dev	8.4	7.0	2.7	16.5
k_{300}	11.4	12.3	7.9	17.3
std-dev	9.6	6.9	3.3	18.6
F_{30}	1.016	1.010	1.008	1.016
std-dev	0.007	0.005	0.005	0.007
F_{300}	1.023	1.015	1.009	1.023
std-dev	0.013	0.006	0.004	0.010
T_{30}	0.114	0.286	0.011	0.234
std-dev	0.375	0.302	0.413	0.343
T_{300}	0.095	0.350	-0.052	0.154
std-dev	0.351	0.285	0.401	0.375

Tabelle 1: Merkmale der magnetischen Suszeptibilität (k in 10^{-3} SI) für die Dykes, die Übergangsbereiche (Transitional), die Sills und Lava Flows bei einer Feldamplitude von 30 A m^{-1} und 300 A m^{-1} .

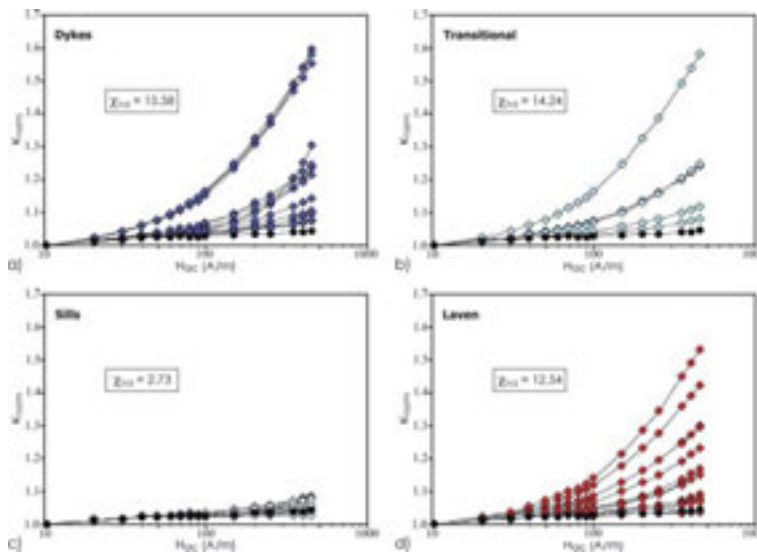


Abbildung 1: Magnetische Suszeptibilität mit zunehmender Feldstärke H_{ac} (k normiert auf $H_{ac} = 10 A m^{-1}$) für a) Dykes; b) Übergänge (Transitional) von Dykes zu Sills und Lava Flows; c) Sills; d) Lava Flows. Zum Vergleich wurde eine Probe mit reinem Magnetit (Magnetit-Standard) dazu geplottet. Der durchschnittliche χ_{Hd} -Wert (Feldstärkenabhängigkeit der magnetischen Suszeptibilität in Prozent, ermittelt aus den Messungen bei einer Feldamplitude von 30 und 350 $A m^{-1}$) für die verschiedenen Probengruppen ist ebenfalls angegeben.

sotropie (P') gelistet. T und P' sind die Parameter, die üblicherweise zur Beschreibung der AMS-Ellipsoide benutzt werden (Jelinek 1981).

Die MS ist für die effusiven Lavagesteine am höchsten, wobei die höchsten Werte den Proben aus dem Lavasee zuzuordnen sind. Die Suszeptibilität nimmt von den effusiven Gesteinen zu den Dykes ab und zeigt die geringsten Werte für die Sills. Für die Messungen in den beiden Feldamplituden gibt es einen deutlichen Unterschied in den Beträgen der MS, mit größeren Unterschieden in Laven und Dykes im Vergleich zu den Sills. Dies steht mit der unterschiedlichen Zusammensetzung der Titanomagnetite in Beziehung und weist auf einen geringen Ti-Anteil in den Sills im Gegensatz zu

den Dykes und Laven hin (Abb. 1). Betrachtet man den gesamten Datensatz, so wird für abnehmende Feldamplituden ein Trend zu geringeren Suszeptibilitäten und isotroperen Strukturen deutlich (Abb. 2).

Messungen bei Feldstärken, die im nicht linearen Bereich liegen, haben offensichtlich auf den Grad der magnetischen Anisotropie einen großen Einfluss, der mit der Zusammensetzung der Titanomagnetite variiert. Generell ist der Grad der Anisotropie bei magmatischen Fließstrukturen eher gering ($P' < 1.1$, Tarling & Hrouda 1993). Der Einfluss der Feldstärkenabhängigkeit kann also den Betrag der ‚wahren‘ magnetischen Anisotropie überschreiten. Der Vergleich der AMS-Ellipsoide für Mes-

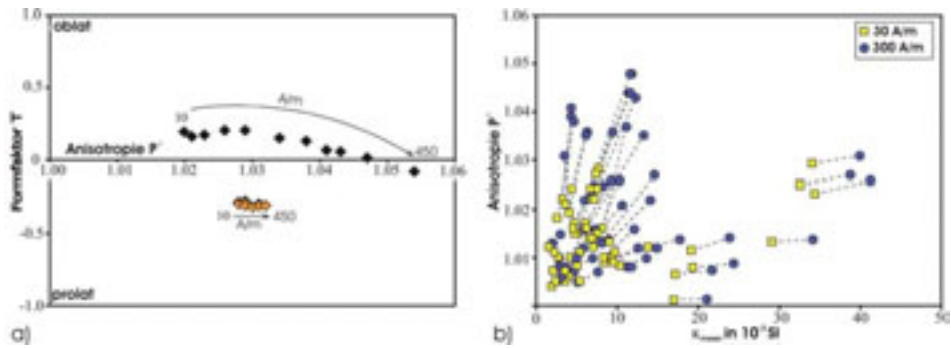


Abbildung 2: In a) ist die Änderung des Formfaktors und der Anisotropie mit zunehmender Feldstärke dargestellt. Die grau gezeichnete Probe enthält einen geringen Ti-Anteil und die schwarze einen hohen; in b) ist für Proben aus den Dykes der Grad der Anisotropie gegen die Suszeptibilität für Messungen bei einer Feldstärke von 30 und 300 A m⁻¹ aufgetragen.

sungen im linearen und nicht linearen Bereich zeigt diesen dramatischen Effekt. Es bleibt aber dennoch ein Unterschied in der MS und P' zwischen Sills, Dykes und Laven, der sich auch in den Suszeptibilitäten in Tab. 1 widerspiegelt. Dies gibt einen Hinweis auf unterschiedliche Fließeigenschaften und Abkühlungsraten der verschiedenen vulkanischen Körper.

Schlussbemerkung

Diese Studie macht den Einfluss der Feldstärkenabhängigkeit auf die MS und AMS in Titanomagnetit-führenden Gesteinen deutlich. Die Auswirkung der Zusammensetzung auf die MS muss also beachtet werden, wenn man magnetische Anisotropien von verschiedenen Typen vulkanischer Gesteine miteinander vergleicht und wenn man den Grad der Anisotropie dazu verwendet, um Informationen über die Fließdynamik einer Lava zu erhalten. Die Auswertung der gemessenen Daten ergibt eine lineare Beziehung zwischen $\Delta P'$ ($P' 300 \text{ A m}^{-1} - P' 30 \text{ A m}^{-1}$)

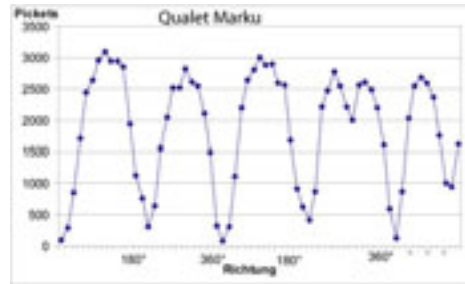
und den χ_{hd} -Werten (Feldstärkenabhängigkeit in %). Aus diesem Graph kann ein Korrekturfaktor bestimmt werden, mit dem die Anisotropiedaten in Titanomagnetit-führenden Gesteinen korrigiert werden können. Ansonsten wird für ferromagnetische, basaltische Gesteine vorgeschlagen, die AMS im Bereich der linearen Beziehung zwischen Magnetisierung und angelegtem Feld zu messen, also bei Feldern $< 100 \text{ A m}^{-1}$.

Literatur

- Canon-Tapia E, Walker GPL & Herrero-Bervera E (1997) The internal structure of lava flows: insights from AMS measurements II: Hawaiian pahoehoe, toothpaste lava and 'a'a. *J. Volcanol. Geotherm. Res.* 76, 19–46
- Canon-Tapia E & Pinkerton H (2000) The anisotropy of magnetic susceptibility of lava flows: an experimental approach. *J. Volcanol. Geotherm. Res.* 98, 219–233
- de Wall H (2000) The field-dependence of ac susceptibility in titanomagnetites: implications for the anisotropy of magnetic susceptibility. *Geophys. Res. Lett.* 27, 2413–2416
- Jackson M, Moskowitz B, Rosenbaum J & Kissel C (1998) Field-dependence of AC susceptibility in titanomagnetites. *Earth Planet. Sci. Lett.* 157, 129–139

Jelinek V (1981) Characterization of the magnetic fabrics of rocks. *Tectonophysics* 79, 63–67

Tarling DH & Hrouda F (1993) *The Magnetic Anisotropy of Rocks*. Chapman & Hall, London, p 217



Empirische Feldstudien über elektromagnetische Emissionen in Gesteinen unter aktiven Krustenspannungen

Vortrag

C.-D. Reuther¹ Elmar Moser¹

Einleitung

In den vergangenen Jahren wurden von den Mitgliedern unseres Departments mehrere Feldstudien über elektromagnetische Emissionen in tektonisch aktiven Regionen durchgeführt. Die Untersuchungsgebiete lagen in Südspanien, Sizilien, Malta, Eger-Graben/Tschechische Republik und die Provence/Frankreich als auch in Süd-Chile.

Theoretische Grundlagen

Das Ziel dieser Untersuchungen war die Erfassung der größten horizontalen Spannungs-Richtung in der oberen Erdkruste. Dazu wurden die Intensität des elektromagnetischen Feldes in Bezug zu der Orientierung einer Richtantenne gemessen (Abb. 1). Diese Ergebnisse wurden mit aktiven Stress-Richtungen verglichen die aus Doorstopper-Messungen, Bohrloch-Randausbrüchen, Herdflächenlösungen

Abbildung 1: Typische Messkurve einer elektromagnetischen Messung zur Richtungsbestimmung der maximalen horizontalen Krustenspannung

und neotektonischen Strukturanalysen gewonnen wurden. Die Richtungen der größten Horizontalspannungen stimmen sehr gut mit der Orientierung der maximalen elektromagnetischen Emission überein.

Die elektromagnetische Emission von Gesteinen unter tektonischer Spannung beruht auf dem Prinzip der Ladungsverschiebung im molekularen Maßstab. Dabei wird in dem Gestein eine kurzzeitige Ladungstrennung und damit ein Dipol erzeugt. Dieser strahlt sowohl bei seiner Entstehung als auch beim folgenden Ladungsausgleich eine gerichtete elektromagnetische Welle ab. Dabei stehen die elektrische und die magnetische Komponente senkrecht aufeinander, haben aber dieselbe Orientierung im Raum. Die Ladungstrennung wird wahrscheinlich durch Mikrorisse hervorgerufen, aber auch der Einfluss von piezoelektrischen und piezomagnetischen Effekten kann nicht ausgeschlossen werden. Daher werden hier nur die empirischen Daten präsentiert und kein spezifisches Modell für die Entstehung der elektromagnetischen Strahlung definiert.

¹ Department für Geowissenschaften, Universität Hamburg, Bundesstrasse 55, 20146 Hamburg

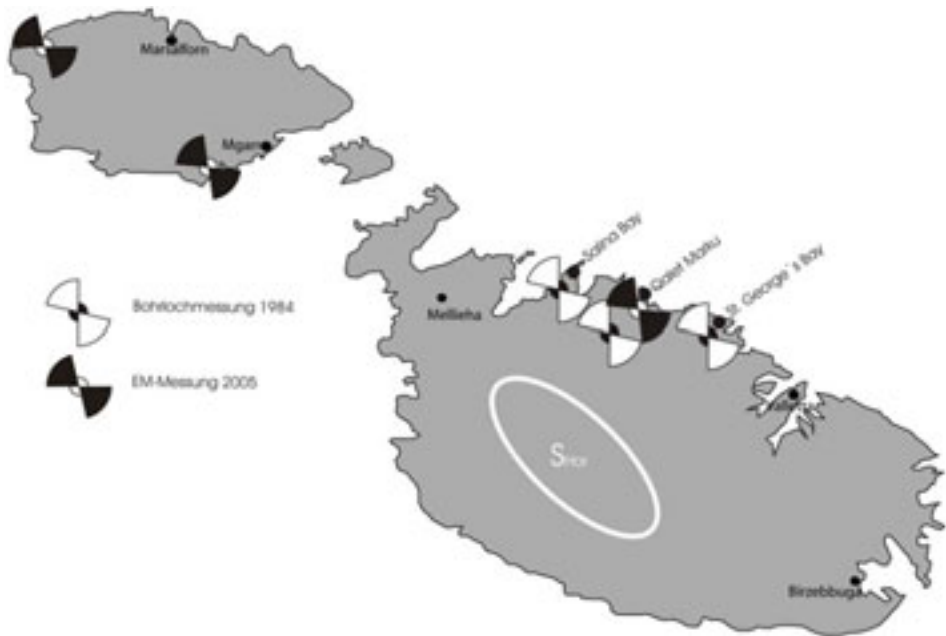


Abbildung 2: Vergleich von Bohrlochmessungen und elektromagnetischen Messungen zur Krustenspannungsbestimmung auf Malta

Empirische Ergebnisse

In Südspanien wurden 2002 und 2005 EM-Messungen durchgeführt um die Reproduzierbarkeit der Messmethode zu zeigen. Die Ergebnisse der beiden Messkampagnen stimmen innerhalb der Messgenauigkeit dieser Methode überein und zeigen eine größte Horizontalspannung in NW-SE-Richtung (140°). Dies ist in guter Übereinstimmung mit der tektonischen Gesamtsituation im westlichen Mittelmeerraum. Sowohl auf Sizilien als auch auf Malta wurden die EM-Messungen mit Bohrlochmessungen aus den 1980er Jahren verglichen. Beide Methoden erbrachten dieselben Ergebnisse in Bezug auf die Richtung der horizontalen Hauptspannung (Abb. 2) und fügen sich auch in die großräumige tektonische Spannungssituation ein. Eine besonders erwähnenswerte Bege-

benheit tritt in Ost-Sizilien auf wo eine tektonische Flexur ein anderes lokales Spannungsfeld hervorruft als in den restlichen Teilen Siziliens (Reuther et al., 2002). Leider ist es bei der Spannungsbestimmung mittels elektromagnetischer Emissionen noch nicht möglich den Absolutbetrag der Spannung zu ermitteln wie es bei den Bohrlochmessungen der Fall war. Die Ergebnisse aus der Tschechischen Republik können sowohl mit der Mikroriss-Theorie als auch mit dem piezoelektrischen Effekt erklärt werden. Die mit den unterschiedlichen Theorien ermittelten Hauptspannungsrichtungen stehen in einem Winkel von 90° zueinander. Beide Lösungen können im geologischen Kontext erklärt werden und daher kann mit diesem Datensatz die Frage der Entstehung der Mikrorisse nicht erklärt werden. Die

auf Basis von Mikrorissen als Ursache der elektromagnetischen Strahlung ermittelte horizontale Hauptspannungsrichtung stimmt gut mit Herdflächenlösungen im tschechischen Schwarmbebengebiet überein. Der piezoelektrische Ansatz würde ein theoretisch mögliches regionalgeologisches Modell mit einer Übertrittssituation zweier gestaffelter Horizontalstörungen nachweisen. Die Spannungsbestimmung in der Provence (Südfrankreich) zeigt eine NNW-SSE Richtung der maximalen Horizontalspannung. Diese Richtung wurde durch neotektonische Strukturanalysen und neueste geodätische Vermessungen (Jouanne et al., 2001) andererseits bestätigt. Südchile ist eine tektonisch sehr aktive Gegend in der mit neotektonischen Untersuchungen basierend auf Strukturanalysen verschiedene regionale/lokale Krustenspannungsfelder ermittelt wurden. Diese Spannungsdomänen sind durch Kompressions-, Extensions-, Vertikal- und Horizontal- Tektonik gekennzeichnet. Die Messung der elektromagnetischen Emissionen bestätigte die unterschiedlichen Spannungsfelder in den jeweiligen Regionen.

Literatur

- Jouanne F, Hippolyte JC, Gamond JF & Martinod J (2001) Current deformation of the Digne Nappe (southwestern Alps) from a comparison between triangulation and GPS data. *Geophysical Journal International* 144, 432–440
- Reuther CD, Obermeyer H, Reicherter K, Reiss S, Kaiser A, Buchmann T, Adam J, Lohrmann J & Grasso M (2002) Neotektonik und aktive Krustenspannungen in Südost Sizilien und ihre Beziehungen zur regionalen Tektonik im Zentralen Mittelmeer. *Mitteilungen des Geologisch-Paläontologischen Instituts der Universität Hamburg* 86, 1–24

Structural contacts in the Late Paleozoic accretionary wedge of central Chile and their tectonic significance for the evolution of the accretionary complex *Vortrag*

Peter P. Richter¹ Uwe Ring² Arne P. Willner³ Bernd Leiss⁴

The Chilean accretionary wedge is part of a Late Paleozoic subduction complex that developed during subduction of the Pacific plate underneath South America. The wedge is commonly subdivided into a structurally lower Western Series and an upper Eastern Series. Understanding the contact between both series has been a long standing problem and is fundamental for the understanding of the evolution of the wedge system. We show the progressive development of structures and finite strain from the least-deformed rocks in the eastern part of the Eastern Series of the accretionary wedge to higher grade schist of the Western Series at the Pacific coast. Upright chevron folds of sedimentary layering are associated with a penetrative axial-plane foliation, S_1 . As the F_1 folds became slightly overturned to the west, S_1 was folded about recumbent open F_2 folds and an S_2 axial-plane foliation developed. Near the contact between the Western and Eastern series S_2 represents a prominent subhorizontal transposition foliation. Towards the structural deepest units in the west

¹ Institut für Geowissenschaften, Johannes Gutenberg-Universität, 55099 Mainz, Germany

² Department of Geological Sciences, Canterbury University, Christchurch, New Zealand

³ Institut für Geologie, Mineralogie und Geophysik, Ruhr-Universität, 44870 Bochum, Germany

⁴ Zentrum für Geowissenschaften, Universität Göttingen, Göttingen, Germany

the transposition foliation became progressively flattened. Finite-strain data as obtained by R_f/ϕ analysis in meta-greywacke and X-ray texture goniometry in phyllosilicate-rich rocks show a smooth and gradual increase in strain magnitude from east to west. There is no evidence for normal faulting or significant structural breaks across the contact. We interpret the progressive structural and strain evolution between both series to reflect a continuous change in the mode of accretion in the subduction wedge. Before ca. 320–290 Ma the rocks of the Eastern Series were frontally accreted to the Andean margin. Frontal accretion caused horizontal shortening and upright folds and axial-plane foliations developed. At ca. 320–290 Ma the mode of accretion changed and the rocks of the Western Series were underplated below the Andean margin. This basal accretion caused a major change in the flow field within the wedge and gave rise to vertical shortening and the development of the penetrative subhorizontal transposition foliation.

Origin of Central Andean collapse calderas *Vortrag*

Ulrich Riller¹

Regional strains in tectonically active volcanic provinces may have a profound influence on the mode of collapse caldera formation. Conversely, the deformation pattern, more specifically, the symmetry of plan-view strain fields imparted to caldera floors may assist in elucidat-

ing the regional deformation active during caldera formation. The symmetry of plan-view strain fields is chiefly controlled by the mode of floor subsidence, particularly whether subsidence is uniform, symmetric or asymmetric, portraying collapse mechanisms known respectively as plate, downsag and trapdoor. Plate and downsag subsidence generates centro-symmetric strain fields characterized by radial and concentric discontinuities and subvolcanic dikes. Such strain fields appear to develop preferably where magma pressure controls collapse. By contrast, rectilinear horizontal strain fields form under unidirectional stretching and generate normal faults and subvolcanic dikes transverse to the stretching direction. Rectilinear strain fields are typical for trapdoor subsidence but also for straight orogenic belts and suggests that the formation of both may be related. This was tested for six central Andean collapse calderas that formed between 10.5 and 2 Ma and are located on prominent NW–SE striking fault zones.

A combined geochronological and structural analysis of the Miocene Negra Muerta Caldera in particular was designed to better understand caldera formation associated with the prominent Olacapato – El Toro Fault Zone. Rb–Sr ages of the caldera outflow facies indicate that caldera formation occurred in two volcano-tectonic episodes. The first episode commenced with explosive eruption of the 9.0 ± 0.1 Ma andesitic Acay Ignimbrite followed by a period of volcanic quiescence and moderate tectonic activity. Dominant volcanic and tectonic activity occurred during the second episode, which is bracketed by eruption of the 7.6 ± 0.1 Ma rhyolitic Toba 1 Ignimbrite and effusive discharge

¹ Humboldt-Universität Berlin, Museum für Naturkunde, Invalidenstrasse 43, 10115 Berlin

of the 7.3 ± 0.1 Ma rhyodacitic to andesitic lava flows. Structural relationships between rocks of the Negra Muerta Volcanic Complex and collapse-induced normal faults, notably NE-striking normal faults, agree with simultaneous volcanic activity and floor subsidence of the caldera during the second episode. Floor subsidence was achieved by tilting on an outward dipping reverse fault to the northwest of the caldera floor around a hinge zone located south of the caldera floor. This induced horizontal extension of the caldera floor and was accomplished by fragmentation of, and intrusion of dikes into, the floor. Collapse-induced and post-collapse fault populations of the caldera do not differ significantly in the directions of their axes of maximum extension and are in this respect kinematically compatible with left-lateral slip on the nearby Olacapato – El Toro Fault Zone. This furnishes evidence for a kinematic control by prominent faults on the formation of collapse calderas in the central Andes.

Similar to the Negra Muerta Caldera, other Central Andean calderas adhere to a rectilinear strain field pointing to trapdoor subsidence and uniform stretching sub-parallel to the orogen axis. The colinearity of Neogene orogen-scale stretching direction deduced from the geometry of large-scale folds and faults with stretching evident from collapse-induced strain fields suggests that caldera formation in the southern central Andes was assisted, if not controlled, by regional tectonism. This implies that rectilinear strain fields of collapse calderas may serve as indicators of regional paleostain imparted to upper crustal rock at the time of collapse caldera formation.

Identification of upper-crustal discontinuities using dip curvature analysis of isostatic residual gravity: examples from the central Andes *Poster*

Ulrich Riller¹ Hans-Joachim Götze²
Sabine Schmidt² Robert Trumbull³
Fernando Hongn⁴ Ivan Petrinovic⁴

Structural analysts are often faced with the problem of identifying prominent structural discontinuities covered by post-tectonic sedimentary or volcanic rocks. Gravity fields are often used to delineate the trace of buried discontinuities but are frequently found to be too crude to localize discontinuities adequately. Here, we introduce the importance of dip curvature of the isostatic residual gravity for identifying upper-crustal discontinuities. The relationship between Bouguer gravity, isostatic residual gravity and its dip curvature, first-order structural elements and distribution of Neogene volcanic rocks was examined in the central Andean plateau, more specifically, the southern Altiplano and the Puna. In the southern Altiplano, strong positive Bouguer gravity corresponds to areas affected by late-Cenozoic faulting and large-scale folding of upper crust. Dip curvature analysis of isostatic residual gravity shows that elongate zones of maximum curvature correspond remarkably well with the structural grain defined by first-order folds and faults. Similarly, isostatic residual gravity in the Puna is

¹ Museum für Naturkunde der Humboldt-Universität zu Berlin, Invalidenstrasse 43, 10115 Berlin, Germany ² Universität Kiel, Germany ³ GeoForschungsZentrum Potsdam, Germany ⁴ CONICED and Universidad Nacional de Salta, Argentina

largely controlled by prominent, upper-crustal structures but also by the distribution of Miocene and younger volcanic rocks. The Central Andean Gravity High, in particular, is confined by Neogene volcanic rocks and is mostly associated with areas of low topography, i.e., fault-bounded, internally-drained basins. Dip curvature analysis of the isostatic residual gravity field shows that elongate zones of maximal curvature correlate with the strike of prominent Neogene faults. Our study suggests that such analysis constitutes an important tool for imaging upper-crustal structures, even those which are not readily apparent at surface. For example, upper-crustal faults in the Salar de Atacama area, the presence of which is suggested by the dip curvature of residual gravity, offers a plausible explanation as to the pronounced angular departure of the volcanic belt from its overall meridional trend and its narrowing south of the salar. In contrast to previous interpretations, our study suggests that gravity anomalies of the Central Andes arise chiefly from late Cenozoic volcanism and tectonism. Furthermore, dip curvature analyses of gravity fields bear a great potential for elucidating first-order structural elements of deformed upper-crustal terranes such as the modern Andes.

Geotechnical characterization of trench- and slope sediments off Southern Chile: preliminary results *Vortrag*

Georg Roeser¹ Jan H. Behrmann¹
Achim Kopf²

Introduction

To understand seismogenesis in shallow parts of subduction zones, it is vital to know about strength and frictional parameters of subducted sediment. For this purpose, PETROTEC, as part of the TIPTEQ-Project, gathers geotechnical data for sediments deposited on the incoming Nazca Plate, the trench and the slope off the southern Chilean coast during the last 5 Ma, and whose equivalents are now being underthrust into the seismogenic zone beneath South America (Fig. 1).



Figure 1: Principle of sampling the southern Chile Trench for geotechnical purposes.

Material comes from gravity cores collected during R/V SONNE Cruises SO181 (Flüh E. & Grevemeyer I (Editors) 2005), SO102 (Hebbeln D, Wefer G, et al. 1995) and SO156 (Hebbeln D, et al. 2001), as well as from ODP Leg 141 (Behrmann JH, et al. 1992) drill cores (Fig. 2).

¹ University of Freiburg, Albertstrasse 23b, D-79104 Freiburg i. Brsg., Germany ² DFG research center ocean margins, University of Bremen, Loebener Str., D-28359 Bremen

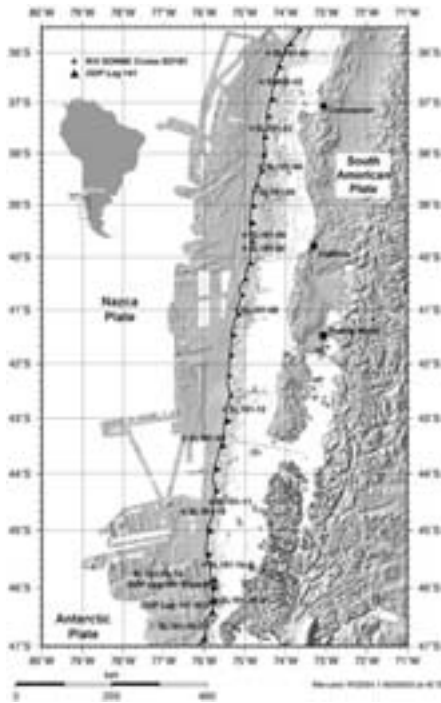


Figure 2: Swath bathymetric map of the southern Chile Trench between 36°S and 47°S, after Flüh E & Grevemeyer I (Eds) (2005), with gravity core sampling localities, and ODP Leg 141 drill sites.

Sediment strength and frictional properties are determined by triaxial testing, ring shear testing and direct shear testing.

First results from triaxial testing show that Young's moduli are much lower (3–20 kPa) in comparison to diatom-rich muds from equivalent depths in the Japan Trench area (180–240 kPa; Roller et al 2003). Internal angles of friction from ring shear testing, direct shear testing, and triaxial testing yielded coherent results. Values from ring shear testing differ depending on material, normal stress and shear velocity, and vary from 9° to 34°. With increasing

shear velocity, there is at first a decrease of the internal angle of friction, followed by an increase. Values from direct shear testing range up to 27° and angles of friction determined from triaxial testing show values of about 10° to 20°.

Results from ring shear testing show compliance to the rate- and state-variable friction law as described by Scholz (1998). Fig. 3 shows two examples of shear stress *vs.* time diagrams. In diagram a), the material shows velocity weakening behaviour at low normal stress (up to 4 MPa). Material from another specimen shown in diagram b), however, shows velocity strengthening behaviour at low (1 MPa) and high (8 MPa) normal stress, but velocity weakening behaviour at intermediate normal stress values (4 MPa). Preliminary data show no pattern or a connection between velocity weakening/strengthening behaviour and different normal stress values. Stick-slip behaviour is observed at high shear velocities, not depending on normal stress (Fig. 3b).

In addition to sediment strength properties, permeabilities were determined on the basis of consolidation data during triaxial testing. Values range from 1.0953×10^{-8} to $8.7 \times 10^{-10} \text{ m s}^{-1}$. Average permeability is 10^{-9} m s^{-1} , an expected value for marine clays to silts.

We discuss possibilities to extrapolate laboratory data (up to 40 MPa effective stress, equivalent to 1.5 km depth) to upper seismogenic zone conditions (equivalent to 100–150 MPa effective stress).

Results so far raise questions: what causes different velocity strengthening/weakening behaviour at varying normal stress values and in which way is seismogenesis affected?

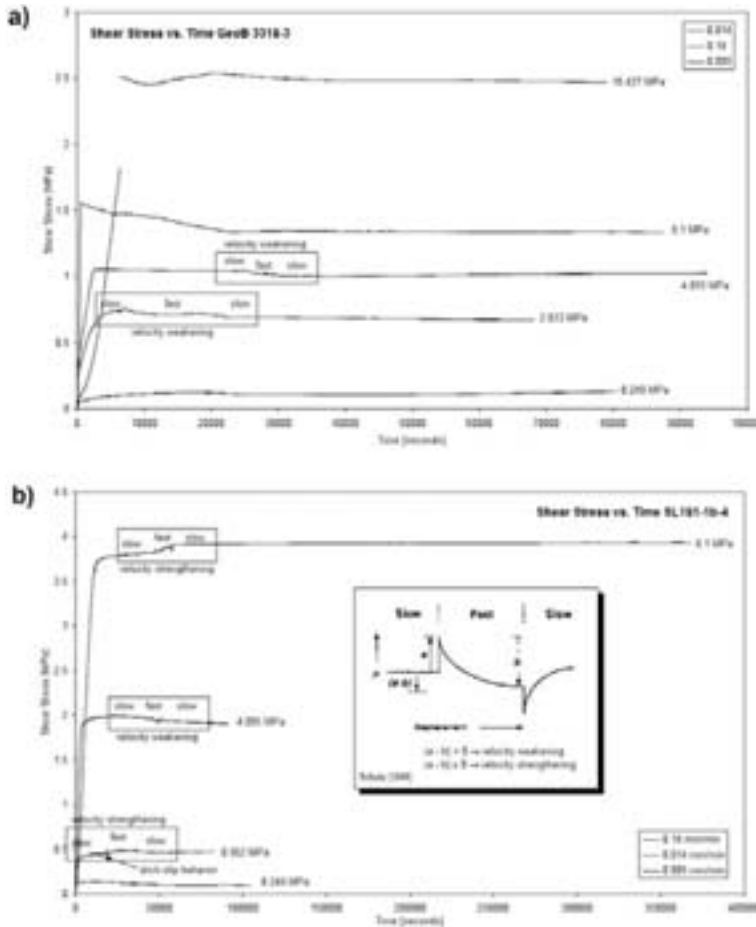


Figure 3: Shear stress *vs.* time diagrams, derived from ring shear testing, showing the rate- and state-variable friction law (Box after Scholz (1998)).

References

- Behrmann JH, et al. (1992) Chile Triple Junction. Proc. ODP, Init. Rept. (Pt. A) 141, 1–708
- Flüh E & Grevemeyer I (ed) (2005) FS Sonne Cruise Report SO181. IFM Geomar Report Nr. 2 March 2005, p 102
- Hebbeln D, Wefer G, et al. (1995) Cruise Report of R/V SONNE Cruise 102, Valparaiso — Valparaiso, 9.5.-28.6.1995. Berichte, Fachbereich Geowissenschaften, Universität Bremen, 68, pp 126
- Hebbeln D, et al. (2001) PUCK: Report and preliminary results of R/V SONNE Cruise SO156, Valparaiso — Talcahuano, 29.3-14.5.2001. Berichte, Fachbereich Geowissenschaften, Universität Bremen, 182, pp 195
- Roller S, Pohl C & Behrmann JH (2003) Data report: Triaxial shear strength investigations of sediments and sedimentary rocks from the Japan Trench, ODP Leg 186. In: Suyehiro K, Sacks IS, Acton GD, & Oda M (ed) Proc. ODP, Sci. Results, 186, 1–19 [Online]
- Scholz CH (1998) Earthquakes and friction laws. *Nature* 391, 37–42

Geowissenschaftliche Bedeutung von Mikrorissen in Kristallingesteinen *Poster*

Joerg Ruedrich¹ Axel Vollbrecht¹

In Kristallingesteinen (Magmatite, Metamorphite, Migmatite) sind Mikrorisse allgegenwärtig. Ihre Entstehung ist auf unterschiedliche treibende Kräfte (i.W. Tektonik, Thermik) und Mechanismen wie z.B. volumetrische Verformung oder plastische Rissinitiierung zurückzuführen (z.B. Vollbrecht et al. 1999). Die heute in oberflächennahen Kristallingesteinen zu beobachtenden Mikrorisspopulationen repräsentieren i.d.R. die Summe verschiedener geologischer Ereignisse in unterschiedlichen Krustenstockwerken, wobei generell die jüngsten Generationen das höchste Erhaltungspotential besitzen. Abhängig von den jeweiligen stofflichen Rahmenbedingungen (Wirtsminerale, Krustenfluide) zeigen die Mikrorisse unterschiedliche Ausbildungsformen (offen, verheilt, versiegelt), die häufig gemeinsam in einem Gestein auftreten und damit komplexe, mehrphasige Entwicklungen dokumentieren (Abb. 1a).

Analysen von natürlichen und experimentell erzeugten Rissen belegen, dass die überwiegende Anzahl als Zugrisse zu interpretieren sind, d.h. sie werden primär senkrecht zur kleinsten Normalspannung angelegt. Zusätzlich ist bekannt, dass Mikrorisse innerhalb größerer Gesteinsvolumina meistens in Form von mehreren richtungs-konstanten Scharen auftreten (Abb. 1b) und damit den Gesteinen ein Anisotropieelement aufprägen. Das Beispiel in Abb. 1b zeigt zusätzlich, dass die Bildung der

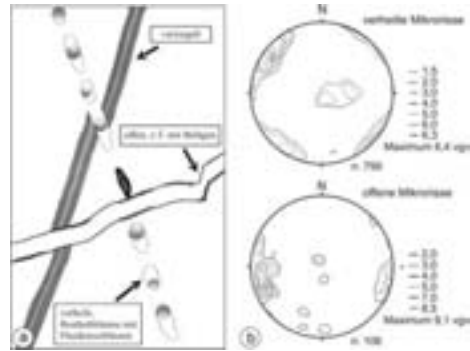


Abbildung 1: Unterschiedliche Mikrorisszustände (a) und Quarz-Mikrorisse im Sultz Granit (b); Belegungsdichtediagramm Schmidt'sches Netz untere Halbkugel; vgv = vielfaches der Gleichverteilung; n = Anzahl der gemessenen Risse, aus Schild et al. (1998).

verheilten und offenen Mikrorisse unter verschiedenen Spannungsrichtungen stattfand.

Aufgrund der genannten Eigenschaften besitzen Mikrorisse sowohl für die Rekonstruktion geodynamischer Entwicklungen als auch für die Interpretation der physikalischen/mechanischen Gesteinseigenschaften besondere Bedeutung. Das Vernetzungsschema in Abb. 2 zeigt, welche Informationen aus Mikrorissen durch Verknüpfung verschiedener analytischer Methoden gewonnen werden können. Beispielhaft seien folgende Forschungs- und Anwendungsfelder genannt:

1. Geodynamik

Mikrorisse stellen zum einen sensible (Paläo-) Spannungsindikatoren dar, zum anderen erlauben die Rissfüllungen (Fluide, Minerale) z.T. weitreichende Rückschlüsse auf die Entwicklungsgeschichte des Gesteins. In günstigsten Fällen kann durch eine Datierung der

¹ Geoscience Centre University Göttingen, Goldschmidtstr. 3, 37077 Göttingen

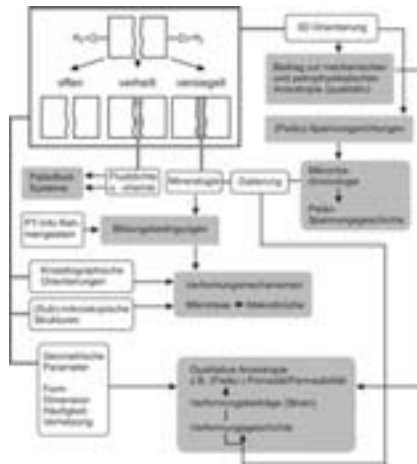


Abbildung 2: Beziehungen zwischen Analytik und Informationspotential von Mikrorissen.

Rissmineralisate in Verbindung mit einer detaillierten Richtungsanalyse eine Chronologie der Spannungsrichtungen rekonstruiert werden (z.B. Vollbrecht et al. 1994). Anhand von Fluideinschlüssen in verheilten Mikrorissen und Indexmineralen in versiegelten Rissen kann zusätzlich für die jeweiligen Spannungsrichtungen eine Druck/Temperaturabschätzung vorgenommen werden (z.B. Schild et al. 1998).

2. Gesteinseigenschaften in situ

Verschiedene geophysikalische Krustenanomalien können u.a. durch ein gehäuftes Auftreten von orientierten Mikrorissen erklärt werden (z.B. Dämpfung und Polarisierung von seismischen Wellen; z.B. Weiss 1998). Die durch vernetzte Risspopulationen erzeugten Gesteinspermeabilitäten stellen bedeutende Wegsamkeiten für Krustenfluide dar. Dies ist u.a. für den gerichteten penetrativen Stoff- und konvektiven Wärmetransport durch die Gesteinsma-

trix von Bedeutung. Die Ausrichtung und der Vernetzungsgrad von Mikrorissen ist z.B. auch ein wichtiger Faktor für die Beurteilung geothermischer Reservoirs, da prä-existierende Mikrorisse die Ausbreitungsrichtung und Dimension von künstlich stimulierten Makrobrüchen (Wärmeaustauschflächen) erheblich beeinflussen.

3. Eigenschaften als Werkstein

Das richtungsabhängige Festigkeitsverhalten wird u.a. durch die bevorzugte Orientierung von Mikrorissen diktiert. Dies gilt insbesondere für Gesteine, die keine weiteren planaren Vorzeichnungen wie stofflicher Lagenbau oder Schieferung aufweisen (z.B. Ruedrich 2003). Der Beitrag von Mikrorissen zur inneren Oberfläche ist für das Verwitterungsverhalten vieler Werksteine von Bedeutung. So stellen Mikrorisse u.a. Wegsamkeiten und Angriffsflächen für korrosive Agenzien dar (Ruedrich 2003). Hinsichtlich der physikalischen Verwitterungsprozesse stellen Mikrorisse in den ansonsten dichten Kristallingesteinen den Porenraum dar, in dem Eis- oder Salzkristallisation und dadurch induzierte Spannungen zur Gefügeentfestigung führen (z.B. Doehne 2002).

Literatur

- Doehne E (2002) Salt weathering: Context and insights. In: S. Siegesmund, T. Weiss and A. Vollbrecht (eds): Natural stones, weathering phenomena, conservation strategies and case studies. Geological Society Special Publication 205, 43–56
- Ruedrich J (2003) Gefügekontrollierte Verwitterung natürlicher und konservierter Marmore. Dissertation, Universität Göttingen, <http://webdoc.sub.gwdg.de/diss/2003/ruedrich/ruedrich.pdf>, pp 158
- Schild M, Vollbrecht A, Siegesmund S, Reutel C (1998) Microcracks in granite cores from

EPS-1 drillhole, Soultz-Sous-Forêts. Paleostress directions, paleofluids and crack-related V_p -anisotropies. *Geologische Rundschau* 86, 775–785

Vollbrecht A, Dürrast H, Kraus J, Weber K (1994) Paleostress directions deduced from microcrack fabrics in KTB core samples and granites from the surrounding field. *Sci. Drilling* 4, 233–241

Vollbrecht A, Stipp M, Olesen, NØ (1999) Crystallographic orientation of microcracks in quartz and inferred deformation processes — a study on gneisses from the German Continental Deep Drilling (KTB). *Tectonophysics* 303, 279–297

Weiss T (1998) Gefügeanisotropie und ihre Auswirkung auf das seismische Erscheinungsbild: Fallbeispiele aus der Lithosphäre Süddeutschlands. *Geotektonische Forschungen* 91, pp 156

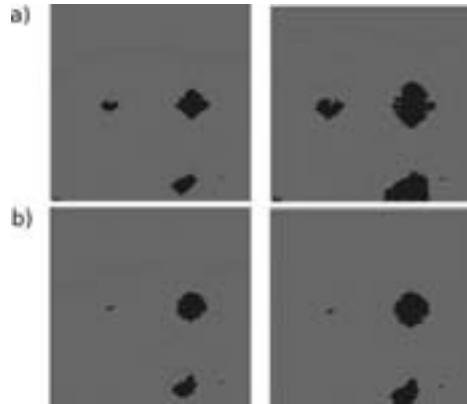


Figure 1: Spinel (black) growing within olivine (grey) in a computer simulation. In run a) the reaction is sluggish due to a low high activation energy. Run b) uses a high activation energy. The resolution is 100×100 particles, the system size is 0.5 mm

Influence of viscosity on the growth of high pressure phases in computer experiments

Poster

Till Sachau¹ Daniel Koehn¹

Introduction

The general aim of the project is the examination of microstructures that develop under HP conditions in computer experiments. Starting point is an interest in the dynamics of HP phase transitions, as for instance the probably catastrophic phase-change event of olivine to spinel in the upper mantle. This is either explained by large overpressure or failure during the development of micro-structures during the growth of the spinel phase. Experimental results on this subject are rare, and do not lead by themselves to a deeper insight into

the complicated stress/strain/volume-change/micro-crack relationships of the transition. We developed a central force spring model, where particles can undergo a phase change using parameters of olivine and spinel. The algorithm is capable of simulating the local growth of the mentioned phases on the basis of direction-dependant rate laws.

In the current context newtonian viscosity is added to the previously solely elastic system, since under HP/HT conditions the viscous flow within the material will have a large influence on the distribution of elastic energies, which in turn have an important influence on the driving force of the transition. Thus we are dealing with a visco-elastic system, which will be subjected to time-dependant strain.

¹ Institut für Geowissenschaften, Universität Mainz

Mechanism

A solely brittle rock will fracture if a certain yield stress is reached, while a rock that behaves only viscously, deforms like a fluid and will compensate stress by flow. Combining these properties leads to a viscoelastic model, which is elastic for small strain rates but viscous for large ones. Whether or not a rock will fracture or flow depends therefore on the interplay of these properties. In the context of stress-driven rapid phase transitions, this means a large viscous deformation during deformation previous to the reaction, and brittle fracturing during the rapid volume reduction after the reaction started. The system itself is sensitive to the starting conditions, which will be influenced by the reduced differential stresses due to viscous flow. An important role in the development of microstructures plays also the velocity of the transition, since this controls the interplay with the latent heat release and the subsequent heat conduction (see Fig. 1).

Structural record of an oblique impact: the central uplift of the Upheaval Dome impact structure, Utah, USA

Vortrag

Dirk Scherler¹ Thomas Kenkmann²
Andreas Jahn²

Introduction

Most asteroids strike their target at an oblique angle (Pierazzo & Melosh 2000). The common criterion for identifying craters formed by an oblique impact is the pattern of the ejecta blanket. On Earth, however, ejecta blankets are rarely preserved and morphological, structural, geophysical as well as depositional criteria were used to infer an oblique impact (e.g. for Chicxulub, Schultz & D'Hondt 1996, Ries-Steinheim, Stöffler et al. 2003, Mjöl-nir & Tsikalas 2005). However, the significance of such criteria in predicting impact angle or direction is a matter of debate (*c.f.* Schultz & Anderson, 1996, Ekholm & Melosh 2001). Particularly, it is not yet known whether there is an influence of the impact angle on the displacement field during the collapse of large transient cavities, and thus, the final crater. For most impact angles, the shape of the final crater is controlled by its size. At a critical diameter (ca. 2–5 km on Earth), simple bowl shaped craters are getting gravitationally unstable and collapse to form complex craters, with a flat floor and a terraced rim (Melosh 1989). During collapse, the crater floor rises to form a

¹ Institut für Geowissenschaften, Universität Potsdam, Karl-Liebknecht-Straße 24/25, D-14476 Golm ² Institut für Mineralogie, Museum für Naturkunde, Humboldt Universität zu Berlin, Invalidenstraße 43, D-10115 Berlin

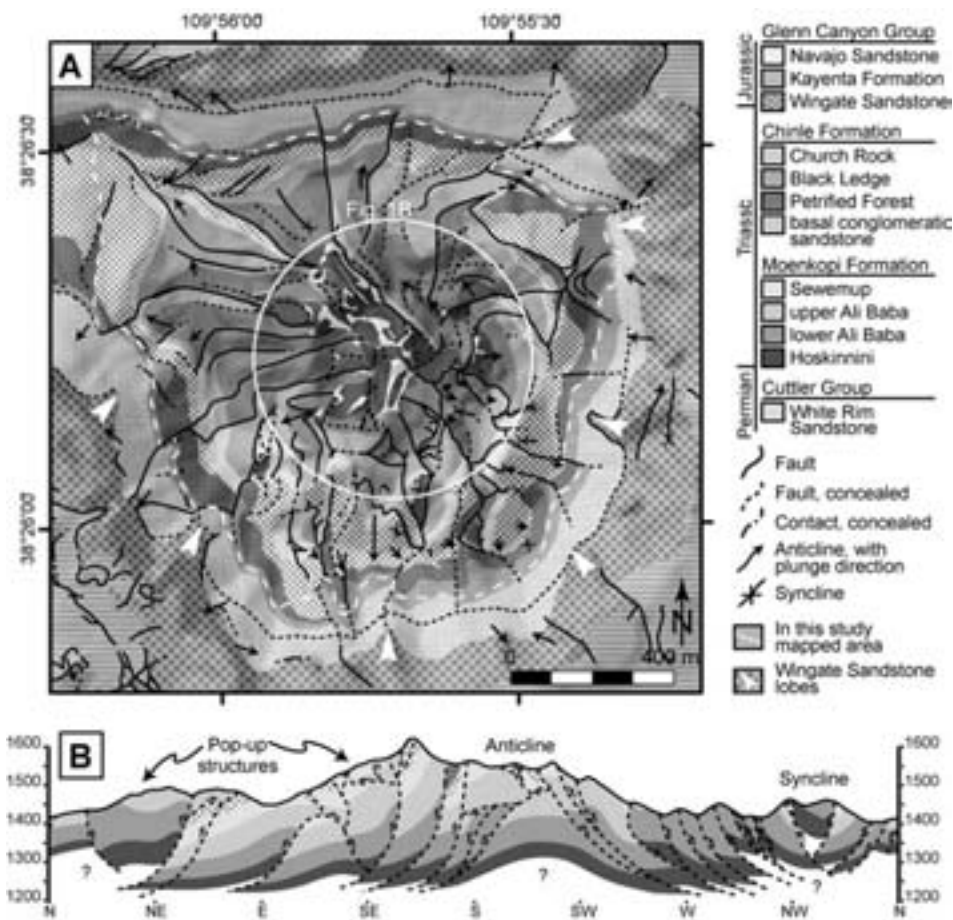


Figure 1: (A) Geological map of the central topographic depression of the Upheaval Dome impact structure. (B) Circular schematic cross section, trace as given in A. Variable thickness of the units mainly due to dip of strata out of the plane of intersection.

central uplift, that may or may not be visible as a central peak, or, when the peak in turn collapses, as a peak ring at yet larger diameters.

Results and Discussion

We present structural details from the central uplift of the Upheaval Dome impact structure, in SE Utah, that are diagnostic of the kinematics during crater collapse and central uplift formation.

A characteristic imbrication of thrust slices towards the southeast (see Fig. 1), the pattern of strata orientation within the central uplift, dominant radial faults that accommodated NW–SE shortening and an elliptical bedding outline indicate, that the displacement field during crater collapse has not been axial symmetric. Instead, an additional lateral component, roughly towards the southeast, is preserved in the internal

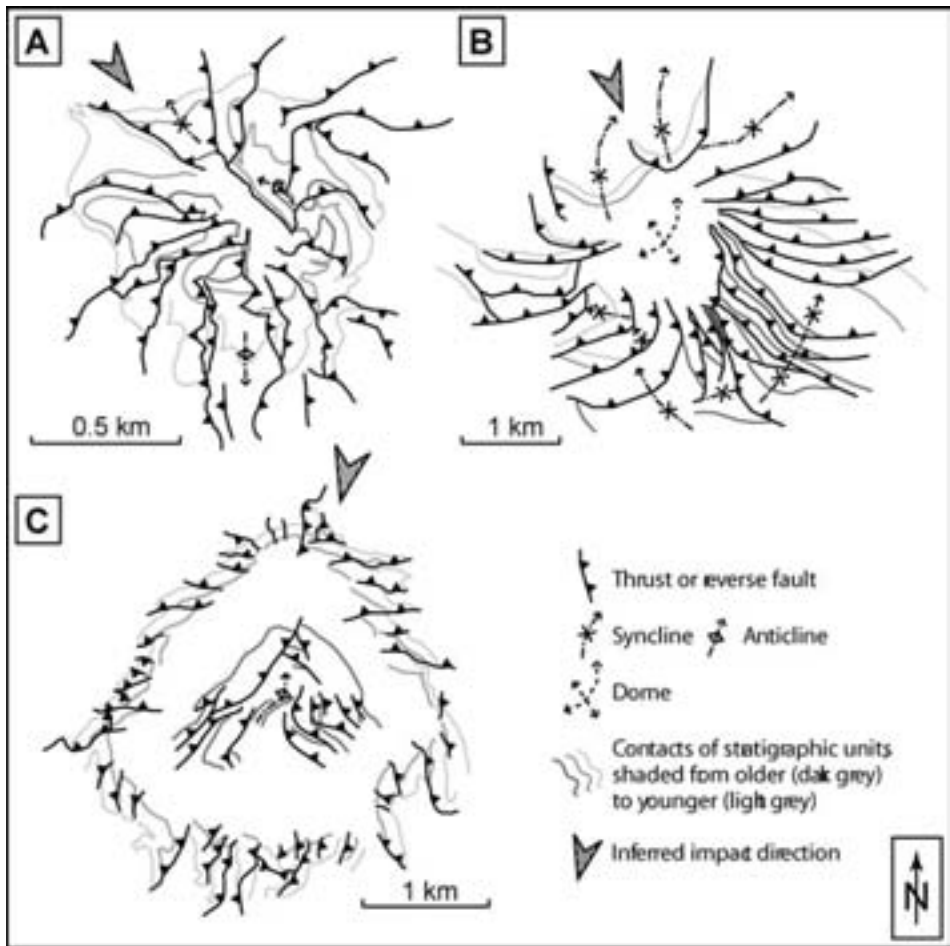


Figure 2: Simplified sketches of faults and contacts from the innermost part of the central uplifts of eroded complex craters in sedimentary target rocks: (A) Upheaval Dome, United States, D ca. 5.3 km, (B) Spider, Australia, D ca. 12 km (after Shoemaker & Shoemaker 1996), (C) Gosses Bluff, Australia, D ca. 24 km (after Milton et al. 1996).

structure of the central uplift. The structural asymmetries are largest in the core of the central uplift and disappear outwards, thereby preserving the large-scale circular shape of the main structural elements (rim monocline, ring syncline). We propose, that this lateral component reflects a shift in the onset of crater collapse and the migration

of the uplifting crater floor downrange (*c.f.* Kenkmann et al. 2005). Comparison with numerical models of oblique impacts supports this view (Shuvalov 2003, Shuvalov & Dypvik 2004) and further suggests, that the asymmetric displacement fades in the later stages of central uplift formation, which provides an explanation for the largely circular

appearance of complex impact craters. Fault patterns, that are strikingly similar to that in the innermost part of Upheaval Dome, can be identified in other impact structures (Fig. 2) and may serve as general criteria for identifying the impact direction of deeply-eroded impact structures.

References

- Ekholm AG & Melosh HJ (2001) Crater features diagnostic of oblique impacts: The size and position of the central peak. *Geoph Res Lett* 28:623–626
- Gault D & Wedekind JA (1978) Experimental studies of oblique impacts. *Proc Lunar Planet Sci Conf* 9:3843–3875
- Kenkmann T, Jahn A, Scherler D & Ivanov BA (2005) Structure and formation of a central uplift: A case study at the Upheaval Dome impact crater, Utah. *Geol Soc Am Spec Pap* 384:85–115
- Melosh HJ (1989) *Impact Cratering — A Geologic Process*. New York: pp 145
- Milton DJ, Glikson AY & Brett R (1996) Gosses Bluff — a latest Jurassic impact structure, central Australia. Part 1: Geological structure, stratigraphy, and origin. *AGSO Journal of Australian Geology & Geophysics* 16, 453–486
- Pierazzo E & Melosh HJ (2000) Understanding Oblique Impacts from Experiments, Observations, and Modeling. *Ann Rev Earth Planet Sci* 28, 141–167
- Schultz PH & Anderson RR (1996) Asymmetry of the Manson impact structure: Evidence for impact angle and direction, *Geol Soc Am Spec Pap* 302, 397–417
- Schultz PH & D’Hondt S (1996) Cretaceous-Tertiary (Chicxulub) impact angle and its consequences. *Geology* 24, 963–967
- Shoemaker EM & Shoemaker CS (1996) The proterozoic impact record of Australia. *AGSO Journal of Australian Geology & Geophysics* 16:379–398.
- Shuvalov VV (2003) Cratering process after oblique impacts, Third International Conference on Large Meteorite Impacts, Nördlingen, Contribution #4130
- Shuvalov VV & Dypvik H (2004) Ejecta formation and crater development of the Mjölñir impact, *Meteoritics Planet Sci* 39, 467–479
- Stöffler D, Artemieva NA & Pierazzo E (2002) Modeling the Ries-Steinheim impact event and the moldavite strewn field, *Meteoritics Planet Sci* 37, 1893–1907
- Tsikalas F (2005) Mjölñir crater as a result of oblique impact: Asymmetry evidence constrains impact direction and angle. In: C Koeberl & H Henkel (eds) *Impact Tectonics*, Berlin, 285–306

Experimental study of the evolution of fault gouge in layered sand–clay sequences

Poster

Joyce Schmatz¹ Peter Vrolijk² Janos L. Urai¹ Steffen Giese³ Martin Ziegler³ Wouter van der Zee⁴

This study focuses on clay smear processes during fault gouge evolution in sand-clay sequences at depths up to 2 km. A clay-rich fault gouge can dramatically lower the fault’s permeability, and prediction of this process is therefore relevant in groundwater modelling and hydrocarbon geology (Fulljames et al. 1997, Yielding et al 1997, van der Zee et al. 2003, 2005).

We constructed an ‘underwater’ sandbox to deform layered sand-clay models of 20 × 40 × 20 cm above a 70°-dipping rigid basement fault (Fig. 1). The experiments are run completely water-saturated to allow deformation of wet

¹ Geologie-Endogene Dynamik, RWTH Aachen, Germany

² ExxonMobil Upstream Research Co., Houston, TX, USA

³ Geotechnik im Bauwesen, RWTH Aachen, Germany

⁴ GeoMechanics International, Mainz, Germany



Figure 1: Sandbox-apparatus. Water-saturated setup of layered sand-clay experiment. Stage: Immediately after deformation.

clay and cohesionless sand. The basement fault moves at 20 to 120 mm h⁻¹ to a maximum offset of 60 mm. We use quartz sand with grain size between 0.1 to 0.4 mm and an illite-rich clay with a water content between 28 and 55 wt.%. Water content of the clay is used to control its shear strength and state of consolidation. We defined three strength classes: *soft clay* (up to 55 wt% water), *normal clay* (around 40 wt% water) and *firm clay* (less than 30 wt% water). *Soft* and *firm clay* represent underconsolidated and overconsolidated endmembers, respectively. The *normal clay* is in equilibrium with the overburden load. In a number of experiments 0.25–10 wt% ‘Portland Cement’ was added to the clay to make it strong and brittle. Material properties were carefully characterized by a series of geotechnical measurements.

Our sandbox experiments are governed by two important boundary conditions. The basement is a well-defined plate

acting as a rigid guide compared to the properties of the sediment. The interface on top of the model material is either water or aluminum plates pre-cut along the kinematically ideal plane. These two points of discontinuity in the boundary velocity field initiate a deformation band curving away from the kinematically preferred plane. On the other hand, the boundary plates force the two deformation bands to join into a continuous zone. Results of ten series of experiments will be presented. We systematically studied the effect of clay strength, thickness, number and position of the clay layers and thickness of the cover sand.

Around 300 high resolution digital images for each experiment were processed into time-lapse movies and analyzed using PIV (Particle Image Velocimetry). PIV calculates the displacement field (Fig. 3) at the scale of individual sand grains, and allows calculation of all components of the incremental strain field. The main effects of the different parameters are as follows:

- i) absence of the top pre-cut plate makes the fault zone much wider, and renders the formation of a continuous clay gouge more difficult.
- ii) in models containing soft clay and a pre-cut top plate, a continuous clay smear is formed irrespective of the details of geometry, and deformation approaches simple shear with mechanical mixing of sand and clay (Fig. 2)
- iii) lateral clay injection is a rare process in our experiments, even for soft clay;
- iv) stiff clay behaves in a brittle fashion, fault motion is associated with

rotation of rigid blocks and no continuous clay gouge is formed (Fig. 2);

- v) for the same amount of clay in the sequence the presence of many thin layers prefers the formation of a continuous clay gouge.

High resolution PIV shows details of the initial phase of deformation, when elastic strain is overprinted by plastic strain and localization (Fig. 3). This shows that the structure of the later defor-

mation bands is already present in the models after the first increment of deformation.

The validity of statistical methods to predict fault seal by a clay gouge (SGR — Shale Gouge Ratio, CSP — Clay Smear Potential) was examined critically. Our results clearly show that these methods can be unreliable if the effects of clay properties and geometry are not included in the analysis.

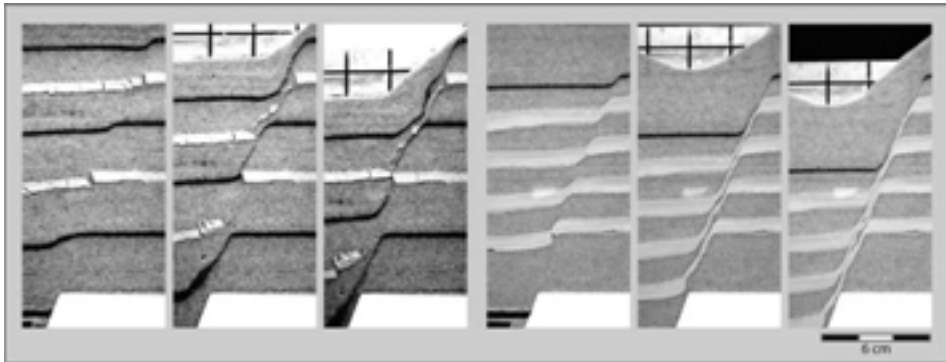


Figure 2: Image sections of experimental results. Images 1–3 show three stages (16, 24 and 50 mm offset) of deformation of sequence with two cemented clay layers. Images 4–6 show the same stages for setup with four soft clay layers.

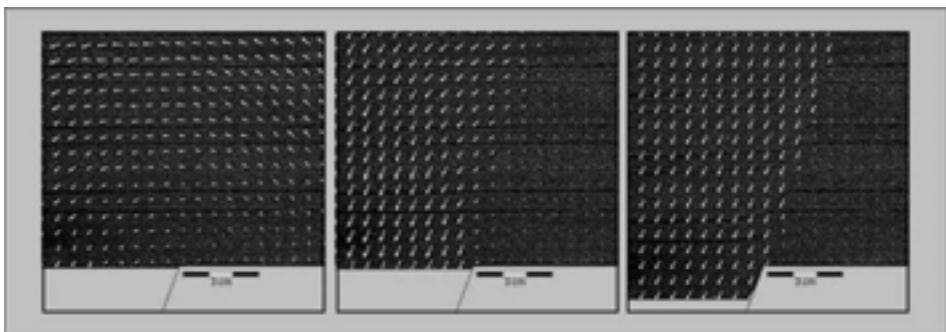


Figure 3: PIV-results for a water-saturated sand experiment. Vector field points to elastic behaviour in the initial phase followed by plastic strain with localization of a fault zone (last image).

References

- Fulljames JR, Zijerveld LJJ, et al. (1997) Fault seal processes: systematic analysis of fault seals over geological and production time scales, In Moeller-Pedersen, & Koester AG, Hydrocarbon Seals, NPF special publication 7: 51-59
- Horsfield, WT (1977) An experimental approach to basement-controlled faulting. *Geologie en Mijnbouw* 56(4): 363-370
- Van der Zee W, Urai JL & Richard PD (2003) Lateral clay injection into normal faults. *GeoArabia* 8(3): 501-522
- Van der Zee, W. & Urai, JL (2005) Processes of normal fault evolution in a siliciclastic sequence: a case study from Miri, Sarawak, Malaysia. *Journal of Structural Geology* 27(12): 2281-2300
- Yielding G, Freeman B, et al. (1997) Quantitative Fault Seal Prediction. *AAPG Bulletin* 81(6): 897-917

Measurement of calcite crystallographic-preferred orientations by magnetic anisotropy and comparison to diffraction methods

Vortrag

Volkmar Schmidt¹ Ann M. Hirt¹
Luigi Burlini² Bernd Leiss³ Jens M. Walter⁴

AMS as a petrofabric tool

The anisotropy of magnetic susceptibility (AMS) of rocks reflects the preferred orientations of minerals. Therefore AMS is a quick and easy way to characterize rock fabrics (Hrouda 1982,

¹ Institute of Geophysics, ETH Zurich, 8093 Zurich, Switzerland

² Geological Institute, ETH Zurich, 8092 Zurich, Switzerland

³ GZG, University of Göttingen, Göttingen, Germany

⁴ Forschungszentrum Jülich, Jülich, Germany

Borradaile 1988); the obtained result is also called the magnetic fabric of the rock. The method has been often used to measure the orientation of ferromagnetic minerals, mainly magnetite, but in recent studies it has been increasingly used to measure textures of paramagnetic minerals as phyllosilicates (Lüneburg et al. 1999, Cifelli et al. 2004).

AMS of calcite textures A further application is the measurement of diamagnetic textures, especially calcite textures. Calcite is suitable for the AMS method, because it has a high magnetic anisotropy with the minimum susceptibility along the crystallographic c-axis. Therefore a preferred orientation of the c-axes, which can be induced by deformation, generates a magnetic fabric. The relationship between AMS and deformation of marbles has been investigated in laboratory (Owens & Bamford 1976) and field studies (de Wall et al. 2000). However, the diamagnetic fabric of calcite is relatively weak and easily overprinted by paramagnetic and ferromagnetic phases. In natural carbonate rocks the ferromagnetic and the paramagnetic subfabrics should be separated to assure a correct interpretation of the AMS. This separation can be made by torque measurements in high fields at different temperatures (see Schmidt et al., this volume).

Textures of artificial calcite-muscovite aggregates

To test how well AMS reflects the actual mineral texture, we produced a series of artificial calcite-muscovite aggregates. Powders made from Carrara marble and muscovite single crystals were mixed in different proportions and compacted uniaxially at room temperature

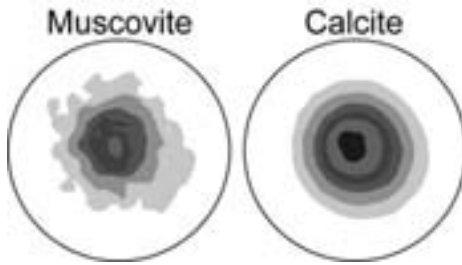


Figure 1: Example of neutron diffraction pole figures (equal-area, lower hemisphere projection). Compaction direction is normal to the pole figure. Lowest contour line is equal to 1.0 multiple of random distribution (m.r.d.); contour interval is 0.25 m.r.d.

to obtain a texture. The samples were further compacted hydrostatically to reduce the porosity and to improve the mechanical properties. The samples show a c-axis preferred orientation of the calcite and muscovite along the compaction direction (Fig. 1). The textures were measured with different methods as AMS, X-ray diffraction and neutron diffraction and the results are compared. Sample volumes of more than 11 cm^3 were used to measure AMS as well as neutron diffraction; the same specimens could be used for both methods.

Low- and high-field AMS measurements were made on all samples. The high-field measurements reflect more accurately the weak dia/paramagnetic fabrics. A nearly perfectly oblate AMS ellipsoid with minimum susceptibility axis sub-parallel to the compression direction developed even at very low pressures, and the principle axes of the AMS ellipsoid are co-axial with the calcite fabric ellipsoid. A general increase in AMS is observed with an increase in compaction. The quantitative correlation between the strength of the texture and the AMS will be investigated in the

future. Moreover the separation of magnetic sub-fabrics will be tested on these artificial samples. The first results show that AMS can reflect the textures of the individual phases in a multiphase rock.

Literatur

- Borradaile GJ (1988) Magnetic-susceptibility, petrofabrics and strain. *Tectonophysics* 156:1–20
- Cifelli F, Mattei M, Hirt AM & Gunther A (2004) The origin of tectonic fabrics in ‘undeformed’ clays: The early stages of deformation in extensional sedimentary basins. *Geophys Res Lett* 31: Art. No. L09604
- De Wall H, Bestmann M & Ullemeyer K (2000) Anisotropy of diamagnetic susceptibility in Thassos marble: A comparison between measured and modeled data. *J Struct Geol* 22:1761–1771
- Hrouda F (1982) Magnetic-anisotropy of rocks and its application in geology and geophysics. *Geophysical Surveys* 5:37–82
- Lüneburg CM, Lampert SA, Lebit HD, Hirt AM, Casey M & Lowrie W (1999) Magnetic anisotropy, rock fabrics and finite strain in deformed sediments of SW Sardinia (Italy). *Tectonophysics* 307:51–74
- Owens BH & Bamford D (1976) Magnetic, seismic, and other anisotropic properties of rock fabrics. *Phil Trans R Soc Lond Ser A* 283:55–68

Separation of magnetic subfabrics by high-field, low-temperature torque measurements

Poster

Volkmar Schmidt¹ Ann M. Hirt¹ Pascal Rosselli¹

The anisotropy of magnetic susceptibility (AMS) can serve as a good indicator of strain in deformed carbonate rocks with diamagnetic susceptibility (Owens and Rutter 1978; de Wall 2000). However, the magnetic fabric due to the diamagnetic carbonate minerals is usually very weak and interpretation of the AMS in these rocks is often complicated by the presence of paramagnetic and ferromagnetic phases which overprint the diamagnetic subfabric. For this reason contributions from ferromagnetic and paramagnetic minerals to the AMS should be separated for a reliable interpretation of the AMS. Ferromagnetic contributions to the AMS can be separated by high-field measurements, using a torque magnetometer (Martin-Hernandez and Hirt 2001). The remaining paramagnetic and diamagnetic contributions can be discriminated by their different temperature dependencies. The paramagnetic susceptibility increases as an inverse function of temperature, whereas the diamagnetic part remains constant. Altogether, AMS measurements at high fields and low temperatures allow for the discrimination of all three subfabrics.

Test measurements with the high-field torque magnetometer at liquid nitrogen temperature were performed. It is possible to keep the specimens at low temperature over the measurement period us-

ing a cryostat. The main problem is the suppression of mechanical disturbances during the measurement so that the sensitivity of the instrument is retained. The torque of paramagnetic minerals increases strongly at low temperature which results in an amplification of the paramagnetic subfabric. The quantitative separation of diamagnetic and paramagnetic subfabric is under investigation. The result is promising when there is a significant diamagnetic signal.

References

- De Wall H, Bestmann M & Ullemeyer K (2000) Anisotropy of diamagnetic susceptibility in Thassos marble: A comparison between measured and modeled data. *J Struct Geol* 22, 1761–1771
- Martin-Hernandez F & Hirt AM (2001) Separation of ferrimagnetic and paramagnetic anisotropies using a high-field torsion magnetometer. *Tectonophysics* 337, 209–221
- Owens WH & Rutter EH (1978) The development of magnetic susceptibility anisotropy through crystallographic preferred orientation in a calcite rock. *Phys Earth Planet Inter* 16, 215–222

Microstructural analysis of the RWTH-1 cores in thin-sections

Vortrag

Katerina Scholz¹ Janos L. Urai¹ Ute Trautwein² Peter A. Kukla²

Introduction

The Aachen RWTH-1 well was drilled to 2544 m TVD for geothermal purposes

¹ Institute of Geophysics, ETH Zurich, 8093 Zurich, Switzerland

¹ Geologie-Endogene Dynamik, RWTH Aachen, Germany ² RWTH Aachen, Department of Geology, Germany



Figure 1: Stretched crystals of quartz and chlorite. Note how the quartz crystal from the matrix gets involved in the vein build up and indicates a distinct direction of grain growth. The dark spotted areas in the vein itself are fluid inclusion trails. What do they tell us about the vein growth? Sample from 1447.5 m TVD.



Figure 2: This vein gives an example of a vein on which the ‘crack seal’ models given so far can be critically tested on. How did the various minerals quartz, chlorite and calcite get deposited in one vein? Sample from 1392.5 m TVD.

and gives substance to extensive geoscientific research. It is located in a hydrothermally and seismically active area of the Aachen Anticline, 500 m NW of the Aachen Overthrust and 420 m ENE of the Laurensberg Fault. The main focus of this PhD work is the structural and microtectonic analysis of the cores sampled.

For 94% of the total well length the collected cuttings give information of the lithology and stratigraphy of the subsurface. A total of 145.5 m was cored in three different intervals. A complete set of wireline measurements including high resolution borehole image allow mapping of fractures and folds, and linking the core to the logs. About 100 core samples were selected for detailed microstructural analysis.

First results

Microstructural analysis of veins formed in Mode I and II fractures shows a wide range of structures, depending on host

rock lithology, fluid composition and opening history. Four different vein generations have been interpreted based on overprinting relationships (Fig. 1).

The first of these is interpreted to have formed during burial, under conditions of increasing pore pressure. The subsequent generations are interpreted to belong to the Variscan compression event. Microstructures vary considerably, between fibrous antitaxial calcite veins in siltstone, uniaxial stretched crystals in siltstone, blocky calcite veins in carbonate, and multiphase chlorite-quartz-calcite veins with spectacular syntaxial fibrous microstructures. This last type of veins which was formed at lower greenschist facies conditions allow a critical test of the available models of crack-seal vein evolution (Fig. 2). We present computer models of syntaxial crystal growth during delocalized cracking in a polyphase vein which may explain the observed microstructures. In a later event part of the veins were deformed into cataclasites under conditions of high shear stress.

The role of the Ranotsara Zone in southern Madagascar for Gondwana correlations

Poster

Guido Schreurs¹ Jörg Giese¹ Alfons Berger¹ Edwin Gnos¹

Introduction

The Precambrian basement of southern Madagascar was reworked at high-grade metamorphic conditions during the East African Orogen (EAO of Stern, 1994) that formed during assembly of Gondwana in late Neoproterozoic/early Paleozoic times. At the end of the EAO, Madagascar is generally thought to be sandwiched between southern India and eastern Africa. Constraints on its paleoposition are often inferred from similarities in structural features on now dispersed continental fragments, in particular high-strain zones. Major zones with (sub)vertical foliation planes can be traced over hundreds of kilometres in southern Madagascar (Fig. 1) and have been interpreted as major vertical ductile shear zones (e.g. Windley et al. 1994; Martelat, 1998). The NW–SE trending Ranotsara Zone (dashed rectangle in Fig. 1) is regarded as an intracrustal mega strike-slip shear zone with a sinistral sense of shear that formed at the end of the Proterozoic (e.g. Nicollet, 1990; de Wit et al., 2001). A large number of studies have used the Ranotsara Zone to propose Gondwana reconstructions. The Ranotsara Zone has been correlated with various ductile shear zones in southern India, e.g. with the Bhavani Shear Zone or the Moyar Shear Zone (Katz & Premoli, 1979),



Figure 1: Foliation traces in the Precambrian basement of southern Madagascar. The dashed rectangle outlines the Ranotsara Zone that previously has been interpreted as a mega strike-slip shear zone and has been used in Gondwana correlations.

the Palghat-Cauvery Shear Zone (de Wit et al., 1995), the Karur-Kamban-Painavum-Trichur Shear Zone (de Wit et al., 2001; Ghosh et al. 2004) or with the Achankovil Shear Zone (Windley et al., 1994; Martelat, 1998).

Within Madagascar, the Ranotsara Zone has been correlated along strike with the more N–S trending Bongolava Zone in central-western Madagascar (Hottin 1976), and the Bongolava-Ranotsara Zone has been further traced into the Surma Shear Zone (Windley et al. 1994) and its along-strike continuation, the Aswa Shear Zone in eastern Africa (Müller 2000). Chetty (2003) suggested that the Ranotsara Zone is

¹ Institute of Geological Sciences, Baltzerstraße 1–3, CH-3012 Bern, Switzerland

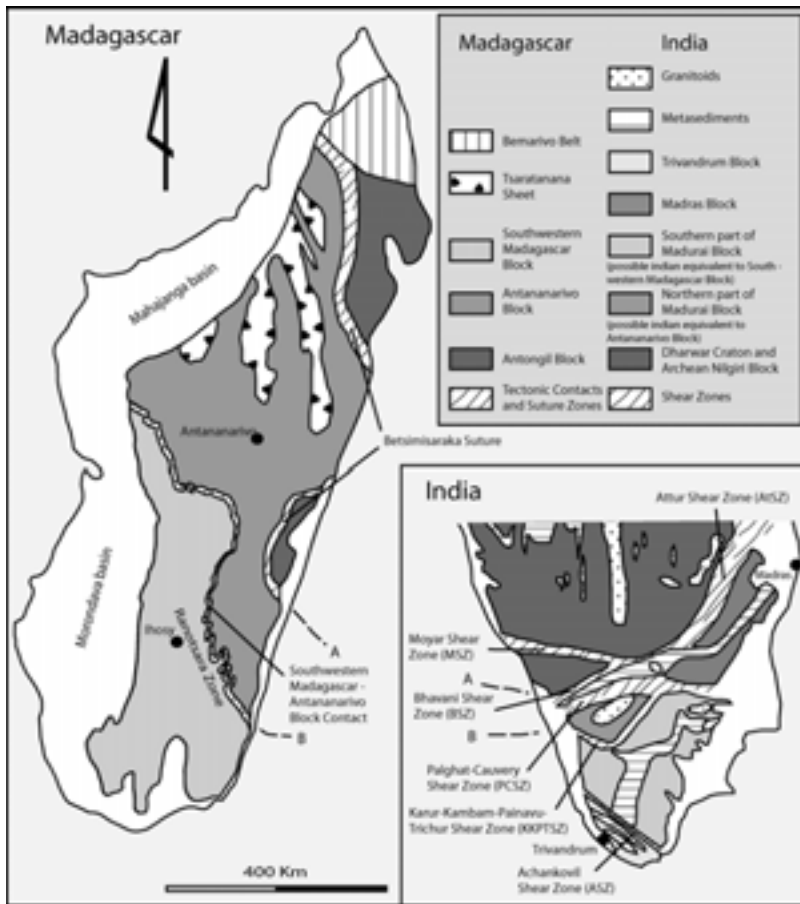


Figure 2: Major tectonic units in Madagascar and southern India. The dashed lines, numbered A and B, indicate possible correlations between ductile shear zones in Madagascar and India. Tectonic units in northern Madagascar are after Collins et al. (2000). The southwestern Madagascar block probably consists of different tectonic units comprising rocks that are predominantly of Proterozoic age. Shear zones in southern India compiled after Meissner (2001) and Ghosh et al. (2004).

not only a mega shear zone, but also a terrane boundary separating a region with Archean crust to the north from a region with Neoproterozoic crust to the south. Our remote sensing and field studies of southern Madagascar indicate that the Ranotsara Zone is neither a major terrane boundary nor an intra-crustal mega strike-slip shear zone and

therefore can not be used as a ‘piercing point’ in Gondwana reconstructions. In the immediate vicinity of the Ranotsara Zone, the basic regional pattern consists of a high-grade gneissic foliation produced during one or more deformation stages (grouped in D₁), which is refolded during a D₂ phase of upright folding with subvertical axial

planes. The steeply dipping composite foliation traces generally strike N–S, except in the Ranotsara Zone where they are ‘sinistrally’ deflected into a NW–SE orientation. Subhorizontal NW–SE trending lineations in the Ranotsara Zone have been previously interpreted as stretching lineations and used as evidence for the presence of a major strike-slip shear zone. However, detailed field studies indicate that subhorizontal lineations in the Ranotsara Zone are in fact intersection lineations and hence do not represent evidence for a tectonic transport direction. In addition, there is no evidence for a gradient in shear deformation gradient across the Ranotsara Zone nor is there a newly developed foliation parallel to it. Lithologies can be traced across the Ranotsara Zone and are — as the composite foliation traces — slightly deflected. In addition, the Precambrian basement rocks in and around the Ranotsara Zone are affected by brittle faulting that is often parallel to the gneissic foliation. Apatite fission track data also indicate that brittle reactivation occurred along the Ranotsara Zone (Seward et al. 2004).

In satellite images it is often difficult to distinguish brittle from ductile lineaments, and especially along the Ranotsara Zone previous workers may have interpreted brittle lineaments as evidence for an along-strike continuation of the ductile Ranotsara Zone towards the SE. Although the Ranotsara Zone can not be used for correlating Madagascar with other continental fragments of Gondwana, a major ductile shear zone further N appears to be useful for Gondwana correlations. This shear zone brings metasedimentary rocks of the Ikalamavony Group and Itremo Group (both part of what we refer to as the south-

western Madagascar Block) in contact with the Antananarivo Block (Fig. 2) and was subsequently affected by the D₂ phase of upright folding (Fig. 1). Preliminary mapping and interpretation of existing geological maps indicate that this tectonic contact remains N of the Ranotsara Zone and can not be traced across it. This suggests that both the Antananarivo Block and the Antongil Block further east (the latter has affinities with the Archean Dharwar craton in India) are restricted to the area N of the Ranotsara Zone and may have acted as an indenter during (transpressional?) Gondwana assembly producing a syn-tactical bend (flexure) across the Ranotsara Zone. On the basis of this tectonic interpretation we propose that the contact between the Antananarivo Block and the southwestern Madagascar Block can possibly be traced into the Karur-Kamban-Painavum-Trichur Shear Zone in southern India (Fig. 2).

References

- Chetty TRK, Vijay P, Narayana BL & Giridhar GV (2003) Structure of the Nagavali Shear Zone, Eastern Ghats Mobile Belt, India: Correlation in the East Gondwana Reconstruction. *Gondwana Research* 6, 215–229
- Collins AS, Razakamanana T & Windley BF (2000) Neoproterozoic crustal-scale extensional detachment in central Madagascar: implications for extensional collapse of the East African orogen. *Geological Magazine* 137, 39–51
- de Wit MJ, Vitali E & Ashwal L (1995) Gondwana Reconstruction of the East Africa - Madagascar - India - Sri Lanka - Antarctica fragments revised. Centennial Geocongress, extended abstracts, vol. 1, Geological Society of South Africa, 218–221
- de Wit MJ, Bowring SA, Ashwal LD, Randianasolo LG, Morel VPI & Rabeloson RA (2001) Age and tectonic evolution of Neoproterozoic ductile shear zones in southwest-

- ern Madagascar, with implications for Gondwana studies. *Tectonics* 20, 1–45
- Ghosh JG, deWit MJ & Zartman RE (2004) Age and tectonic evolution of Neoproterozoic ductile shear zones in the Southern Granulite Terrain of India, with implications for Gondwana studies. *Tectonics* 23, TC3006, doi:10.1029/2002TC001444
- Hottin G (1976) Présentation et essai d'interprétation du Précambrien de Madagascar. *Bull. Bur. Rech. Géol. Mineral., Deuxième Série, Sect. IV, 2*, 117–153
- Katz MB & Premoli C (1979) India and Madagascar in Gondwanaland: a fit based on Precambrian tectonic lineaments. *Nature* 1791, 312–315
- Martelat JE (1998) Evolution of Thermomecanique de la croute inferieure du Sud de Madagascar. Ph.D. Thesis, Université Blaise Pascal Ū Clermont-Ferrand II; France
- Meissner B (2001) Tektonometamorphe Entwicklung von Scherzonen im praekambrischen Basement Suedindiens: Sm-Nd-, Rb-Sr- und U-Pb-Isotopenuntersuchungen an den Moyar-, Bhavani-, Palghat- und Kollegal-Scherzonen. Dissertation, Ludwig-Maximilians-Universität Muenchen
- Mueller BGJ (2000) The evolution and significance of the Bongolava-Ranotsara shear zone, Madagascar. Ph.D. Thesis, Rand Afrikaans University, Johannesburg, South Africa
- Nicollet C (1990) Crustal evolution of the granulites of Madagascar. In: Vielzeuf, D, Vidal, P. (eds). *Granulites and Crustal Evolution* Kluwer Academic Publishers, 310–291
- Seward D, Grujic D & Schreurs G (2004) An insight into the breakup of Gondwana: Identifying events through low-temperature thermochronology from the basement rocks of Madagascar. *Tectonics* 23/3, TC3007 doi:10.1029/2003TC001556
- Stern RJ (1994) Arc assembly and continental collision in the Neoproterozoic East African Orogen: Implications for the consolidation of Gondwanaland. *Annu. Rev. Earth. Planet. Sci.* 22, 319–351
- Windley BF, Razafiniparany A, Razakamanana T & Ackermann D (1994) Tectonic framework of the Precambrian of Madagascar and its and its Gondwana connections: A review and reappraisal. *Geol. Rundschau* 83, 642–659

Kinematics of the SEMP-fault in the western Tauern Window (Stillupp Valley)

Poster

Susanne Schneider¹
 Claudio Rosenberg¹

Introduction

The working area is located in the Stillupp Valley (Tirol, Austria), where the western termination of the SEMP-fault (Salzach, Ennstal, Mariazell, Puchberg), overprints the northernmost margin of the Zentralgneiss. This sinistral shearzone, which has a length of about 300 km, and causes a lateral displacement of 60 km (Linzer et al. 2002), marks part of the northern border of the Tauern Window.

Macroscopic Structures

The northern part of the study area shows a penetrative, mylonitic foliation, which strikes ENE–WSW, dips subvertically, and contain flat-lying, but generally WSW-dipping stretching lineations. This mylonitic zone, which has a width of approximately 2 km is systematically associated with shear bands and σ -clasts, indicating a sinistral sense of shear. Occasionally, shear bands are also contained in the YZ plane of deformation, where they indicate a S-side-up sense of shear. Besides mostly in this part the deformation of the rocks is overprinted by brittle tectonics. South of the mylonitic zone, the foliation is folded by isoclinal folds with axial planes subparallel to the foliation described above. These folds can be correlated to the upright, large-amplitude

¹ Freie Universität Berlin, Malteserstr 74–100, 12249 Berlin Germany

folds, which form the three gneiss cores of the western Tauern Window. Further south, folds become more open, with axial planes dipping gently southward. We attribute these folds to the early Alpine phase of shortening, which affected the Zentral Gneiss (e.g. Lammerer 1988), before doming of the Tauern Window. This area is also affected by ductile shear zones of several meters width and a periodic distance of about 100 m. These shear zones strike WSW–ENE, dip steeply southwards and show a S-side-up sense of shear, indicated by the foliation drag and shear bands.

Microscopic Structures

On the basis of the quartz microstructures a gradient in the deformation temperature across the sinistral shear zone can be inferred. Quartz grains in the northernmost samples were deformed by dislocation glide associated with incipient bulging recrystallization. Towards the South, the deformation and recrystallization mechanisms of quartz show a transition to dislocation creep and sub-grain rotation recrystallization, followed by dislocation creep and grain boundary migration at the southernmost end of the sinistral shear zone. This change in the deformation and recrystallization mechanisms goes together with a grain size increase of the new grains from ca. 0.04 mm in the North to ca. 0.12 mm in the South. The folded foliation south of the sinistral shear zone shows a high-temperature fabric, characterized by dynamic recrystallization of quartz. Hence, there is no evidence for a static overprint separating the first and the second phase of folding.

Interpretation

In summary, the structures and microstructures described above suggest that the upright folds of the western Tauern Window formed during shearing along the SEMP Fault, which becomes ductile as it enters the northern margin of the Tauern Window. In addition, a pronounced, southward increase in structural level, as exposed across the strike of the shear zone, points to a transpressive type of deformation. Therefore, in addition to a left-lateral displacement, the SEMP Fault accommodates a vertical S-side-up component of displacement, which contributes to the exhumation of the Tauern Window.

References

- Lammerer B (1988) Thrust-regime and transpression-regime tectonics in the Tauern Window (Eastern Alps). *Geologische Rundschau* 77, 143–156.
- Linzer H-G, Decker K, Peresson H, Dell’Mour R, & Frisch W (2002) Balancing orogenic float of the Eastern Alps. *Tectonophysics* 354, 211–237.

Cadomian and Variscan metamorphic events in the Léon Domain (Armorican Massif) resolved by trace element analysis in monazite and garnet *Poster*

Bernhard Schulz¹ Erwin Krenn² Fritz Finger² Helene Brätz³ Reiner Klemd³

The question, whether crustal domains are allochthonous terranes or not is crucial for plate tectonic models of the Ibero-Armorican segment of the Variscan belt. The Léon Domain in the Armorican Massif appears as a displaced crustal block as it bears a resemblance to the South Armorican Domain of the internal Variscan belt (Le Corre et al. 1989). In the central part of the Léon, the amphibolite-facies Conquet-Penze Micaschist Unit (CPMU) overlies the high-grade Lesneven Gneiss Unit (LGU). At the base of the LGU, a high-pressure stage at 700°C/>13 kbar, recorded by garnet-clinopyroxene assemblages in eclogites was followed by a high-temperature event at 800°C/8 kbar with garnet and cordierite in aluminous paragneisses. Maximal temperatures in the upper parts of the LGU were 630°C/6 kbar. In the micaschists of the Conquet-Penze Unit, microstructures indicate a crystallization of garnet and then staurolite during the development of S₁ and S₂ foliations. Zoned garnet in assemblages with staurolite recorded prograde P–T paths from 490–610°C at 5–8 kbar in the upper and at 6–9 kbar in the lower parts of the CPMU (Fig. 1A, B). The foliation S₂ was over-

printed by shear bands with a top-to-SW directed normal sense of shear, corresponding to a dextral strike-slip movement (Balé & Brun 1986).

A younger population of monazite with variable Y contents displays Variscan Th-U-Pb ages (EMP dating method) between 340 and 300 Ma (Fig. 1C). In contrast, an older population of Cadomian monazite at 552–517 Ma is uniformly rich in Y and was observed in samples with only few or even no garnet. As the 330–340 Ma Saint Renan-Kersaint granite postdates the foliations S₁ and S₂ with peak metamorphic assemblages one can conclude that 340–300 Ma Variscan monazites should postdate garnet crystallization. In metapelites, the crystallization of garnet and accessory xenotime and monazite are linked by reactions with net transfer of Y. Trace-elements in garnet were analyzed by LA-ICPMS. Garnet Y, HREE and Li are low in high-grade gneisses. In amphibolite-facies micaschists strong zonations of Y and HREE are observed. Like Mn, both Y and HREE decrease from garnet core to rim at increasing temperature when garnet appears with xenotime and monazite, which are consumed. At low temperatures, xenotime is supposed to be a stable phase. In some samples, the Y is very low in the Mn-rich cores of garnet which crystallized at low temperatures. The Y contents strongly increase toward the inner rims, indicating that Y was initially bound in xenotime and/or monazite and then liberated by the breakdown of these phases under prograde metamorphic conditions. This suggests that high-Y Cadomian monazite crystallized previous to the garnet and at high temperatures. Presumably, garnet did not crystallize at the Cadomian

¹ Institut für Mineralogie, Brennhausgasse 14, 09596 Freiberg/Sachsen ² Abteilung für Mineralogie, Hellbrunner Str. 34, A-5020 Salzburg
³ Institut für Mineralogie, Am Hubland, 97074 Würzburg

event due to coeval low-pressure conditions, but at Variscan medium pressures. Whatever, Cadomian monazite dates a distinct thermal event. One could speculate on a contact metamorphism in the vicinity of intrusions like the Pointe des Renards metagranitoid or a Cadomian regional low-pressure metamorphism as it was described from the St. Malo and Fougères units of the adjacent North Armorican Cadomian Domain (Ballèvre et al. 2001).

P-T paths in combination with the monazite ages underline that the central

Léon units represent a normal crustal pile which was underthrust towards the SE or E beneath the Central Armorican Domain during a Variscan collision, as proposed by Rolet et al. (1986). Then, the range of Variscan monazite ages is linking this event to a Late-Carboniferous stage with overprinting of the S_1 - S_2 -structures by dextral shearing. The finding of Cadomian remnants does not support a South Armorican provenance. The Léon units were rather parts of a suture zone along the northern boundary of the Armorican microplate,

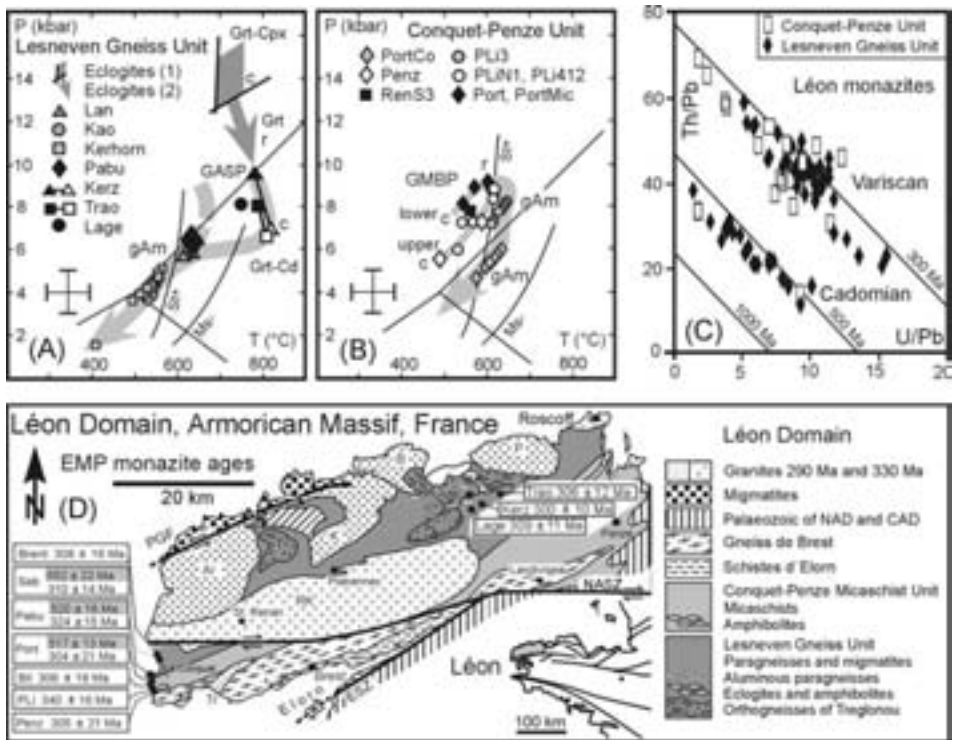


Figure 1: (A, B) P-T paths from the Léon. Garnet-clinopyroxene equilibria (Grt-Cpx) and relative evolution derived from garnet zonation trend. Data from green amphiboles (gAm). Data from garnet-sillimanite-plagioclase-quartz (GASP) and garnet-cordierite (Grt-Cd) equilibria, calculated with garnet core (c) compositions. Data from garnet-muscovite-biotite-plagioclase-quartz equilibria in micaschists (GMBP); prograde P-T paths derived from garnet core-to-rim (c, r) zonations. (C, D) Th-U-Pb monazite ages.

hence related to the margin of a former Rheic Ocean between Armorica and Avalonia.

References

- Balé P, Brun, JP (1986) Les complexes métamorphiques du Léon (NW Bretagne): un segment du domaine éo-hercynien sud armoricain translaté au Dévonien. *Bulletin Société Géologique de France* 1986/3, 471–477
- Ballèvre M, Le Goff E, Hébert R (2001) The tectonothermal evolution of the Cadomian belt of northern Brittany, France: a Neoproterozoic volcanic arc. *Tectonophysics* 331,19–43
- Le Corre C, Bale P, Georget Y (1989) Le Léon: un domaine exotique au Nord-Ouest de la chaîne varisque armoricaine (France). *Geodynamica Acta* 3/2, 57–71
- Rolet J, Le Gall B, Darboux JR, Thonon P, Gravelle M (1986) L' évolution géodynamique dévono-carbonifère de l' extrémité occidentale de la chaîne hercynienne d' Europe sur le transect Armorique - Cornwall. *Bull Soc Géol France* 1986-8/1, 43–54

Evolution and structure of the Upper Rhine Graben — quantitative insights from numerical modelling approaches

Vortrag

Michael Schwarz¹

Introduction

The Upper Rhine Graben forms the major segment of the Cenozoic Rift system of Western Europe. Although the rift was the target of many seismic and geological investigations, the style of lithospheric extension below the inferred faults, the depth to detachment,

¹ Geologisches Institut, Universität Freiburg, Albertstr. 23B, 79104 Freiburg i. Breisgau

and the amounts of horizontal extension and lateral translation are still being debated. In this study, the date base to the Upper Rhine Graben was subjected to a finite element approach in order to include thermomechanical processes of the lithosphere as well as erosion and sedimentation. The study concentrated on the consequences of extension and lateral translational events on the structure and evolution in terms of basin geometry, sediment layer thicknesses, Moho elevation, and shoulder uplift on a lithospheric scale. The numerical approach was three dimensional in order to incorporate the lateral crustal heterogeneities in the Upper Rhine area and the varying ambient stress field.

The thermomechanical simulation of a real rift requires the knowledge of the parameters controlling its structure and evolution. Furthermore, field data are needed for assessing the modelling results. Both preconditions could be met by the production of comparative data sets as well as by a parameter study before the modelling of the rift evolution. The critical validation of the research level allowed the extraction of the parameters to be determined. The results of the parameter study already gave some cues on the points of controversy mentioned above.

In anticipation of the parameter study, a hypothesis on continental rifting processes was formulated. It describes the consequences of the potential factors controlling the vertical displacements of the graben, shoulder, and Moho under simplified conditions. Opposite to other concepts, the hypothesis also takes into account the mechanical behaviour of faults as a primary factor. The numerical results of the parameter study were compared with the forecasts of the hy-

pothesis in order to identify additional processes acting in the more complex setting of the Upper Rhine Graben area. Moreover, the comparison allowed disclosing functional relationships between the vertical displacements and the controlling parameters. Apart from these insights in the continental rifting process the parameter variations rendered some important results specific to the Upper Rhine rift system. They are in detail:

- i) The vertical displacements in the rift system are controlled primarily by the friction, depth, and geometry of the border faults in the brittle domain. The consequences of the temperature and rheology in the creep regime are of minor importance. The same holds for the effects of the erosion and sedimentation.
- ii) The boundary faults are sub-listric down to maximum depth of 15 to 16 km. The geometry of the faults remains the same during the rifting. In the pre-rift setting, they flatten from a dip angle of around 65° to some 40° at greater depth. Beneath, the deformation is accommodated by ductile creep without a need for discrete shear zones in the lower crust and upper mantle.
- iii) The apparent frictional coefficients mostly lie around 0.3 bis 0.4, but at every point on the fault surfaces lower than 0.5.
- iv) There are no crustal horizons where a considerable restoration of the isostatic equilibrium takes place.
- v) High viscosities can be excluded at any depth in the lower crust. The variability of the lower crustal compositions is of no consequence for the rift evolution.
- vi) The upper crustal creep behaviour can be simulated only with much higher viscosities as it is predicted by the quartzite rheology. The requirement can be followed by using the creep parameters of a felsic granulite.

These results were put into the actual modelling of the Rhine Graben evolution. Therein, the implementation of the thermomechanical processes and the balancing on a lithospheric scale allowed reconstructing the vertical displacements of the graben, Moho, and shoulder over time. The comparative data sets are matched with a rift evolution in two phases. An extension being approximately orthogonal to the Rhine Graben is replaced by lateral translation which leads to a reactivation of the rift in a sinistral sense. The horizontal extension of 7.5 to 8.5 km and a sinistral displacement across the entire graben of 4.5 km at most are necessary in order to accommodate the sedimentary thicknesses. Dextral and sinistral displacements along the border faults take place during the period of orthogonal extension as well. These displacements are located at the fault segments where the friction coefficients change laterally due to a switch of the rift polarity. There, the graben block is extended parallel to the graben accompanied by a reduction of the principal stress in the same direction which causes the lateral displacements.

The conduction keeps pace with the advection of heat at any time during the rift evolution. There is no need for a thermal input of subcrustal ori-

gin for initiation of the rift. No thermal anomaly is created by the rifting in the Upper Rhine Graben area. The modelling results confirmed the ideas of the graben as an example of a passive rift.

The numerical outcomes can serve as decision guidance for solving conflictive positions about the geodynamics of the graben system. The fit between model and reality gives preferences for an evolution of the graben in two periods with different kinematics. The lateral displacements calculated in the study lie at the upper end of values which are inferred from structural and geophysical observations in the Rhine Graben region. Other stretching directions than orthogonal would result to additional strike-slip displacements above this threshold and, therefore, have to be declined. In the period of lateral translation during the Neogene, the regional strike slip setting disintegrates into different tectonic regimes along its strike. The configuration resembles the recent kinematics in the Rhine Graben region. Thus, the study approves the assumption of regional stress field being nearly constant since the beginning of the Miocene.

The modelling results refer only to periods of sedimentary record. They contain no information about the tectonosedimentary evolution in times with hiatuses. The hiatuses are located predominantly in the period of rift-parallel translation. This is at conflict with the calculated displacements which are already at the top of the values inferred for the Upper Rhine Graben from other observations. However, the results show that the graben subsidence, especially in a strike slip regime, is highly sensitive to the mechanical properties of the border faults and their orientation

to the local stress field. Slight modifications of these factors can result in a sticking behaviour of these faults over large distances which may account for the hiatuses.

Apart from continental rifting, southwestern Germany was affected by the migration of the Alpine peripheral forebulge into the Rhine Graben region. The modelling outcome permits separating the vertical displacements due to rifting from those related to the bulging processes. Future thermomechanical modelling studies require an implementation of these processes in order to achieve a holistic reconstruction of all geodynamic processes which were active in the Upper Rhine Graben area during the Cenozoic. Therefore, this study is regarded only as a first step to understand the interaction between extension, and lateral translation in a spatially and temporally varying stress field with a pre-existing structural inventory.

Die neogene Entwicklung des zentralen Tien Schan, Kasachstan. Erste Ergebnisse von Apatit-Spaltspurdaterungen und morphotektonischer Analyse von Satellitendaten *Poster*

Nadine Seib¹ Jonas Kley¹ Ralf Freitag¹ Thomas Voigt¹

Einführung

Der Tien Schan ist ein etwa E-W erstrecktes, rund 2500 km langes und bis

¹ Institut für Geowissenschaften, Universität Jena, Burgweg 11, 07749 Jena

250 km breites Gebirge in Zentralasien. Einzelne Gipfel sind über 7000 m hoch. Obwohl durch die Kollision Indiens mit Asien entstanden, ist der Tien Schan ein Intraplatten-Orogen, dessen Hebung lange nach dem Beginn der Kollision vor 50 Ma und weit nördlich der Suture einsetzte (Sobel & Dumitru 1997). Von Tibet ist der Tien Schan durch das kaum deformierte Tarim-Becken getrennt (Abb. 1).

Hohe und schroffe Topographie, starke Seismizität (Molnar & Ghose 2000) und GPS-Daten zeigen, dass das Orogen auch heute sehr aktiv ist (Abdrakhmatov et al. 1996, Reigber et al. 2001). Der Tien Schan nimmt gegenwärtig etwa 40% der Gesamtkonvergenz Indiens mit Asien auf. Die Struktur des Tien Schan wird dominiert von E–W-streichenden, nach N und S gerichteten Überschiebungen (Avouac et al. 1993, Yin et al. 1998), die sich meist deutlich in der Morphologie äußern. Auffallend ist die großräumige Gliederung des Orogens durch NW–SE-streichende dextrale Blattverschiebungen, die auch in das nördliche Vorland reichen (Tapponnier & Molnar 1979). Den Unterbau des Tien Schan bildet ein paläozoisches Akkretionsorogen (Zonenshajin et al. 1990). Im Mesozoikum entstand eine ausgedehnte Fastebene. In der späten Kreide oder dem frühen Tertiär setzte die Ablagerung kontinentaler Serien ein, die im jüngeren Känozoikum sehr mächtig werden. Die synorogenen Sedimente liegen manchmal konkordant, oft aber auch deutlich winkeldiskordant auf dem paläozoischen Sockel. In beiden Fällen bilden sie häufig asymmetrische Falten, die oft mit Störungen verknüpft sind. Geländestufen und ein starker Einfluss auf die Entwicklung des Entwässerungsnetzes weisen viele Störungen als gegenwärtig



Abbildung 1: Lage und Hauptstörungssysteme des Tien Schan, stark vereinfacht

aktiv aus. Unser Untersuchungsgebiet liegt im Südosten Kasachstans. Es umfasst die Nordflanke des Tien Schan und seinen zentralen Teil mit den höchsten Erhebungen. Im Untersuchungsgebiet liegt das nach E propagierende Ende eines seismisch aktiven Störungssystems, das weiter westlich die nördliche Randstörung des Gebirges bildet, wo es unter der Millionenstadt Almaty (Alma-Ata) verläuft und eine ernste Bedrohung darstellt. Die Entwicklung dieses Störungssystems soll über verschiedene Zeitskalen mit verschiedenen Methoden untersucht werden.

Apatit-Spaltspurdaten

Erste Apatit-Spaltspurdatierungen aus Graniten und granitischen Gneisen zeigen zwei deutlich getrennte Bereiche (Abb. 2).

Die niedrigen, durch aktive Störungen begrenzten Bergzüge im N haben mesozoische Abkühlalter. Diese Bereiche haben seit dem Mesozoikum keine starke Exhumierung erlebt. Auch die Bedeckung durch känozoische Vorlandsedimente war nicht mächtig genug, um die beprobten Gesteine über die Schließungstemperatur des Apatit-Spaltspurssystems (ca. 110°C) zu erwär-

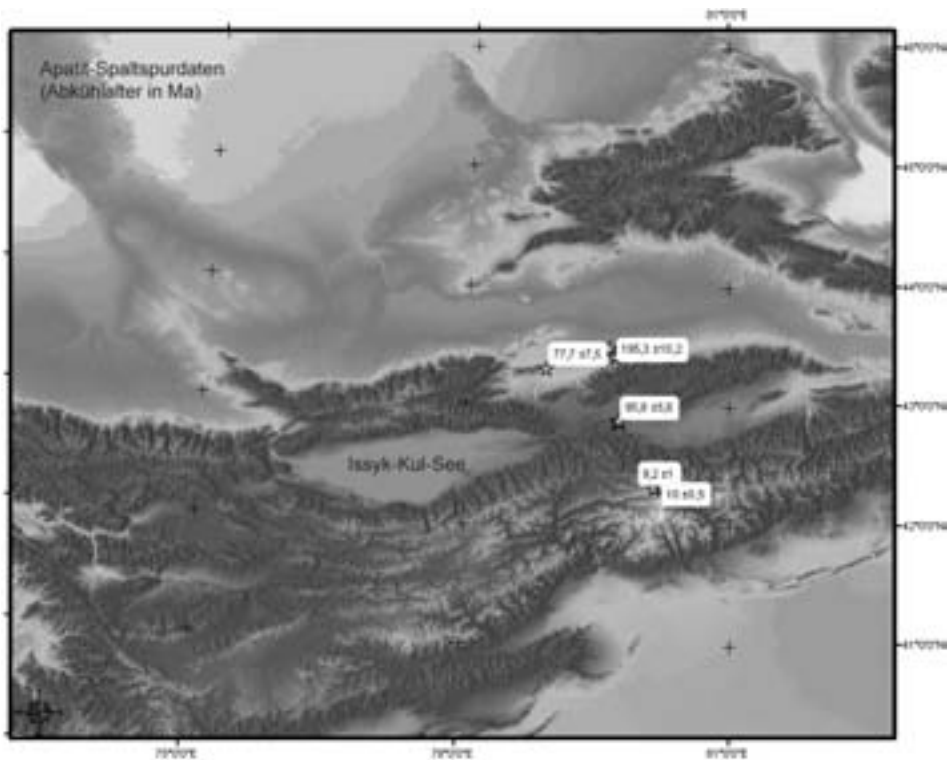


Abbildung 2: Probenahmepunkte und Ergebnisse der Spaltspur-Thermochronologie

men. Weiter südlich treten junge Alter von ca. 10 Ma auf. Hier wurde nach 10 Ma eine Überdeckung von ca. 3–4 km Mächtigkeit abgetragen, die vermutlich aus alten Gesteinen des Gebirgskerns bestand. Die Spurlängenverteilung in diesen Proben deutet auf rasche Exhumierung und Abkühlung. Die heute seismisch aktive Randstörung wurde wahrscheinlich erst später angelegt. Weitere Spaltspuruntersuchungen sollen Exhumierungsalter aus dem höchsten Teil des Gebirges und aus dem Hangendblock der Randstörung bei Almaty liefern. Außerdem soll die Grenze zwischen dem stark und dem schwach exhumierten Bereich (Abb. 2) durch zusätzliche Datierungen genauer festgelegt werden,

um die Hebung einem bestimmten Störungssystem zuordnen zu können.

Morphotektonische und strukturgeologische Untersuchungen aus Satellitendaten

Große Teile des Untersuchungsgebiets sind entweder zu trocken oder liegen zu hoch für dichten Bewuchs. Sie eignen sich deshalb ideal für Methoden der Fernerkundung, mit denen große Gebiete rasch untersucht, vom Boden aus nur schwer erkennbare Strukturen erfasst und Geländeuntersuchungen gezielt geplant werden können. Bisher haben wir Landsat TM7-Szenen und die digitalen Höhenmodelle aus 90 m-SRTM

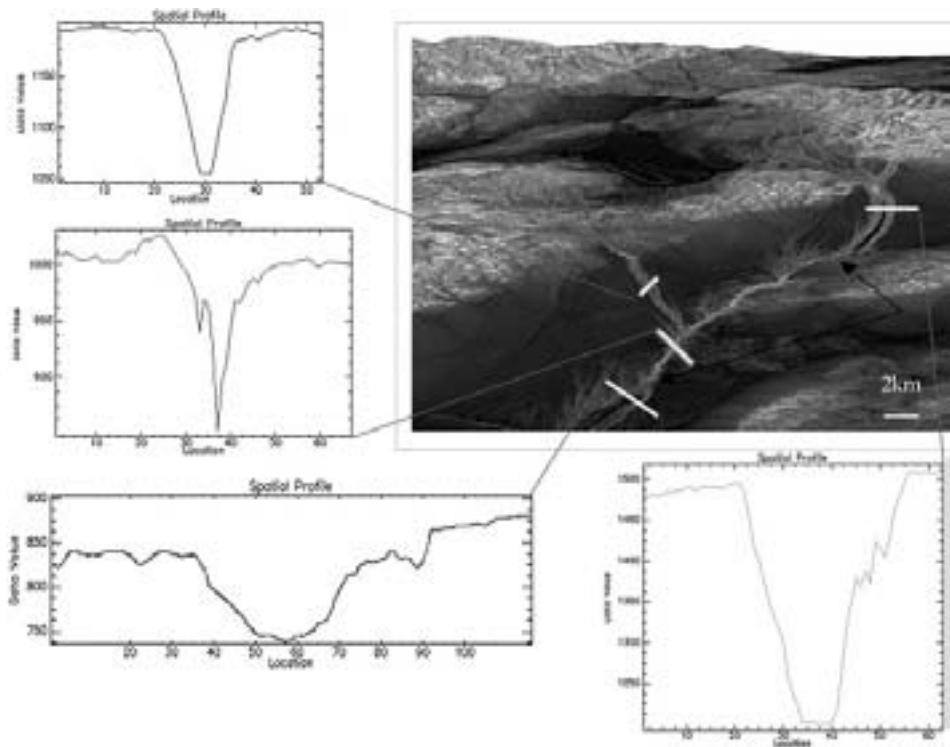


Abbildung 3: 'Profile Convexity' der SRTM Daten und verschiedene Formen von Talquerschnitten in einem Teil des Untersuchungsgebiets. Ebene Talböden und Kerbtäler sind deutlich kontrastiert. Der am stärksten eingeschnittene V-förmige Flussabschnitt (zwischen Pfeilen) deutet auf schnelle Hebung des querenden Hügelszugs. Starkes lokales Relief (hell) korreliert hier deutlich mit aktiv sich hebenden Bereichen

(Shuttle Radar-)Daten benutzt. Direkte strukturgeologische Beobachtungen aus diesen Daten sind versetzte geologische oder morphologische Elemente und Faltenbau. Bearbeitete Landsat-Daten zeigen durch wesentlich verbesserte Auflösung der Stratigraphie selbst in Gebieten mit geringem Geländere relief deutlich großräumige Falten neogener Sedimente, die bisher nicht kartiert waren. Die Hebung der Gebirgszüge steuert im Zusammenspiel mit Klimaschwankungen die Ablagerung alluvialer Fächer, die Ausbildung von Talprofilen und die Bildung von Terras-

sen. Das Entwässerungsnetz ist oft der sensibelste Anzeiger aktiver Deformation. Die Bearbeitung der SRTM Daten erlaubt die Analyse verschiedenster morphologischer Parameter mit statistischen und/oder manuellen Verfahren. Abb. 3 zeigt als Beispiel eine Analyse der Konvexität der Oberflächen.

Die Verbindung von Landsat- und SRTM-Daten ermöglicht eine sehr gute Visualisierung und verbesserte Interpretation der räumlichen Zusammenhänge von Strukturen und Geländeformen. Die meisten wissenschaftlichen Arbeiten waren bisher auf den chinesischen Ti-

en Schan im Osten und Kirgistan im Westen konzentriert. Der zentrale Tien Schan in Kasachstan ist bis heute eine wenig untersuchte Region. Die hier vorgestellten Arbeiten sind nur ein erster Schritt zu weiteren Forschungen. Sie zeigen aber schon jetzt, wie wirkungsvoll die eingesetzten Methoden sind.

Literatur

- Abdrakmatov KY, et al. (1996) Relatively recent construction of the Tien Shan inferred from GPS measurements of present-day crustal deformation rates. *Nature* 384, 450–453
- Avouac JP, Tapponnier P, Bai M, You H & Wang G (1993) Active thrusting and folding along the northern Tien Shan and late Cenozoic rotation of the Tarim relative to Dzungaria and Kazakhstan. *J Geophys Res* 98(B4), 6755–6804
- Molnar P & Ghose S (2000) Seismic moments of major earthquakes and the rate of shortening across the Tien Shan. *Geophysical Research Letters* 27(16), 2377–2380
- Reigber C et al. (2001) New space geodetic constraints on the distribution of deformation in Central Asia. *Earth and Planetary Science Letters* 191, 157–165
- Sobel ER & Dumitru TA (1997) Thrusting and exhumation around the margins of the western Tarim basin during the India-Asia collision. *J Geophys Res* 102(B3), 5043–5063
- Tapponnier P & Molnar P (1979) Active faulting and Cenozoic tectonics of the Tien Shan, Mongolia and Baykal regions. *J Geophys Res* 84, 3425–3459
- Yin A, Nie S, Craig P & Harrison TM (1998) Late Cenozoic tectonic evolution of the southern Chinese Tian Shan. *Tectonics* 17(1): 1–27
- Zonenshajn LP, Kuzjimin MI & Napatov LM (1990) Plate tectonics of the U.S.S.R. territory. *Nedra* 1990, pp 334 (in Russian)

Texturanalysen von Halitmyloniten aus den Salzstrukturen Gorleben, Morsleben und Teutschenthal *Poster*

Torben Seidel¹ Bernd Leiss¹ Yvonne Küster² Klaus Ullemeyer³ Michael Schramm²

Das Verständnis der Mechanismen und der Prozesse der Gefügeentwicklung und die damit verbundene Charakterisierung der anisotropen physikalischen Eigenschaften von natürlich deformiertem Steinsalz sind von grundlegender Bedeutung. So lassen sich damit u.a. Aussagen zur Entwicklung von Salzstrukturen vom mikroskopischen bis zum regionalen Maßstab machen, aber auch wichtige Parameter u.a. für den Kavernenbau oder die Endlagerung toxischer Stoffe in Salzstrukturen gewinnen. Ein wichtiger Gefügeparameter ist dabei die kristallographische Vorzugsorientierung (Textur). In der Literatur gibt es im Gegensatz zu Deformationsexperimenten und numerischen Simulationen relativ wenige Untersuchungen natürlicher deformierter Steinsalze (für einen Überblick siehe Scheffzük 1999). Die meisten der bislang untersuchten Proben sind Einzelproben und sind nicht nach mylonitischen oder rekristallisierten Steinsalzgesteinen unterschieden (u.a. Schwerdtner 1966, 1968, Goemann & Schumann 1977, Ertel 1987). Aussagen sind daher nicht zwingend repräsentativ und eine Charakterisierung der gesamten Salinarstruktur nicht möglich.

¹ Geowissenschaftliches Zentrum der Universität Göttingen (GZG), Goldschmidtstr. 3–5, D-37077 Göttingen ² Bundesamt für Geowissenschaften und Rohstoffe (BGR) Hannover, Stilleweg 2, D-30655 Hannover ³ Geologisches Institut, Universität Freiburg, Albertstr. 23-B, D-79104 Freiburg



Abbildung 1: Zentraler Teil des südlichen permischen Beckens mit den dort entwickelten Salzstöcken und -kissen (Abb. nach Lokhorst 1999). Der Rand des Beckens ist durch einen Fazieswechsel der Zechstein 2 Karbonate vom Beckenhang (grau) zum Beckeninneren (hellgrau) hin gekennzeichnet. Die Lokationen der beprobten Bohrkern von Gorleben, Morsleben und Teutschenthal sind vermerkt.

Ziel unserer Arbeiten ist daher eine strukturbezogene (Falten, Scherzonen etc.) Gefügecharakterisierung durch Korrelation von Kornformanalysen, Texturen, makroskopischen Strukturen im dm- bis 10er Meter Bereich und der gesamten Salzstruktur. In einer ersten Studie wurde auf Bohrkern der Bundesanstalt für Geowissenschaften und Rohstoffe in Hannover zurückgegriffen. Die Proben stammen aus durchteuften Scherzonen, d.h. Bereichen mit signifikanten Kornlängungen, die auf Verformung zurückgeführt werden. Es wurden Bohrkern aus den Salzstrukturen von Gorleben, Morsleben und Teutschenthal in Norddeutschland beprobt (Abb. 1). Die Gesamtintensität der Verformung nimmt von Teutschenthal bis Gorleben

zu, d.h. in Teutschenthal liegt eine Salzkissenstruktur, in Gorleben eine Diapirstruktur vor.

Steinsalzgesteine sind immer vergleichsweise grobkörnig und Halit ist optisch isotrop. Eine systematische quantitative und volumenbezogene Texturanalyse ist damit vor allem mit der Neutronenbeugung sinnvoll, da Neutronen in Materie relativ schwach absorbiert werden und daher größere Probenvolumina durchstrahlt werden können. Besonders geeignet ist dabei der Neutronentexturmessplatz SKAT am Vereinigten Institut für Kernforschung in Dubna, Russland, da dort Probenvolumina mit bis zu 5 cm Durchmesser gemessen werden können. (Ullemeyer et al. 1998).

Als Probenkörper wurden daher Zylinder mit einem Durchmesser von 5 cm bzw. Würfel mit einer Kantenlänge von 5 cm präpariert. Das Probenkoordinatensystem wurde unabhängig vom Gefüge, aber in Bezug zur Bohrkerngeometrie festgelegt. Die z-Richtung ist parallel zur Bohrrichtung, x parallel und y senkrecht zum Medianschnitt des Bohrkerns orientiert. Die Flächenanschnitte in Abb. 2 sind nicht zwingend parallel zur Foliation und zur Mineralstreckungslineation orientiert, da diese am Bohrkern nicht immer eindeutig ersichtlich sind.

Die Gefüge aus Gorleben und Morsleben zeigen deutliche Kornformanisotropien (Abb. 2a, b). Während die Proben aus Gorleben Kornlangachsen zwischen 1 mm und bis zu 10 mm aufweisen, zeigen die Morslebenproben Kornlangachsen zwischen 1 mm und 5 mm. In beiden Lokationen liegen die abgeschätzten Kornachsenverhältnisse bei 1:2 bis 1:2.5. Die Korngrenzen sind gerade bis leicht verzahnt. Bei den Proben aus Teutschenthal lassen sich keine bzw. nur

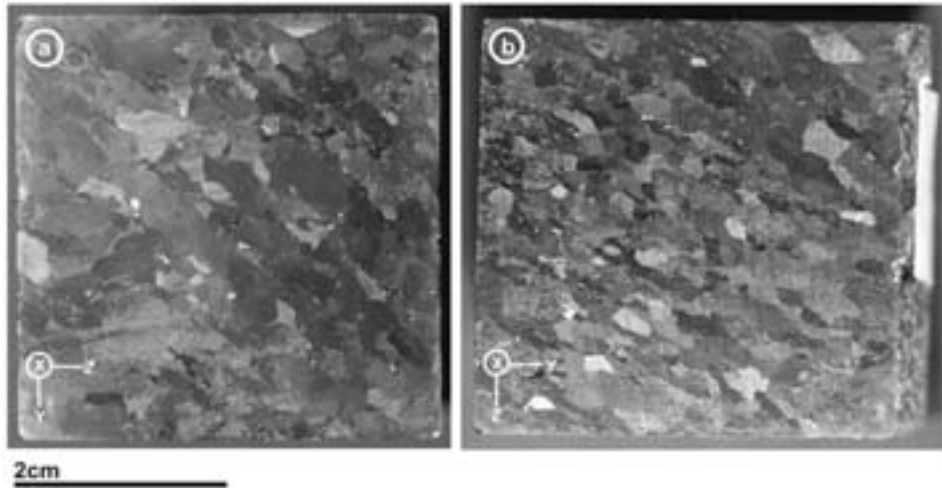


Abbildung 2: Flächenanschnitte der Proben a) Gorleben und b) Morsleben.

sehr schwache Kornlängungen nachweisen. Der mittlere Korndurchmesser beträgt ca. 3 mm. Die Korngrenzen sind bei diesen Proben etwas stärker verzahnt.

Die quantitativen Neutronentexturmessungen zeigen für alle vier Proben keine kristallographischen Vorzugsregelungen. Da die bislang aus der Literatur bekannten Regelungen im Steinsalz in der Regel sehr schwach sind, wurden Untergrund- und -Detektorkorrekturen sehr genau überprüft und Einzelmaxima in den Polfiguren mit Hilfe der Texturkomponentenmethode auf kristallographische Kompatibilität überprüft. Es konnten jedoch keine, auch nicht sehr schwache Regelungen festgestellt werden.

Obwohl die anisotropen Kornformgefüge klare Hinweise auf plastische Verformung geben, können über die Texturanalyse keine Hinweise auf intrakristalline Gleitsysteme als Verformungsmechanismen gefunden werden. Zur Diskussion steht ein Verformungsprozess

ohne intrakristallines Gleiten, d.h. Lösung/Fällung bzw. Diffusion, oder eine postdeformative Entregelung. Laufende Untersuchungen sollen zeigen, ob und in welchen Strukturen der Salzstöcke Texturen auftreten.

Literatur

- Ertel A (1987) Neutronographische Texturuntersuchung an Salinargesteinen aus Kalisalzlagerstätten der DDR. Dissertation Karl-Marx Univ. Leipzig, pp 94
- Goemann U & Schumann H (1977) Röntgenographische Gefüge-Untersuchung an einer orientiert entnommenen Probe von grobkörnigem Steinsalz. *Tschermaks Mineral. Petrogr. Mitt.* 24, 179–190
- Lokhorst A (ed) (1999) NW European gas atlas CD-Rom. Bundesanstalt für Geowissenschaften und Rohstoffe Hannover.
- Scheffzyk C (1999) Neutronographische Texturanalysen und Mikrostrukturuntersuchungen natürlicher und triaxial verformter Halite. Dissertation RWTH Aachen, Scientific Technical Report STR99/15, GeoForschungsZentrum Potsdam.
- Schwerdtner WM (1966) Preferred Orientation of Halite in a 'Salt Seismogram'. *Proc.*

Second. Symp.on Salt 1965, Northern Ohio Geol. Soc., Cleveland, 70–84

Schwerdtner WM (1968) Intragranular gliding in domal salt. *Tectonophysics* 5, 353–380

Ullemeyer K, Spalhoff P, Heinitz J, Isakov NN, Nikitin AN & Weber K (1998) The SKAT texture diffractometer at the pulsed reactor IBR-2 at Dubna: experimental layout and first measurement. *Nuclear Instruments and Methods in Physics Research A*412, 80–88

Mikrostruktur und Textur nach Scherverformungsversuchen an Hämatiterzen *Poster*

Heinrich Siemes¹ B. Klingenberg¹ E. Rybacki² M. Naumann² Jens M. Walter³ Ekkehard Jansen³ Karsten Kunze⁴

Einführung

Die Beziehungen zwischen der Mikrostruktur und der kristallografischen Vorzugsorientierung (Textur) von Hämatiterzen der gebänderten Eisenerzformation (BIF) in Brasilien wurden in vielen Veröffentlichungen behandelt, z.B. Quade et al. 2000, Rosière et al. 2001, Bascou et al. 2002. Polfiguren dieser Hämatiterze zeigen kreisförmige bis elliptische c-Achsen-Maxima, die um den Pol der Foliation liegen. Die Pole der Prismenflächen liegen auf Großkreisen in der Foliationsebene und die Maxima auf diesen fallen mit der Lineation zusammen. Die Entstehung dieser Regelung wird auf Scherverformungs-

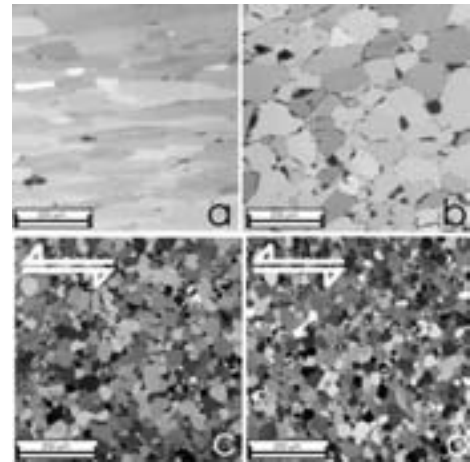


Abbildung 1: Mikrostruktur von natürlich (a,b) und experimentell verformtem (c,d) Hämatiterz, a) Brucutu, Minas Gerais, Brasilien, b) Andrade, Minas Gerais Brasilien, c) 1000°C, $\gamma = 3.8$, Peripherie der Probe, d) 1000°C, $\gamma = 0.0$, Zentrum der Probe.

prozesse zurückgeführt. Bei experimentellen Stauchversuchen an polykristallinem Hämatit gab es Anzeichen der Bildung eines c-Achsenmaximums senkrecht zur Kompressionsrichtung (Siemes et al. 2003). Da zu vermuten war, dass Gleiten parallel zur Basis des Hämatits Ursache der Regelung ist, wurden die Gleitmechanismen an experimentell verformten Hämatiteinkristallen bestimmt (Siemes et al. 2006). In diesem Beitrag werden neue Scherexperimente an polykristallinen Hämatitaggregaten vorgestellt.

Konzeption der Versuche

Zunächst wurden drei Torsionsversuche in einer Hochdruck-Hochtemperatur-Apparatur (Paterson & Olgaard, 2000) konzipiert, um zu prüfen, ob und wie diese Versuche sich mit Hämatiterz

¹ Institut für Mineralogie und Lagerstättenlehre, RWTH Aachen, D-52056 Aachen ² Geoforschungszentrum Potsdam, Deformation und Rheologie, D-14473 Potsdam ³ Mineralogisches Institut, Universität Bonn, Forschungszentrum Jülich, D-52425 Jülich ⁴ Geologisches Institut, ETH Zürich, CH-8092 Zürich

realisieren lassen. Als Versuchsmaterial wurde ein Hämatiterz von Sishen, Südafrika, gewählt, das fast ungerichtet ist und eine Kristallitgröße von 5–60 Mikrometer aufweist (Siemes et al. 2003). Proben (Durchmesser 14 mm, Länge 10 mm) mit einer 0,5 mm dicken Nichteisen-Schutzhülle wurden in ein Jacket aus Eisen oder aus Kupfer eingebracht, das die Probe vom Druckmedium Argongas trennt. Bei Temperaturen von 1000°C bis 900°C wurden bei 400 MPa allseitigem Druck, mit einer Torsionsrate von $6 \times 10^{-5} \text{s}^{-1}$, in 30-Stunden-Versuchen Scherverformungen von 3,8 bis 4,0 erreicht. Eine Schutzhülle aus Silber-Palladium in einem Eisenjacket erwies sich als die geeignete Versuchsanordnung, um Hämatit mit nur geringer Magnetitbildung zu verformen. Inzwischen wurden weitere Versuche bei Temperaturen bis hinunter zu 800°C gefahren.

Erste Ergebnisse

Der Hämatit ist bei 1000°C zu einem gleichförmigen polygonalen Korngefüge rekristallisiert (Abb. 1c,d), das sich auch bei natürlich verformten Erzen findet (Abb. 1b). Die Korngrößen weisen dabei keine Unterschiede über die Probenquerschnitte (Abb. 1c,d) auf, obwohl die finite Scherverformung von Null im Zentrum der Probe bis zum maximalen Wert an der Peripherie variiert. Neutronentexturmessungen (Jansen et al. 2000) im Probenbereich mit der stärksten Verformung und EBSD-Messungen (Kunze et al. 1993) ergaben für die (0003)-Polfigur ein zentrales, elliptisches Maximum im Pol der Scherebene. In der (11 $\bar{2}$ 0)-Polfigur befindet sich auf dem Grundkreis ein Maximum, das die Orientierung der Scherrichtung angibt. Die (10 $\bar{1}$ 4)-Polfigur, die zwei bananenförmige

Maxima (Quade 1988) unterschiedlicher Höhe aufweist, lässt auf den Schersinn schließen. Diese Polfiguren stimmen weitgehend mit Polfiguren natürlich verformter Hämatiterze überein. Im Gegensatz zum homogenen Korngefüge besitzt die Textur einen grossen Gradienten von nahezu regellos im Zentrum (undeformiert) zu stark geregelt am Rand (maximaler Scher-Strain). Die Beobachtungen unterstützen die Vermutung, dass Hämatiterz bevorzugt durch Versetzungsgleiten auf $\{0001\} \langle 1\bar{2}10 \rangle$ mit simultaner dynamischer Rekristallisation deformiert.

Danksagung Die zur Zeit laufenden Experimente werden von der Deutschen Forschungsgemeinschaft gefördert.

Literatur

- Bascou J, Raposo MIB, Vauchez A & Egydio-Silva M (2002) Titanohematite lattice-preferred orientation and magnetic anisotropy in high-temperature mylonites. *Earth and Planetary Science Letters* 198, 77–92
- Jansen E, Schäfer W, Kirfel A, (2000) The Jülich neutron diffractometer and data processing in rock texture processing. *Journal of Structural Geology* 22, 1559–1564
- Kunze K, Wright SI, Adams BL & Dingley DJ (1993) Advances in automatic EBSD single orientation measurements. *Textures and Microstructures* 20, 41–54
- Paterson MS & Olgaard DL (2000) Rock deformation tests to large shear strains in torsion. *Journal of Structural Geology* 22, 1341–1358
- Quade H (1988) Natural and simulated (10.4) pole figures of polycrystalline hematite. *Textures and Microstructures*, 8–9, 719–736
- Quade H, Rosière CA, Siemes H & Brokmeier H-G (2000) Fabrics and textures of Precambrian iron ores from Brazilian deposits. *Zeitschrift für angewandte Geologie, Sonderheft* 1, 155–162
- Rosière CA, Siemes H, Quade H, Brokmeier H-G & Jansen EM (2001) Microstructures, textures and deformation mechanisms in hema-

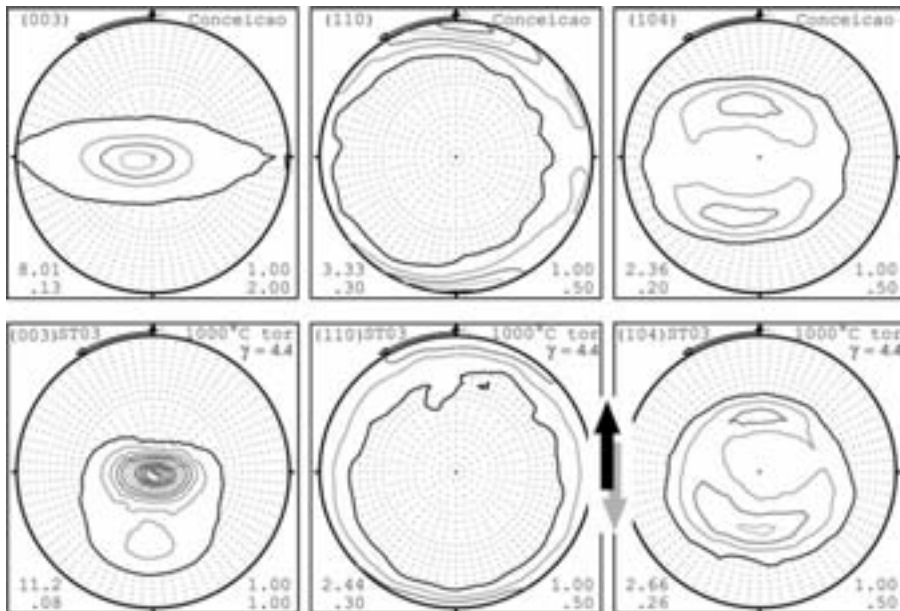


Abbildung 2: (0003)-, $(11\bar{2}0)$ - und $(10\bar{1}4)$ -Polfiguren von natürlich und experimentell verformtem Hämatiterz, a) Conceição, Minas Gerais, Brasilien, b) Polfiguren parallel zur Scherebene, Scherrichtung etwa NS, Schersinn N.

tite. Journal of Structural Geology 23, 1429–1440

Siemes H, Klingenberg B, Rybacki E, Naumann M, Schäfer W, Jansen E & Rosière CA (2003) Texture, microstructure, and strength of hematite ores experimentally deformed in the temperature range 600° to 1100°C and at strain rates between 10^{-4} and 10^{-6} s $^{-1}$. Journal of Structural Geology 25, 1371–1391

Siemes H, Klingenberg B, Rybacki E, Naumann M, Schäfer W, Jansen E & Kunze K (2006) Glide systems of hematite single crystals in deformation experiments. Ore Geology Reviews (accepted)

Syn-kinematic magma ascent and batholith inflation (Sierra de San Luis/Argentina) Vortrag

André Steenken¹ Siegfried Siegesmund² Mónica G. López de Luchi¹ Augusto Rapalini³ Klaus Wemmer²

The measurement of the anisotropy of the magnetic susceptibility (AMS) is

¹ Instituto de Geocronología y Geología Isotópica (INGEIS), Ciudad Universitaria, 1428 Buenos Aires, Argentina ² Geoscience Centre of the University of Göttingen (GZG), Goldschmidtstr. 3, 37077 Göttingen, Germany

³ Instituto de Geofísica Daniel Valencio (INGEODAV), Departamento de Ciencias Geológicas, Facultad de Ciencias Exactas y Naturales, Universidad de Buenos Aires, CONICET, Pabellón 2, Ciudad Universitaria, 1428 Buenos Aires, Argentina

now routinely used since more than four decades in the analyses of rock fabrics in granitic rocks (e.g. Stacy 1960, Henry 1975, Gleizes et al. 1993). Even though the intensity of fabrics in granitoids is often weakly developed the significance of orientation and shape of crystals is the same like in other deformed rock types. By revealing the distribution of fabrics in plutonic rocks one of the still ongoing discussions in granite tectonics may be addressed: How did those sometimes voluminous batholiths were inflated in the middle crust? We are presenting magnetic fabric data on a series of Devonian batholiths that intruded the polyphase deformed metaclastites of the Sierra de San Luis (32°10'–33°20' S / 65°15' – 66°20' W) in central Argentina. Regional considerations on the tectonic regime during the emplacement of the batholiths are inferred from combined field, microstructural and AMS observations.

Geological background

The proto-Andean basement outcropping in the Sierras Pampeanas experienced a polyphase magmatometamorphic history during the Ediacaran/Early Palaeozoic resulting from the accretion of different crustal fragment to Gondwanas southwestern margin (Ramos 1988). The final manifestation of this history is the emplacement of voluminous, elliptical granodioritic to syenogranitic composite batholiths in the Sierra de San Luis and the Sierras de Córdoba during the Early/Middle Devonian (Fig. 1).

There exists discordance on the regional stress field that enabled the magma ascent during this period. According to Llambías et al. (1998) the Devonian magmatism is the result of the collapse

of the Famatinian orogen whereas Sims et al. (1998) emphasised the relation of the Devonian batholiths with the continual subduction followed by the collision of the Chilenia Terrane with the western outboard of Gondwana.

The Devonian batholiths

Detailed fabric studies on the largest batholiths in the Sierra de San Luis, i.e. the La Totorá, Renca and Las Chacras-Potrerrillos batholiths were carried out. The studies comprised systematic field surveys, microstructural observations and anisotropy of magnetic susceptibility (AMS) measurements. Microstructural studies indicate that the batholith rocks are mainly characterised by magmatic microstructures with limited sub-magmatic to high temperature sub-solidus deformation. Magmatic foliations are defined by the planar arrangement of tabular feldspar and biotite. The local appearance of intracrystalline fractures in the feldspar filled with fine-grained granitic melt point to the syn-kinematic emplacement of the batholiths. Continued deformation below the solidus is accommodated by feldspar recrystallisation as indicated by sub-grain boundaries. Recrystallisation of quartz at low temperatures, leading to the formation of quartz ribbons is observed in the SE sector of the Las Chacras-Potrerrillos batholith only. Shear indicators point to sinistral as well as dextral sub-horizontal displacement. All three batholiths possess concentric foliation patterns that along the margins show a steep inclination. The average magnetic foliation patterns in the studied plutons agree well with the macroscopic fabrics measured in the field indicating that the AMS-data can be used to study the orientation of fabric

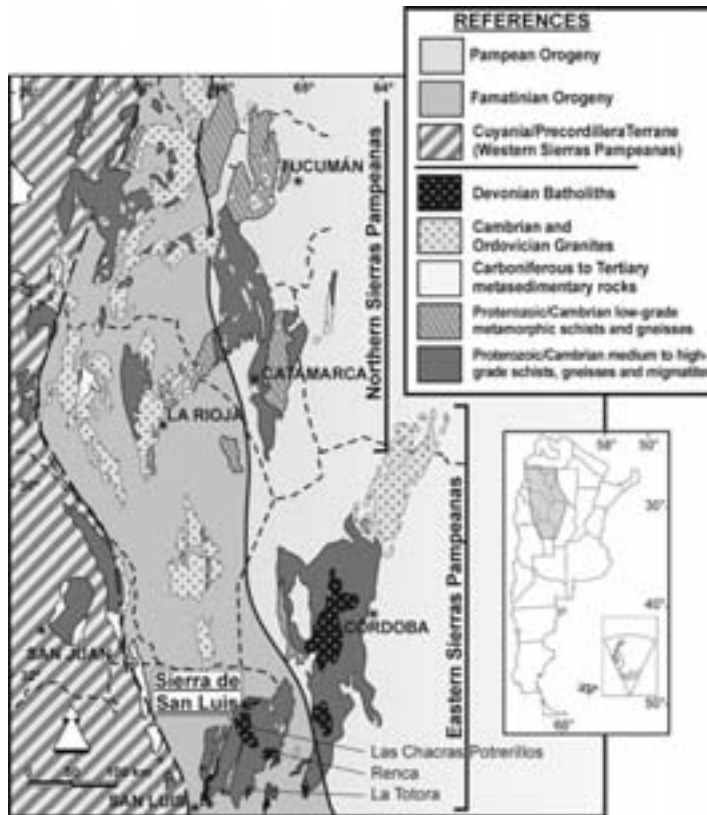


Figure 1: Schematic map of the southern section of the Sierras Pampeanas. The Devonian magmatism is restricted to the basement complexes of the Sierra de San Luis and the Sierras de Córdoba

elements. However, a bulk susceptibility (K_{vol}) of up to 8000×10^6 in almost all granitic sub-units indicates a predominance of ferromagnetic contributions to the bulk susceptibility. Therefore biotite fabrics of selected samples were used to calculate a theoretical AMS tensor (Siegsmund et al. 1995) that was compared to the measured AMS fabric, indicating acceptable accordance in the directional data but do not necessarily support the shape of the magnetic fabric ellipsoid. Most foliations and lineations reflect magmatic flow and their attitude

is linked to the interference between regional deformation and batholith inflation, i.e. fabrics may be due to regional strain in combination with the internal dynamics of the magma bodies. Magnetic lineations either are sub-vertical or follow the NNE–SSW trend that is also documented by the linear fabrics of their hosts (Fig. 2).

Results

It is proposed that the opening of transtensional pull-apart structures controls those shallow dipping lin-

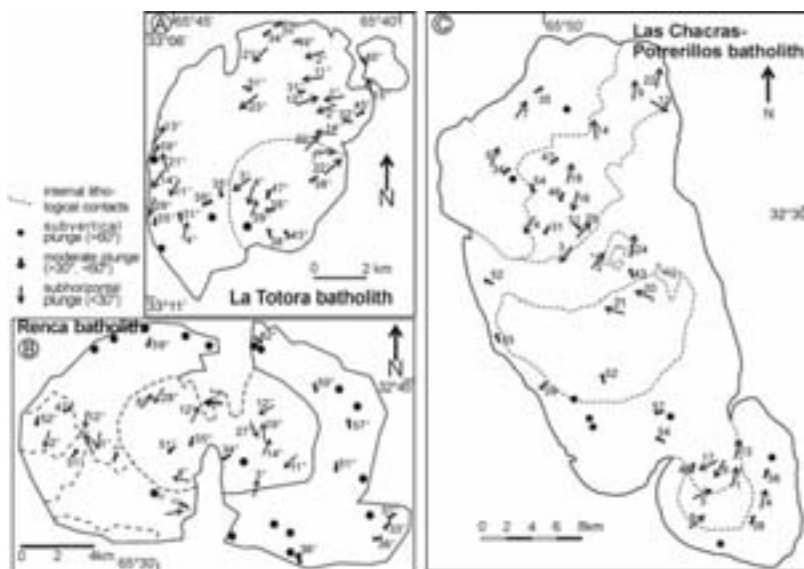


Figure 2: Orientation of magnetic lineations for the La Totora, Renca and Las Chacras-Potreriillos batholiths. Note that except for the marginal part of the Renca batholith, most lineations tend to be sub-horizontal or shallowly plunging.

eations during batholith inflation. K/Ar and Ar/Ar muscovite data from regional shear zones at ~ 360 Ma (Sims et al. 1998, Steenken et al. 2004) support the idea of a syn-kinematic magma ascent and batholith inflation following the direction of extension in a transpressional tectonic framework (Fig. 3). It turns out that the Devonian batholiths intruded the basement syn-kinematically with respect to the Achaian deformational cycle.

References

- Henry, B (1975) Microtectonique et anisotropie de susceptibilité et magnétique du massif tonalitique des Riesenferner-Vedrette di Ries (Frontiere Italo-Autrichienne). *Tectonophysics* 27: 155-165
- Gleizes, G, Nédélec, A, Bouchez, JL, Autran, A, Rochette, P (1993) Magnetic susceptibility of the Mont-Louis Andorra Ilmenite-Type Granite (Pyrenees): A new tool for the petrographic characterisation and regional mapping of zone granite plutons. *Journal of Geophysical Research* 98: 4317-4331
- Llambías EJ, Sato A, Ortiz Suárez A, Prozzi C (1998) The granitoids of the Sierra de San Luis. Geological Society of London, Special Publication 142: 325-341
- Ramos VA (1988) Late Proterozoic-Early Paleozoic of South America — a collisional history. *Episodes* 11: 168-174
- Siegsmund S, Ullemeyer K, Dahms M (1995) Control of magnetic rock fabrics by mica preferred orientation: a quantitative approach. *Journal of Structural Geology* 17: 1601-1613
- Sims JP, Ireland TR, Camacho A, Lyons P, Skirrow RG, Stuart-Smith PG, Miró R (1998) U-Pb, Th-Pb and Ar-Ar geochronology from southern Sierras Pampeanas, Argentina: Implications for the Palaeozoic tectonic evolution of the western Gondwana margin. Geological Society of London, Special Publication 142: 235-258
- Stacey FD (1960) Magnetic anisotropy of igneous rocks. *Journal of Geophysical Research* 65: 2429-2442

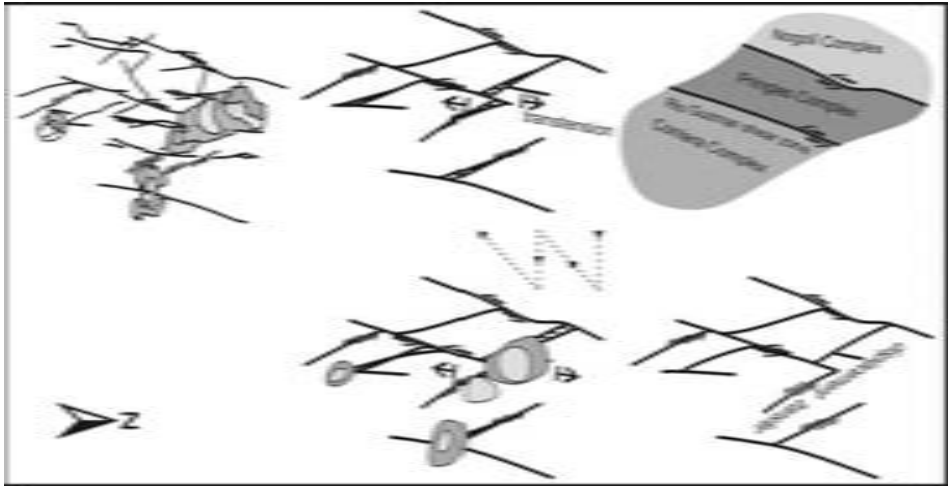


Figure 3: Comic strip illustrating the syn-tectonic emplacement of the major Devonian granitoids in the Sierra de San Luis. Schematic depiction of the major tectonic strike slip faults connected with the ‘space-creation’ for the magma ascent. The development of a secondary set of NNW trending sinistral strike slip faults leads to the counter clockwise step over of the sinistral displacement along the Río Guzmán and related NNE-SSW trending shear zones. NNE directed crustal extension would allow the formation of magma conduits and subsequent magma accommodation in a transtensional setting.

Steenken A, López de Luchi MG, Siegesmund S, Wemmer K, Pawlig S (2004) Crustal provenance and cooling of the basement complexes of the Sierra de San Luis: An insight into the tectonic history of the proto-Andean margin of Gondwana. *Gondwana Research* 7: 1171–1195

Deformation der karbonatischen Espanola-Formation im zentralen Teil der Sudbury-Impaktstruktur, Kanada

Poster

Elisabeth Steffes¹ Ulrich Riller²
Daniel Doman²

Archaische Granitoide und paläoproterozoische Metasedimente der *Huronian Supergroup* werden von dem schüsselförmigen und partiell erodierten 1.85 Ga alten Impaktschmelzkomplex der Sudbury-Impaktstruktur überlagert. Huronische Metasedimente und deren basaler Kontakt zum granitoid-

¹ Freie Universität Berlin, Institut für Geologische Wissenschaften, Malteser Str. 74–100, D-12249 Berlin ² Humboldt-Universität zu Berlin, Museum für Naturkunde, Invalidenstr. 43, 10115 Berlin

den Grundgebirge stehen in einer Entfernung bis zu 15 km von dem lagigen Komplex und um diesen herum steil. Obwohl diese Steilstellung durch die Bildung eines impakt-induzierten Zentralberges erklärt werden kann, ist unklar, ob orogene Verformung vor dem Impakt an der Steilstellung beteiligt war. Um hierüber Aufschluss zu gewinnen, wurden die basalen Huronischen Einheiten, insbesondere die karbonatische Espanola Formation und deren benachbarte Metakonglomerate und Metasandsteine, nordöstlich des Impaktschmelzkomplexes strukturell untersucht. Aufgrund der Nähe der metasedimentären Einheiten (ca. 5 km) zu dem 2,5 km mächtigen Schmelzkomplex wurde daher auch dessen möglicher thermischer Einfluss auf die Metasedimente untersucht.

Die Espanola Formation ist durch einen engen Lagenbau gekennzeichnet, der durch deutliche Unterschiede in der Korngröße und der Mineralzusammensetzung bestimmt wird. Dunkle Lagen sind feinkörnig und enthalten Erze und unterscheiden sich von helleren Lagen, die an Quarz und Feldspat angereichert sind. Messungen der Orientierung von Schichtflächen, planaren und linearen Mineralgefügen, sowie Faltenachsen wurden an insgesamt 360 Stationen durchgeführt und dienen zusammen mit lithologischen Beobachtungen der Erstellung einer detaillierten Strukturkarte. Entgegen älterer Kartierungen, zeigt diese, dass die Espanola-Formation nicht diskontinuierlich auftritt, sondern im Gegensatz zu ihren siliziklastischen und mechanisch kompetenteren Nachbareinheiten im Dezimeter- bis 10er-Meter-Bereich stark verfaltet ist. Eine strukturelle Detailkartierung zeigt insbesondere einen asymmetrischen Faltenbau, der durch flach ESE-einfallende

Achsen und steile WNW–ESE streichende Achsenebenen gekennzeichnet ist. Minerallineationen sind parallel zu Kleinfaltenachsen. Desweiteren zeichnet sich die Espanola Formation durch eine achsial-planare Drucklösungsschieferung aus. Diese strukturellen Befunde belegt einen orogenen Ursprung der Faltung. Die Überprägung von Kleinfalten durch Pseudotachylitzonen belegt desweiteren, dass der asymmetrische Faltenbau bereits vor dem Impaktereignis angelegt wurde. Inwieweit dieser Faltenbau durch impaktinduzierte Verformung modifiziert, insbesondere rotiert, wurde, ist noch unklar.

Mikrostrukturelle Untersuchungen, z.T. mithilfe des Kathodoluminiszenzmikroskopes, zeigen, dass planare und lineare Mineralgefüge durch eine deutliche Vorzugsorientierung von Kalzit definiert sind. Jedoch ist Kalzit nahezu vollständig durch eine polygonale Ausbildung seiner Korngrenzen mit 120°-Tripelpunkten gekennzeichnet. Dies zeigt, dass planare Kalzitgefüge durch eine statische Rekristallisation überprägt wurden. Im Gegensatz dazu waren die siliziklastischen Nachbareinheiten der Espanola Formation lediglich einer dynamischen Rekristallisation von Quarz ausgesetzt. Dies bedeutet, dass die Gesteine thermische unter statischen Bedingungen in einem Temperaturfenster von mindestens 150°C, der Rekristallisationstemperatur von Kalzit, und höchstens 300°C, der Rekristallisationstemperatur von Quarz, überprägt wurden. Ursache für die lokale, statische Überprägung ist aller Wahrscheinlichkeit nach der nahegelegene Impaktschmelzkomplex. Dies birgt wichtige Konsequenzen für die Abschätzung der ursprünglichen Ausdehnung dieses Komplexes.

The effect of water, temperature and strain rate on the dislocation creep microstructure, recrystallized grain size and flow stress of quartz

Vortrag

Michael Stipp¹ Jan Tullis² Harald Behrens³

Since the work of Griggs & Blacic (1965) it is well known that the crystal plastic flow strength of ‘wet’ quartz samples is much lower than that of ‘dry’ samples deformed at the same conditions, and the general effect of water on dislocation creep microstructures has been documented (e.g. Hirth & Tullis 1992), but its effect on the recrystallized grain size has not been quantified. The recrystallized grain size is the most reliable and most easily measurable microstructural feature to derive flow stresses from natural mylonites (e.g. White 1979, Kohlstedt et al. 1980). In a recent experimental study, a well-constrained recrystallized grain size piezometer for quartz (Stipp & Tullis 2003) was calibrated using natural as-is quartzites; the use of a molten salt cell at high confining pressure (1.5 GPa) in a Griggs-type apparatus allowed good stress resolution (Green & Borch 1989). There has been some debate as to whether there is any independent effect of water on the recrystallized grain size piezometer. Two laboratory studies on olivine aggregates (at different pressures) report contradictory results; van der Wal et al. (1993) found that the recrystallized grain size

piezometer is independent of the water content, whereas Jung & Karato (2001) observed a water-dependence of the piezometer.

In this study, we have investigated changes in the recrystallized grain size and other deformation microstructures of quartz within dislocation creep regimes 2 and 3 of Hirth & Tullis (1992). Deformation experiments on Black Hills quartzite with three different initial water contents (as-is, water-added and vacuum-dried) were carried out in order to evaluate the effect of water on the recrystallized grain size / flow stress piezometer. Samples were deformed in axial compression at temperatures of 750° to 1100°C, strain rates between $2 \times 10^{-7} \text{ s}^{-1}$ and $2 \times 10^{-4} \text{ s}^{-1}$ and strains up to 46% using a molten salt assembly in a Griggs apparatus. An increase of the initial water content at otherwise constant deformation conditions caused a decrease in flow stress, an effect known as hydrolytic weakening. The total water content of the starting material was analyzed by Karl Fischer Titration (KFT) and Fourier Transform Infrared (IR) spectroscopy, and quenched samples were analyzed microstructurally and by IR. Changes in the dynamic recrystallization microstructure correlate with changes in flow stress, but there is no independent effect of temperature, strain rate or water content. IR absorption spectra of the deformed samples indicate that different water contents were maintained in the three sample sets throughout the experiments. For quantitative determination of the water content in the deformed samples a new IR calibration was developed, based on KFT analysis of the starting material.

A comparison with previously used

¹ Geologisches Institut, Universität Freiburg, Albertstr. 23b, D-79104 Freiburg ² Department of Geological Sciences, Brown University, PO Box 1846, Providence, USA ³ Institut für Mineralogie, Universität Hannover, Callinstraße 3, D-30167 Hannover

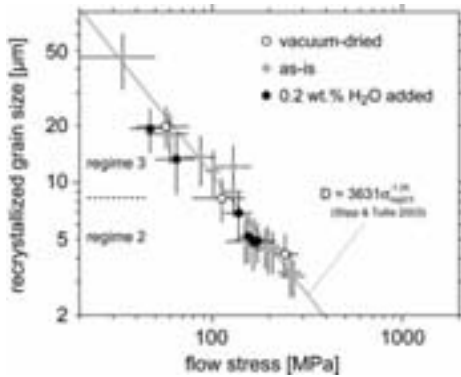


Figure 1: Recrystallized grain size/flow stress data from the water-added, as-is and vacuum-dried samples plotted together with the least squares fit calibration of the recrystallized grain size piezometer of dislocation creep regimes 2 and 3 (Stipp & Tullis 2003, equation is indicated).

IR calibrations (e.g. Paterson 1982) demonstrates that the latter systematically underestimate the water content of Black Hills quartzite. Only relative differences in water content within a sample set are reliable when solely using these previous IR calibrations. However, relative differences within the sample set indicate that the amounts of water measured within the vacuum-dried ($\sim 260 \pm 40$ ppm H_2O), the as-is ($\sim 340 \pm 50$ ppm H_2O) and the water-added ($\sim 430 \pm 110$ ppm H_2O) samples are significantly smaller than the initial content of the quartzite ($\sim 640 \pm 50$ ppm H_2O , each with our IR calibration). We assume that this initially puzzling result was caused by a redistribution of the water content during experimental deformation and/or during IR sample preparation. Decrepitation of aqueous fluid inclusions and transport of the water via microcracking or dislocation pipe

diffusion are presumed to produce an increase of the free fluid phase along the grain boundaries, which probably controls water fugacity and flow stress during the experiments. The differences in water content before and after the experiments can largely be explained by loss of water during IR sample preparation. Initial differences in water content between the three sample sets were maintained during experimental deformation. A comparison of the three sample sets shows that vacuum-dried as well as water-added samples have the same recrystallized grain size/flow stress relationship as the piezometer determined for as-is samples by Stipp & Tullis (2003). Hence, no independent effect of water on the piezometric relationship has been detected (Fig. 1; Stipp et al., in press), and paleostress estimates on natural mylonites need not consider differences in water content when applying the recrystallized grain size piezometer of quartz.

References

- Green HW II & Borch RS (1989) A new molten-salt cell for precision stress measurement at high pressure. *Eur. J. Mineral.* 1, 213–219
- Griggs DT & Blacic JD (1965) Quartz: Anomalous weakness of synthetic crystals. *Science* 147, 292–295
- Hirth G & Tullis J (1992) Dislocation creep regimes in quartz aggregates. *J. Struct. Geol.* 14, 145–159
- Jung H & Karato S-I (2001) Effects of water on dynamically recrystallized grain-size of olivine. *J. Struct. Geol.* 23, 1337–1344
- Kohlstedt DL & Weathers MS (1980) Deformation induced microstructures, paleopiezometers and differential stresses in deeply eroded fault zones. *J. Geophys. Res.* 85, 6269–6285
- Paterson MS (1982) The determination of hydroxyl by infrared-absorption in quartz, silicate-glasses and similar materials. *Bull. Mineral.* 105, 20–29

- Stipp M & Tullis J (2003) The recrystallized grain size piezometer for quartz. *Geophys. Res. Lett.* 30(21), 2088, doi:10.1029/2003GL018444
- Stipp M, Tullis J & Behrens H (in press) The effect of water on the dislocation creep microstructure and flow stress of quartz, and implications for the recrystallized grain size piezometer. *J. Geophys. Res.*
- van der Wal D, Chopra P, Drury M & Fitz Gerald J (1993) Relationship between dynamically recrystallized grain size and deformation conditions in experimentally deformed olivine rocks. *Geophys. Res. Lett.* 20, 1479–1482
- White S (1979) Grain and sub-grain size variations across a mylonite zone. *Contrib. Mineral. Petrol.* 70, 193–202

Magnetische Suszeptibilitätsmessungen an Gängen vom Ostrand des Hauzenberger Granitplutons — Bayerischer Wald

Poster

Verena Streit¹ Helga de Wall¹ Carlo Dietl²

Einführung

Am Ostrand des Hauzenberger Plutons im südlichen Bayerischen Wald treten Ganggesteine auf, die spät- bis postvariskische Granitoide und ihre Rahmengesteine (anatektische und diatektische Gneise) durchschlagen. Die Intrusion der Gänge wurde auf 307 Ma datiert (Siebel, pers. comm.). Sie stellen somit das jüngste magmatische Ereignis mit deutlichem zeitlichen Hiatus

¹ Institut für Geologie, Julius-Maximilians-Universität Würzburg, Pleicherwall 1 D-97070 Germany ² Geologisch-Paläontologisches Institut, Johann-Wolfgang-Goethe-Universität Frankfurt am Main, Senckenberganlage 32-34 D-60054

zur Platznahme der Granitplutone des Bayerischen Waldes zwischen 316 und 324 Ma (Propach 2000) dar. Die Hauptverbreitung dieser Ganggesteine liegt in einem herzynisch verlaufenden Zug von Oberndorf im Nordwesten über Waldkirchen zum Oberfrauenwald und weiter nach Wegscheid im Südosten. Die Gänge streichen in den zwei Hauptrichtungen WNW–ESE (etwa 140°), also in etwa parallel zum Bayerischen Pfahl, sowie annähernd N–S (etwa 170°). Die Gänge stehen generell saiger und haben Mächtigkeiten von wenigen dm bis zu 15 m.

Ergebnisse

An 14 Gängen wurden im Gelände und Labor die magnetische Suszeptibilität gemessen. Im Gelände wurden dabei Gangprofile mit einem tragbaren Kappameter (KT-6, Geofyzica Brno) registriert. Im Labor wurde neben der Volumenssuszeptibilität auch die Anisotropie der magnetischen Suszeptibilität (AMS) mit einer Kappabrücke KLY-4S (AGICO, Brno) bestimmt.

Die Suszeptibilitätswerte zeigen starke Schwankungen im Wertebereich von 10^{-4} bis 10^{-2} SI. Träger der magnetischen Suszeptibilität ist in den ferromagnetischen Proben (10^{-2} SI) Magnetit, in den paramagnetischen Proben (10^{-4} SI) ist Biotit/Hornblende für die Suszeptibilität verantwortlich. Bei den Gangprofilen fällt eine starke Variation der Werte innerhalb der einzelnen Gänge auf. Dabei können folgende Fälle unterschieden werden (Abb. 1):

- i) geringe Suszeptibilitätswerte am Gangrand und Anstieg zum Zentrum hin;
- ii) hohe Suszeptibilitätswerte am Gangrand und Abfall zum Zentrum hin;

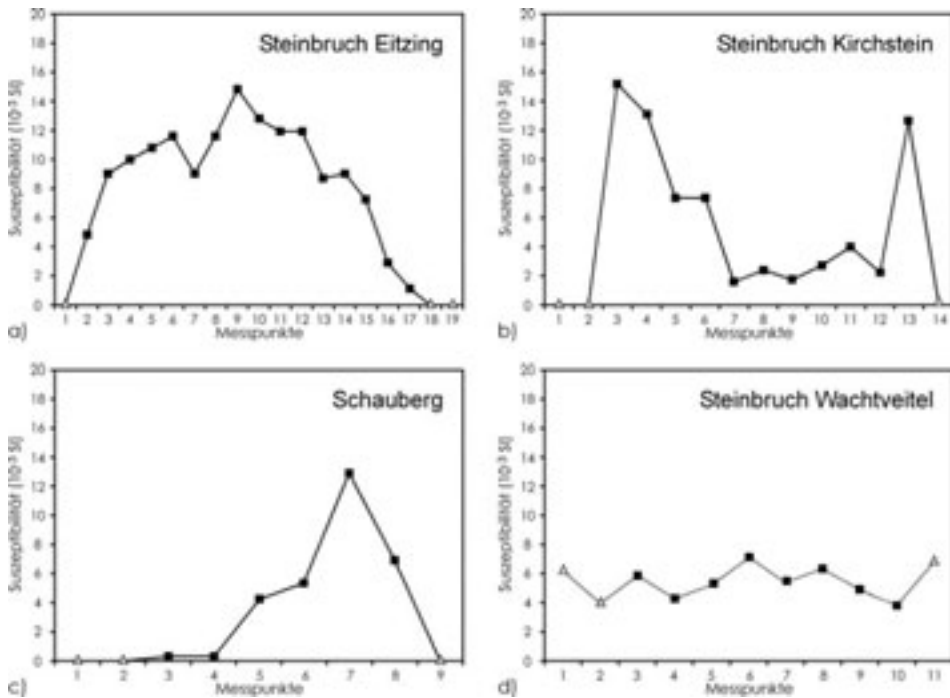


Abbildung 1: Suszeptibilitätsschwankungen an Gangprofilen, gemessen mit einem Handkappameter, Dreiecke repräsentieren Messungen in dem Nebengestein, Messungen an den Gängen sind durch Quadrate dargestellt.

- iii) bei einem Gang steigen die Suszeptibilitätswerte von einer Gangseite zur anderen kontinuierlich an;
- iv) nur wenige Gänge zeigen ein konstantes Suszeptibilitätsprofil.

Variationen der Suszeptibilität in Gangprofilen werden in der Literatur mehrfach beschrieben und können auf unterschiedliche Ursachen (Korngrößeneffekte durch Abschreckung, Alterationseffekte) zurückgeführt werden.

Messungen der AMS reflektieren generell die Ganggeometrie. In 27 Proben steht k_{min} senkrecht zur Gangwand (normales Gefüge). In nur drei Proben steht k_{max} senkrecht zur Gangwand (inverses Gefüge). Bemerkenswert ist ei-

ne für Ganggesteine relativ hohe Anisotropie, die bis hin zu Werten von $P' = 1,15$ reicht. Während in Proben mit niedrigen Anisotropien (P' kleiner als 1,05) die Geometrie des magnetischen Gefüges von prolat bis oblat variiert, haben Proben mit höheren Anisotropien generell oblate Gefüge. Sowohl bei konventioneller Interpretation (magnetische Lineation liegt parallel der Transportrichtung, z.B. Ellwood 1978) als auch bei Anwendung der von Geoffroy et al. (2002) vorgeschlagenen Schnittgeometrie von planaren Gefügen, ergeben sich stark variierende horizontale bis vertikale Magmaffiefrichtungen.

Literatur

- Ellwood B B (1978) Flow and emplacement direction determined for selected basaltic bodies using magnetic susceptibility anisotropy. *Earth Planet. Sci Lett* 41, 254–264
- Geoffroy L, Callot J P, Aubourg C & Moreira M (2002) Magnetic and plagioclase linear fabric discrepancy in dykes: a new way to define the flow vector using magnetic foliation. *Terra Nova* 14, 183–190
- Propach G, Baumann A, Schulz-Schmalschlager M & Grauert B (2000) Zircon and monazite ages of Variscan granitoid rocks and gneisses in the Moldanubian zone of eastern Bavaria, Germany. *N. Jb. Geol. paläont. Mh.* 2000, 345–377

Kinematic 3D Retro-Deformation of Fault Blocks Picked from 3D Seismics

Poster

David C. Tanner¹ Tina Lohr² Charlotte M. Krawczyk² Onno Oncken² Heike Endres³ Ramin Samiee³ Henning Trappe³ Peter A. Kukla⁴

Introduction

Movement on fault planes causes a large amount of smaller-scale deformation, ductile or brittle, in the area surrounding the fault. Much of this deformation is below the resolution of reflection seismics (i.e. sub-seismic, <10m displacement), but it is important to determine this deformation, since it can make up a large portion of the total

¹ Geowissenschaftliches Zentrum der Georg-August-Universität Göttingen, Abteilung Strukturgeologie und Geodynamik, Goldschmidtstr. 3, D-37077 Göttingen
² GFZ Potsdam, Telegrafenberg, D-14473 Potsdam
³ TEEC, Burgwedelerstr. 89, D-30916 Isernhagen
⁴ RWTH Aachen, Geol. Institut, Willnerstr. 2, D-52056 Aachen

bulk strain, for instance in a developing sedimentary basin. Calculation of the amount of sub-seismic strain around a fault by 3-D geometrical kinematic retro-deformation can also be used to predict the orientation and magnitude of these smaller-scale structures. However, firstly a 3-D model of the fault and its faulted horizons must be constructed at a high enough resolution to be able to preserve fault and horizon morphology with a grid spacing of less than 10m. Secondly, the kinematics of the fault need to be determined, and thirdly a suitable deformation algorithm chosen to fit the deformation style. Then by restoring the faulted horizons to their pre-deformation state (a ‘regional’), the moved horizons can be interrogated as to the strain they underwent. Since strain is commutative, the deformation demonstrated during this retro-deformation is equivalent to that during the natural, forward deformation.

Working area

Our working area is located within the northern part of the Lower Saxony Basin. This structural unit is a part of the post-Variscan Central European Basin System. We use 3-D, depth-converted, reflection seismics provided by RWE-DEA AG, Hamburg for this investigation. The seismic database covers an area of ca. 15 × 10 km² and extends down to 7.5 km depth. This is deep enough to reveal the subcrop of Upper Carboniferous and stratigraphically-higher strata.

Construction of a 3-D model

Our particular interest is the Rotliegend strata of this area. The Rotliegend

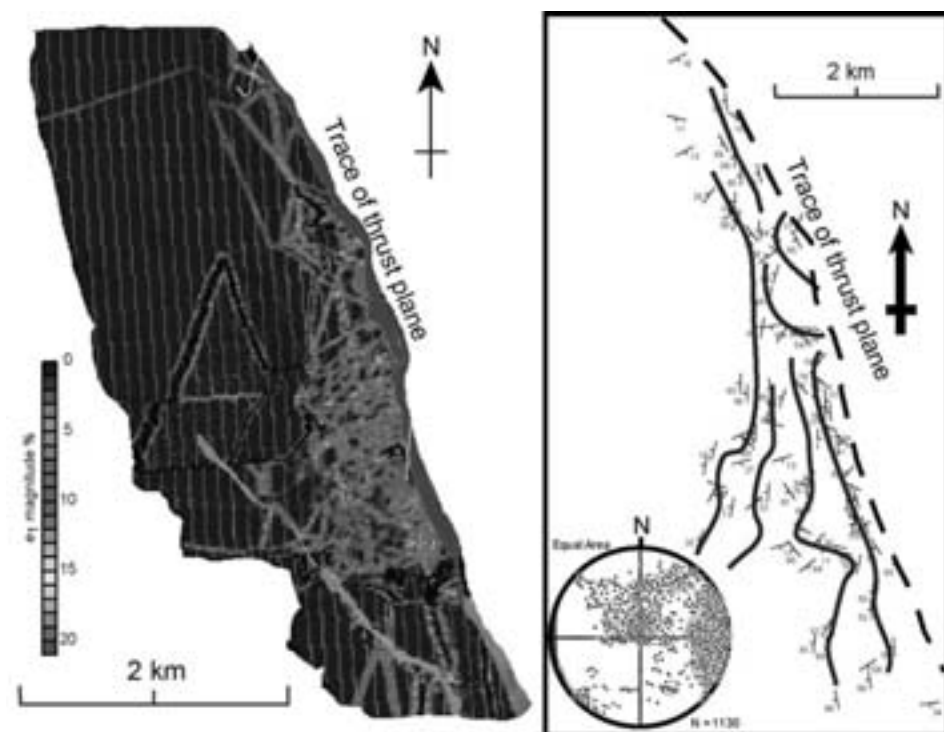


Figure 1: Left: Map view of the hanging-wall of a Rotliegend thrust after retro-deformation, colour-coded for magnitude of the major strain (e_1). Lighter greys are higher strain. Right: Map view of the hanging-wall of the thrust after retro-deformation, showing trajectories (and dip and strike data) of the e_2 - e_3 plane, and thus the expected orientation of extensional fractures, caused by thrusting. Insert shows lower hemisphere, equal-area stereonet of poles to the e_2 - e_3 planes.

mainly consists of aeolian and fluvial sandstones, which form an onshore hydrocarbon play. The Top Rotliegend surface lies between 4.5 and 5.7 km depth in the studied area. First, the Top Rotliegend surface was picked at a high resolution, as were fault surfaces which displaced Top Rotliegend and lower strata. Displacement of the Top Rotliegend varies from 0–250 m, mainly caused by normal faulting. These surfaces were then gridded in GoCAD, and then transferred to the Midland Valley software package 3DMove for retro-

deformation.

Retro-deformation

For retro-deformation modelling we used the algorithms ‘inclined shear’ for normal faults and ‘fault-parallel flow’ for reverse faults, respectively. In the former, the hanging-wall volume of a fault is sheared at an oblique angle to the fault surface, and thus strain is directly attributable to fault curvature. In the latter method, all horizon surface nodes move parallel to the fault surface (as the name suggests), and therefore

strain is also related to fault curvature. Figure 1 demonstrates an example of retro-deformation (using the ‘fault-parallel flow’ algorithm) of a thrust within the Rotliegend, and shows the strain tensor values and orientations which occurred in the surrounding strata. We propose the values of the strain tensor, and thus the magnitude of the strain, are equivalent after retro- or forward deformation. For this example, the e_1 -magnitude ranges from 0–20%, but the highest strain intensities are constrained to within 700 m of the fault generally, and up to 1 km locally (Fig. 1). We propose that the e_1 -magnitude can be correlated to the density, and that the e_2 – e_3 plane can be correlated to the orientation, of small-scale structures.

Acknowledgements We thank RWE-DEA AG, Hamburg for allowing us to use their 3D seismic database and borehole data for this project. The project is part of the DFG SPP 1135; we acknowledge DFG grants TA 427/1 and KR 2073/1.

Two-dimensional finite element models of convective heat transfer in the upper crust — implications for the interpretation of fission-track data

Poster

Zoltan Timar-Geng¹ Andreas Henk¹
 Andreas Wetzel²

Fission-track (FT) thermochronology is a tool routinely used for studies of surface denudation because of its sensitivity to the low temperatures found in the uppermost part of the crust. FT ages and associated track length distributions are regularly interpreted assuming a steady-state temperature field and only conductive heat transfer. However, application of the method to thermochronological studies based on such interpretations may lead to invalid conclusions, if the temperatures at a certain depth had actually varied with time. For example, the convective transfer of heat by hydrothermal fluids can cause transient thermal events within the upper crust. In particular, fluid circulation along fault zones can result in substantial convective heat transport and cause temperature anomalies in the adjacent rocks (Zuther & Brockamp 1988, Fleming et al. 1998, Lampe & Person 2002, Bächler et al 2003). As a consequence, any refined interpretation of FT data requires a thorough understanding of the upper crustal temperature field and its evolution through time.

The main objective of this study is to assess quantitatively how convective heat transport influences the upper crustal

¹ Geologisches Institut, Universität Freiburg, Albertstr. 23b, D-79104 Freiburg

² Geol.-Paläont. Institut, Universität Basel, Bernoullistr. 32, CH-4056 Basel

temperature field as well as the cooling ages and track length distributions observed in apatite FT data. Modelling utilizes Finite Element techniques and the software FEFLOW, respectively. In-depth parameter studies (including fault geometry, erosion rate, hydraulic potential, hydraulic and material properties) are conducted on two-dimensional (cross-sectional) models of fault zones. After evaluating the relative importance of different variables relevant to fluid circulation in a palaeogeothermal system, the time-temperature (tT) histories of particle points are tracked as erosion moves them closer to surface. These tT-paths are used in a forward modelling approach to determine the expected FT age and track length distributions. For each parameter study, a corresponding set of FT parameters is produced, thus, providing a catalogue of FT ages and track length distributions, which will help to interpret real data sets.

One of the goals of the project is to investigate the regional impact of convective heat transport on the interpretation of FT data and other thermal data from the Black Forest (SW-Germany). The modelling techniques outlined above will be applied to field data from the Baden-Baden and Offenburg troughs in the northern and central Black Forest.

References

- Bächler D, Kohl T & Rybach L (2003) Impact of graben-parallel faults on hydrothermal convection; Rhine Graben case study. *Phys. Chem. Earth*, 28, 431–441
- Fleming CG, Couples GD & Hazeldine RS (1998) Thermal effects of fluid flow in steep fault zones. In: Jones G, Fisher QJ & Knipe RJ (eds) *Faulting, fault sealing and fluid flow in hydrocarbon reservoirs*. *Geol. Soc. London, Spec. Publ.* 147, 217–229
- Lampe C & Person M (2000) Episodic hydrothermal fluid flow in the Upper Rhine-graben (Germany). *Journal of Geochemical Exploration*, 69/70, 37–40
- Zuther M & Brockamp O (1988) The fossil geothermal system of the Baden-Baden trough (Northern Black Forest, Germany). *Chem. Geol.* 71, 337–353

Microstructural evidence of impact-induced crystal-plastic deformation and post-shock annealing of quartz

Vortrag

Claudia A. Trepmann¹

John G. Spray²

Introduction

During impact, rocks at the surface and accessible depths encounter extreme conditions. The hydrostatic component of the shock wave-associated stress, the so-called shock pressure, can reach several tens of GPa in the central part of the structure. The shock pressure can cause the transformation of target minerals into their high pressure modifications or amorphous phases. The role of the deviatoric component of the shock wave-associated stress during shock-metamorphism is only poorly understood. Shock effects in quartz are particularly useful for providing information on the conditions during deformation, given the widespread occurrence of this mineral in the Earth's

¹ Institut für Geologie, Mineralogie und Geophysik, Ruhr-Universität Bochum, Germany, Collaborative Research Center 526 ² Planetary and Space Science Centre, Department of Geology, University of New Brunswick, Canada

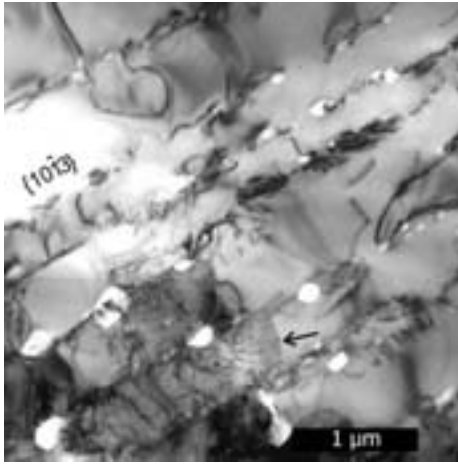


Figure 1: Bright field TEM micrograph showing rhombohedral PDFs that comprise dislocations and fluid inclusions.

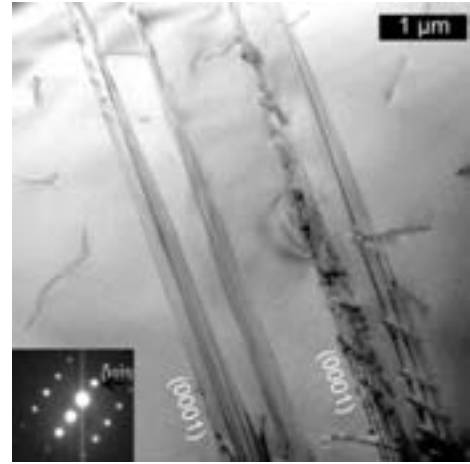


Figure 2: Bright field TEM micrographs showing inclined Brazil twin boundaries in (0001) representing basal PDFs. Note partial dislocations within the boundaries.

crust and its comprehensive experimental calibration. Two distinct types of quartz microstructure in charnockitic target rocks and quartz veins of the Charlevoix impact structure are compared and contrasted in order to distinguish shock-induced microstructures that indicate a high hydrostatic stress component of the shock wave-associated stress from those that indicate a high deviatoric component, as well as associated microstructures that were generated during post-shock relaxation.

Type 1 microstructure

The dominant shock effects in the type 1 microstructure in charnockites at ca. 2–4 km from the centre of the structure are planar deformation features (PDFs) parallel to rhombohedral planes of quartz. The rhombohedral PDFs comprise a high density of dislocations and fluid inclusions, as revealed by transmission electron microscopy (TEM) (Fig. 1). They have

been interpreted as the result of water-assisted, post-shock crystallisation of the amorphous phase along rhombohedral planes, initially generated during shock compression (e.g. Goltrant et al. 1992, Leroux et al. 1994, Leroux & Doukhan 1996). The abundance of different sets of these PDFs indicates a high hydrostatic component of the shock wave-associated stress (ca. 10–15 GPa). Evidence of crystal-plastic deformation due to high deviatoric stresses is absent. Post-shock recovery is indicated by the actual microstructure of rhombohedral PDFs, dislocations in climb configuration and well-ordered low angle grain boundaries.

Type 2 microstructure

In contrast, PDFs parallel to the basal plane are predominant in the type 2 microstructure developed in rocks at ca. 4–9 km from the centre of the structure, whereas rhombohedral PDFs are rare.

This indicates a lower hydrostatic stress component (ca. 7–8 GPa) compared to the type 1 microstructure, which correlates with a radial decrease in recorded peak shock pressure. The basal PDFs are revealed by TEM to represent mechanical Brazil twins (Fig. 2), which give evidence for crystal-plastic deformation at high deviatoric stresses. In the type 2 microstructure, numerous deformation bands, strong undulose extinction and cataclastic zones at the optical scale, as well as glide-dislocations and microcracks at the TEM scale, occur in association with basal PDFs, and are therefore also interpreted to be shock-induced. Post-shock recovery is indicated by the occurrence of small elongate subgrains with low angle grain boundaries paralleling low-index planes.

Conclusions

Although mechanical Brazil twins in the basal plane are common in naturally-shocked quartz (e.g. Goltrant et al. 1991, Leroux et al. 1994), shock-induced crystal-plastic deformation of quartz is generally considered to be ineffective due to the high rates of loading during shock (e.g. Langenhorst 1994). However, the type 2 microstructure records highly heterogeneous and localised glide-controlled deformation accompanied by twinning and microcracking. Glide-controlled deformation of quartz is characteristic of high stress and strain rate conditions, e.g. during co-seismic loading (Trepmann & Stöckhert 2003). Therefore, this crystal-plastic deformation is interpreted to be due to high deviatoric stresses and high loading rates during shock.

The dominant occurrence of rhombohedral PDFs in the type 1 microstructure, in contrast to their rare occurrence in

the type 2 microstructure in combination with the abundance of mechanical Brazil twins, indicates that the deviatoric component of the shock wave-associated stress increases relative to the hydrostatic component with increasing distance from the centre of the impact structure. This relationship has also been reported from other impact structures (Leroux et al. 1994; Leroux & Doukhan 1996).

Post-shock recovery is indicated in the type 1 microstructure by the actual microstructure of rhombohedral PDFs, dislocations in climb configuration and well-ordered low angle grain boundaries, as well as in the type 2 microstructure by the occurrence of small elongate subgrains with low angle grain boundaries paralleling low-index planes. This has probably taken place during annealing shortly after the impact event at quasi-static conditions and still sufficiently high post-shock temperatures, rather than during a separate regional thermal event.

References

- Goltrant O, Cordier P & Doukhan J-C (1991) Planar deformation features in shocked quartz; a transmission electron microscopy investigation: *Earth Planet. Sci. Lett.* 106, 103–115
- Goltrant O, Leroux H, Doukhan J-C & Cordier P (1992) Formation mechanisms of planar deformation features in naturally shocked quartz. *Phys. Earth Planet. Inter.* 74, 219–240
- Langenhorst F (1994) Shock experiments on pre-heated quartz: II. X-ray and TEM investigations. *Earth Planet. Sci. Lett.* 128, 683–698
- Leroux H & Doukhan J-C (1996) A transmission electron microscope study of shocked quartz from the Manson impact structure. in 'The Manson Impact Structure, Iowa: Anatomy of an Impact Crater', C Koerber, RR Anderson, (eds) Boulder, Colorado, Geol. Soc. Am. Spec. Paper 302, 267–274

- Leroux H, Reimold WU & Doukhan J-C (1994)
A TEM investigation of shock metamorphism in quartz from the Vredefort dome, South Africa. *Tectonophysics* 230, 223–239
- Trepmann CA & Stöckhert B (2003) Quartz microstructures developed during non-steady state plastic flow at rapidly decaying stress and strain rate. *J. Struct. Geol.* 25: 2035–2051

Quartz microstructures in nature and experiment — evidence of rapid plastic deformation and subsequent annealing

Poster

Claudia A. Trepmann¹ Bernhard Stöckhert¹ Dorothée Dorner² Martina Küster¹ Klaus Röller¹

Quartz microstructures produced in short-term deformation and annealing experiments are compared with those in naturally deformed vein quartz in cores from the Long Valley Exploratory Well (Long Valley Caldera, California). The experiments are designed to simulate

- i) co-seismic deformation of quartz in the uppermost plastosphere and
- ii) annealing during post-seismic stress relaxation.

The experiments are performed in a modified Griggs type solid medium apparatus. Natural polycrystalline quartz samples (grain size on the order of millimetres) are deformed at a temperature of 400°C, a confining pressure of 2 GPa,

¹ Institut für Geologie, Mineralogie und Geophysik, Ruhr-Universität Bochum, Germany, Collaborative Research Center 526 ² Max-Planck-Institut für Eisenforschung, Düsseldorf, Germany

and strain rates of ca. 10^{-4} s^{-1} . The differential stress reaches 2–4 GPa and the irreversible axial shortening is typically a few percent. In some experiments the samples have subsequently been annealed for ca. 14–15 h at elevated temperatures of 800–1000°C and low stresses (quasi-hydrostatic or non-hydrostatic conditions). The confining pressure has been chosen to keep the sample in the stability field of α -quartz. The samples, which have not been annealed after deformation, show deformation bands that are characterised by a crystallographic misorientation of up to 25° to the host quartz grain. The deformation bands vary in thickness and can grade into fractures. Transmission electron microscopy reveals a high density of straight dislocations arranged into subparallel arrays in the vicinity of a deformation band. The density of free dislocations decreases with distance from the deformation band. Microstructures in deformed samples annealed at 900–1000°C and quasi-hydrostatic conditions are characterised by strings of isometric grains with a diameter of ca. 10–50 μm that show no crystallographic preferred orientation. In one experiment, in which the sample has been annealed at non-hydrostatic conditions subsequent to deformation, shear zones have developed that are characterised by elongate, small grains with a diameter of up to 30 μm . The grains are preferentially oriented with their $\langle c \rangle$ axes in a plane perpendicular to the shear zone. These shear zones are interpreted to have formed during deformation at non-hydrostatic annealing with dynamic recrystallisation. In contrast, the strings of isometric grains in the experiments with quasi-hydrostatic annealing are suspected to be due to static

recrystallisation from a highly damaged zone generated during high-stress deformation, as observed in the non-annealed samples. These microstructures compare well with those observed in naturally deformed vein quartz from the Long Valley Exploration Well, with independent evidence of episodic deformation due to co-seismic loading. Comparison of experimental and natural record provides insight into processes, conditions, length and time scales characteristic for the episodic loading and relaxation in the middle crust driven by seismic activity in the upper crust. Such insight may be crucial for the appropriate inversion of geodetic results and the interpretation of aftershocks.

Neutron time-of-flight texture measurements in Dubna: Status and developments

Vortrag

Klaus Ullemeyer¹ Jan H. Behrmann¹

Introduction

The multidetector texture diffractometer SKAT (from Russian: *Spektrometer Kolitshestvennovo Analiza Tekstury*) at the pulsed reactor IBR-2 in Dubna, Russia, started operation in March 1997 and is open for users from all countries. Application of time-of-flight (TOF) diffraction to texture measurements offers the opportunity to record complete diffraction patterns, i.e., to measure several pole figures simultaneously (Fig. 1(a)). To allow high spectral resolution for measurements on

¹ Geologisches Institut, Universität Freiburg, Albertstr. 23B, D-79104 Freiburg

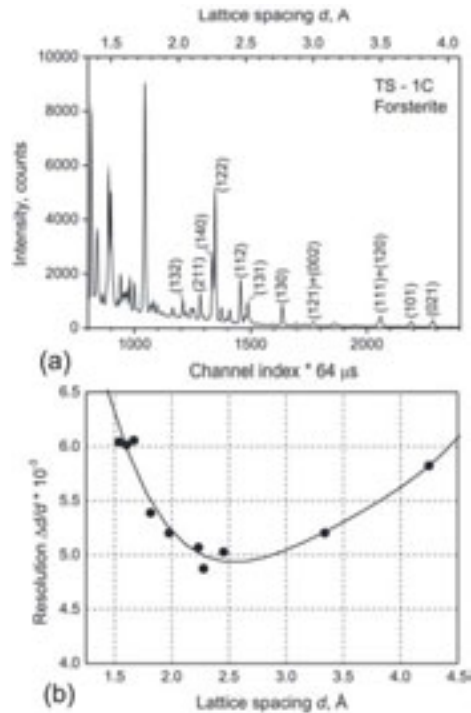


Figure 1: (a) Time-of-flight diffraction pattern of olivine (forsterite). Some Bragg reflections are indicated. (b) Best possible experimental resolution $\Delta d/d$, determined on quartz powder sample.

polyphase geological samples with many diffraction patterns, the instrument was placed at the end of an over 100 m long flight path. In this paper, we will summarize advantages and disadvantages of the SKAT, as well as intended improvements.

Characteristics of the SKAT — advantages and disadvantages

The main characteristics of the SKAT are as follows (Ullemeyer et al. 1998, Fig. 2):

- 19 detector modules are arranged around the incident neutron beam

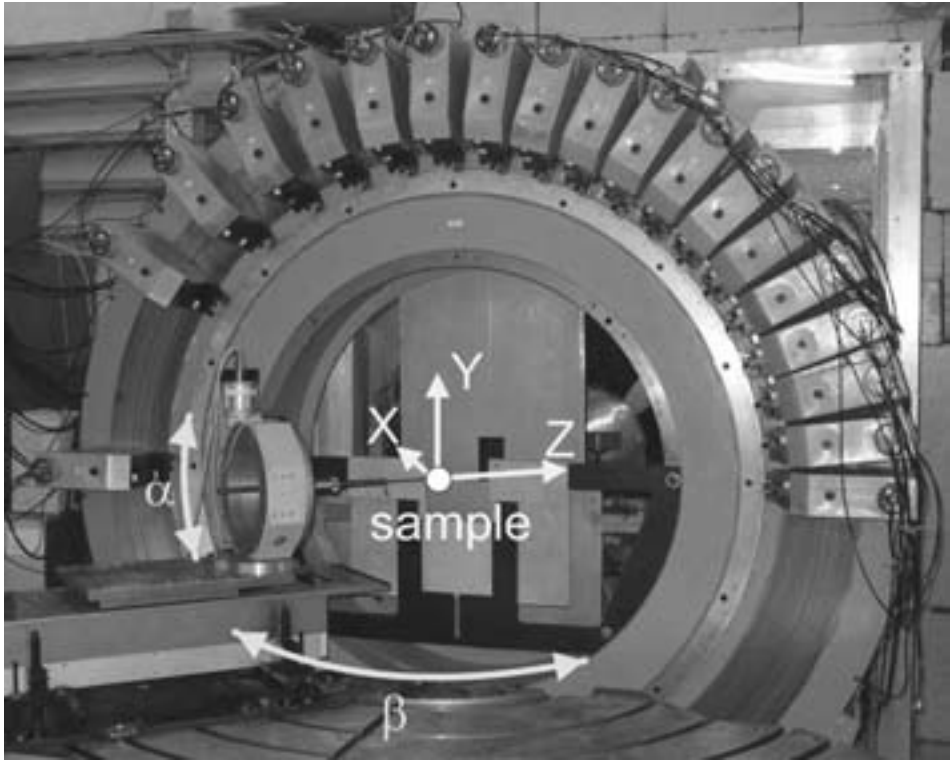


Figure 2: Photograph of the SKAT. Planned sample motions around X (α) and Y (β) are indicated.

- at a unique angle of $2\Theta = 90^\circ$. Particular Bragg peaks are assigned to one and the same neutron wavelength λ , hence, all λ and Θ dependent intensity corrections may be avoided.
- The sample is positioned in the centre of the detector ring and rotated around an horizontal axis Z at an angle of 45° with respect to the incident neutron beam. Supposing that the detector modules include an angular range of 180° , complete pole figures may be measured by a single sample revolution (measurements are fast).
 - The goniometer angle of 45° allows installation of axial symmetric sample environment with minimum restrictions to the incident and diffracted beams.
 - Due to the long flight path, high resolution may be achieved by collimation of the diffracted beam (Fig. 1 (b)).
 - The beam cross section of $50 \times 85 \text{ mm}^2$ allows application of large sample volumes.
- Although the SKAT is well-suited for the measurement of bulk textures on geological samples, restrictions are valid.

Due to the pulse repetition rate of 5 Hz at the IBR-2 reactor, the maximum accessible lattice spacing d_{max} is restricted to about 4.9 Å. This may be sufficient for texture analyses even on three-phase samples (e.g., carbonate rocks consisting of calcite + dolomite + quartz). On the other hand, successful texture analysis may be hampered (e.g., in case of ultrabasic rocks or phyllosilicate-bearing gneisses).

Intended upgrading of the SKAT

Expansion of accessible d -range improves the possibilities for texture measurements. From Bragg's law,

$$\lambda = 2d \sin \Theta$$

and invariability of λ follows that expansion of d_{max} may be achieved by decrease of 2Θ only. We consider construction of a second detector system with $2\Theta = 65^\circ$, keeping the old detector system for alternative use. Accessible d -range extends to about 6.5 Å, allowing access to more non-overlapped Bragg reflections. Inevitable deterioration of resolution $\Delta d/d$ by about 15–20% (compare to Fig. 1(b)) appears to be acceptable. In addition, the scanning possibilities will be improved by two more sample rotations around an horizontal and a vertical axis, respectively (Fig. 2). Thus, the recording of orientational data even for alternative methods of quantitative texture analysis (Bernstein et al. 2005) will be possible. Upgrading of the SKAT is scheduled contemporaneously with modernization of the IBR-2 reactor (2007–2009).

Acknowledgements Operation of the SKAT is supported by the German Ministry of Education and Research

through grant 03DU03FB. Valuable support of the Frank Laboratory of Neutron Physics – Joint Institute of Nuclear Research (Dubna) is also gratefully acknowledged.

Literatur

- Bernstein S, Hielscher R & Schaeben H (2005) The Generalized Spherical Radon Transform and Its Application in Texture Analysis. Preprint 2005-2, Fakultät für Mathematik und Informatik, TU Bergakademie Freiberg
- Ullemeyer K, Spalhoff P, Heinitz J, Isakov NN, Nikitin AN & Weber K (1998) The SKAT texture diffractometer at the pulsed reactor IBR-2 at Dubna: experimental layout and first measurements. Nucl Instr Meth Phys Res A412, 80–88

Neotectonics in the Swiss Alps — A late Alpine to post-glacially active fault at the Gemmi Pass Vortrag

Michaela Ustaszewski¹ Adrian Pfiffner¹ Marco Herwegh¹

Introduction

The area of the central and western Swiss Alps reveals not only the highest uplift rates of Switzerland (1.5 mm a⁻¹ near Brig, Schlatter & Marti 2002), but also shows a strong concentration of earthquakes (e.g. Deichmann et al. 2004). This raised the question, whether the region hosts any linear topographic expressions that can be attributed to motion along potentially seismogenic faults. The area was therefore chosen for the investigation of

¹ Institute of Geological Sciences, University of Bern, Baltzerstrasse 1–3, CH-3012 Bern, Switzerland

postglacially active lineaments. Firstly, aerial photographs from the entire area were searched for linear features, which could be of gravitational or tectonic origin. Subsequently, selected lineaments were visited in the field to study their origin. We found scarce but positive evidence for neotectonic fault movements. One particular lineament that exhibited the most promising exposures was investigated in greater detail. This lineament is a prominent NW–SE striking fault located at the Gemmi Pass, runs perpendicularly to the regional fold axes and cuts through the Helvetic nappe stack. The position and orientation of the fault discounts gravitational reactivation. A close examination of the fault rocks reveals a long term evolution of this fault starting already at a late stage of Alpine nappe emplacement and related deformation.

Late Alpine deformation

The fault is characterized by a high density of fault-parallel joints and veins, which become less abundant away from the fault zone. Initially the fault originated as a–c joints forming an array with variable widths of 10–20 m. With progressive deformation, the joints connected in the center of the array generating a major 1–3 m wide large-scale fault zone. Deformation associated dilatancy and the presence of a fluid resulted in filling of the newly formed cavities by calcite. Cathodo-luminescence on the vein filling shows zonation and subsequent disruption by brittle deformation as is indicated by the existence of discrete cataclastic areas. Several cycles of veining and brittle deformation can be observed. Changes in cathodofacies suggest variations in fluid chemistry pointing to episodic fluid pulses.

The youngest deformation features in these fault rocks are micro-scale faults impregnated by iron-hydroxide bearing minerals. Kakirites are absent, which suggests that they have a low preservation potential in carbonate rocks. This could be due to syndeformational dissolution of the fine grained fault gouge, or recent erosion.

Postglacial deformation

The fault crosses a small (ca. 60 × 30 m) postglacial, sediment-filled depression, which was targeted for a large trench (15.4 m long, 2 m wide and up to 2.2 m deep) in order to verify its postglacial reactivation. The trench bottom reached limestone bedrock almost all along the trench (x in Fig. 1). It delineates a basin, which deepens towards the north-east. The base of the sediment-fill of this depression is made of an up to 1.5 m thick dark brown moraine layer. The moraine material consists partly of lodgment till (h in Fig. 1), partly of transported till (e, f and g in Fig. 1). Large rock boulders (up to 1 m in diameter) were found in the till material. A very constant 20 to 30 cm thick, fine-grained (silt to fine sand fraction), yellow layer, for which the working term ‘loess’ is used (d in Fig. 1), was sedimented on top of the moraine. It has a sharp upper contact, whereas the basal contact to the moraine material is sometimes unclear. This yellow layer delineates the basin form as well. An up to 1.5 m thick grey-brown B horizon (b in Fig. 1) of soil is overlaying the yellow loess layer. It consists of brown fine-grained silt material intercalated by numerous sand and grit lenses, and up to 7 m continuous clay bands, which are up to 5 cm thick (c in Fig. 1). This horizon shows onlap-structures onto the loess at both sides

of the basin. The uppermost 5 to 15 cm are made up by the active soil layer, the A horizon (a in Fig. 1). A cataclastic fault zone disrupts the partly karstified limestone bedrock from meter 6.4 to 6.8 m. This 40 cm wide zone is split in the middle by an open joint or fault plane. No surface displacement was seen on the bedrock surface. Right above this fault zone, the about 50 cm thick moraine layer does not show any disturbances. However, the yellow loess layer, which represents a very continuous horizon in the trench with a clear upper surface, is heavily disrupted, incorporating moraine material from below and displaying flame-like structures and up to 5 cm large vertical displacements at its upper boundary (Fig. 2).

These structures can not be explained by any sedimentary or erosional processes. The overlying B horizon does not seem to be displaced at all, thus sealing the movement. These observations indicate strike-slip kinematics, which would also be favored by the recent stress-field. Samples for OSL-dating of the Loess layer and the B horizon were taken in order to limit the age of the movement.

Conclusion

To summarize, this example of an active fault allows studying active and ancient deformation structures/processes that occurred at shallow and greater depth, respectively. We expect that the episodic cycles of brittle deformation and fluid pulses forming veins and catclasites equivalent to the older structures observed at the surface, were on going at a few kilometers depth during

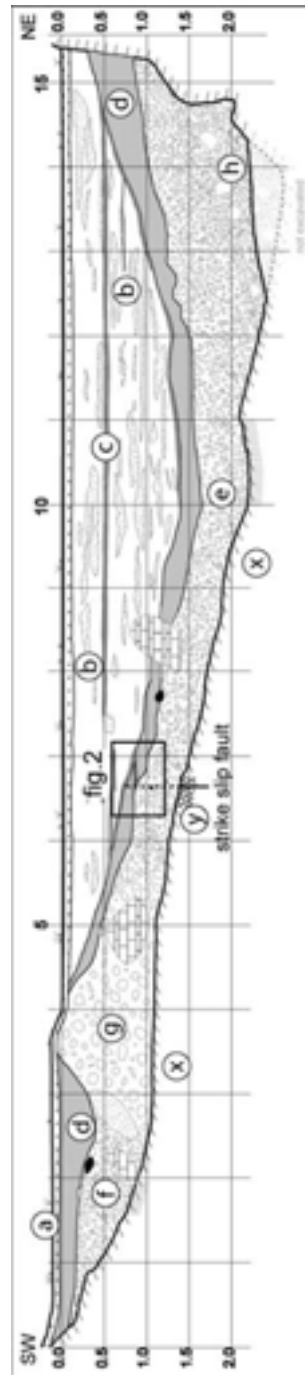


Figure 1: Trench-log. (a — soil horizon A, b — soil horizon B, c — clay bands in soil horizon B, d — fine-grained yellow ‘loess’ layer, e, f + g — transported moraine material, h — lodgment till, x — limestone bedrock, partly karstified, y — cataclastic zone)

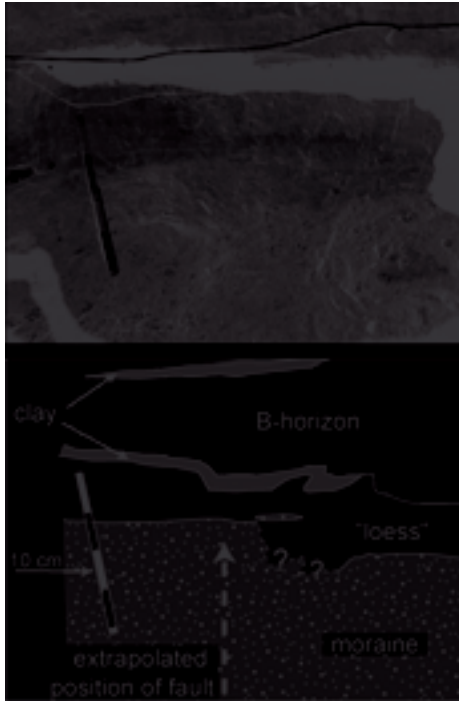


Figure 2: Photo and sketch of a detail of Fig. 1 showing the disrupted zone in the loess layer.

the time of post-glacial activity. Given the regional seismicity pattern we conclude that such veining and cataclasite formation at depth is still recurring and in concert with this earthquake activity.

References

- Schlatter A & Marti U (2002) Neues Landeshoehennetz der Schweiz LHN95. Vermessung, Photogrammetrie, Kulturtechnik 1, 13–17
- Deichmann N, et al. (2004) Earthquakes in Switzerland and surrounding regions during 2003. *Eclogae geologicae Helvetiae* 97-3, 447–458

Discrimination of different volcanic rock units by magnetic properties — geothermal field at Reykjanes peninsula (SW-Iceland) *Poster*

C. Vahle¹ A. Kontny¹ F. Dietze¹
H. Audunsson²

The geothermal field at Reykjanes peninsula is located at the boundary where the submarine Reykjanes Ridge passes over into the rift zone of southwestern Iceland. The geothermal field coincides with a magnetic low in the aeromagnetic anomaly map and is situated within a dense NE–SW fissure and fault zone. Surface geology is characterized by different historic fissure eruptions (youngest from 1226 AD), shield lava (12.5–14.5 ka) and intercalated pillow basalt–hyaloclastite ridges probably formed during the last glacial episode (14.5–20 ka). During a field magnetic study in the vicinity of the geothermal field in summer 2005 different volcanic rock units have been sampled to correlate rock magnetic and magneto-mineralogical properties with magnetic field intensity. Additionally, measurements on a dense dolerite intrusion, recovered from the RN–19 borehole (2245–2248 m depth) in May 2005 within the frame of IDDP, should shed light on the influence of crustal rocks on the total magnetic field intensity.

Generally, the natural remanent magnetization and magnetic susceptibility, measured on rock specimen, is high, ranging between 2.5 and 33.6 A m^{-1} and $2\text{--}37 \times 10^{-3} \text{ SI}$, respectively. The high NRM coincides with the mag-

¹ Geol.-Pal. Institute, Ruprecht-Karls-University, INF 234, 69120 Heidelberg, Germany

² Technical University of Iceland, Hofdabakka 9, 110 Reykjavik, Iceland

netic high outside the geothermal field. The Koenigsberger ratios (Q) are also high (12–132) for all surface samples, indicating the predominance of remanent magnetization. Most of the study area is covered by strongly magnetic Stampahraun (1226 AD) and Skalafell (8–11.5 ka) pahoehoe and block lava stemming from fissure eruptions. The rock magnetic characteristics of these flows are quite similar, whereas the older flow (Skalafell) shows stronger scattering. The pillow lava and especially the picritic Haleyjabunga shield lava show lower NRM intensity and magnetic susceptibility. The NRM of the doleritic dike sample from RN-19 drilling is rather low ($5.4\text{--}8.8\text{ A m}^{-1}$) but susceptibility is high ($32.5\text{--}34.5 \times 10^{-3}\text{ SI}$), indicating large grain sizes, formed during typically slow cooling of an intrusion. First temperature dependent magnetic susceptibility data indicate homogeneous Ti-rich titanomagnetite ($T_c = 60\text{--}240^\circ\text{C}$), pure magnetite ($T_c = 580^\circ\text{C}$) and an irreversible titanomaghemite with T_c at about 450°C in the area of the magnetic low. The occurrence of magnetite and the low-temperature behavior of k_T curves below -150°C indicate exsolution textures typically forming during high-temperature oxidation. Our observation, that high crustal magnetization is related to the youngest flow along the rift axis is in agreement with observations of the central anomaly magnetization high from mid-ocean ridges (e.g. Schouten et al. 1999).

References

Schouten H, Tivey MA, Fornari DJ & Cochran JR (1999) Earth and Planetary Science Letters 169, 37–50

Kinematics and deformation structures in a crustal-scale shear zone on Kea (W. Cyclades, Greece) *Poster*

Klaus Voit¹ Bernhard Grasemann¹
Erich Draganits³ Michael A. Edwards¹
Monika Müller¹ Christoph Iglseder¹
Konstantin Petrakakis² Ulrike Exner¹

It is generally agreed upon that the exhumation of metamorphic rocks in the Aegean is caused by post orogenic extension in the late Oligocene to early Miocene. This extension is in principle largely accommodated by low-angle crustal detachment faulting possibly resulting in the formation of metamorphic core complexes (MCC).

Here, we present data from recent structural investigations on the island of Kea in the W. Cyclades, Greece. Our work focussed in the north of the island. Of the ca. 270 m total structural thickness that was mapped, the entire section of rocks are highly strained. Exhumation during progressive deformation is recorded by the transition from ductile to brittle/ductile to brittle conditions. The regional characteristics and types of deformation structures vary depending on the protolith and the intensity of strain.

The lower portions comprise albite blast-bearing greenschist gneiss that becomes intensely folded structurally upwards and then changes through increasing strain and decreasing temperatures into a fine-grained greenschist-

¹ Department of Geodynamics and Sedimentology, Structural Processes Group, University of Vienna, A-1090 Vienna, Austria ² Department of Geodynamics and Sedimentology, University of Vienna, A-1090 Vienna, Austria ³ Institute for Engineering Geology, Vienna University of Technology, A-1040 Vienna, Austria

bearing internal gneiss lamellae.

This central unit of fine-grained greenschist comprises a series of interlayered cm- to m-scale marbles and compositionally varying schist layers. These host structural features such as macroscopic S-C fabric, lensoidal to angular boudins. All sections are overprinted by polyphase brittle/ductile to brittle deformation. Also present are brittle fault zones that are concentrated on rheologically-distinct weak layers. These layers often contain serpentinite lenses and talc. Additionally, cataclasites with slickensides and Riedel-fractures are present in these zones. A high density of syn-post mylonitic quartz veins are present as well as distinctive ultramylonite (graphitic) shear zones testifying diffusive mass transfer and solution/precipitation mechanisms during deformation. Late stage fluid-related activity resulted in alterations and mineralizations including a conspicuous ankeritization of dolomitic megaboudins.

The uppermost portion comprises a 10's m thick marble-ultramylonite with dolomite lenses at its base that forms very coherent km-long blocks. The competency contrast between the marble-ultramylonite layer and the underlying fine-grained greenschists is frequently marked by a metre-scale zone of very high strain as indicated by the presence of sheath folds. Within the marble-ultramylonite, a-type flanking folds represent the last stage of deformation.

The lineations show a NNE-SSW-direction on mostly NE-dipping foliation planes (with an average dip of 30°). All ductile (SC' or SCC', clasts with monoclinic symmetry, shear bands, SPO and LPO in quartz mylonites), brittle/ductile (rotated veins, flanking

structures, asymmetric boudinage) and brittle (Riedel fractures, slickensides) shear sense indicators show a consistent top to SSW direction. Although the low-angle fault system in the northern part of Kea has the current orientation of a thrust, in analogy to other metamorphic core complexes (e.g. Serifos) we speculate that the fault zone is part of an up-warped extensional crustal scale detachment.

The low-angle extensional faulting related structures are overprinted by younger and possibly still active steeply dipping conjugate fault zones, which strike NNE-SSW and NW-SE respectively. A possible regional genetic link with the actively widening Gulf of Corinth is subject of further investigations.

Komplexe Verformung von Metaquarziten im Umfeld kleinräumiger Granitintrusionen — Ergebnisse einer Vorstudie im Paläoproterozoikum der Västervik Region (SE-Schweden) *Poster*

Axel Vollbrecht¹ Bernd Leiss¹ Anja Thust¹

Das Untersuchungsgebiet liegt im Übergangsbereich zwischen den Svekofeniden und der Transskandinavischen Magmatischen Zone (Abb. 1a), welcher als Teil einer Paläoproterozoischen E- bis NE-abtauchenden Subduktionszone interpretiert wird (z.B. Be-

¹ Geowissenschaftliches Zentrum der Georg-August-Universität Göttingen, Goldschmidtstr. 3, 37077 Göttingen

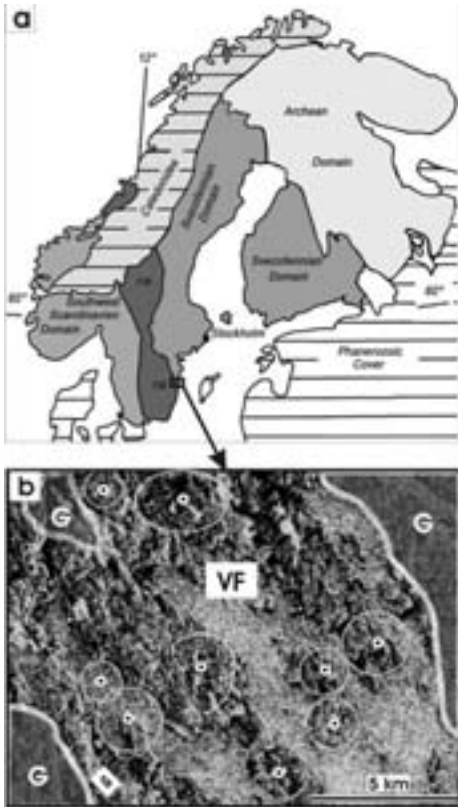


Abbildung 1: Geologischer Rahmen
 a: Gliederung des Baltischen Schildes (aus Nolte 2006, in Vorb.) mit Lage des Untersuchungsgebiets (Rahmen)
 b: Radar-Satellitenbild für ein Gebiet NW Västervik; VF-Ausstrichbereich Västervik-Formation, G-Ausstrichbereiche Granitoiden; Punkte und Ringe zeigen vermutete Ringstrukturen.

unk & Page 2001). Im heutigen tiefkrustalen Erosionsniveau sind im Wesentlichen mehrere Generationen von Granitoiden aufgeschlossen, die etwa im Zeitraum 1850–1650 Ma (z.B. Åhäll & Larson 2000) in die zuvor gefalteten Metasedimente und Metavulkanite der paläo-Proterozoischen Västervik-Formation intrudierten. Dabei kam es,

in Abhängigkeit von der primären Lithologie der Schichtenfolge, zu unterschiedlichen Formen kontaktmetamorpher und migmatischer Überprägungen bis hin zur Bildung anatektischer Granite. Innerhalb dieser migmatisch/anatektischen Bereiche stellen Metabasite und Metaquarzite schmelzresistente Horizonte der ursprünglichen Abfolge dar.

Nordwestlich von Västervik zeigen entsprechende Metaquarzite lokal komplexe, z.T. nicht-zylindrische Falten im m- bis 10er m-Maßstab, die sich deutlich von der einfacheren, großmaßdimensionierten Faltung in dieser Region abheben. Aufgrund von ersten Ergebnissen einer Vorstudie und einer Diplomkartierung wird angenommen, dass diese Strukturen durch Intrusionen von Mini-Lakkolithen in tiefere Niveaus der Västervik-Formation erzeugt wurden. Schwach entwickelte Ringstrukturen im Radar-Satellitenbild, deren Konturen z.T. durch jüngere Störungen überprägt wurden, bilden vermutlich entsprechende Aufwölbungen innerhalb der Quarzit-Schichtfolgen ab (Abb. 1b). Dabei führte ein lokal erhöhter Wärmestrom zunächst zu einer Reduzierung der Fließfestigkeit der Quarzite, was wiederum die nachfolgende Aufwölbung der Lakkolithe begünstigte. Die damit verbundene Hochtemperaturverformung der Quarzite erzeugte neben den komplexen Faltenstrukturen auch durchgreifende mylonitische Gefüge und Texturen (Abb. 2a und c). Innerhalb dieser Mylonite belegen granitische Dykes und Sills (letztere z.T. spröde/duktile verformt) die räumliche Nähe von Granitoiden im Untergrund.

Weitgehend nicht-zylindrische Falten mit sub-horizontalen Faltenachsenflächen (Abb. 2e) sowie sub-vertikale

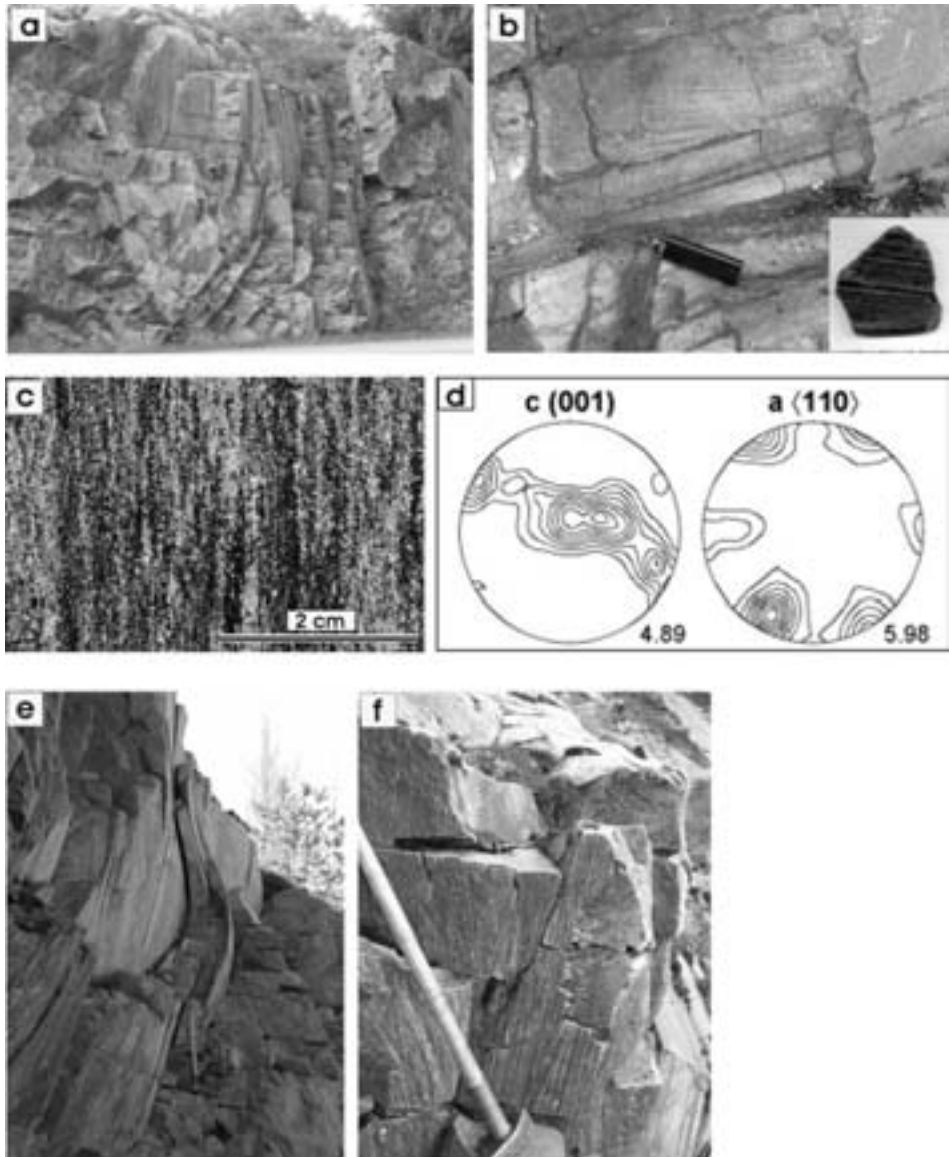


Abbildung 2: Strassenaufschluß Almvik

- a: Gefaltete Quarzit-Mylonite
- b: Reliktische Schrägschichtung in nicht mylonitisierten Metaquarziten
- c: Mikrogefüge eines Quarzit-Mylonits (Schnitt senkrecht zur mylonitischen Foliation und parallel zum Streckungslinear)
- d: Quarztextur (Neutronen-Texturen für Schnittlage wie bei c)
- e: Falten mit subhorizontaler Faltenachsenfläche, die dem Kollapsstadium zugeordnet werden.
- f: Subvertikale Harnischlineare.

Harnischlineare (Abb. 2f) auf fast allen steil stehenden s-Flächen werden als spät angelegte Kollapsstrukturen an den Flanken der Aufwölbungen gedeutet. Die andernorts in den Quarziten der Västervik-Formation oft sehr gut erhaltenen Sedimentstrukturen (vor allem Schrägschichtung; z.B. Russel 1967) treten hier innerhalb der Mylonite nur noch in Form von geschonten, scharf abgegrenzten ‚Porphyroklast-Schollen‘ auf (Abb. 2b).

Danksagung Für anregende Diskussionen während gemeinsamer Geländebegehungen danken wir K. Wemmer und I. Kleinhanns. Die bislang vorliegenden Neutronen-Texturmessungen führte dankenswerter Weise K. Ullemeyer am Vereinigten Institut für Kernforschung in Dubna durch.

Literatur

- Åhäll K-I & Larson SÅ (2000) Growth related 1.85–1.55 Ga magmatism in the Baltic shield; a review addressing to tectonic characteristics of Svecofennian, TIB 1-related, and Gothian events. *GFF* 122, 193–206
- Beunk FF & Page LM (2001) Structural evolution of the accretional continental margin of the Paleoproterozoic Svecofennian orogen in southern Sweden. *Tectonophysics* 339, 67–92
- Nolte N (2006, in Vorb.) Geologische Kartierung granitoider und metamorpher Gesteine SW†Törnfall, Västervik-Region (SE-Schweden). unveröff. Diplomkarierung, Universität Göttingen
- Russell RV (1967) Paleocurrent analysis in the deltaic Precambrian meta-sedimentary rocks from Västervik, Sweden. *GFF* 89, 105–115

Structural investigation and strain analysis of a polyphase flower structure in the Lower Saxony Basin, Germany

Poster

Lars Wagner¹ Tina Lohr² David C. Tanner³ Charlotte M. Krawczyk² Onno Oncken²

Introduction

The Lower Saxony Basin (LSB) is a part of the post-Variscan Central European Basin System. We used a 3-D reflection seismic dataset in the northern LSB, provided by RWE-DEA AG, Hamburg (*c.f.* Lohr et al. submitted) for our investigation, which is concerned with the detailed structural and kinematic analysis of a flower structure within Mesozoic strata. This data is used in turn to determine input parameters for further 3-D geometrical retro-deformation. The retro-deformation verifies our assumptions about the structure and tectonic processes, and gives further information about sub-seismic strain distribution with respect to the branch faults of the flower structure.

Structural and kinematic analysis

In a preliminary step, *structural analysis* was carried out to ensure our interpretation of the investigated flower structure was correct. We analysed it by using the criteria of Harding (1990). The investigated structure shows a planar, steeply-dipping main fault zone

¹ Department of Geology, University of Gießen, Senkenbergstraße 3, D-35390 Gießen

² GeoForschungsZentrum Potsdam, Telegrafenberg, D-14473 Potsdam ³ Department of Structural Geology and Geodynamics, Geoscience Centre, University of Göttingen, Goldschmidtstraße 3, D-37077 Göttingen

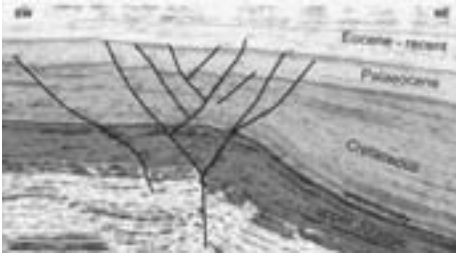


Figure 1: Interpreted 2-D seismic cross-section of the flower structure (width of figure ca. 4 km, depth from 0–3.5 s TWT). An earlier Upper Cretaceous compressive stage leads to reduced sedimentation towards the central part of the structure. The following Paleocene extension led to increased sedimentation and reduction of displacement in the deeper parts of the branch faults.

which indicates wrench tectonics, and also divergent branch faults at higher levels; both features are characteristics of a flower structure (Fig. 1). In addition, competing structural interpretations could be ruled out. For example, the collapsed crest of an anticline would not show a deeper main fault zone. Furthermore, cross-sections at varying distances from a nearby Zechstein salt diapir to the SE of this structure show no change in structural style, suggesting salt tectonics was not the main driving force for the tectonic evolution of the flower structure. The structure shows a polyphase synsedimentary evolution, with a compressive stage from Late Cretaceous up to earliest Tertiary, followed by extension during the later Tertiary (Fig. 1).

The main goal of the *kinematic analysis* was to determine the transport vector as one of the input parameters for later retro-deformation. In this example, direct determination of the transport vector was not possible because

of the lack of suitable markers, and also of the polyphase tectonic history of this structure. Instead, minimum transport distances are defined on fault planes by the cutoff relationships of sedimentary horizons. Additional kinematic indication is given by the topography of the branch fault planes, which shows strongly-corrugated morphologies (Fig. 2, 3). These asymmetrically-shaped corrugations have an amplitude of some ten meters and a spacing of approximately 1000 meters. Their axes, which indicate the direction of tectonic transport (Needham et al. 1996), show less than 20° deviation from the dip azimuth of the fault plane (Fig. 3). As a consequence of this, the post-Paleocene evolution of the flower structure seems to have been mainly dominated by extensional tectonics, since lateral transport is negligible. Indications for splitting of the strike-slip and dip-slip components to different branch faults was not found, since all of the fault planes show steeply-dipping curvature lineations.

Restoration and strain analysis

We perform 3-D geometrical retro-deformation of the fault displacement using the Midland Valley 3DMove software. For this, input parameters such as heave distance, transport direction, and inclined shear vector were obtained from the previous structural and kinematic analysis. Iterative tests of some of the parameters and the use of different restoration algorithms provide an indication of the reliability of our modelling and give some insights on their effect on the distribution of sub-seismic strain distribution (Fig. 4).

The 3D retro-deformation points to a strong correlation between fault sur-

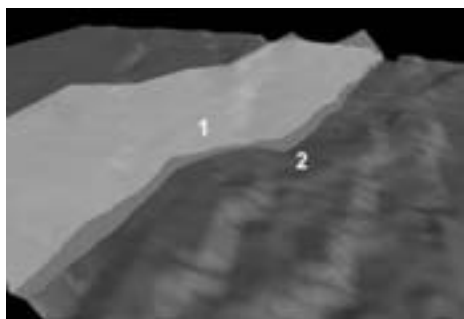


Figure 2: Branch fault planes, showing a strongly-corrugated morphology.

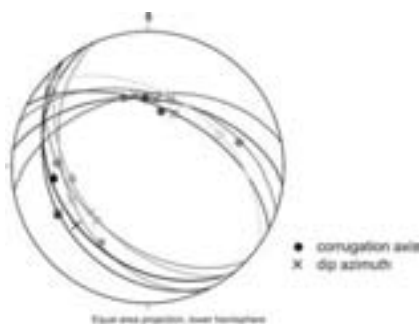


Figure 3: Stereonet-diagram with dip azimuth (crosses) and corrugation axis direction (circles) of branch fault planes (great circles). Calculation of the displacements and dipping angles of the branch fault planes, typically between $40\text{--}50^\circ$, allows to calculate the minimum extension amount of 240 m, or 10%, with respect to Base Tertiary level's width of 2400 m.

face morphology and strain distribution in the hanging wall, especially above ramp structures and with respect to fault surface corrugations. Furthermore, the strain distribution also depends strongly on the angular differences between the orientation of corrugation axes and transport direction. The modelling shows that deviations of more than $20\text{--}30^\circ$ between transport direction and corrugation axis may lead to

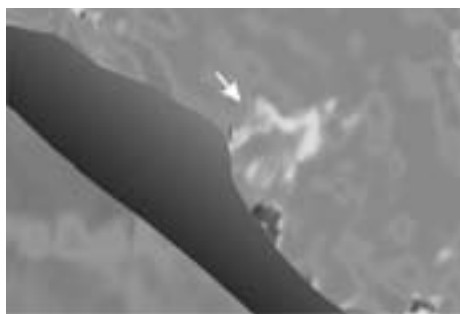


Figure 4: Greyscale map showing the relationship between strain accumulation (light grey — highest strain (15%) in the hanging wall of the Base Tertiary horizon and the fault surface morphology. View from top, fault plane dips toward upper right.

significant higher strain amounts. This is in agreement with the modelling results of Needham et al. (1996), in their analysis of North Sea faults. The use of different restoration algorithms shows only few differences (and therefore the results shown here are representative) in amount and distribution of sub-seismic strain in our models. That is, we predict strains of 10–15% (e_1 magnitude) within 200 m of the faults, extending to 400 m above ramp structures.

Conclusions

Using the criteria of Harding (1990), we established the flower structure nature of the investigated structure. Our investigation demonstrates that this flower-structure has undergone a polyphase evolution, with compression in the Upper Cretaceous and predominately extension during Paleocene to Eocene times. The minimum amount of this extension is 240 m, with respect to the Base Tertiary level. There is no evidence for wrench tectonics in the latter tectonic stages. The 3D retro-

deformation points to a strong correlation between fault surface topography and strain distribution, but the strain value also depends strongly on the angular difference between the corrugation axes of fault planes and transport directions. In our models, the use of different restoration algorithms shows only few differences in amount and distribution of sub-seismic strain. The modelling show that deviations of more than 20–30° between transport direction and fault plane corrugation axis may lead to significant higher strain amounts in the hanging-wall.

Acknowledgements We thank RWE-DEA AG, Hamburg for allowing us to use their 3D seismic database and borehole data for this project. The project is part of the DFG SPP 1135; we acknowledge DFG grants TA 427/1 and KR 2073/1.

References

- Harding TP (1990) Identification of wrench faults using subsurface structural data: criteria and pitfalls. *AAPG Bull* 74, 10
- Lohr T, Krawczyk CM, Tanner DC, Samiee R, Endres H, Trappe H, Oncken O & Kukla PA (under review) Structural evolution of the NW German Basin over time from 3-D reflection seismic data — a case study at the border between Lower Saxony Basin and Pompeckj Block. Submitted to *Journal of Structural Geology*
- Needham DT, Yielding, G & Freeman B (1996) Analysis of fault geometry and displacement patterns In: Buchanan, PG & Nieuwland, DA (eds) *Interpretation, Validation and Modelling*. *Geol Soc Sec Publ* 99

The importance of lithological heterogeneity of the Onaping Formation for understanding post-impact deformation of the Sudbury Impact Structure, Canada

Poster

Andrea Wittek¹ Ulrich Riller² Lutz Hecht²

The suevitic Onaping Formation overlies the layered Main Mass of the 1.85 Ga Sudbury Igneous Complex (SIC) of the Sudbury Impact Structure, Ontario. The Formation consists of four Members, namely from top to bottom, the Black, the Green, the Gray and the Basal. Post-impact NW-SE shortening during the Penokean Orogeny (ca. 1.9–1.75 Ga) affected the Onaping Formation and led to the lobate shape of the SIC in plan view. In order to investigate the possible fold origin of the NE-lobe of the SIC, a field-based structural analysis of the Onaping Formation was conducted in the Frenchman Lake area. The analysis is based on structural measurements at 580 stations and encompasses the orientation of mineral shape fabrics as well as their intensity. In addition to these quantities, lithological variation and metamorphic overprint of the Onaping Formation was examined. Special attention was paid thereby to the Green Member since previous workers stated that it forms a continuous unit at the base of the Black Member.

Individual Members of the Onaping For-

¹ Freie Universität Berlin, Institut für Geologische Wissenschaften, Malteser Strasse 74-100, 12249 Berlin ² Humboldt-Universität Berlin, Institut für Mineralogie, Invalidenstrasse 43, 10115 Berlin

mation differ in mineral composition, size and abundance of clasts as well as in color and texture of the matrix, the latter one of which ranges from cryptocrystalline to coarse-grained as well as in the content of felsic minerals. Overall, grain size of the matrix as well as size and content of clasts increase from the top of the Onaping Formation towards its base. The Green Member is well apparent by the presence of angular mineral aggregates, composed chiefly of chlorite. Therefore, these aggregates became known as 'chloritic shards' and possibly represent original fragments of melt particles. In the Frenchman Lake area, the Green Member forms a 70–100 m thick, discontinuous band, whereby the strike of its contacts at surface varies highly. By contrast, intra-formational lithological contacts of the lower units of the Onaping Formation are rather straight.

Microscopic inspection of samples from the Black, Green and Gray Members shows that mineral shape fabrics are chiefly defined by chlorite and epidote. This points to post-impact deformation under lower greenschist-facies metamorphic conditions. Deformation of the Onaping Formation varies greatly with position. This is indicated by the orientation and intensity of planar mineral shape fabrics. Fabric intensity was visually estimated and is based on the shape-preferred alignment of matrix minerals and clasts. It varies as a function of the mineralogical composition and grain size of the matrix, as well as in distance to the NE-lobe. More specifically, fabric intensity increases towards the top of the Onaping Formation suggesting that mechanical strength during deformation of the Formation increased toward its lower contact. This is corrob-

orated by the variation in strike of intra-formational lithological contacts, which are straight at the base but highly irregular towards the top of the Formation, and may well account for the discontinuous nature of the Green Member.

An increase in shape fabric intensity is also apparent towards the east. Similarly, the strike of planar shape fabrics becomes more uniform in this direction, i.e., NE–SW, which is axial-planar to the acute bisectrix of the NE-lobe. This may indicate that the effect of folding of the SIC on the fabric development in the Onaping Formation decreases towards the west. The planar shape fabrics also display a progressive change in their overall strike from NE–SW in the NE-lobe to ENE–WSW towards the west of the lobe. This change in strike can be explained by the curvature of the fold axis of the NE-lobe. Despite the strong heterogeneity of deformation in the Frenchman lake area, the orientation in, and gradients in intensity of, planar shape fabrics in the Onaping Formation are consistent with a fold origin of the NE-lobe, which formed under lower greenschist-metamorphic conditions.

Late stage evolution of the Serifos Metamorphic Core Complex (Cyclades, Greece)

Poster

András Zámolyi¹ Bernhard
 Grasemann¹ Erich Draganits²
 Konstantin Petrakakis³ Christoph
 Iglšeder¹ Christian Rambousek¹
 Ulrike Exner¹ Klaus Voit¹ Monika
 Müller¹

Introduction

The island of Serifos is located in the Western Cyclades within the Attic-Cycladic metamorphic belt. It represents the westward continuation of an arcuate belt of Metamorphic Core Complexes with intrusions of late syn-post tectonic intrusions younging from East (e.g. Naxos main activity ca. 12 Ma) to West (e.g. Serifos with 9–8 Ma). In scientific discussions the dominance of probably continuous extension since ca. 30 Ma (e.g. Jolivet & Faccenna, 2000) and the presence of Metamorphic Core Complexes (Lister et al. 1984) is accepted. The speculated roll-back of the subducting plate possibly started due to the slowing down of absolute plate convergence rate between Africa and Eurasia. This model is attractive, because it would also explain the shift from a compressional Andean-type regime to an extensional Mariana-type regime (Jolivet & Faccenna 2000). Contrary to the kinematic directions reported from the Central and Eastern Cyclades, the movement of the hanging

wall of the Serifos Metamorphic Core Complex is south directed. The island's main part is occupied by an undeformed granodiorite. Early granitic intrusions intruded into low-grade M₂-crystalline rocks that have been overprinted to as high as amphibolite facies conditions due to contact metamorphism. Parts of these rocks (gneisses and amphibolites) as well as the early intrusions are deformed to mylonites (Grasemann et al. 2004).

Structural observations

A striking feature is found in the south-western part of the Serifos Metamorphic Core Complex, where a SW-dipping brittle surface cuts through the gneiss-marble lithology forming a prominent morphological fault scarp. During higher greenschist facies metamorphic deformation, the marbles acted as a weak layer between deforming areas of more rigid gneisses. They show a fine-grained homogenous recrystallized microstructure with crystal-preferred orientation. Structures indicating high strain like sheath folds are recorded within the marble with south dipping fold axes. In contrast to the marble-ultramylonites, centimeter to meter scale gneiss lenses act as boudins within the marble-ultramylonite. Deformation is characterized by overall extension (chocolate-tablet boudinage) with stretching directions NW–SE and NE–SW, respectively. Carbonatic metaconglomerate layers with oblate components and pressure solutions indicate a considerable amount of pure shear. The shear sense of the main ductile shear zone is top to the SSW, also indicated by SCC' fabrics and sigma clasts. Subsequent brittle deformation overprinted certain layers of the

¹ Department of Geodynamics and Sedimentology, Structural Processes Group, University of Vienna, Austria ² Institute for Engineering Geology, Vienna University of Technology, Austria ³ Department of Geodynamics and Sedimentology, University of Vienna, Austria

marble-ultramylonite, forming a continuous, decimeter to meter thick marble layer immediately below the prominent morphologic brittle fault scarp, showing a mature stage of cataclastic reworking and high content of mica and silica. We find two generations of cataclasites: subvertical and low angle cataclasites. The subvertical generation grades into decimeter thick non-cohesive cataclasites. In the hanging wall of the brittle surface block rotations can be observed, whereas in the footwall horst and graben structures occur.

Conclusion

Two main phases can be recognized from the above mentioned:

- i) a phase of ductile to brittle-ductile deformation represented by the decimeter thick interlayered marble-gneiss shear zone and
- ii) a purely brittle phase represented by thick cataclastic horizons and an ankeritic dolomite surface forming the prominent morphological scarp.

This shear zone likely represents the final stage in the evolution of the Serifos Metamorphic Core Complex and is an excellent outcrop rarely found on the islands of the Cyclades.

Literatur

- Grasemann B, Petrakakis K, Iglseder C, Ramboisek C, Zámolyi A & Draganits E (2004) The Serifos Metamorphic Core Complex (Western Cyclades, Greece). 5th International Symposium on Eastern Mediterranean Geology, Thessaloniki, Greece, 14–20 April 2004
- Jolivet L & Faccenna C (2000) Mediterranean extension and the Africa–Eurasia collision, *Tectonics*, 19-6, 1095–1106

- Lister GS, Banga G & Feenstra A (1984) Metamorphic core complex of Cordilleran type in the Cyclades, Aegean Sea, Greece, *Geology*, 12, 221–225

Tertiäre Landoberflächen in Mitteldeutschland als Anzeiger tektonischer Bewegungen — Eine Rekonstruktion mittels Einsatz von Geo-Informationssystemen *Poster*

Ina Zander¹

Arbeitshypothese

Aus der Verteilung und Lage tertiärer und quartärer Ablagerungen in Mitteleuropa lassen sich tertiäre Paläooberflächen rekonstruieren. Die spätere Verstellung dieser Oberflächen erlaubt es, die vertikalen Krustenbewegungen der jüngeren und jüngsten geologischen Vergangenheit zu quantifizieren. Diese Hebungs- und Senkungsbewegungen sind nur wenig durch die lokale Heraushebung der mitteldeutschen Mittelgebirge beeinflusst. Sie sind vor allem die Folge sehr großräumiger Verstellungen der Erdkruste zwischen Nordsee und Fichtelgebirge, bei denen Prozesse im Erdmantel einen entscheidenden Einfluss im großräumigen (mitteleuropäischen) Maßstab haben.

Untersuchungsgebiet

Das Untersuchungsgebiet liegt im Zentrum des im heutigen Sprachgebrauch als Mitteldeutschland bekannten Dreiländerecks Thüringen — Sachsen —

¹ Institut für Geowissenschaften, Friedrich-Schiller-Universität Jena, Burgweg 11, 07749 Jena

Sachsen-Anhalt. Geographisch gesehen, umfasst es Ausschnitte aus einer Vielzahl von naturräumlichen Einheiten mit unterschiedlichen morphologischen Erscheinungsformen: Mittelgebirge, Hügellandschaften und Senken sind vertreten. Doch trotz dieser Vielgestaltigkeit ist von Süden nach Norden deutlich eine Abnahme der Höhe und eine Verflachung des Reliefs erkennbar.

Regionalgeologisch betrachtet, liegt der Untersuchungsraum am Südrand der Mitteleuropäischen Tertiärsenke. Die tertiären Ablagerungen bestehen hier überwiegend aus Meeresablagerungen, untergeordnet aus Flussablagerungen von zum Teil unsicherer zeitlicher Einstufung. Beschränkten sich die Ablagerungen und die Bildung von Kohleflözen anfangs auf Subrosionssenken, wurden sie im Verlauf des Tertiärs im Bereich der Leipziger Tieflandsbucht und im Weißelsterbecken flächendeckend. Die diese Sedimentation ermöglichenden Transgressionen werden unter anderem auf weiträumige Senkungen (Eismann 2002, Standke 2002) zurückgeführt, die die Leipziger Tieflandsbucht mit dem Nordwestdeutschen Becken und damit mit der tertiären Nordsee verbanden. Die Bedeckung des Grundgebirges bzw. der mesozoischen Gesteine mit tertiären und quartären Ablagerungen im Süden und Südwesten des Untersuchungsgebietes ist heute nur noch sehr lückenhaft erhalten. Teilweise blieben diese Sedimente hier nur in Subrosionssenken bewahrt. Nach Norden bzw. Nordosten nimmt die Häufigkeit und die Mächtigkeit der känozoischen Bildungen zu. Im Raum der Leipziger Tieflandsbucht geht der Flickenteppich aus känozoischen Sedimenten über in eine nach Norden hin mächtiger werdende, geschlossene Decke. Aber

nicht nur die Sedimentation sondern auch die Erosionsprozesse des zeitweilig sehr feuchtwarmen Klimas während Kreide und Tertiär hinterließen zum Teil tief reichende Verwitterungsrinden prä-tertiärer Gesteine, die weitere greifbare Zeugen des Tertiärs bzw. der Kreidezeit darstellen (Migón & Lidmar-Bergström 2001, Unger & Schramm 1966).

Zielsetzung

Über ein Jahrhundert hinweg sind, entsprechend dem wachsenden Wissensstand, verschiedene Modelle entstanden, die die morphologische Entwicklung der tertiären Ablagerungsräume der Leipziger Tieflandsbucht und insbesondere ihrer südlich angrenzenden Gebiete (z. T. bis hin zum Fichtelgebirge) zu erklären suchten (v. Freyberg 1923, Penck 1924, Philippi 1910, Steinmüller 1974). In neueren Arbeiten wird neben früheren Erkenntnissen neueres fachübergreifendes Wissen (Spaltspurdaten zur Exhumierungs- und Hebungsgeschichte, Erkenntnisse zum Klima und zum meso-känozoischen Verwitterungsgeschehen: Saprolitisierung) integriert. Peterek (2002) diskutiert für sein Modell einen Entstehungsmechanismus, der mit der Heraushebung von Thüringer Wald und Thüringer Schiefergebirge in Verbindung steht. Prä-existente tektonische Strukturen werden durch Kompressionsprozesse reaktiviert, die zur Heraushebung der beiden Mittelgebirge führen. Dieser Mechanismus steht im direkten Zusammenhang mit Bewegungen von Platten der Lithosphäre. Peterek veranschlagt für diese Bewegung einen Zeitraum, der von der Unterkreide bis deutlich in das Tertiär hineinreicht. Untersuchungen im Harz (Voigt et al. 2004) legen jedoch nahe, dass die Inversionsbewegungen schon in

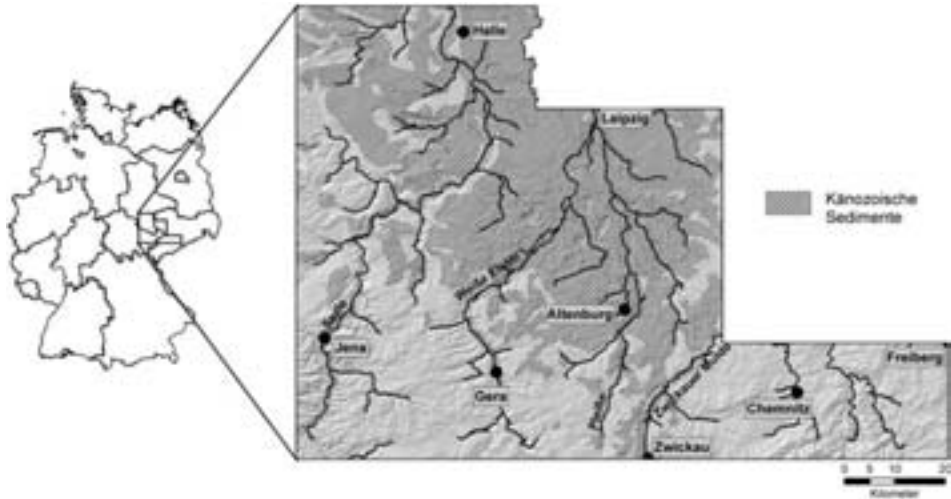


Abbildung 1: Lage des zentralen Untersuchungsgebietes. Die Karte zeigt ein Digitales Geländemodell zusammen mit der Verbreitung känozoischer Ablagerungen.

der Oberkreide weitgehend beendet waren. Die durch zunehmende Mächtigkeit der tertiären Sedimente bis in die Nordsee (Scheck-Wenderoth & Lamarque 2005, Ziegler 1990) belegte Verstellung scheint auch zu großräumig, um durch Inversionstektonik verursacht zu sein. Das hieße, das kein zwingender Zusammenhang mit kollidierenden Bewegungen von Lithosphärenplatten bestehen müsste, sondern eine direkte Verknüpfung mit Massenverlagerungen und thermischen Vorgängen im Mantel besteht, die zur Verstellung und Verbiegung der überlagernden Lithosphärenplatte(n) führen und auch für den tertiären Vulkanismus verantwortlich sein könnten.

Mit dieser Arbeit soll ein Beitrag zur Erforschung der Antriebsmechanismen geleistet werden, die hinter der Bildung der oben beschriebenen Geomorphologie des Untersuchungsgebietes stecken. Im Einzelnen sind folgende Arbeiten geplant:

Im beschriebenen Untersuchungsgebiet sollen die Tertiär-Relikte in ihrer Lage, Mächtigkeit und zeitlichen Einordnung erfasst werden. Aufbauend darauf soll die jetzt verstellte, deformierte (?) und zum großen Teil erodierte mesozoisch-känozoische Verebnungsfläche rekonstruiert werden. Zur Durchführung der Rekonstruktion muss ermittelt werden, ob tektonische Vorgänge und/oder Salzauslaugung (Subrosion) zur Bildung bzw. Erhaltung der tertiären Ablagerungen führten. Die Rekonstruktion der Paläolandoberfläche soll die Bilanzierung des erodierten Volumens sowie die Quantifizierung großräumiger Hebungen und Senkungen der Erdkruste während des Känozoikums ermöglichen. Durch die Einbindung der gewonnenen Ergebnisse in den geologischen Rahmen Mitteleuropas sollen Rückschlüsse auf die tektonischen Vorgänge in Erdkruste und Erdmantel gezogen werden.

Daten und Methoden

Bei der Arbeit wird überwiegend auf vorhandene mittel- bis kleinmaßstäbige, digitale Fach- und Basisdaten zurückgegriffen: Dies sind vor allem Digitale Geländemodelle (ATKIS-DGMs, SRTM-Daten, GTOPO30) sowie Digitale Geologische Karten. Diese Daten werden durch Informationen aus weiteren Quellen (z.B. Karten, Bohrungsdaten, Berichte, Karten, Geländebegehungen) ergänzt. Die genannten Daten besitzen deutliche qualitative und quantitative Unterschiede, die einen erheblichen Aufbereitungsaufwand erfordern, bevor sie ihrem eigentlichen Zweck zugeführt werden können. So können z.B. Kartenwerke mit vergleichbarem Maßstab aus verschiedenen Bundesländern voneinander abweichen in den Datengrundlagen (Art, Anzahl), der Aktualität, der unterschiedlichen Darstellung gleicher fachlicher Inhalte. Hinzu erkommt die Digitalisierung der zur Ergänzung notwendigen analogen Daten. Anschließend soll mit Hilfe von GIS- und 3D-Modellierungssoftware durch die Verbindung von topographischen und geologischen Daten die rezente Lage der tertiären Reliktflächen modelliert werden. Höhen- und Hanglage der tertiären Reliktflächen sollen im Zusammenhang mit ihren stratigraphischen Informationen (Alterstellungen) Abschätzungen sowohl über ihre relative Versetzung zueinander als auch über ihre Gesamtverstellung während des Känozoikums ergeben (siehe auch Geomorphologische Analyse). Zusätzlich sollen die Quartärbasis und die Tertiärbasis in ihrer rezenten Lage hergestellt werden. Die Modellierung der vermuteten Lage der präquartären (tertiären) und der prätertiären Landoberfläche sollen die Abschätzung des Volu-

menaustrags während des Tertiärs und des Quartärs ermöglichen. Für Teilbereiche des Untersuchungsgebietes soll mittels Frequenz-Zerlegung (Fourier-Analyse) und Wellenlängen-Filterung durchgeführt werden: Die sehr unruhige Oberfläche dieser Teilgebiete ist vermutlich sowohl durch tektonische Vorgänge als auch durch Ablaugung von Salzgesteinen im Untergrund (Subsion) entstanden. Beide Prozesse verformen die ehemalige Landoberfläche in unterschiedlichen Wellenlängenbereichen. Daher soll die Analyse Aufschluss über tektonische und subsosive Anteile der Landschaftsformung sowie über deren Beziehung zueinander geben. Ferner soll eine isostatische Modellierung auf zwei Traversen durchgeführt werden, die vom Untersuchungsgebiet bis in die Nordsee reichen. Die Daten des Untersuchungsgebietes werden hierzu mit den sehr viel weniger detaillierten, sehr kleinmaßstäbigen Daten aus dem ‚Tektonischen Atlas Nordwestdeutschlands‘ zusammengeführt. Diese Schnitte durch die Erdkruste, in die die Höhenlage der rezenten Landoberfläche, die erodierten und sedimentierten Volumina, sowie die Mächtigkeit und die durchschnittlichen Dichten der Erdkruste und der Mantellithosphäre mit einfließen, sollen mit Hilfe der Isostatischen Modellierung Rückschlüsse auf die großräumigen tektonischen Vorgänge in Erdkruste und Erdmantel zulassen.

Literatur

- Eissmann L (2002) Tertiary geology of the Saale-Elbe-Region. *Quaternary Science Reviews* 21, 1245–1274
- von Freyberg B (1923) Die tertiären Landoberflächen in Thüringen. *Fortschritte der Geologie und Paläontologie* 6, Berlin, pp 77
- Migón P & Lidmar-Bergström K (2001) Weathering mantles and their significance for

- geomorphologicalevolution of central and northern Europe since the Mesozoic. *Earth-Science Reviews* 56: 285–324
- Penck W (1924) Die morphologische Analyse. Ein Kapitel der physikalischen Geologie. J. Engelshorns Nachf, Stuttgart, 283
- Peterek A (2002) Neotektonische und morphostrukturelle Entwicklung des Thüringer Waldes und Thüringischen Schiefergebirges - Überblick und Ausblick. *Zeitschrift für Geologische Wissenschaften* 30, 277–292
- Philippi E (1910) Über die präoligocäne Landoberfläche in Thüringen. *Zeitschrift der Deutschen Geologischen Gesellschaft* 62 (Abhandlungen und Monatsberichte), 305–404
- Scheck-Wenderoth M & Lamarche J (2005) Crustal memory and basin evolution in Central European Basin System — new insights from a 3D structural model. *Tectonophysics* 397/1-2, 143–165
- Standke G (2002) Das Tertiär zwischen Leipzig und Altenburg. In: *Beiträge zur Geologie von Thüringen* 9, 41–73
- Steinmüller A (1974) Die präpleistozäne Morphogenese des östlichen Thüringer Schiefergebirges und südöstlich angrenzender Gebiete. *Zeitschrift für Geologische Wissenschaften* 2, 37–59
- Unger KP & Schramm H (1966) Alttertiäre Rotlehme auf Muschelkalk in NE-Thüringen. *Jahrbuch der Geologie* 2, Berlin, 521–535
- Voigt T, von Eynatten H & Franzke HJ (2004) Late Cretaceous Unconformities in the Subhercynian Cretaceous Basin (Germany). *Geologica Polonica Acta* 54, 675–696
- Ziegler PA (1990) *Geological Atlas of Western and Central Europe*. Shell, Den Haag

Jetzt auch Publikationsplattform
www.GEO-LEO.de
 Virtuelle Fachbibliothek und Internetportal



- > Geowissenschaften
- > Bergbau
- > Geographie
- > Thematische Karten



The Clean Lab Company		PicoTrace
Equipment for Trace Element and Isotope Analysis		
Wolfsgarten 7	TEL: + 49 - (0)5594 - 9 31 31	Email: info@picotrace.de
D-37120 Bovenden	FAX: + 49 - (0)5594 - 9 31 90	Internet: www.picotrace.de

Autorenverzeichnis

Präsentierende Autorinnen und Autoren in Fettdruck.

- Almeida, Harrizon Lima de, **3**
Andrew, Ruth, **6**
Angerer, Thomas, **9**, 123
Audunsson, H., 238
Auer, Andreas, 48
Austrheim, Haakon, 121
- Bartelsen, Tobias, 167
Battaglia, Maurizio, 16
Bechstädt, Thilo, 125
Beck, Andre, **12**
Behrens, Harald, 222
Behrmann, Jan H., 96, 182, 233
Bense, Frithjof, **16**
Berger, Alfons, 20, 198
Bissen, Raphael, **18**
Brätz, Helene, 203
Brodhag, Sabine, **20**
Bücker, Carsten, 87
Buck, Roger, 145
Burchardt, Steffi, **21**, **24**, **25**, 61, 119
Burliga, Stansilaw, 90
Burlini, Luigi, 194
Buurman, Nils, **27**
- Cao, Shuyun, 135
Castellarin, Alberto, 45
Chatziliadou, Maria, **30**
Cotza, Gianluca, **33**
Craddock, John, 108
- Danišik, Martin, 45
Davaa, Buyan, **34**, 63
de Wall, Helga, 12, 48, 151, 173, 224
Deckert, Hagen, **36**, **38**
Dietl, Carlo, 224
- Dietze, F., 238
Dobmeier, Christoph, 84
Doman, Daniel, **40**, 220
Dorner, Dorothee, 232
Draganits, Erich, 143, 239, 248
Dresmann, Horst, **42**
Dunkl, István, **45**
Dworazik, Nina, **48**
- Ebert, Andreas, **50**
Edwards, Michael A., 143, 172, 239
Ehrlich, Ralf, **52**
Endres, Heike, 226
Ertl, Gabriele, 16
Exner, Ulrike, 239, 248
von Eynatten, Hilmar, 45
- Færseth, Roald, 52
Finger, Fritz, 203
Fischer, Mario, **56**
Fiseli, Jochenl, 85
Freitag, Ralf, **58**, 98, 207
Friese, Nadine, 21, **61**, 119
Frisch, Wolfgang, 45
Froitzheim, Nikolaus, 170
Fügenschuh, Bernhard, 42, 73
- Gaedicke, Christoph, 58
Gaich, Heiko, 106
Geerdts, Peter, 34, **63**
Gessner, Klaus, 36, **66**
Geyer, Adelina, 79
Giba, Marc, 85
Giese, Jörg, **198**
Giese, Steffen, 191
Glodny, Johannes, 108, 122

- Glotzbach, Christoph, **67**
 Gnos, Edwin, 198
 Gröger, Heike R., **73**
 Götze, Hans-Joachim, 181
 Grasemann, Bernhard, 33, 143, 172, 239, 248
 Greiling, Reinhard O., 9, 70
 Grimmer, J.C., **72**
 Gross, Christian J., **75**
 Gudmundsson, Agust, 6, 21, 24, 61, **79**, **81**, 93, 119, 130, 164, 167

 Handy, Mark R., 84
 Hansen, Bent T., 56
 Hauten, Sarah, **84**
 Hecht, Lutz, 246
 Heidelbach, Florian, 91
 Heinemann, Niklas, **85**
 Henk, Andreas, 18, 34, 63, 228
 Herwegh, Marco, 20, 50, 235
 Hilgers, Christoph, 30, **87**, **90**
 Hirt, Ann M., 91, 156, 194, 196
 Hoffmann, Stefan, **93**, 167
 Hofmann, Kai, 40
 Hongn, Fernando, 181

 Ibele, Tobias, **96**
 Iglseider, Christoph, 143, 172, 239, 248

 Jähne, Fabian, 58, **98**
 Jahn, Andreas, 188
 Jansen, Ekkehard, 170, 214
 Jonas, Philipp S., **101**
 Jones, P.A., 66

 Kenkmann, Thomas, **103**, 188
 Kiechl, Eva, **106**
 van der Klauw, Sebastiaan, 146
 Klein, Thomas, **108**
 Kleinhanns, Ilka C., 56
 Klemd, Reiner, 203
 Kley, Jonas, 146, **207**
 Klimczak, Christian, **111**
 Klingenberg, B., 214
 Koehn, Daniel, **112**, 187
 Kolb, J., 137

 Kontny, A., 238
 Kopf, Achim, 182
 Kouankap, Nono Gus D., **113**, **115**, **116**
 Kracke, Tobias, 25
 Krawczyk, Charlotte M., 226, 243
 Krbetschek, Matthias, 58
 Krenn, Erwin, 203
 Kruhl, Jörn H., 132, 159
 Krumbholz, Michael, 21, 61, **119**
 Kück, Jochem, 12
 Kühn, Alexander, **121**, **122**
 Küster, Martina, 232
 Küster, Yvonne, 211
 Kukla, Peter A., 196, 226
 Kuntcheva†, Boriana, 132
 Kunze, Karsten, 132, 214
 Kurz, Walter, 106

 Laukamp, Carsten, **123**, **125**
 Leiss, Bernd, 25, **128**, 156, 161, 179, 194, 211, 240
 Letourneur, Ludovic, **130**
 Lichtenberger, Marco, 70
 Liebl, Christoph, **132**
 Liu, Junlai, **135**
 Lögering, M.J., **137**
 Lohr, Tina, 226, 243
 López de Luchi, Mónica G., 216

 Martin, Ulrike, 48, 173
 McEnroe, Suzanne, 91
 Meyer, F.M., 137
 Molli, Giancarlo, 25, 161
 Mora, Andrés, **141**
 Moser, Elmar, **177**
 Müller, Christian, 93, 167
 Müller, Monika, **143**, 239, 248

 Nagel, Thorsten, 145
 Naumann, M., 214
 Németh, Karoly, 48, 173
 Neubert, Jana, **146**
 Nietzsche, Thomas, **151**
 Nüchter, Jens-Alexander, **155**

 Obermeyer, Hennes, 70

- Oelrich, Asdis, 167
 Oncken, Onno, 226, 243
 Otto, Michael, **156**
- Parra, Mauricio, 141
 Passchier, Cees, 112
 Pennock, Gill, 90
 Peternell, Mark, **159**
 Petrakakis, Konstantin, 143, 172, 239, 248
 Petrinovic, Ivan, 181
 Petzel, Volker, 125
 Pfaar, Rüdiger, **161**
 Pfiffner, Adrian, 20, 50, 235
 Philipp, Sonja L., 24, 81, 93, **164, 167**
 Picotti, Vincenzo, 45
 Pleuger, Jan, **170**
- Rabitsch, Robert, 106
 Rahn, Meinert, 67
 Rambousek, Christian, **172, 248**
 Ranten, Colin D., 101
 Rapalini, Augusto, 216
 Reinecker, John, 67
 Renard, François, 112
 Renk, Daniela, **173**
 Reuther, C.-D., 27, 177
 Richter, Peter P., **179**
 Riller, Ulrich, 40, 111, **180, 181, 220, 246**
 Ring, Uwe, 38, 122, 179
 Robinson, Peter, 91
 Röller, Klaus, 232
 Roeser, Georg, **182**
 Rolf, Christian, 48, 151
 Roller, Sybille, 170
 Rosenberg, Claudio, 201
 Rosselli, Pascal, 196
 Ruedrich, Joerg, **185**
 Ruiz, Amarildo Salina, 3
 Rybacki, E., 214
- Sachau, Till, **187**
 Samiee, Ramin, 226
 Scherler, Dirk, **188**
 Schlöder, Zsolt, 90
- Schmatz, Joyce, **191**
 Schmid, Stefan M., 73
 Schmidt, Sabine, 181
 Schmidt, Volkmar, 91, 156, **194, 196**
 Schmittbuhl, Jean, 112
 Schneider, Susanne, **201**
 Scholz, Katerina, **196**
 Schramm, Michael, 211
 Schreurs, Guido, 198
 Schulz, Bernhard, **203**
 Schwarz, Michael, **205**
 Schwarzbauer, J., 137
 Seib, Nadine, 207
 Seidel, Torben, **211**
 Siegesmund, Siegfried, 216
 Siemes, Heinrich, **214**
 Sindern, Sven, 30
 Sjøholm, Jorunn, 52
 Smørdal Lien, Kari, 52
 Spiegel, Cornelia, 67
 Spottke, Ina, 42
 Spray, John G., 229
 Steenken, André, **216**
 Steffes, Elisabeth, **220**
 Stipp, Michael, 85, **222**
 Stöckhert, Bernhard, 155, 232
 Strecker, Manfred, 141
 Streit, Verena, **224**
 Sverdrup, Einar, 52
 Sylvestre, Ganno, 116
- Tanner, David C., **226, 243**
 Thäter, Denise, 167
 Thöni, Martin, 33
 Thust, Anja, 240
 Timar-Geng, Zoltan, 42, **228**
 Tischler, Matthias, 73
 Toussaint, Renaud, 112
 Trappe, Henning, 226
 Trautwein, Ute, 196
 Trepmann, Claudia A., **229, 232**
 Trumbull, Robert, 181
 Tullis, Jan, 222
- Ullemeyer, Klaus, 128, 211, **233**

Urai, Janos L., 87, 90, 191, 196

Ustaszewski, Michaela, **235**

Vahle, C., **238**

Vogler, Marc, 34, 63

Voigt, Thomas, 207

Voit, Klaus, 143, **239**, 248

Vollbrecht, Axel, 3, 16, 185, **240**

Vrolijk, Peter, 191

Wagner, Lars, **243**

Walter, Jens M., 156, 161, 170, 194, 214

Wemmer, Klaus, 216

Wetzels, Andreas, 42, 228

Wilde, A.S., 66

Willner, Arne P., 179

Winkler, Gerfried, 106

Witteck, Andrea, 246

Zámolyi, András, 143, 172, **248**

Zander, Ina, 249

van der Zee, Wouter, 191

Ziegler, Martin, 191

Zulauf, Gernold, 108

Øye, Vibeke, 52

Adressenverzeichnis

Almeida, Harrizon de Lima

harrizonla@cpd.ufmt.br – Dep. Geologia
Geral, Universidade Federal de Mato
Grosso-ICET/DGG

Andrew, Ruth

randrew@gwdg.de – Geowissenschaft-
liches Zentrum der Georg-August-
Universität Göttingen, Goldschmidtstr.
3, 37077 Göttingen

Angerer, Thomas

thomas.angerer@urz.uni-heidelberg.de –
Geologisch-Paläontologisches Institut,
Universität Heidelberg, Im Neuenheimer
Feld 234

Audunsson, H.

Technical University of Iceland, Hofda-
bakka 9, 110 Reykjavik, Iceland

Auer, Andreas

Institut für Geologie, Julius-
Maximilians-Universität Würzburg,
Pleicherwall 1 D-97070, Germany

Austrheim, Haakon

hakon.austrheim@geo.uio.no – Physics of
Geological Processes (PGP), University
of Oslo, PO Box 1048 Blindern, 0136 Os-
lo, Norway

Bartelsen, Tobias

tobias_bartelsen@web.de – Geowissen-
schaftliches Zentrum der Georg-August-
Universität Göttingen, Goldschmidtstr.
3, 37077 Göttingen

Battaglia, Maurizio

mbattag@gwdg.de – Geowissenschaft-
liches Zentrum der Georg-August-
Universität Göttingen, Goldschmidtstr.
3, 37077 Göttingen

Bechstädt, Thilo

bechstaedt@uni-hd.de – Geologisch-
Paläontologisches Institut, Universität
Heidelberg, Im Neuenheimer Feld 234

Bechtold, Michel

spechtold@unister.de – Geowissenschaft-
liches Zentrum der Georg-August-

Universität Göttingen, Goldschmidtstr.
3, 37077 Göttingen

Beck, Andre

andre.beck@geologie.uni-wuerzburg.de –
Institut für Geologie, Pleicherwall 1,
97070 Würzburg

Behrens, Harald

h.behrens@mineralogie.uni-hannover.de –
Institut für Mineralogie, Universität
Hannover, Callinstr. 3, D-30167 Han-
nover

Behrmann, Jan H.

jan.behrmann@geologie.uni-freiburg.de
– Geologisches Institut, Universität
Freiburg, Albertstr. 23B, D-79104
Freiburg

Bense, Frithjof

f.bense@geo.uni-goettingen.de – Geo-
wissenschaftliches Zentrum der Georg-
August-Universität Göttingen, Gold-
schmidtstr. 3, 37077 Göttingen

Berger, Alfons

berger@geo.unibe.ch – Institute of Geo-
logical Sciences, Baltzerstraße 1–3, CH-
3012 Bern, Switzerland

Bissen, Raphael

raph234@hotmail.com – Geologisches In-
stitut der Albert-Ludwigs-Universität
Freiburg i. Br.

Blatt, Axel

axel.k.blatt@geolo.uni-giessen.de – Justus-
Liebig-Universität Gießen, Zur Hainerde
26

Brätz, Helene

Institut für Mineralogie, Am Hubland,
97074 Würzburg

Brodhag, Sabine

Brodhag@geo.unibe.ch – Institut für Geo-
logie, Universität Bern, Schweiz

Buck, Roger

Lamont Doherty Earth Observatory, Pa-
lisades, NY, USA

Bücker, Carsten

Shell E&P, Houston, USA

Burchardt, Steffi

sburcha@gwdg.de – Geowissenschaftliches Zentrum der Georg-August-Universität Göttingen, Goldschmidtstr. 3, 37077 Göttingen

Burliga, Stansilaw

Wroclaw University, Department of Structural Geology, ul. W. Cybulskiego 32, 50-205 Wroclaw, Poland

Burlini, Luigi

luigi.burlini@erdw.ethz.ch – Geological Institute, ETH Zurich, 8092 Zurich, Switzerland

Buurman, Nils

buurman@geowiss.uni-hamburg.de – Department für Geowissenschaften, Universität Hamburg, Bundesstraße 55, 20146 Hamburg

Cao, Shuyun

jliu@cugb.edu.cn – State Key Laboratory of Geological Processes and Mineral Resources, China University of Geosciences, Beijing 100083, China

Castellarin, Alberto

castello@geomin.unibo.it – University of Bologna, Italy

Chatziliadou, Maria

chatziliadou@iml.rwth-aachen.de – Institut für Mineralogie und Lagerstättenlehre, RWTH-Aachen, Germany

Cotza, Gianluca

Gianluca.c@gmx.net – Department of Geodynamics and Sedimentology, Structural Processes Group University of Vienna, Althanstrasse 14, Vienna A-1090, Austria

Craddock, John

craddock@macalaster.edu – Macalaster College, Geol. Dept., St. Paul, 1600 Grand Ave., Mn 55105

Danišik, Martin

martin.danisik@uni-tuebingen.de – University of Tübingen, Germany

Davaa, Buyan

buyan_arvijikh@hotmail.com – Geologisches Institut, Universität Freiburg Albertstrasse 23b, D-79104 Freiburg, Germany

Deckert, Hagen

deckert@uni-mainz.de – Institut für Geowissenschaften, Johannes Gutenberg-Universität, Becherweg 21, 55099 Mainz, Germany

Dietl, Carlo

C.Dietl@em.uni-frankfurt.de – Geologisch-Paläontologisches Institut, Johann-Wolfgang-Goethe-Universität Frankfurt am Main, Senckenberganlage 32-34 D-60054

Dietze, F.

Geol.-Pal. Institute, Ruprecht-Karls-University, INF 234, 69120 Heidelberg, Germany

Dobmeier, Christoph

Freie Universität Berlin, Department of Earth Sciences, Malteserstr. 74-100, 12249 Berlin

Doman, Daniel

daniel.doman@museum.hu-berlin.de – Humboldt-Universität zu Berlin, Museum für Naturkunde, Invalidenstr. 43, 10115 Berlin

Dorner, Dorothee

Max-Planck-Institut für Eisenforschung, Düsseldorf, Germany

Draganits, Erich

erich.draganits@tuwien.ac.at – Institute for Engineering Geology, Vienna University of Technology, A-1040 Vienna, Austria

Dresmann, Horst

Horst.Dresmann@unibas.ch – Geologisch-Palaeontologisches Institut, University of Basel, Switzerland

Dunkl, István

istvan.dunkl@geo.uni-goettingen.de – Geowissenschaftliches Zentrum der Georg-August-Universität Göttingen, Goldschmidtstr. 3, 37077 Göttingen

- Dworazik, Nina**
ndorazik@gmx.de – Institut für Geologie, Julius-Maximilians-Universität Würzburg, Pleicherwall 1 D-97070, Germany
- Ebert, Andreas**
ebert@geo.unibe.ch – Institut für Geologie, Universität Bern, Schweiz
- Edwards, Michael A.**
michael.edwards@univie.ac.at – Department of Geodynamics and Sedimentology, Structural Processes Group, University of Vienna, A-1090 Vienna, Austria
- Ehrlich, Ralf**
ralf.ehrlich@1petro.com – Ener Petroleum ASA, Lysaker Torg 5, 1325 Lysaker (Oslo), Norway
- Endres, Heike**
TEEC, Burgwedelerstr. 89, D-30916 Isernhagen
- Ertl, Gabriele**
ertl_gabi@yahoo.de – Geowissenschaftliches Zentrum der Georg-August-Universität Göttingen, Goldschmidtstr. 3, 37077 Göttingen
- Exner, Ulrike**
ulrike.exner@univie.ac.at – Department of Geodynamics and Sedimentology, Structural Processes Group, University of Vienna, A-1090 Vienna, Austria
- von Eynatten, Hilmar**
hilmar.von.eynatten@geo.uni-goettingen.de – Geowissenschaftliches Zentrum der Georg-August-Universität Göttingen, Goldschmidtstr. 3, 37077 Göttingen
- Færseth, Roald**
Norsk Hydro ASA, PO Box 7190 Bergen, Norway
- Finger, Fritz**
Abteilung für Mineralogie, Hellbrunner Str. 34, A-5020 Salzburg
- Fischer, Mario**
mariofischer@gmx.at – Geowissenschaftliches Zentrum der Georg-August-Universität Göttingen, Goldschmidtstr. 3, 37077 Göttingen
- Fiseli, Jochenl**
jochenfiseli@web.de – Geologisches Institut, Universität Freiburg, Albertstr. 23b, D-79104 Freiburg
- Freitag, Ralf**
ralf.freitag@uni-jena.de – Friedrich-Schiller-Universität Jena, Institut für Geowissenschaften, Burgweg 11, 07749 Jena
- Friese, Nadine**
nfriese@gwdg.de – Geowissenschaftliches Zentrum der Georg-August-Universität Göttingen, Goldschmidtstr. 3, 37077 Göttingen
- Frisch, Wolfgang**
wolfgang.frisch@uni-tuebingen.de – University of Tübingen, Germany
- Froitzheim, Nikolaus**
niko.froitzheim@uni-bonn.de – Geologisches Institut, Universität Bonn, Nußallee 8, 53115 Bonn
- Fügenschuh, Bernhard**
bernhard.fuegenschuh@uibk.ac.at – Institut für Geologie und Paläontologie, Universität Innsbruck, Innrain 52, Bruno Sander Haus, 6020 Innsbruck, Austria
- Gaedicke, Christoph**
Bundesanstalt für Geowissenschaften und Rohstoffe
- Gaich, Heiko**
heiko.gaich@tugraz.at – Institute of Applied Geosciences, Graz, Austria
- Geerds, Peter**
peter_geerds@yahoo.com – Geologisches Institut, Universität Freiburg Albertstrasse 23b, D-79104 Freiburg, Germany
- Gessner, Klaus**
kgessner@cyllene.uwa.edu.au – School of Earth and Geographical Sciences, University of Western Australia, 35 Stirling Highway, Crawley WA 6008, Australia

Geyer, Adelina

Institute of Earth Science, Jaume Almera, Barcelona, Spain

Giba, Marc

marc.giba@gmx.net – Geologisches Institut, Universität Freiburg, Albertstr. 23b, D-79104 Freiburg

Giese, Jörg

giese@geo.unibe.ch – Institute of Geological Sciences, Baltzerstraße 1–3, CH-3012 Bern, Switzerland

Giese, Steffen

Geotechnik im Bauwesen, RWTH Aachen, Germany

Glodny, Johannes

glodny@gfz.postdam.de – GeoForschungsZentrum Postdam, Telegrafenberg C2, 14473 Potsdam

Glotzbach, Christoph

christoph.glotzbach@uni-tuebingen.de – Institut für Geowissenschaften, Eberhard-Karls-Universität Tübingen

Gnos, Edwin

gnos@geo.unibe.ch – Institute of Geological Sciences, Baltzerstraße 1–3, CH-3012 Bern, Switzerland

Götze, Hans-Joachim

Universität Kiel, Germany

Grasemann, Bernhard

bernhard.grasemann@univie.ac.at – Department of Geodynamics and Sedimentology, Structural Processes Group, University of Vienna, A-1090 Vienna, Austria

Greiling, Reinhard O.

er8@ix.urz.uni-heidelberg.de – Geologisch-Paläontologisches Institut, Universität Heidelberg, Im Neuenheimer Feld 234, 69120 Heidelberg

Grimmer, J.C.

grimmer@urz.uni-hd.de – Geologisch-Paläontologisches Institut, Ruprecht-Karls Universität Heidelberg, Im Neuenheimer Feld 234, 69120 Heidelberg

Gross, Christian J.

cgross@gwdg.de – Geowissenschaftliches Zentrum der Georg-August-Universität Göttingen, Goldschmidtstr. 3, 37077 Göttingen

Gröger, Heike

heike.groeger@unibas.ch – Geologisch Paläontologisches Institut, Universität Basel, Bernoullistrasse 32, 4056 Basel, Switzerland

Gudmundsson, Agust

Agust.Gudmundsson@gwdg.de – Geowissenschaftliches Zentrum der Georg-August-Universität Göttingen, Goldschmidtstr. 3, 37077 Göttingen

Handy, Mark R.

Freie Universität Berlin, Department of Earth Sciences, Malteserstr. 74-100, 12249 Berlin

Hansen, Bent T.

bhansen@gwdg.de – Geowissenschaftliches Zentrum der Georg-August-Universität Göttingen, Goldschmidtstr. 3, 37077 Göttingen

Hauten, Sarah

sarahhauten@hotmail.com – Freie Universität Berlin, Department of Earth Sciences, Malteserstr. 74-100, 12249 Berlin

Heidelberg, Florian

Florian.Heidelberg@uni-bayreuth.de – Bayerisches Geoinstitut, University of Bayreuth, 95440 Bayreuth, Germany

Heinemann, Niklas

niklasheinemann@compuserve.de – Geologisches Institut, Universität Freiburg, Albertstr. 23b, D-79104 Freiburg

Henk, Andreas

henk@geologie.uni-freiburg.de – Geologisches Institut, Universität Freiburg, Albertstr. 23b, D-79104 Freiburg

Herwegh, Marco

herwegh@geo.unibern.ch – Institute of Geological Sciences, University of Bern,

- Baltzerstrasse 1–3, CH-3012 Bern, Switzerland
- Hilgers, Christoph**
c.hilgers@ged.rwth-aachen.de – Geologie-Endogene Dynamik, RWTH- Aachen, D-52056 Aachen, Germany
- Hirt, Ann M.**
hirt@mag.ig.erdw.ethz.ch – Institute of Geophysics, ETH Zurich, 8093 Zurich, Switzerland
- Hoffmann, Stefan**
s.hoffmann@geo.uni-goettingen.de – Geowissenschaftliches Zentrum der Georg-August-Universität Göttingen, Goldschmidtstr. 3, 37077 Göttingen
- Hofmann, Kai**
kayhofmann@gmail.com – Freie Universität Berlin, Institut für Geologische Wissenschaften, Malteserstrasse 74–100, D-12249 Berlin
- Hongn, Fernando**
CONICED and Universidad Nacional de Salta, Argentina
- Ibele, Tobias**
tobiasibele@web.de – Geologisches Institut, Universität Freiburg, Albertstr. 23B, D-79104 Freiburg
- Iglseder, Christoph**
christoph.iglseder@univie.ac.at – Department of Geodynamics and Sedimentology, Structural Processes Group, University of Vienna, A-1090 Vienna, Austria
- Jahn, Andreas**
andreas.jahn@museum.hu-berlin.de – Institut für Mineralogie, Museum für Naturkunde, Humboldt Universität zu Berlin, Invalidenstrasse 43, D-10115 Berlin
- Jansen, Ekkehard**
e.jansen@fz-juelich.de – Mineralogisches Institut, Universität Bonn, Forschungszentrum Jülich, D-52425 Jülich
- Jähne, Fabian**
fabian_jaehne@web.de – Friedrich-Schiller-Universität Jena, Institut für Geowissenschaften, Burgweg 11, 07749 Jena
- Jones, P.A.**
School of Earth Sciences, James Cook University Townsville QLD 4811, Australia
- Kenkmann, Thomas**
thomas.kenkmann@museum.hu-berlin.de – Institut für Mineralogie, Museum für Naturkunde, Humboldt-Universität Berlin, Invalidenstrasse 43, 10115 Berlin
- Kiechl, Eva**
ekiechl@sbbox.tugraz.at – Institute of Applied Geosciences, Graz, Austria
- van der Klauw, Sebastiaan**
klauw@ercosplan.com – Ercosplan – Ingenieurgesellschaft Geotechnik und Bergbau mbH, Arnstädter Strasse 28, 99096 Erfurt, Germany
- Klein, Thomas**
tklein@em.uni.frankfurt.de – Johann Wolfgang Goethe-Universität, Senckenberganlage 32-34, 60325 Frankfurt am Main
- Kleinhanns, Ilka C.**
ilka@geo.uni-goettingen.de – Geowissenschaftliches Zentrum der Georg-August-Universität Göttingen, Goldschmidtstr. 3, 37077 Göttingen
- Klemd, Reiner**
Institut für Mineralogie, Am Hubland, 97074 Würzburg
- Kley, Jonas**
jonas.kley@uni-jena.de – Friedrich-Schiller-University, IGW, Burgweg 11, 07749 Jena, Germany
- Klimczak, Christian**
christian.klimczak@museum.hu-berlin.de – Freie Universität Berlin, Institut für Geologische Wissenschaften, Malteser Strasse 74-100, D-12249 Berlin
- Klingenberg, B.**
Institut für Mineralogie und Lagerstättenlehre, RWTH Aachen, D-52056 Aachen

Koehn, Daniel

koehn@mail.uni-mainz.de – Tectonophysics, Institut of Geosciences, University of Mainz, Becherweg 21, 55099 Mainz, Germany

Kolb, J.

kolb@rwth-aachen.de – Institut für Mineralogie und Lagerstättenlehre, RWTH Aachen, Wüllnerstr. 2, D-52056 Aachen

Kontny, A.

Geol.-Pal. Institute, Ruprecht-Karls-University, INF 234, 69120 Heidelberg, Germany

Kopf, Achim

akopf@uni-bremen.de – DFG research center ocean margins, University of Bremen, Loebener Str., D-28359 Bremen

Kouankap, Nono Gus D.

Kouankap@yahoo.fr – Université de Yaoundé I, Département des Sciences de la Terre, BP : 812 Yaoundé-Cameroun

Kracke, Tobias

Geowissenschaftliches Zentrum der Georg-August-Universität Göttingen, Goldschmidtstr. 3, 37077 Göttingen

Kraus, Jurgen

jkraus@mac.com – Canadian Tectonics, 2011 20th Ave SW, Calgary, Alberta, Canada T2T

Krawcyk, Charlotte M.

lotte@gfz-potsdam.de – GFZ Potsdam, Telegrafenberg, D-14473 Potsdam

Krbetschek, Matthias

Sächsische Akademie der Wissenschaften

Krenn, Erwin

Abteilung für Mineralogie, Hellbrunner Str. 34, A-5020 Salzburg

Kruhl, Jörn H.

kruhl@tum.de – Tectonics and Material Fabrics Section, Technische Universität München, D-80290 München, Germany

Krumbholz, Michael

krumbholz_gesch@freenet.de – Geowissenschaftliches Zentrum der Georg-August-Universität Göttingen, Goldschmidtstr. 3, 37077 Göttingen

Kühn, Alexander

kuehna@uni-mainz.de – Institut für Geowissenschaften, Becherweg 21, Universität Mainz, D-55099 Mainz, Germany

Kukla, Peter

kukla@geol.rwth-aachen.de – RWTH Aachen, Geol. Institut, Wüllnerstr. 2, D-52056 Aachen

Kuntcheva, Boriana[†]

Tectonics and Material Fabrics Section, Technische Universität München, D-80290 München, Germany

Kunze, Karsten

kunze@erdw.ethz.ch – Geologisches Institut, ETH Zürich, CH-8092 Zürich

Kurz, Walter,

walter.kurz@tugraz.at – Institute of Applied Geosciences, Graz, Austria

Kück, Jochem

Geo-Forschungs-Zentrum Potsdam, Telegrafenberg, 14473 Potsdam

Küster, Martina

Institut für Geologie, Mineralogie und Geophysik, Ruhr-Universität Bochum, Germany, Collaborative Research Center 526

Küster, Yvonne

Y.Kuester@bgr.de – Bundesamt für Geowissenschaften und Rohstoffe (BGR) Hannover, Stilleweg 2, D-30655 Hannover

Laukamp, Carsten

carsten.laukamp@urz.uni-heidelberg.de – Geologisch-Paläontologisches Institut, Universität Heidelberg, Im Neuenheimer Feld 234

Leiss, Bernd

bleiss1@gwdg.de – Geowissenschaftliches Zentrum der Georg-August-Universität Göttingen, Goldschmidtstr. 3, 37077 Göttingen

Letourneur, Ludovic

letourneur_ludovic@yahoo.fr – Geowissenschaftliches Zentrum der Georg-August-

- Universität Göttingen, Goldschmidtstr. 3, 37077 Göttingen
- Lichtenberger, Marco**
mlichten@ix.urz.uni-heidelberg.de – Geologisch-Paläologisches Institut, Heidelberg University, Im Neuenheimer Feld 234, 69120 Heidelberg, FR Germany
- Liebl, Christoph**
christoph.liebl@mytum.de – Tectonics and Material Fabrics Section, Technische Universität München, D-80290 München, Germany
- Link, Klemens**
klemens.link@geolo.uni-giessen.de – Justus-Liebig-Universität Gießen, Gäßchen 25, 63667 Geiß-Nidda
- Liu, Junlai**
jliu@cugb.edu.cn – State Key Laboratory of Geological Processes and Mineral Resources, China University of Geosciences, Beijing 100083, China
- Lögering, M.J.**
markus.loegering@iml.rwth-aachen.de – Institut für Mineralogie und Lagerstättenlehre, RWTH Aachen, Wüllnerstr. 2, D-52056 Aachen
- Lohr, Tina**
lohr@gfz-potsdam.de – GFZ Potsdam, Telegrafenberg, D-14473 Potsdam
- López de Luchi, Mónica G.**
deluchi@ingeis.uba.ar – Instituto de Geocronología y Geología Isotópica (INGEIS), Ciudad Universitaria, 1428 Buenos Aires, Argentina
- Martin, Ulrike**
umartin@geologie.uni-wuerzburg.de – Institut für Geologie, Julius-Maximilians-Universität Würzburg, Pleicherwall 1 D-97070 Germany
- McEnroe, Suzanne**
Suzanne.McEnroe@ngu.no – Geological Survey of Norway, N-7040, Trondheim, Norway
- Meyer, F.M.**
m.meyer@rwth-aachen.de – Institut für Mineralogie und Lagerstättenlehre, RWTH Aachen, Wüllnerstr. 2, D-52056 Aachen
- Molli, Giancarlo**
gmolli@dst.unipi.it – Dipartimento di Scienze della Terra, Università di Pisa and CNR, Centro di Studio Geologia Strutturale e Dinamica dell'Appennino, Via San Maria 53, 56126 Pisa, Italien
- Mora, Andrés**
mora@geo.uni-potsdam.de – Institut für Geowissenschaften, Universität Potsdam, 14415 Potsdam, Germany
- Moser, Elmar**
elmar_moser@hotmail.com – Department für Geowissenschaften, Universität Hamburg, Bundesstraße 55, 20146 Hamburg
- Motagh, Mahadi**
motagh@gfz-potsdam.de – GFZ Potsdam, Telegraphenberg, Sektion 2.1, 14473 Potsdam
- Müller, Christian**
Geowissenschaftliches Zentrum der Georg-August-Universität Göttingen, Goldschmidtstr. 3, 37077 Göttingen
- Müller, Monika**
geomail@gmx.at – Department of Geodynamics and Sedimentology, Structural Processes Group, University of Vienna, A-1090 Vienna, Austria
- Münn, Sebastian**
smuenn@ifm-geomar.de – IFM-Geomar Kiel, Wischofstr. 1-3, 24148 Kiel
- Nagel, Thorsten**
tnagel@uni-bonn.de – Geologisches Institut Bonn, Nußalle 8, 53115 Bonn
- Naumann, M.**
Geoforschungszentrum Potsdam, Dept. Deformation und Rheologie, D-14473 Potsdam

Nemeth, Karoly

K.Nemeth@massey.ac.nz – Geological Institute of Hungary, 14 Stefania St., Budapest H-1143, Hungary

Neubert, Jana

JanaNbt@aol.com – Friedrich-Schiller-University, IGW, Burgweg 11, 07749 Jena, Germany

Nitzsche, Thomas

t.nitzsche@gga-hannover.de – Institut für Geowissenschaftliche Gemeinschaftsaufgaben (GGA) Hannover

Njiekak, Gautier

g.njiekak@em.uni-frankfurt.de – J.W.G. Universität Frankfurt a. Main, Senkenberganlage 32-34, Postfach 11 19 32, 60325 Frankfurt a. M.

Nommensen, Lisa

lisa.nommensen@web.de – Universität Freiburg, Runzstr. 6

Nüchter, Jens-Alexander

jens.nuechter@ruhr-uni-bochum.de – Institut für Geologie, Mineralogie und Geophysik, Ruhr-Universität Bochum, Germany, Collaborative Research Center 526

Obermeyer, Hennes

hennes.obermeyer@inka.de – Gesellschaft für Erkundung und Ortung, Yorckstraße 36, 76185 Karlsruhe, FR Germany

Oelrich, Asdis

asdis_oelrich@hotmail.com – Geowissenschaftliches Zentrum der Georg-August-Universität Göttingen, Goldschmidtstr. 3, 37077 Göttingen

Oncken, Onno

oncken@gfz-potsdam.de – GFZ Potsdam, Telegrafenberg, D-14473 Potsdam

Otto, Michael

motto4@gwdg.de – Geowissenschaftliches Zentrum der Georg-August-Universität Göttingen, Goldschmidtstr. 3, 37077 Göttingen

Parra, Mauricio

mauricio@geo.uni-potsdam.de – Institut für Geowissenschaften, Universität Potsdam, 14415 Potsdam, Germany

Passchier, Cees

Tectonophysics, Institut of Geosciences, University of Mainz, Becherweg 21, 55099 Mainz, Germany

Pennock, Gill

Utrecht University, Faculty of Earth Sciences, 3508 TA Utrecht, The Netherlands

Peternell, Mark

mark.peternell@tum.de – Tectonics and Material Fabrics Section, Technische Universität München, D-80290 München, Germany

Petrakakis, Konstantin

konstantin.petrakakis@univie.ac.at – Department of Geodynamics and Sedimentology, University of Vienna, A-1090 Vienna, Austria

Petrinovic, Ivan

CONICED and Universidad Nacional de Salta, Argentina

Petzel, Volker

vpetzel@mme.gov.na – Geological Survey of Namibia, 1 Aviation Road, Windhoek, Namibia

Pfaar, Rüdiger

rpfaar@gwdg.de – Geowissenschaftliches Zentrum der Georg-August-Universität Göttingen, Goldschmidtstr. 3, 37077 Göttingen

Pfiffner, Adrian

pfiffner@geo.unibern.ch – Institute of Geological Sciences, University of Bern, Baltzerstrasse 1–3, CH-3012 Bern, Switzerland

Philipp, Sonja L.

Sonja.Philipp@geo.uni-goettingen.de – Geowissenschaftliches Zentrum der Georg-August-Universität Göttingen, Goldschmidtstr. 3, 37077 Göttingen

- Picotti, Vincenzo**
picotti@geomin.unibo.it – University of Bologna, Italy
- Pleuger, Jan**
jan.pleuger@uni-bonn.de – Geologisches Institut, Universität Bonn, Nußallee 8, 53115 Bonn
- Rabitsch, Robert**
robert.rabitsch@tugraz.at – Institute of Applied Geosciences, Graz, Austria
- Rahn, Meinert**
Meinert.Rahn@hsk.de – Hauptabteilung für die Sicherheit der Kernanlagen, Villigen-HSK, CH
- Rambousek, Christian**
christianrambousek@hotmail.com – Department of Geodynamics and Sedimentology, Structural Processes Group, University of Vienna, Austria
- Rapalini, Augusto**
rapalini@gl.fcen.uba.ar – Instituto de Geofísica Daniel Valencio (INGEODAV), Departamento de Ciencias Geológicas, Facultad de Ciencias Exactas y Naturales, Universidad de Buenos Aires, CONICET, Pabellón 2, Ciudad Universitaria, 1428 Buenos Aires, Argentina
- Reinecker, John**
john.reinecker@uni-tuebingen.de – Institut für Geowissenschaften, Eberhard-Karls-Universität Tübingen
- Renard, François**
LGIT-CNRS-Observatoire, Université J. Fourier BP 53, F-38041 Grenoble, France
- Renk, Daniela**
dany.renk@freenet.de – Institut für Geologie, Julius-Maximilians-Universität Würzburg, Pleicherwall 1 D-97070 Germany
- Reuther, C.-D.**
reuther@geowiss.uni-hamburg.de – Department für Geowissenschaften, Universität Hamburg, Bundesstraße 55, 20146 Hamburg
- Richter, Peter P.**
prichter@uni-mainz.de – Institut für Geowissenschaften, Johannes Gutenberg-Universität, 55099 Mainz, Germany
- Riller, Ulrich**
ulrich.riller@museum.hu-berlin.de – Museum für Naturkunde der Humboldt-Universität zu Berlin, Invalidenstrasse 43, 10115 Berlin, Germany
- Ring, Uwe**
uwe.ring@canterbury.ac.nz – Department of Geological Sciences, Canterbury University, Christchurch, New Zealand
- Robinson, Peter**
Peter.Robinson@ngu.no – Geological Survey of Norway, N-7040, Trondheim, Norway
- Rolf, Christian**
r.rolf@gga-hannover.de – Institut für Geowissenschaftliche Gemeinschaftsaufgaben (GGA) Hannover
- Röller, Klaus**
Institut für Geologie, Mineralogie und Geophysik, Ruhr-Universität Bochum, Germany, Collaborative Research Center 526
- Roeser, Georg**
georg.roeser@geologie.uni-freiburg.de – University of Freiburg, Albertstrasse 23b, D-79104 Freiburg i. Brsg., Germany
- Roller, Sybille**
sybille.roller@uni-bonn.de – Geologisches Institut, Universität Bonn, Nußallee 8, 53115 Bonn
- Rosselli, Pascal**
Institute of Geophysics, ETH Zurich, 8093 Zurich, Switzerland
- Ruedrich, Joerg**
joerg.ruedrich@geo.uni-goettingen.de – Geowissenschaftliches Zentrum der Georg-August-Universität Göttingen, Goldschmidtstr. 3, 37077 Göttingen
- Ruiz, Amarildo Salina**
Dep. Geologia Geral, Universidade Federal de Mato Grosso-ICET/DGG

Rybacki, E.

Geoforschungszentrum Potsdam, Deformation und Rheologie, D-14473 Potsdam

Sachau, Till

sachau@uni-mainz.de – Institut für Geowissenschaften, Universität Mainz

Samiee, Ramin

TEEC, Burgwedelerstr. 89, D-30916 Isernhagen

Scherler, Dirk

dirk@geo.uni-potsdam.de – Institut für Geowissenschaften, Universität Potsdam, Karl-Liebknecht-Straße 24/25, D-14476 Golm

Schleder, Zsolt

Geologie-Endogene Dynamik, RWTH-Aachen, D-52056 Aachen, Germany

Schmatz, Joyce

joyce_schmatz@web.de – Geologie-Endogene Dynamik, RWTH Aachen, Germany

Schmid, Stefan M.

stefan.schmid@unibas.ch – Geologisch Paläontologisches Institut, Universität Basel, Bernoullistrasse 32, 4056 Basel, Switzerland

Schmidt, Sabine

Universität Kiel, Germany

Schmidt, Volkmar

schmidt@mag.ig.erdw.ethz.ch – Institute of Geophysics, ETH Zurich, 8093 Zurich, Switzerland

Schmittbuhl, Jean

IPG Strasbourg, UMR 7516 CNRS, 5 Rue Descartes, F-67084 Strasbourg Cedex, France

Schneider, Susanne

sanne5@web.de – Freie Universität Berlin. Institut für geologische Wissenschaften, FR Geologie, Malteserstr. 74-100, 12249 Berlin

Scholz, Katerina

k.scholz@ged.rwth-aachen.de – Geologie-Endogene Dynamik, RWTH Aachen, Germany

Schramm, Michael

M.Schramm@bgr.de – Bundesamt für Geowissenschaften und Rohstoffe (BGR) Hannover, Stilleweg 2, D-30655 Hannover

Schreurs, Guido

schreurs@geo.unibe.ch – Institute of Geological Sciences, Baltzerstraße 1–3, CH-3012 Bern, Switzerland

Schulz, Bernhard

Bernhard.Schulz@mineral.tu-freiberg.de – Institut für Mineralogie, Brennhausgasse 14, 09596 Freiberg/Sachsen

Schwarz, Michael

michael.schwarz.@geologie.uni-freiburg.de – Geologisches Institut, Universität Freiburg, Albertstr. 23B, 79104 Freiburg i. Breisgau

Schwarz, Stefan

stefan_goe@web.de – Geowissenschaftliches Zentrum der Georg-August-Universität Göttingen, Goldschmidtstr. 3, 37077 Göttingen

Schwarzbauer, J.

Institut für Mineralogie und Lagerstättenlehre, RWTH Aachen, Wüllnerstr. 2, D-52056 Aachen

Seib, Nadine

nadine.seib@uni-jena.de – Institut für Geowissenschaften, Universität Jena, Burgweg 11, 07749 Jena

Seidel, Torben

tseidel@gwdg.de – Geowissenschaftliches Zentrum der Georg-August-Universität Göttingen, Goldschmidtstr. 3, 37077 Göttingen

Siegesmund, Siegfried

ssieges@gwdg.de – Geoscience Centre of the University of Göttingen (GZG), Goldschmidtstr. 3, 37077 Göttingen, Germany

Siemes, Heinrich

siemes@rwth-aachen.de – Institut für Mineralogie und Lagerstättenlehre, RWTH Aachen, D-52056 Aachen

Sindern, Sven

sindern@rwth-aachen.de – Institut für Mineralogie und Lagerstättenlehre, RWTH-Aachen, Germany

Sjøholm, Jorunn

Norsk Hydro ASA, PO Box 7190 Bergen, Norway

Smørdal Lien, Kari

Norsk Hydro ASA, PO Box 7190 Bergen, Norway

Spiegel, Cornelia

cornelia.spiegel@uni-tuebingen.de – Institut für Geowissenschaften, Eberhard-Karls-Universität Tübingen

Spottke, Ina

Geologisch-Palaeontologisches Institut, University of Basel, Switzerland

Spray, John G.

Planetary and Space Science Centre, Department of Geology, University of New Brunswick, Canada

Steenken, André

asteenk@gwdg.de – Instituto de Geocronología y Geología Isotópica (INGEIS), Ciudad Universitaria, 1428 Buenos Aires, Argentina

Steffes, Elisabeth

elnino@zedat.fu-berlin.de – Freie Universität Berlin, Institut für Geologische Wissenschaften, Malteser Str. 74–100, D-12249 Berlin

Stipp, Michael

michael.stipp@geologie.uni-freiburg.de – Geologisches Institut, Universität Freiburg, Albertstr. 23b, D-79104 Freiburg

Stöckhert, Bernhard

Bernhard.stoeckhert@ruhr-uni-bochum.de – Institut für Geologie, Mineralogie und Geophysik, Ruhr-Universität Bochum, Germany, Collaborative Research Center 526

Strecker, Manfred

strecker@geo.uni-potsdam.de – Institut für Geowissenschaften, Universität Potsdam, 14415 Potsdam, Germany

Streit, Verena

verena_streit@yahoo.com – Institut für Geologie, Julius-Maximilians-Universität Würzburg, Pleicherwall 1 D-97070 Germany

Sverdrup, Einar

Ener Petroleum ASA, Lysaker Torg 5, 1325 Lysaker (Oslo), Norway

Sylvestre, Ganno

Université de Yaoundé I, Département des Sciences de la Terre, BP : 812 Yaoundé-Cameroun

Tanner, David C.

dtanner@gwdg.de – Geowissenschaftliches Zentrum der Georg-August-Universität Göttingen, Goldschmidtstr. 3, 37077 Göttingen

Thäter, Denise

denise.thaeter@web.de – Geowissenschaftliches Zentrum der Georg-August-Universität Göttingen, Goldschmidtstr. 3, 37077 Göttingen

Thöni, Martin

martin.thoeni@univie.ac.at – Department of Geodynamics and Sedimentology, Structural Processes Group University of Vienna, Althanstrasse 14, Vienna A-1090, Austria

Thust, Anja

— Geowissenschaftliches Zentrum der Georg-August-Universität Göttingen, Goldschmidtstr. 3, 37077 Göttingen

Timar-Geng, Zoltan

zoltan.timar-geng@geologie.uni-freiburg.de – Geologisches Institut, Universität Freiburg, Albertstr. 23b, D-79104 Freiburg

Tischler, Matthias

m.tischler@unibas.ch – Geologisch Paläontologisches Institut, Universität Basel, Bernoullistrasse 32, 4056 Basel, Switzerland

Toussaint, Renaud

IPG Strasbourg, UMR 7516 CNRS, 5

- Rue Descartes, F-67084 Strasbourg Cedex, France
- Trappe, Henning**
TEEC, Burgwedelerstr. 89, D-30916 Isernhagen
- Trautwein, Ute**
trautwein@geol.rwth-aachen.de – RWTH Aachen, Department of Geology, Germany
- Trepmann, Claudia A.**
Claudia.Trepmann@rub.de – Institut für Geologie, Mineralogie und Geophysik, Ruhr-Universität Bochum, Germany, Collaborative Research Center 526
- Trumbull, Robert**
GeoForschungsZentrum Potsdam, Germany
- Tullis, Jan**
jan_tullis@brown.edu – Department of Geological Sciences, Brown University, PO Box 1846, Providence, USA
- Ullemeyer, Klaus**
klaus.ullemeyer@geologie.uni-freiburg.de – Geologisches Institut, Universität Freiburg, Albertstr. 23B, D-79104 Freiburg
- Urai, Janos L.**
j.urai@ged.rwth-aachen.de – Geologie-Endogene Dynamik, RWTH Aachen, Germany
- Ustaszewski, Michaela**
ustaszewski@geo.unibern.ch – Institute of Geological Sciences, University of Bern, Baltzerstrasse 1-3, CH-3012 Bern, Switzerland
- Vahle, C.**
carsten_vahle@urz.uni-heidelberg.de – Geol.-Pal. Institute, Ruprecht-Karls-University, INF 234, 69120 Heidelberg, Germany
- Vogler, Marc**
vomarc@arcor.de – Geologisches Institut, Universität Freiburg Albertstrasse 23b, D-79104 Freiburg, Germany
- Voigt, Thomas**
thomas.voigt@uni-jena.de – Institut für Geowissenschaften, Universität Jena, Burgweg 11, 07749 Jena
- Voit, Klaus**
klaus_voit@gmx.at – Department of Geodynamics and Sedimentology, Structural Processes Group, University of Vienna, A-1090 Vienna, Austria
- Vollbrecht, Axel**
avollbr@gwdg.de – Geowissenschaftliches Zentrum der Georg-August-Universität Göttingen, Goldschmidtstr. 3, 37077 Göttingen
- Vrolijk, Peter**
ExxonMobil Upstream Research Co., Houston, TX, USA
- Wagner, Lars**
LWagner@gmx.com – Department of Geology, University of Gießen, Senkenbergstraße 3, D-35390 Gießen
- de Wall, Helga**
DeWall@geologie.uni-wuerzburg.de – Institut für Geologie, Julius-Maximilians-Universität Würzburg, Pleicherwall 1 D-97070 Germany
- Walter, Jens M.**
j.walter@fz-juelich.de – Mineralogisches Institut, Universität Bonn, Forschungszentrum Jülich, D-52425 Jülich
- Wemmer, Klaus**
kwemmer@gwdg.de – Geowissenschaftliches Zentrum der Georg-August-Universität Göttingen, Goldschmidtstr. 3, 37077 Göttingen
- Wetzel, Andreas**
Geol.-Paläont. Institut, Universität Basel, Bernoullistr. 32, CH-4056 Basel
- Wilde, A.S.**
School of Earth Sciences, Monash University Clayton, VIC 3400, Australia
- Willner, Arne P.**
Institut für Geologie, Mineralogie und Geophysik, Ruhr-Universität, 44870 Bochum, Germany

Winkler, Gerfried

gerfried.winkler@joanneum.at – Joanneum
Research, Institute of Water Resources
Management, Graz, Austria

Wittek, Andrea

andrea.wittek@gmx.net – FU Berlin, Mal-
teserstr. 74-100, 12249 Berlin

Zámolyi, András

a_zamolyi@gmx.at – Department of Geo-
dynamics and Sedimentology, Structural
Processes Group, University of Vienna,
Austria

Zander, Ina

ina.zander@uni-jena.de – Institut für
Geowissenschaften, Friedrich-Schiller-
Universität Jena, Burgweg 11, 07749
Jena

van der Zee, Wouter

GeoMechanics International, Mainz,
Germany

Ziegler, Martin

Geotechnik im Bauwesen, RWTH Aa-
chen, Germany

Zulauf, Gernold

g.zulauf@em.uni-frankfurt.de – Johann
Wolfgang Goethe-Universität, Sencken-
berganlage 32-34, 60325 Frankfurt am
Main

Øye, Vibeke

Norsk Hydro ASA, PO Box 7190 Bergen,
Norway

Seit nunmehr 20 Jahren findet regelmäßig alle zwei Jahre das Symposium "Tektonik, Struktur- und Kristallingeologie" statt. Die Tagung soll insbesondere jungen Nachwuchswissenschaftlern die Möglichkeit bieten, ihre Ergebnisse zu diskutieren und einem breiten Fachpublikum vorzustellen.

In diesem Jahr wird schon TSK 11 durchgeführt – zum zweiten Mal nach 1994 wieder in Göttingen.



Tübingen 1986



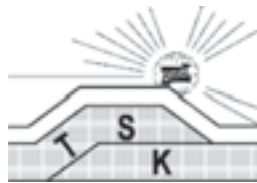
Erlangen 1988



Graz 1990



Frankfurt 1992



Göttingen 1994



Salzburg 1996



Freiberg 1998



Freiberg 2000



Erlangen 2002



Aachen 2004



Göttingen 2006



GEORG-AUGUST-UNIVERSITÄT
GÖTTINGEN